

CONTRIBUTION TO THE STUDY OF  
TENSION PILES  
UNDER CYCLIC LOADING

by

ALAIN MARCEL GOULOIS

Dipl. Ing., Ecole Centrale de Paris  
(1976)

M.S., University of Wisconsin - Madison  
(1976)

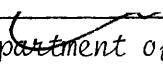
Submitted to the Department of  
Civil Engineering  
in Partial Fulfillment of the Requirements of the Degree of

Doctor of Philosophy  
at the  
Massachusetts Institute of Technology  
December 1982.

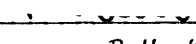
© Alain M. Goulois, 1982

The author hereby grants to M.I.T. ~~permission~~ to reproduce and  
to distribute copies of this ~~thesis~~ document in whole or in part.

Signature of Author

  
Department of Civil Engineering, December 1982.

Certified by

  
R.V. Whitman, Thesis Supervisor.

Accepted by

  
F. Morel, Chairman, Department Committee.  
MASSACHUSETTS INSTITUTE  
OF TECHNOLOGY

Archives DEC 09 1983 Archives

LIBRARIES

CONTRIBUTION TO THE STUDY OF  
TENSION PILES  
UNDER CYCLIC LOADING

by

Alain Marcel Goulois

Submitted to the Department of Civil Engineering  
on December 13, 1982 in partial fulfillment of the  
requirements for the Degree of Doctor of Philosophy

ABSTRACT

This thesis focuses on the study of a single tension pile embedded in clay and subjected to undrained cyclic loading conditions of the type experienced by Tension Leg Platform foundations during a storm. The proposed methodology makes possible the following of the soil-pile contact degradation and the estimation of the resulting redistributions of stresses and strains occurring during the passage of the storm as well as the vertical displacements of the foundation.

Three stages are distinguished. First a theoretical study of the cyclic behavior of a class of elasto-plastic models (Iwan models) used to represent the pile and the soil is presented. Then the effects of average stresses on the cyclic behavior of Plastic Drammen Clay are discussed. The results of 12 constant volume stress-controlled direct simple shear (DSS) tests are used to introduce a new format of presentation allowing for easy interpolations and extrapolations of the data over a wide range of stresses. Finally the development of the computer code TLPIL is detailed. It integrates the mechanical model and the soil degradation data into an analytical tool leading to estimates of the cyclic behavior of tension piles which are in general agreement with experimental evidence. Parametric studies reveal the benefits from having a stiff pile, and suggest that present regulations are adequate for the particular configurations and soil studied.

Thesis Supervisor : R.V. Whitman  
Title : Professor of Civil Engineering

à Dominique,  
Carlos,  
Félix,  
Adriano,  
Marie-Agnès,  
Steve,  
Suzanne,  
Jano,  
Barbara,  
Colette,  
Claire,  
Philippe,  
Paul,  
Pierrot,  
Patrice,  
David,  
Hayan,  
John,  
Hugo,  
Marthe,  
Aziz,  
Michèle,  
Jean-Pierre,  
Rémi,  
Sylvie,  
Elisabeth,  
Albert,  
Guy,  
Claudine,  
Victor,  
Christiane,  
Pierre,  
Anne,  
Simone,  
Judy,  
Andrée,  
Roland,  
Minoru,  
Marc,  
Gouriche,  
Sandrine,  
Ameline,  
Yogi,  
Bobby,  
Adèle,  
Serge,  
Georgette,  
Jean-Jacques,  
Nicole,

Waldemar,  
Isabelle,  
Nicolas,  
Bernard,  
Madeleine,  
Hélène,  
Lu,  
Samih,  
Maurice,  
Jean,  
Sylvianne,  
Michael,  
Yves,  
Miguel,  
Marcel,  
Franco,  
Huguette,  
Chantal,  
Stanley,  
Claude,  
Marie,  
Marcelle,  
Joe,  
Odette,  
Pedro,  
Renée,  
Georges,  
Alain,  
Ghilaine,  
Mike,  
Karin,  
Roger,  
Allin,  
Martine,  
Alfredo,  
Jean-Luc,  
Michel,  
Christine,  
Patrick,  
Réjane,  
Lucien,  
Francis,  
Bill.  
...

ACKNOWLEDGMENTS.

The author wishes to express his deepest appreciation to the Societe Nationale Elf Aquitaine for suggesting and sponsoring this research in an ideal atmosphere of trust. He is particularly thankful to Mr. Claude Cochard, Mr. Reynald Bonmati, and Mr. Charles Vernet for their constant support.

Professor Robert V. Whitman has advised the author throughout his work. His acute engineering judgment and the sharpness of his comments have been invaluable, as was his human support in difficult moments. Professors Charles C. Ladd and Amr S. Azzouz have provided continuous guidance as members of the doctoral committee. The author is very grateful for their assistance and their availability in times of heavy professional commitments.

Dr. Kaare Hoeg and his colleagues of the Norwegian Geotechnical Institute, and especially Suzanne Lacasse, Knut Andersen and Kjell Karlsrud, have actively contributed to this thesis which was truly initiated while the author was a Fellow at N.G.I.. Their support has been faultless, as was their friendship, and the testing program would never have been realized without them.

Joe Goss, Steve Hale, Mike Morrison and Yogi have tremendously helped the author in the presentation of this thesis despite the considerable obstacles created by gallicisms and handwriting. But the true burden of this work rested on the shoulders of Dominique who has made it all possible.

Cambridge, December 1982.

TABLE OF CONTENTS.

		<u>Page No.</u>
TITLE PAGE	.....	1
ABSTRACT	.....	2
ACKNOWLEDGEMENTS	.....	5
TABLE OF CONTENTS	.....	6
LIST OF TABLES	.....	11
LIST OF FIGURES	.....	12
Chapter 1	<u>THE PROBLEM AND ITS CONTEXT</u> .....	24
1.1	<u>BACKGROUND OF THE RESEARCH SUBJECT</u> .....	24
1.1.1	<u>Deep water production</u> .....	24
1.1.2	<u>The tension leg platform (TLP)</u> .....	25
1.1.3	<u>The TLP Foundation</u> .....	28
1.2	<u>THE PRESENT THESIS</u> .....	32
1.2.1	<u>Statement of objectives</u> .....	32
1.2.2	<u>Research orientation</u> .....	32
1.2.3	<u>Thesis organization</u> .....	37
Chapter 2	<u>STATE-OF-THE-ART</u> .....	38
2.1	<u>TENSION PILES UNDER STATIC LOADING</u> .....	39
2.2	<u>CYCLIC LOADING ON TENSION PILES</u> .....	49
2.3	<u>MODELS</u> .....	61
2.3.1	<u>Soil behavior under cyclic loading</u> .....	61
2.3.2	<u>Models of tension piles under cyclic loading</u> ...	64
A.	<u>Implicit procedures</u> .....	65
B.	<u>Explicit procedures</u> .....	68
C.	<u>Conclusions</u> .....	73

Chapter 3	<u>THE PILE MODEL</u> .....	74
3.1	<u>FUNCTION OF THE PILE MODEL</u> .....	74
3.2	<u>FIRST DESCRIPTION OF THE PILE MODEL</u> .....	78
3.3	<u>BEHAVIOR OF THE PILE MODEL UNDER CYCLIC LOADING</u> ..	81
3.3.1	<u>An introductory example</u> .....	81
3.3.2	<u>Masing's rules and Iwan models</u> .....	87
3.3.3	<u>Properties of Iwan models</u> .....	88
	A. <u>The Prandtl body</u> .....	92
	B. <u>The generalized P-body and the infinite P-body</u> ..	96
	C. <u>Iwan models and Random assemblies</u> .....	106
	D. <u>A physical analog to Iwan models</u> .....	107
	E. <u>A few extensions of Persoz's results</u> .....	111
3.3.4	<u>Shakedown analysis</u> .....	118
	A. <u>Melan's theorem</u> .....	119
	B. <u>A simple pile model</u> .....	123
3.4	<u>BACK TO THE DESCRIPTION OF THE PILE MODEL</u> .....	126
Chapter 4	<u>CONTRIBUTION OF AVERAGE SHEAR STRESSES TO</u> <u>THE CYCLIC DEGRADATION OF CLAY</u> .....	135
4.1	<u>BACKGROUND</u> .....	135
4.2	<u>TEST CONDITIONS</u> .....	148
4.2.1	<u>Equipment</u> .....	148
	A. <u>The DSS apparatus</u> .....	148
	B. <u>The height control mechanism</u> .....	150
	C. <u>The data acquisition system</u> .....	150
4.2.2	<u>Clay and specimen</u> .....	152
4.2.3	<u>Loading program</u> .....	154

		<u>Page No.</u>
Chapter 4.2.3.A.	<u>Consolidation</u> .....	155
	<u>B. Drained shear and creep</u> .....	155
	<u>C. Cyclic loading</u> .....	156
4.3	RESULTS OF THE CYCLIC TESTING .....	158
4.4	SYNTHESIS OF THE RESULTS .....	173
4.4.1	<u>Iso-<math>\gamma_c</math> and iso-<math>\gamma_{ave}</math> networks</u> .....	174
4.4.2	<u>Degradation of the iso-<math>\gamma_c</math> network</u> .....	186
4.4.3	<u>Degradation of the iso-<math>\gamma_{ave}</math> network</u> .....	187
4.5	COMMENTS AND INTERPRETATIONS .....	198
4.5.1	<u>Shape of the strain contour diagrams</u> .....	198
	<u>A. The first cycle of loading</u> .....	198
	<u>B. After the first cycle</u> .....	207
4.5.2	<u>Interpretations of the variable cyclic tests</u> ...	208
	<u>A. Andersen's procedure</u> .....	208
	<u>B. Extension to <math>\gamma_{ave} \neq 0</math></u> .....	211
4.6	SUMMARY .....	215
Chapter 5	<u>TLPILE : THE ANALYTICAL TOOL</u> .....	216
5.1	MODIFICATION OF THE SOIL-PILE PARAMETERS .....	216
5.2	NUMERICAL ASPECTS OF THE PILE MODEL .....	223
5.3	SOIL DEGRADATION DATA BASE .....	230
5.4	ORGANISATION OF TLPILE AND ITERATION SCHEME ....	237



		<u>Page No.</u>
5.5	EXAMPLES OF APPLICATION OF TLPILE .....	244
5.5.1	<u>Presentation of the examples</u> .....	244
5.5.2.	<u>The basic example</u> .....	249
<u>A.</u>	<u>Description of the input</u> .....	249
<u>B.</u>	<u>Static loadings</u> .....	249
<u>C.</u>	<u>Cyclic loading</u> .....	252
5.5.3	<u>Variations around the basic example</u> .....	257
<u>A.</u>	<u>A geometric parameters</u> .....	257
a)	<u>Thickness</u> .....	257
b)	<u>Diameter</u> .....	260
c)	<u>Choice of template</u> .....	263
<u>B.</u>	<u>Safety parameters</u> .....	265
5.5.4	<u>Conclusions</u> .....	267
Chapter 6	<u>SUMMARY, CONCLUSIONS AND RECOMMENDATIONS</u> .....	270
6.1	SUMMARY .....	270
6.1.1	<u>Recapitulation of objectives</u> .....	270
6.1.2	<u>Contributions</u> .....	270
<u>A.</u>	<u>The Pile Model</u> .....	271
<u>B.</u>	<u>The soil degradation data</u> .....	272
<u>C.</u>	<u>TLPILE</u> .....	273
6.2	CONCLUSIONS AND RECOMMENDATIONS .....	276
References	.....	283
Appendix 3	<u>SHAKEDOWN ANALYSIS</u> .....	291
3.A	INTRODUCTION .....	291
3.B	SHAKEDOWN ANALYSIS .....	294

		<u>Page No.</u>
3.B.1	<u>Background</u> .....	294
3.B.2	<u>Terminology</u> .....	299
3.B.3	<u>Theorems</u> .....	303
3.C	EXAMPLES OF APPLICATION OF SHAKEDOWN ANALYSIS .	309
3.C.1	<u>Presentation of the examples</u> .....	309
3.C.2	<u>No separation : the "pile foundation" case</u> ....	311
3.C.3	<u>Separation : the superficial foundation case</u> ..	321
Appendix 4	<u>COMPLEMENTARY EXPERIMENTAL RESULTS</u> .....	329
4.A	GENERAL DATA .....	329
4.B	PREPARATION AND INDEX PROPERTIES.....	332
4.C	CONSOLIDATION, SHEAR AND CREEP .....	338
4.D	CYCLIC LOADING .....	345
4.E	COMPARISON OF TESTS (2) AND (12) .....	358
Appendix 5	<u>LISTINGS OF COMPUTER PROGRAMS AND DATA FILE</u> ...	363
5.A	SUBROUTINE CYCDEG .....	363
5.B	PROGRAM TLPILE .....	372
5.C	DATA FILE FOR EXAMPLE <u>/1/</u> .....	396

LIST OF TABLES

<u>Table No.</u>	<u>Title</u>	<u>Page No.</u>
3.3.1	Mathematical models for symmetric loading .....	90
4.2.1	Origin of the clay .....	152
4.2.2	Summary of test conditions .....	157
4.3.1	Essential test parameters at all stages of loading .....	160
4.3.2	Shear stresses applied .....	161
5.5.1	Definition of examples .....	248
5.5.2	Various definitions of the ultimate capacities and factors of safety .....	267
6.1.1	Summary .....	275

LIST OF FIGURES.

<u>Fig. No.</u>	<u>Title</u>	<u>Page No.</u>
1.1.1	Tension leg platform for Hutton field .....	27
1.2.1	Schematic of the force applied to the top of the foundation .....	33
1.2.2	Shear stresses during cycling .....	34
2.1.1	Measured versus calculated ultimate capacities in tension .....	41
2.1.2	Correlation of ultimate friction capacities in tension and in compression .....	43
2.1.3	Sustained tension loading - history of the pile top displacement ( 31 ) .....	46
2.1.4	French recommendations for the testing of piles ....	47
2.1.5	Plancoët tension pile : load-deflection curves and creep-curves from static tests $S_2$ and $S_3$ . Determination of the creep load. (After Puech and Jezequel  89 ) .....	48
2.2.1	Load - Displacement response under cyclic loading - Empire test site. (After Kraft et al.  56 ) .....	51
2.2.2	a) Types of loadings applied to the Plancoët pile. b) Time history of the pile top displacement during test C21. c) Load distributions in the pile during test C21. (After Puech  89 ,  86 ) .....	52

LIST OF FIGURES (Continued)

<u>Fig. No.</u>	<u>Title</u>	<u>Page No.</u>
2.2.3	a) Time history of the pile top displacement during test C12.	
	b) Time history of the pile top displacement during test C11.	
	c) Time history of the pile top displacement during test T2. (After Puech  86 ) .....	53
2.2.4	Comparison of static and cyclic creep loads - Plancoët Pile .....	55
2.2.5	Comparison of time histories of top pile displacements at Cran and at Plancoët. (After Puech  87 ) .....	55
2.2.6	Cyclic loading applied to the pile head. (After McAnoy et al.  70 ) .....	57
2.2.7	Pile head displacements (a) cyclic amplitude (b) mean. (After McAnoy et al.  70 ) .....	58
2.2.8	Load distributions. (After McAnoy et al.  70 ) ....	59
2.3.1	Schematics of implicit and explicit treatments of cyclic degradation .....	62
3.1.1	Explicit scheme .....	75
3.1.2	Loading at pile top .....	75
3.2.1	Pile Model .....	79

LIST OF FIGURES (Continued)

<u>Fig. No.</u>	<u>Title</u>	<u>Page No.</u>
3.3.1	A simple Iwan Model .....	82
3.3.2	Introductory example, first loading curve .....	84
3.3.3	Introductory example, successive loadings .....	85
3.3.4	Extended Masing Rules .....	89
3.3.5	Decomposition in series and parallel of an Iwan Model .....	91
3.3.6	Riener's rheological tree .....	92
3.3.7	Typical St Venant body stress-strain diagram ....	93
3.3.8	An unacceptable Hooke body stress-strain diagram ..	94
3.3.9	Schematic of the Prandtl body .....	95
3.3.10	First deformation curve .....	95
3.3.11	Geometrical interpretation of Equation 3.2 .....	97
3.3.12	Unloading from the first deformation curve .....	99
3.3.13	Slope discontinuity at A .....	102
3.3.14	Stabilization to a closed loop .....	103
3.3.15	Example of stabilization under regular cyclic loading .....	105

LIST OF FIGURES (Continued)

<u>Fig. No.</u>	<u>Title</u>	<u>Page No.</u>
3.3.16	A physical analog to a P-body .....	108
3.3.17	Physical analog of a generalized P-body .....	110
3.3.18	Example of stabilization under regular cyclic loading .....	112
3.3.19	Analog of an asymmetric P-body .....	113
3.3.20	Construction of the asymmetric first deformation curves .....	115
3.3.21	Cyclic responses of an elasto plastic element ...	119
3.3.22	Graphical decomposition of the stress .....	121
3.3.23	Changes of stresses .....	122
3.3.24	Simple pile model .....	123
3.3.25	Recap of the results of the pile example .....	125
3.4.1	"t-z" curves. (From Ref. [22]) .....	126
3.4.2	Stress strain relationships for DSS specimen at several distances away from the pile corresponding to pile loading conditions. (Private communication from Kavvadas) .....	129
3.4.3	Construction of "t-z" curve .....	131

LIST OF FIGURES (Continued)

<u>Fig. No.</u>	<u>Title</u>	<u>Page No.</u>
3.4.4	Algorithm used in the decomposition in Prandtl bodies .....	132
3.4.5	Update of Figure 3.1.1 .....	133
4.1.1	Rigid pile in uniform NC clay exhibiting normalized behavior $\tau_{ave} = \tau_{cons}$ .....	136
4.1.2	Combinations of $\tau_{ave}$ and $\tau_c$ causing failure .....	138
4.1.3	Combinations of $\tau_{ave}$ and $\tau_c$ causing different strains - Vicksburg silty clay .....	140
4.1.4	Loading patterns .....	140
4.1.5	Cyclic strength contours .....	142
4.1.6	Optimum resistance value of $\tau_{ave}$ .....	143
4.1.7	Shear loading and notations .....	145
4.1.8	Test stress range .....	146
4.2.1	The experimental set up .....	149
4.2.2	Description of profile for Danviksgt.50301, Drammen. (After N.G.I.) .....	151
4.2.3	Loading schedule .....	154



LIST OF FIGURES (Continued)

<u>Fig. No.</u>	<u>Title</u>	<u>Page No.</u>
4.2.4	Pulse shape .....	156
4.3.1	Relative positioning of the tests and summary of results .....	159
4.3.2	Results of tests ①, ③, ⑦ and ⑪ .....	165
4.3.3	Results of tests ④ and ⑧ .....	166
4.3.4	Results of tests ⑤ and ⑥ .....	167
4.3.5	Results of tests ② and ⑫ .....	168
4.3.6	Results of test ⑨ .....	169
4.3.7	Results of test ⑩ .....	170
4.3.8	Comparison between test ⑧ and segments of tests ⑨ and ⑩ .....	171
4.3.9	Degradation of the cyclic shear modulus .....	172
4.4.1	Andersen's results   2   .....	175
4.4.2	a) Section of iso- $\gamma_c$ network at N = 50 cycles ...	176
	b) Section of iso- $\gamma_{ave}$ network at N = 50 cycles ...	177
4.4.3	a) Section of iso- $\gamma_c$ network at N = 100 cycles ...	178
	b) Section of iso- $\gamma_{ave}$ network at N = 100 cycles ..	179

LIST OF FIGURES (Continued)

<u>Fig. No.</u>	<u>Title</u>	<u>Page No.</u>
4.4.4	a) Section of iso- $\gamma_c$ network at N = 200 cycles ....	180
	b) Section of iso- $\gamma_{ave}$ network at N = 200 cycles ...	181
4.4.5	a) Section of iso- $\gamma_c$ network at N = 500 cycles ....	182
	b) Section of iso- $\gamma_{ave}$ network at N = 500 cycles ...	183
4.4.6	a) Section of iso- $\gamma_c$ network at N = 1000 cycles ....	184
	b) Section of iso- $\gamma_{ave}$ network at N = 1000 cycles ..	185
4.4.7	a) Sections of iso- $\gamma_c$ surface for $\gamma_c = 0.15\%$ at various numbers of cycles .....	188
	b) Sections of iso- $\gamma_c$ surface for $\gamma_c = 0.25\%$ at various numbers of cycles .....	189
	c) Sections of iso- $\gamma_c$ surface for $\gamma_c = 0.5\%$ at various numbers of cycles .....	190
4.4.8	a) Sections of iso- $\gamma_{ave}$ surface for $\gamma_{ave} = 2.5\%$ at various numbers of cycles .....	191
	b) Sections of iso- $\gamma_{ave}$ surface for $\gamma_{ave} = 3\%$ at various numbers of cycles .....	192
	c) Sections of iso- $\gamma_{ave}$ surface for $\gamma_{ave} = 4\%$ at various numbers of cycles .....	193
	d) Sections of iso- $\gamma_{ave}$ surface for $\gamma_{ave} = 6\%$ at various numbers of cycles .....	194
4.4.9	a) Sections of the iso- $\gamma_c$ network at N = 100 and N = 1000 .....	195
	b) Sections of the iso- $\gamma_{ave}$ network at N = 100 and N = 1000 .....	196

LIST OF FIGURES (Continued)

<u>Fig. No.</u>	<u>Title</u>	<u>Page No.</u>
4.5.1	a) Effective stress paths for undrained static simple shear tests. (After Andersen   2  ) ....	200
	b) Stress-strain curves for undrained static DSS tests .....	200
4.5.2	Stress strain relationships for plastic Drammen clay .....	201
4.5.3	Undrained DSS on Lierstranda quick clay with consolidation under $\tau_{cons} \neq 0$ . (After Bjerrum and Kenney   11  ) .....	202
4.5.4	Use of asymmetric P-bodies to model effect of consolidation under $\tau_{cons}$ .....	203
4.5.5	Estimation of $\gamma_{ave}$ at $N = 1$ .....	205
4.5.6	Comparison of iso- $\gamma_{ave}$ networks .....	206
4.5.7	Andersen's procedure .....	209
4.5.8	Use of data base in Andersen's procedure .....	210
4.5.9	Prediction of test ⑨ Andersen's procedure with fit on $\gamma_{ave}$ .....	213
4.5.10	Prediction of test ⑩ Andersen's procedure with fit on $\gamma_{ave}$ .....	214

LIST OF FIGURES (Continued)

<u>Fig. No.</u>	<u>Title</u>	<u>Page No.</u>
5.1.1	a) Storm loading on Illite ( $\tau_{ave} = 0$ ). b) Storm loading on Bentonite ( $\tau_{ave} = 0$ ) .....	218
5.1.2	Andersen's procedure. Use of the N = 1 curve .....	219
5.1.3	a) Static loading after cycling. (After Andersen   2  ). b) Construction of stress-strain relationships after cycling .....	220
5.1.4	Modification of the stress-strain relationship with cycling .....	222
5.1.5	Artifice used to impose the permanent displacement to the "fixed" reference .....	222
5.2.1	a) P-body and the equivalent linear force and internal forces. b) Stress-strain diagram explaining the equivalence .....	223
5.2.2	Relative position of the result of the elastic solution with respect to the starting and yield points .....	224
5.2.3	Example of determination of the next P-body to yield ..	225
5.2.4	Global numbering and global stiffness matrix .....	226
5.2.5	Flow chart of Pile Model computations .....	226

LIST OF FIGURES (Continued)

<u>Fig. No.</u>	<u>Title</u>	<u>Page No.</u>
5.2.6	Numerical check of the behavior of the Pile Model subjected to a loading similar to the one of Figure 3.3.15 .....	228
5.3.1	a) Section of iso- $\gamma_c$ network at N = 5000 cycles (Estimated) .....	231
	b) Section of iso- $\gamma_c$ network at N = 5000 cycles (Estimated) .....	232
5.3.2	a) Discretization of iso- $\gamma_c$ network at N = 100 .....	233
	b) Discretization of iso- $\gamma_{ave}$ network at N = 100 ...	234
5.3.3	Partial axisymmetric view of the iso- $\gamma_{ave} = 4\%$ network .....	235
5.3.4	Simplified flow-chart of subroutine CYCDEG .....	236
5.4.1	Iteration scheme .....	239
5.4.2	Basic variables used in TLPILE (1) .....	241
5.4.3	Basic variables used in TLPILE (2) .....	242
5.4.4	Flow chart of TLPILE .....	243
5.5.1	Force displacement curve to failure, basic example ...	250
5.5.2	a) Force distribution in pile, static loading	
	b) Shear stress distribution on pile static loading ..	251

LIST OF FIGURES (Continued)

<u>Fig. No.</u>	<u>Title</u>	<u>Page No.</u>
5.5.3	a) Force-displacement at pile top, example <u>/1/</u> . b) History of displacement at pile top, example <u>/1/</u> ...	254
5.5.4	a) Force distribution in pile, example <u>/1/</u> , lower load level. b) Shear stress distribution on pile, example <u>/1/</u> , lower load level .....	255
5.5.5	a) Force distribution in pile, example <u>/1/</u> , upper load level. b) Shear stress distribution on pile, example <u>/1/</u> , upper load level .....	256
5.5.6	a) Force-displacement at pile top, example <u>/5/</u> uniform wall thickness of 3". b) History of displacement at pile top, example <u>/5/</u> uniform wall thickness of 3" .....	258
5.5.7	a) Shear stress distribution in pile, example <u>/1/</u> uniform wall thickness of 2". b) Shear stress distribution in pile, example <u>/5/</u> uniform wall thickness of 3" .....	259
5.5.8	a) Force-displacement at top, example <u>/6/</u> pile diameter 48". b) History of displacement at pile top, example <u>/6/</u> pile diameter 48" .....	261
5.5.9	a) Force distribution in pile, example <u>/6/</u> pile diameter 48".	

LIST OF FIGURES (Continued)

<u>Fig. No.</u>	<u>Title</u>	<u>Page No.</u>
5.5.9	b) Shear stress distribution on pile, example $\overline{16}$ pile diameter 48" .....	262
5.5.10	a) Force-displacement at top, example $\overline{13}$ 12-pile template b) History of displacement at pile top, example $\overline{13}$ 12-pile template .....	264
5.5.11	Force displacement relationships and histories of the displacement at the pile top for various values of the factor of safety F.S. ....	266
5.5.12	Permanent displacement versus factor of safety F.S. ..	268
6.2.1	Potential domains of application of soil degradation data .....	280

## 1 THE PROBLEM AND ITS CONTEXT

The Tension Leg Platform is certainly one of the favorite topics in the offshore industry today because it might be the best option to produce oil in deep waters\*...

### 1.1 BACKGROUND OF THE RESEARCH SUBJECT

Most of the major oil companies have been involved for several years now in the preliminary engineering of the Tension Leg Platform (TLP). What are their motivations ? What exactly is a TLP ? And what type of problems will the geotechnical engineer be faced with ? Such are some of the key questions we should first consider.

#### 1.1.1 Deep water production

Deep water discoveries of oil and gas have been made over the last years, the presence of which cannot be ignored in today's energy-avid society. Exploration techniques are now very well mastered to water depths of some 3 000 feet and the first drilling by 6 000 feet of water is seriously envisioned. New leases of blocks in deep water are made in large number every year. In the United States the government, which had been until now limiting these leases to some parts of Southern California, the Gulf of

---

\* The term "deep" waters is very much dependent on the environmental conditions ; in the Gulf of Mexico it could be depths greater than 1000 ft, while in the North Sea "deep" water would start around 650 ft.



Mexico and some East coast areas, has recently announced its intention to issue exploration permits along the entire coast line. And this trend is not limited to the US ; Norway has discovered major reservoirs by deep waters and important new fields are thought to exist in Easter Canada, Western Australia, in the Mediterranean sea, etc ...

The very difficult environment associated with large water depths has required the development of totally new concepts in parallel with extensions of the traditionnal jacket supports. But, as water depth increases, the cost of the latter becomes prohibitive and their dynamic behavior becomes problematic (their natural frequencies approaching the peak of the sea wave spectrum), leaving the whole field open for innovation.

One way to minimize the impact of environmental loading is to use compliant structures (the natural frequencies of which will be much smaller than the peak of the sea wave spectrum). Four main concepts are presently considered : semi-submersibles with catenary mooring, guyed towers, articulated towers and tension leg platforms. Discussions of the pros and cons of each concept can be found for example in Huslid et al., 1982 [47]. At the present time, feasibility studies have a tendency to favor the TLP over the others and this explains the tremendous interest shown by the industry for this new concept, which will now be described in some detail.

#### 1.1.2 The Tension Leg Platform (TLP)

The tension leg platform has best been described by CONOCO engineers as "a huge upside-down pendulum, with buoyancy replacing gravity". The

---

\* "Hutton's TLP-CONOCO Reveals The Shape of Thing To Come", Offshore Engineer, Feb. 1980.

Tension Leg Platform is composed of two parts : a floating structure and an anchorage system of vertical "legs" attached to the sea bed. These legs are always in tension - even in the worst environment conditions - and insure that the buoyancy of the platform is always in excess of its displacement\*. As a direct consequence the structure will have a very high vertical rigidity, and essentially no heave motion. One such structure is represented in Figure 1.1.1 : it is the first production TLP to be constructed and will be installed on the Hutton field in the Northern North Sea in 1983 by CONOCO\*\*. This figure clearly shows the groups of legs positioned at the four corners of the deck. There are four legs per corner connecting to the same foundation template, and therefore a total of 16 legs for the entire structure. The network of conductors visible in the center part of the structure, in between the deck and the production template, corresponds to the production risers and the injection lines. This network is itself maintained in constant tension, which is one of the key advantages of the TLP as it minimizes fatigue in the risers, eliminates the need for large heave compensators, and permits the installation of the well heads on the deck. Other advantages of the TLP concept include :

- . a very limited sensitivity to water depth,
- . the fact that it is an "early production system", - wells can be predrilled before the installation of the structure and be producing immediately after installation, which is very rapid since the whole

---

\* Weight of the water displaced by the structure.

\*\* See "Evolution of the Tension Leg Platform Technology" by J.A. Mercier  
|74 |.

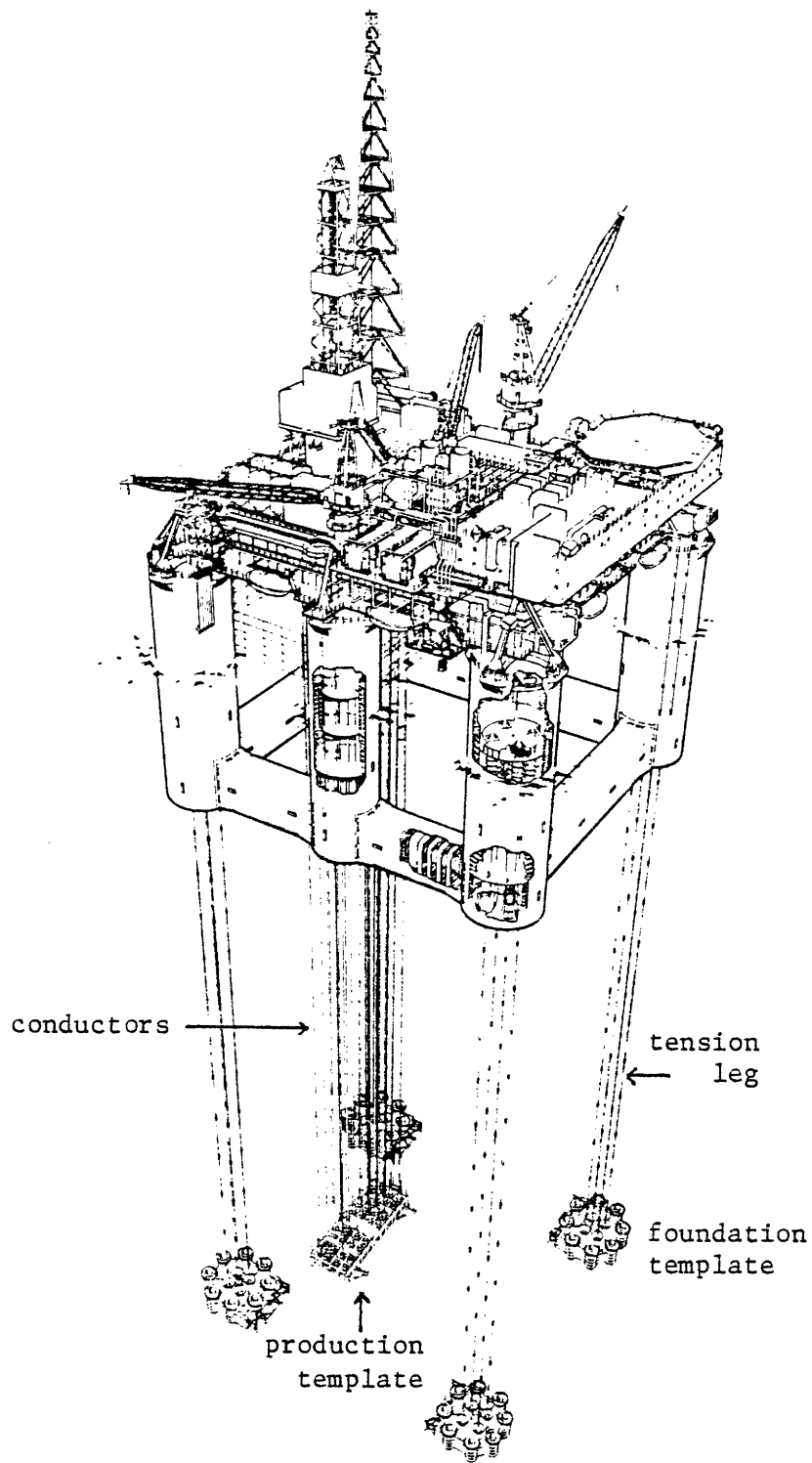


Figure 1.1.1 Tension leg platform  
for Hutton field.

- floating structure can be towed to the site fully equipped, - and the foundation templates can be preinstalled -
- . that it is operational 90 % of the time,
  - . and that it can be salvaged at the end of production.

There are also problems associated with this new concept. The behavior of the risers and of the tension members under hydrodynamic conditions and fatigue is certainly the most complex of these issues. In the design stage the structure is also quite sensitive to weight, but it is the foundation problem which will mostly draw our attention. This is a situation where the foundation becomes a major issue affecting the feasibility of an offshore project as a whole\*.

### 1.1.3 The TLP Foundation

What type of loading will the Hutton TLP apply to its foundations ?  
The newest information (Mercier |74|) indicates, per foundation template\*\* :

- . a mean load, due to pretension, of 3 550 tonnes\*\*\*.
- . a maximum load of 8 700 tonnes,
- . and a minimum of  $\approx 0$  tonne.

The actual foundation design calls for 8 piles per foundation template ( $\emptyset$  72 in, driven 60 m and grouted to the template sleeves). The horizontal forces should remain less than 10 % of these vertical forces and at this level are not considered to present a significant problem.

---

\* This situation can be compared with the design of the Ekofisk reservoir, the first gravity structure in the North Sea.

\*\* The weight of the legs has been considered, but not the weight of the foundation template itself. These loads are deduced from loads at the surface.

\*\*\*Tonnes will always refer to metric tonnes.

The very nature of this loading has proved to be a psychological handicap. Quite naturally designers have started worrying about the behavior of the foundation with relation to its ability to withstand " $10^8$  load reversals during its 20 year design life", about creep, about possible large permanent displacements under extreme loading conditions, about "pullout" etc ... All concerns which can be associated to the "nail-out-of-the-wall" syndrome. The technical press has also given a large echo to this wide-spread preoccupation :

"... Cyclic loading superimposed on the static pretension load of TLPs represents one of the most complex and challenging areas for geotechnical research and development. Cyclic loading may have a detrimental effect on the side friction of tension piles. Elastic elongation of the pile under cyclic loading leads to two-way cyclic loading and heavy degradation of strength along the upper part of the pile, and further down the pile one-way cycling may tend to increase creep velocity..."

(Petroleum Engineer, May 1982)\*

"... A major influence in the overall feasibility of the TLP concept is how the seabed soil around anchor piles would perform under cyclic loading in tension...". (Offshore Engineer, Feb. 1980)\*\*

One may wonder why only piles have been mentioned as potential solutions. Gravity foundations have also been considered : in such systems

---

\* "Deep Water Operations Demand Safe, Stable Anchoring" by Olsen O.A. et al.  
\*\* Rep.

large masses in the foundation templates insure a total security against the fatigue effects previously mentioned. It provides a good example of the "change of statistical universe" advocated by De Mello in his Rankine Lecture |73|. It also presents the advantage of having a better understood behavior.

However the gravity option presents major disadvantages. The installation of gravity templates in large water depths and with tolerances\* of a few inches on the positioning is a fantastic task. The necessary support vessels, cranes, etc... represent an enormous mobilization cost and new techniques would have to be tested. There are two more good reasons for the lack of enthusiasm of the industry : first, piles are a proven technique and offshore civil engineering is conservative, and secondly the "drillers" have total priority, and they don't like the idea of having these monstrous templates restricting the area available around the wells.

The final choice is however a question of economics and of course of site conditions.

"... Both gravity and piled anchorage schemes provide viable solutions technically and economically... However it has been confirmed that a pile solution offers the more versatile system to suit a larger range of field situations\*\*...".

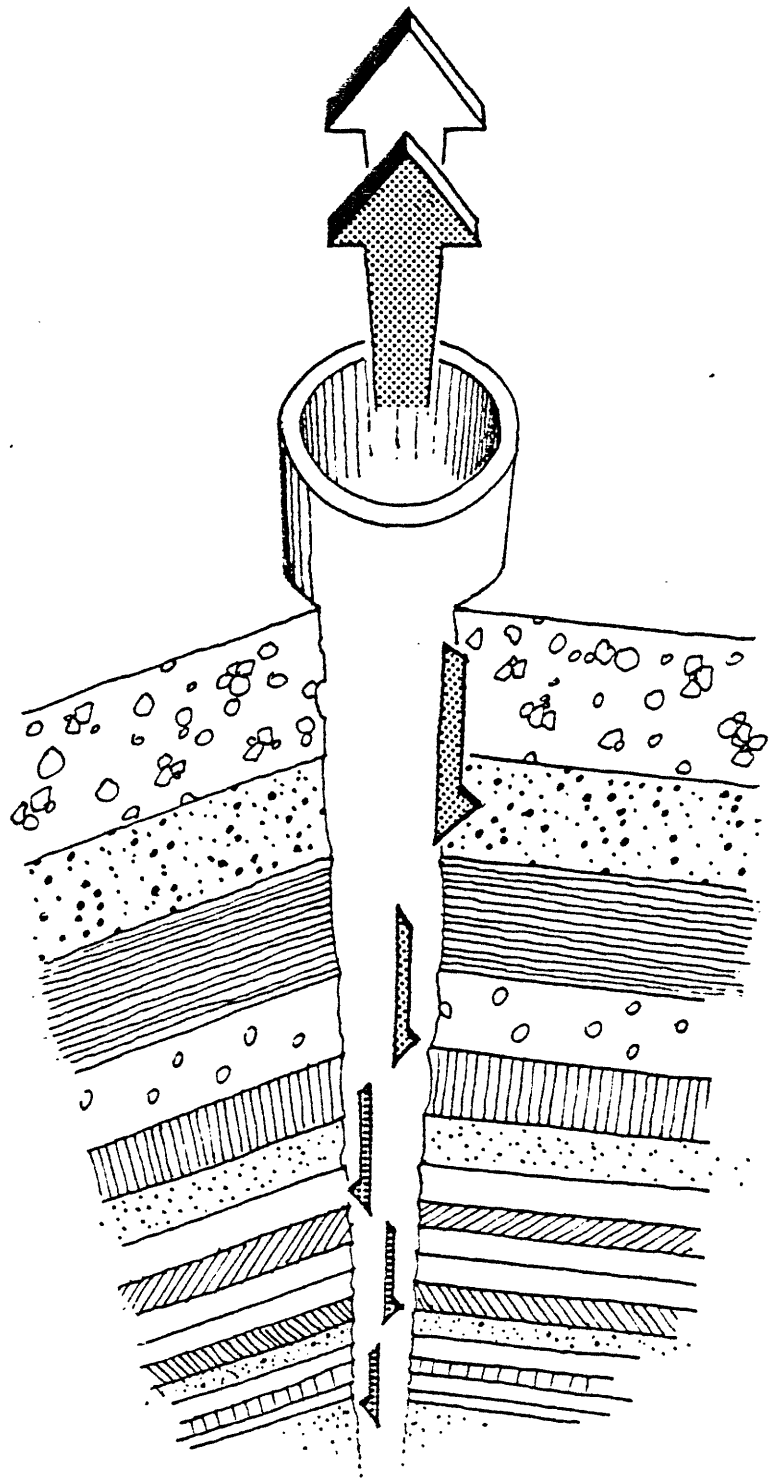
---

\* The levelness of the set of the four templates is a key requirement as well as their relative positioning. Mercier, during the discussion of his paper |74|, has talked of "a distance between diagonals equal to within 1.5 meters".

\*\* Perret G.R. and Webb R.M., OCT 3881, p. 264, 1980 "Tethered Buoyant Platform Production System".

As a matter of fact more and more engineers are thinking today of using hybrid solutions which will include both piles and gravity.

Let us now see how this thesis will attempt to contribute to our understanding of TLP foundations.



## 1.2 THE PRESENT THESIS

### 1.2.1 Statement of objectives

In an effort to improve our understanding of the basic behavior of a TLP pile foundation during the passage of a storm, this work has focused on the study of a single tension pile embedded in clay and subjected to undrained cyclic loading conditions.

The objective of the research is to contribute to the development of methodology that will ultimately allow us to follow the evolution of the pile-soil contact degradation and to estimate the redistributions of stresses and strains occurring during the storm as well as the resulting displacements of the foundation.

### 1.2.2 Research orientation

As a matter of introduction to the present thesis it may be useful to present the logic of the research with simple ideas based on plain engineering judgment.

Whereas the pile-soil system is a very complex one, the examination of the problem at-hand reveals a comparatively simple pattern of loading. The external force,  $P$ , applied to the top of the foundation is not only in permanent tension but it is also characterized by fluctuations,  $P_{cyc}$ , imposed by the sea state around a mean value,  $P_{ave}$ , which can be, in a first approximation, considered as constant with time (Figure 1.2.1).



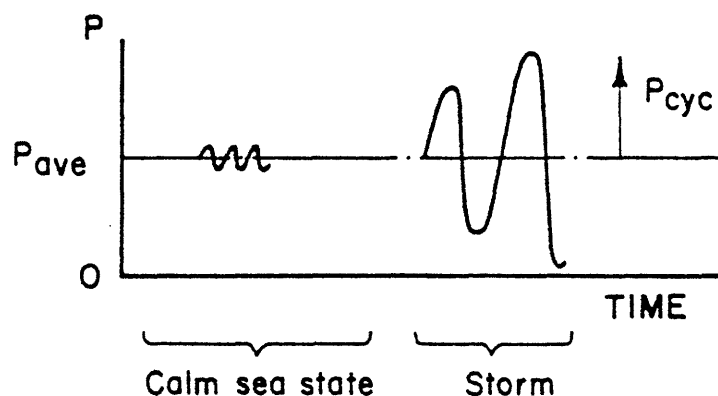


Figure 1.2.1 Schematic of the force applied to the top of the foundation.

Consequently the overall system is force-controlled, and it seems thus logical to envision the analysis of the local pile-soil behavior from a stress-controlled point of view. Intuitively it is apparent that the value of  $P_{ave}$ , as compared with the pile ultimate capacity, may have a critical impact on the overall behavior of the foundation. A given value of  $P_{ave}$  can be associated with various shear stress distributions\*, each one corresponding to a different history of loading. During calm sea states, and along a large part of the pile, one expects that the soil will creep and consolidate and therefore modify its physical characteristics, so that a particular average shear stress distribution,  $\tau_{cons}$ , will develop. Thus this calm sea period will directly affect the pile behavior during the next storm. During the

---

\* Shear stresses applied on the soil immediately adjacent to the pile, on a surface parallel to the pile surface and in the pile direction.

passage of this storm the shear stress distribution will change. At a given time one can think in terms of a distribution  $\tau_{\max}$  associated with the maximum value of  $P$  during the cycle,  $P_{\max}$ , and another distribution  $\tau_{\min}$  corresponding to  $P_{\min}$ . The mean of these two distributions will be called  $\tau_{\text{ave}} = (\tau_{\max} + \tau_{\min}) / 2$ ; while the fluctuation around this mean is termed  $\tau_c = (\tau_{\max} - \tau_{\min}) / 2$  as shown in Figure 1.2.2.

The distribution of  $\tau_{\text{ave}}$  at an instant during the storm will usually be different from that of  $\tau_{\text{cons}}$ , the shear stress distribution at the end of consolidation, but both will nonetheless be in equilibrium with  $P_{\text{ave}}$ . Along a large part of the pile, shearing will thus occur with a significant mean value  $\tau_{\text{ave}}$ . It can furthermore be expected that a large range of values of  $\tau_{\text{ave}}$  and  $\tau_c$  will be encountered along the pile. Based on these preliminary observations we may now envision the research directions in some more details.

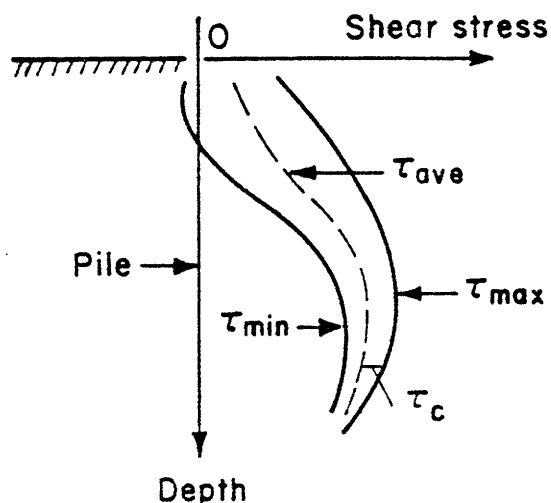


Figure 1.2.2 Shear stresses during cycling.

There are essentially three research topics which must be properly tackled if we want to be able to reasonably understand the behavior of such a tension pile :

1. We need a pile-soil model that will insure the compatibility of the displacements of the pile and of the soil as well as the equilibrium of the forces in the whole system. The estimation of the shear stress distributions previously mentioned is a direct result of the application of such a model. The choice of the soil-pile parameters, which describe the contact between the soil and the pile, is certainly one of the most delicate problems ; in the case of static loadings imposed to the pile, the profession has already developed methodologies for making such a choice, but very little is known when the loading is more complex and involves successive unloadings and reloadings. An additional problem may stem from the fact that with a given set of soil-pile parameters the pile-soil model may accumulate permanent displacements and residual stresses at each successive application of a cyclic loading at its top. It will be of paramount importance to properly understand the behavior of the model under cyclic loading if we want to be able to differentiate between this phenomenon and the effect of the "soil cyclic degradation" which is the object of the next point.
2. The soil fatigues under cyclic loading, and as a direct consequence the characteristics of the soil-pile contacts (the soil-pile parameters) change with time. The term "degradation" will refer to this modification

of physical properties due to the repetition of loading.

It is a fundamental point of this thesis that the average shear stresses existing along the pile before and during the storm should be considered amongst the governing parameters of the degradation. However the introduction of two new parameters ( $\tau_{\text{cons}}$  and  $\tau_{\text{ave}}$ ), in an area of soil mechanics where classically only  $\tau_c$  is considered, is a formidable complication, and one must restrict the problem to a more practical formulation. The simplest starting point is to study the cyclic behavior of the soil under a constant value of average shear stress, i.e. with  $\tau_{\text{ave}} = \tau_{\text{cons}}$ , which corresponds to adopting at the local level a characteristic of the global loading,  $P_{\text{ave}} = \text{constant}$ . Our objective will be to accumulate a relevant set of experimental data on the fatigue of clay under cyclic loading with  $\tau_{\text{ave}} = \tau_{\text{cons}}$ , while covering the wide range of stresses encountered along the pile.

3. The third issue is to integrate the pile-soil model and the degradation data into a consistent engineering tool. One needs to properly define how the soil degradation affects the pile-soil parameters and how our limited data base can be used while the distributions of  $\tau_{\text{max}}$  and  $\tau_{\text{min}}$  change as a cyclic force  $P$  is applied to the pile top. Finally the elaboration of an iteration scheme that respects the physical characteristics of the phenomenon and properly integrates the pile-soil model and the degradation data is a key requirement of the procedure.

All these issues must be considered in detail if we intend to develop a rational means of studying the behavior of the tension pile under cyclic loading.

### 1.2.3 Thesis organization

Chapter 2 presents an overview of the state-of-the art on the design, testing and modeling of tension piles under cyclic loading. The emphasis is placed on the test data obtained on instrumented piles tested in-situ and on the analysis of theoretical models which generated the first impulses of the present work.

Chapter 3 analyzes in detail the chosen pile-soil model, called the "Pile Model", by providing a complete description of its behavior under cyclic loading and in the absence of degradation of the soil-pile parameters. The methodology used to estimate the soil-pile parameters from the local soil properties is also described at this stage.

Chapter 4 details the program of tests which was carried out in order to gather information on the degradation of Plastic Drammen Clay under cyclic loading with  $\tau_{ave} = \tau_{cons}$ . This chapter also reports these results in a format allowing for easy interpolation and extrapolation of the data to a wide range of stress conditions.

Chapter 5 then integrates the results of the two previous chapter into a computational computer tool called TLPILE and presents examples of its application to a typical offshore pile.

Chapter 6 summarizes the key contributions of this thesis and indicates new directions for research.

•—————•

## 2. STATE OF THE ART

The present chapter summarizes the information gathered in the technical literature on topics directly related to the behavior of tension piles under cyclic loading. We shall focus our attention on three issues :

1. static pile tests, and more specifically the equivalence of skin friction in clay for tension and compression and the effect of sustained loading on piles,
2. cyclic tests on tension piles, with the main emphasis placed on in-situ testing, and
3. theoretical models presently available to follow/explain/predict the behavior of tension piles under cyclic loading.

Additional information on the cyclic behavior of clays relevant to our problem is provided in Chapter 4.

## 2.1 TENSION PILES UNDER STATIC LOADING

The least that can be said at the present time is that our experience with tension piles is limited, and it could be added that for piles under constant tension it is almost inexistent. Over the years the interest for tension piles has essentially been associated with the foundations of high voltage transmission towers, with those of high rise buildings and, more recently, those of offshore jacket platforms. In all these cases the nature of the loading is alternatively compressive and tensile and the mean loading is compressive. Let us now review the information gathered from static tension tests run in connection with the development of these structures.

The foundations of transmission lines involve very short concrete-cast-in-situ bored piles. Sowa [95], who presented in 1980 an extensive review on this subject, has concluded that in the case of cohesive soils the ultimate pulling capacity of these piles could be reasonably well estimated from the relationship between the cohesion  $c_a$  and the undrained shear strength as proposed by Tomlinson. However in view of the scatter he recommended "a suitable factor of safety to be selected", as well as pulling tests on important projects. In the case of sandy soils he concluded that the scatter of K values is significant and that "it is not possible to select a value of K with a sufficient degree of confidence to estimate the pulling capacity of cast-in-situ piles in sandy soils" and pulling tests were strongly recommended.

Driven piles have been frequently tested in tension but only a few tests have been reported in the literature. Nearly all the piles that were studied had an embedded length smaller than 80 ft with an average size of roughly 50 ft. Very different types of testing procedures were used, from long-term

sustained loading of several hours or days to quick tests of a few minutes. Most of the piles tested were steel pipe piles but one also finds precast concrete and H-piles.

In 1980, Olsen at the University of Texas at Austin started research funded by the American Petroleum Institute, whose objective is to compile and analyze the maximum number of pile load tests of any type (compression, tension, or both). In this study the observed ultimate capacities are compared with those predicted by the various methods presently in use in offshore design, namely for clays :

- . the API RP 2A method,
- . the  $\alpha$  method of Tomlinson,
- . the  $\beta$  method of Burland,
- . and the  $\lambda$  method,

and for sands :

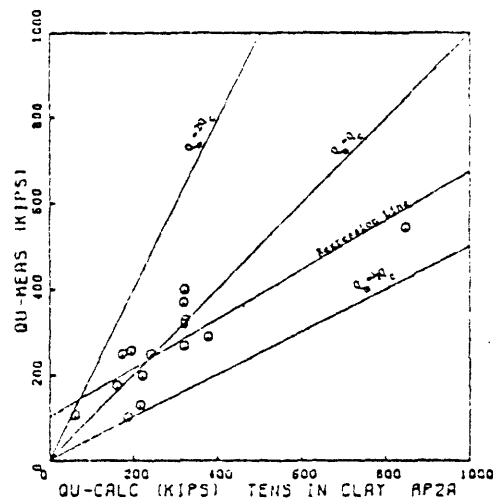
- . the N-value method.

Figure 2.1.1 gives an overview of the results obtained from tension tests. The top diagram relates to clay and the RP 2A method and the bottom one to sand. The abscissa corresponds to the calculated value of the ultimate pulling capacity and the ordinate refers to the measured value.

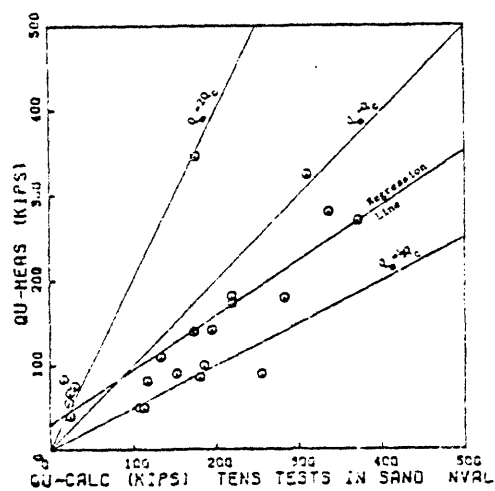
On the basis of all the tests analyzed, Olson concluded that :

1. in clay the RP 2A method gives the most consistent agreement between calculated and measured ultimate capacities,
2. the prediction is far better for clay than for sands. A typical factor of safety, against ultimate failure, to be applied in clay would be two while a factor of three should be applied to sands,
3. we seem to consistently overestimate the calculated value of the





a) in clay



b) in sand

Figure 2.1.1 Measured versus calculated ultimate capacities in tension.

ultimate capacities for the higher loads as shown by the slopes of the regression lines (this observation was systematic with all the test results).

These results indicate that the level of accuracy in the estimation of the tension capacities is quite comparable to that traditionally obtained in compression thereby justifying the procedure recommended by API. The RP 2A code | 1 | does not differentiate between skin friction in tension and in compression in the case of clay, nor does the Canadian Foundation Engineering Manual |18| or the "Rules for the Design, Construction and Inspection of Offshore Structures" established by DnV |26|. Furthermore all these codes suggest the application in clay of the same factors of safety in compression and in tension.

To further document the equivalence tension - compression Figure 2.1.2 shows measured values of ultimate friction capacities for piles in clay tested in both compression and in tension (Chan |19|, Cox et al. |21|). It can be seen that these results correlate very well, another indication that the ultimate skin friction in clay can be taken as equal in compression and in tension. (The results of Cox et al. also show that residual stresses may play some role since the first type of test applied (compression or tension) seems to give consistently a higher ultimate friction than the second one). The ultimate base resistance in the compression tests was estimated from the RP 2A recommendation ( $q_u = 9c_u$ ).

The estimation of the ultimate pulling capacity of piles in sand is a more controversial topic. The failure mechanisms in sand are much more affected by surface effects and as a result several theories predict a different behavior in compression and in tension (Janbu |51|). The codes

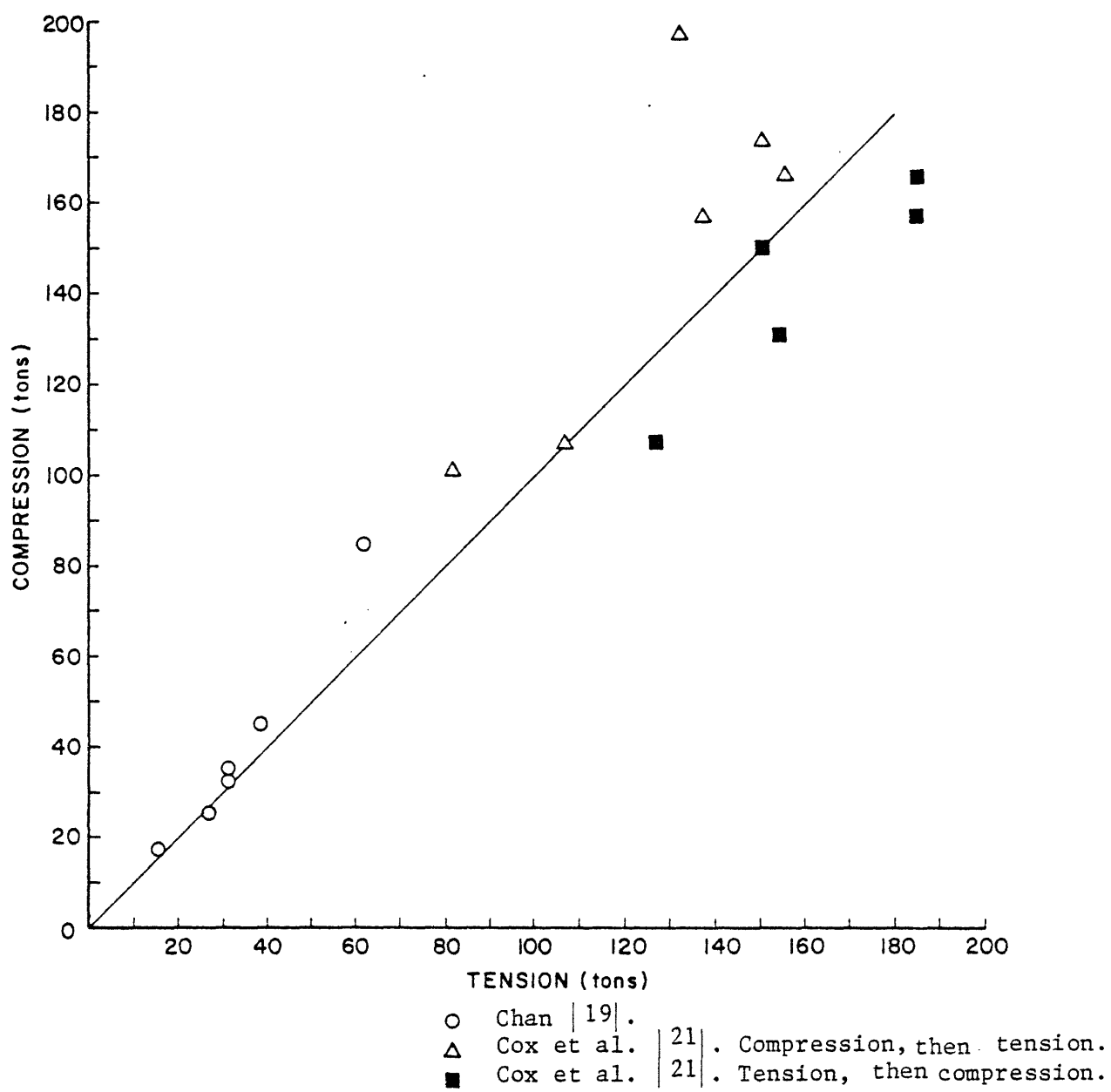


Figure 2.1.2 Correlation of ultimate friction capacities in tension and in compression.

recognize this possible difference and RP 2A limits the value of K to 0.5 while the others simply state that the skin friction in tension should be chosen different from that in compression.

Another very interesting topic is that of sustained loading on piles. Until now we have only discussed the ultimate pile capacity but significant displacements may be accumulated when the pile is subjected to a sustained loading lower than its ultimate capacity. There is very little information available on this subject for tension piles, and this is quite unfortunate since this phenomenon is of great interest in the study of TLP foundations.

Gallagher and St John [31] have reported results of sustained tension loading on piles in the form of time versus pile head displacements for different loads applied (Figure 2.1.3). The ultimate pulling capacity of this pile is roughly 120 tonnes. It appears that for a load greater than approximately 90 tonnes (75 % of the ultimate pulling capacity) there is a change in the pattern of increase of the displacement with time leading to creep failure.

The type of tests reported in Figure 2.1.3 have been directly included in the French recommendations for the testing of piles [27]. Figure 2.1.4 recaps the principal aspects of this procedure. Each load step is applied for a period of 90 minutes (sometimes 60 minutes) during which the displacement is recorded on a log scale (diagram 1). The different rates obtained for each load are then plotted (diagram 3) and usually show a marked transition between a quasi-linear increase at low loads and a sharp rate increase at high loads. The transition load is called the creep load ("charge de fluage"). The acceptable load is then defined from this creep load by application of an adequate factor of safety (usually 1.4).

This procedure has been applied on tension piles by Puech and Jezequel | 89|. Figure 2.1.5 shows that in their example the creep load \* corresponded to 75 % of the ultimate pulling capacity - as in the case of Gallagher and St John -. For a much longer period of application of the load (larger than 100 or 90 minutes of the preceding examples) we may find that the creep load is lower than given by these procedures. There is unfortunately no information available on this critical issue.

---

\* This creep load is estimated from 60-minute load steps.

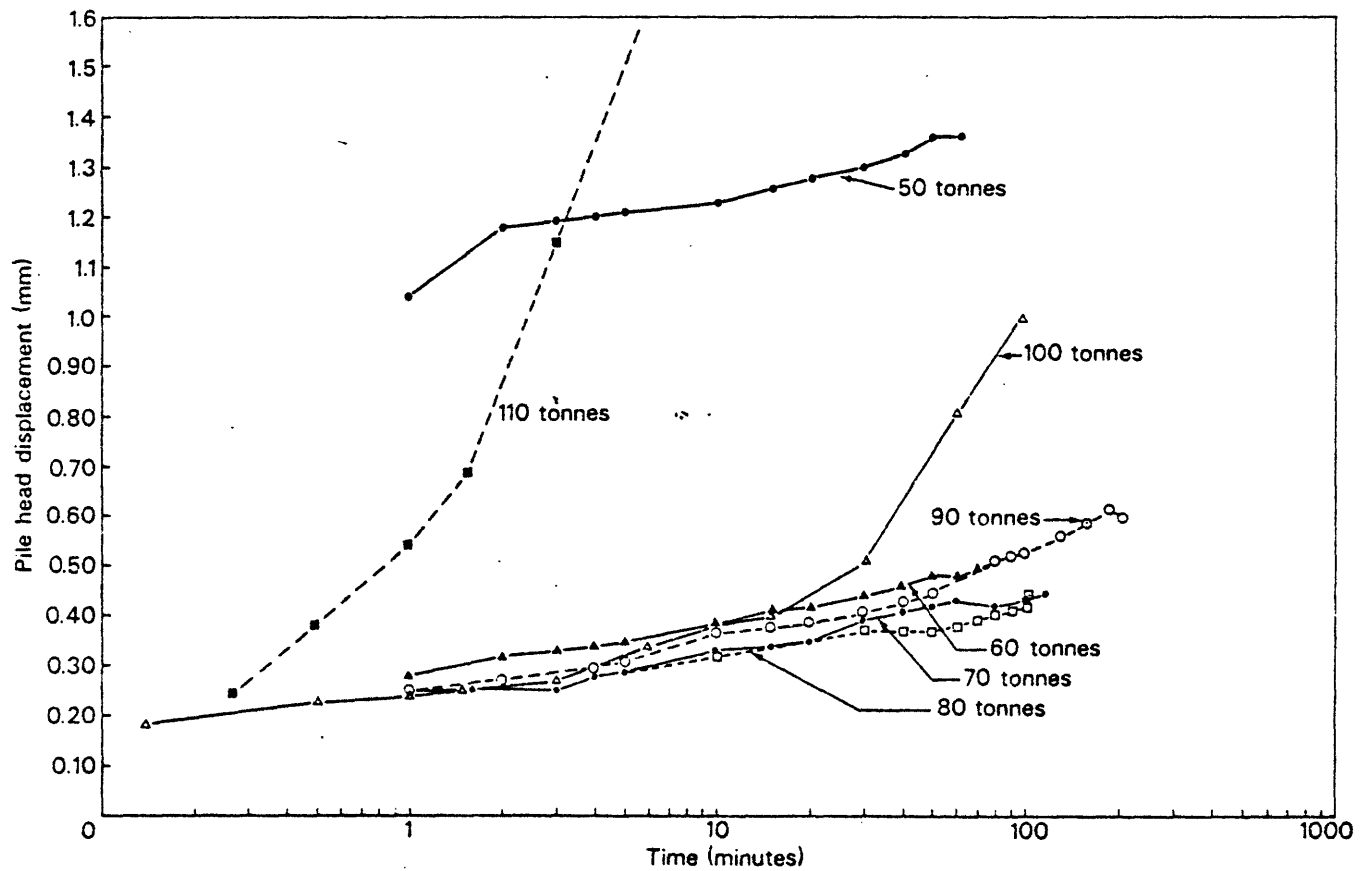


Figure 2.1.3 Sustained tension loading - history of the pile top displacement.

(After Gallagher and St John [31]).

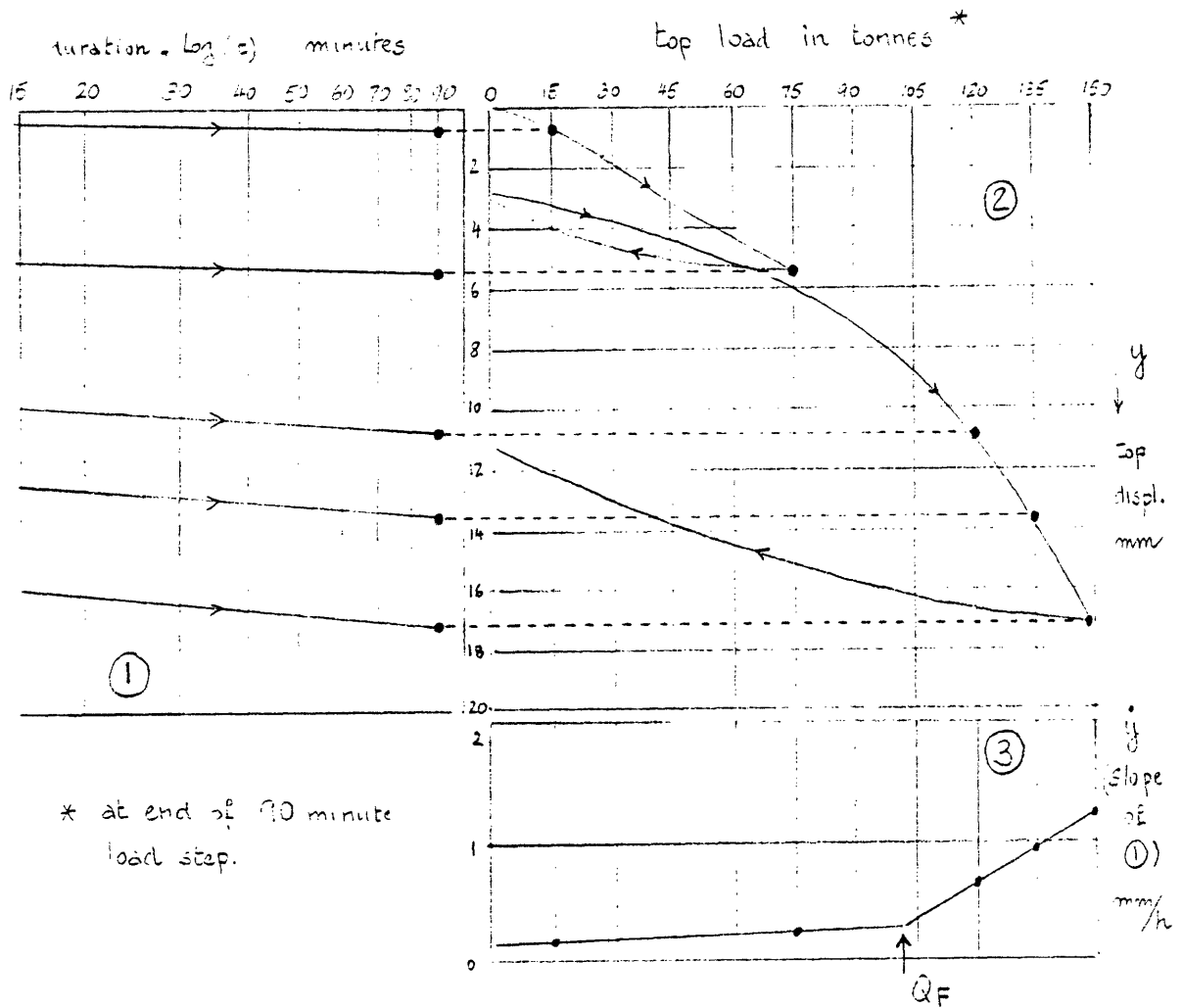
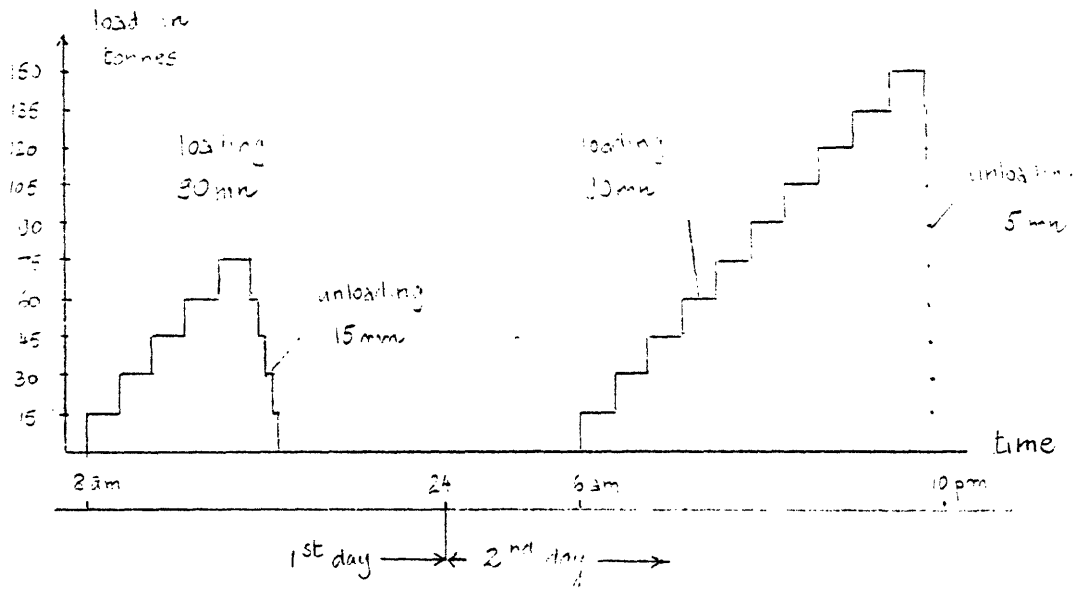


Figure 2.1.4 French recommendations for the testing of piles.

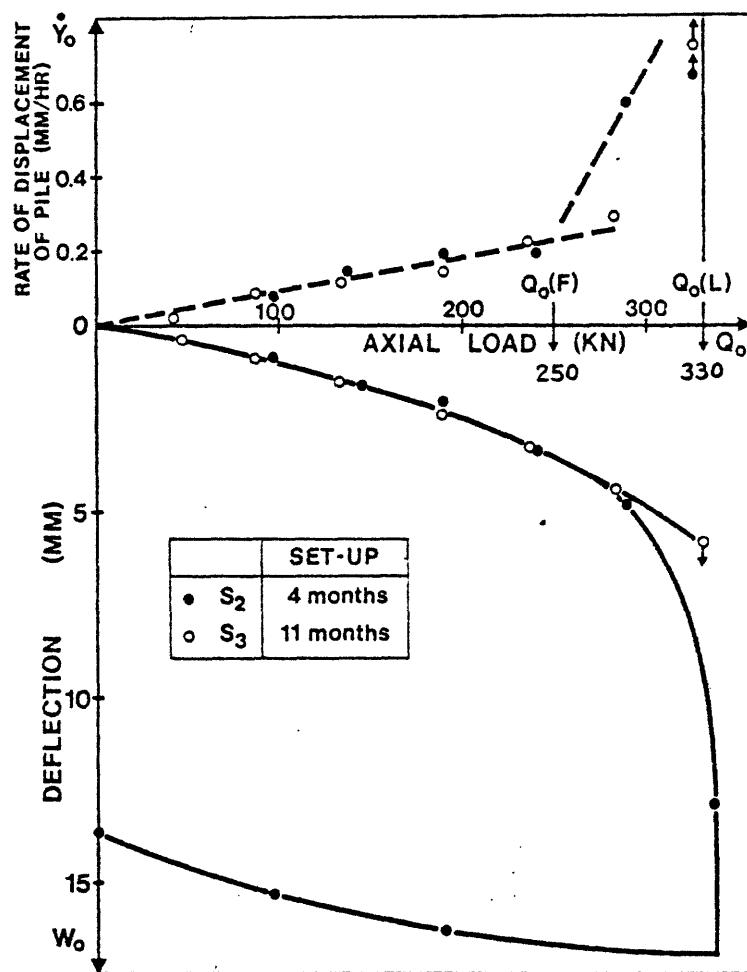


Figure 2.1.5 Plancoet tension pile - load-deflection curves and creep-curves from static tests S<sub>2</sub> and S<sub>3</sub>. Determination of the creep load.

(After Puech and Jezequel [89]).



## 2.2 CYCLIC LOADING ON TENSION PILES

This review focuses on in-situ testing of piles but for reasons of completeness we should first comment on the tests which have been run on model piles of small dimension\*. Many researchers have tested such model piles under cyclic loading (usually under controlled strain conditions)\*\* and some under both cyclic loading and tension [88]. Overall it is extremely difficult to interpret these tests which are very affected by test conditions. The shafts used are very stiff compared to actual piles and as a consequence the study of the redistribution of stresses during cycling is difficult, if not impossible. The results are erratic and often contradictory (for example in the evaluation of excess pore pressures during cycling [84]), and their extrapolation to actual pile sizes is extremely delicate. Overall it is felt that the model tests do not constitute yet a satisfactory source of information for the design of TLP foundations and we shall focus uniquely on in-situ piles of more practical sizes (diameters of 20 to 50 cm and length of 5 to 17 m). Note that even with these piles the application of the results will require significant extrapolations for offshore piles of 1.5 m-diameter and 100 m-length.

These are numerous problems associated with in-situ testing of piles under cyclic loading the least of which is certainly not the proprietorship of the data. These tests are extremely costly and their results are kept in some secrecy. The discussion that will follow is based on the few papers which have been released in the literature but it does not represent an accurate image of what is really known. Four test programs have been reported : the "Empire test program" in the USA [56], the BRE test program in Great

---

\* Usually in the laboratory.

\*\* [33], [82], [44], [8], [13], [96], [5], [67].

Britain ([31], [70]), the NGI test program in Norway [52], and the IFP test program in France ([89], [86], [87]), all of them being funded by oil companies.

These tests are very complex to run, they require a sophisticated instrumentation and some key choices of procedure to be made. Apart from the choice of the pile and of the soil one has to select an installation procedure (driving or jacking), the number of cyclic tests to be run on each pile, the duration of the rest periods between tests, the loading period, shape, amplitude, duration, etc... The number of parameters is such that the results should be treated case by case.

It is very important to notice that none of these programs have considered the application of a sustained average tension load prior to testing. In other words the piles were cycled from zero-load conditions.

Kraft et al. ([56], and also Cox et al. [21]) have reported in 1981 some of the results obtained at the Empire Test Site in 1975 on four 14 " (35.6 cm) -diam, open-ended, sections of steel pipe piles driven into strong underconsolidated clays at depths varying from 150 ft to 360 ft. Their tests were composed of various combinations of tension, compression and cyclic loadings. In many cases, and in the own words of the authors, "qualitative rather than quantitative conclusions (had) to be drawn from the test data". These tests were load-controlled. Typical load-displacement responses under cyclic loading are given in Figure 2.2.1. The one-way cyclic loading applied did not affect the ultimate capacity, but large displacement began to accumulate when the maximum load reached 80 % of the static capacity. It can be observed from Figure 2.2.1 that the cyclic stiffness of the pile was not significantly affected by the cyclic loading.

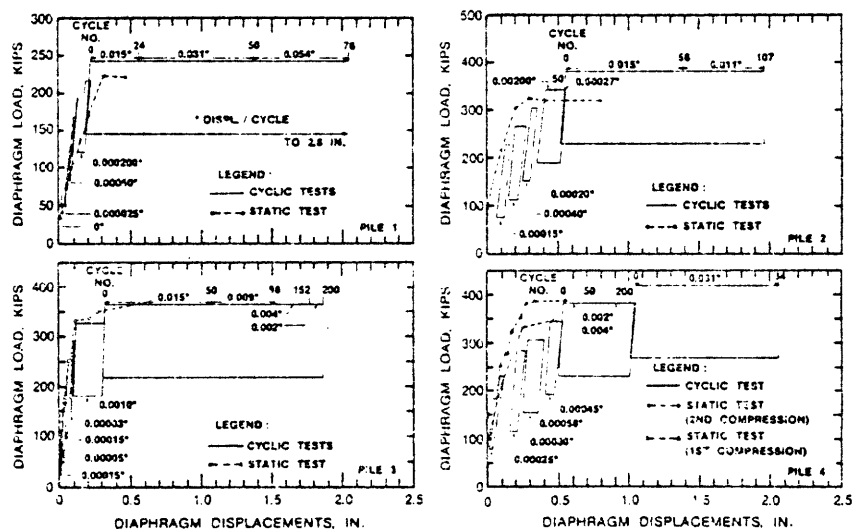


Figure 2.2.1 Load - Displacement response under cyclic loading - Empire test site.

(After Kraft et al. [56]).

Puech et al. ([86], [87], [89]) have reported very interesting results on a 13 m long closed-ended steel pipe pile driven into recent deposits of marine sediments including compressible silts, loose sands and silty clays. (Plancoet site) Figure 2.2.2.a shows the type of loadings applied to this pile : static (S), cyclic (C) and storm (T). (The static tests corresponds to those of Figure 2.1.5). Figures 2.2.2.b and 2.2.3.a to c give the displacements of the top of the pile as a function of the number of cycles for 4 tests called C21, C12, C11 and T2.

Tests C21 and C12 (Figures 2.2.2.b and 2.2.3.a) have the same maximum loads (defined from the creep load,  $Q_o (F)_s$ , of Figure 2.1.5) of  $Q_o (max) = 0.52 Q_o (F)_s$ , and they both show a steady accumulation of the deformation with no indication of future stabilization. Test C11 (Figure 2.2.3.b) has a lower maximum load of  $Q_o (max) = 0.42 Q_o (F)_s$  and shows a clear tendency to

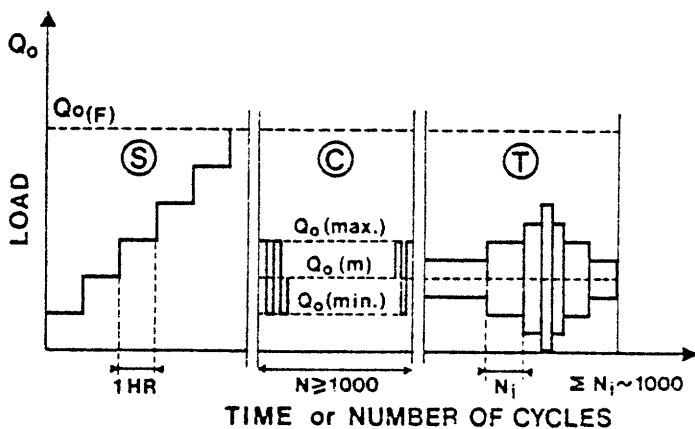


Figure 2.2.2.a Types of loadings applied to the Plancoet pile.

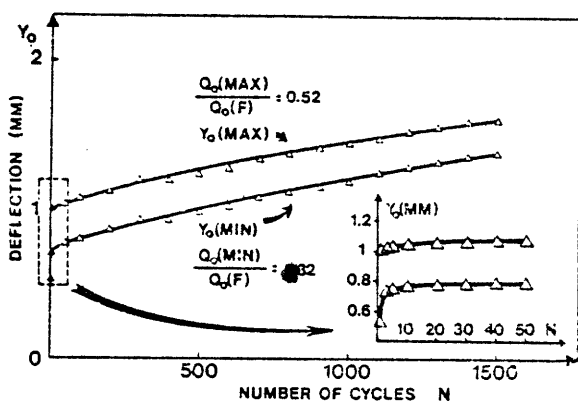


Figure 2.2.2.b Time history of the pile top displacement during test C21.

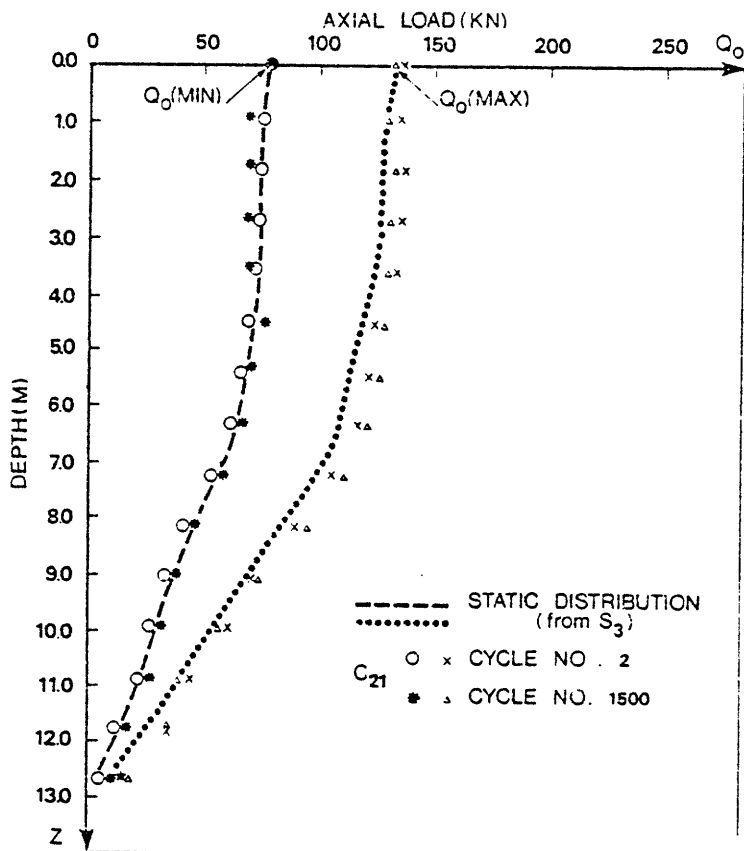


Figure 2.2.2.c Load distributions in the pile during test C21.

(After Puech [89], [86]).

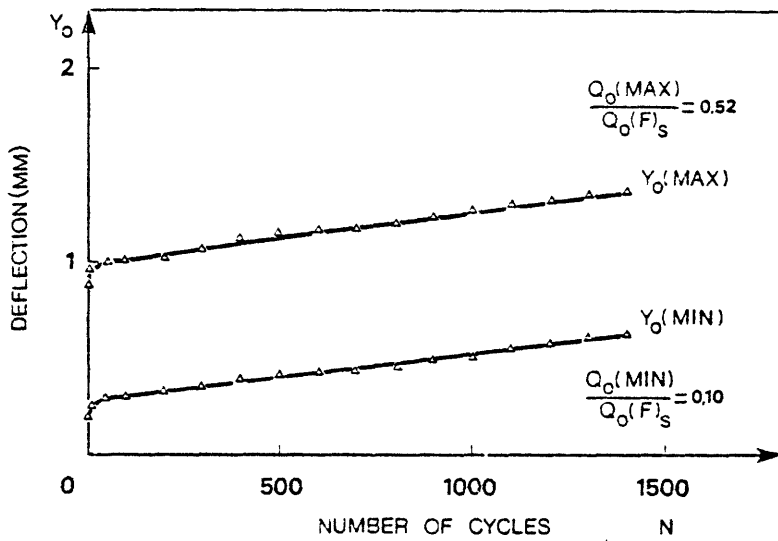


Figure 2.2.3.a Time history of the pile top displacement during test C12.

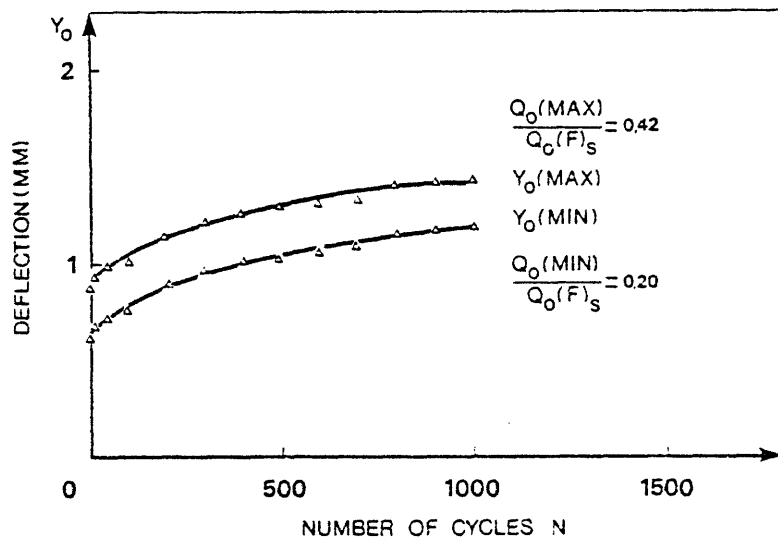


Figure 2.2.3.b Time history of the pile top displacement during test C11.

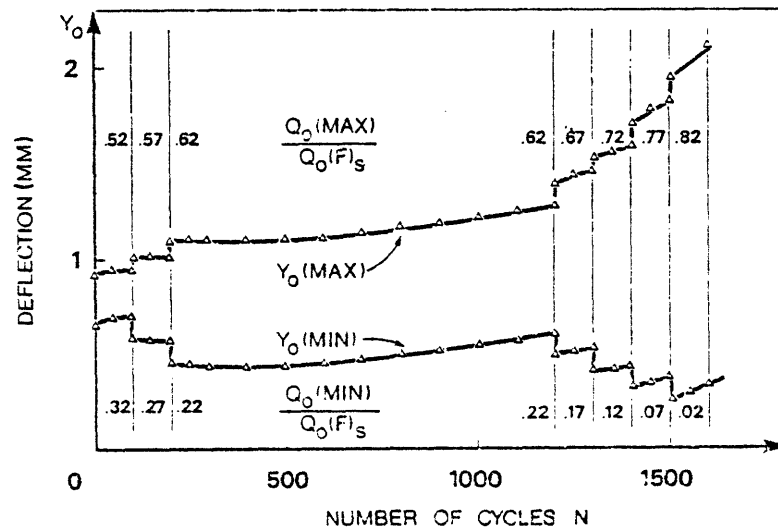


Figure 2.2.3.c Time history of the pile top displacement during test T2.

(After Puech |86|).

stabilize. The middle of Test T2 (Figure 2.2.3.c) has the highest  $Q_o$  (max) of all and shows a marked acceleration of the displacement with time. Puech considers the maximum load as the crucial parameter of the loading and suggests that the range of acceptable loads be limited to  $Q_o$  (max)  $< 0.6 Q_o$  (F)<sub>s</sub> (and therefore  $Q_o$  (max)  $< 0.45 Q_{ult}$ ) with this type of soil.

It can also be observed from these tests that the cyclic stiffness of the pile does not change much with the cycling. In the preceding figures the curves corresponding to the maximum and minimum load stay parallel to each other, even in the case of the storm loading (Figure 2.2.3.c).

Puech also pointed out that the first 50 cycles or so are not representative of the long term behavior (see insert in Figure 2.2.2.b), and may lead to unsafe conclusions. Figure 2.2.2c shows the load distributions in the pile during test C21 at cycles # 2 and 1500 and compares them to the static distributions of test S3. There is a clear transfer of the load towards the tip of the pile under the maximum load, but under the minimum load the cyclic and static distributions are essentially identical.

Puech also defines a cyclic creep load by considering the rate of displacements of the pile (under the maximum load), and compares it to the static creep load of Figure 2.1.5 (see Figure 2.2.4). The cyclic creep load is found to be equal to 60 % of the static creep load.

Puech et al. [87] also reported some preliminary results obtained with a 17 m piles driven in an homogeneous slightly overconsolidated ( $OCR \approx 2$ ) plastic clay (Cran site). It appears that the behavior of the pile under cyclic loading is strongly affected by the nature of the soil. Figure 2.2.5 compares the evolution of the top displacement with time for two sets, one at Plancoet and one at Cran, having similar cyclic loadings.

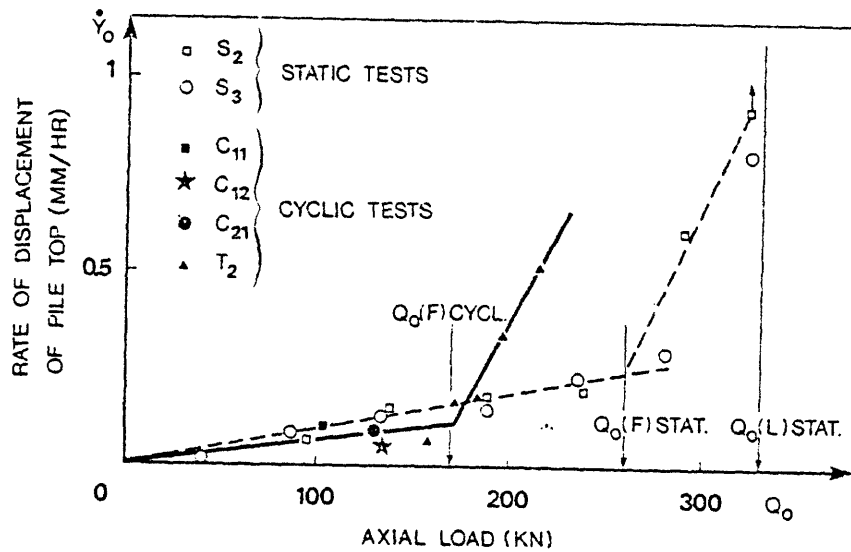


Figure 2.2.4 Comparison of static and cyclic creep loads - Plancoet Pile.

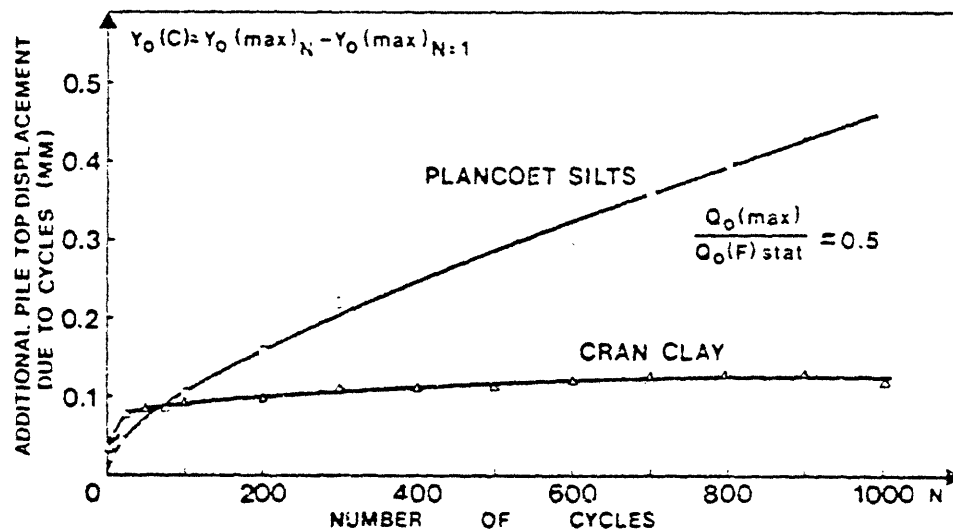


Figure 2.2.5 Comparison of time histories of top pile displacements at Cran and at Plancoet.

(After Puech | 87|).

It is clear that the Cran pile shows a much lower rate of increase of the displacement than the Plancoet pile. Puech suggests that the cyclic creep load for the Cran pile is approximately equal to the static creep load.

Mc Anoy, Cashman and Purvis [70] also reported interesting results from the BRE test program. Four piles were jacked into an overconsolidated till to a penetration of 9.9 meters. The loading applied to one of the pile, and presented in Figure 2.2.6, is of particular interest. Three cyclic tension tests were performed. The evolution of the top displacement with the number of cycles is given in Figure 2.2.7 where the top diagram represents the cyclic component and the bottom one the mean component of the displacement. It is clear that the cyclic component is not affected by the cycling, and that rupture occurs in an average deformation mode (test B, lower diagram). Figure 2.2.8 gives the load distributions along the pile at specific cycles and in the static case. The cyclic distribution is not very affected by the cycling and actually the only difference seems to be a slight increase in the load taken at the tip of the pile.

In conclusion, it can be said that the published results agree on several points :

1. the cyclic stiffness of the pile is not greatly affected by the cyclic loading even around failure,
2. the shape of the stress distributions along the pile do not significantly vary during loading but there is a clear indication of a shift of load towards the tip of the pile,
3. the nature of the soil is a controlling factor,



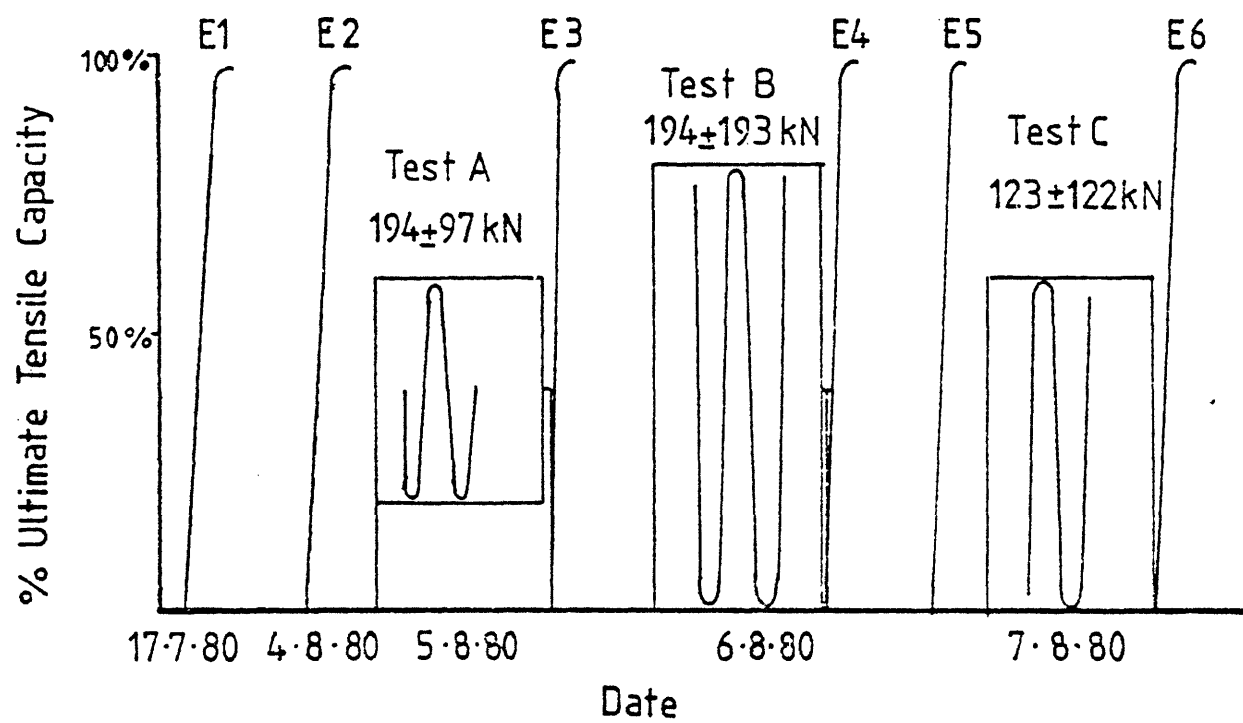


Figure 2.2.6 Cyclic loading applied to the pile head.

(After McAnoy et al. [70]).

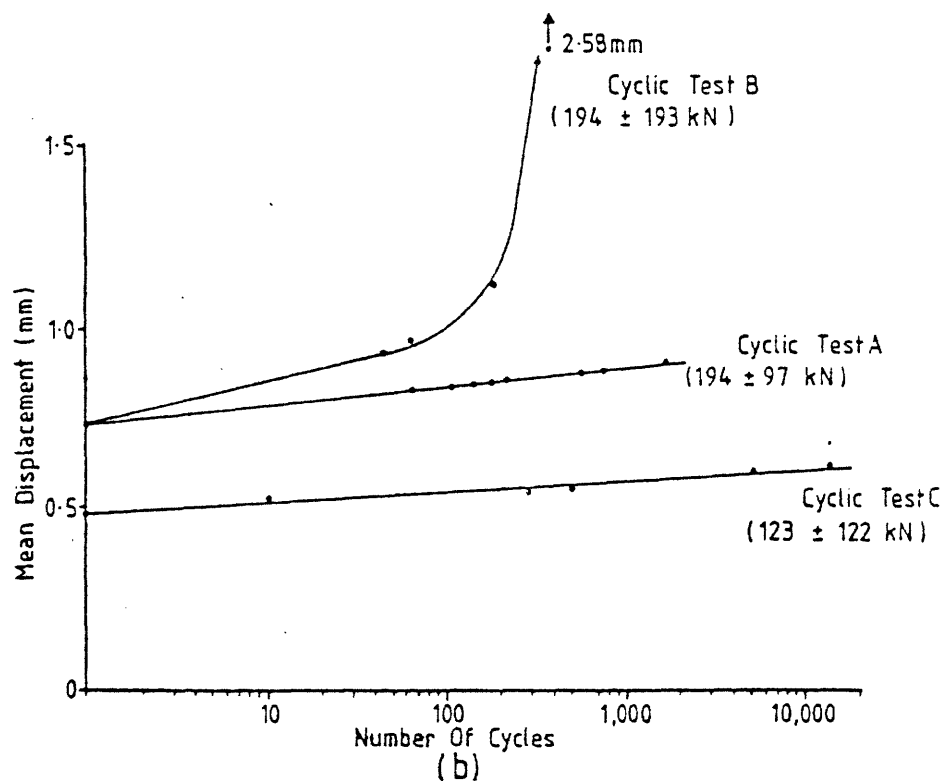
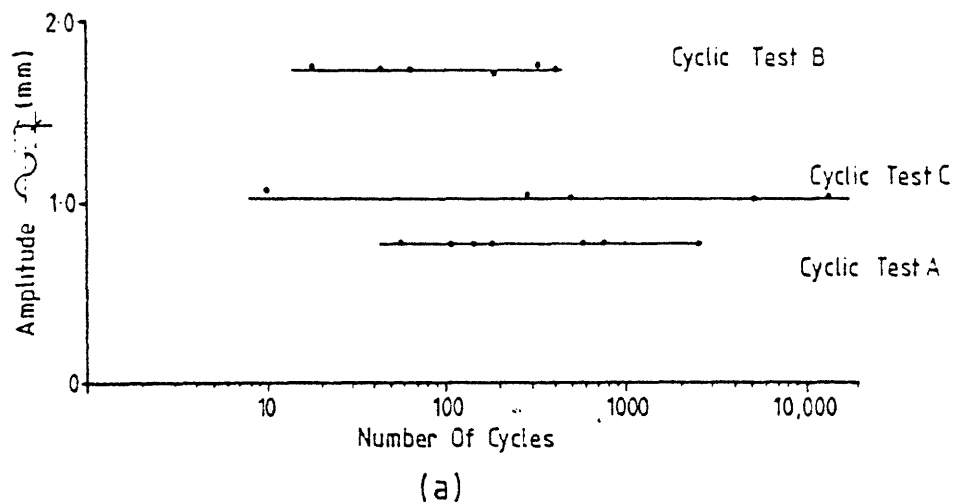


Figure 2.2.7 Pile head displacements (a) Cyclic amplitude (b) Mean.

(After McAnoy et al. [70]).

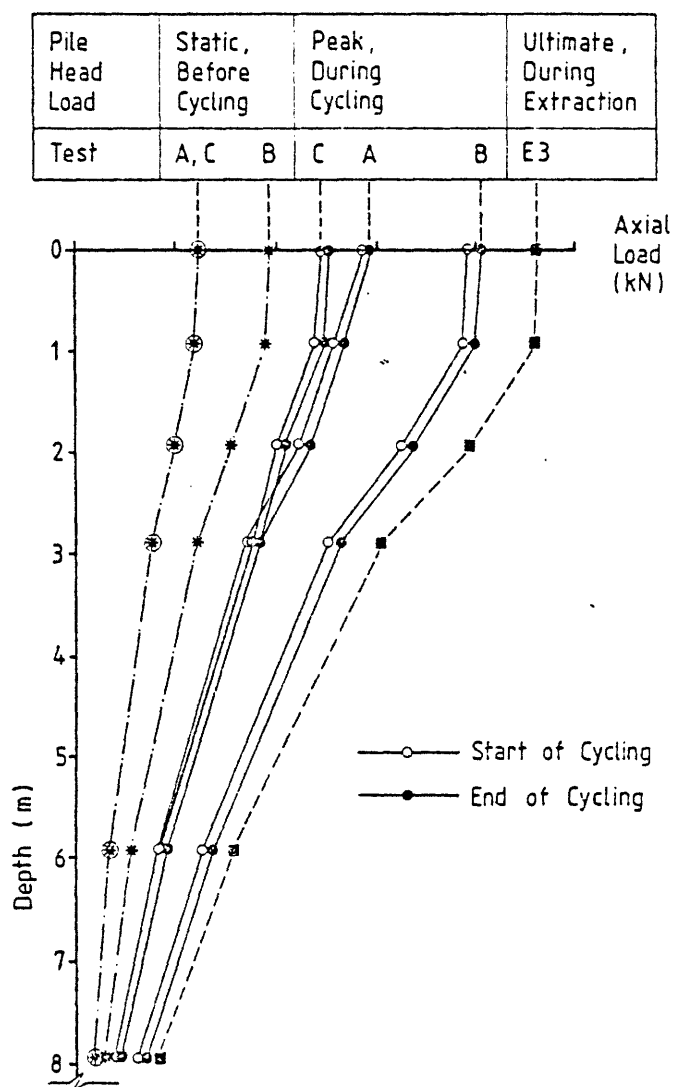


Figure 2.2.8 Load distributions.

(After McAnoy et al. [70]).

4. cycling with  $Q_o \text{ max} < 0.5 Q_{ult}$  seems to lead to stabilization in all cases.

Kraft et al. adequately concluded their paper by the following words :

"(These tests) demonstrate the influences that the combined but complex interaction of loading rate, number of load cycles, magnitude of cyclic load, loading history, and magnitude of sustained load have on pile performance. Each of these factors influences pile performance in a complex manner, and their individual and combined effects can be significant. In view of the complex loading history of these piles, conclusions are more qualitative than quantitative".

These conclusions are applicable to all the preceding tests, and invite the researchers to have humility in attempting to model a very imperfectly understood phenomenon.

## 2.3 MODELS

The models which have been proposed for the analysis of tension piles under cyclic loading will now be reviewed after a brief discussion of the cyclic soil models on the basis of which they are developed.

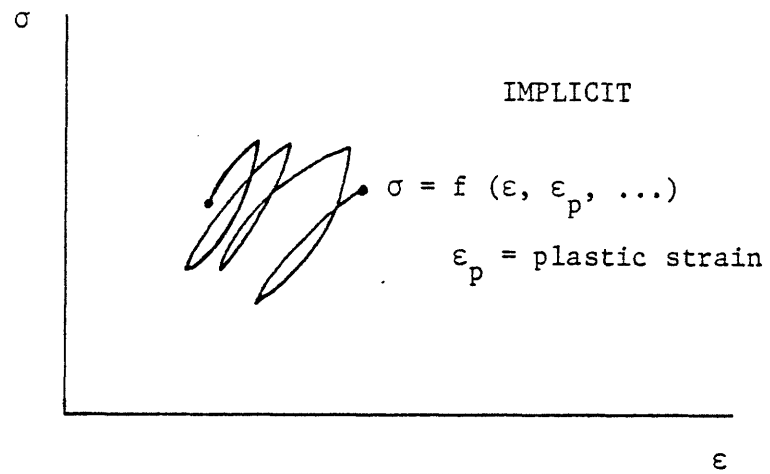
### 2.3.1 Soil behavior under cyclic loading

The adaptation of monotonic\* models to consider cyclic loading has been pursued over the past few years from two very different point of views. The first option is to aim at developing general constitutive models which would ultimately describe the complete cyclic behavior of the soil whereas the second adopts a cruder, and less ambitious, approach based on degradation laws obtained from simplified loading conditions and used to approximate the evolution of the monotonic model parameters at a few points of the cyclic history. The first category of models can be termed "implicit" since the treatment of the degradation is inherently contained in the governing equations of the model, while the second category can be called "explicit" in order to emphasize the necessity of providing specific information characterizing the degradation over a whole period of cycling in addition to the description of the (monotonic) model in itself.

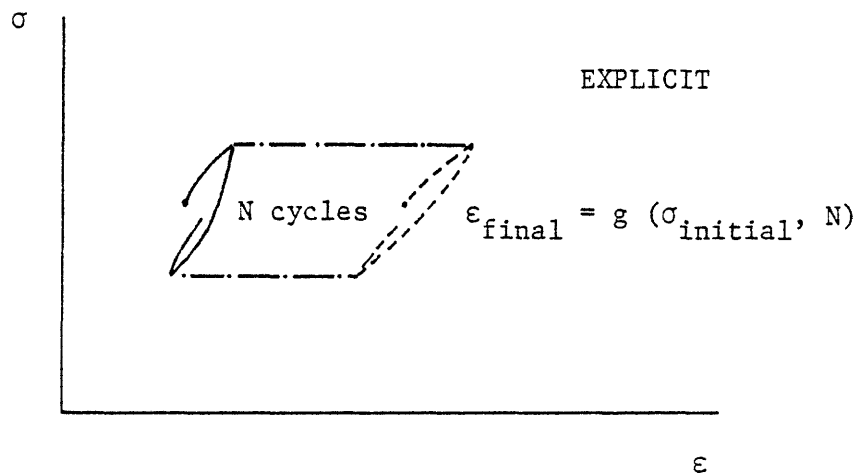
In the implicit models the cumulative effect of the degradation is usually represented by a measure of the plastic deformation that directly affects the constitutive parameters of the basic monotonic model (Figure

---

\*Monotonic in constast to cyclic, but usually involves unloading and reloading.



(a)



(b)

Figure 2.3.1 Schematics of implicit and explicit treatments of cyclic degradation.

2.3.1.a. One example of such approach is given by Prevost [85] who adopted the "length of the plastic deviatoric shear strain trajectory", called " $\lambda$ " in his model, as the degradation variable controlling the evolution of the sizes of the yield surfaces and the values of the plastic moduli in his anisotropically hardening model based on Mroz's concept of a "field of hardening moduli". The effect of the number of cycles in such a model is itself implicit since it is only indirectly represented by the build-up of plastic strains. Other examples of implicit models include the ones proposed by Hujeux and Aubry [46], Lassoudiere et al. [60] and Darve and Labanieh [24]\*. The implementation of any of these models requires a step-by-step analysis of the loading with severe implications of cost and complexity as they usually involve the use of elaborate finite element programs. At the present time these techniques can be used with confidence for only a few number of cycles. They should be viewed essentially as research tools permitting a detailed comparison with experimental results.

The second group of models considers the effect of complete periods of cycling under simplified loading conditions (e.g. controlled stresses) and makes use of explicit relationships between these cyclic loads and the plastic strains obtained at a given number of cycles (Figure 2.3.1.b). Several of these techniques can be related to the "cyclic pseudo creep" of Meimon and Hicher [71], Boulon et al. [16], or the viscoelastic formulation of Urzua [101]. Marr et al. [64] presented a comprehensive review of the work done at MIT in this direction on the basis of equations fitted on the results of numerous triaxial tests run on sand (Hedberg [38] and Hadge

---

\* See Darve and Labanieh [24] for a complete bibliography.

| 35|) and showed practical applications of these models to the prediction of the permanent deformations of foundations. One of the handicaps of these techniques is the bias introduced by the fitting procedures. Marr. et al. | 64| fit their equations over a limited range of the experimental results and as a consequence the rate of permanent strain accumulation that they use decreases with each additional cycle, which is not very realistic close to failure. To overcome this difficulty Andersen | 1 |\* makes a direct use of the test results in his graphical representation thereby eliminating the need for a fit by functional relationships. In general these explicit models do not require the use of complex constitutive laws. They simply involve the adjustment of the (monotonic) model parameters to reflect the effects of cyclic loading at the end of each loading sequence, but of course they are constrained by fixed loading conditions. When large number of cycles are considered their use is inevitable but they require some engineering judgment when used to obtain quantitative estimates since they may overly simplify, or distort, the predictions by lack of respect for equilibrium and compatibility requirements.

### 2.3.2 Models of tension piles under cyclic loading

The nature of the loading imposed by a storm should dictate the use of an explicit procedure since the number of cycles is usually of the order of 1000, distributed in packages of different intensities. Yet some researchers have used implicit schemes (Matlock and Foo | 68 |, Bea et al. | 9 | as will be shown immediatly.

---

\* See Chapter 4 for a discussion of this procedure.



### 2.3.2.A. Implicit procedures

The first procedure that should be discussed consists in using an equivalent monotonic pile model\* ; it is the simplest and yet probably the most popular approach in the profession. During the BOSS'79 Conference, Bea and Audibert | 9 | made the following observations after "a study of cyclic axial load effects on pile behavior based on a review of published pile load test case histories" :

" ... There appeared to be a definite trend toward decreasing (pile) capacity with increased number of cycles. The decreased capacity tends toward an asymptotic value ranging from 0.80 and 0.90 of the static capacity ... It can thus be concluded that the axial capacity of a pile is only negligibly affected by cyclic loads. However, cumulative deformations ... can become extremely large ... It is suggested ... that the sum of static and cyclic axial loads be kept below 80 percent (of the ultimate static axial capacity) in order to avoid large cumulative settlements ...".

Since these suggestions have been made it has often been proposed that equivalent monotonic pile models be used on the basis of the following criteria :

- . the average limiting skin friction is to be multiplied by a factor  $k_{cy} = 0.85$  to take into account the effect of cyclic loading on the ultimate capacity, and

---

\* Strictly speaking it is a degenerate model where the degradation per se is simply not considered, and it is classified amongst the implicit models only for convenience.

. the mobilized skin friction along any section of the pile is to be kept below a maximum of 80 percent of its limiting value (even though, in our opinion this requirement may prove too constraining for flexible offshore piles).

Let us quickly skip this very primitive "model" to consider more seriously the effects of the degradation.

The first real implicit procedure was proposed by Matlock and Foo |68| in 1980 and was meant to permit the adaptation of the pile driving code DRIVE 7 to consider cyclic loading. Their basic model of the pile-soil system is very similar to the one that will be used in this thesis, and consists, in the words of the authors, of "an assembly of elasto-plastic sub-elements at each node (used) to represent any desired non-linear inelastic behavior of the axial support"\*.

Let us quote from their description of the degradation model :

"In the present program, a degradation procedure is applied to each elasto-plastic sub-element separately. A degradation factor  $\lambda$  is applied to the ultimate plastic resistance of each sub-element only on the occurrence of a full reversal of the direction of slip of that sub-element\*\*. In addition to the initial ultimate resistance  $Q_u$  (of the sub-element) and the factor  $\lambda$ , the user specifies a lower-bound resistance  $Q_{min}$  which is asymptotically approached as degradation proceeds. Whenever the reduction is applied, the existing ultimate resistance  $Q_1$  is degraded to a new ultimate resistance  $Q_2$  according to the following relationship :

---

\* This is not exactly true as shall be shown in Chapter 3.

\*\* Local "alternate plasticity" in the terminology of shakedown analysis (Chapter 3).

$$Q_2 = (1 - \lambda) (Q_1 - Q_{\min}) + Q_{\min} .$$

Then the authors added :

"At present, there is limited knowledge about such degradation"

which is an understatement.

At the BOSS'82 Conference, Bea et al. [10] adopted apparently an even cruder procedure :

"In order to speed up degradation so as to minimize computer time (sic), the selected cyclic degradation law was formulated as follows : under each cycle the soil shear strength, or shear transfer along the pile shaft, decreased by 50 % of the value in excess of the fully degraded strength, which was selected to be 50 % of the undisturbed initial shear strenght ".

It is probable however that Bea et al. were in fact using the procedure of Matlock and Foo with  $\lambda = 0.5$  and  $Q_{\min} = 0.5 Q_{\text{initial}}$ , with an alternate plasticity criterion and not degradation at each cycle. The total lack of evolution of this model in these two years clearly underlines its limits : how do we select  $\lambda$  and  $Q_{\min}$  ? Is the evolution of the degradation satisfactorily represented by a constant value of  $\lambda$  ? etc ... Until these questions are properly answered we see no reason to recommend the use of this artificial model.

The latest example of an implicit scheme used to model a tension pile under cyclic loading is furnished by Lassoudiere et al. [60]. In their case the loading is restricted to a few cycles only and a good agreement with

experiments is obtained. Their degradation procedure involves hyperbolic relationships between the deviatoric hardening variables and the plastic strains. Unfortunately much more effort will be necessary to permit the use of such procedures for a moderately large number of cycles (100), but it is certainly a direction of research that should be considered in the case of extreme loadings.

### 2.3.2.B. Explicit procedures

It is convenient to distinguish between the developments involving finite element codes and those using much simpler one-dimensional models.

Boulon et al. [14-16] and Puech et al. [87] report extensive works on pile models capable of representing the soil behavior under a large range of loading and drainage conditions. The implementation of these models requires the elaboration of complex finite element codes integrating soil models of the type of Darve's incremental law (Darve [23]) with specific slip boundary elements. These formulations however do not escape the difficulties associated with the definition of the initial state of stress before loading (and it should be noted that their treatment of this problem is quite crude when compared with the developments made in this domain by MIT researchers (Baligh, Levadoux, Kavvadas)). The explicit formulation of the degradation, called the "extrapolation relationship", used by Boulon et al. is of the form

$$\epsilon_{\text{plastic}} = \frac{N}{a + bN}$$

where  $\epsilon_{\text{plastic}}$  is the irreversible strain and N the number of cycles. Due to its simplified form, this extrapolation is only valid over a limited

range of number of cycles. In practice it seems that these models can be calibrated to accurately represent a posteriori the soil-pile behavior (Puech et al. |87|) but it is still much too early to use them with confidence in class-A quantitative predictions. These complex and costly models have very weak points and it can be argued whether it is really justified to use such a juxtaposition of powerful computational tools and fancy equations when key elements of the problem, such as the initial stress conditions or the extrapolation relationship, are oversimplified.

Much simpler models of the pile-soil interaction may lead to results that are just about as satisfactory. The idea is to develop procedures that have uniform degrees of sophistication in each of their constitutive elements : pile-soil interaction definition, degradation laws, loading description, initial state of stresses, etc ... Since they will be simpler and less costly such models will offer the big advantage of permitting sensitivity analyses to be made thereby significantly improving our qualitative understanding of the overall system.

In other words it may be far more instructive to consider an approach specifically designed to study the problem from a sound qualitative point of view rather than to insist on developing only cumbersome and perhaps misleading quantitative procedures.

Such has been the approach of Poulos |80-84| who has been attempting to adapt his own computer codes, which are based on an unidimensional representation of the pile-soil system and on Mindlin's equation (Mattes and Poulos |69|), to consider the cyclic degradation of soil. Poulos made serious efforts to gather information but the scarcity of the data forced him to

elaborate a "semi empirical approach" in which engineering judgment was used to patch results from different sources into a composite data bank. Since this work is at the origin of the development of our own procedure it shall now be analyzed in some detail.

The objective of Poulos is to estimate the "apparent" stiffness and the ultimate capacity of the pile after undrained cycling. In order to do this he originally used a simplified effective stress analysis (Poulos |2, 3|) based on an approximate formulation of the evolution of the pore pressure during constant-stress DSS cycling (Van Eekelen and Potts |102|) in combination with normalized properties obtained from monotonic results (SHANSEP, Ladd and Foott |59|). But this first attempt proved to be somewhat unsuccessful\* and was abandoned to the benefit of a more versatile total stress analysis. He then gathered information on the evolution of cyclic stiffness with number of cycles in two-way\*\* constant strain undrained tests run on San Francisco Bay Mud (Idriss et al. |48|), and on the evolution of the undrained shear strength as a function of the cyclic shear strain level as given by Lee and Focht |61|. Only in his last article does Poulos (Poulos |84|) introduce the effect of the number of cycles on this strength degradation. All these experimental results were expressed in terms of normalized cyclic strains thereby requiring the (subjective) evaluation of "critical cyclic strains" as references. It is fundamental to recognize that the degradation represented by these data is only associated with cyclic shear strains and with symmetric

---

\* Poulos estimates that the pore pressure build up is only one of the elements of the degradation and that the progressive destruction of the contacts in the soil skeleton is not taken into account by the effective stress analysis.

\*\* Symmetric straining around the origin.

loadings around  $\varepsilon = 0$ , and that consequently no average shear strains or average shear stresses are considered. Thus such a formulation cannot be used to study the evolution of the displacements of the pile during cyclic loading since no provision is made for the accumulation of permanent deformation with each cycle.

Let us now consider the iteration procedure used by Poulos assuming for a moment that his data are satisfactory.

"The detailed analysis procedure is as follows :

1. First estimates of soil modulus  $E_s$  (and) ultimate skin friction are chosen at each element (e.g., the values for static loading).
2. The pile is analyzed for the maximum load  $P_{\max}$ , and the distribution of shear stress and displacement along the pile is determined.
3. The pile is similarly analyzed for the minimum load  $P_{\min}$ .
4. The cyclic shear stress  $\tau_c$  and the cyclic displacement  $\rho_c$  are determined from the two foregoing analyses by subtracting the minimum values from the maximum values.
5. For the specified number of cycles and the appropriate level of cyclic shear stress, the following determinations are made : displacement or cyclic shear strain at each element (depending on the type of degradation analysis being performed) ; the change in soil modulus ; and ultimate skin friction ...

6. The new modulus and ultimate skin friction values are compared with the estimated values, and if the difference is greater than a specified tolerance, new values are selected and steps 2 to 6 repeated until the desired degree of convergence is attained.
7. The cyclic deflection, the mean deflection, and the values of ultimate skin friction ... are thus obtained, from which the available ultimate load capacity after cycling may be readily calculated".

The first four steps are quite acceptable, even though it is not clear whether step 3 is carried out considering the residual stresses created at step 2, as it should be. In step 5 it is not easy to see how the data bank as previously described can be used with cyclic shear stresses as input. But far more debatable is the iteration procedure described in step 6. Why should we expect to have agreement within a "specified tolerance" between estimated and final values of the modulus and of the ultimate skin friction ? The modification of the estimated values at each iteration masks their significance : if they are estimates of the final values - as seems to be indicated by the convergence criterion - why do we subject them to the degradation of the complete cycling at each time ? It is really difficult to understand why and where such an iteration procedure converges, if it does\*.

---

\* This iteration procedure has been systematically applied in all Poulos' papers, which rules out a possible redaction error.



### 2.3.2.C. Conclusions

There are good reasons for wanting to develop a simple explicit procedure, and Poulos' approach has been considered as one of the better adapted ones (Gallagher and St John [31]), but there are also obvious improvements which can be made in the description of the soil degradation and in the iteration procedure employed. There are also experimental motivations for rejecting a model such as Poulos' as it is. In a paper recently presented at Austin in 1982 Mc Anoy et al. ([70]) made the following observations based on in-situ pile test results :

"No change in cyclic displacement occurred within any of the three tests, indicating that there was no degradation of cyclic soil modulus, contrary to the suggestion of Poulos (1980) that cyclic shear degradation was a function of stress level and number of cycles. It is particularly surprising that no degradation occurred during test B, especially when the pile was failing ...".

As we shall see later, this phenomenon can be clearly explained on the basis of the test results and of the analysis to be presented in this thesis.

\_\_\_\_\_.

### 3. THE PILE MODEL

#### 3.1 FUNCTION OF THE PILE MODEL

The Pile Model is one of the elements of the procedure which is proposed to study the behavior of a tension pile under cyclic loading. The two other constituents of this procedure are the Soil Degradation data (which will be treated in Chapter 4), and the algorithm of Chapter 5 integrating the Pile Model and the Soil Degradation data into an analytical tool : the computer code TLPILE.

What is the rolé of the Pile Model ? For a given set of soil-pile parameters, initial conditions (plastic displacements, residual stresses) and loading, the Pile Model estimates the distributions of forces and displacements existing in the pile and in the soil around it. The Pile Model insures that these displacements are compatible and that the forces are in equilibrium.

The procedure that will be developed is founded on a explicit scheme of the type presented in section 2.3. Thus the pile is analyzed at only a few intermediate cycles of the loading and between each of these analyses the evolution of the soil-pile parameters with cyclic loading are estimated from soil degradation data obtained under simplified loading conditions (based on the stress distributions estimated during the last application of the Pile Model). In other words the cyclic degradation affects the pile behavior through the soil-pile parameters but these parameters are fixed whenever the Pile Model is used.

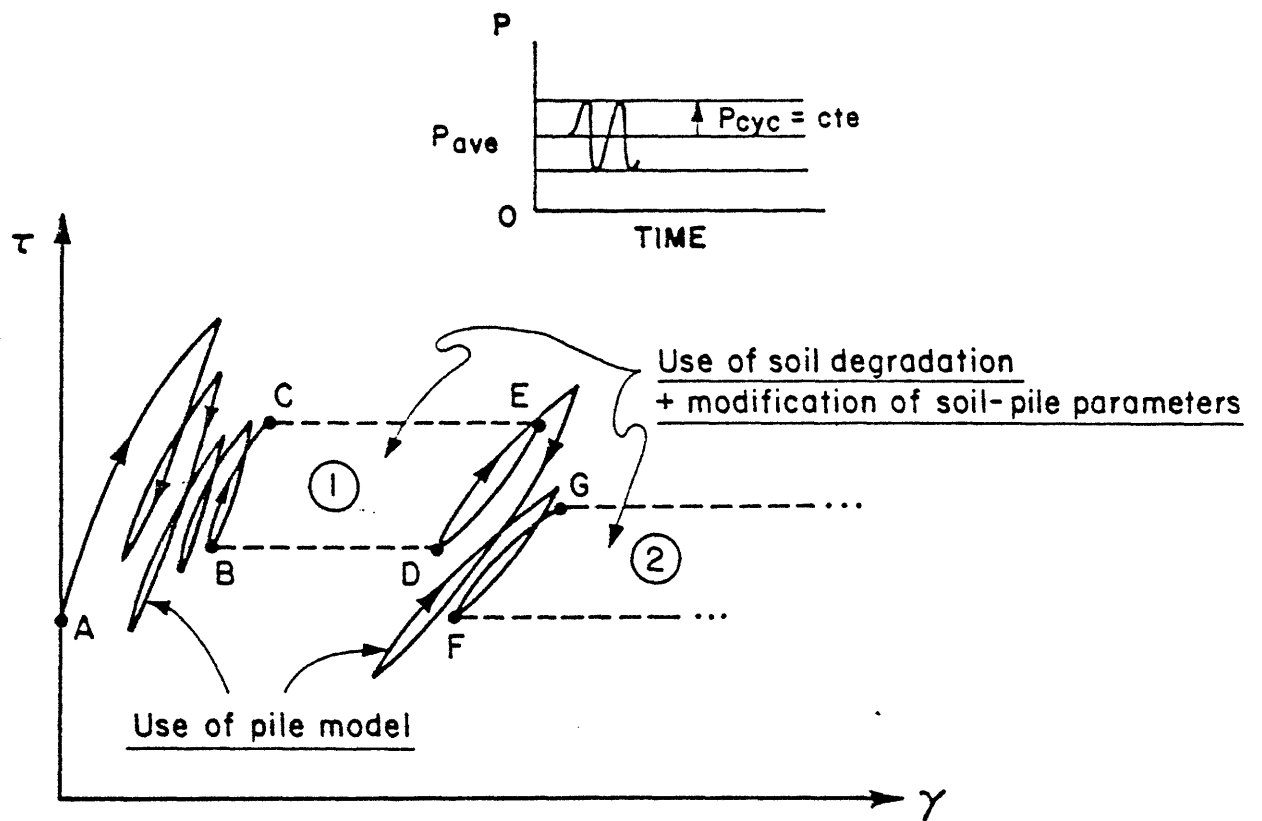


Figure 3.1.1 Explicit scheme.

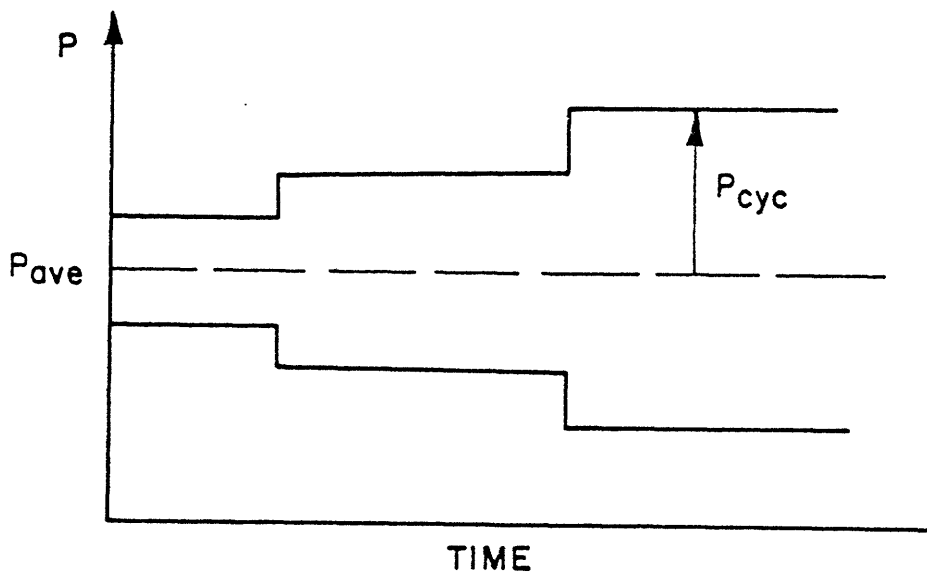


Figure 3.1.2 Loading at pile top.

The schematic stress-strain diagram of Figure 3.1.1 may help in presenting this procedure. Suppose we are at some point located along the pile and we wish to follow the evolution of the stresses and strains as a cyclic load is applied at the top of the pile ( $P_{ave}$  and  $P_{cyc}$  are constant). Upon the first application of the load the soil leaves its initial position A. Based on the soil-pile parameters estimated at point A, the Pile Model can be used to trace the local stress-strain curve over a few cycles. We should not, however, pursue this analysis too far since in practice soil degradation will occur and the soil-pile parameters of point A will no longer be representative. Thus the analysis is stopped at point C. The explicit representation of the soil degradation is then introduced : the stress range that has just been estimated by the Pile Model ( $\tau(B)$ ,  $\tau(C)$ ) is applied to the soil for a specific number of cycles (zone 1 of Figure 3.1.1). The soil-pile parameters are then modified to account for this degradation and the Pile Model is used again to estimate the new distributions of stresses and strains (from points D, E to F, G), before a new package of cycling (still under  $P_{cyc}$ ) is applied (zone 2). The evolution of the pile under  $P_{cyc}$  is therefore modeled by a succession of controlled stress approximations.

When the value of  $P_{cyc}$  is changed during the loading such as in Figure 3.1.2 the Pile Model is used to estimate the changes in stress and strain distributions. We must therefore distinguish between the use of the Pile Model at changes of  $P_{cyc}$  and its use corresponding to intermediate cycles under a given value of  $P_{cyc}$ . In both cases the resulting effects at the local level are similar to the transition between points E, D and points F, G of Figure 3.1.1. The local stressing at these transitions is "irregular"

but it may become "cyclic" after a while (i.e. repeat itself). One of the key issues in the discussion of the Pile Model is to understand these irregular transitions. Are we going to reach a cyclic stabilization ?, and, if so, when is it going to occur ?, and after how much strain ?. In other words can the Pile Model constitute a mechanism leading to an accumulation of deformation (even though the soil-pile parameters are maintained constant) ? Can a tension pile, modeled in the specific Pile Model which we shall use as a linear element and embedded in a soil represented by assemblages of springs and slip elements of constant characteristics, be pulled out by application at its top of a cyclic loading which never reaches the pile's ultimate capacity ? These are a few of the questions which shall be addressed in this chapter.

### 3.2 FIRST DESCRIPTION OF THE PILE MODEL

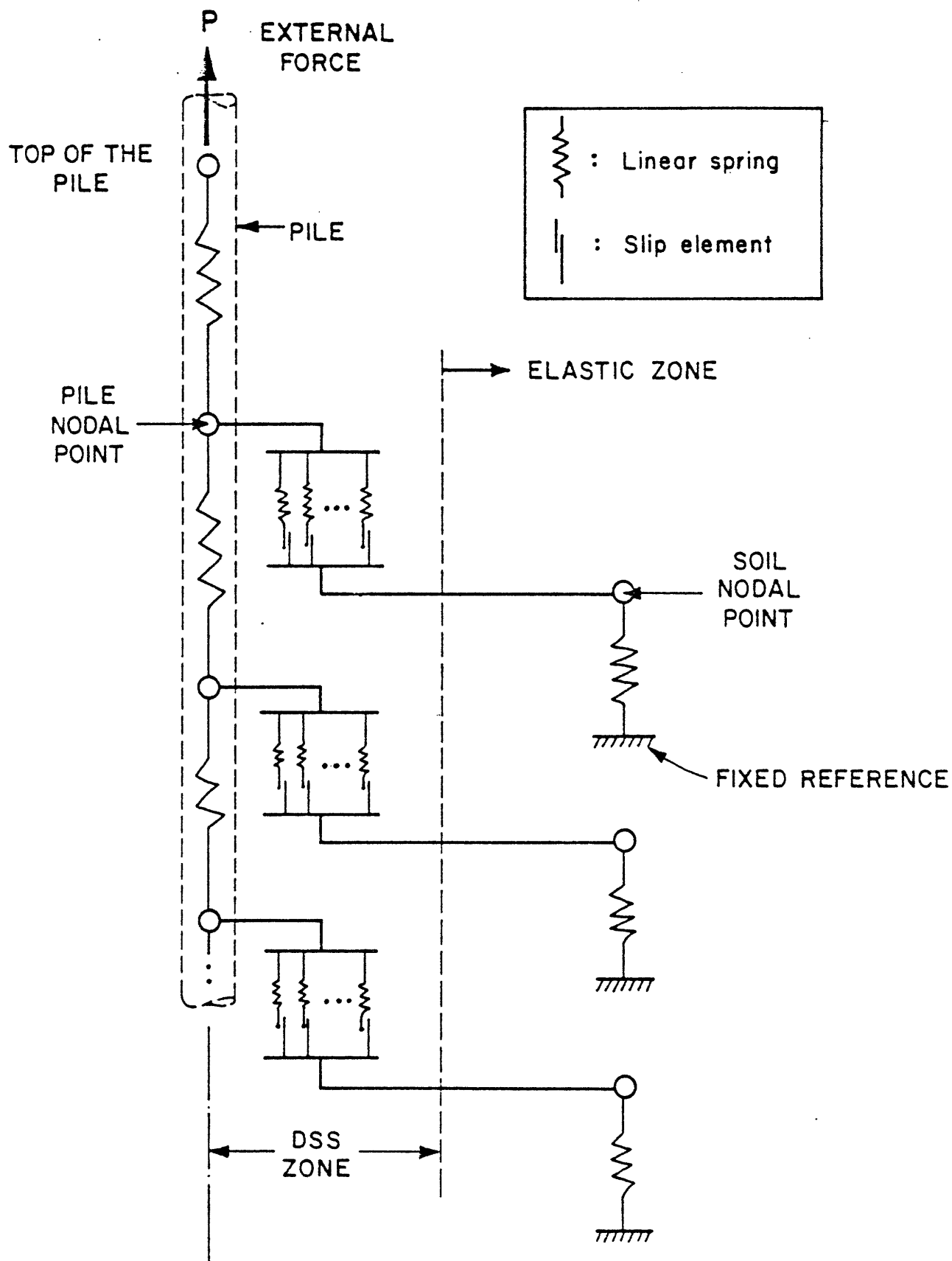
The Pile Model is an unidimensional assemblage of linear springs and slip elements as shown schematically in Figure 3.2.1. The pile itself is modeled by a discrete number of linear springs connected at pile nodal points. Each pile nodal point is in turn connected to a soil nodal point through a discrete set of springs and slip elements placed in series and in parallel while the soil nodal point is itself linked to a fixed reference by a linear spring. The first connection (pile-soil) represents the DSS\* zone : a nonlinear inelastic domain located directly around the pile that experiences all of the plastic strain. The second link (soil-soil) corresponds to the elastic zone around the DSS zone\*\*. No connection exists between the soil nodal points apart from the pile itself (this corresponds to Winkler's assumption). The stiffness coefficients of the springs together with the yield strengths of the slip elements constitute the "soil-pile parameters". (In chapter 5 we shall introduce imposed displacements to the "fixed references" to which the elastic zone springs are attached. This will be done by both adding very stiff springs in series with the elastic zone springs and by imposing large internal forces. These additions do not modify the overall behavior of the pile Model under irregular loading).

The Pile Model which has just been described has been used previously in a slightly simpler form by Chan, Matlock and Foo (|19|, |68|). It is a direct application of models proposed many years ago (|100| and section 3.3)

---

\* Direct Simple Shear.

\*\* A discussion of this DSS zone-elastic zone concept is presented in section 3.4.

Figure 3.2.1 Pile Model.

and commonly called Iwan models. These models are assemblages of springs and slip elements decomposable in branches in series and in parallel. In its discrete form (a finite number of springs and slip elements) an Iwan model permits a multilinear approximation of the loading\*, unloading and reloading of a material obeying Masing's rules (see section 3.3). This approximation applies reasonably well to soil (Pyke |90|). In the jargon of Plasticity Theory, Iwan models can be used to represent the kinematic hardening (without isotropic hardening) of elasto-plastic bodies admitting multiple nested yield surfaces.

Further aspects of the description of the Pile Model will be presented in section 3.4 on the basis of the theoretical understanding of its cyclic behavior. These additional comments will concern the compatibility of our Pile Model with the "t-z" curve concept and the procedure used to choose the soil-pile parameters, and to define the DSS zone elements.

---

\* Loading applies to the initial loading.  
Unloading means decreasing the load.  
Reloading means increasing the load after an unloading.



### 3.3 BEHAVIOR OF THE PILE MODEL UNDER CYCLIC LOADING

#### 3.3.1 An introductory example

The following example serves two purposes : it introduces, using a simple assemblage, some of the key ideas of the next sections and it constitutes a reference that the reader can use later on to put in concrete form the future theoretical developments. Despite the elementary nature of this example, tracing out the response of the assemblage is still a complex matter which may be difficult to follow at first reading.

We shall focus on the behavior of one DSS zone assemblage and follow its evolution under a preselected irregular (and ultimately cyclic) loading. This Iwan model is composed of four elasto-perfectly plastic (EPP) springs placed in parallel as shown in Figure 3.3.1. Each EPP spring is modeled by a linear spring and a slip element placed in series. All the slip elements are symmetric, i.e. their stress\* thresholds (yield strengths) are the same in extension and in compression. Originally all the EPP springs are in an unstressed and unstrained condition (point 0 in Figure 3.3.2). As the load is applied to the Iwan model it responds linearly until we reach the stress threshold in EPP spring # 1 (point 1). Since the strain is common to all EPP springs the first one to yield is the one with the lowest strain threshold (stress threshold divided by the EPP stiffness). When the load is increased after EPP spring # 1 has yielded we simply replace it by its constant yield strength. The global stiffness of the Iwan model is now equal to the initial

---

\* We shall work with stresses, but forces may be used equivalently.

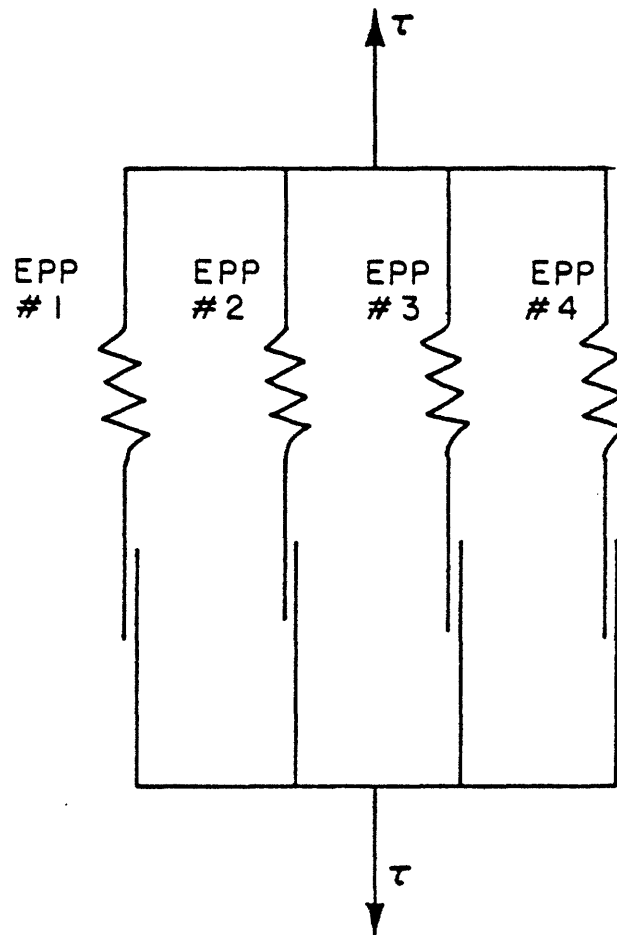


Figure 3.3.1 A simple Iwan Model.

stiffness minus the stiffness of EPP spring # 1. The next EPP spring to yield is number 2 (at point 2) which has the next lowest strain threshold, etc... In Figure 3.3.2 the procedure has been carried on to point A where EPP springs 1, 2 and 3 have all yielded. Now we are going to decrease the load applied to the Iwan model. Upon unloading all the EPP springs immediately re-enter their elastic domains (see Figure 3.3.3). The plastic strains remain unchanged until one EPP spring yields (at point 4). The first EPP spring to yield during this unloading is also number 1 but it first has to pass through to a no-stress condition before it is stressed in the direction of the unloading (point 4 on diagram 3.3.3.b) i.e. this yielding will require twice the amount of straining that was necessary to cause yield from the original position (in this case where  $\tau_A$  is selected to be twice  $\tau_1$ , this yielding occurs on the strain axis). This property is true for all the EPP springs. The order of yielding during unloading is the same as during loading. Since the stiffnesses remain the same and the incremental straining to yielding is twice its value during the original loading, the whole unloading curve can be deduced from the loading curve by applying a scaling factor of two.

Let us now stop the unloading at point B and start reloading to point C (Figure 3.3.3). Along the path BC the order of yielding is again the same as it was during the original loading. The shape of this reloading is identical to that of the unloading curve from A towards B. Now we unload from point C to follow the path CD. At point D, EPP spring 2 is still in its elastic domain (point D on diagram 3.3.3.c).

We now reload once again to point C (path DC). The increment of strain required to yield EPP spring # 2 is then given by the difference of  $\gamma(C)$  and

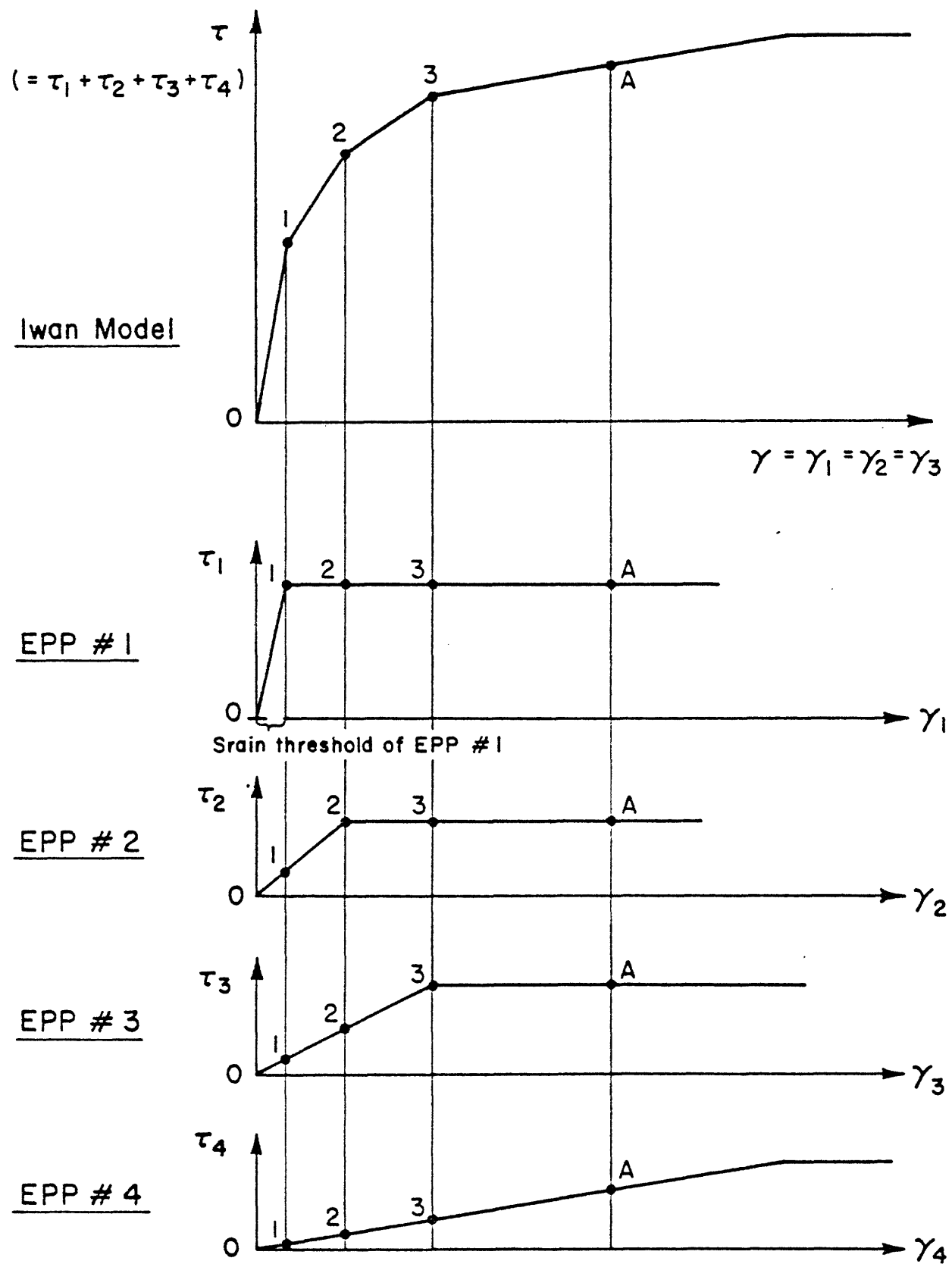


Figure 3.3.2 Introductory example, first loading curve.

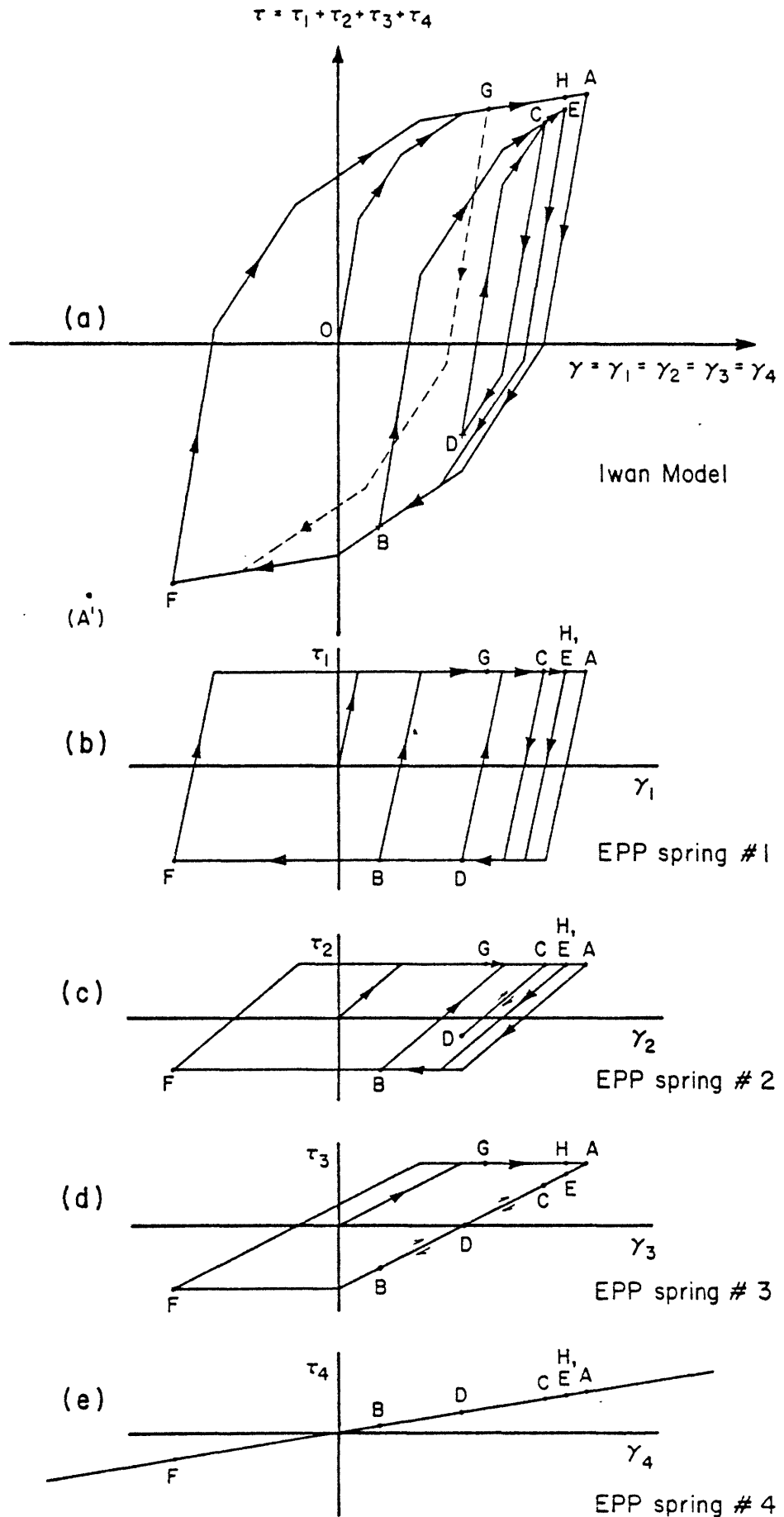


Figure 3.3.3 Introductory example, successive loadings.

$\gamma(D)$ , (see path DC on diagram 3.3.3.c), which is less than twice the strain threshold of EPP spring # 2. Next we continue the reload past point C to point E. Note that the shape of the reloading curve on path DCE (diagram 3.3.3.a) is not identical to that of the reloading curve along path BCE and cannot be obtained from the original loading curve by using a scaling factor of two as before.

Let us now unload from point E to point F. The unloading curve will pass through point B. The EPP spring # 3 will yield for  $\gamma = 0$  (this is a coincidence) (diagram 3.3.3.d) and evidently E was in the elastic domain of this spring. As a result the unloading curve along path EBF is not identical to the original loading curve by using a scaling factor of two. (This situation is exactly similar to the previous reloading along path DCE).

From point F we now reload to point G (where  $\tau(G) = \tau(E)$ ). At point F all the springs are either yielding or have never yielded, and the same is true at point G. The reloading curve along path FG is identical to the original loading curve up to  $\tau(G)$  expanded by a scaling factor of two.

Now we unload from point G. This unloading curve from point G will pass through point F (represented by a dotted line in Figure 3.3.3), and furthermore its shape will also be identical to the original curve when a scaling factor of two is used. If the stress  $\tau$  is cycled from now on between  $\tau(F)$  and  $\tau(G)$  the stress strain curve will describe a closed loop which is symmetrical with respect to its center and such that its branches can be obtained from the original loading curve by using a scaling factor of 2.

Another way of looking at this loading sequence is to see it as a cyclic loading, with  $\tau$  varying between  $\tau(E)$  and  $\tau(F)$ , applied to the system

after it is at point D. The first branch of the closed loop is described by the path obtained between the second and the third extreme values of  $\tau$  ( $\tau(E)$  is the first,  $\tau(F)$  the second and  $\tau(G)$  the third). In other words the determination of the closed loop requires the analysis of the loading through three successive loading peaks, i.e. one and one half cycles of loading. As will be shown in the following sections this example is characteristic of the cyclic behavior of the Iwan models.

### 3.3.2 Masing's rules and Iwan models

The Iwan models are entirely defined by their original loading curves (there are two such curves, one in extension and one in compression, both starting from the unstressed and unstrained condition). In this section these "first deformation curves" are assumed to be known.

What are Masing's rules ? They are rules which permit one to estimate the unloading and reloading behavior of a material knowing only its loading curve, as we shall now see. The utilization of the results of a monotonic test to predict material behavior under irregular loading is a classical topic in theoretical mechanics which has been traditionally approached in the past from two different directions |90| : through standard mathematical models on the one side, and through mechanical analogs on the other.

The mathematical models articulate themselves on sets of rules which have been experimentally established for some materials and are assumed to hold for others. The most widely accepted set of such rules was suggested by Masing |66|, and states that 1 the shear modulus on each loading reversal assumes a value equal to the initial tangent modulus for the initial loading curve (Figure 3.3.4.a), and that; 2 the shape of the unloading or reloading curves is the same as that of the initial loading curve, except that the scale is enlarged by a factor of two (Figure 3.3.4.b). Application of these rules allows behavior under symmetric cyclic loadings to be described by means of a single

analytical function\*.

In order to study the behavior under irregular loading two more rules must be added : 3 the unloading and reloading curves should follow the initial loading curve if the previous maximum shear strain is exceeded (Figure 3.3.4.c), and 4 if the current unloading or reloading curve intersects the curve described in a previous unloading or reloading, the stress-strain relationship follows this previous curve (Figure 3.3.4.d). The set of these four rules is called the extended Masing rules.

Obviously, keeping track of the behavior under irregular loading becomes a very tedious problem as it requires the memorization of the entire past history.

The mechanical models involve the study of rheological analogs. Among them are the Iwan models which offer the remarkable properties of adhering to all four of Masing's extended rules and of inherently "memorizing" the relevant portion of the past loading history so that no bookkeeping is required to comply with both the third and the fourth rules above. The proof of these facts is the object of the next section.

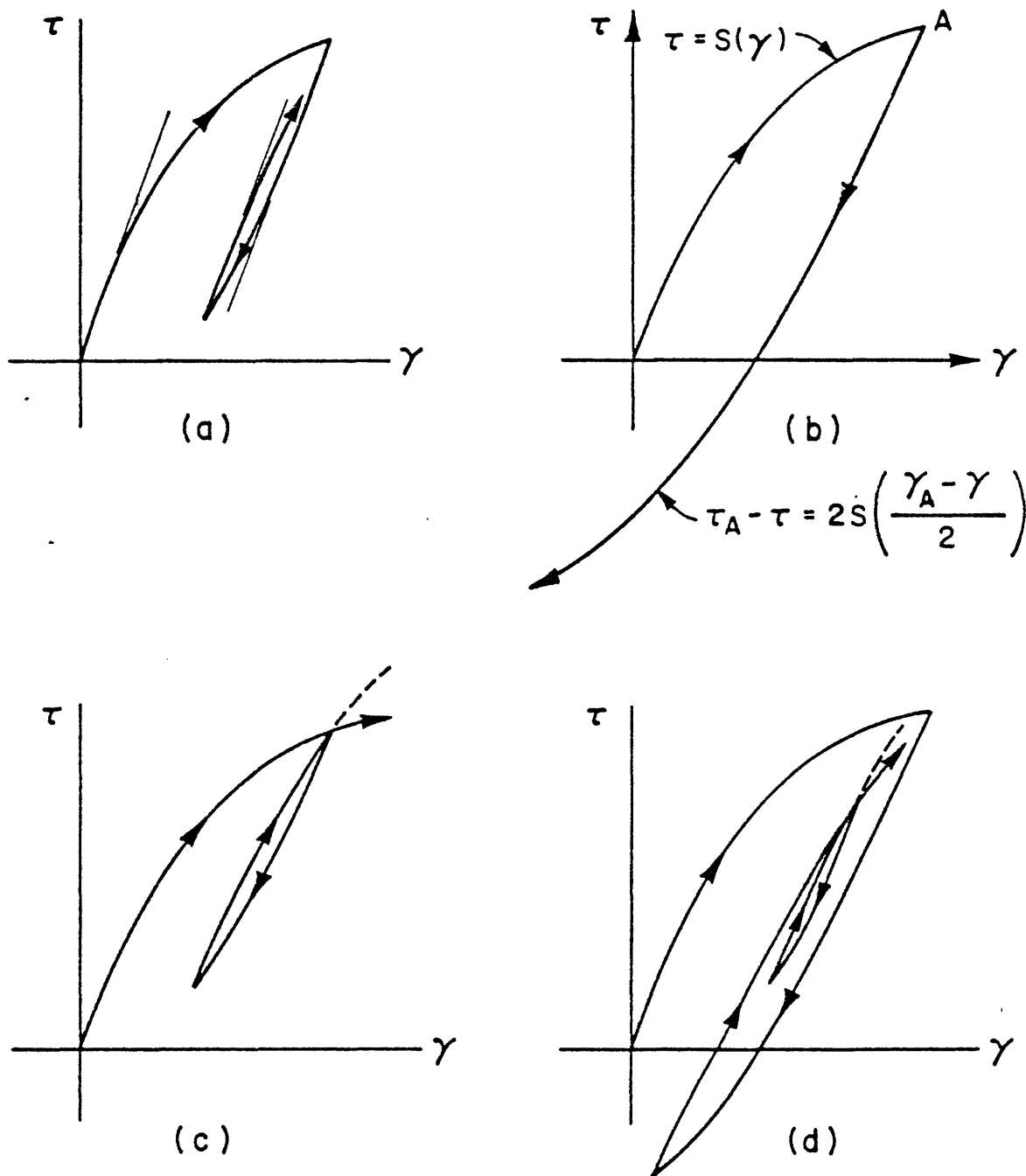
### 3.3.3 Properties of Iwan models

As already mentioned Iwan models are assemblages of springs and slip elements placed in any order but always decomposable into branches in series and in parallel. Figure 3.3.5 shows an example of both an Iwan model assemblage and a random assemblage that does not qualify as an Iwan model. Iwan models placed in series or/and in parallel constitute an Iwan model in itself. The dotted lines of Figure 3.3.5.a show how the whole assemblage can be gradually reduced to a single Iwan model.

---

\* For instance, the Davidenkov-class models and the Ramberg-Osgood-class models in Table 3.3.1.



Figure 3.3.4 Extended Masing Rules.

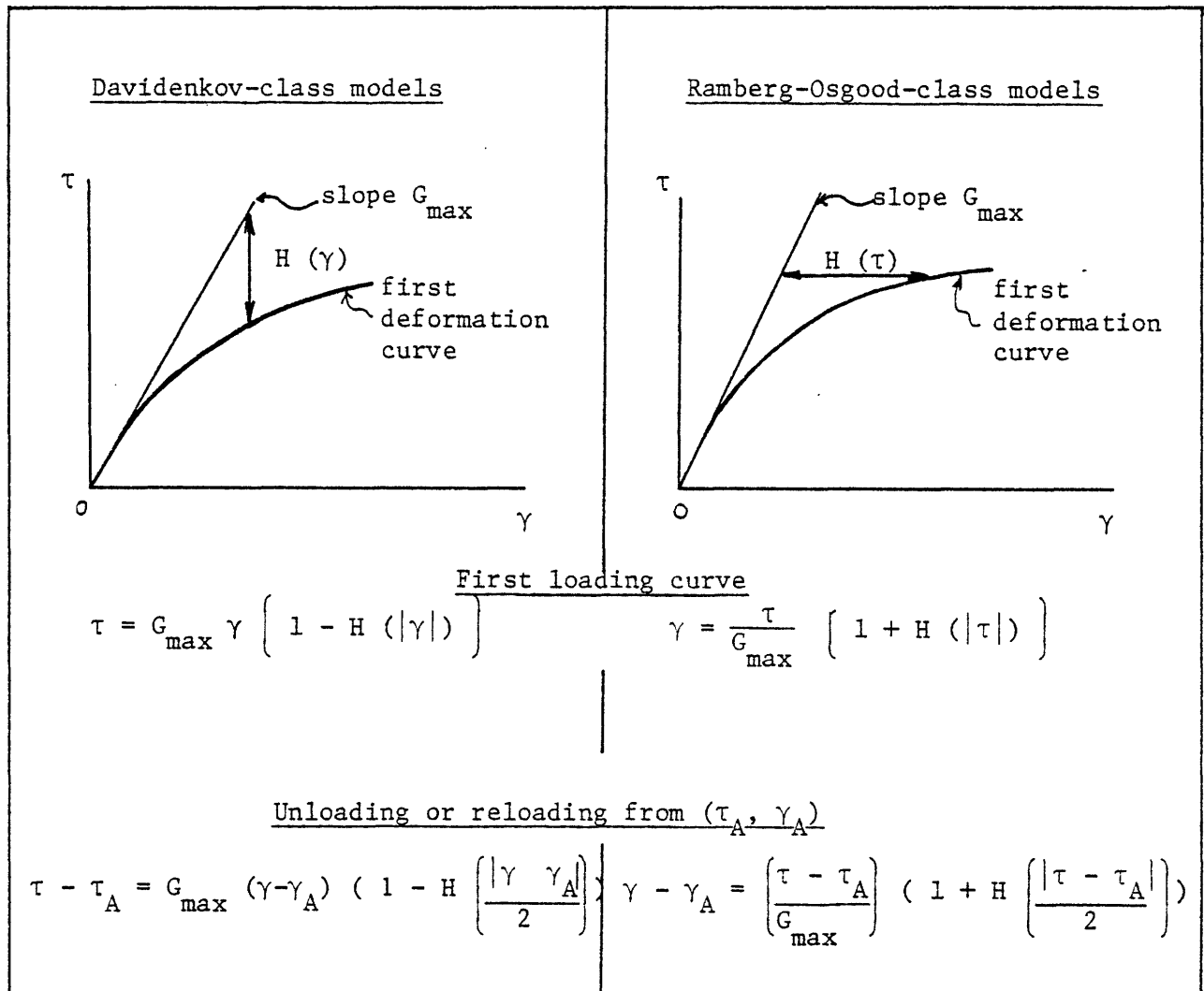


Table 3.3.1 Mathematical models for symmetric loading.

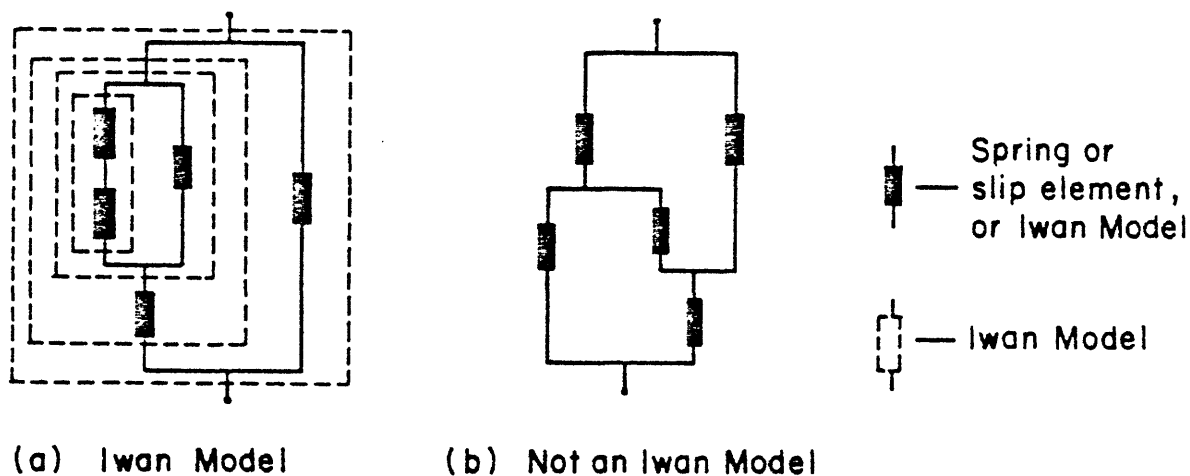


Figure 3.3.5 Decomposition in series and parallel of an Iwan Model.

The definition of Iwan models can be extended to an infinite number of springs and slip elements as shall be shown later. Figure 3.2.1 shows that the Pile Model is an Iwan model.

W.D. Iwan was the first to recognize that the models which bear his name are not his creation [50]. Masing used similar models as early as 1926, as did Prandtl, Duwez, Drucker and Ivlev among others over the years. Timoshenko suggested this approach in 1930 [100], and Persoz [78] had presented many of the results, which shall be considered later on here, in 1958. This last paper was published in French, and as a result, received little attention in this country. Since then the French school, lead by Mandel, has produced numerous results concerning the study of rheological bodies, greatly generalizing the Iwan models [49]. Finally, let it be pointed out that Iwan models have already been widely used in geotechnical engineering, particularly in areas related to earthquake engineering and in the study of piles [67], as was previously mentioned.

### 3.3.3.A. The Prandtl body

The basic constituent of Iwan models is a spring in series with a slip element. Unfortunately, this constituent is the object of a varied and confusing terminology. Earlier in this chapter, we used the term elasto-perfectly-plastic (EPP) spring, but this name is not recognized in rheology. Iwan calls it a Jenkin element - and he is about the only one to do so -. Hereafter, we shall adopt the name "Prandtl body", abbreviated P-body, as used by Riener [92] in his tree of rheological bodies which is partly reproduced in Figure 3.3.6.

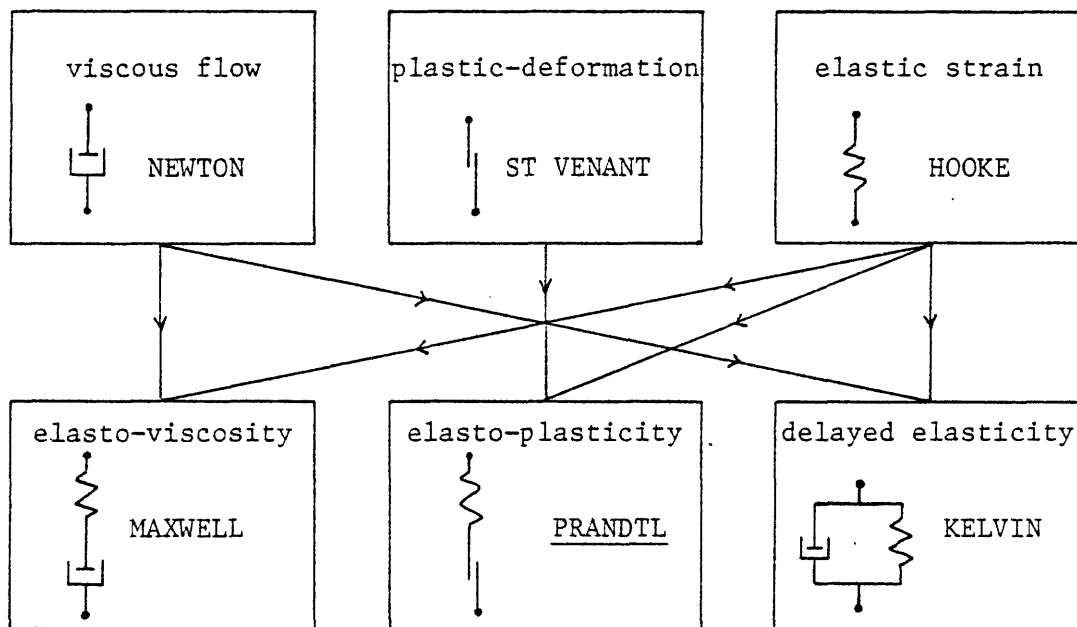


Figure 3.3.6 Riener's rheological tree.

While the St Venant body in Figure 3.3.6 is associated with perfect plasticity and the Hooke body with linear elasticity, the Prandtl body represents elasto-plasticity and is composed of a St Venant body in series with a Hooke body.

The St Venant body, also called a "rigid-plastic" or "slip" element, is characterized by a stress threshold differentiating immobility from plastic flow. Strictly speaking this threshold should be the same for "compression" and "extension" but one also uses the term of St Venant body when the two thresholds are different. A typical stress-strain diagram for a St Venant body is shown in Figure 3.3.7.

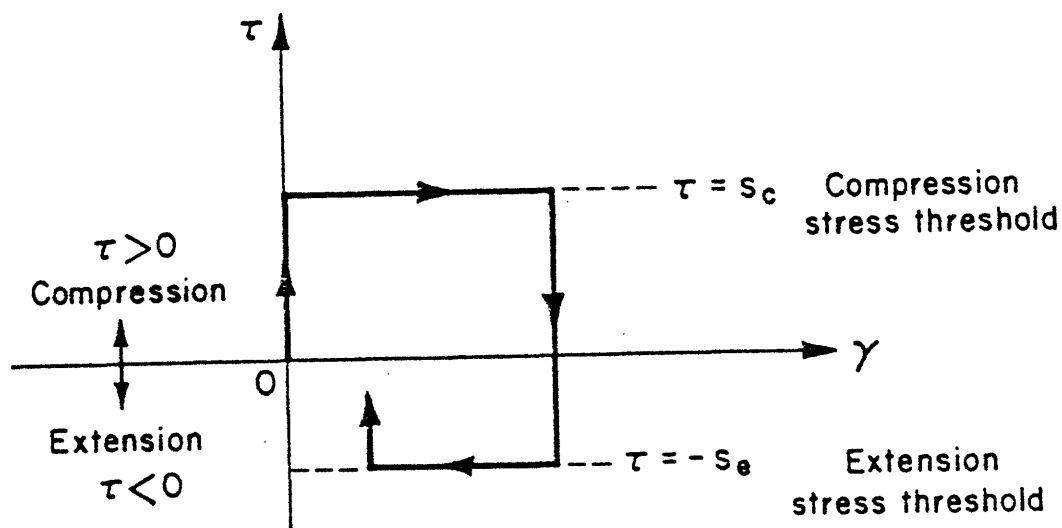


Figure 3.3.7 Typical St Venant body stress-strain diagram.

The Hooke body on the other hand is associated with only one value of the modulus of elasticity,  $E$ . The stress-strain diagram of Figure 3.3.8 is therefore not acceptable.

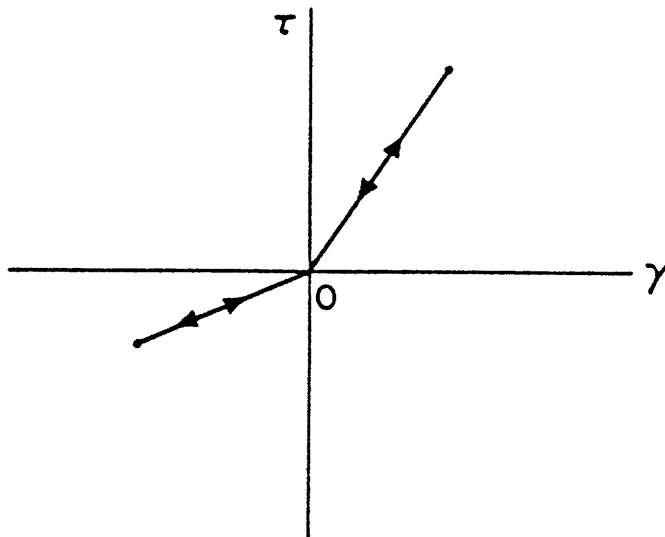


Figure 3.3.8 An unacceptable Hooke body stress-strain diagram.

In a Prandtl body the same stress  $\tau$  acts on both constitutive elementary bodies and the deformation  $\gamma$  is the sum of the elementary deformations,  $\gamma_e$  for the Hooke body, and  $\gamma_p$  for the St Venant body, as shown in Figure 3.3.9.

The "first-deformation" curve (or "first-loading" curve, "skeleton" curve, "backbone" curve) is the combination of the two stress-strain relationship obtained by both compressing the Prandtl body from the origin ( $\gamma = 0, \tau = 0$ ) and by extending it from the origin, as shown in Figure 3.3.10.

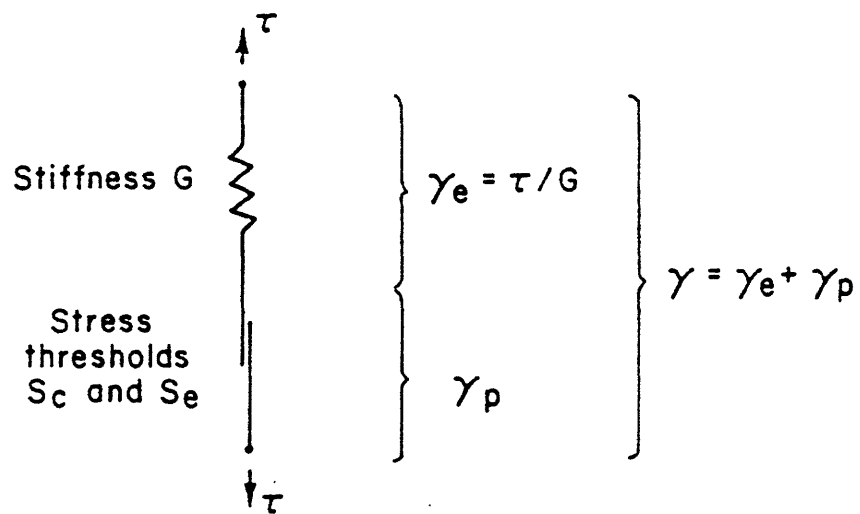


Figure 3.3.9 Schematic of the Prandtl body.

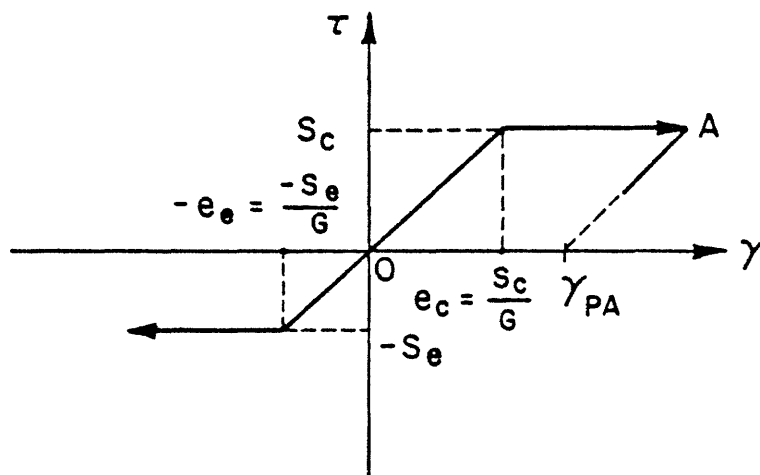


Figure 3.3.10 First deformation curve.

As can be seen in this figure, if the constitutive St Venant has two different stress threshold values, the Prandtl body will have two strain thresholds,  $e_c$  and  $e_e$ , defined from the first deformation curve.

When  $\tau = s_c$ , for example, the strain becomes indeterminate. If the stress is released from a point A where  $\gamma_p = \gamma_{pA}$ , the St Venant body freezes so that  $\gamma_p$  remains equal to  $\gamma_{pA}$  until further yielding occurs. The plastic deformation,  $\gamma_p$ , can be associated with the system's "memory" of its complete past history.

### 3.3.3.B. The generalized P-body and the infinite P-body

The generalized Prandtl body is an association of a finite number of P-bodies placed in parallel, while the infinite P-body will be its extension to an infinite number of P-bodies. Only the properties of the latter need to be studied, but the generalized P-body is usually the one used in practical applications.

We shall assume for the moment that each St Venant body has the same stress thresholds in compression and in extension, so that each P-body is characterized by one value of the strain threshold. We must now generalize the notion of modulus that was introduced earlier. The density distribution of the modulus,  $g''(e)$ , is such that  $\int g''(de)de$  is the sum of the moduli corresponding to a strain threshold between  $e$  and  $e + de$ .

The equation of the first-deformation curve is obtained by separating the P-bodies which are still elastic at a given value of the common strain  $\gamma$  from those that are not. The global stress  $\tau$  can be expressed by Equation 3.1.



$$\tau = \underbrace{\gamma \int_{\gamma}^{\infty} g''(e) \, de}_{\text{elastic part}} + \underbrace{\int_0^{\gamma} e \, g''(e) \, de}_{\text{plastic part}} \quad \text{Eq. 3.1}$$

which can also be written as :

$$\tau = \gamma g'(\infty) - g(\gamma) \quad \text{Eq. 3.2}$$

with  $g'(x) = \int_0^x g''(e) \, de$  and  $g(x) = \int_0^x g'(e) \, de$ .

The term  $g'(\infty) = \int_0^{\infty} g''(e) \, de$  is the initial modulus of the infinite P-body. The geometrical interpretation of Equation 3.2 is shown in Figure 3.3.11 and should be compared with the Davidenkov-class models of Table 3.3.1.

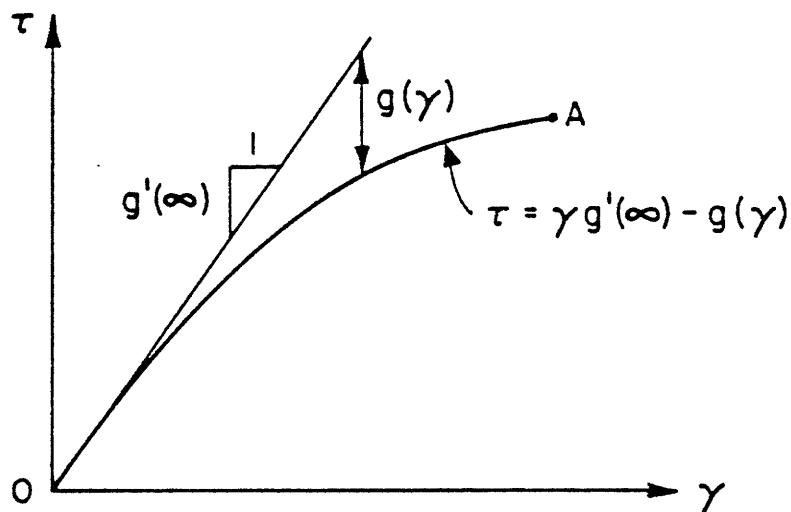


Figure 3.3.11 Geometrical interpretation of Equation 3.2.

Equation 3.2 will be functionally represented by :

$$\tau = S(\gamma), \text{ which gives the first deformation curve.}$$

Let us now consider unloading from a point A ( $\gamma_A, \tau_A$ ) belonging to the first deformation curve (Figure 3.3.11). Upon the first sign of strain release all the St Venant bodies will suddenly freeze and the system will recover its original global modulus (Cf. first Masing rule). At point A (Figure 3.3.12) all the P-bodies that have previously yielded have a stress equal to their stress threshold. Upon unloading, any of these P-bodies can thus tolerate a change of strain equal to twice the value of their strain threshold before they start yielding in the opposite direction. At the same time the P-bodies that have not yielded at point A will remain elastic for any strain change smaller than  $2 \gamma_A$ . The order of yielding during unloading will be the same as during the first deformation loading, i.e. by increasing value of strain threshold. The global stress change for a change of strain smaller than  $2 \gamma_A$  will then be given by equation 3.3.

$$\tau_A - \tau = (\gamma_A - \gamma) \int_{(\gamma_A - \gamma)/2}^{\infty} g''(e) de + 2 \int_0^{(\gamma_A - \gamma)/2} e g''(e) de. \quad \text{Eq. 3.3}$$

The first term on the right corresponds to the P-bodies which have not yielded during the unloading, and for which, therefore,  $2 e > \gamma_A - \gamma$ .

Equation 3.3 will not apply if  $\gamma_A - \gamma$  becomes larger than  $2 \gamma_A$ , since at that strain P-bodies which had never yielded previously may start yielding. In fact, as soon as  $\gamma_A - \gamma$  becomes equal to  $2 \gamma_A$  one reaches the symmetric point, A', of point A with respect to the origin, and therefore the first deformation curve. This can be clearly seen by recognizing the fact that Equation 3.3 can be written as :

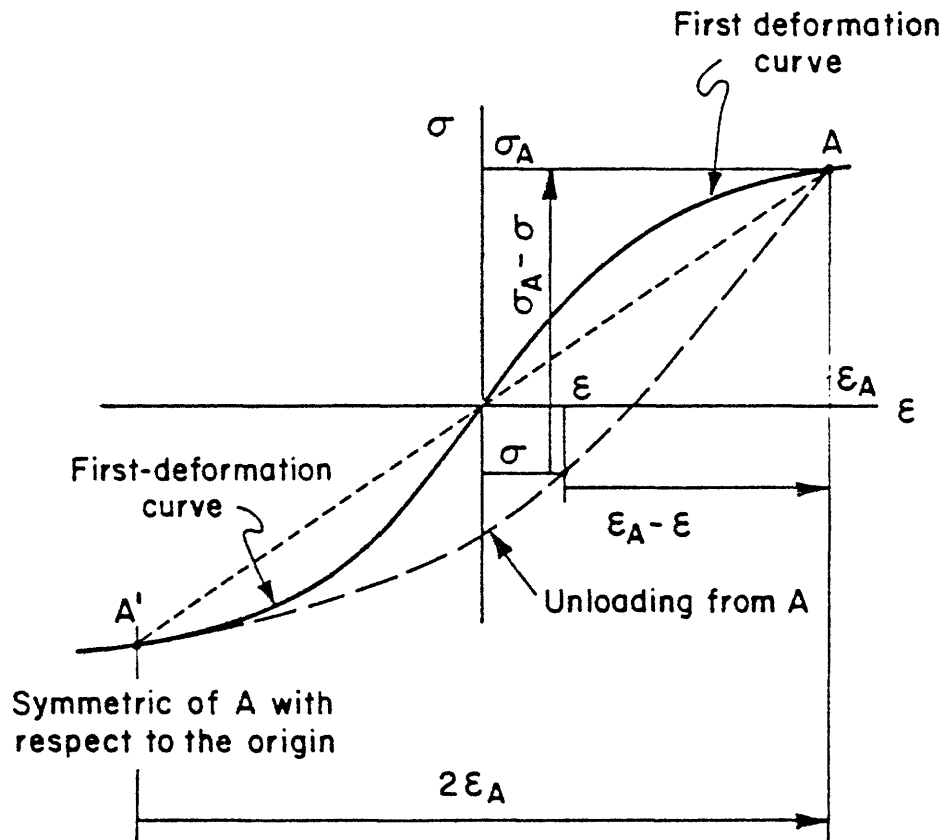


Figure 3.3.12 Unloading from the first deformation curve.

$$\tau_A - \tau = \left[ \gamma_A - \gamma \right] g'(\infty) - 2 g \left[ (\gamma_A - \gamma) / 2 \right] \text{ or}$$

$$\tau_A - \tau = 2 S \left[ \gamma_A - \gamma / 2 \right] \quad \text{Eq. 3.4}$$

When  $\gamma = -\gamma_A$ ,  $\tau_A - \tau = 2 \tau_A$ , i.e.  $\tau = -\tau_A$ .

At point A' all the P-bodies which had previously yielded have now yielded back. The situation is exactly symmetrical to that of point A and if the unloading is pursued past A' the characteristic point  $(\gamma, \tau)$  will follow the first deformation curve (3rd Masing rule). One can also observe that the slope of the unloading curve at A' is continuous since :

$$\left( \frac{d\tau}{d\gamma} \right)_{\gamma=-\gamma_A} = S' \left[ \frac{\gamma_A - \gamma}{2} \right]_{\gamma=-\gamma_A} = S' \left[ \gamma_A \right] = S' \left[ -\gamma_A \right].$$

Let us now reload from any point B  $(\gamma_B, \tau_B)$  of the previous unloading curve. All the St Venant bodies will freeze and, once again, the same order of yielding will be respected. One must however be cautious since there are now three categories of P-bodies to be considered : 1) those which have yielded in both directions, 2) those which have yielded in only one direction, and 3) those which have not yet yielded. If point B is on the first deformation curve in extension, and therefore past A', there will be no P-body in the second category, but this is not the case if B is in between A and A'. In this case, and in our particular example (loading path OAB), the P-bodies in the second category will remain elastic during reloading until  $\gamma = \gamma_A$ . this is due to the fact that at point A all of the P-bodies were at their threshold stresses. Thus, for the present reloading and for  $\gamma - \gamma_B$  less than or equal to  $\gamma_A - \gamma_B$ , one has :

$$\tau - \tau_B = (\gamma - \gamma_B) \int_{\frac{\gamma - \gamma_B}{2}}^{\infty} g''(e) de + 2 \int_0^{\frac{\gamma - \gamma_B}{2}} e g''(e) de \quad \text{Eq. 3.5}$$

$$\tau - \tau_B = 2 S \left( \frac{\gamma - \gamma_B}{2} \right). \quad \text{Eq. 3.6}$$

Evidently for  $\gamma = \gamma_A$  one gets  $\tau = \tau_A$ , therefore one has a closed loop between A and B that is symmetrical with respect to its center. Equation 3.6 can also be rewritten as :

$$\tau_c = S(\gamma_c) \quad \text{Eq. 3.7}$$

$$\text{with } \tau_c = \frac{\tau_A - \tau_B}{2} \quad \text{and} \quad \gamma_c = \frac{\gamma_A - \gamma_B}{2}.$$

In the coordinate system oriented at the center of the closed loop, the summits of the loop belong to a curve identical to the first-deformation curve, (whatever the position of A and B).

If the reloading is now continued beyond point A the characteristic point will follow the first deformation curve since the P-bodies which had yielded during AB will have yielded back during BA. If B is not on the first deformation curve (in extension) there will be a discontinuity in the slope at point A between the reloading curve and the first deformation curve, as shown in Figure 3.3.13.

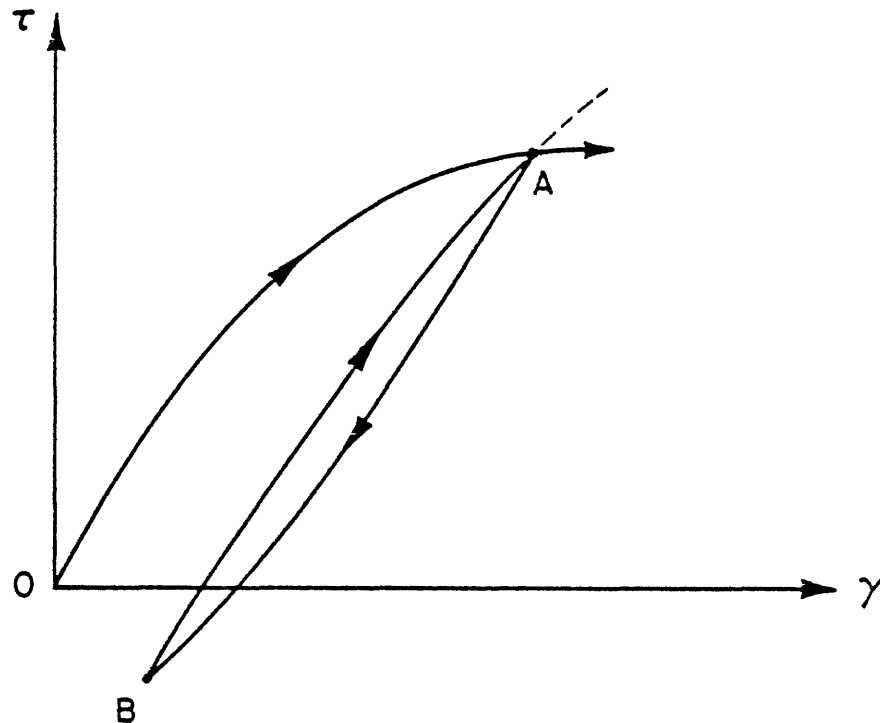


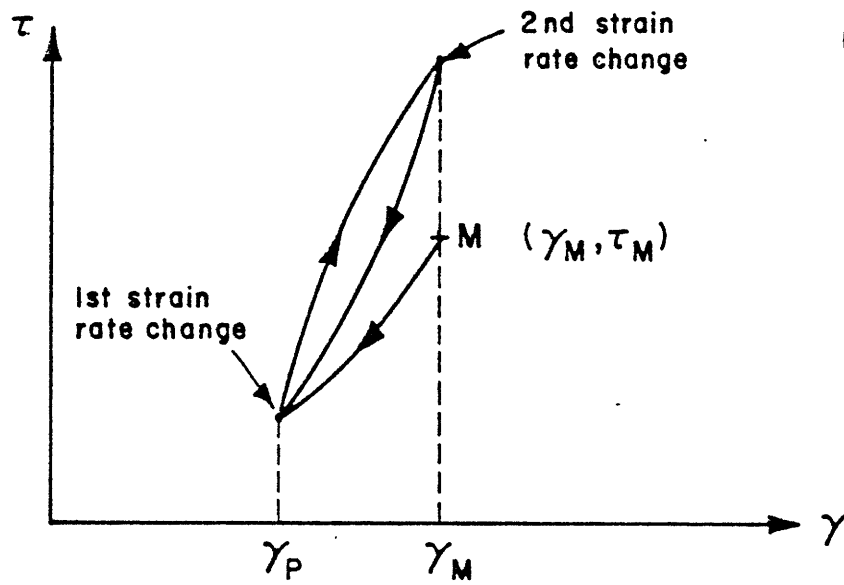
Figure 3.3.13 Slope discontinuity at A.

The properties of the cycle ABA have been known for some time [72]. But how many of these properties can be associated with any cyclic loading? Persoz [78] has proved the following general rules which are valid for any infinite P-body :

1. the convexity of the first deformation curve is always turned toward the strain axis,
2. any cyclic loading applied to an infinite P-body at a position M ( $\gamma_M, \tau_M$ ) such that either  $\gamma$  is varied between  $\gamma_M^*$  and  $\gamma_P$ , or  $\tau$  is varied between  $\tau_M$  and  $\tau_P$ , will result in a stabilized closed cycle as soon as the strain-rate, or the stress-rate, will have changed sign once (Figure 3.3.14a),
3. this closed cycle will be convex and symmetric with respect to its center. Furthermore if the first-deformation curve can be

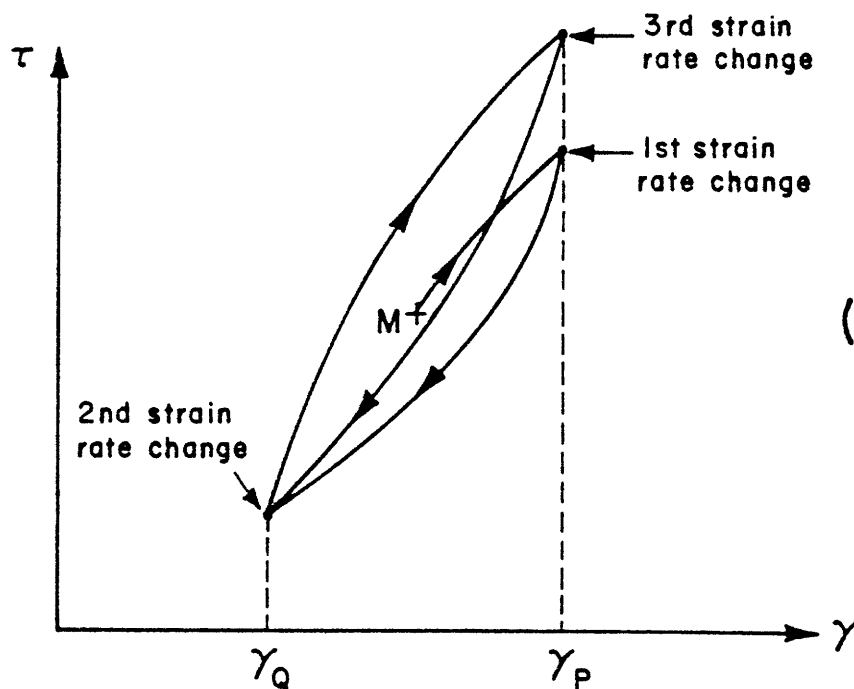
---

\* Note that the loading involves the coordinates of point M itself, see Figure 3.3.14a.



(a)

Loading with

 $\dot{\gamma} \in (\dot{\gamma}_M, \dot{\gamma}_P)$ .

(b)

Loading with

 $\dot{\gamma} \in (\dot{\gamma}_P, \dot{\gamma}_Q)$ .Figure 3.3.14 Stabilization to a closed loop.

written as  $\tau = S(\gamma)$ , the unloading branch from the top of the cycle  $(\gamma_T, \tau_T)$  will be given by  $(\tau_T - \tau) = 2 S \left( \frac{\gamma_T - \gamma}{2} \right)$ , and the reloading from the bottom  $(\gamma_B, \tau_B)$  by :

$$(\tau - \tau_B) = 2 S \left( \frac{\gamma - \gamma_B}{2} \right).$$

As a consequence one might observe that for a general cyclic loading characterized by  $\gamma \in (\gamma_P, \gamma_Q)^*$ , or  $\tau \in (\tau_P, \tau_Q)$ , the stabilization to a closed loop having the above mentioned properties will occur, at the very latest, after the second sign change of the strain rate, or of the stress rate. Practically speaking, this means that the closed loop will have as its summits the points corresponding to the second and third changes of strain rate or stress rate. The complete description of the behavior of the infinite P-body under regular cyclic loading will require the determination of three successive extrema, i.e. one-and-one-half cycles of loading. An example is shown in Figure 3.3.15 and should be compared to Figure 3.3.3.

One should also stress that as a direct consequence of the third property, with  $\tau_c = \frac{\tau_T - \tau_B}{2}$ , and  $\gamma_c = \frac{\gamma_T - \gamma_B}{2}$  one has :

$$\tau_c = S(\gamma_c)$$

independent of the values of  $\tau_{ave} \left( \tau_{ave} = \frac{\tau_T + \tau_B}{2} \right)$  and  $\gamma_{ave} \left( \gamma_{ave} = \frac{\gamma_T + \gamma_B}{2} \right)$ .

---

\* See Figure 3.3.14b.



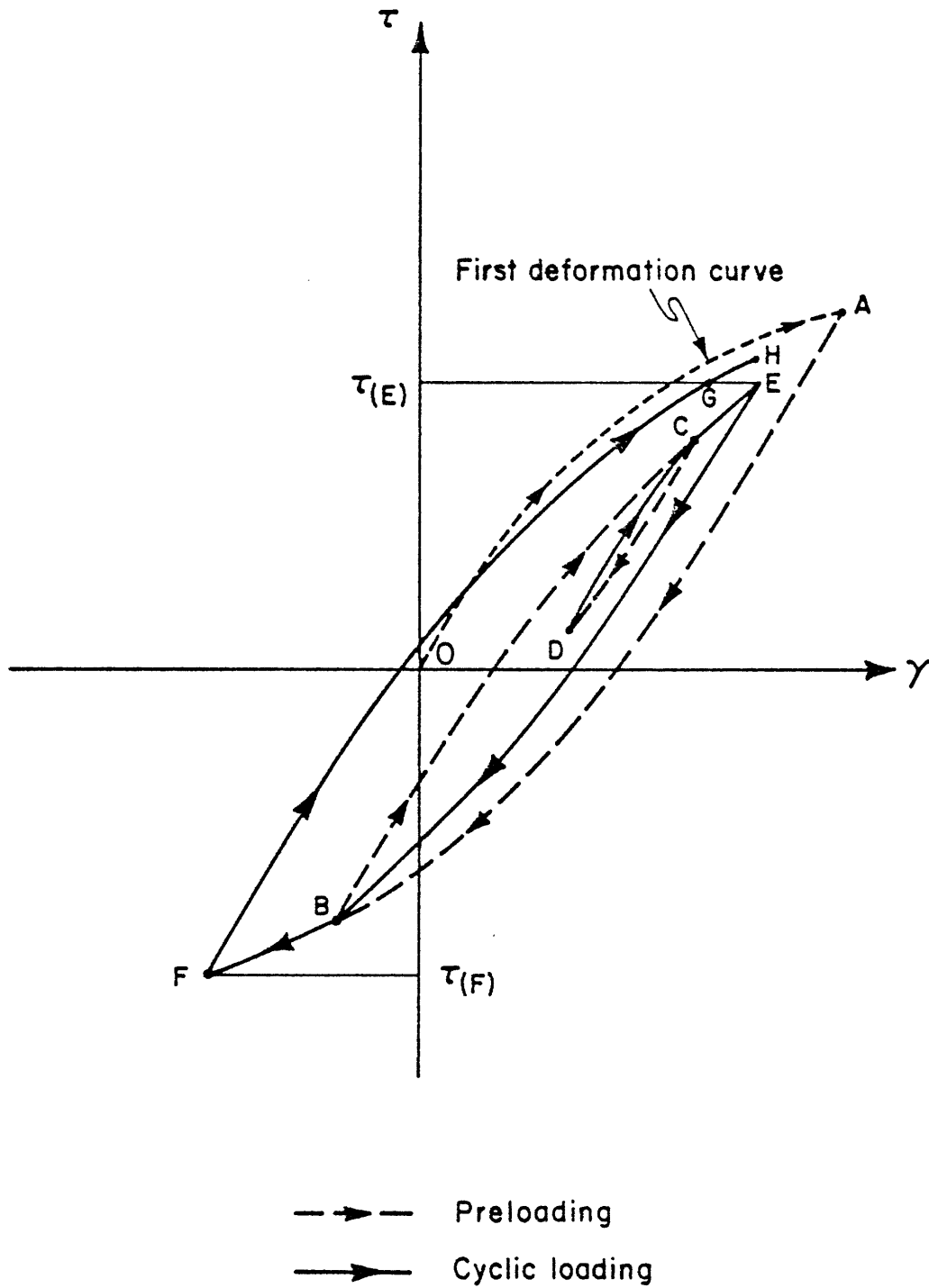


Figure 3.3.15 Example of stabilization under regular cyclic loading.

### 3.3.3.C. Iwan models and Random assemblies

Now, can these observations be extended to any Iwan model ?

The answer is yes (Persoz |79|\*).

To prove these properties we simply need to show that any Iwan model can be seen as an infinite (or a generalized) P-body. This proof is recursive. First it is observed that two infinite P-bodies placed in parallel constitute an infinite P-body. Then, in a second stage, we show that when placed in series they also behave exactly like an infinite P-body. Each branch of the model can thus be represented by an infinite P-body and gradually the whole Iwan model is replaced by a infinite P-body.

Other observations can then be made :

- the variation of stress or strain in an elementary component is a non-decreasing function of the variation of stress or strain applied to the whole assemblage,\*\*
- a closed loop on the stress-strain diagram of the Iwan model corresponds to a closed loop at the element level.

These results indicate that the Pile Model will never be "pulled out" by a cyclic loading applied at its top and that the irregular response under cyclic loading will stabilize after one-and-one-half cycles of loading etc...

Finally one may ask the question : what do we know of the behavior of random assemblies under cyclic loading ? These assemblies have been extensively studied by Mandel and his co-workers (Mandel |63|, Halphen |37|,

---

\* But the observation he made stating that "any cycle of stress corresponds to a cycle of strain" is wrong.

\*\*In other words an increase (resp. decrease) in the stain or stress applied to the whole assemblage cannot result in a decrease (resp. increase) of strain or stress at the elementary level.

Nguyen Quoc Son [76] and Zarka [103]) who have arrived at the following observations :

1. stabilization to a closed loop under regular cyclic loading occurs after one cycle\* or it does not occur at all,
2. ratchetting is possible (see Section 3.3.4),
3. the limiting state, when it exists, is generally a function of the initial state.

At this level of complexity we reach the domain of present research.

Let us now return to the study of Iwan models but this time looking at them from another angle which may prove helpful to further enhance our understanding of their behavior under cyclic loading.

#### 3.3.3.D. A physical analog to Iwan models

Since it has been shown that Iwan models and infinite P-bodies are equivalent concepts we shall restrict the discussion to the latter.

For the time being we will maintain the use of true St Venant bodies (equal properties in extension and in compression). Let us reconsider the stress-strain diagram of a P-body in Figure 3.3.16a. Assume there is a third dimension, called  $t$ , as shown in Figure 3.3.16b. The plane  $(\gamma, t)$  is used only for plotting an annulus of diameter equal to twice the strain threshold. The center of this annulus is always located along the  $\gamma_{axis}$ , and originally corresponds to point 0 of Figure 3.3.16b. As the loading is increased from the origin to point A we remain in the elastic domain, and the position of the annulus is unchanged. At point B the strain  $\gamma$  or rather

---

\* "One-and-one half" cycles.

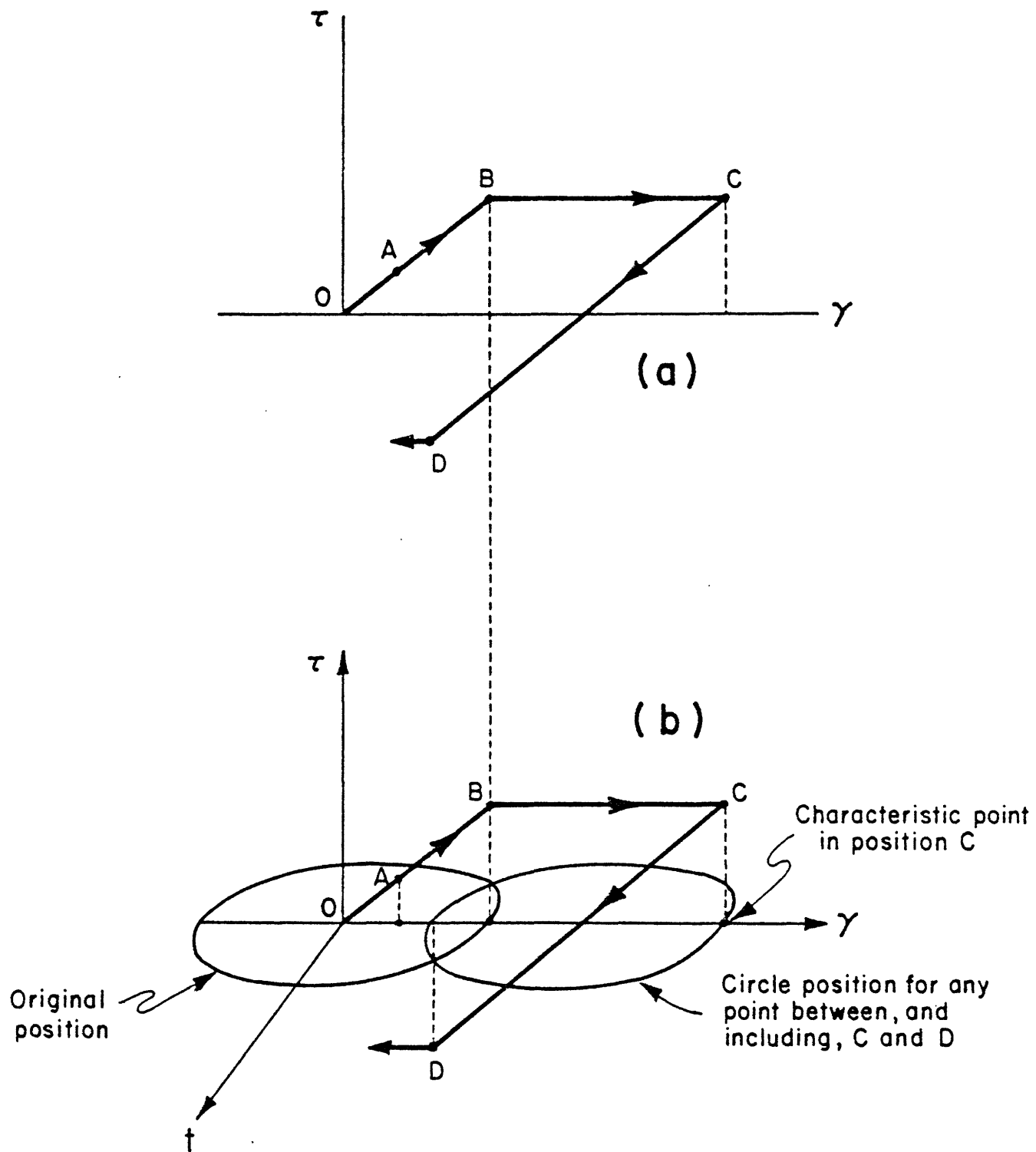


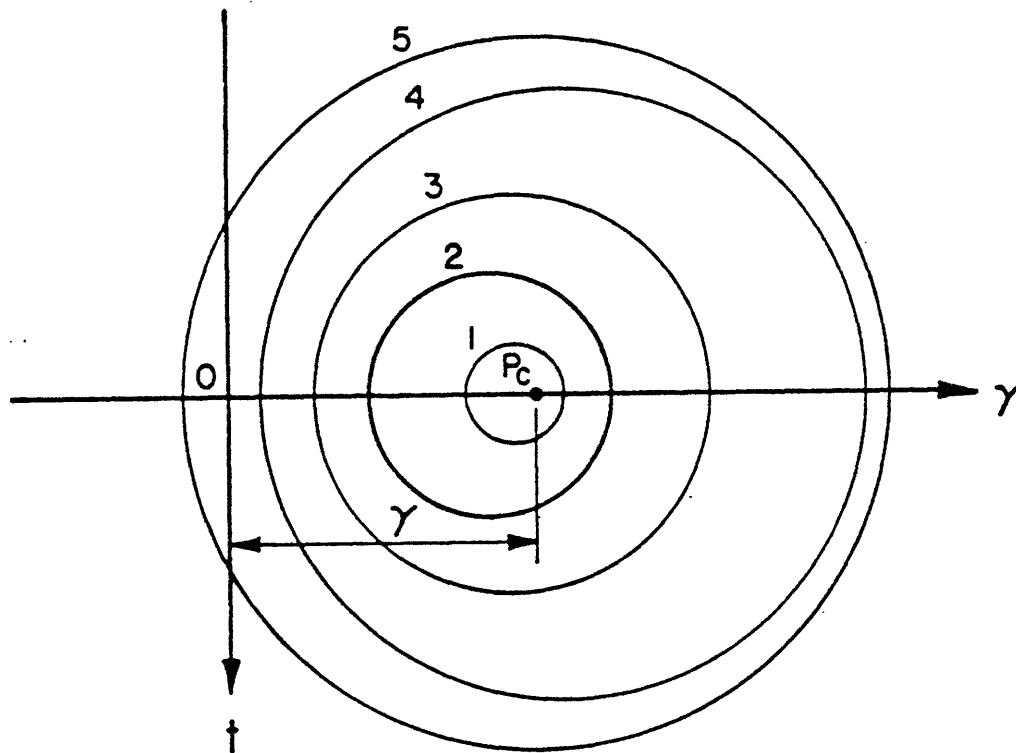
Figure 3.3.16 A physical analog to a P-body.

the characteristic point which is the projection of point B on the  $\gamma$  axis, touches the annulus. The characteristic point is constrained to stay in or on the annulus the diameter of which is constant. As yielding occurs the annulus is thus translated by the characteristic point until the loading is reversed (point C). Then, between C and D the annulus remains immobile. A new translation in the opposite direction will occur when the P-body begins to yield again at point D. The annulus may be thought of as a yield surface, the translation representing kinematic hardening. There is no isotropic hardening since the diameter remains constant. The annulus is only a convenient representation, its use being to represent a constant distance (its diameter), and the dimension  $t$  is just an artifice. The position of the center of the annulus gives at all times the plastic strain  $\gamma_p$  of the Prandtl body.

Let us now consider what will be the mechanical analog of a generalized P-body. Since the strains are common to the assemblage we can use the same characteristic point but now we shall have a set of nested annuli of different sizes such as those in Figure 3.3.17.

Again each annulus is representing a P-body and its diameter is equal to twice the P-body strain threshold. Again the locations of the centers of these annuli give the plastic strains of their associated P-bodies. Now, how does the analog model work ?

As the global strain  $\gamma$  is varied the characteristic point,  $P_c$ , will carry with it all the annuli with which it comes into contact. Upon reversing the sign of the strain rate, the contact will be broken before new contacts are made in the direction of straining. Each time an annulus is carried by



● Characteristic point

Figure 3.3.17 Physical analog of a generalized P-body.

the characteristic point some plastic yielding occurs since the position of the annulus center is modified.

Figure 3.3.18 is an example of a complete cycle of straining. The initial position of the assemblage is given in Figure 3.3.18a. At its right, on Figure 3.3.18b, one extreme of the straining has been reached. Annuli 1, 2, 3 and 4 have been moved by the characteristic point, but annulus 5 has not been touched. In Figure 3.3.18c the other extreme of the straining is obtained. Now the five first annuli have moved. If we then re-impose the first extreme, as in Figure 3.3.18d, the behavior stabilized to a symmetric cycle. Note however that the change from b to c is quite different from that occurring between c and d. The latter change defines the stabilized cycle. In other words we need to reach the situation of Figure 3.3.18d to know what the stabilized cycle will be. These results are perfectly analogous to the properties of the preceding section (and could be directly compared to Figure 3.3.15).

### 3.3.3.E. A few extensions of Persoz's results

What new properties can be derived from this annuli representation ? In the case of a generalized P-body such as the one represented in the previous figures it can be easily understood that the system can be restored to its virgin condition (with the characteristic point and all the centers of the annuli positioned at the origin) by applying as many strain changes as it has off-centered annuli (P-body with non-zero plastic strain). Of course, the P-bodies are restored in decreasing order of their strain threshold. An infinite P-body could similarly be restored by an infinite number of strain changes of decreasing amplitudes around the origin.

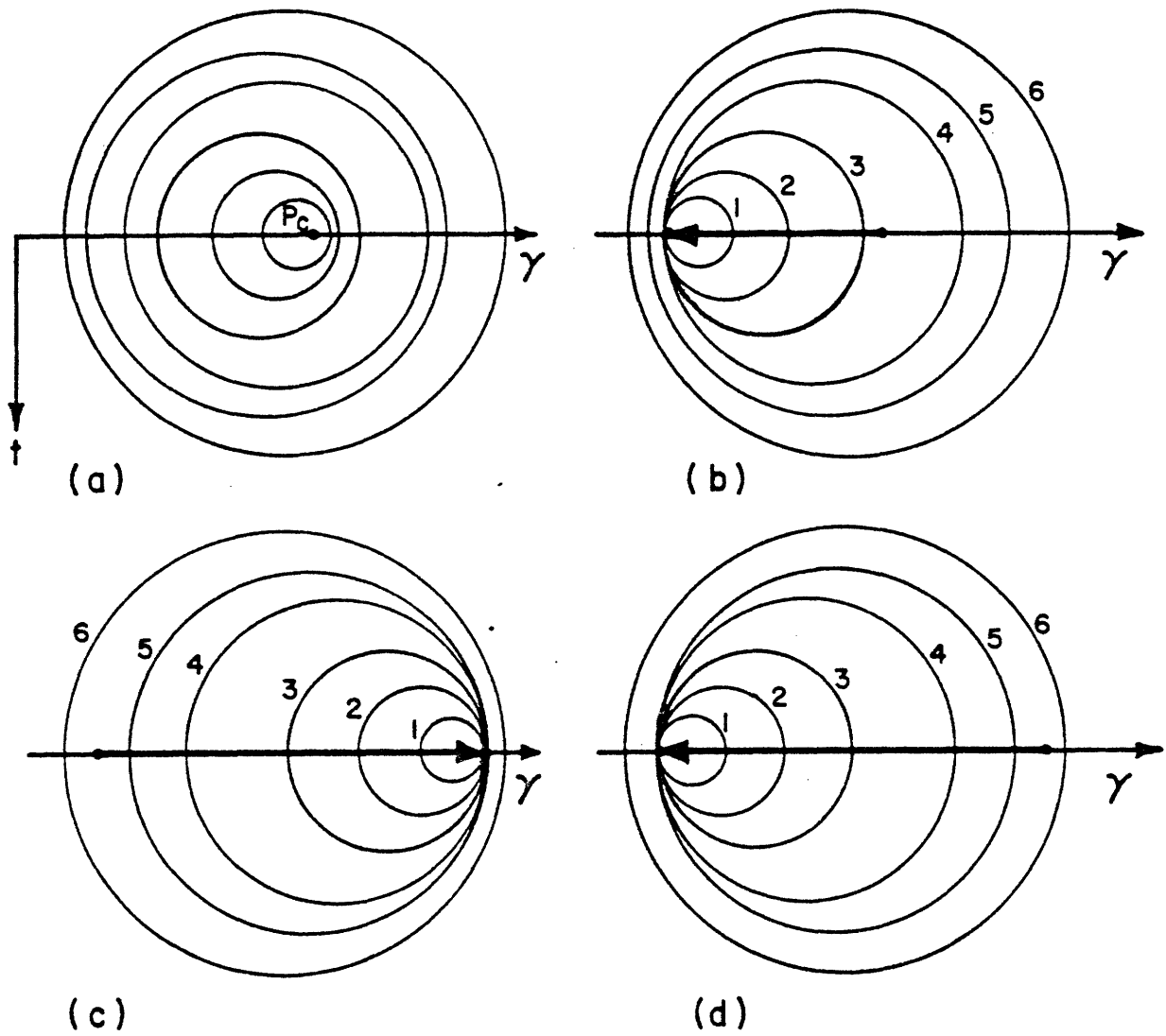


Figure 3.3.18 Example of stabilization under regular cyclic loading.



What would happen if the plastic strain of each P-body were not necessarily associated with the center of each annulus but with a point,  $Q$ , of fixed coordinate with respect to the annulus, and placed inside the annulus along the line of the centers (see Figure 3.3.19) ?

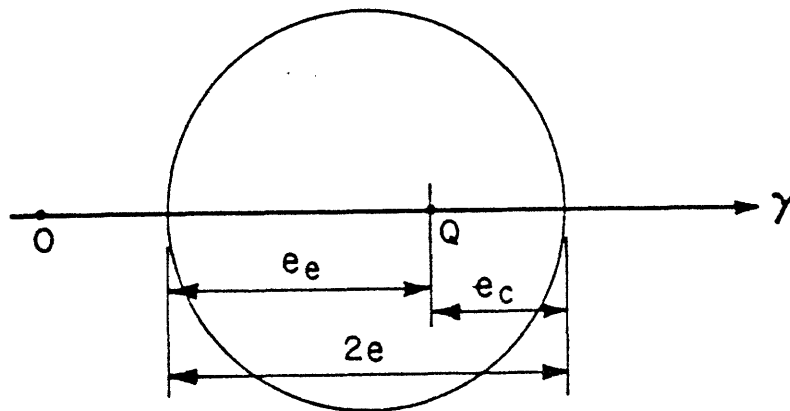


Figure 3.3.19 Analog of an asymmetric P-body.

The evolution of the annuli with the movement of the characteristic point would not be changed at all and it can be seen that stabilization to a closed loop would occur in one-and-one-half cycles under a regular cyclic straining. The original condition (virgin condition) of the system would be different since it would exhibit an asymmetry : the centers of the annuli

would no longer be positioned at the origin, they would be replaced there by the points Q. The first deformation curve in compression would be different from that in extension. Obviously this situation corresponds to the case of asymmetric St Venant bodies. During one of the branches of a closed loop cycle, the amount of plastic strain for each P-body will be the same as that of a symmetric P-body such that  $e = (e_e + e_c)/2$  and this plastic deformation will start at exactly the same position of the characteristic point. The closed loops of the two systems - the asymmetric infinite P-body and the symmetric infinite P-body defined by the previous relation - have therefore the same shape ! All the properties introduced earlier are applicable to an asymmetric infinite P-body, except for the use of the first deformation curve to describe the closed loop. Even though the infinite P-body is asymmetric, the closed loop will be symmetric with respect to its center.

In the case of asymmetric P-bodies it is thus obvious that the second Masing rule does not apply but there is always a function S such that the branches of the closed loop between A and B are given by the relationships previously described. It is also interesting to note that the first Masing rule will not apply when the first deformation curve does not have a continuous slope at the origin (which is now possible).

Let us now consider a specific type of asymmetric infinite P-body which will be used in the pile analysis. Initially one defines a symmetric first-deformation curve which corresponds to a reference symmetric infinite P-body. The associated function is  $\tau = S(\gamma)$ .

The first deformation curve of the asymmetric P-body is then given by

$$\tau = \lambda S \left( \frac{\gamma}{\lambda} \right) \quad \text{in compression, and by :}$$

$$\tau = \mu S \left( \frac{\gamma}{\mu} \right) \quad \text{in extension.$$

Figure 3.3.20 shows these two curves together with the geometric constructions which permit to derive them from the symmetric  $\tau = S(\gamma)$  curve.

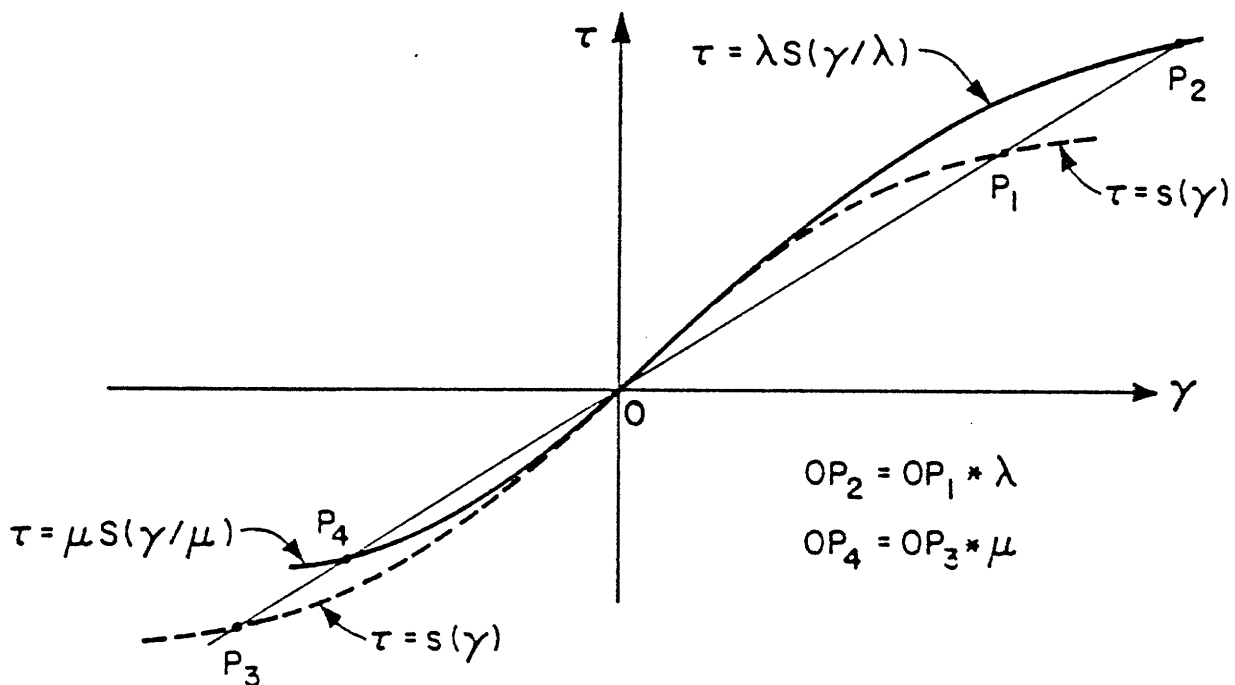


Figure 3.3.20 Construction of the asymmetric first deformation curves.

In the case of the symmetric infinite P-body we again define  $(g''(e)de)$  as the sum of the moduli corresponding to a strain threshold  $e$  between  $e$  and  $e + de$ . In the case of the asymmetric infinite P-body we use a new variable,  $e'$ , which is the sum of the strain thresholds in compression and in extension,  $e' = e_c + e_e$ . Then we define  $h''(e')de'$  as the sum of the moduli corresponding to  $e'$  between  $e'$  and  $e' + de'$ .

With our particular construction of the asymmetric infinite P-body we have :

$$h''(e')de' = g''(e)de$$

with

$$e' = (\lambda + \mu) e.$$

Thus on the unloading branch of a closed loop between A and B one will have a change of strain defined by:

$$\tau_A - \tau = (\gamma_A - \gamma) \int_{\gamma_A - \gamma}^{\infty} h''(e')de' + \int_0^{\gamma_A - \gamma} e' h''(e')de'$$

or,

$$\tau_A - \tau = (\gamma_A - \gamma) \int_{\frac{\gamma_A - \gamma}{\lambda + \mu}}^{\infty} g''(e)de + \int_0^{(\gamma_A - \gamma)/(\lambda + \mu)} (\lambda + \mu) e g''(e)de$$

and upon integrating,

$$\tau_A - \tau = (\gamma_A - \gamma) g'(\infty) + (\lambda + \mu) g \left( \frac{\gamma_A - \gamma}{\lambda + \mu} \right)$$

Hence :

$$\left( \frac{\tau_A - \tau}{\lambda + \mu} \right) = S \left( \frac{\gamma_A - \gamma}{\lambda + \mu} \right)$$

Similarly one can show that during reloading from B,

$$\frac{\tau - \tau_B}{\lambda + \mu} = S \left( \frac{\gamma - \gamma_E}{\lambda + \mu} \right)$$

In particular, if  $\lambda + \mu = 2$  these expressions become equal to those characterizing the closed loop of the symmetric infinite P-body.

It should however be observed that an assemblage of asymmetric P-bodies, each of the type described earlier (i.e. obtained from a symmetric first-loading curve by scaling) does not usually have this property. That is, the overall force-deformation relation for a cycle cannot be obtained by scaling the overall force-deformation curve for first loading. Rather, this assemblage constitutes a standard asymmetric Iwan model.

We now conclude our theoretical presentation of Iwan models with a final remark. The Pile Model that we have considered has only one source of external variable loading, the force P applied at its top. All we have shown is that the structure that exists between the top and the reference base could be treated as an Iwan model. Now if other external variable forces were applied at different points on this structure the previous conclusions would not apply globally to the Pile Model. Such is the case for example with piles under dynamic loading.

### 3.3.4 Shakedown analysis

In the course of this research shakedown analysis was the first body of theory that was considered in order to study the behavior of Iwan models under cyclic loading. At the time the properties of Iwan models were not known to the author and it seemed logical to turn to a branch of engineering specifically concerned with the behavior of elasto-plastic structures under irregular loading. Since it now appears that shakedown analysis is becoming a source of real interest in the profession [43], it was decided to present here a short discussion of what was learned concerning the potential and the limitations of these little-known techniques. Some complementary information is given in Appendix 3.

Let us consider an elasto-plastic element subjected to a regular cyclic loading expressed in terms of stress. There are essentially four types of possible responses as shown in Figure 3.3.21 in order of complexity :

a) a purely elastic response, b) a stabilization to a linear elastic response, called elastic shakedown, c) a stabilization to a closed loop response called alternate plasticity and d) an accumulation of plastic strain at each cycle without stabilization, called ratchetting. The previous terminology is perfectly valid on the global level of structure composed of elasto-plastic elements\*. Global elastic shakedown can be locally associated with either purely elastic response or elastic shakedown, and in general global responses may include all forms of simpler local responses.

Shakedown analysis aims at determining the range of loading ultimately leading to elastic shakedown. However, shakedown analysis will never permit one to establish when (in how many cycles) this limiting stage can be reached.

---

\* See Appendix 3.B for detailed terminology.

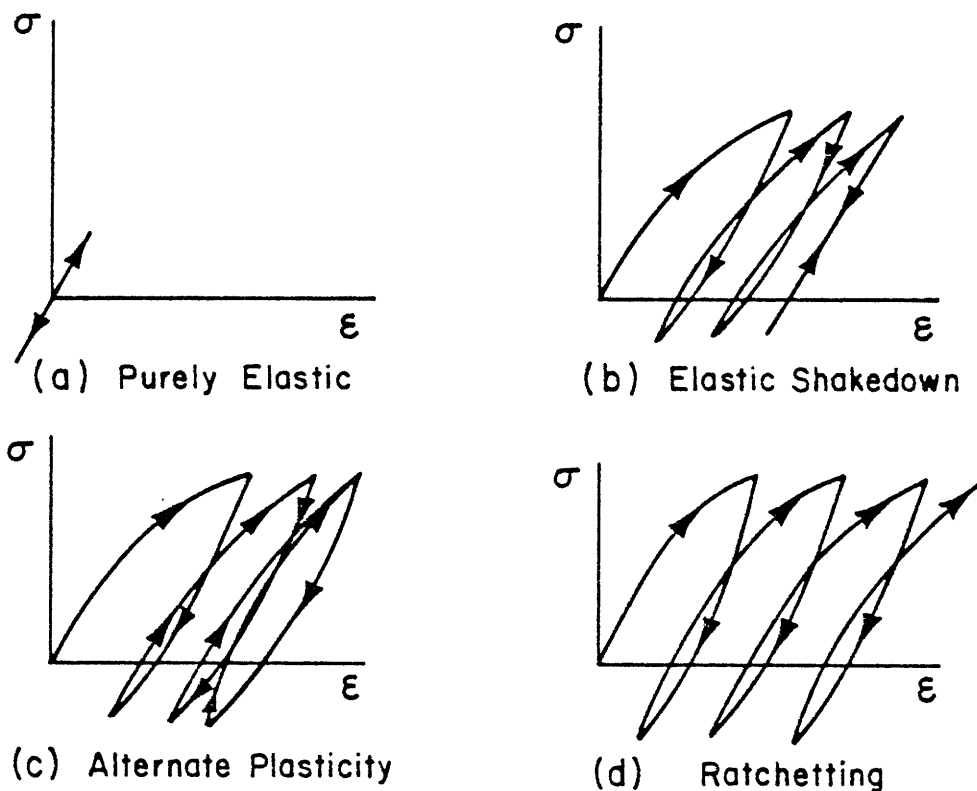


Figure 3.3.21 Cyclic responses of an elasto plastic element.

#### 3.3.4.A. Melan's theorem

Let us consider a structure  $S$ , and the set of external forces to which it is subjected,  $X(t)$ . Let  $\sigma^E(t)$  be the artificial stress distribution resulting from the application of  $X(t)$  if  $S$  were perfectly elastic. A stress distribution  $\rho$  will be termed statically admissible if it satisfies

the equations of equilibrium everywhere in  $S$  and at its boundary. By definition a residual stress distribution,  $\rho$ , is statically admissible with no external forces applied. Let us finally define  $\phi(\sigma) = 0$  as the equation of the yield surface at each point.

The fundamental theorem of shakedown analysis, Melan's static theorem, states that [65] :

The structure will shakedown if, and only if, any time-independent distribution of residual stress,  $\bar{\rho}$ , can be found such that :

$$\phi \{ \sigma^E(t) + \bar{\rho} \} < 0 \text{ everywhere.} \quad \text{Eq. 3.8}$$

"In essence, this states that if the structure can shakedown, then it will shakedown", as Hodge [42] most beautifully put it.

It is easy to show that any stress distribution  $\sigma(t)$ , which is statically admissible with  $\chi(t)$ , can be disassembled into the sum of the artificial elastic stress distribution  $\sigma^E(t)$  and a residual stress distribution  $\rho(t)$

$$\sigma(t) = \sigma^E(t) + \rho(t) \quad .$$

Thus if the structure shakes down there will be a time independent residual stress distribution  $\rho_0$  such that in the elastic shakedown state

$$\sigma(t) = \sigma^E(t) + \rho_0 \quad .$$

It is very important to see that  $\rho_0$  is dependent on the loading history, and that the time independent residual stress distribution of Melan's theorem does not have to be equal to  $\rho_0$ .

Let us consider a graphical representation of the theorem. For convenience the stress space is represented by the axes  $x_i, x_j$ , and in this



space of the residual stress distribution is represented by the curve C.

The yield condition  $\phi(\sigma) = 0$  can also be written as :

$$\phi \left[ \rho(t) - \{-\sigma^E(t)\} \right] = 0,$$

so that the residual stress  $\rho(t)$  is constrained to remain inside the volume V "centered" on the point  $(-\sigma_i^E, -\sigma_j^E)$  as shown in Figure 3.3.22.

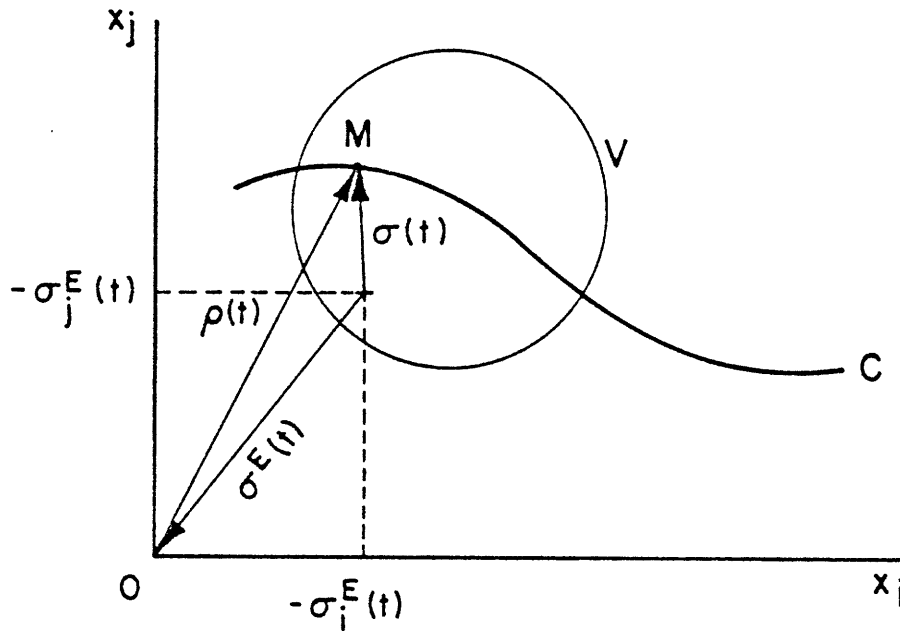


Figure 3.3.22 Graphical decomposition of the stress.

For an elasto-perfectly-plastic structure the equation of V relative to origin  $(-\sigma_i^E(t), -\sigma_j^E(t))$  is  $\phi(\sigma) = 0$ , and is therefore independent of  $\sigma^E(t)$ . As the loading changes, so does the position of  $\sigma^E(t)$  and the volume is translated accordingly, as seen in Figure 3.3.23.

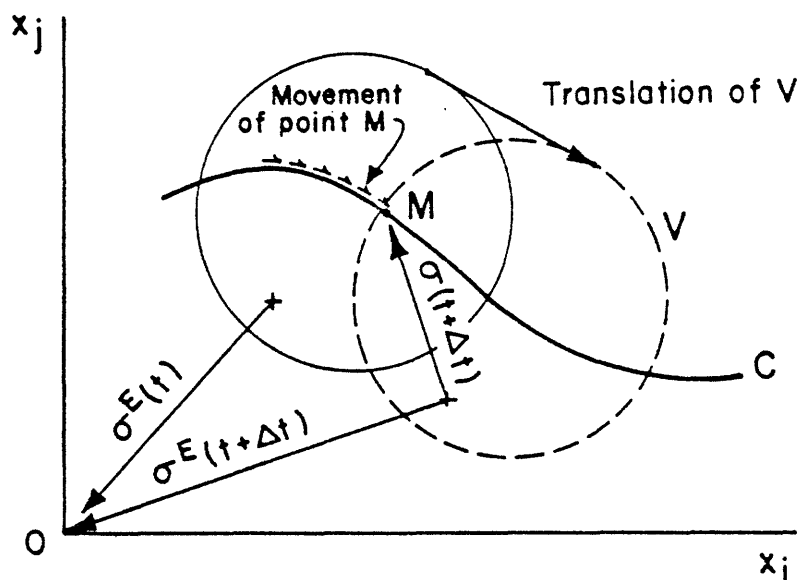


Figure 3.3.23 Changes of stresses.

The residual stress distribution will only change when the point  $M$  comes into contact with  $V$ , at which stage it will be carried away by the boundary of  $V$  along curve  $C$ . Upon reversal of the loading the point  $M$  will be immobilized until further yielding occurs. This representation shows a clear similarity to the physical analog of Iwan models presented earlier (with the exception that it is now the surface that moves the characteristic point).

Melan's theorem states that if there is one point belonging to  $C$  that remains inside  $V$  as the loading proceeds then shakedown will occur.

Hopefully, this graphical representation will have shown that the idea behind Melan's theorem is rather simple. However, the use of the theorem is not. Whereas it is easy to deal with  $\sigma^E$ , it is sometimes difficult to find a residual stress distribution satisfying Melan's theorem.

In some cases it is simpler to define the shakedown domain by studying the boundary between elastic shakedown and alternate plasticity, as will be shown in the following example.

### 3.3.4.B. A simple pile model

Consider an elastic pile embedded in an elasto-perfectly plastic soil. The pile model is defined in Figure 3.3.24 as an infinite Iwan model.

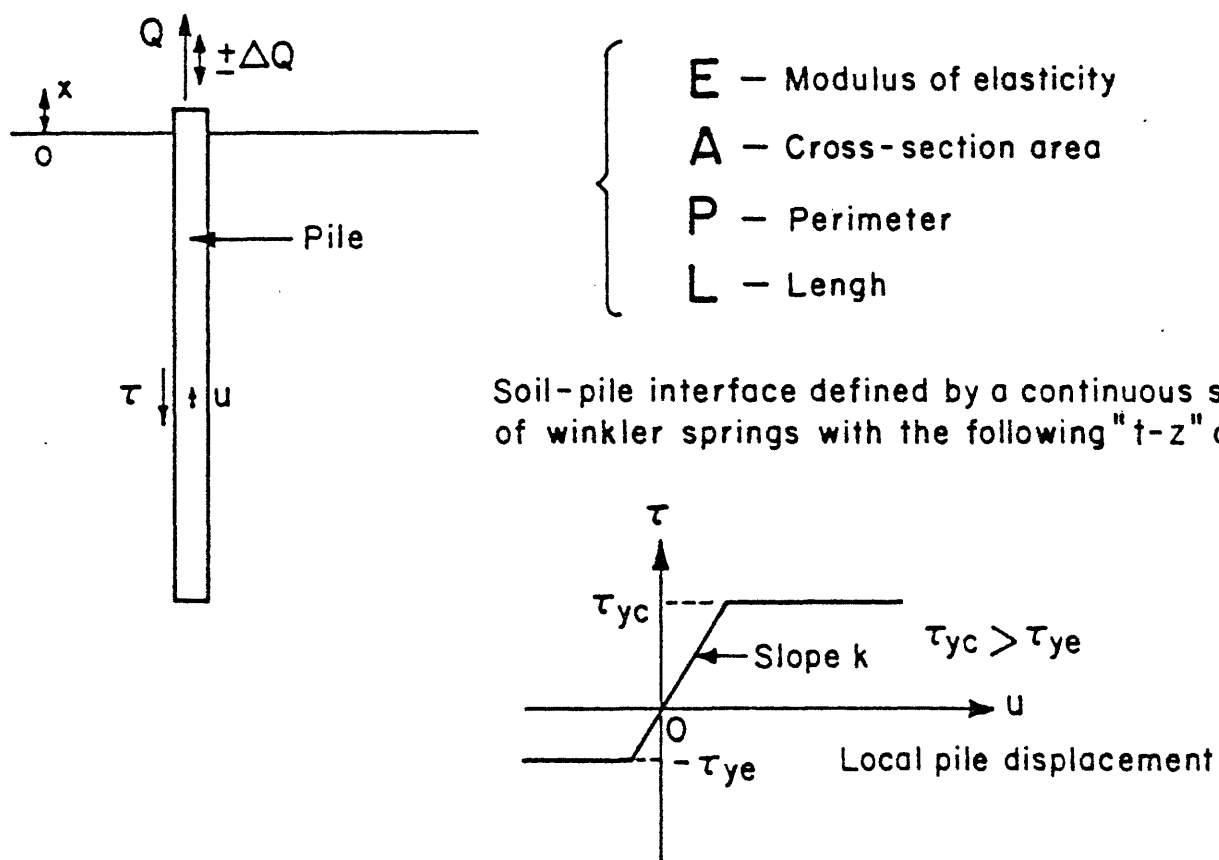


Figure 3.3.24 Simple pile model.

The value of  $k$  is assumed constant along the whole pile as well as the values of  $\tau_{yc}$  and  $\tau_{ye}$ .

The equation of equilibrium characterizing the elastic solution is :

$$E A \frac{\partial^2 u}{\partial x^2} - P k u = 0.$$

Which gives the elastic solution :

$$\tau^E(t, x) = \frac{Q(t)}{PL} \frac{\lambda L}{\text{th}\lambda L} (\text{ch } \lambda x + \text{th } \lambda L \text{ sh } \lambda x)$$

where  $\lambda^2 = Pk/EA$ .

The purely elastic range is defined by :

$$\frac{Q + \Delta Q}{PL} \frac{\lambda L}{\text{th}\lambda L} < \tau_{yc} \quad \text{and} \quad \frac{Q - \Delta Q}{PL} \frac{\lambda L}{\text{th}\lambda L} > -\tau_{ye}$$

where it is assumed that there were no initial residual stresses.

Melan's theorem can be used to establish the equation of the boundary between elastic shakedown and alternate plasticity. On the boundary there exists a residual stress distribution  $\bar{\rho}(x)$  such that :

$$\tau_{\max}^E(x, t) + \bar{\rho}(x) = \tau_{yc}$$

and

$$\tau_{\min}^E(x, t) + \bar{\rho}(x) = -\tau_{ye}$$

Hence by difference :

$$\tau_{\max}^E(x, t) - \tau_{\min}^E(x, t) = \tau_{yc} + \tau_{ye}$$

which can be written as :

$$2 \frac{\Delta Q}{PL} \frac{\lambda L}{\text{th}\lambda L} (\text{ch } \lambda x + \text{th } \lambda L \text{ sh } \lambda x) = \tau_{yc} + \tau_{ye}$$

(where the portion in parenthesis is a maximum at  $x = 0$ ).

Therefore the boundary is defined by :

$$\frac{\Delta Q}{PL} \frac{\lambda L}{\text{th}\lambda L} = \frac{\tau_{yc} + \tau_{ye}}{2}$$

Since one knows that only pure elasticity, elastic shakedown and alternate plasticity can occur for this Iwan model a complete description of the pile

behavior under cyclic loading can be given as in Figure 3.3.25. :

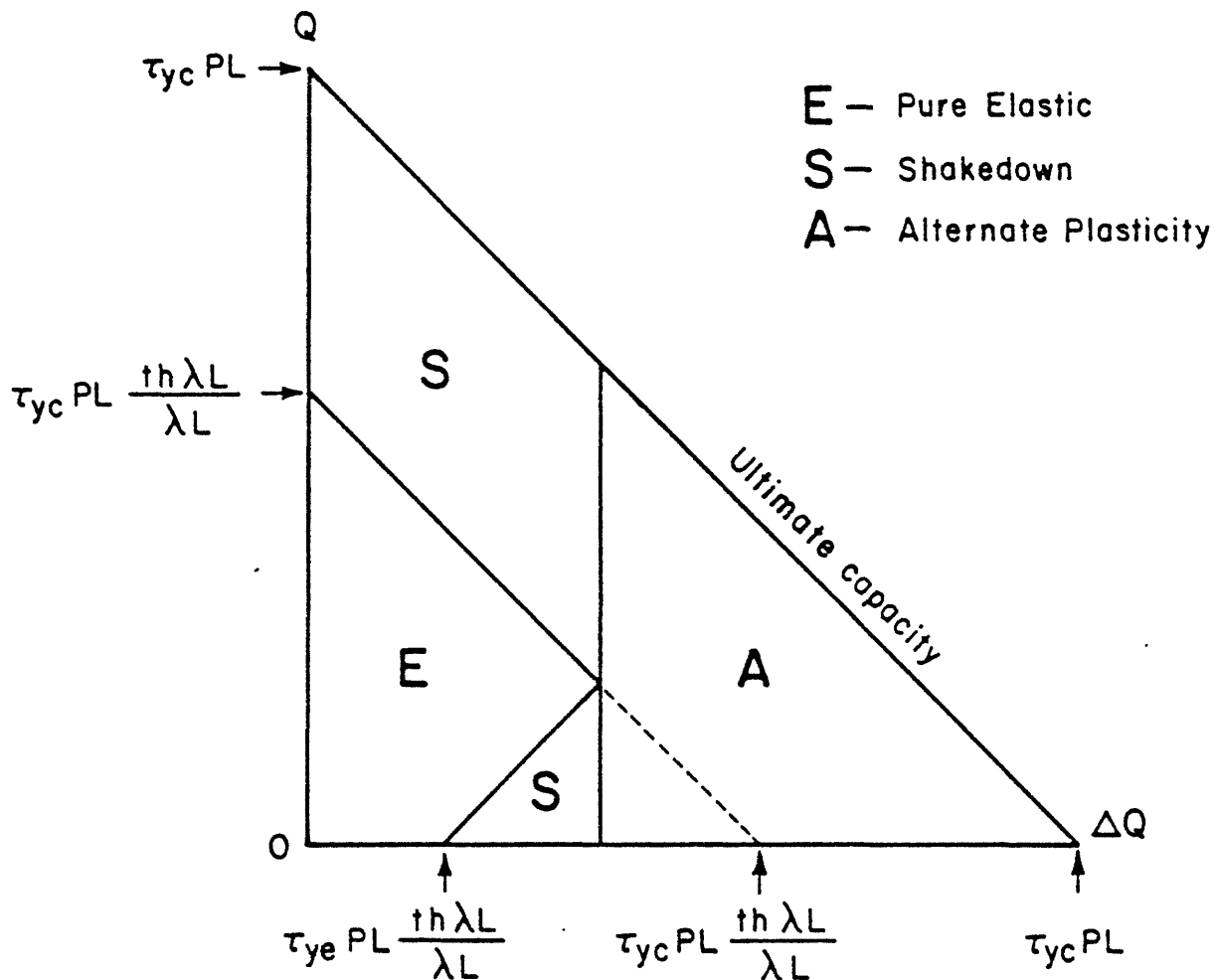


Figure 3.3.25 Recap of the results of the pile example.

Even though this is an over-simplified example, it shows the kind of results that can be obtained from shakedown analysis for the type of pile models of interest. The information it provides is far less complete than the one deduced from the study of Iwan models. Applications of shakedown analysis to the case of two independent external forces are given in Appendix 3.A.

### 3.4 BACK TO THE DESCRIPTION OF THE PILE MODEL

The composite action of the DSS zone and of the elastic zone on a pile nodal point is traditionally handled through the concept of "t-z" curves. These "t-z" curves are relationships between the absolute displacement,  $d_i$ , of the pile nodal point # i and the force,  $f_i$ , applied by the soil at this nodal point. Such curves have been evaluated from monotonic tests on piles [22] and have been semi-empirically adapted to the analysis of the axial behavior of piles in clay and sand in general [57]. An example of a set of "t-z" curves for clay is presented in Figure 3.4.1:

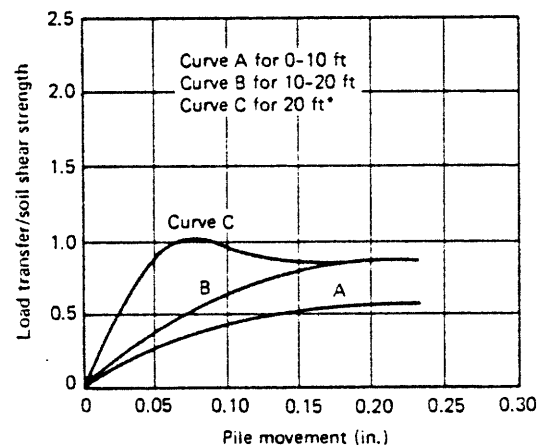


Figure 3.4.1 "t-z" curves.

(From Ref. [22]).

It is important to recognize that the "t-z" curves were originally established without consideration of the residual stresses existing before loading was applied. The use of the "t-z" curves therefore implicitly assumes that these residual stresses can be ignored during the loading. In other words the "t-z" curves are treated as first-loading curves. The "t-z" curves are in effect the first loading curves of the Iwan models composed of the DSS zone assemblages and the elastic zone springs.

The construction of "t-z" curves is an empirical procedure. The first step is to estimate the ultimate skin friction along the pile. Quoting from Kraft et al. [57], " $\tau_{\max}$  is computed in the same way as it would be for shaft friction in pile capacity computations, but some discretion should be used to select the distribution of  $\tau_{\max}$  along the pile". This very delicate stage can, unfortunately, not be avoided. In a second step an estimate of the original slope of the "t-z" curve is made on the basis of elastic theory [91]. Analysis of the shearing of concentric cylinders of soil yields the following relationship :

$$z = \frac{\tau_o r_o}{G} \ln \left( \frac{r_m}{r_o} \right),$$

where, z is the displacement,

$\tau_o$  the shear stress at the pile wall,

$r_o$  the pile radius,

G the soil shear modulus,

$r_m$  the distance from the pile axis to a boundary where displacements are considered to be zero.

It is usually assumed that  $r_m$  is of the order of 10 to 20  $r_o$ , so that  $\left( \frac{r_m}{r_o} \right)$  will vary between 2 and 3. The initial slope of the "t-z" curve for a

unit length of pile is therefore taken as  $\frac{2 \pi G}{\lambda}$  where  $\lambda$  varies between 2 and 3. The shape of the "t-z" curve between the origin and the ultimate value of t is still not well defined. Many researchers [70] have found that the "t-z" curve exhibited an almost elasto-perfectly-plastic behavior. One very consistent observation made on experimental "t-z" curves is that mobilization of the ultimate skin friction occurs for pile displacements of the order of 1 % of the pile diameter [70]. In clay the range of  $z_{\max}/2 r_o$  seems to be between 0.5 % and 1 %. It is important to note that this relationship was obtained over a very limited range of pile diameters and it is only assumed to hold for different pile diameters [70] such as those encountered offshore.

The estimation of "t-z" curves by a rational analysis is one of the objectives of present research on the behavior of piles. This work requires the study of the stress and strain conditions existing during installation, consolidation and loading [7]. Kavvadas [53] recently studied the case of a pile in normally consolidated Boston Blue Clay (BBC) on the basis of both the strain path method [7] - used to model the installation - and of a new soil model [53]. Figure 3.4.2 presents some stress-strain relationships corresponding to direct simple shear undrained conditions computed\* at different distances from the pile wall. Several observations can be drawn from this figure. First the ultimate skin friction predicted by this model corresponds to approximately 50 % of the  $CK_{\circ} UDSS$  shear strength on NC Boston Blue clay (for which  $\tau_{\text{strength}}/\bar{\sigma}_{vo} \approx 0.22$ ), i.e. the  $\alpha$ -factor is equal to 0.5

---

\* These results are theoretical.



Direct simple shear.  
(Loading of pile).

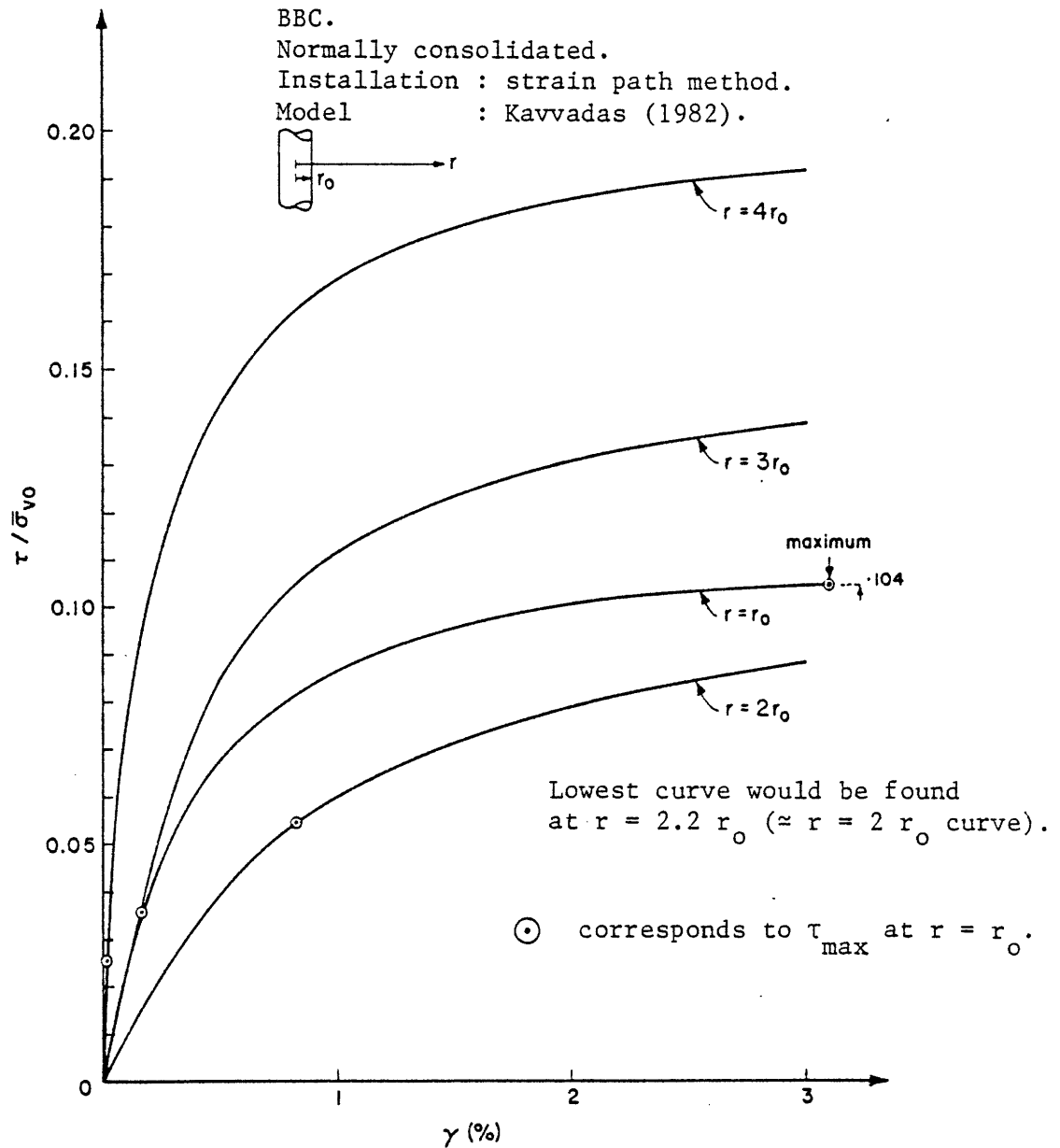


Figure 3.4.2 Stress strain relationships for DSS specimen at several distances away from the pile corresponding to pile loading conditions.

(Private communication from Kavvadas).

(if the DSS strength is taken as the value of  $C_u$  in  $\alpha = C_a/C_u$ ,  $C_a$  being the adhesion or the ultimate skin friction). Secondly, there is a marked variation of the stress-strain diagrams with distance from the pile wall.

One way of interpreting these predictions is to consider the stress distribution existing when the ultimate skin friction is reached. A good estimation of the shear stress distribution away from the pile is given by  $\tau r = \tau_0 r_0$ , where  $r_0$  is the pile radius,  $\tau_0$  the shear stress at the pile wall and  $\tau$  the shear stress at a distance  $r$  from the pile axis. The relationship allows us to locate the points corresponding to  $\tau_0 = \tau_{\text{strength}}$  along each curve of Figure 3.4.2. The plotting of these points indicates clearly that the soil remains essentially linear elastic as close as one radius away from the pile wall ( $r = 2 r_0$ ). In other words these results justify the distinction we have made in the Pile Model between the DSS zone and the elastic zone.

This observation leads to the proposal of a simple construction for the "t-z" curve. The DSS zone is associated with a DSS stress-strain relationship normalized to the ultimate skin friction - let us call it  $\tau = f(\gamma)$  - while the elastic zone has a shear modulus  $G^*$ . The stiffness of the elastic zone is taken as  $2 \pi G/\lambda$ . Let us now consider Figure 3.4.3.

The displacement of the DSS zone is equal to the DSS strain,  $\gamma$ , multiplied by the DSS zone width. This width is adjusted so that the ultimate skin friction is obtained for a total displacement  $z$  roughly equal to 1 % of the pile diameter. The displacement of the DSS zone is then given by :  $z_{\text{dss}} = \gamma * \text{width}_{\text{DSS}} = f^{-1}(\tau) * \text{width}_{\text{DSS}}$  or :  $z_{\text{dss}} = f^{-1} \left( \frac{t}{A} \right) * \text{width}_{\text{DSS}}$  with  $A$  equal to the pile surface

---

\* This  $G$  is the equivalent shear modulus of the whole (linear) elastic zone. While the ratio  $G_1/\bar{\sigma}_{vo}$  for  $\gamma = 10^{-3}$  is roughly 100 for NC BBC the (equivalent  $G/\bar{\sigma}_{vo}$ ) was calculated to be 16 when the curves of Figure 3.4.2 are integrated between  $r = r_0$  and  $4 r_0$ .

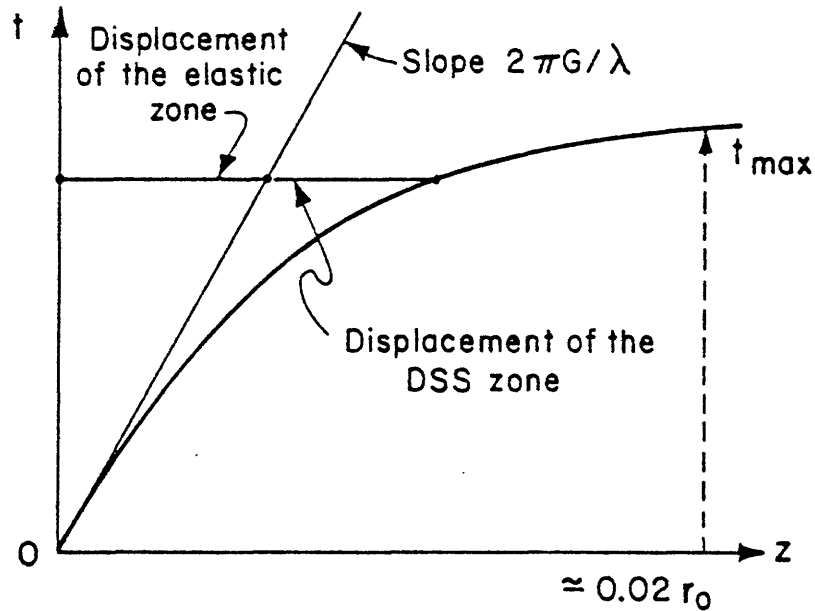


Figure 3.4.3 Construction of "t-z" curve.

area on which  $\tau$  is applied. The equation on the "t-z" curve is then given as a function of t as :

$$z = t * \frac{\lambda}{2 \pi G} + f^{-1} \left( \frac{t}{A} \right) * \text{width}_{\text{DSS}}$$

An almost elasto-perfectly-plastic "t-z" curve of the type previously observed in practice corresponds to a very narrow DSS zone width. The Pile Model is perfectly compatible with this construction. Now the last question we need to answer is : given a stress-strain relationship for the DSS zone how can we construct the Generalized P-body which will represent this zone ?

The answer is quite simple. First integrate the stress-strain curve in the DSS zone by considering the area A on which  $\tau$  is applied and the width of the DSS zone. This yields a force-displacement relationship for each DSS

zone, which is then approximated by a multi-linear curve. The last step is to decompose this multi-linear relationship into elementary elasto-perfectly-plastic springs (or Prandtl bodies, but expressed in terms of forces and displacements). The algorithm used is as follows. At point I of Figure 3.4.4 the change of stiffness is equal to the stiffness of the P-body that just yielded, therefore :

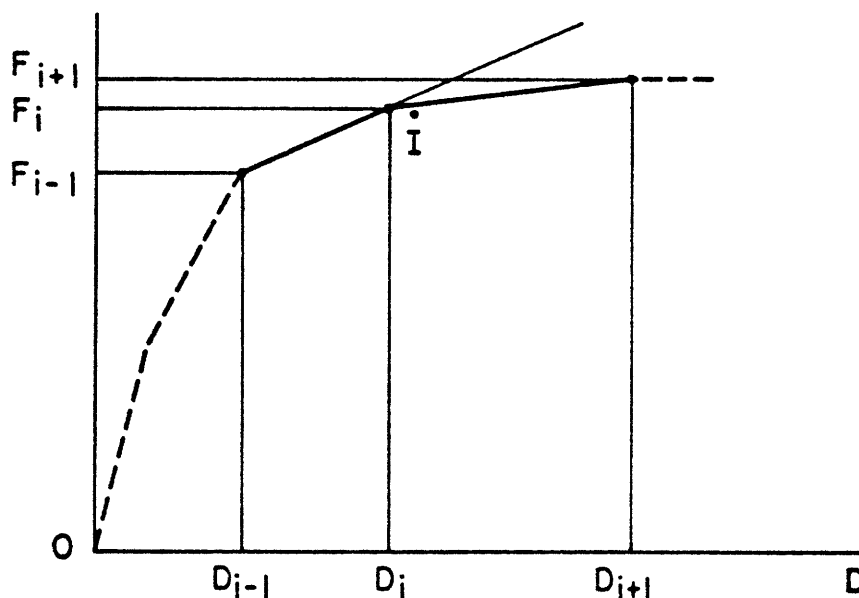


Figure 3.4.4 Algorithm used in the decomposition in Prandtl bodies.

$$K_i = \frac{F_i - F_{i-1}}{D_i - D_{i-1}} - \frac{F_{i+1} - F_i}{D_{i+1} - D_i} .$$

The strength of this P-body is simply equal to  $K_i D_i$ . There are as many P-bodies as there are points where the slope changes.

We have now gathered enough information concerning the Pile Model to envision the next critical element of our procedure : the Soil Degradation data. As a mean of concluding this chapter and introducing the next one, Figure 3.4.5 recaps some of the key information we have obtained by up-dating Figure 3.1.1 and by answering the questions we asked at the beginning of the chapter.

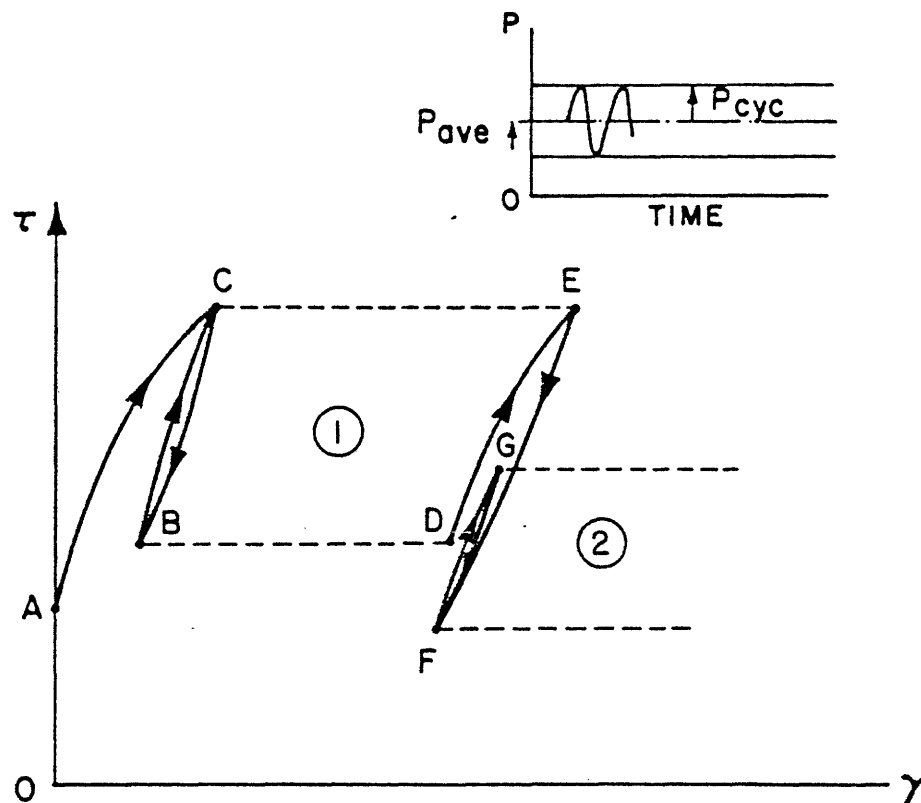


Figure 3.4.5 Update of Figure 3.1.1.

Are we going to reach cyclic stabilization ? and, if so, when is it going to occur ?, and after how much strain ?

Cyclic stabilization to a closed loop, which is convex and symmetrical with respect to its center, occurs after one-and-half cycles of loading. Furthermore, when the pile model is symmetric in tension and in compression the equation of the first-deformation curve is directly applicable to the unloading and reloading branches of the closed loop with a scaling factor of two. The strains accumulated until stabilization are therefore always finite.

Can the pile constitute a mechanism, that is can a tension pile (as represented by the Pile Model) be pulled out by application at its top of a cyclic loading which never reaches the pile's ultimate capacity ?

No, such behavior cannot be represented by the present model. Cyclic degradation will have to be introduced in order to permit this type of evolution to be predicted. Such is the purpose of the next chapter 4, which will detail the soil behavior during periods such as zones (1) and (2) of Figure 3.4.5. Chapter 5 will then explain how the soil-pile parameters are modified to account for the physical changes occurring during one of these periods of cycling, so that the Pile Model can be used again - as shown by curve DEFG - to prepare for a new package of loading.

---

#### 4. CONTRIBUTION OF AVERAGE SHEAR STRESSES TO THE CYCLIC DEGRADATION OF CLAY

##### 4.1 BACKGROUND

As observed in the introductory chapter, an important characteristic of the stress tensor applied to the clay surrounding the piles of a TLP during a storm is the existence of a sustained (or average) shear stresses,  $\tau_{ave}$ , on the very plane where the cyclic shear stresses,  $\tau_c$  are applied. Moreover it was also suggested that the "consolidation" shear stress,  $\tau_{cons}$ , applied during the calm sea state preceding the storm may play an important role as well on the cyclic behavior of this clay.

During the passage of the storm the distributions of  $\tau_{ave}$  and  $\tau_c$  along the pile will change as a result of degradation. However from a practical point of view the composite action of the three shear stresses ( $\tau_{cons}$ ,  $\tau_{ave}$ ,  $\tau_c$ ) - two of them being time dependent - on the cyclic behavior of the clay is yet intractable. Thus some restrictions must be imposed to reduce the number of parameters while hopefully maintaining the essential characteristics of the problem, and our choice in this study is to limit ourselves to the case where  $\tau_{ave} = \tau_{cons}$  throughout the loading.

This situation corresponds to that of an infinitely rigid pile embedded in an uniform profile of normally consolidated clay with normalized behavior (Figure 4.1.1). Since the same shear strain is common to the whole pile, the local shear stresses are proportional to the vertical effective stress  $\sigma'_{vo}$  at all time, and they are also proportional to the force applied to the top of the pile. The average force being constant, it directly results that

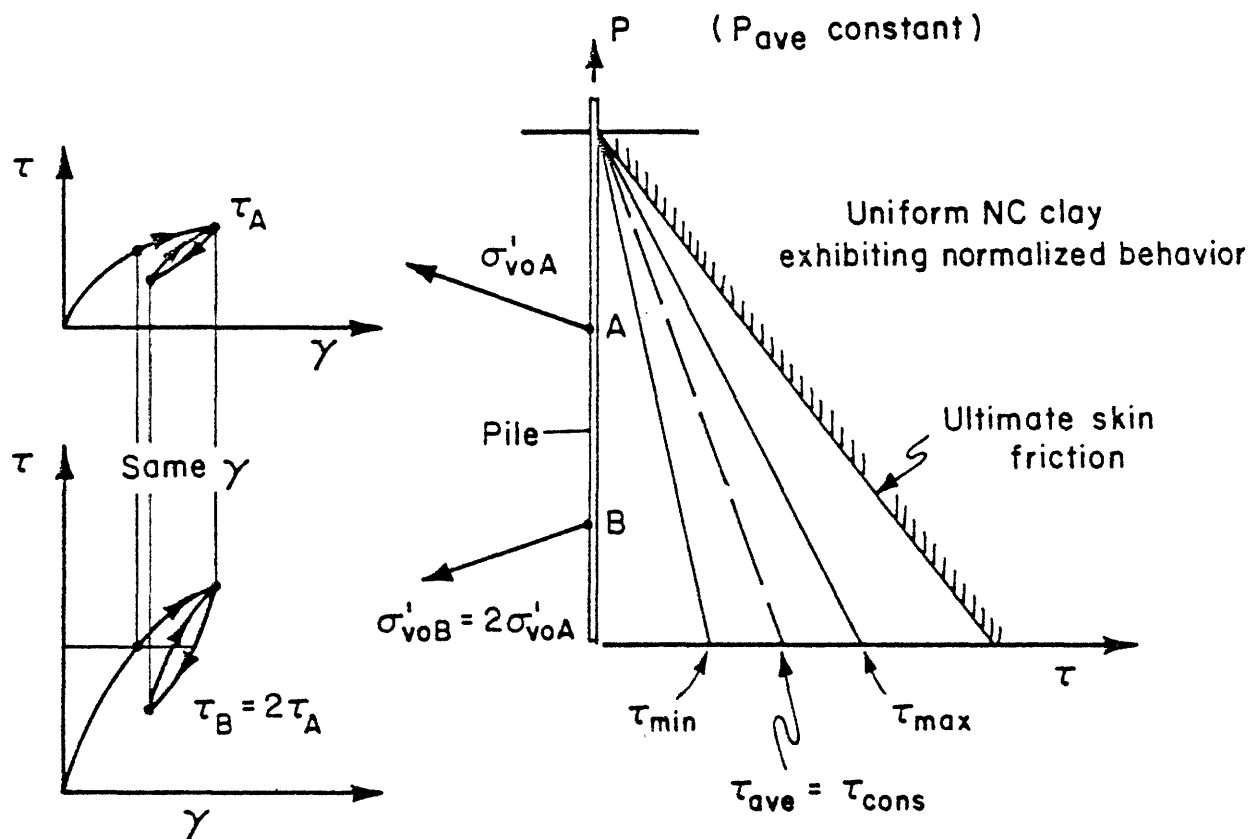


Figure 4.1.1 Rigid pile in uniform NC clay exhibiting normalized behavior  $\tau_{ave} = \tau_{cons}$ .



$\tau_{ave} = \tau_{cons}$  everywhere along the pile. Hence the proposed approach corresponds very well to the case of the stiff piles used in the cyclic tension tests reviewed in Chapter 2. This "rigid pile approach" is viewed as a reasonable starting point but it is clearly understood that future consideration of very flexible piles will require a refinement of this limited data base. It should however be noted that the model which will be presented later does allow for a variation of  $\tau_{ave}$ , and  $\tau_c$ , during the loading, but it will be assumed that for any value of  $\tau_{ave}$  one can use in some way degradation data obtained from a cyclic test run with  $\tau_{cons}$  equal to this very  $\tau_{ave}$ .

Several researchers [94, 39, 41] have already been working on the effect of  $\tau_{ave}$  and  $\tau_{cons}$  on the cyclic behavior of clay but nobody has yet presented a clear description of it or of the  $\tau_{ave} = \tau_{cons}$  case, most of the results being related to only one value of  $\tau_{cons}$  per clay. All of the tests were conducted with cyclic triaxial apparatuses.

In order to clarify the research background let us quickly review some of the key results available today. In a remarkable paper published in 1966, Seed and Chan [94] presented the first extensive report on this subject and actually set much of the presentation framework that will be adopted for the display of our results. Their study was based on a series of CIU triaxial tests run on three NC clays\* by maintaining constant  $\tau_{ave}$  and  $\tau_c$  during each test (which was therefore characterized by a couple  $(\tau_{ave}, \tau_c)$  and  $\tau_{cons} = 0$ ). The results are presented in a set of  $(\tau_{ave}, \tau_c)$  coordinates

---

\* Vicksburg silty clay, Pittsburg sandy clay and San Francisco Bay Mud.

both normalized by the static strength, so that each test is associated with one point, which in turn can be assigned a test variable such as, for example, the number of cycles required to reach failure\*. Lines can then be fitted to represent the conditions of failure in any given number of cycles, as shown in Figure 4.1.2.a and b for  $N = 1, 10$  and  $100$ . When  $\tau_c = 0$ , failure occurs for  $\tau_{ave}$  equal to the static strength, and for a given value of  $\tau_{ave}$  fewer cycles of loading are needed to reach failure as  $\tau_c$  is increased. The ordinate axis corresponds to  $\tau_{ave} = 0$  and hence to a symmetrical application of shear stresses around zero.

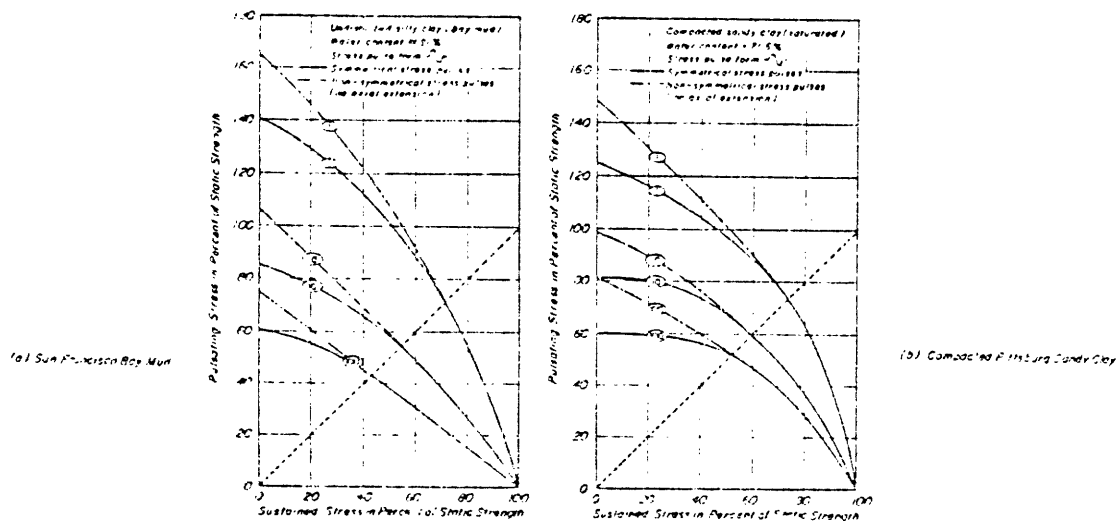


Figure 4.1.2 Combinations of  $\tau_{ave}$  and  $\tau_c$  causing failure.

(|94|).

\* Their definition of failure is not stated explicitly.

It is also interesting to note that all the points placed above the diagonal, i.e. with  $\tau_c > \tau_{ave}$ , correspond to "two way loading" and reversal of the shear stress sign, whereas the points below the diagonal are associated with "one way loading" in which the shear stresses are always of the same sign. The diagonal itself corresponds to  $\tau_{ave} = \tau_c$ , and thus to  $\tau_{min} = 0$ . The cyclic stresses can be larger than the static strength due to the high strain rates used during the cycling.

In place of reporting the number of cycles to failure one can more generally study the number of cycles required to reach any given strain. The resulting fitting lines are shown in Figure 4.1.3 in the case of 10 and 100 cycles, but since these particular results were obtained with an apparatus which could not apply extension to the triaxial specimen all the points positioned above the diagonal should really be reported on the diagonal as for any other test for which  $\tau_{min} = 0^*$ .

Several researchers, among which it is worth mentioning Houston and Herrmann [45], and Hicher [41], have since then presented results concerning the same subject. As schematically shown in Figure 4.1.4, Houston and Herrmann used mostly anisotropically consolidated specimens (with one K value imposed for each clay) whereas Hicher started with isotropically consolidated specimens.

Houston and Herrmann reported their results for four marine clays\*\* of various origins in the same form as Seed and Chan using a  $(\tau_{ave}, \tau_c)$

---

\* Similar results were obtained by Ellis and Hartman [28].

\*\* Atlantic and Pacific hemi-pelagics, Pacific pelagic clay and San Francisco Bay Mud.

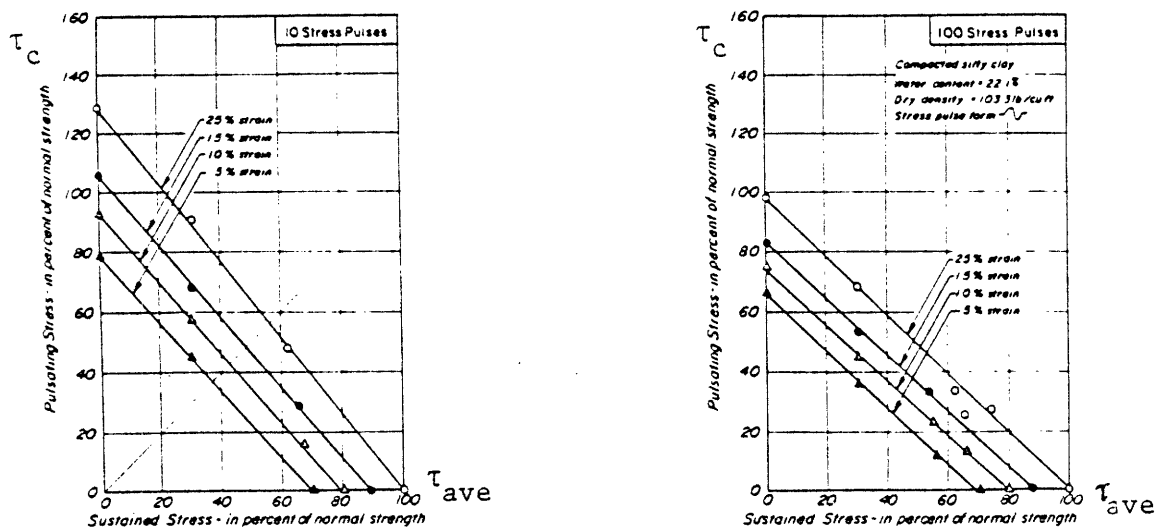


Figure 4.1.3 Combinations of  $\tau_{ave}$  and  $\tau_c$  causing different strains - Vicksburg silty clay. (94).

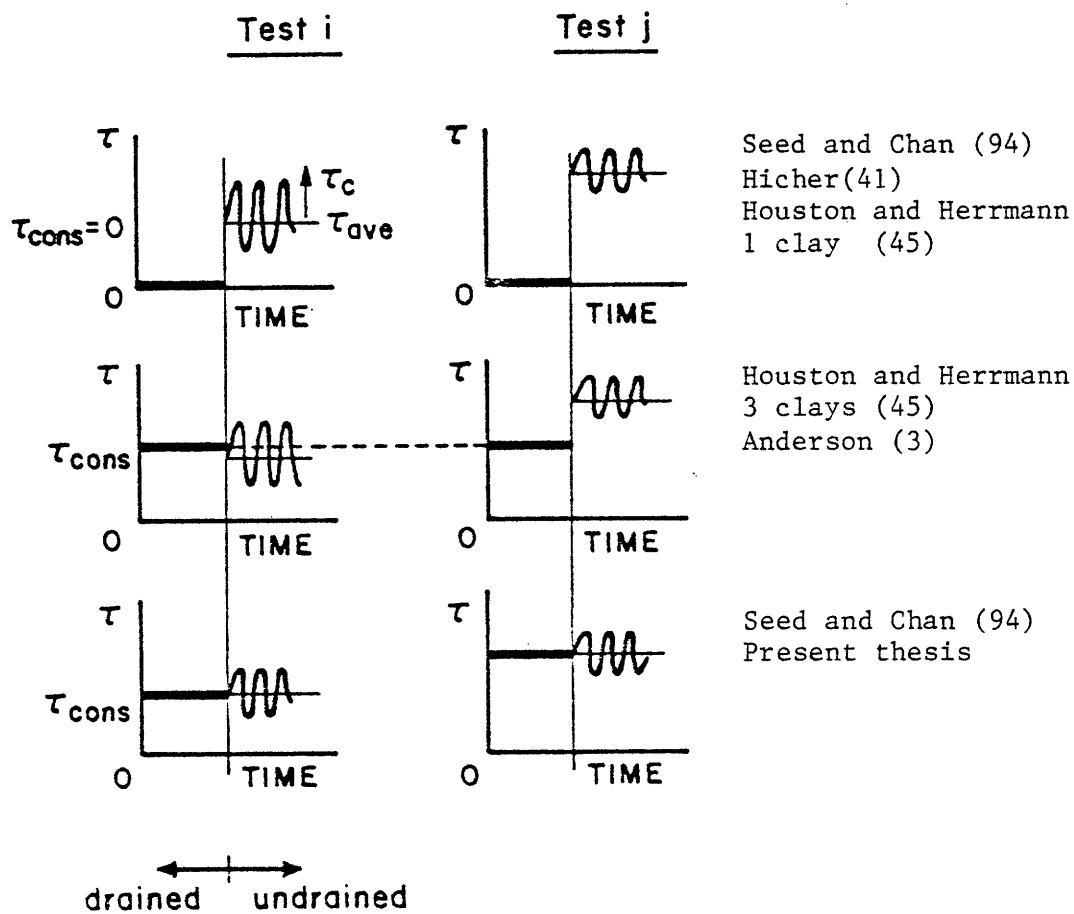


Figure 4.1.4 Loading patterns.

coordinate system and plotting failure\* lines corresponding to three different number of cycles (30, 300 and 30 000), as shown in Figure 4.1.5. For the three clays that were anisotropically consolidated and for each of their failure curves there appears to be an optimum value of  $\tau_{ave}$ , different from zero, at which there is a maximum resistance to cyclic degradation. For the values of K used (0.45 and 0.55) it seems that these maxima occurred for a value of  $\tau_{ave}$  approximately 20 to 25 % lower than  $\tau_{cons}$ , with a tendency for the higher-number-of-cycle-curves to have a higher value of optimum  $\tau_{ave}$ . A possible interpretation of this phenomenon is suggested in Figure 4.1.6 where the maximum-resistance- $\tau_{ave}$  corresponds to an approach of the effective stress strength envelopes simultaneously in extension and in compression, whereas rupture of an anisotropically consolidated specimen sheared around  $\tau_{ave} = \tau_{cons}$  is likely to occur in compression, and for  $\tau_{ave} = 0$ , in extension.

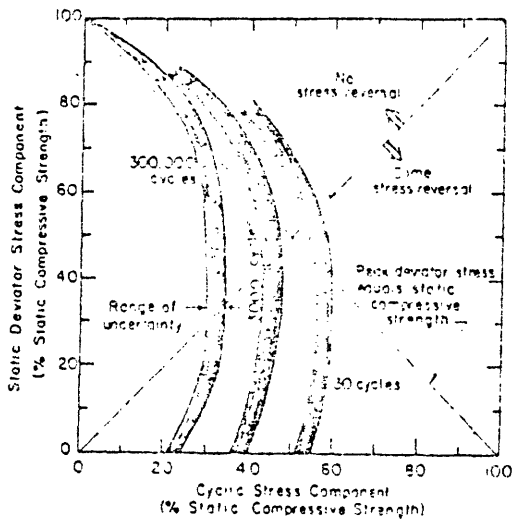
In the case of the San Francisco Bay Mud the failure curves obtained by Houston and Herrmann (Figure 4.1.5.d) are quite similar to those of Seed and Chan (Figure 4.1.2.a) which however show a much quicker degradation\*\*.

It is worth noting that a non-zero  $\tau_{ave}$  value corresponding to a maximum resistance to cyclic degradation may also exist for some isotropically consolidated NC clays. Some evidence of this fact was furnished by Seed and Chan with Vicksburg silty clay [94], and by Hicher [41] with argile noire for which a given value of  $\tau_c$  was found to be more destructive with  $\tau_{ave} = 0$

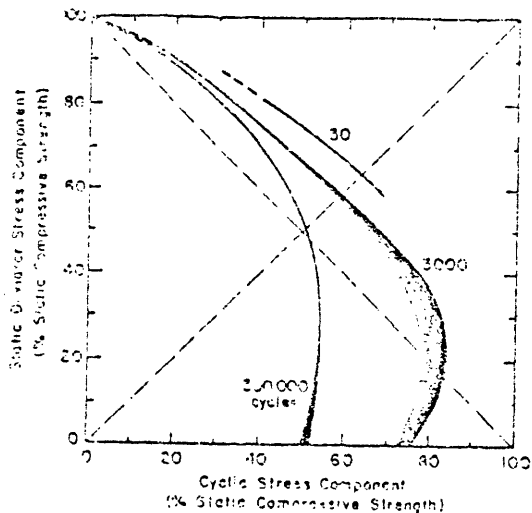
---

\* Defined as 10 % axial strain.

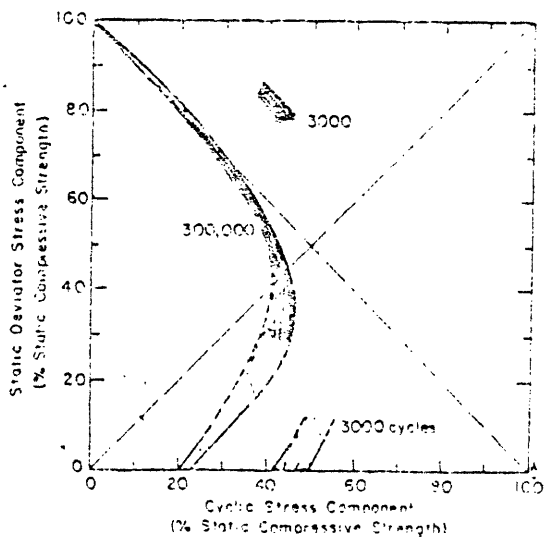
\*\* May be due to a variety of reasons : different definition of failure, different sampling, preparation and testing techniques, etc...



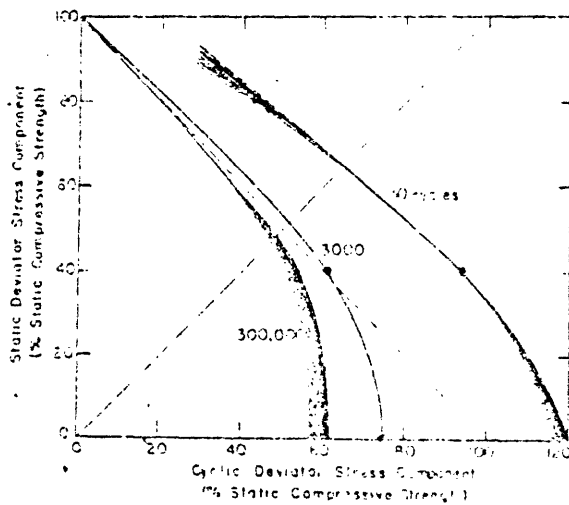
Pacific Hemi-Pelagic Clay.  $K = 0.45$ .



Pacific Pelagic Clay.  $K = 0.55$ .



Atlantic Hemi-Pelagic Clay.  $K = 0.45$ .



San Francisco Bay Mud.  $K = 1.0$ .

Figure 4.1.5 Cyclic strength contours.

(After Houston and Herrmann [45]).

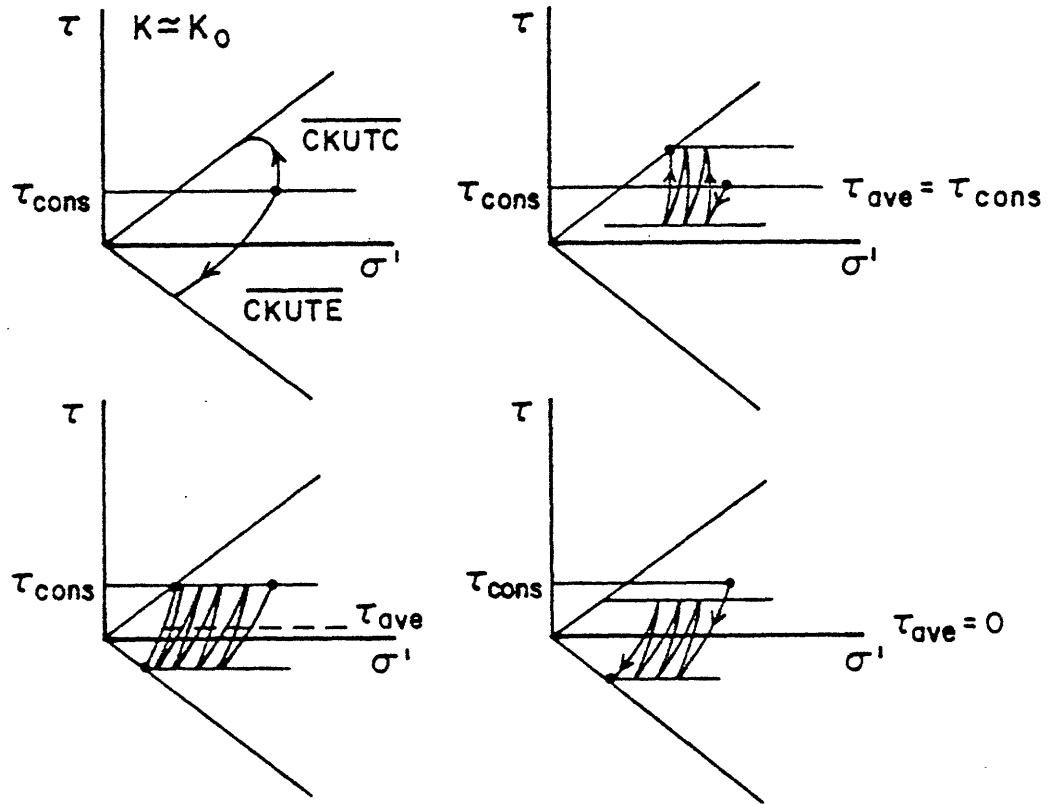


Figure 4.1.6 Optimum resistance value of  $\tau_{ave}$ .

than with  $\tau_{ave} = \tau_c$ , but there is however no clear confirmation of these results.

Hicher also emphasized the fact that, for a given value of  $\tau_{max}$ , the cyclic shearing gets more destructive as the value of  $\tau_c$  increases, which seems to be in agreement with all the available data.

Such is approximately the extent of our understanding of the contribution of  $\tau_{ave}$ ,  $\tau_{cons}$  and  $\tau_c$  to the cyclic behavior of clay. At the present time no information is available for the  $\tau_{ave} = \tau_{cons}$  case for one clay and for more than one value of  $\tau_{cons}$ . However the phenomena that have already been observed may prove useful in the future when deviations from the  $\tau_{ave} = \tau_{cons}$  situation will be studied.

Even though many different clays have been tested under various conditions, a comprehensive synthesis of the available experimental results has not yet been made. This situation can be partly explained by the sensitivity of the results to the nature of the clay and to the applied stress system, but it is also true that very few programs have been large enough, and systematic enough, to present a satisfactory overview of the cyclic behavior of one specific clay. The unchallenged example of such a comprehensive study is the 1975 program led by NGI concerning the repeated loading of Drammen clay under the supervision of Knut Andersen [2, 4]. Yet the 1975 program dealt with limited cyclic loading conditions and the aspect of soil behavior that we are concerned with was not examined even though the original testing program called for tests, later cancelled, of the type that we shall consider. The present program was tailored to fill this specific gap while capitalizing upon the experience previously accumulated by NGI.



In order to meet this objective, a series of simple stress-controlled DSS tests was performed during which  $K_0$ -consolidated specimens were incrementally loaded and allowed to consolidate and creep under a constant shear stress,  $\tau_{\text{cons}}$ . The same specimens were then cyclically sheared at constant volume with an average component of the shear stress,  $\tau_{\text{ave}}$ , equal to  $\tau_{\text{cons}}$ . The time history was modelled after the field conditions. The loading stages are schematically represented in Figure 4.1.7 where one also finds definitions of the notations\* to be used in this work.

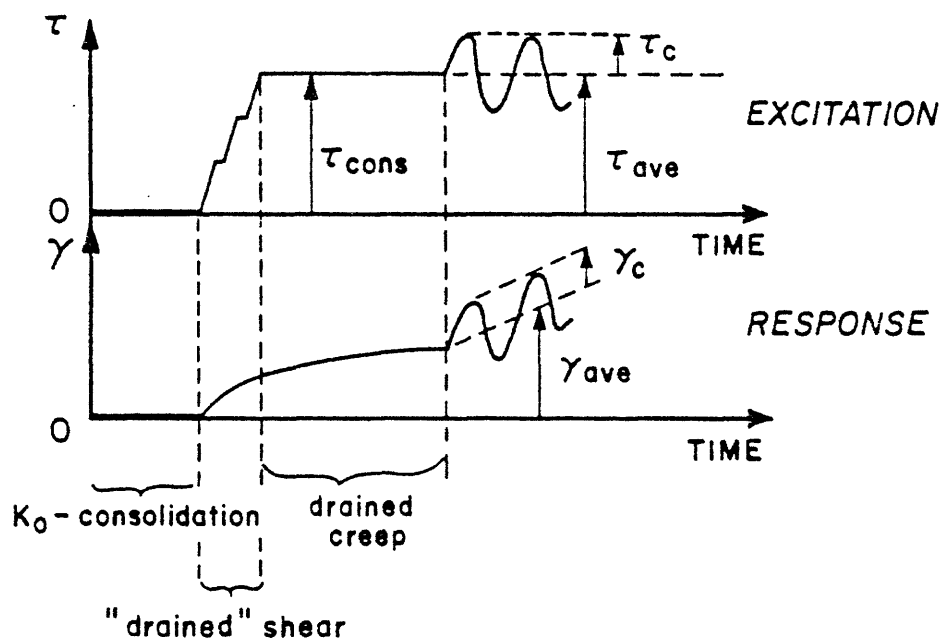


Figure 4.1.7 Shear loading and notations.

\* Note that the deformations are defined by the envelopes.

The average strain  $\gamma_{ave}$  is the total average strain resulting from the application of  $\tau_{cons}$  and from the cyclic degradation. The choice of each test loading characteristics was dictated by our desire to cover a wide range of different couples  $(\tau_{ave}, \tau_c)$ . In order to visualize this range, extensive use will be made throughout this thesis of the plane of Seed and Chan having normalized values of  $\tau_{ave}$  and  $\tau_c$  as axes. The normalizing factor is the DSS shear strength,  $\tau_{strength}$ , of a  $K_0$ -consolidated specimen of undisturbed Drammen clay, with  $\sigma'_{vc} = 4 \text{ kg/cm}^2$  ( $392.4 \text{ kN/m}^2$ ) which was common to all tests. Drammen clay has a normalized behavior with  $(\tau_{strength}/\sigma'_{vo})_{NC} = 0.215$ , so that  $\tau_{strength} = 4 * 98.1 * 0.215 = 84.3 \text{ kN/m}^2$ .

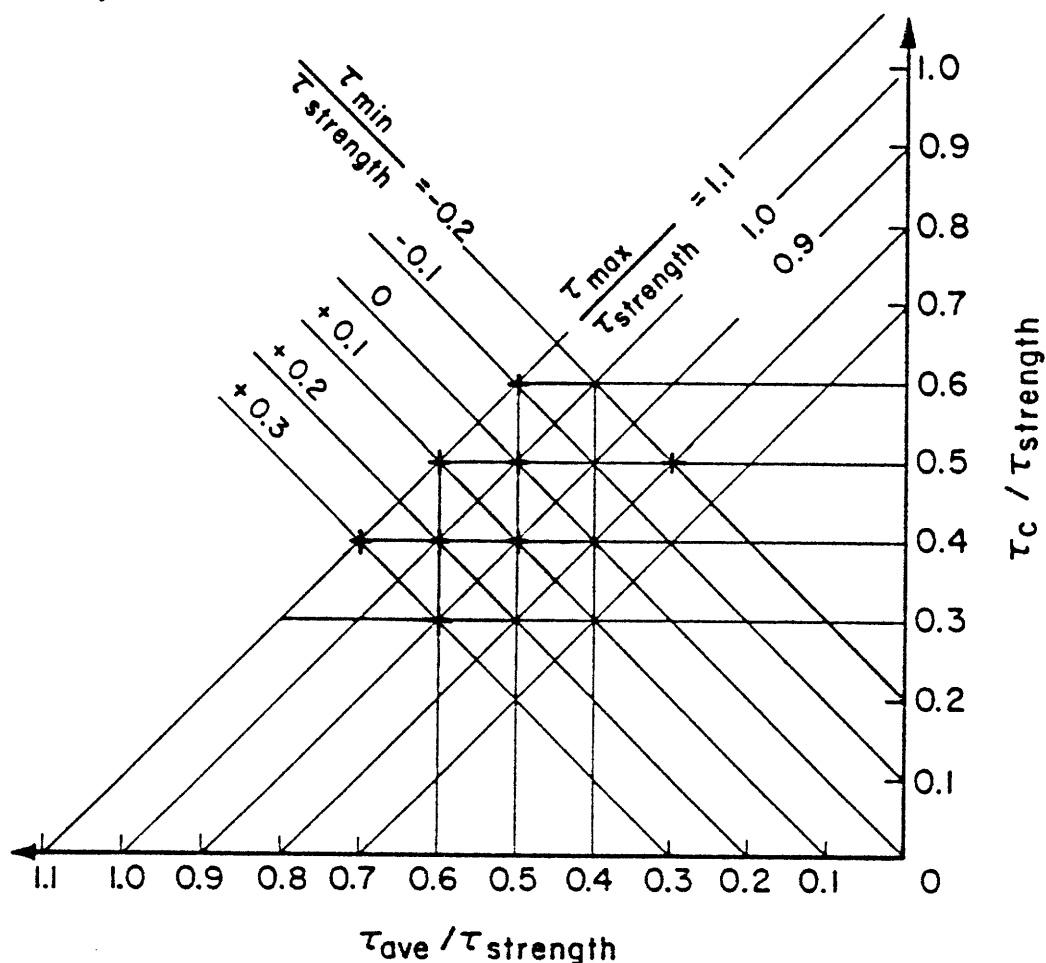


Figure 4.1.8 Test stress range.

Figure 4.1.8 shows the location of the test points in this plane. It is very important to note that the 1975 program covered the behavior of the clay along the vertical axis ( $\tau_c$ -axis). This axis corresponds to a symmetric loading where  $\tau$  varies from  $+\tau_c$  to  $-\tau_c$  which is the case of a classical cyclic DSS test. Values of  $\tau_{\max}$  and  $\tau_{\min}$  can be read directly from the figure.

The organization of chapter 4 pursues the following steps. In the next section we shall comment on the test conditions of the specimens, and the loading program including the  $K_o$ -consolidation, the static shearing, the drained creep, and the cyclic shearing. The results from the cyclic shearing will be the subject of a section of its own, then we shall give a global representation of these results permitting a synthesis of the behavior of the clay over a wide range of loading. Ultimately some comments and interpretations of some key results will be developed. Pertinent data for each step will also be presented in the appendices.

All the tests were run by the author in the laboratory of the Norwegian Geotechnical Institute (NGI) in Oslo.

## 4.2 TEST CONDITIONS

### 4.2.1 Equipment

The equipment is composed of three parts which are first the DSS apparatus adapted for stress-controlled loading, secondly the height control mechanism and finally the data acquisition system. A general view of the set-up is given in Figure 4.2.1 where one can see the classical h.12 Geonor DSS as well as the loading system and the height regulation circuit (LVDT, Regulator and Motor).

#### 4.2.1.A. The DSS apparatus

Two holes were drilled in the base of the apparatus near the center in order to accommodate a set of cables, between the pulleys and the hanger on the right side of the specimen. On the left side of the specimen one sees a contact box, and a piston\* acting under the left hanger. The principle of the application of the cyclic shear is the following. In the configuration of Figure 4.2.1 the left hanger is not in contact with the contact box ; the piston is in its upper position and supports totally the left hanger and its load. The only weights applied on the left are those on the load cell, the contact box and the vertical portion of the cables. These weights can easily be balanced by applying an appropriate counterweight on the right hanger, taking also into account the weight of the right hanger itself and of the vertical sections of the cables\*\*. The additional load applied on the

---

\* In fact we have a set of two pistons, the upper one controlling the "stiffness" of the pulse and the lower one controlling the vertical displacement and the period.

\*\* All the pulleys are virtually frictionless.

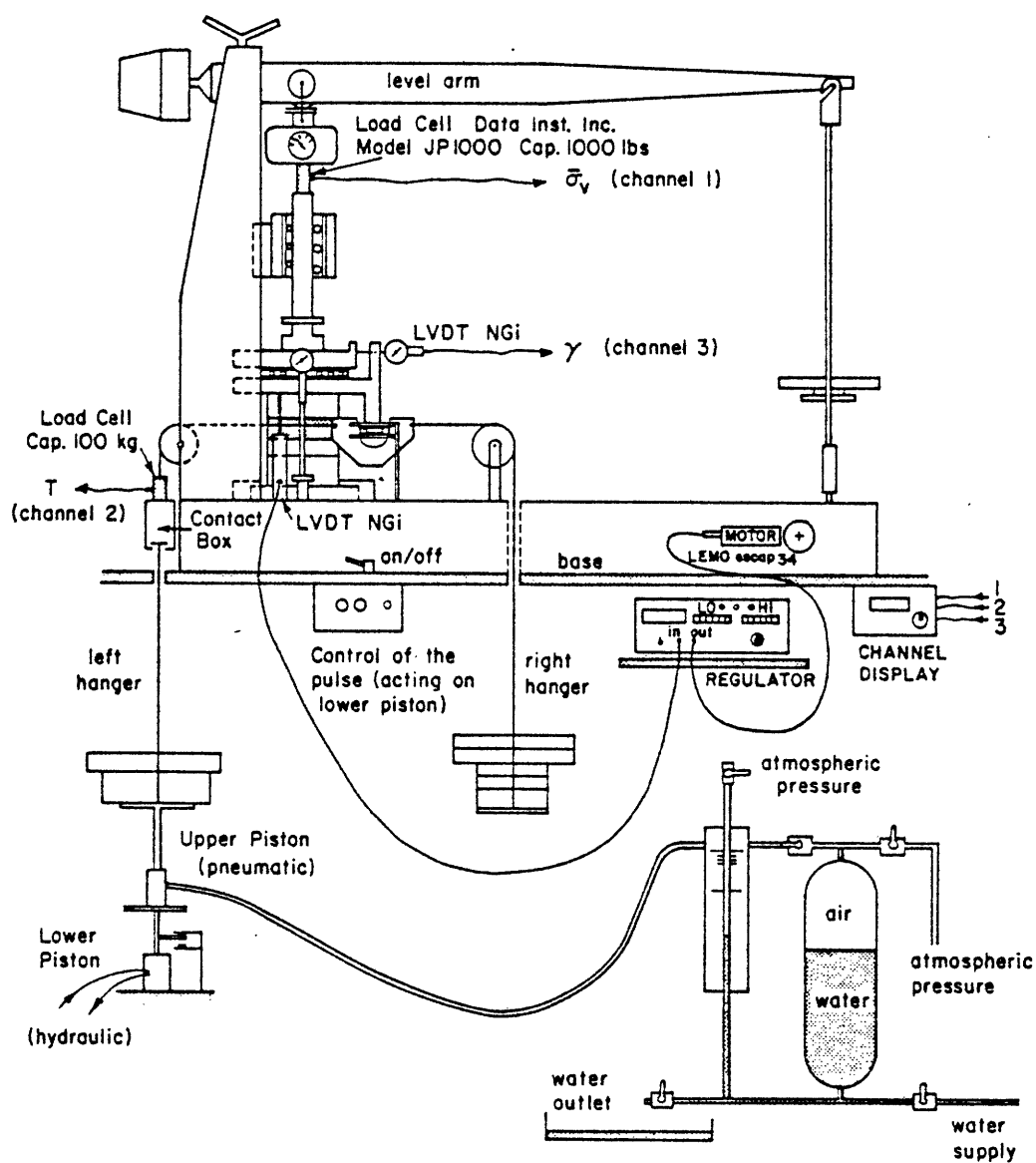


Figure 4.2.1 The experimental set up.

right hanger is applied directly to the specimen and the membrane.

Knowing the correction for the membrane horizontal deformation and the area of the specimen ( $A = 50 \text{ cm}^2$ ) one can easily obtain the shear stress applied to the clay. This shear stress corresponds to  $\tau_{\text{max}}$  since we associate a positive sign to stresses inducing a deformation towards the right.

Let us now imagine that we lower the piston enough to establish contact in the contact box and thus we totally lose contact between the piston and the bottom of the left hanger ; this action insures that the left hanger and its load are now acting against the loads applied on the right. The net resulting stress applied on the clay is  $\tau_{\text{min}}$ . The shape of the pulse (trapezoidal) and the period (10 seconds) are imposed by controlling the displacement, stiffness and speed of the pistons.

#### 4.2.1.B. The height control mechanism

The cyclic loading was imposed at a constant volume. Since the membrane cannot expand much laterally\*, our only concern is to maintain the height of the specimen constant. In order to do this we have placed a vertical LVDT between the base of the apparatus and the top cap; the reading in mV is transmitted to a regulator which will activate the motor when specific bounds are reached. The motor will act directly to modify the displacement of the level arm and thus that of the specimen top. We can control both the range of allowable variation of height and the speed of the corrective action.

#### 4.2.1.C. The data acquisition system

This system is not represented on Figure 4.2.1 but one can see the

---

\* A maximum of 0.2 mm extension of the diameter is accepted.

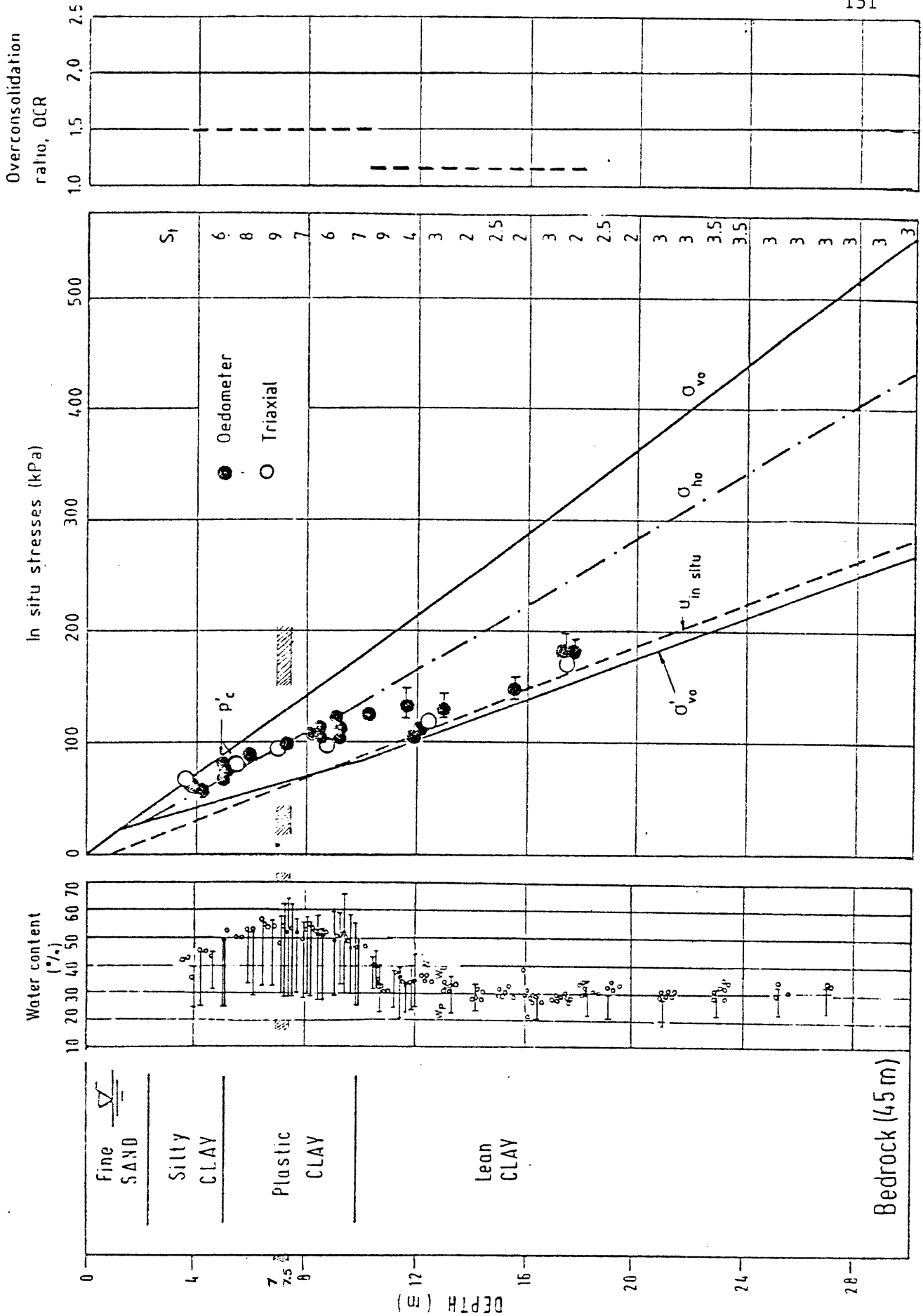


Figure 4.2.2 Description of profile for Danviksgt. 50301, Drammen. (After N.G.I.)

location of the transducers. Three channels are continuously recorded on a strip chart.

Channel 1 corresponds to the vertical load applied to the specimen. This load will be converted into a reading of vertical effective stress and, by difference, into increments of pore pressure during the cyclic loading.

Channel 2 is associated with the load acting on the left side of the specimen. It is used to control the pulse shape and the period.

Channel 3 is connected to a horizontal LVDT giving the lateral displacement of the top cap, and ultimately the lateral deformation.

Two complete set-ups\* were available and have been used in parallel.

#### 4.2.2 Clay and specimen

NGI provided undisturbed plastic Drammen clay from a site and a depth compatible with the 1975 testing program as shown on Table 4.2.1.

	<u>Site</u>	<u>Depth</u>	<u>Sampler diameter</u>
1975 program	Museumsparken, Drammen.	6.6 - 11.2 m	95 mm
1982 program	Danviksgt.50301, Drammen.	7.0 - 7.5 m	200 mm

Table 4.2.1 Origin of the clay.

---

\* Apparatuses # 4 and 5. Note also that the same membrane was always used with the same set-up. The tests with an even (resp. uneven) number were run on apparatus # 5 (resp. 4).



The profile corresponding to the borehole from which the 1982 specimens were obtained is given in Figure 4.2.2. Other site descriptions including a profile of the Museumsparken site (1975 program) and a list of typical Drammen clay properties can also be found in Appendix 4.A. (Some key properties are also reported in the summary of the test conditions of Table 4.2.2).

The cylindrical specimens have an area,  $A$ , of 50 cm<sup>2</sup> and an original height,  $h_0$ , of 16 mm. They were cut with their flat surfaces parallel to the ground surface (perpendicular to the axis of the sampling tube). The porous stones were equipped with 1.3 mm long anti-slippage pins placed in a regular square pattern at 5 mm intervals. The membranes are made in Ni alloy ("iron-nickel") by Geonor. They have an index of rigidity, associated with the wire type and the thickness of the rubber,  $C = 1.3^*$ . Finally the pore water salinity was taken as 25 g/l\*\*. The preparation of the specimens followed exactly the NGI procedures. The originality of the samples was their unusual size : 200 mm in diameter. We worked with two original cakes of clay which each gave six specimens (specimens ① to ⑥ where obtained from cake 39-2, while specimens ⑦ to ⑫ came from cake 39-1). The details of the preparation are given, and commented on, in Appendix 4.B. The index properties obtained at the same time\*\*\* ( $w$ ,  $w_L$ ,  $w_p$ , PI, and fall cone strengths) are reported in Table 4.3.1, Figures 4.B.3 to 4.B.5, and Table 4.B.1. These results show that the two cakes correspond

---

\* To be used in the corrections for membrane deformation, both vertically and horizontally.

\*\* The drainage tubes of the caps are saturated with water before the cyclic loading.

\*\*\* The Atterberg limits were obtained independently by NGI personnel a few days after the end of the testing.

to slightly different clays - and probably to somewhat different disturbances. We shall later come back to this apparent discrepancy.

#### 4.2.3 Loading program

As already mentioned the loading program was designed to simulate a simplified field situation in which a pile is first installed and the soil is allowed to consolidate around it ( $K_o$ -consolidation). The tension legs are then attached to the foundation ("drained" test\*) and the pile is subjected to sustained tension (drained creep) until a storm loading occurs (cyclic loading\*\*). A typical loading schedule is given in Figure 4.2.3.

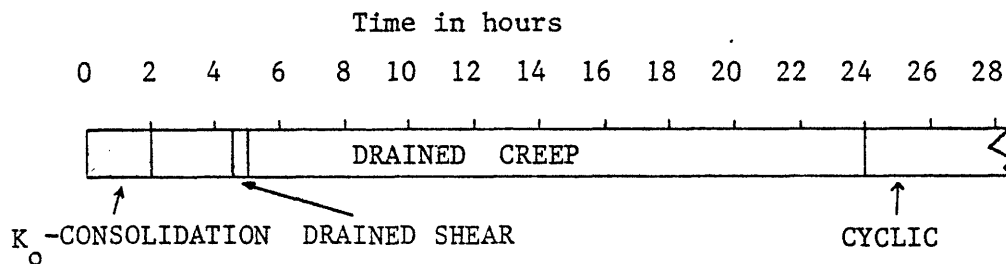


Figure 4.2.3 Loading schedule.

Let us now analyze this loading schedule one step at a time.

\* The term "drained" test is used to describe a loading during which the volume of the specimen is not maintained constant.

\*\* The time required for consolidation being much smaller for piles than for gravity structures, it was considered that the typical large storm would occur after some drained creep.

#### 4.2.3.A. Consolidation

Again the NGI procedure was used. The clay was subjected to a final  $\sigma'_{vc} = 4 \text{ kg/cm}^2$  (392.4 kN/m<sup>2</sup>\*) applied in 4 steps (0.5, 1, 2 and 4 kg/cm<sup>2</sup>). Each step was maintained for 30 minutes except for the last one which lasted 30 minutes + 2 ½ hours, at which time the drained shear was applied. All specimens are normally consolidated. Details of the procedure are given in Appendix 4.C.1. The maximum past pressure\*\* is of the order of 1 kg/cm<sup>2</sup>. The curves ( $\epsilon$  versus  $\log \sigma'_{vc}$ ) of Figure 4.C.1 clearly indicate again a slight difference of behavior between the two cakes. At the high final value of  $\sigma'_{vc}$  used, differences due to sample disturbance are believed to be minimal. It is important to realize that the differences between specimens must have been also observed during the 1975 program\*\*\*. These variations are therefore considered implicit in the results of K. Andersen et al., and as such should not be a source of concern in the present attempt to expand their data base.

#### 4.2.3.B. Drained shear and creep

The shear load applied to the specimen was increased by 4 kg every 6 minutes (the increase of the shear stress was therefore  $4/50 = 0.8 \text{ kg/cm}^2$  (or 7.85 kN/m<sup>2</sup>) every 6 minutes). The maximum shear stress,  $\tau_{cons}$  was attained in roughly 30 minutes. It was then maintained for a total period of 19 hours before the start of the cyclic loading. Details such as the

---

\* Well beyond the maximum past pressure of 100 kN/m<sup>2</sup> (see Figure 4.2.2).

\*\* See discussion on the apparent preconsolidation pressure,  $p_c$ , and aging by Bjerrum L.

\*\*\* No real comment on this question is however available in the literature.

deformations reached at the onset of cyclic loading are given in Appendix 4.C.2.

#### 4.2.3.C. Cyclic loading

The pulse imposed was trapezoidal in shape as shown in Figure 4.2.4 and the period was 10 seconds (except for test 2 and 12 for which the period was 12 seconds). The loading was limited to 2000 cycles or to a failure condition defined either by  $\gamma_{ave}$  reaching 15 %, or  $\gamma_c$  reaching  $\pm 3$  % (based on the end of  $K_o$ -consolidation height). Two types of tests have been realized : 10 simple degradation tests with constant ( $\tau_{ave}$ ,  $\tau_c$ ) and 2 variable cyclic loadings. In an effort to check our capacity to reproduce the results, two of the simple degradation loadings were duplicated, and the first 175 cycles in the variable cyclic tests are also identical. Let us now consider the results of this cyclic program. (A summary of the tests conditions is presented in Table 4.2.2).

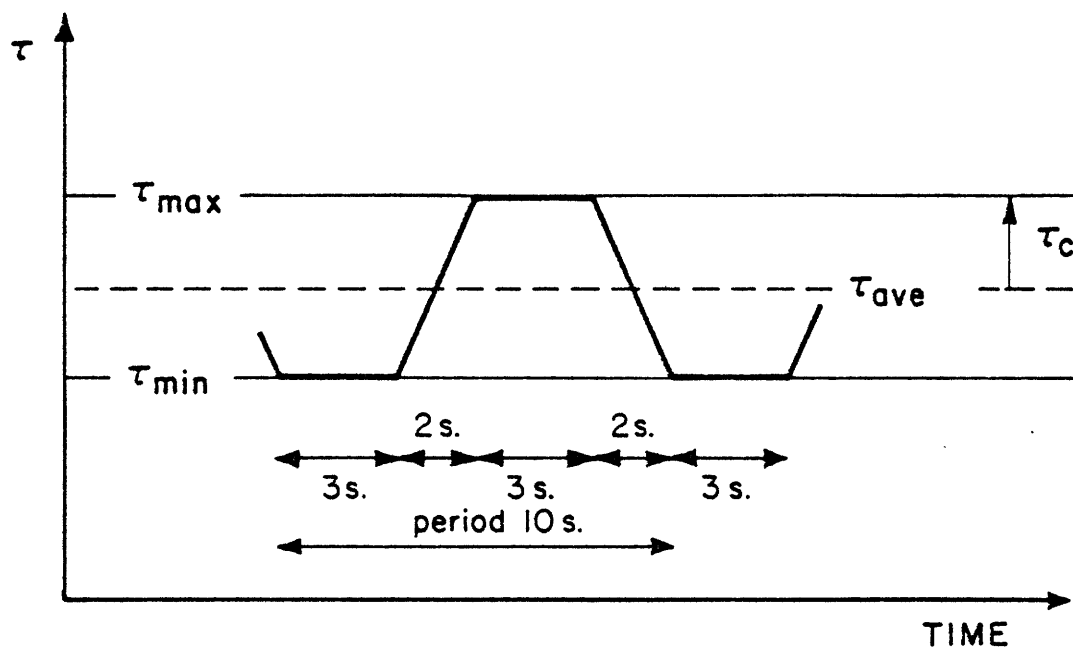


Figure 4.2.4 Pulse shape.

<u>Clay</u>	Plastic Drammen Clay Depth $\approx$ 7.3 m      Salinity 25 g/l $\sigma'_{vo} \approx 0.6 \text{ kg/cm}^2$ $\sigma'_{vm} \approx 1.0 \text{ kg/cm}^2$
<u>Specimen</u>	Initial height: $h = 16 \text{ mm}$ Area: $A = 50 \text{ cm}^2$ Filter pins:      Length = 1.3 mm      Spacing = 5 mm Ni alloy membrane ( $C = 1.3$ )
<u><math>K_o</math>-Consolidation</u>	To a Normally Consolidated State in 4 steps of 30 minutes to $\sigma'_{vc} = 4 \text{ kg/cm}^2$
<u>Drained Shear</u>	2.5 hours after the end of $K_o$ -consolidation $0.08 \text{ kg/cm}^2$ applied every 6 minutes to $\tau_{cons}$
<u>Drained Creep</u>	Under $\tau_{cons}$ and $\sigma'_{vc} = 4 \text{ kg/cm}^2$
<u>Cyclic loading</u>	24 hours after start of $K_o$ -consolidation trapezoidal pulse, period 10 seconds DSS stress-controlled tests with $\tau_{ave} = \tau_{cons}$

Table 4.2.2 Summary of test conditions.

#### 4.3. RESULTS OF THE CYCLIC TESTING

The exact locations of the tests in the  $(\tau_{ave}, \tau_c)$  plane are shown in Figure 4.3.1 ; also reported are the test numbering\* and the eventual failure (F) with their associated number of cycles or the number of cycles at which the test was stopped. Another very useful summary of the program is given in Table 4.3.1 where the essential test parameters have been reported for all stages of the loading. Table 4.3.2 gives the details of the shear stresses applied during each test.

All failures occurred in an "average deformation mode", i.e.  $\gamma_{ave}$  \*\* reached the failure criterion of 15 %. However it should be noted that the cyclic deformation failure criterion of 3 % was simultaneously attained with tests (4), (5) and (6). The number of cycles to failure proved to be rather insensitive to the  $\gamma_{ave}$  failure criterion since rupture - the rapid acceleration of the degradation to the complete destruction of the specimen - occurred over a rather limited number of cycles.

---

\* Which corresponds to the chronological order. The "best" cake was first used, and a simple diamond shape grid was covered by tests (1), (2), (3) and (4). To insure a good link with Andersen's results, the duplicate tests (5) and (6) were run. With the second cake the initial grid was expanded to tests (7) and (8), before the variable cyclic tests (9) and (10) were completed. Finally, since more time was available, test (11) was selected at low stress level and test (12) attempted to duplicate test (2).

\*\* Once again  $\gamma_{ave}$  is the result of the combined effect of the drained creep and the cyclic loading.

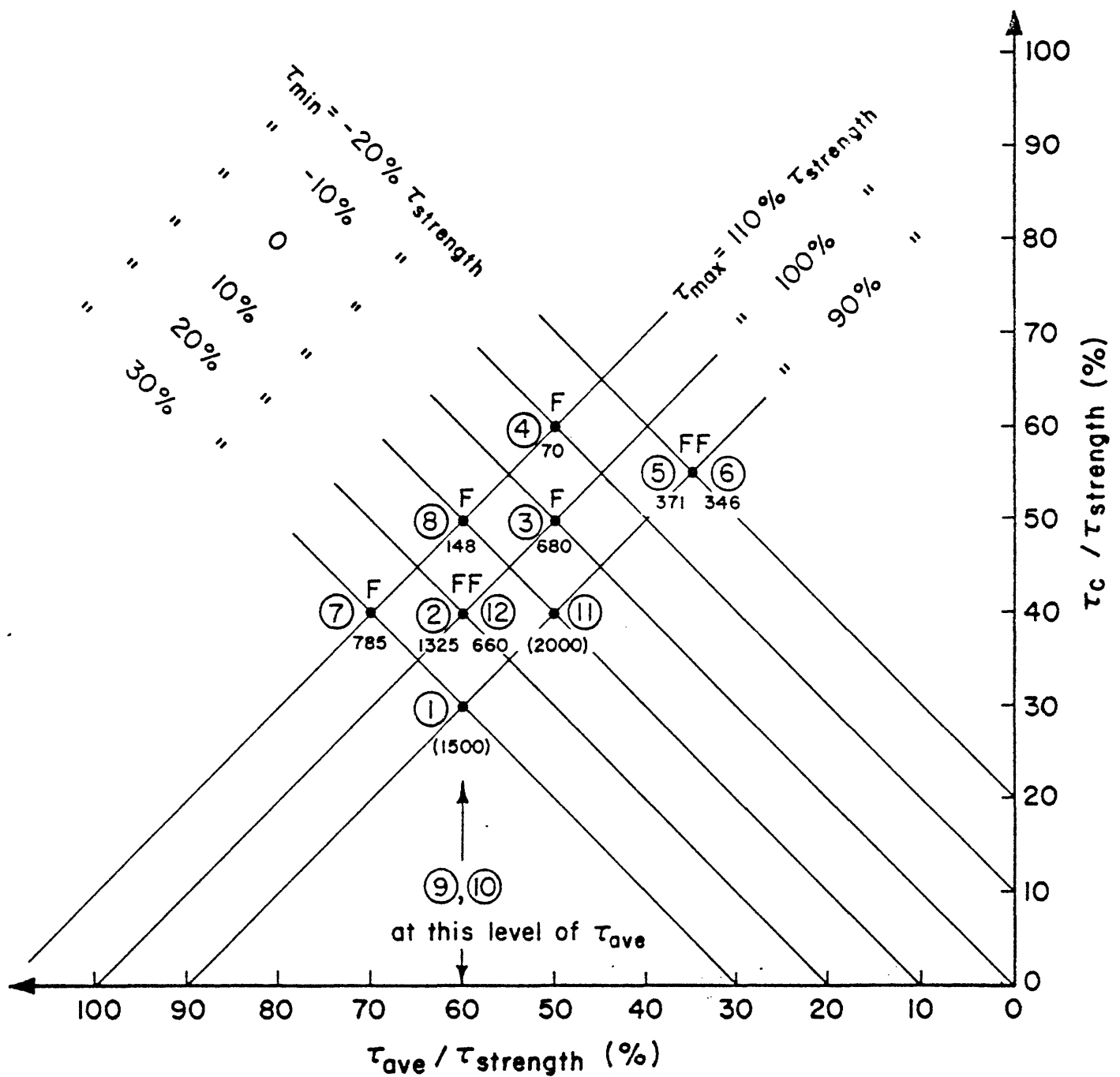


Figure 4.3.1 Relative positioning of the tests and summary of results.

- (2) = test number  
 F = failure  $\left\{ \gamma_{ave} = 15\% \text{ of } (h_o - \Delta h_c) \right\}$   
 1325 = number of cycles to failure  
 (1500) = number of cycles to end of test

Test No.	Date	P R E P A R A T I O N						E N D O F T E S T			C O N S O L I D A T I O N									
		52 <sup>a</sup>	28 <sup>a</sup>	55 <sup>a</sup>	27 <sup>a</sup>	Fall cone	S <sub>u</sub>	S <sub>t</sub>	w	S <sub>u</sub>	S <sub>t</sub>	Loading	K <sub>o</sub>		Unloading		S h e a r			
		w <sub>p</sub>	w <sub>p</sub>	w <sub>L</sub>	I <sub>p</sub>								σ <sub>vc</sub>	ε <sub>v</sub>	σ <sub>vc</sub>	ε <sub>v</sub>	τ <sub>ave</sub>	τ <sub>ave</sub> /τ <sub>hf</sub>	γ <sup>3</sup> <sub>ave</sub>	ε <sub>v</sub>
z	z	z	z	kN/m <sup>2</sup>	z	kN/m <sup>2</sup>	z	kN/m <sup>2</sup>	z	z	kN/m <sup>2</sup>	z	z	z	z	z	z	z		
①	04/03 04	55.0	29.3	59.1	29.8	29.4	6.5	42.0	67.7	-	392.4 <sup>1</sup>	17.6	-	-	50.62	60	2.43	- <sup>b</sup>		
②	04 05	54.4	28.0	58.0	30.0	30.9	6.4	42.1	62.3	-	392.4 <sup>1</sup>	17.4	-	-	50.62	60	2.42	- <sup>b</sup>		
③	05 06	54.6	29.3	59.7	30.4	31.7	5.7	43.0	60.3	-	392.4	17.0	-	-	42.18	50	2.02	19.0		
④	05 06	54.0	28.0	59.1	31.1	34.3	5.6	40.7	70.6	-	392.4	17.1	-	-	42.18	50	1.88	19.3		
⑤	07 08	55.3	28.1	59.7	31.6	29.4	4.6	42.1	63.4	-	392.4	17.0	-	-	29.53	35	1.17	18.8		
⑥	07 08	54.4	27.2	57.6	30.4	33.4	5.3	42.5	60.5	-	392.4	17.4	-	-	29.53	35	1.21	19.1		
⑦	08 09	51.0	26.4	53.6	27.2	26.1	5.8	40.8	47.1	-	392.4	16.2	-	-	59.06	70	3.29	18.4		
⑧	08 09	51.8	27.7	53.1	25.4	33.8	6.5	39.8	45.1	-	392.4	16.0	-	-	50.62	60	2.38	18.1		
⑨	10 11	50.0	26.4	52.5	26.1	33.4	6.8	41.3	82.4	-	392.4	15.6	-	-	50.62	60	2.33	17.5		
⑩	10 11	48.5	27.3	52.2	24.9	32.2	4.9	39.3	54.4	-	392.4	15.6	-	-	50.62	60	2.34	17.5		
⑪	11 12	- <sup>2</sup>	27.0	52.3	25.3	28.7	5.9	40.0	62.3	-	392.4	16.5	-	-	42.18	50	1.84	18.3		
⑫	11 12	50	27.0	52.3	25.3	30.9	4.7	38.4	64.7	-	392.4 <sup>1</sup>	15.4	-	-	50.62	60	2.47	17.2		

Test No.	Estim. <sup>7</sup>	C Y C L I C S H E A R I N G			E n d o f c y c l i n g			u <sub>N</sub>	REMARKS
		τ <sub>hf</sub>	τ <sub>c</sub>	τ <sub>c</sub> /τ <sub>hf</sub>	N	γ <sub>ave</sub> <sup>N</sup>	γ <sub>c</sub> <sup>N</sup>		
		kN/m <sup>2</sup>	kN/m <sup>2</sup>		Cycle	z	z		
①	84.37	25.31	30	1500	2.98	.145	79.5	Apparatus # 4	
②	84.37	33.75	40	1360	20.85	.65	271.7	12 s period. App.5	
③	84.37	42.18	50	710	18.3	1.47	310.8	App.4	
④	84.37	50.62	60	75	21.4	3.20	296.6	App.5	
⑤	84.37	46.40	55	375	17.20	3.85	332.8	App.4	
⑥	84.37	46.40	55	350	19.1	5.52	348.8	App.5	
⑦	84.37	33.75	40	825	20.7	.64	265.3	App.4	
⑧	84.37	42.18	50	155	18.7	1.26	284.0	Failure of regulator, hand-controlled height. App.5	
⑨	84.37	Variable		395	17.6	1.3	278.9	App.4	
⑩	84.37	Variable		460	30.4	0.57	308.7	App.5	
⑪	84.37	33.75	40	2000	4.9	0.30	213.8	12 s period. App.4	
⑫	84.37	33.75	40	700	25.42	0.8	293.7	App.5	

Table 4.3.1.  
Essential test parameters at all stages of loading.

<sup>1</sup> No membrane correction vertically (4 kg for 50 cm<sup>2</sup> specimen).  
<sup>2</sup> Loss of container.  
<sup>3</sup> End of drained shear based on end of K<sub>o</sub> consolidation.

<sup>4</sup> No record.  
<sup>5</sup> Obtained independently by NGI personnel.

<sup>6</sup> From Andersen et al. [2].  
<sup>7</sup> τ<sub>hf</sub> = c'<sub>vo</sub> \* .215  
<sup>8</sup> Mean values plastic Drammen clay.



Test Number	$\tau_{\max}$ kN/m <sup>2</sup>	$\tau_{\min}$ kN/m <sup>2</sup>	$\tau_c/\tau_{st}$ in %	$\tau_c$ kN/m <sup>2</sup>	$\tau_{ave}/\tau_{st}$ in %	$\tau_{ave}$ kN/m <sup>2</sup>	Cycle range
①	75.93	25.31	30	25.31	60	50.62	0 → end
②	84.37	16.87	40	33.75	60	50.62	
③	84.37	0	50	42.18	50	42.18	
④	92.80	- 8.44	60	50.62	50	42.18	
⑤	75.93	- 16.87	55	46.40	35	29.53	
⑥	75.93	- 16.87	55	46.40	35	29.53	
⑦	92.80	25.31	40	33.75	70	59.06	
⑧	92.80	8.44	50	42.18	60	50.62	
⑨	75.93	25.31	30	25.31	60	50.62	0 → 98 300 → 349
	84.37	16.87	40	33.75	60	50.62	100 → 149 174 → 223
	92.80	8.44	50	42.18	60	50.62	150 → 173 225 → 298 350 → end
⑩	75.93	25.31	30	25.31	60	50.62	0 → 101 208 → 307 452 → end
	84.37	16.87	40	33.75	60	50.62	102 → 152 198 → 207 308 → 357
	92.80	8.44	50	42.18	60	50.62	153 → 177 188 → 197 358 → 402 408 → 450
	101.24	0	60	50.62	60	50.62	178 → 187 403 → 407
⑪	75.93	8.44	40	33.75	50	42.18	0 → end
⑫	84.37	16.87	40	33.75	60	50.62	0 → end

Table 4.3.2 Shear stresses applied.

The strip charts generated for each test will not be provided here, but tables presenting the observed deformations and pore pressures at specific numbers of cycles can be found in Appendix 4.D for each test. All the tests were run with a 10 second period except for (2) and (12) for which the period applied was 12 seconds. On the basis of past NGI experience the difference is believed to be of little importance in this study. The results will also be presented in the form of graphs of deformations and pore pressure versus time. On these graphs the mean excess pore pressures have been indicated by dashed lines and are reported in  $\text{kN/m}^2$ . The deformations are represented by the envelopes of  $\gamma_{\max}$  and  $\gamma_{\min}$  (expressed in % of end of  $K_0$ -consolidation height).

The results of the simple degradation tests are reported in Figures 4.3.2 through 4.3.5. Figure 4.3.2 covers the high number of cycles range, while Figure 4.3.3 deals with more rapid failures. Figures 4.3.4 and 4.3.5 relate specifically to the tests which are duplicated. A few observations can be made on the overall behavior;

- ∴ all tests presented a very similar evolution both in deformation and pore pressure,
- ∴ as already mentioned the average component of deformation becomes far larger than the cyclic one, which does not vary much even upon reaching the rupture zone,
- ∴ there is a clear change of curvature of the deformation versus time curves, with the possibility of an intermediate linear region\*,

---

\* This trend can be compared to the evolution of deformation during creep tests.

the pore pressure curves show a very rapid increase followed by a slower, almost linear, region.

It is not very easy to compare the test results amongst themselves in this format of presentation and, a fortiori, to interpolate or extrapolate the results to new stress conditions. As a matter of fact this is precisely our argumentation for developing the interpretation of the next section. The traditional way to compare the tests is to plot on one graph test parameters associated with a constant stress characteristic ( $\tau_{ave}$ ,  $\tau_c$ ,  $\tau_{max}$  or  $\tau_{min}$ ) ; this corresponds to studying tests placed on vertical, horizontal or diagonal lines of Figure 4.3.1. Examples of such a procedure can be found in Appendix 4.E.

Duplicate tests (5) and (6) agreed very well (Figure 4.3.4). They were run on the same cake quarter (see Figure 4.B.2 in Appendix 4.B) and in parallel (i.e. with the same know-how on the part of the author). On the other hand tests (2) and (12) yielded quite different responses (Figure 4.3.5). It has been decided to discard the results of test (12) for two reasons: a marked heterogeneity and a lack of compatibility with neighboring tests. Details of this comparison are presented in Appendix 4.E.

Variable cyclic loading was imposed during tests (9) and (10) by rapidly changing the loads at given values of N on both sides of the DSS apparatus\*. The results of these two tests are presented in Figures 4.3.6 and 4.3.7, and will be analyzed later in this chapter.

---

\* Special thanks to Dr. Suzanne Lacasse.

By comparison, during the 1975 program the cycling was interrupted at each load level change to allow for weight adjustment.

Note the good agreement in the two tests over the first 175 cycles during which the same loading is applied. Also, as a first indication of their coherence with other tests, Figure 4.3.8 shows a comparison between test ⑧ with segments of tests ⑨ and ⑩ corresponding to the same loading. The overall fit appears to be satisfactory. It is also very interesting to observe the marked steps in the evolution of the pore pressure each time the loading is reduced, and the clear increases that occur when the applied stresses recover their past highest value.

A few words should be said on the evolution of the cyclic shear modulus (defined as  $\tau_c/\gamma_c$ ). The curves obtained by K. Andersen for 100 and 1000 cycles are replotted on Figure 4.3.9 together with our data. It should be pointed out that our measurements are less accurate since we are studying a wider range of deformations. It appears however that our results are consistent with the 1975 observations ; they follow the trend and lie below the two lines as should be expected since the level of shearing is higher.

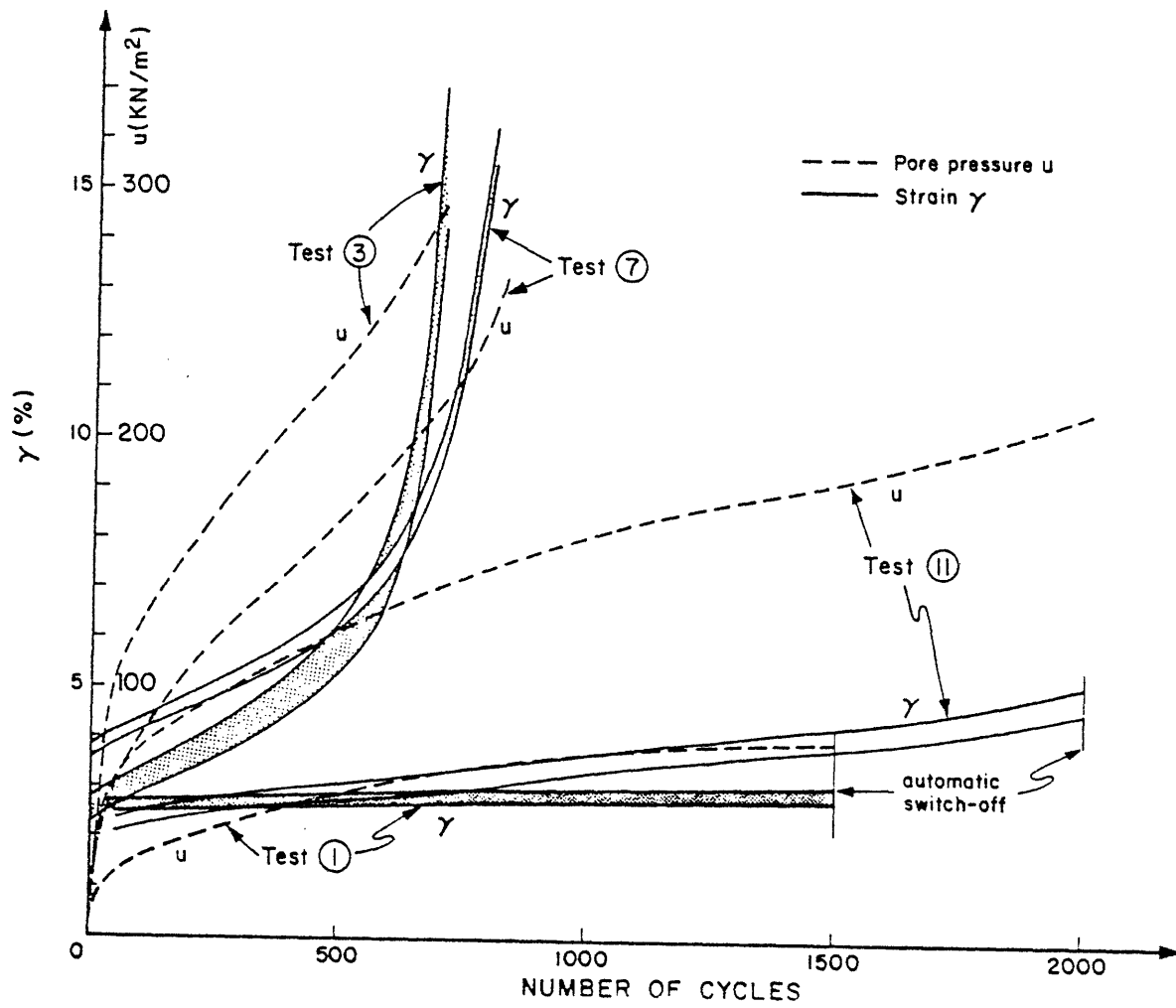


Figure 4.3.2 Results of tests ①, ③, ⑦ and ⑪.

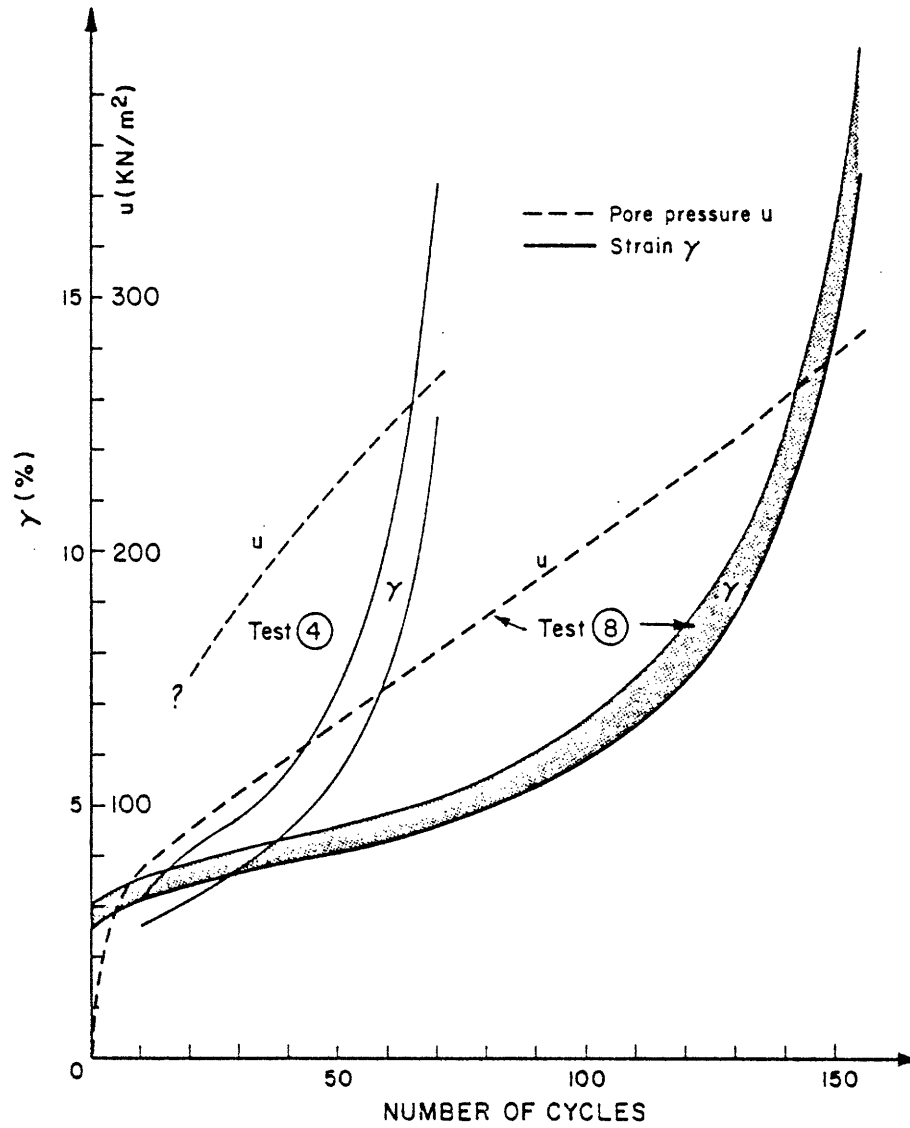


Figure 4.3.3 Results of tests ④ and ⑧.

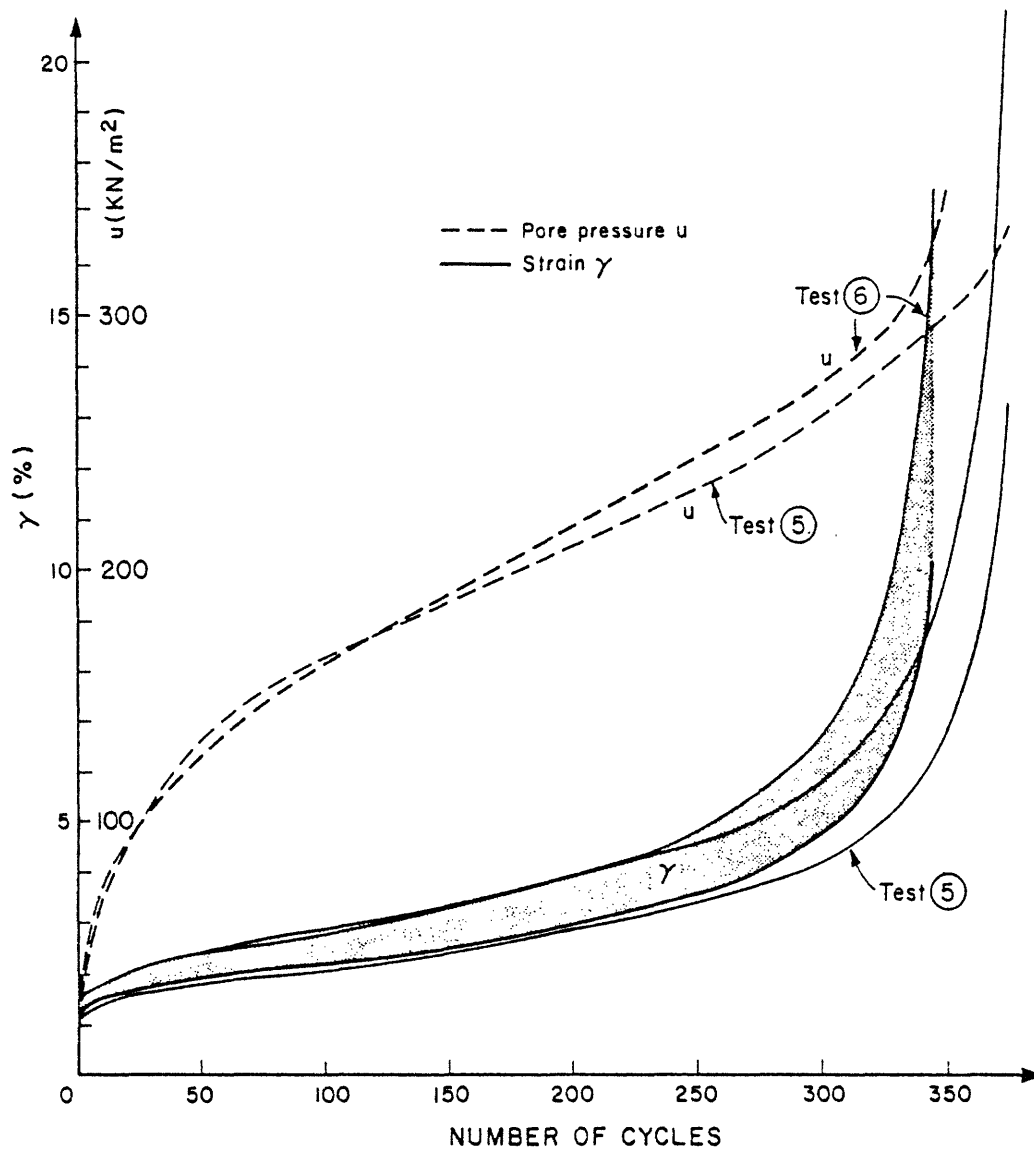


Figure 4.3.4 Results of tests (5) and (6).

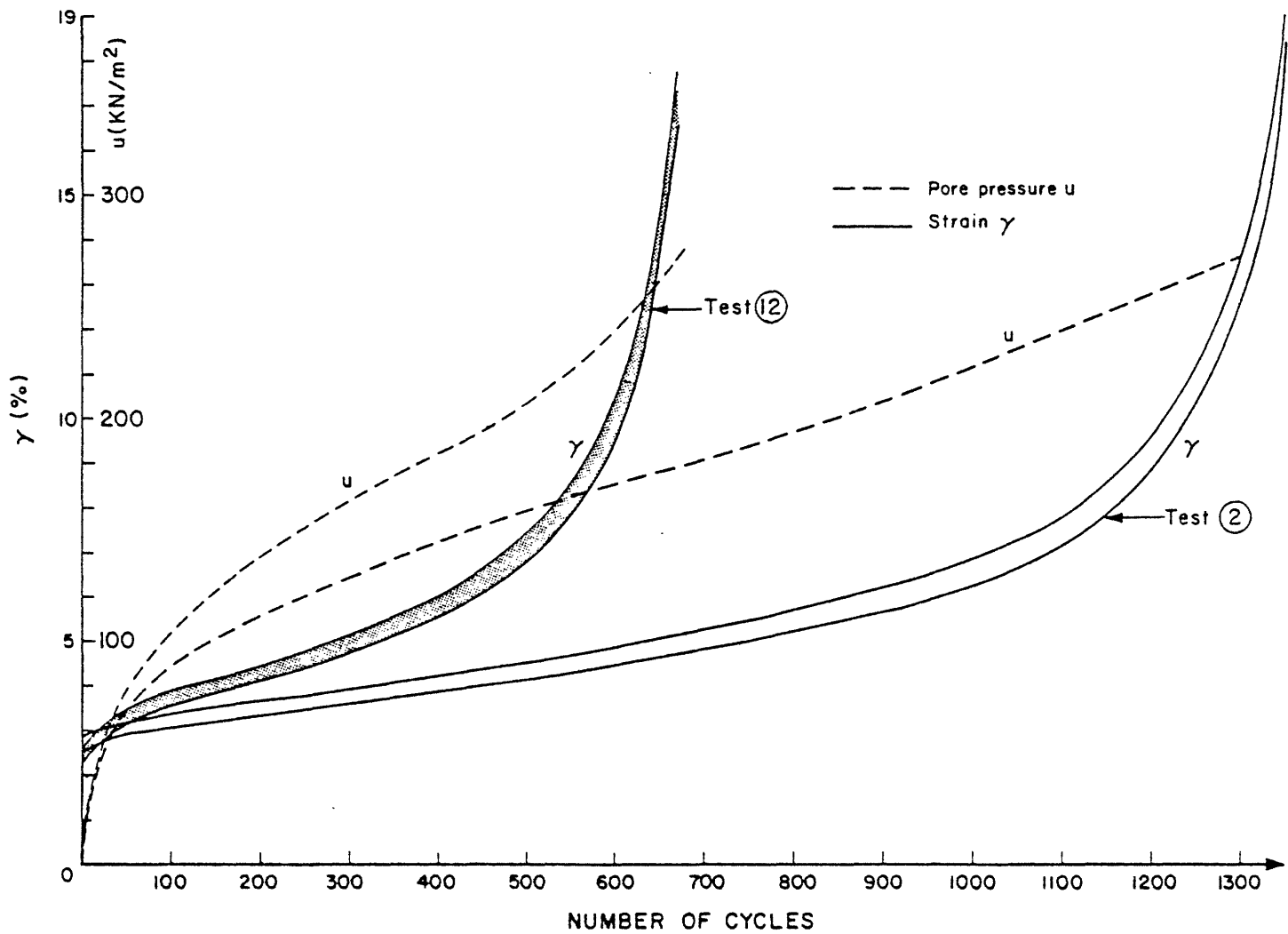


Figure 4.3.5 Results of tests (2) and (12) .



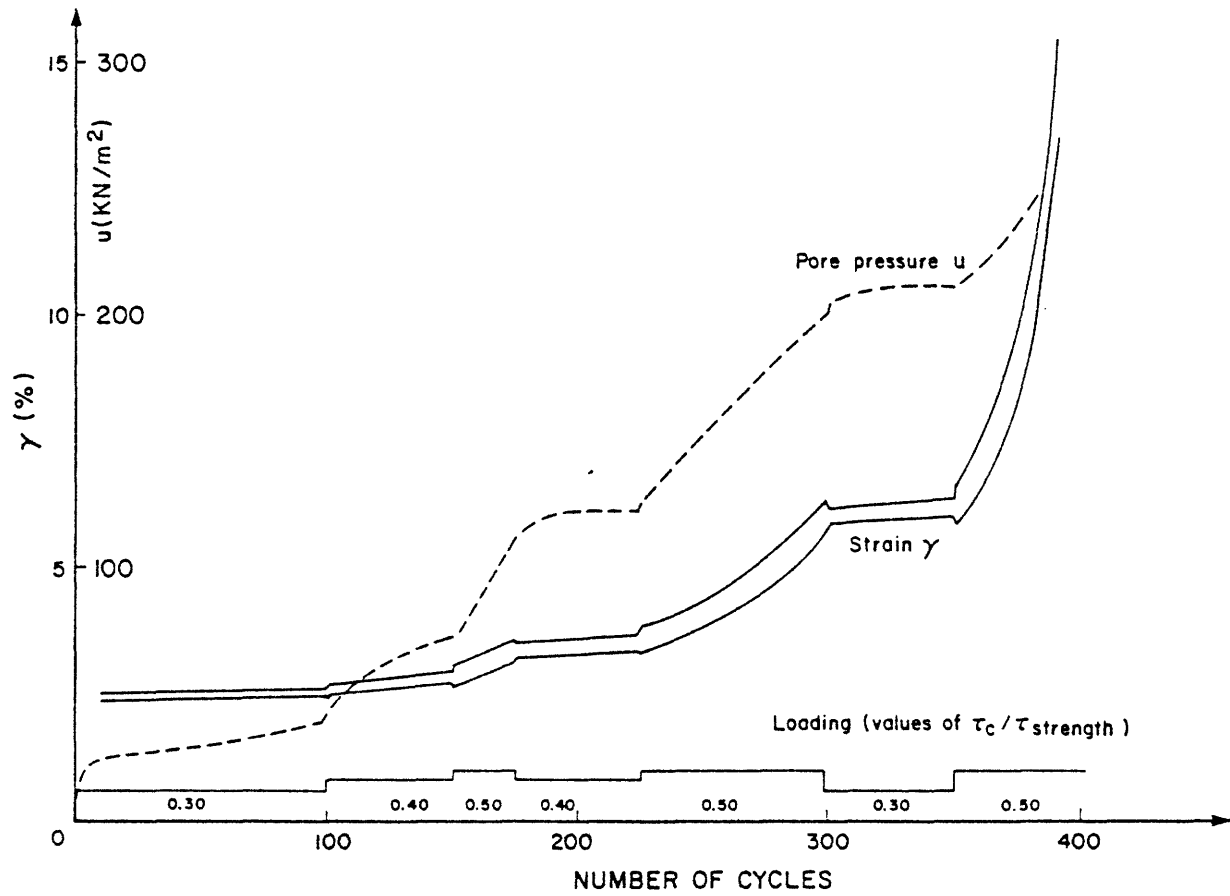


Figure 4.3.6 Results of test ⑨.

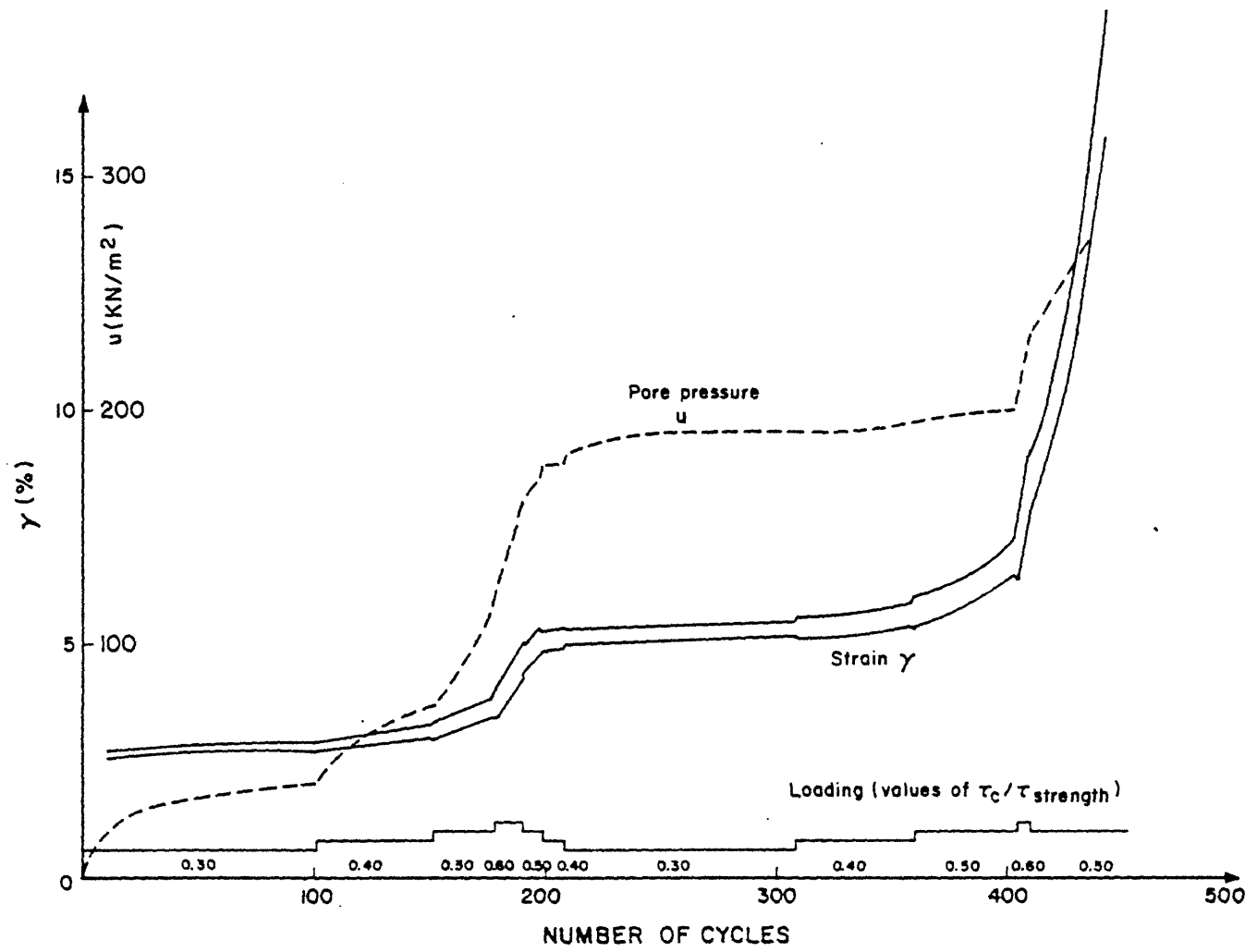


Figure 4.3.7 Results of test (10).

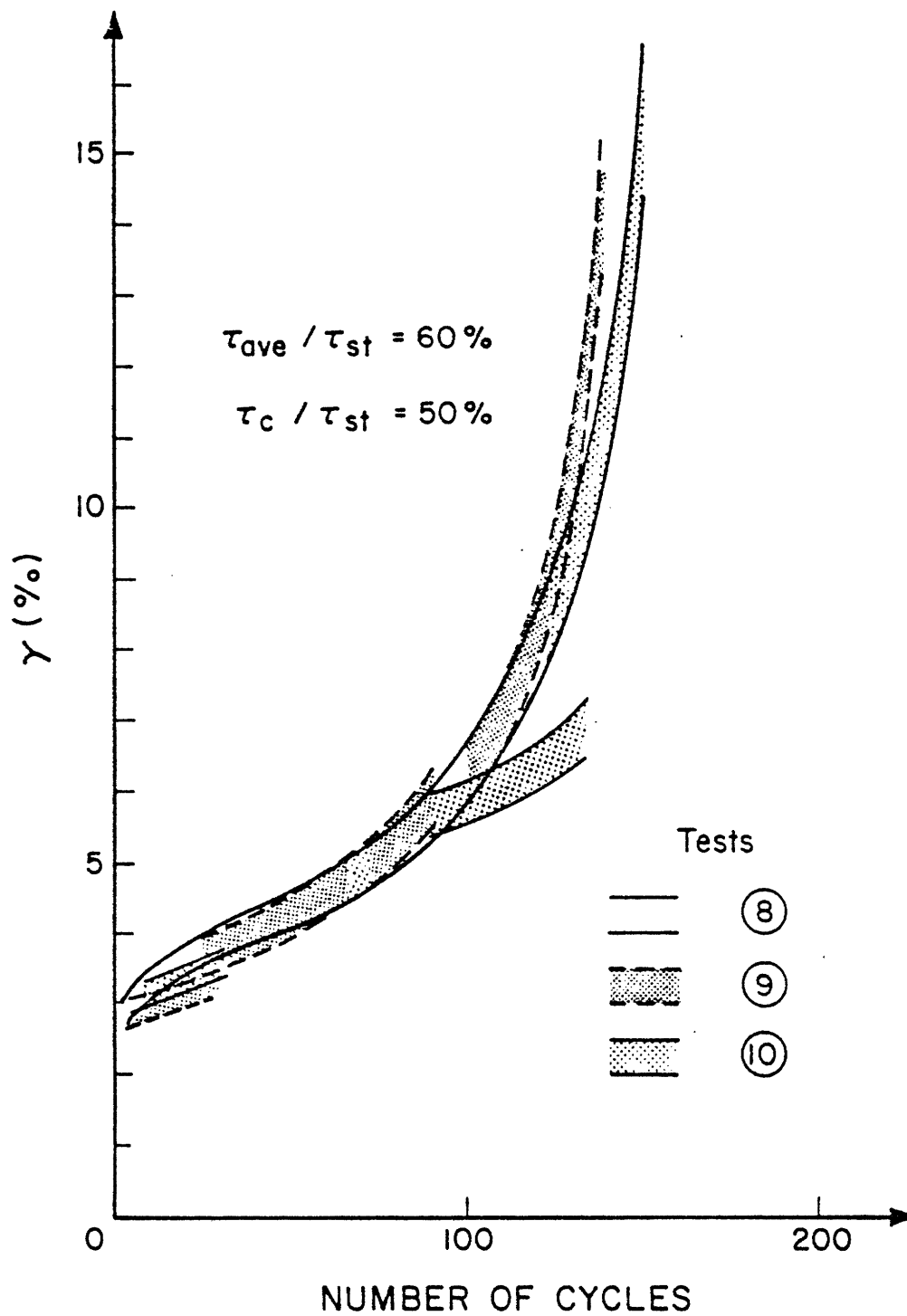


Figure 4.3.8 Comparison between test (8) and segments of tests (9) and (10).

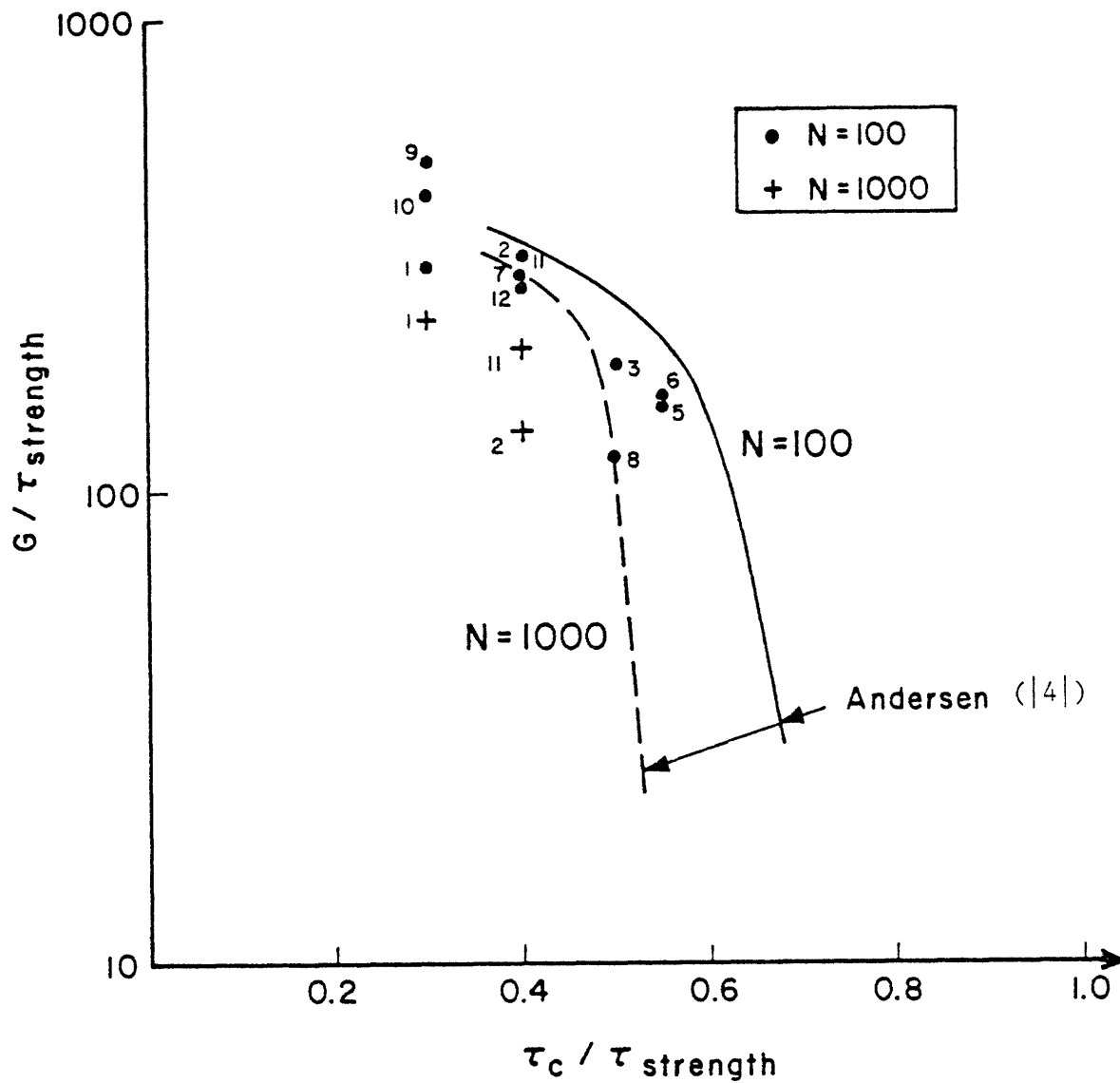


Figure 4.3.9 Degradation of the cyclic shear modulus.

#### 4.4 SYNTHESIS OF THE RESULTS

There is an evident need to organize the previous results in a physically coherent and practical manner. It would certainly be very helpful to find a graphic representation allowing for easy interpolation and even extrapolation from our data base. The concept of 3-D strain contour diagrams can be used in this purpose as shall now be shown.

The 3-D (three dimensional) contour diagrams are simply an extension of Andersen's 1975 strain contour diagrams to a third dimension, the average shear stress. Let us first recall Andersen's plotting procedure. In a (normalized)  $\tau_c$  versus  $\log N$  plane one reports for each test - i.e. along lines of constant  $\tau_c$  - observed values of  $\gamma_c$  at specific  $N$ . Examples of this operation can be seen in Figure 4.4.1. Also shown in the same figure are curves joining points associated with given values of  $\gamma_c$  (e.g. 0.15 % and 0.5 %). These curves form a "strain contour diagram". They can also be seen as S-N curves in a fatigue study.

Since our tests are not characterized by  $\tau_c$  only, but by a couple ( $\tau_{ave}$ ,  $\tau_c$ ), it seems logical to add a third dimension to Andersen's representation : the (normalized)  $\tau_{ave}$  value. The corresponding axis will be perpendicular to Andersen's plane. The same procedure as above can then be used to report experimental readings of  $\gamma_{ave}$ , for example, at given values of  $N$  along a line corresponding to a fixed couple ( $\tau_{ave}$ ,  $\tau_c$ ). By joining points associated with equal  $\gamma_{ave}$  one can then create surfaces. These surfaces form a "3-D strain contour diagram", by analogy with Andersen's appellation. This particular 3-D strain contour diagram will also be referenced to as the iso- $\gamma_{ave}$  (surface) network. Of course similar

surfaces can be obtained for  $\gamma_c$  ; they will form the iso- $\gamma_c$  (surface) network\*.

Since it is not very easy to graphically represent a network of surfaces, cross-sections at specific values of N will be used, which correspond precisely to the planes ( $\tau_{ave}$ ,  $\tau_c$ ) introduced earlier in this chapter. In these planes one will see networks of iso-deformation curves which will also be called - abusively perhaps - the iso- $\gamma_{ave}$  and iso- $\gamma_c$  networks. Let us now study how these networks can be obtained from our data.

#### 4.4.1 iso- $\gamma_c$ and iso- $\gamma_{ave}$ networks

The basic results of section 4.3 are replotted in the form of cross-sections of the 3-D strain contour diagrams for N = 50, 100, 200, 500 and 1000 cycles. At each number of cycles we present the iso- $\gamma_c$  network corresponding to  $\gamma_c = 0.15, 0.25$  and  $0.50$  %, as well as the iso- $\gamma_{ave}$  network for  $\gamma_{ave} = 2.5, 3, 4$  and  $6$  %. Andersen's results, as presented in Figure 4.4.1 are reported on the  $\tau_c$  axis on the iso- $\gamma_c$  networks. It will be seen that they agree very well with our present set of data. Figures 4.4.2 to 4.4.6 show these networks superimposed on the test points with their associated deformation values (underlined). The letter F indicates a specimen failure. As already mentioned these failures occurred in the average deformation mode and should be interpreted as such even on the iso- $\gamma_c$  networks.

The iso- $\gamma_c$  networks are not very sensitive to change in  $\tau_{ave}$ , except for very large values of  $\tau_{max}$  (of the order of 100 % of  $\tau_{strength}$ ). We shall come back on this phenomenon in the next section.

---

\* We could have iso- $\gamma_{max}$ , iso- $\gamma_{min}$ , iso-pore pressure... networks.

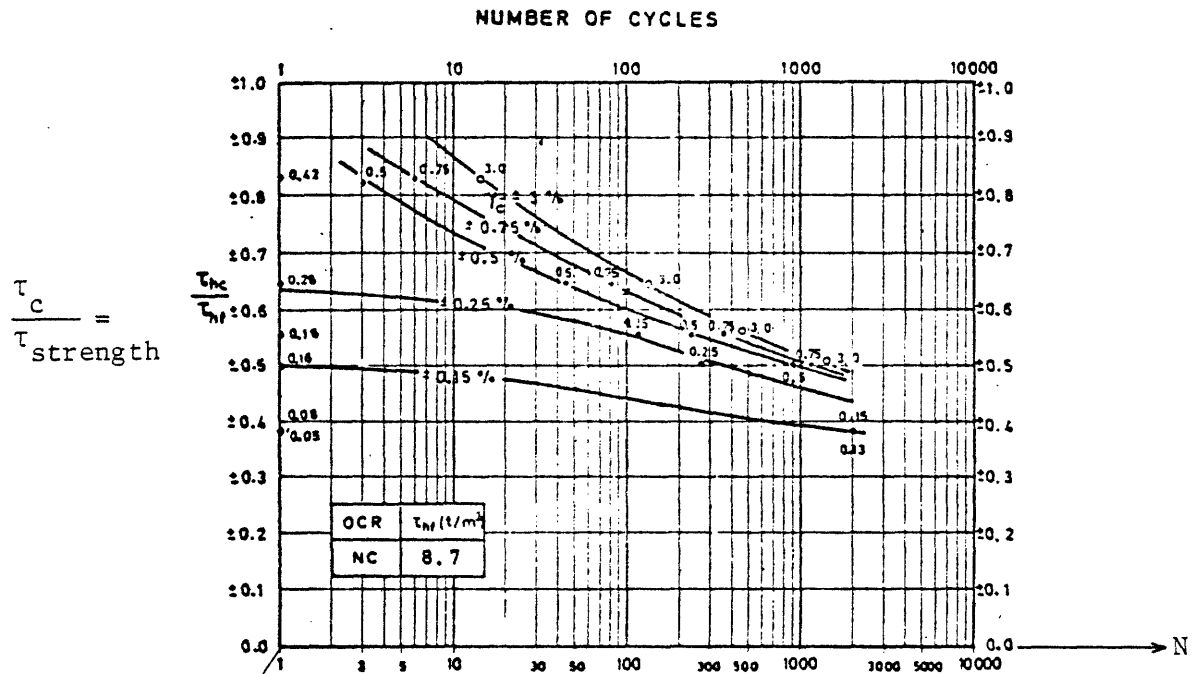


Figure 4.4.1 Andersen's results | 2 |.

(Note :  $\tau_{hf} = \tau_{strength}$ ).

$\frac{\tau_{ave}}{\tau_{strength}}$

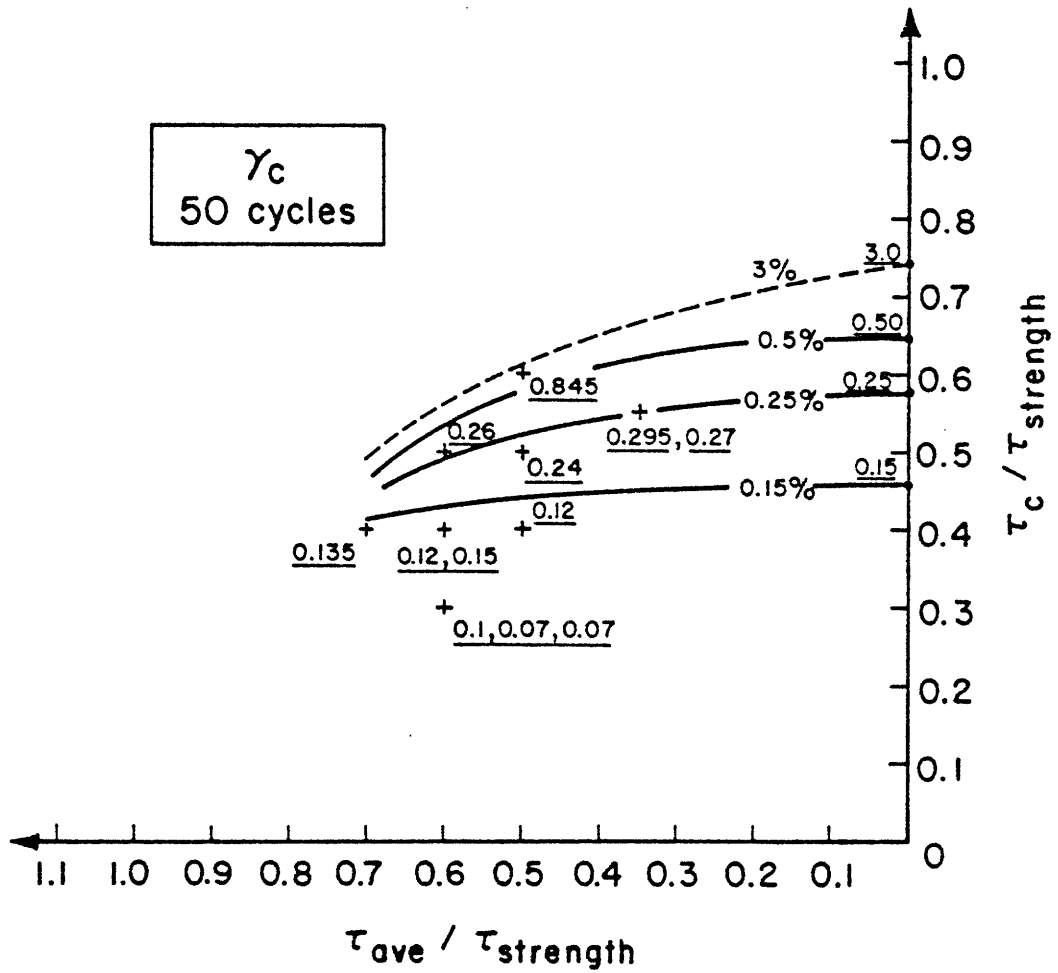


Figure 4.4.2.a Section of iso- $\gamma_c$  network at N = 50 cycles.



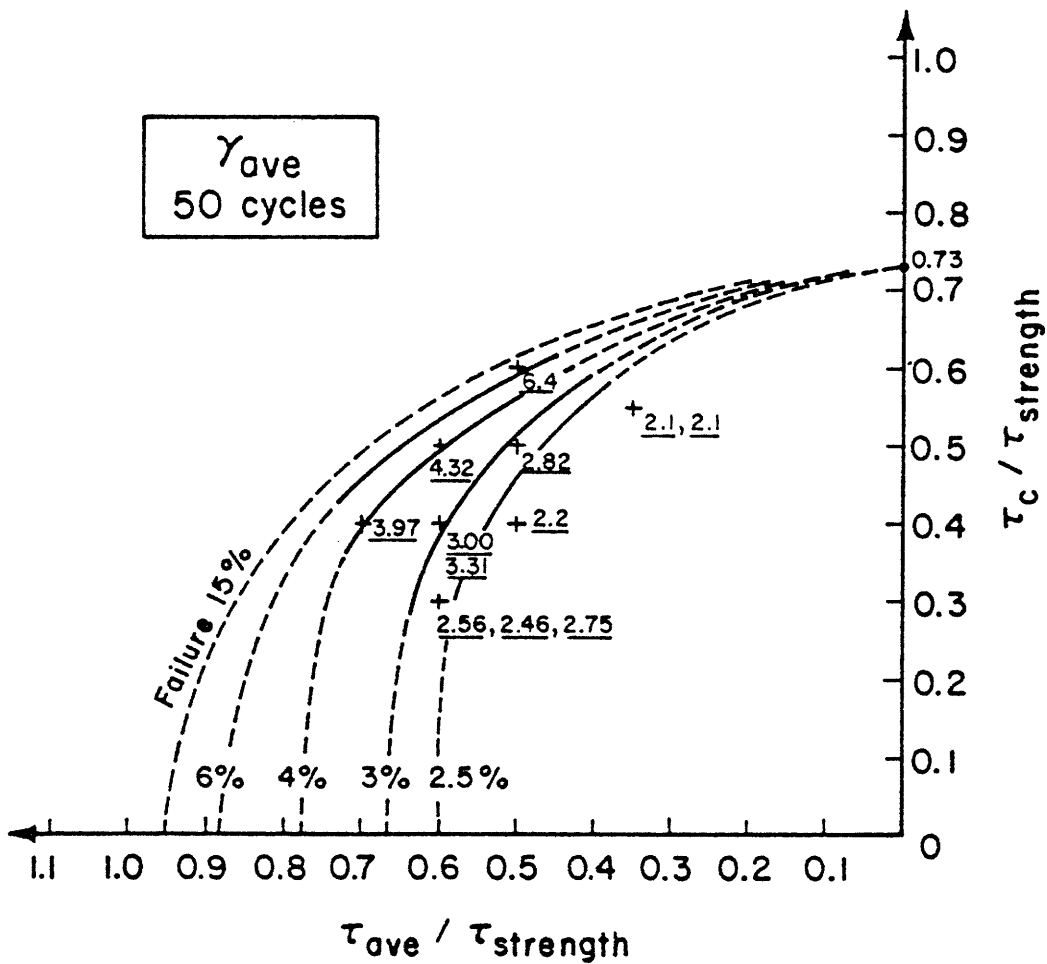


Figure 4.4.2.b Section of iso- $\gamma_{ave}$  network at N = 50 cycles.

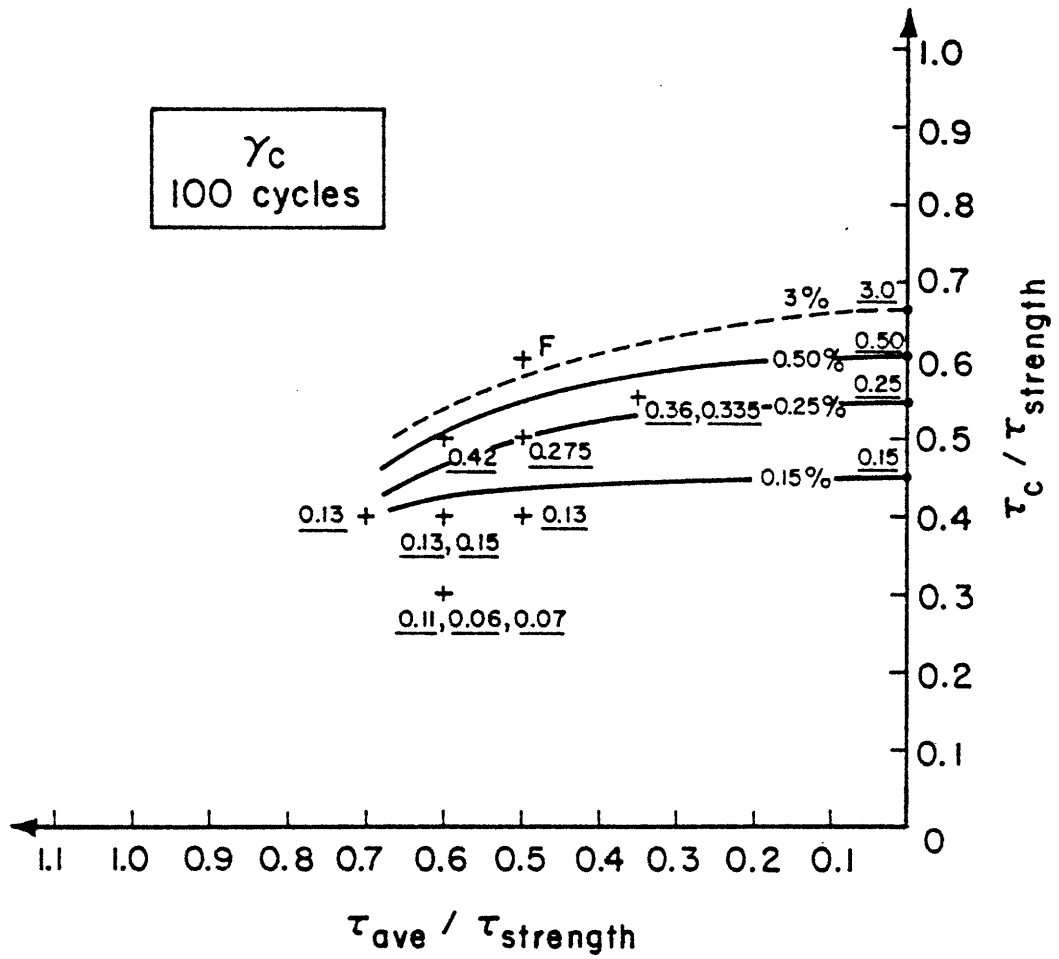


Figure 4.4.3.a Section of iso- $\gamma_c$  network at  $N = 100$  cycles.

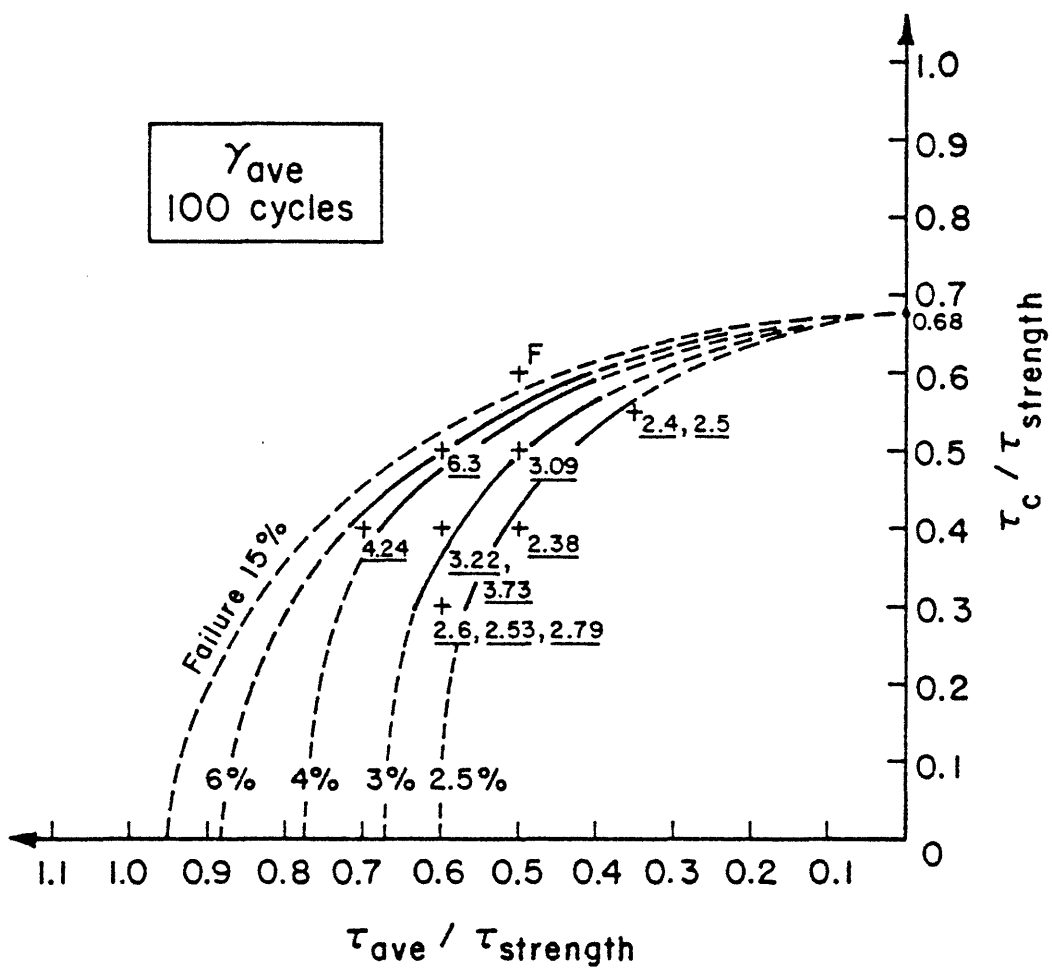


Figure 4.4.3.b Section of iso- $\gamma_{ave}$  network at N = 100 cycles.

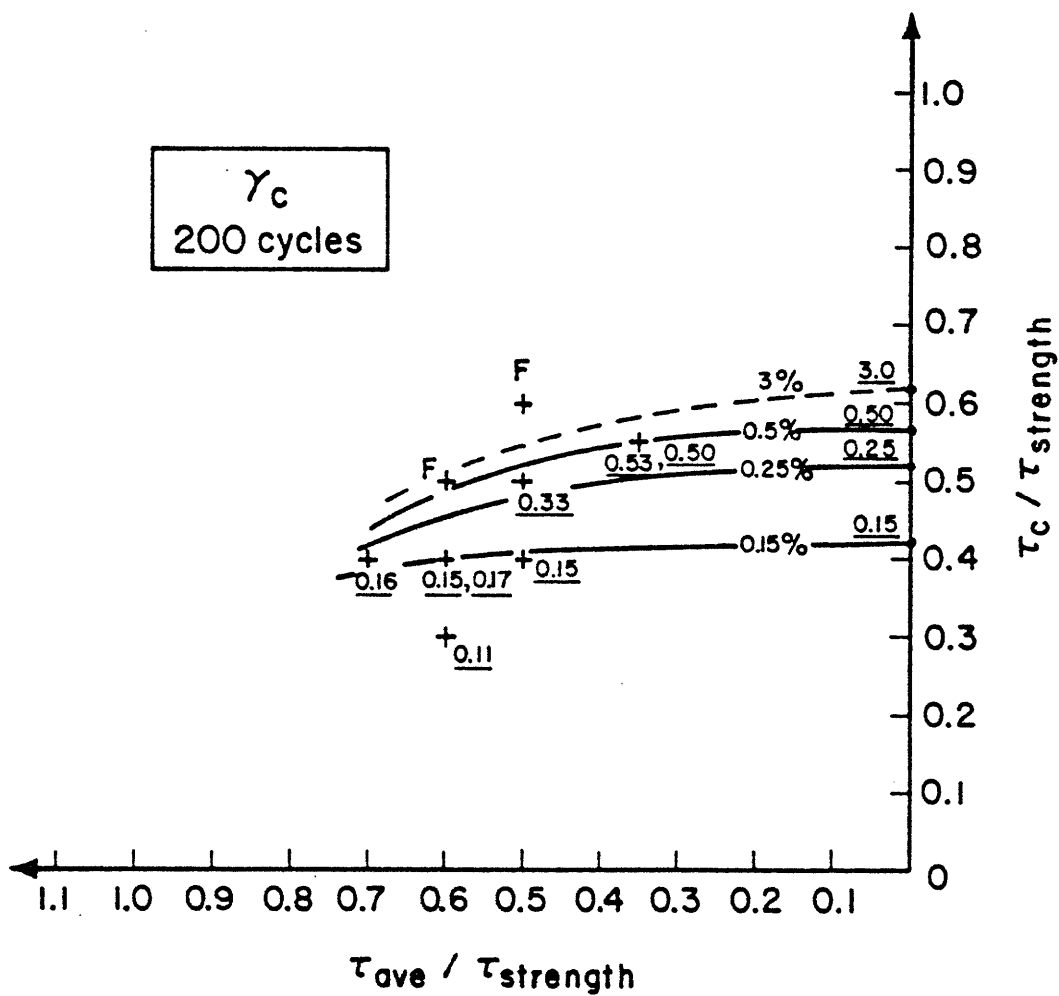


Figure 4.4.4.a Section of iso- $\gamma_c$  network at N = 200 cycles.

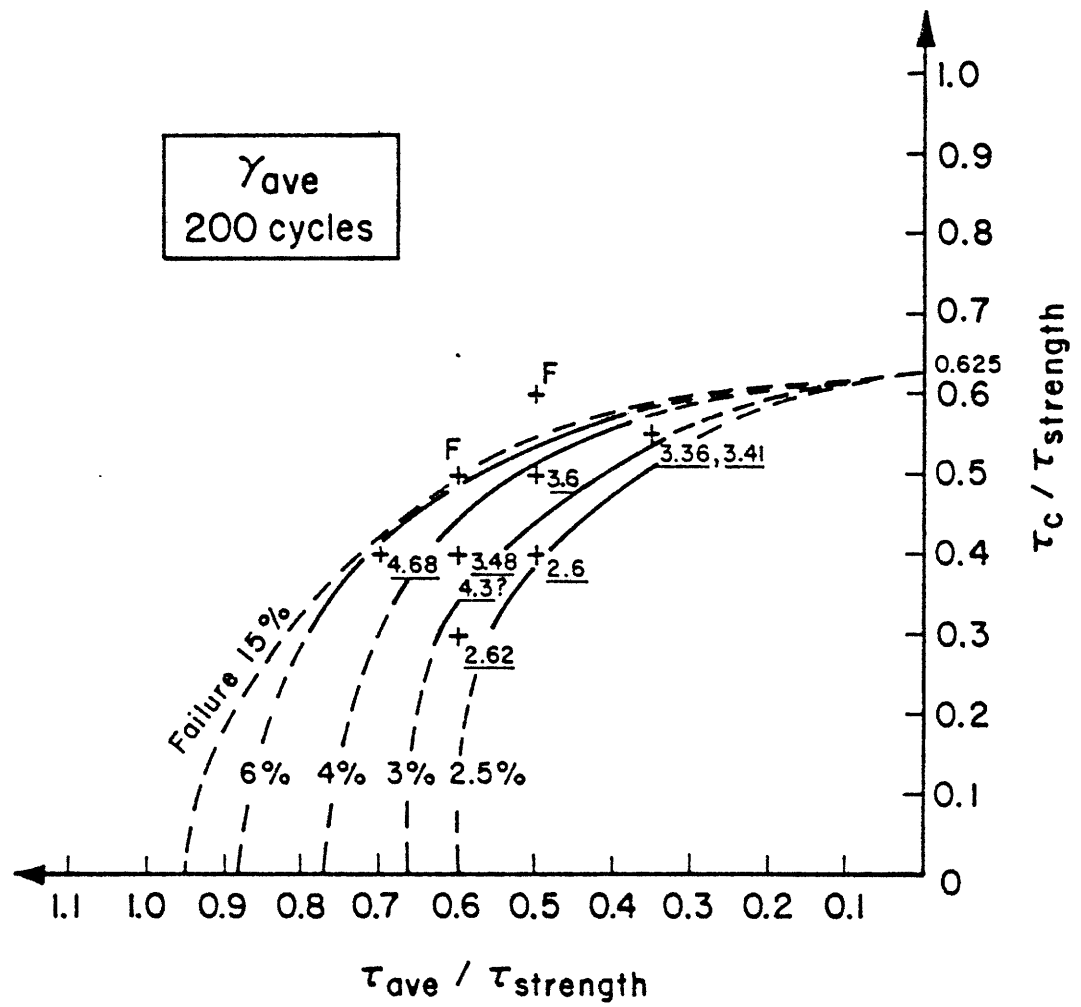


Figure 4.4.4.b Section of iso- $\gamma_{\text{ave}}$  network at  $N = 200$  cycles.

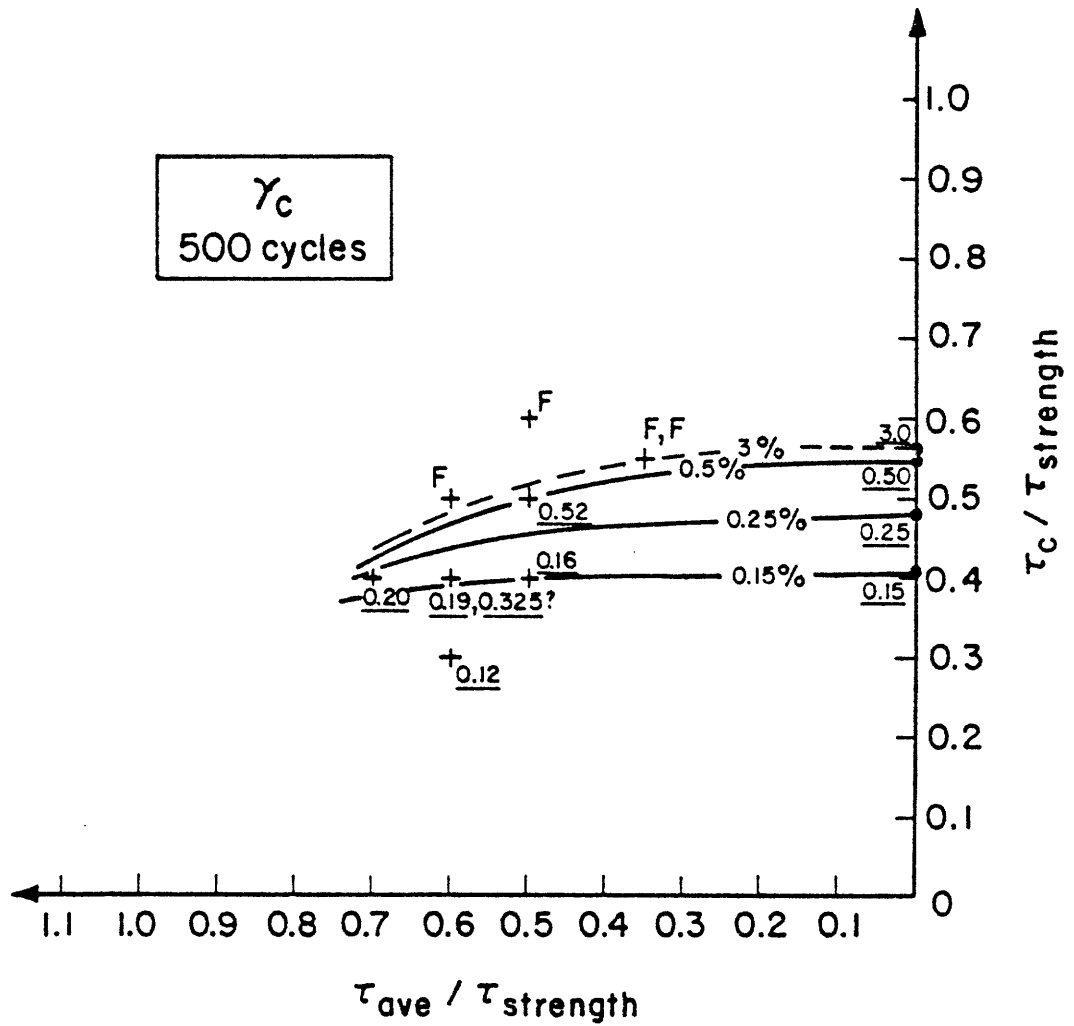


Figure 4.4.5.a Section of iso- $\gamma_c$  network at N = 500 cycles.

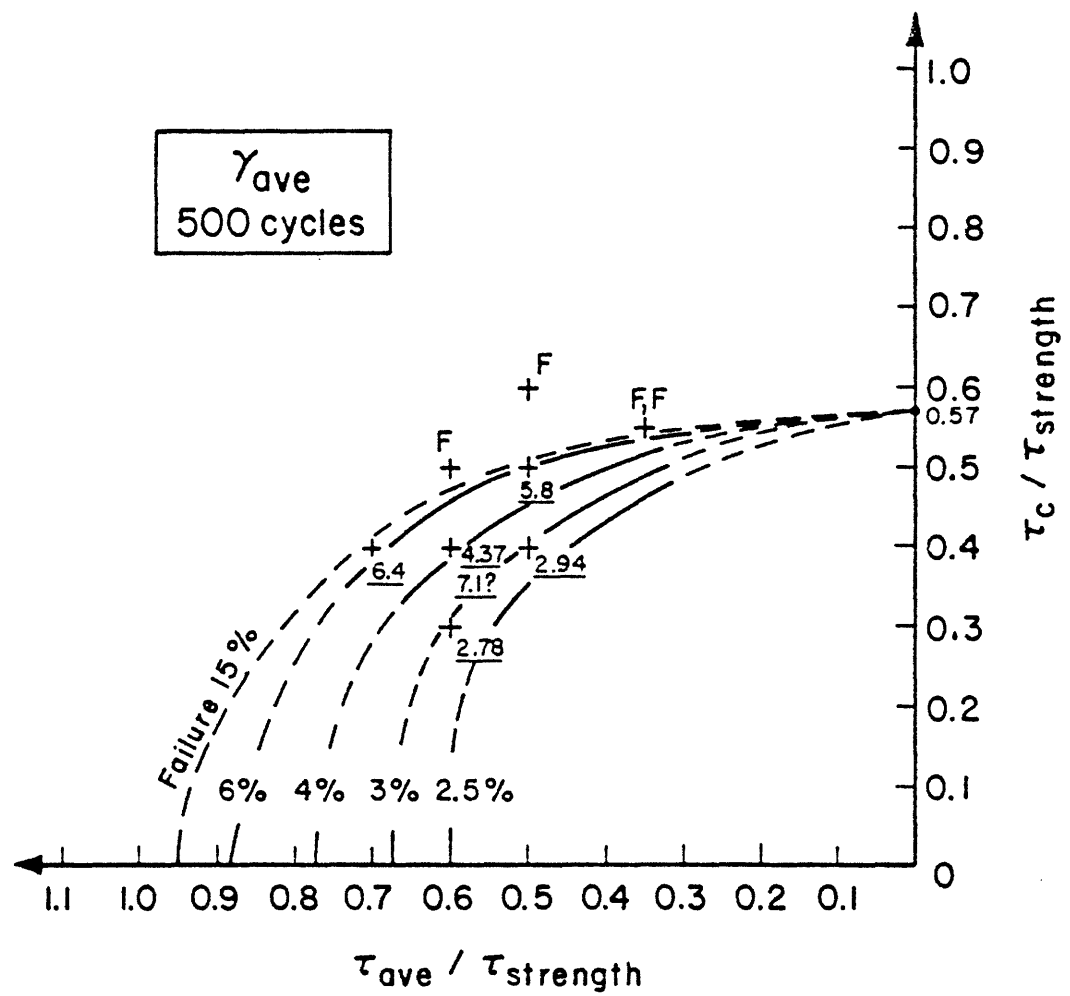


Figure 4.4.5.b Section of iso- $\gamma_{ave}$  network at  $N = 500$  cycles.

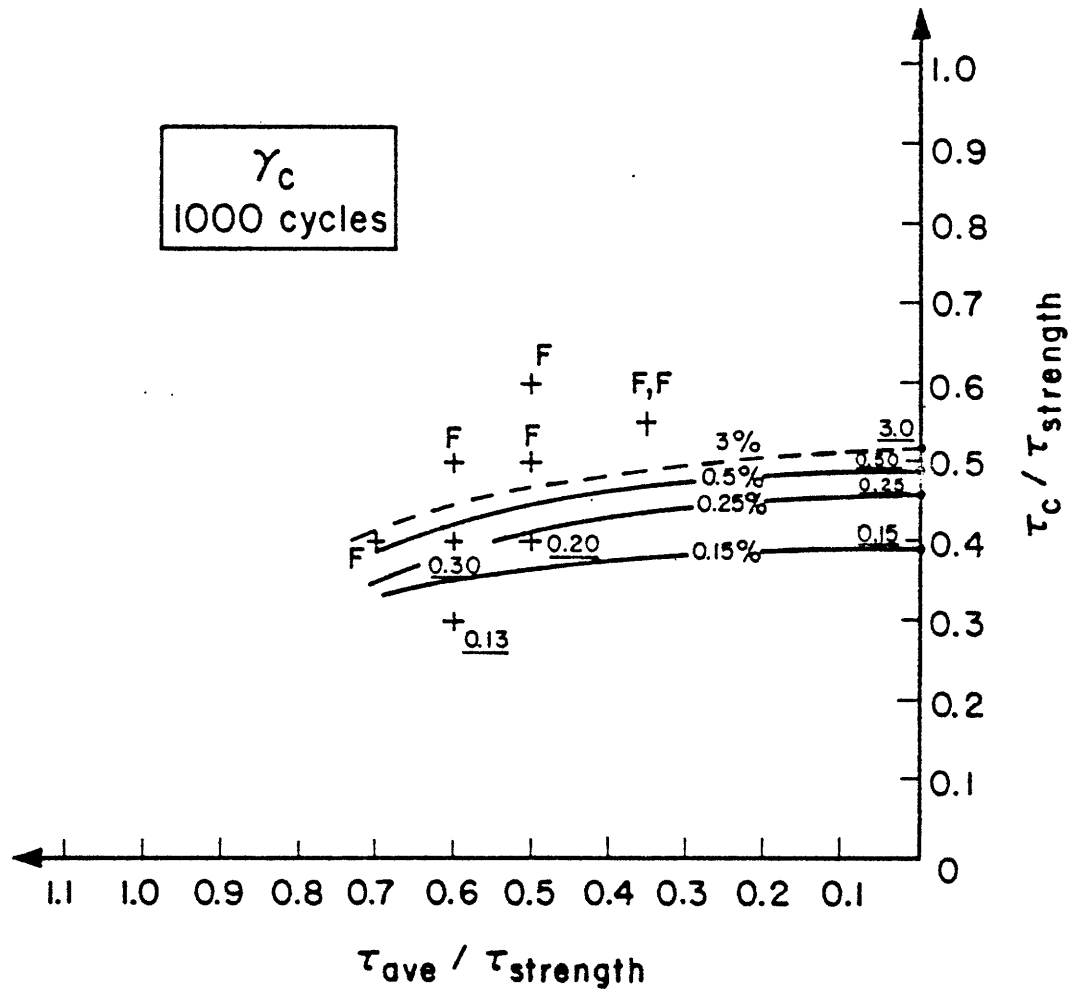


Figure 4.4.6.a Section of iso- $\gamma_c$  network at N = 1000 cycles.



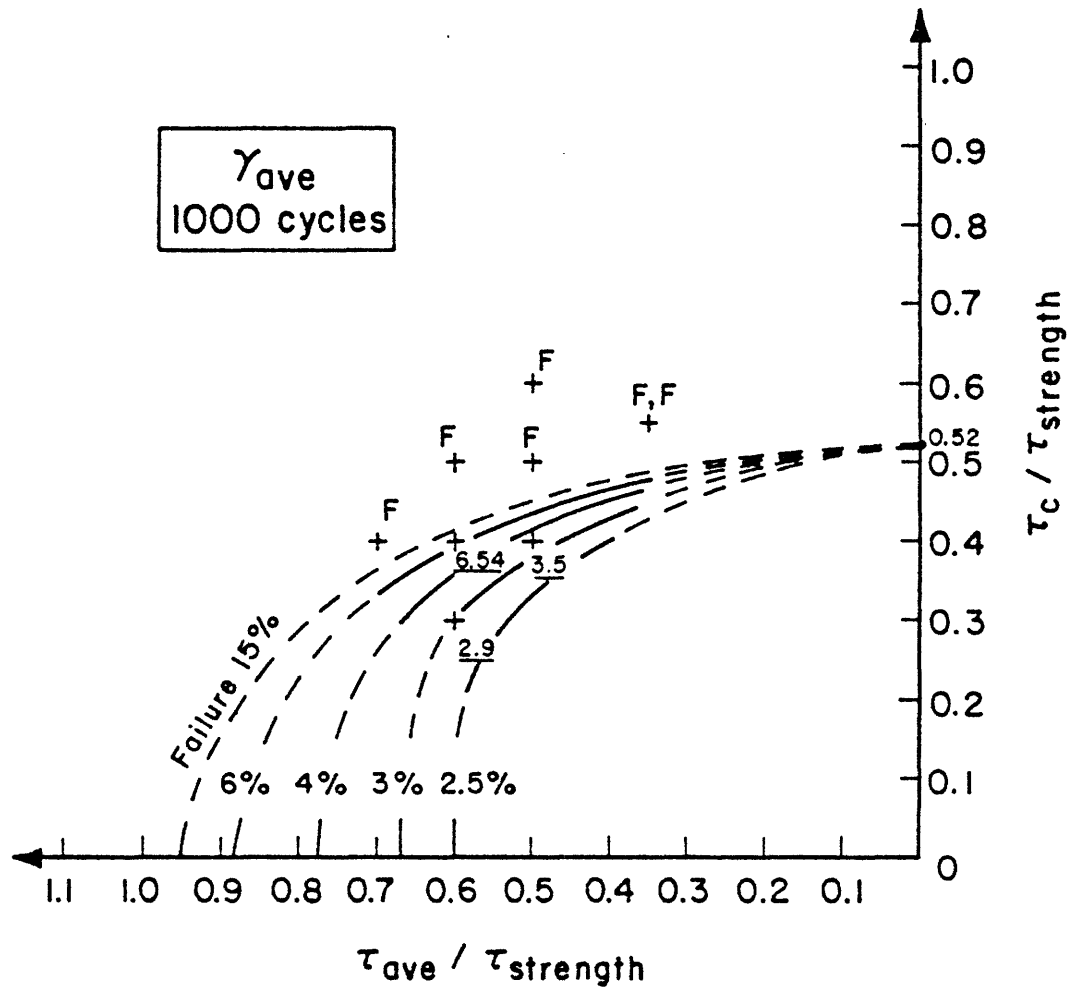


Figure 4.4.6.b Section of iso- $\gamma_{ave}$  network at N = 1000 cycles.

The iso- $\gamma_{ave}$  networks are represented with an accumulation point on the  $\tau_c$ -axis (see also next section for interpretation). It is believed that the locus of the accumulation points corresponds to an imaginary curve on Andersen's plane (Figure 4.4.1) towards which the iso- $\gamma_c$  network converges for large  $\gamma_c$ . Along the  $\tau_{ave}$  axis, and for all N values, the iso- $\gamma_{ave}$  networks are consistent with the deformations obtained at the end of the drained creep, which requires the assumption that the undrained creep occurring during the storm loading is negligible. The locations of the 4 % and 6 % points had to be extrapolated (see Figure 4.C.3). It can also be seen on Figures 4.4.3 through 4.4.6 that curves extrapolating the behavior to  $\gamma_c = 3 \%$  and to  $\gamma_c = 15 \%$  ("failure") have been added (they will be needed to define a complete data base for the future estimation procedure).

#### 4.4.2 Degradation of the iso- $\gamma_c$ network

Let us now consider the degradation with time of each specific iso-deformation curve by first superimposing on one diagram all the iso- $\gamma_c$  curves corresponding to a given  $\gamma_c$  (e.g. 0.5 %). Each of these curves will be indexed by its corresponding number of cycles (50, 100, 200, 500 or 1000). Figures 4.4.8.a to c present the resulting diagrams (for  $\gamma_c = 0.15, 0.25$  and 0.50 %). One can see that :

- the degradation is very consistent. There is no overlapping of the curves, and a rather regular pattern appears.
- the lower is the  $\gamma_c$ , the flatter the curves. There is very little dependence of  $\gamma_c$  on  $\tau_{ave}$  for the lower values of  $\gamma_c$ , and for all  $\gamma_c$  one notes a very flat zone close to the  $\tau_c$  axis.
- the lower is the  $\gamma_c$ , the denser are the curves. It will take a

large number of cycles to reach  $\gamma_c = 0.15\%$  at point P of Figure 4.2.1.a while  $\gamma_c = 0.5\%$  will be obtained more quickly at point Q of Figure 4.4.8.c. The high density of the curves is an indication of stability in the zone located underneath.

#### 4.4.3 Degradation of the iso- $\gamma_{ave}$ network

Similar results are presented in Figures 4.4.8.a to d for the iso- $\gamma_{ave}$  curves. These figures also show a very characteristic pattern. A low values of  $\tau_c$  the iso- $\gamma_{ave}$  curves are seen to be relatively insensitive to changes of  $\tau_c$ . The curves converge very abruptly on the  $\tau_{ave}$  axis. For large values of  $\tau_{ave}$  this zone will probably be controlled by the drained creep under  $\tau_{cons}$  and the undrained creep which should not be neglected (as we have done). More tests are necessary in this zone.

For high values of  $\tau_c$  and low values of  $\tau_{ave}$  the curves seem to maintain their overall shape with a tendency to become flatter as the number of cycles increases. The erosion of the domain of stability (between the network and the axes) is clearly associated with  $\tau_c$  rather than with  $\tau_{max}$ . For a given value of  $\tau_{max}$  there seem to be an optimal value of  $\tau_c$  at which the resistance to degradation is maximum (the iso- $\gamma_{ave}$  curves are tangential to the lines of equal  $\tau_{max}$  at such a point).

These graphs allow for a simple estimation of the number of cycles necessary to reach a selected value of  $\gamma_{ave}$ . Another interesting representation permitting one to appreciate the evolution of the networks with N is given in Figure 4.4.9 where the graphs of Figures 4.4.3 (N = 100) and 4.4.6 (N = 1000) have been superimposed.

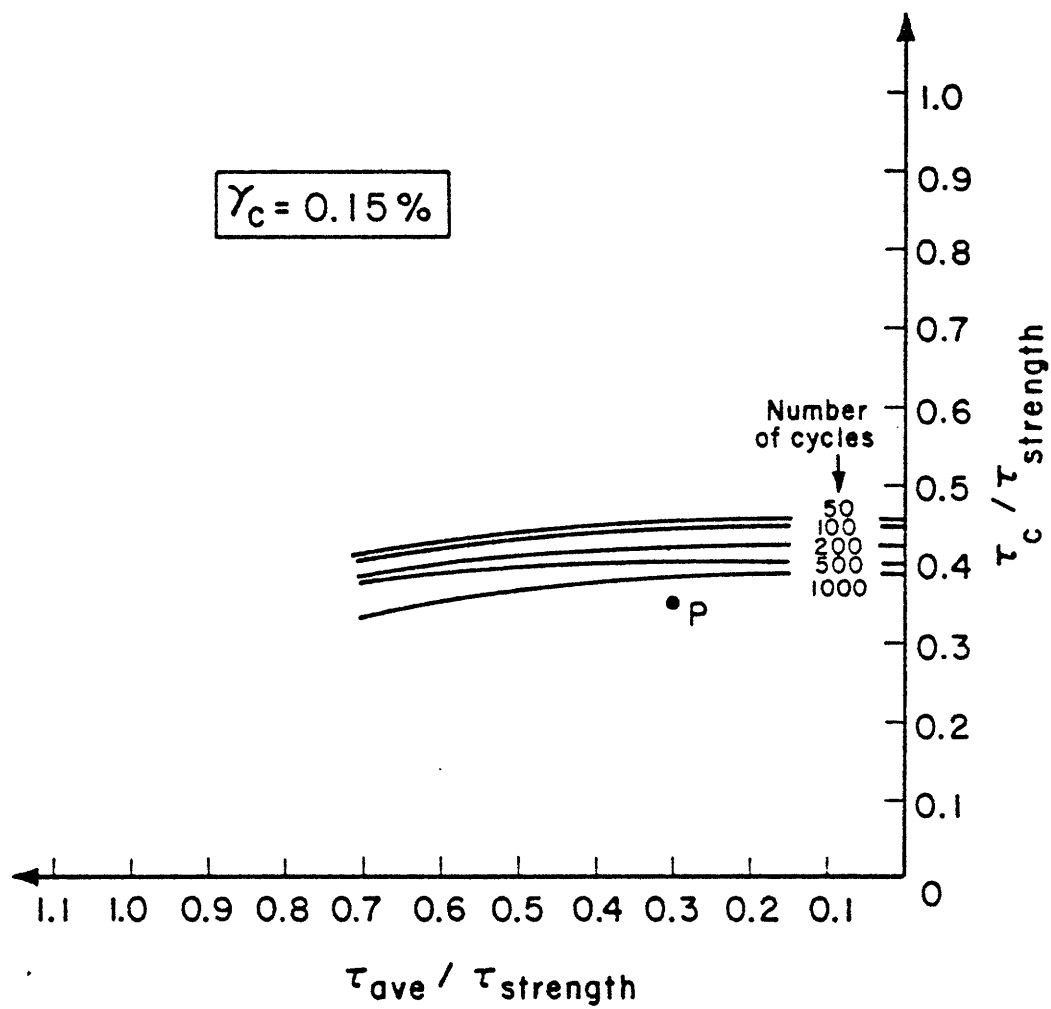


Figure 4.4.7.a Sections of iso- $\gamma_c$  surface for  $\gamma_c = 0.15\%$  at various numbers of cycles.

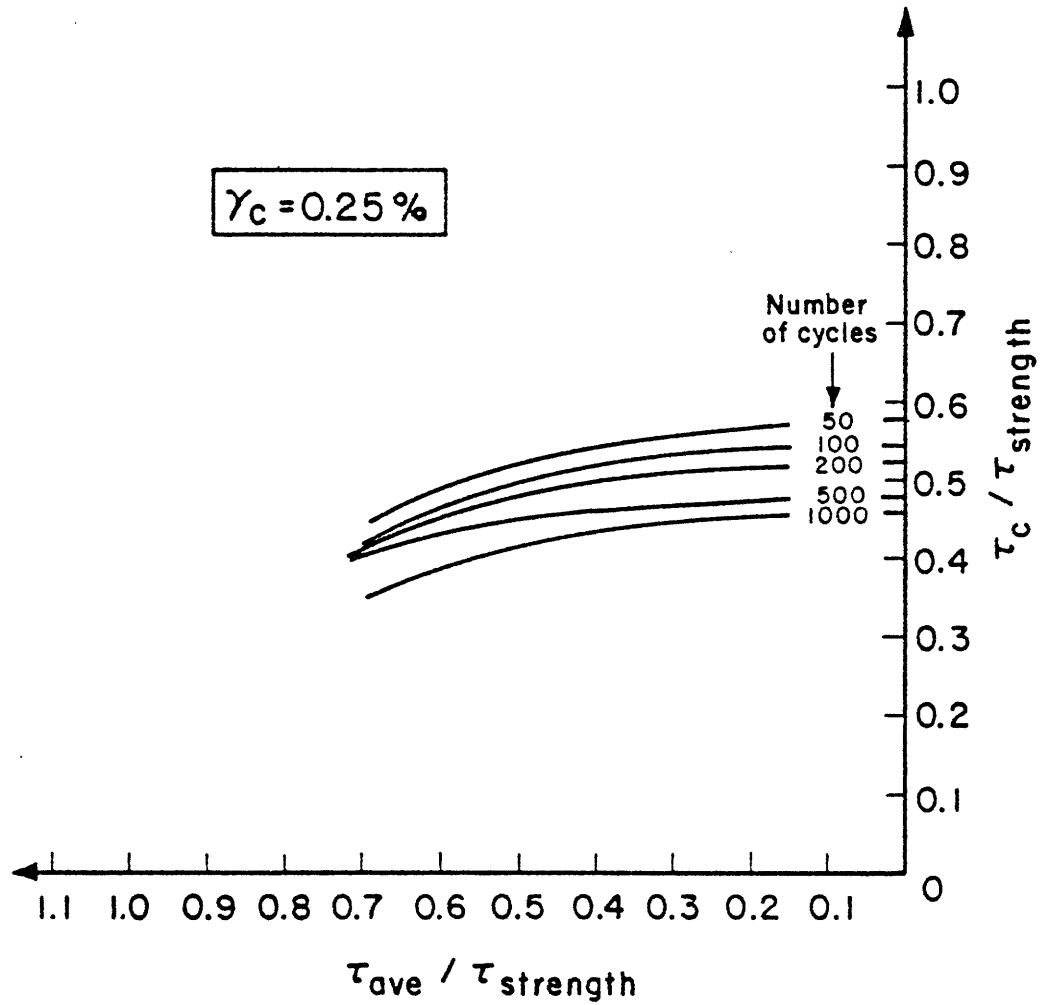


Figure 4.4.7.b Sections of iso- $\gamma_c$  surface for  $\gamma_c = 0.25\%$  at various numbers of cycles.

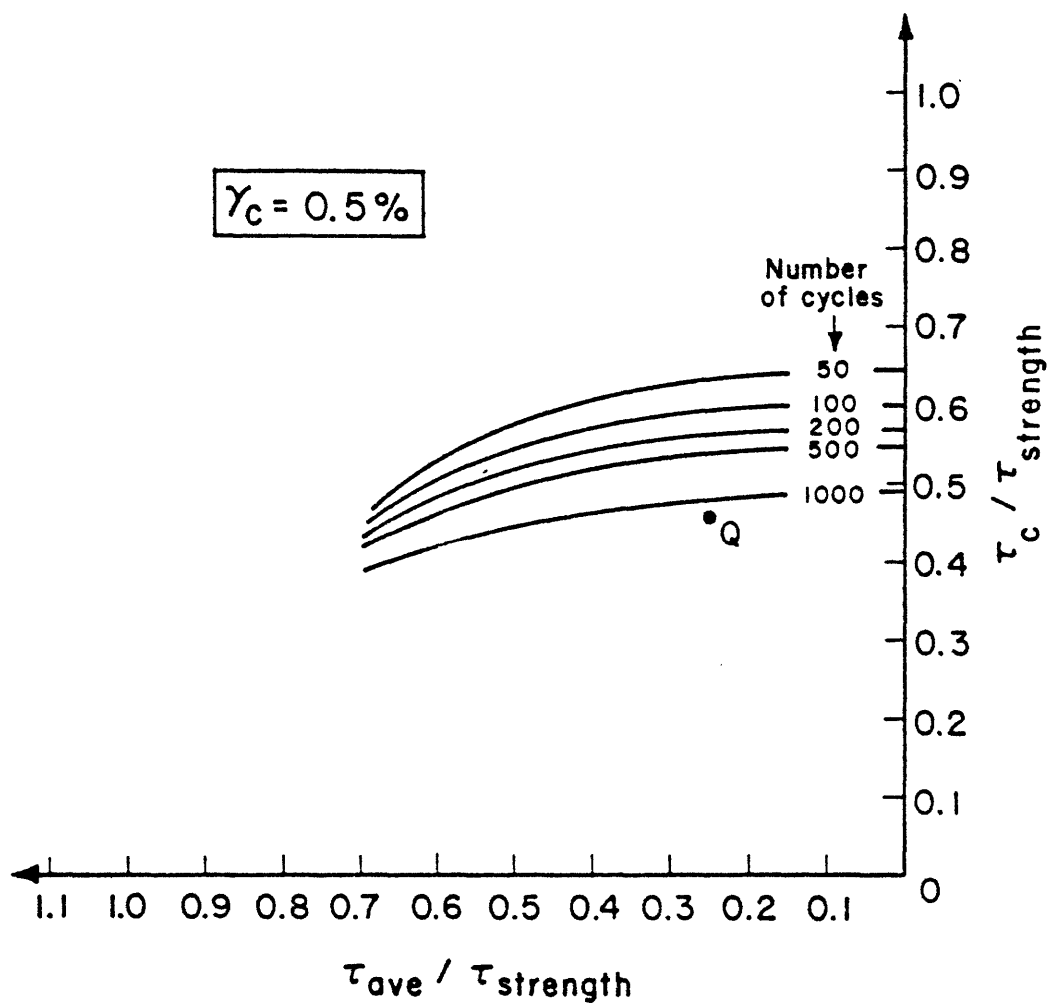


Figure 4.4.7.c Sections of iso- $\gamma_c$  surface for  $\gamma_c = 0.5\%$  at various numbers of cycles.

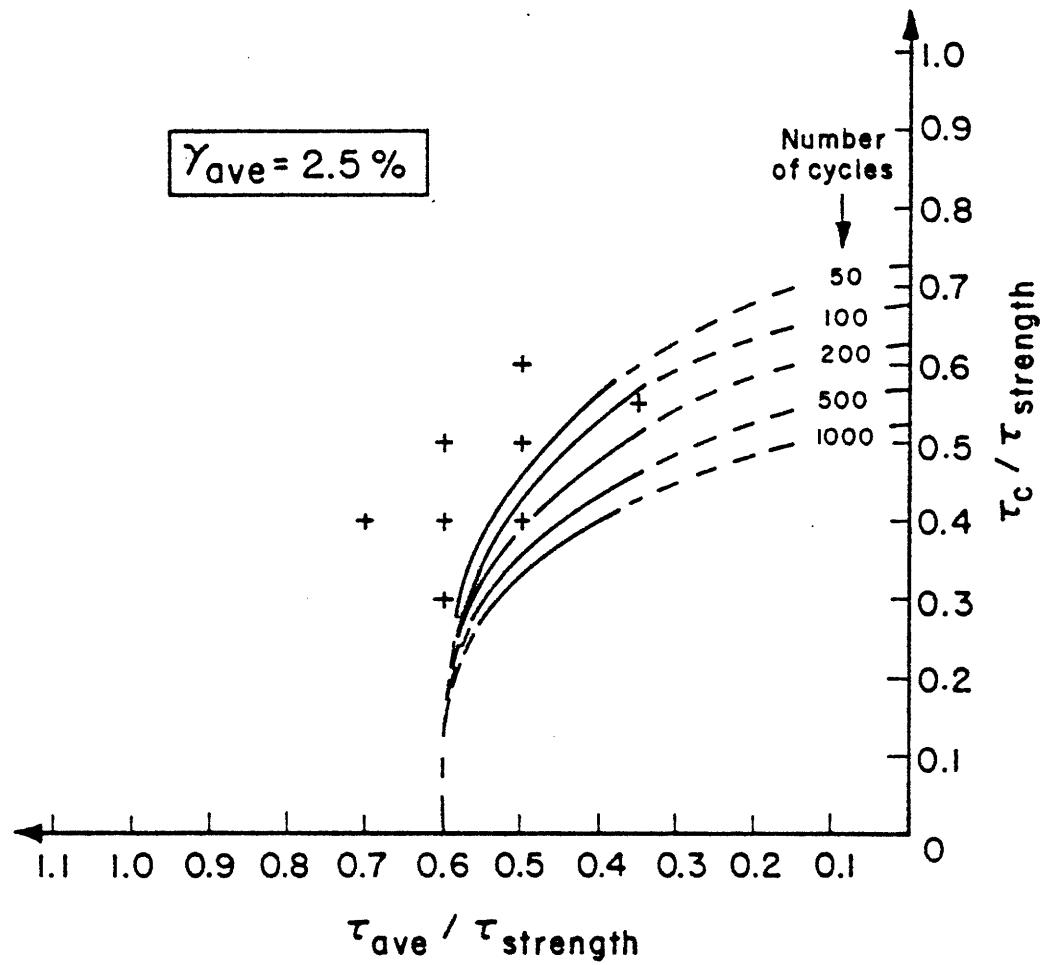


Figure 4.4.8.a Sections of iso- $\gamma_{ave}$  surface for  $\gamma_{ave} = 2.5\%$  at various numbers of cycles.

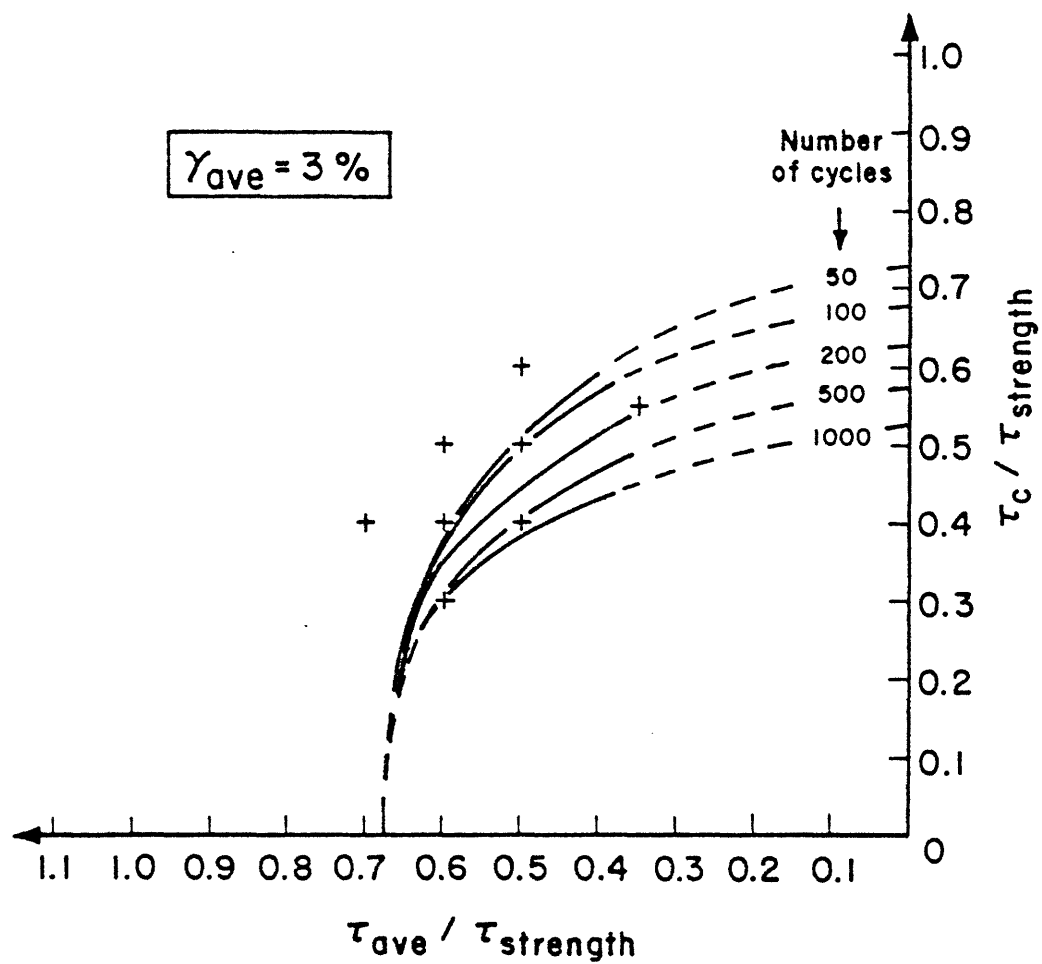


Figure 4.4.8.b Sections of iso- $\gamma_{ave}$  surface for  $\gamma_{ave} = 3\%$  at various numbers of cycles.



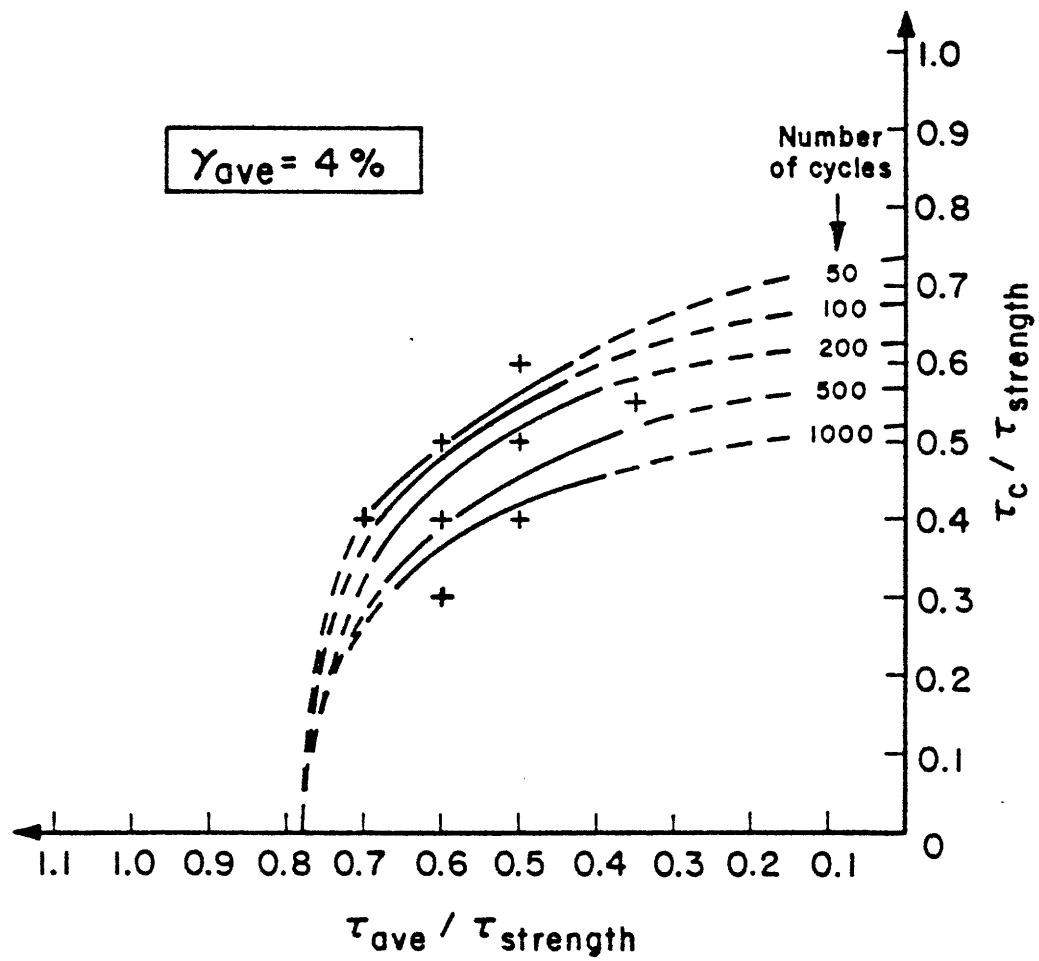


Figure 4.4.8.c Sections of iso- $\gamma_{ave}$  surface for  $\gamma_{ave} = 4\%$  at various numbers of cycles.

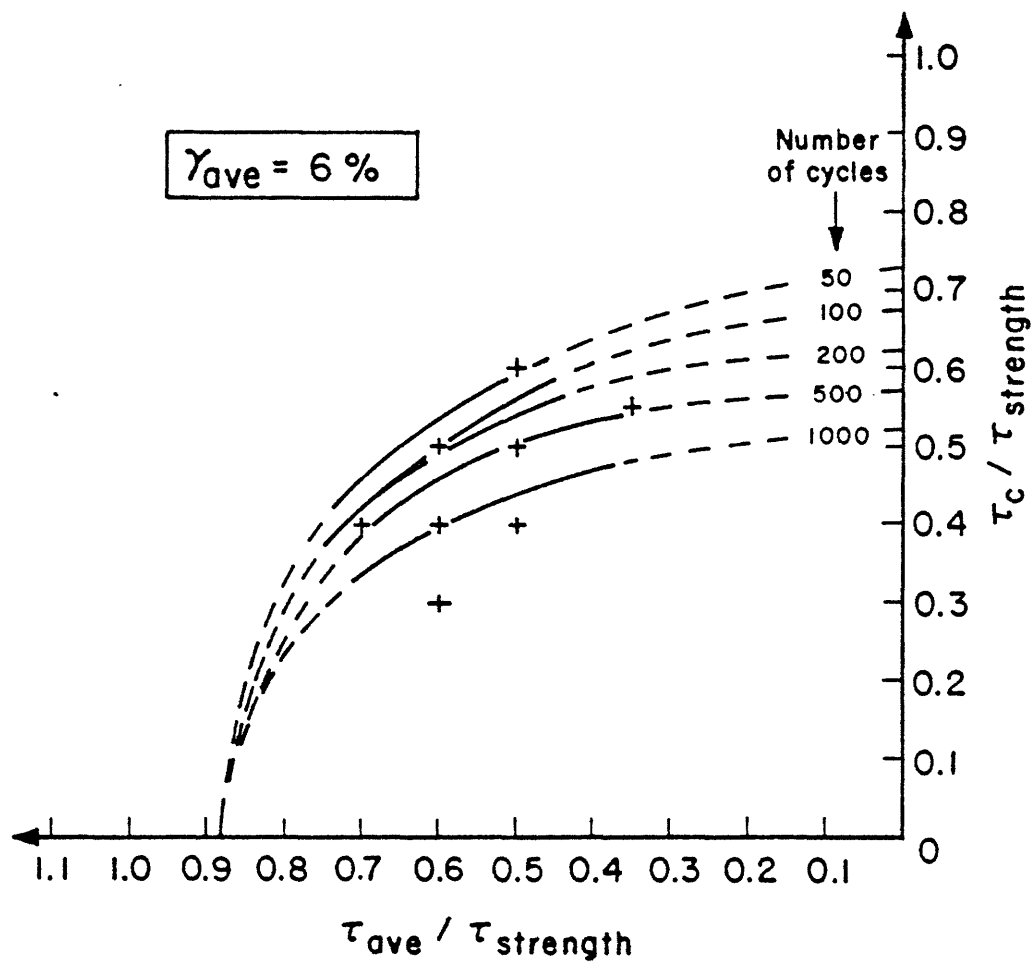


Figure 4.4.8.d Sections of iso- $\gamma_{ave}$  surface for  $\gamma_{ave} = 6\%$  at various numbers of cycles.

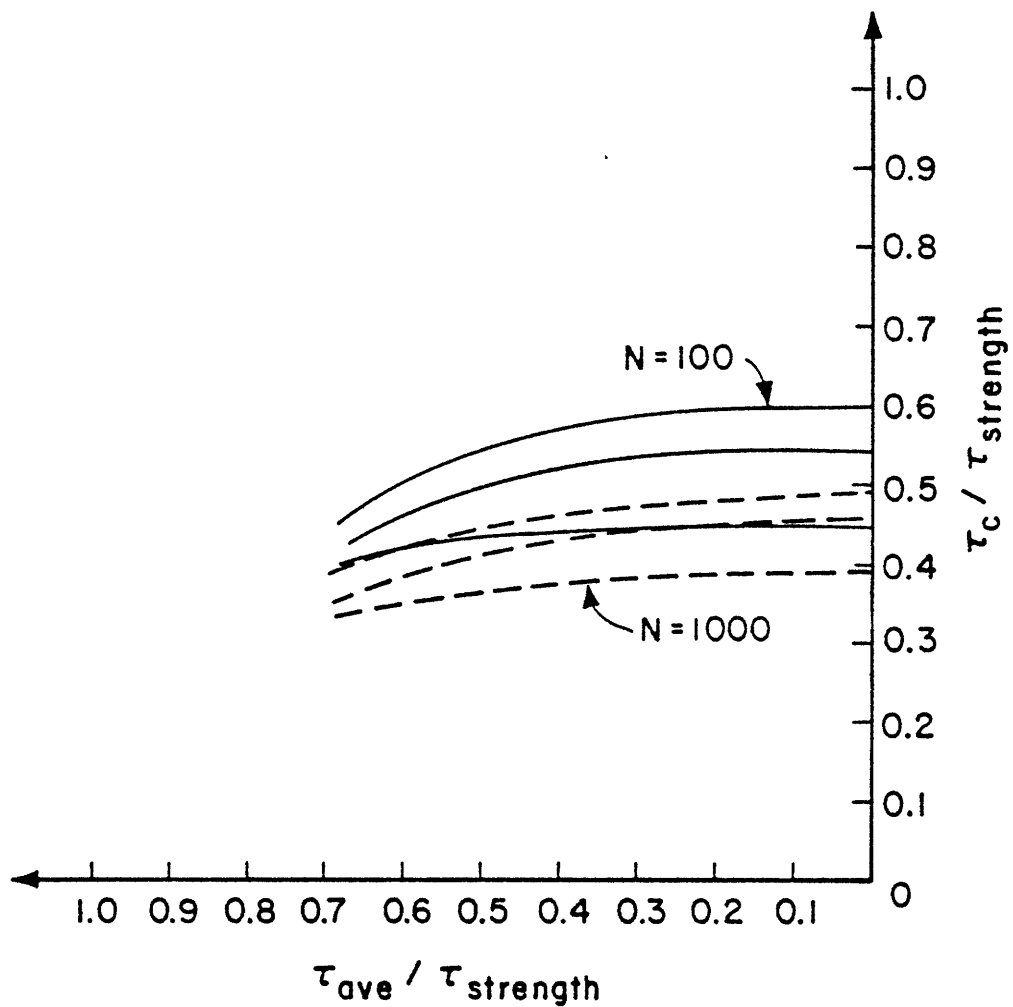


Figure 4.4.9.a Sections of the iso- $\gamma$  network at  $N = 100$  and  $N = 1000$ .

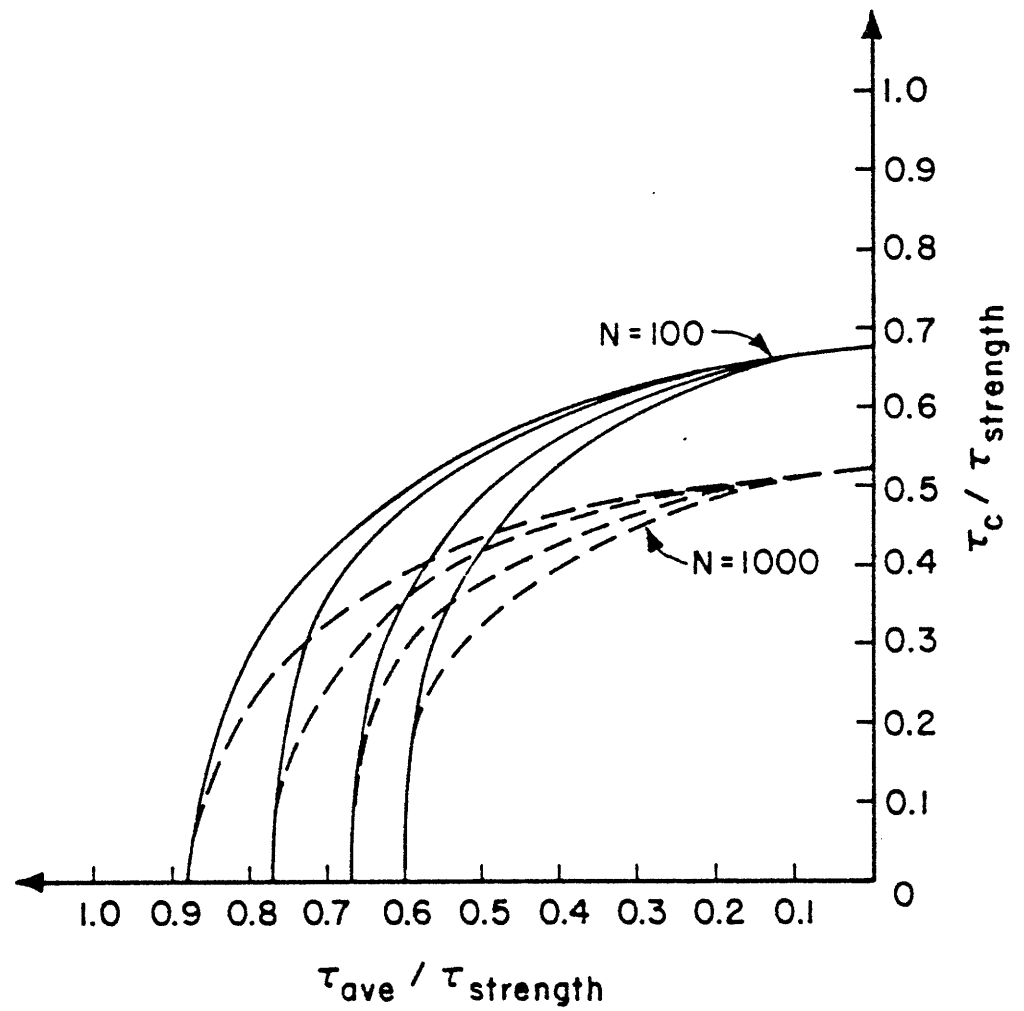


Figure 4.4.9.b Sections of the iso- $\gamma_{ave}$  network at  $N = 100$  and  $N = 1000$ .

With some practice it will be seen that all these representations allow for an easy reading of the clay behavior under our specific test conditions through clear interpolations and extrapolations covering a wide range of loadings.

## 4.5 COMMENTS AND INTERPRETATIONS

The preceding section has introduced ideas concerning the shape of the 3-D strain contour diagrams which merit some comments before we consider the study of the variable cyclic loading tests.

### 4.5.1 Shape of the strain contour diagrams

#### 4.5.1.A. The first cycle of loading

Our data do not permit the construction of the  $N = 1$  deformation networks because very small deformations occurred on the first cycle for the specific loading grid that was selected. The objective of the present paragraph is to estimate these  $N = 1$  networks from the consideration of monotonic stress-strain properties. This estimation will then prove to be useful for explaining some of the characteristics of the networks after the first cycle.

The application of  $\tau_{\text{cons}}$  during the drained creep modifies the stress-strain behavior of the clay. The increase of the shear strength with  $\tau_{\text{cons}}$  and the stiffening of the stress-strain curve for a loading applied in the same direction as  $\tau_{\text{cons}}$  are now well documented for several clays (e.g. Ladd and Edgers [58] for Boston Blue Clay (BBC)). Unfortunately such results are still scarce in the case of the Plastic Drammen Clay. Andersen [2] presented results obtained for two static tests run respectively from  $\tau_{\text{cons}} = 0$  and from  $\tau_{\text{cons}} = 0.35 \tau_{\text{strength}}$  under conditions very similar to ours. The  $\tau$ - $\sigma$  plots and the  $\tau$ - $\gamma$  curves for these two tests are shown in Figure 4.5.1.a and b. It can be seen that there is effectively an increase of the shear strength of approximately 15 % for the anisotropically consolidated specimen,

and only a very slight decrease in the peak deformation from about 6 % to 5 % (note that this deformation is measured from the end of anisotropic consolidation position). The stiffening of the stress-strain curve is not really apparent. Based on this limited information, and on the indication from previous studies that the increase of strength and the decrease in peak deformation can be considered, as a first approximation, as proportional to  $\tau_{\text{cons}}$ , one can estimate\* the stress-strain curves that would be obtained at the end of the drained creep. Figure 4.5.2 shows such estimations for  $\tau_{\text{cons}} / \tau_{\text{strength}} = 0.35, 0.50$  and  $0.60$  in the case of a quick test. The fast test corresponds to a rate of loading compatible with the cycling. The effect of the higher strain rate can be modeled in the present case by a 10 % increase of the shear stress at a given strain, based on the comparison between a typical stress-strain curve (Andersen |4|) and the  $N = 1$  curve given by Andersen |2| (this increase is also compatible with the results of Bea and Audibert |9|). The "19 hour curve" of this diagram is identical to the one of Figure 4.C.3. There is very little information on the behavior of the clay from an anisotropic consolidation state when the shearing is applied in the direction opposite to  $\tau_{\text{cons}}$ . The only report of such a test in the literature is presented by Bjerrum and Kenney |11| in 1967, and is reproduced in Figure 4.5.3. (In the case of Drammen clay there is apparently little strain softening so that we will ignore this aspect of the results).

---

\* These curves are obtained by scaling down the fast undrained test curve, corresponding to  $\tau_{\text{cons}} = 0$ , to fit the peaks which are estimated on the basis of the two diagrams on the right of Figure 4.5.2.

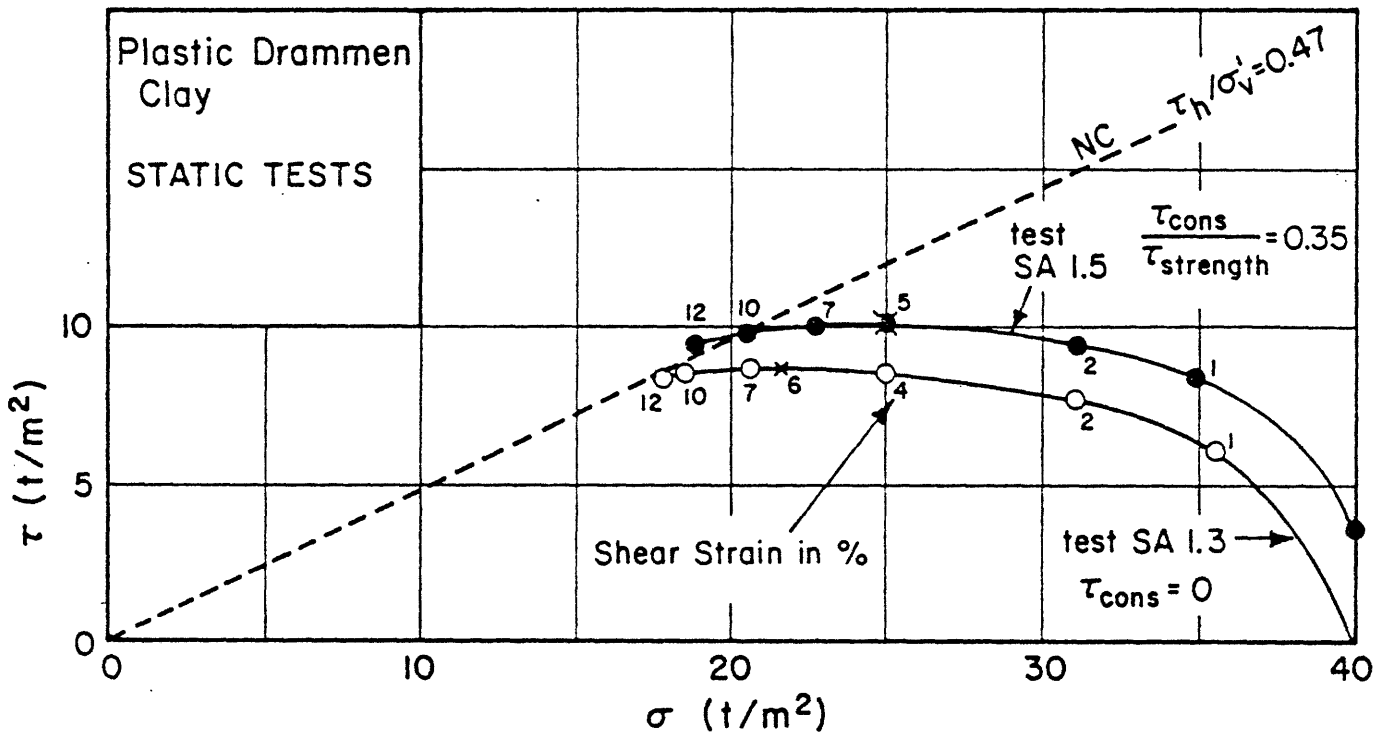


Figure 4.5.1.a Effective stress paths for undrained static simple shear tests.  
(After Andersen [2]).

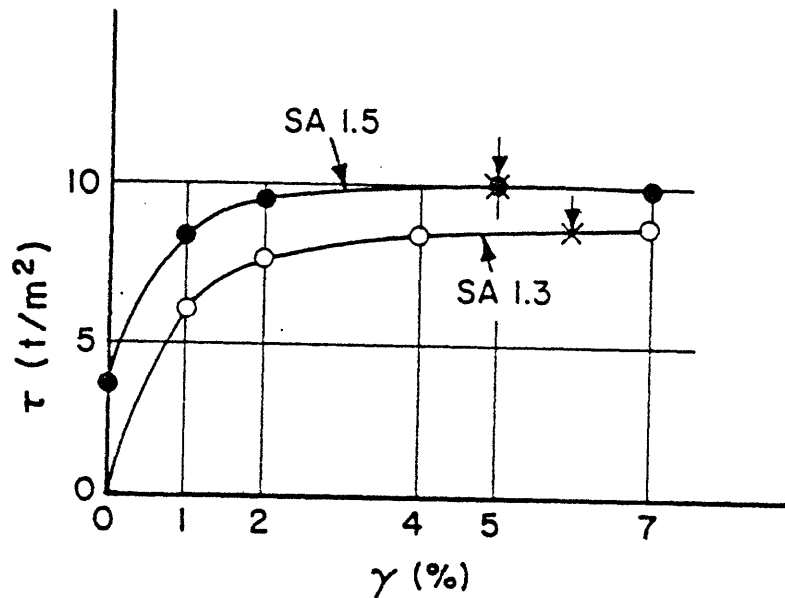


Figure 4.5.1.b Stress-strain curves for undrained static DSS tests.



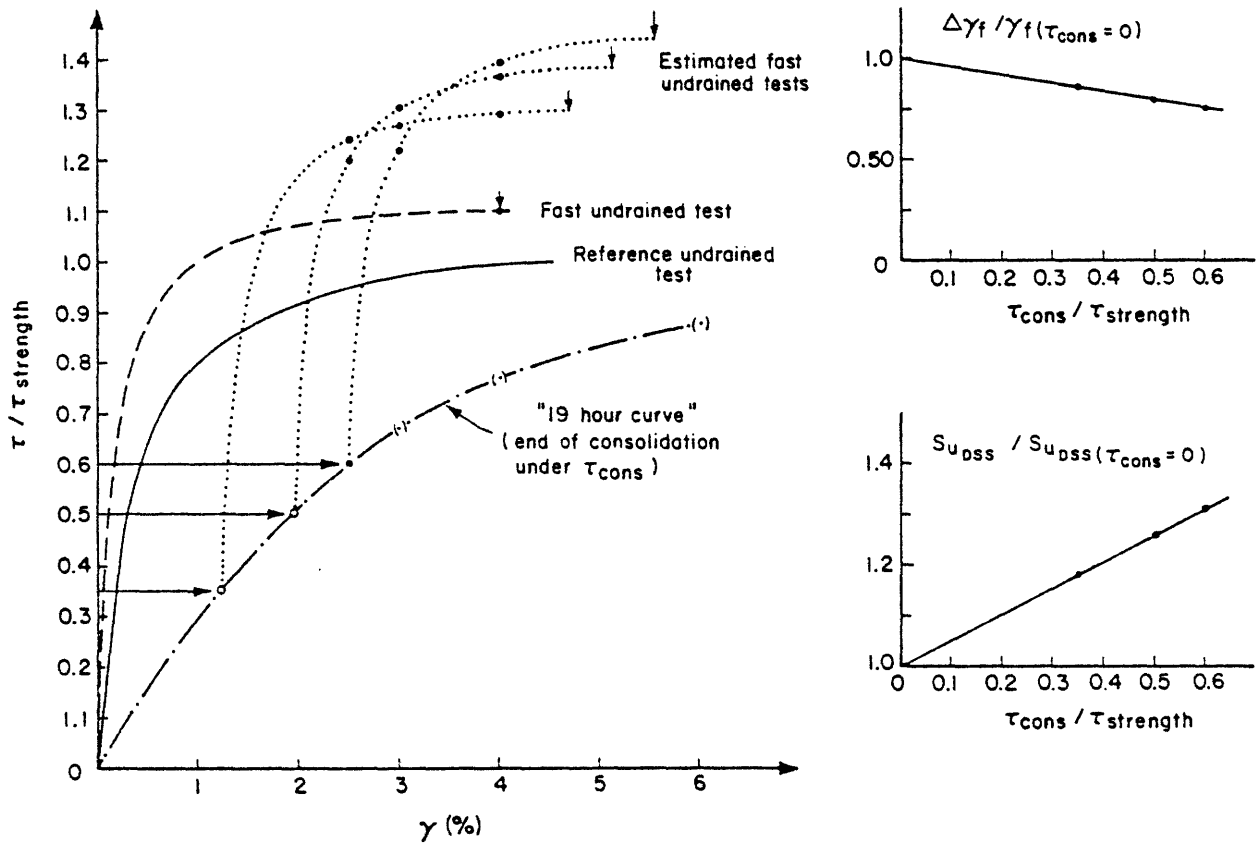
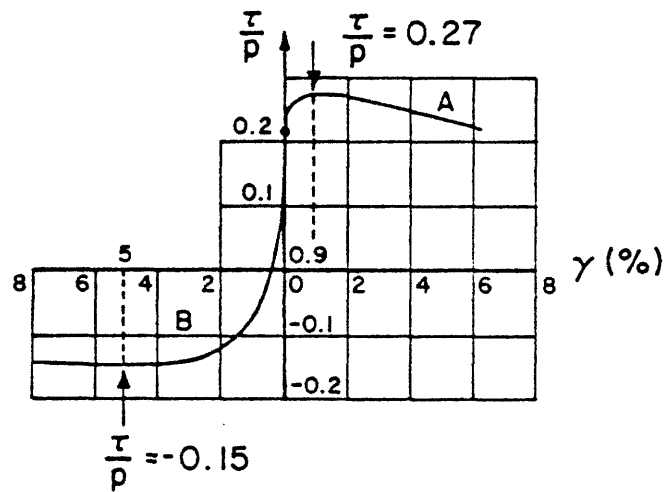
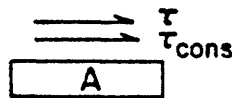


Figure 4.5.2 Stress strain relationships for plastic Drammen Clay.



A Sheared in same direction as the consolidation shear stress.



B Sheared in opposite direction.

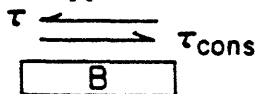


Figure 4.5.3 Undrained DSS on Lierstranda quick clay  
with consolidation under  $\tau_{\text{cons}} \neq 0$ .

(After Bjerrum and Kenney [11]).

The shapes of the two branches A and B up to the peaks are very similar within a scale factor of roughly 6 (the increments of stresses and the increments of strains to the peak are in this ratio :  $\left[ 5/0.9 \approx (0.21 + 0.15) / 0.06 = 6 \right]$ ). Furthermore the absolute difference in strength  $(0.27 + 0.15)$  is approximately equal to twice the strength obtained without  $\tau_{\text{cons}}$  ( $\approx 0.21$ )\*. It appears therefore that the following construction may be useful to estimate the stress-strain curves (first deformation curve of Chapter 3) of an anisotropically\*\* consolidated specimen (see Figure 4.5.4).

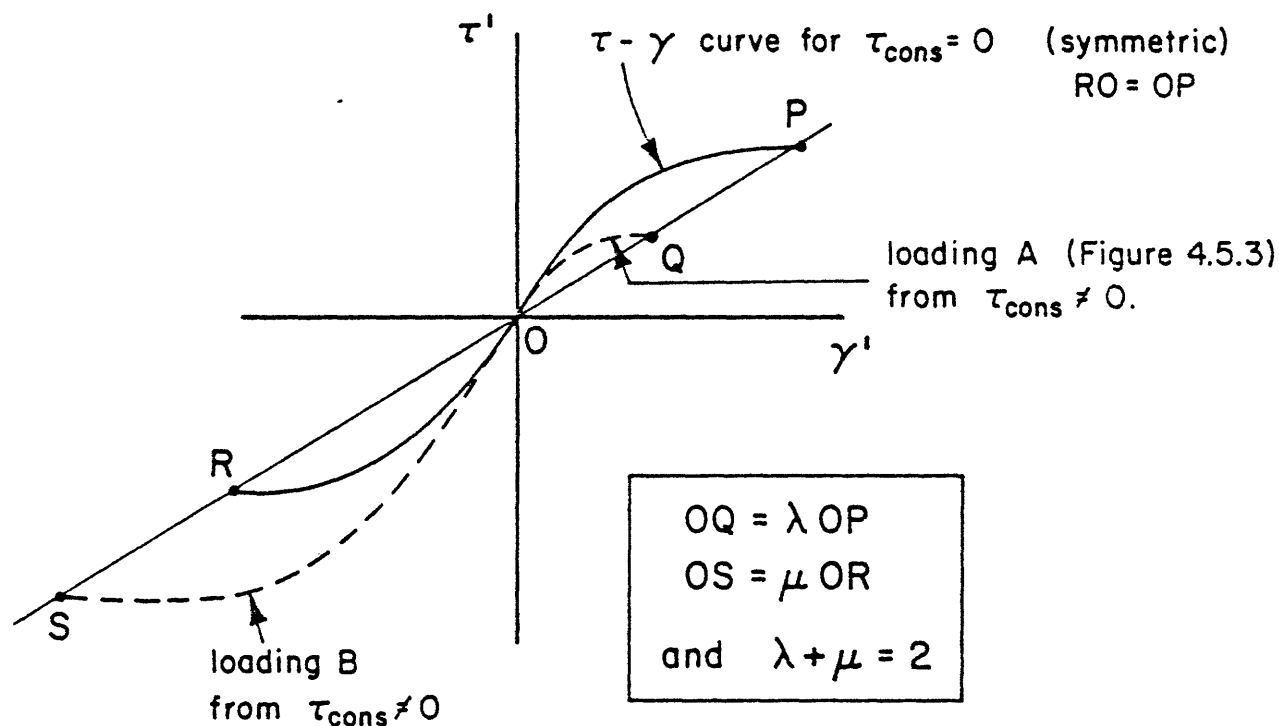


Figure 4.5.4 Use of asymmetric P-bodies to model effect of consolidation under  $\tau_{\text{cons}}$ .

\* The consolidation shear stress was applied during a drained test.

\*\*  $\tau_{\text{cons}} \neq 0$ .

In this figure  $\tau'$  is equal to  $\tau - \tau_{\text{cons}}$  and  $\gamma'$  to  $\gamma - \gamma_{\text{cons}}$ . Distance OQ is obtained by scaling OP by a factor  $\lambda$  while  $OS = \mu OR$ , with  $\lambda + \mu = 2$ . The slope at point O is therefore the same for curves ROP and SOP. In other words, in the case of the Plastic Drammen Clay any fast test curves starting from anisotropic conditions can be very simply estimated from the fast test curve starting from isotropic condition by a symmetry with respect to the origin of the same type as the one that was introduced in section 3.3 followed by a translation to match the post-consolidation position. The associated Iwan models will have the property of sharing the same relationship

$$\tau_c = S(\gamma_c)$$

whatever the value of  $\tau_{\text{cons}}$ .

The trace of the iso- $\gamma_c$  network on the  $N = 1$  plane will therefore be constituted of lines parallel to the  $\tau_{\text{ave}}$  axis.

Let us now return to Figure 4.5.2. For the three values of  $\tau_{\text{cons}}$  that are represented we can easily obtain the  $\gamma_{\text{max}}$  corresponding to a given  $\tau_c$ . This has been done systematically in Figure 4.5.5 for  $\gamma_{\text{max}} = 2.5, 3, 4$  and  $6\%$  where the trace of the iso- $\gamma_{\text{max}}$  network has also been estimated. With the knowledge of the horizontal  $\gamma_c$  network we can then construct point by point the trace of the iso- $\gamma_{\text{ave}}$  network by difference. (To illustrate the procedure on two points let us consider the estimated fast undrained test curve for  $\tau_{\text{cons}}/\tau_{\text{strength}} = 0.60$  in Figure 4.5.5 at  $\gamma = \gamma_{\text{max}} = 4\%$  (point A). This point is obtained for  $\frac{\tau}{\tau_{\text{strength}}} = 1.4$ , so that  $\frac{\tau_{\text{max}}}{\tau_{\text{strength}}} = 1.4$  and  $\frac{\tau_{\text{ave}}}{\tau_{\text{strength}}} = 0.60$  leads to  $\frac{\tau_c}{\tau_{\text{strength}}} = 0.8$  (the corresponding point in Figure

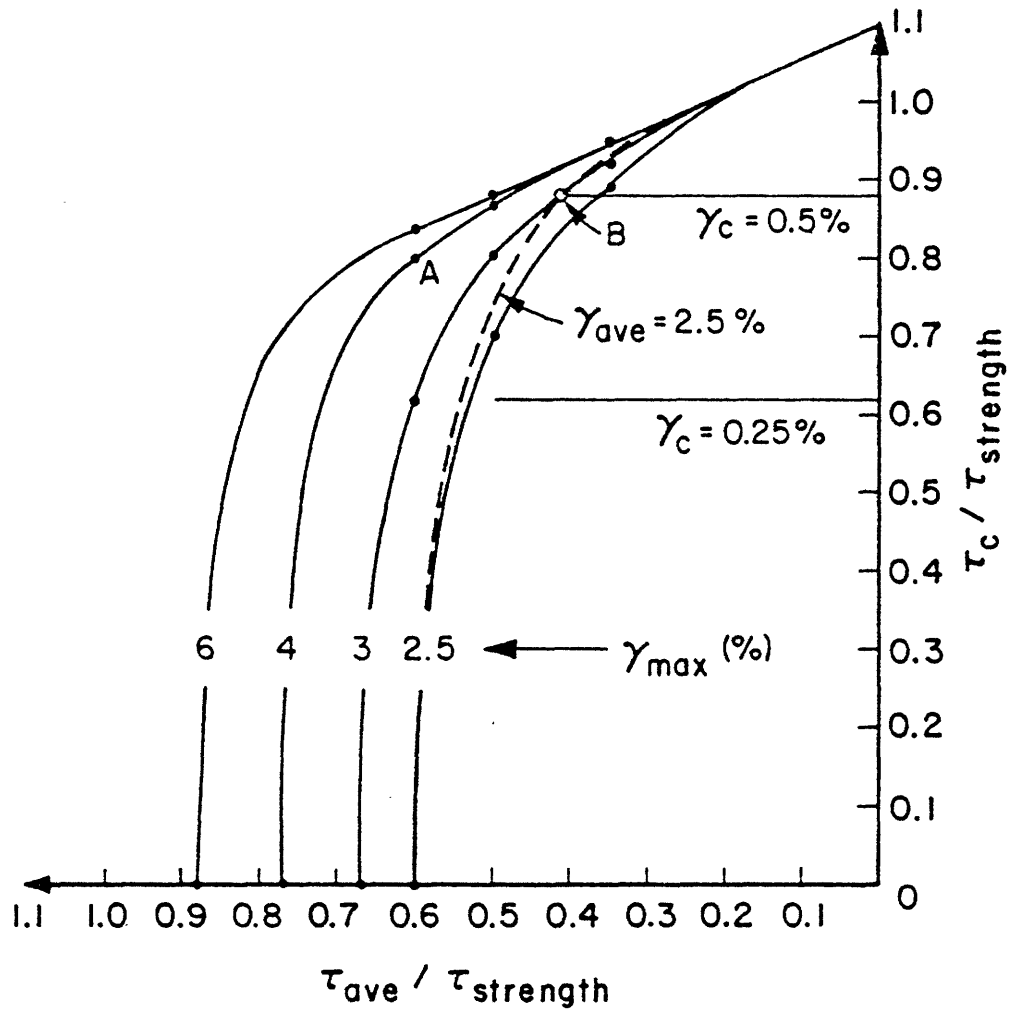


Figure 4.5.5 Estimation of  $\gamma_{\text{ave}}$  at  $N = 1$ .

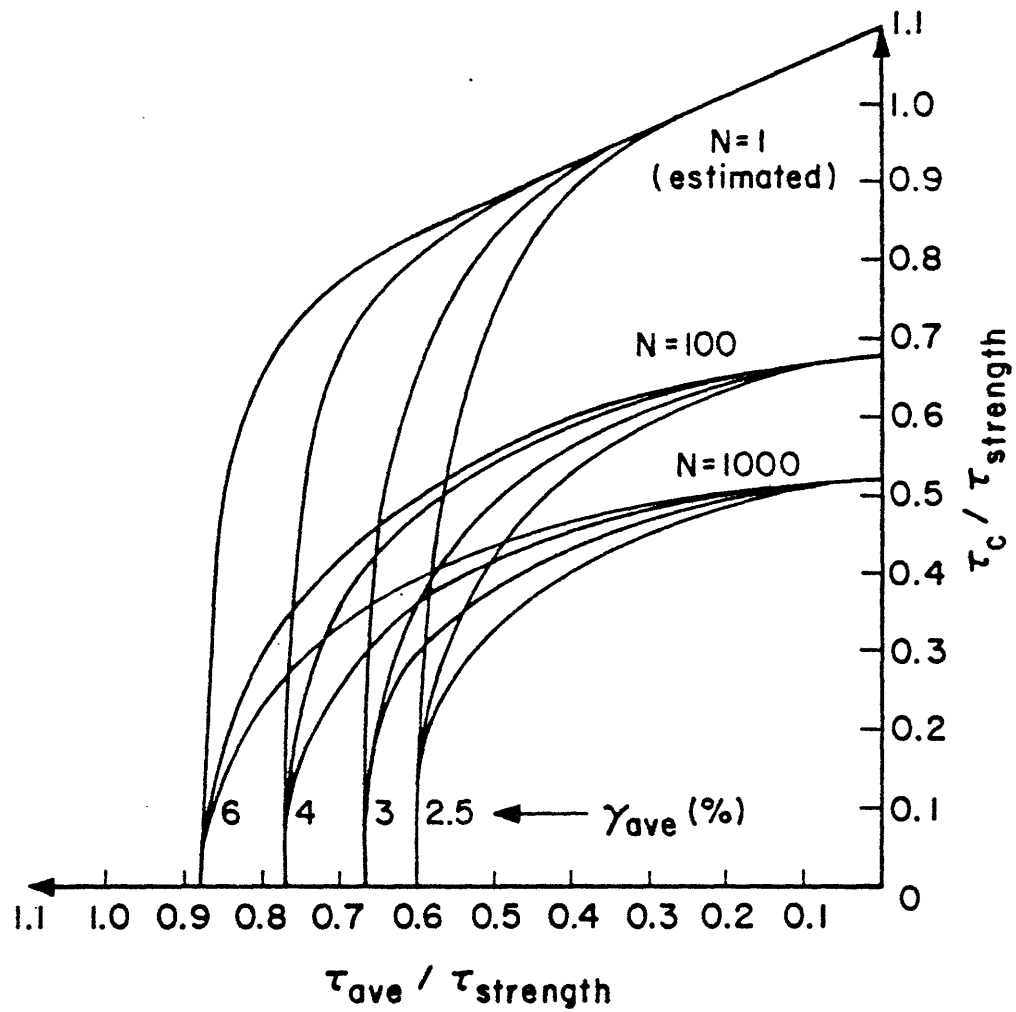


Figure 4.5.6 Comparison of iso- $\gamma_{\text{ave}}$  networks.

4.5.5 is also called A). Point B on Figure 4.5.5 corresponds to  $\gamma_{ave} = 2.5\%$  since it is at the intersection of the  $\gamma_{max} = 3\%$  curve with the  $\gamma_c = 0.5\%$  curve). This estimated iso- $\gamma_{ave}$  network at  $N = 1$  has been reported in Figure 4.5.6 together with the results for  $N = 100$  and  $1000$  of Figure 4.4.10.b.

It is important to note the existence of an accumulation point at  $\tau_c = 1.1 \tau_{strength}$  and  $\tau_{ave} = 0$  in Figure 4.5.5. All the iso- $\gamma_{max}$  curves converge at this point and it should be clear that by construction all the iso- $\gamma_{ave}$  curves must also converge.

#### 4.5.1.B. After the first cycle

The study of Figures 4.4.2 to 4.4.6 has shown that the  $\gamma_c$ -network remained quite independent of the average shear stress  $\tau_{ave}$  for values of  $\tau_{max}$  smaller than approximately  $100\% \tau_{strength}$ . This observation seems to indicate that the use of an asymmetric Iwan model (with  $\lambda + \mu = 2$ ) might be reasonable during the cyclic loading, but of course the characteristics of this Iwan model will change with time.

One of the most delicate ideas introduced in the  $\gamma_{ave}$ -networks of Figures 4.4.2 to 4.4.6 is the existence of an accumulation point on the  $\tau_c$  axis at each  $N$  (and therefore of a locus of accumulation points in the Anderson plane). The interpretation of these points is not as clear as in the  $N = 1$  plane. The idea is that when  $\gamma_c$  becomes very large a very small change of  $\tau_{ave}^*$  may result in a large value of  $\gamma_{ave}$ ; however at the present time this idea cannot be proved and remains a convenient assumption. It has been suggested to us that the network of  $\gamma_{ave}$  might become asymptotic to the  $\tau_c$  axis but it should be recognized that the trace of this same  $\gamma_{ave}$

---

\* From the beginning of the cycling.

network on the  $N = 1$  plane is an absolute bound. In other words a point in the  $N = 1$  plane corresponding to a high value of  $\tau_{\max}$  and a low  $\tau_{\text{ave}}$ , and associated for example with  $\gamma_{\text{ave}} = 4\%$ , can only be associated with a higher value of  $\gamma_{\text{ave}}$  for  $N > 1$ . This does not mean that the  $\gamma_{\text{ave}}$  network will converge exactly at a point, but we think that it will correspond to a small region along the  $\tau_c$  axis that will follow the zone of very large  $\gamma_c$  in pure symmetric shearing ( $\tau_{\text{ave}} = 0$ ) as the number of cycles increases.

#### 4.5.2 Interpretations of the variable cyclic tests

Tests ⑨ and ⑩ of the program have variable cyclic loadings in which  $\tau_{\text{ave}}$  is maintained equal to  $\tau_{\text{cons}}$  but where the value of  $\tau_c$  is changed at selected cycles. The problem then becomes to estimate the evolution of the deformation on the basis of the elementary tests run at constant value of  $\tau_c$ .

##### 4.5.2.A. Andersen's procedure

An approximate procedure of estimation has been proposed with some success by Andersen [3] for the case of  $\tau_{\text{cons}} = 0$ . In essence Andersen assumes that the whole past history of the soil is implicitly included in  $\gamma_c$  ( $\gamma_{\text{ave}}$  is always zero in this case). Let us consider  $\gamma_c = \gamma_{c,N}$  corresponding to the cyclic strain in cycle  $N$  of the loading while  $\tau_c = \tau_{c,N}$  (see Figure 4.5.7). If we change the applied stress at the end of this cycle there will be an immediate change of  $\gamma_c$ , called  $\Delta\gamma_{c,i}$  ( $i$  stands for immediate), corresponding to the stress change from  $\tau_{c,N}$  to  $\tau_{c,N+1}$ . Then if  $\Delta N$  cycles are applied with  $\tau_c = \tau_{c,N+1}$  the resulting  $\gamma_c$  will be  $\gamma_{c,N+\Delta N}$  where :



$$\gamma_{c,N+\Delta N} = \underbrace{\gamma_{c,N}}_{\substack{\text{Cyclic Shear} \\ \text{Strain after} \\ \text{N} + \Delta\text{N} \text{ cycles}}} + \underbrace{\Delta \gamma_{c,i}}_{\substack{\text{Immediate Change} \\ \text{in } \gamma_c \text{ due to change} \\ \text{of } \tau_c \text{ from } \tau_{c,N} \text{ to } \tau_{c,N+1}}} + \underbrace{\Delta \gamma_{c,\Delta N}}_{\substack{\text{Increase in} \\ \text{cyclic strain} \\ \text{due to } \Delta\text{N} \\ \text{cycles under} \\ \text{cyclic shear} \\ \text{stress} \\ \tau_{c,N+1}}}$$

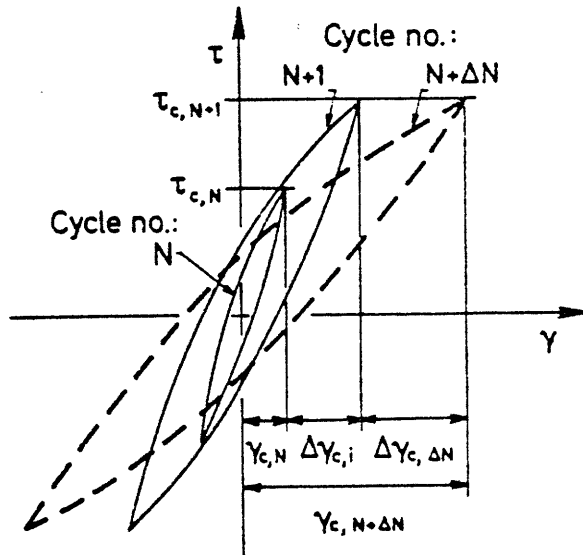


Figure 4.5.7 Andersen's procedure.

Andersen then assumes that :

- the immediate change in shear strain,  $\Delta\gamma_{c,i}$  due to the change in cyclic shear stress,  $\tau_{c,N+1} - \tau_{c,N}$  is the same as the one that would have been obtained in the first load cycle ( $N = 1$ ),
- the increase in cyclic shear strain  $\Delta\gamma_{c,\Delta N}$  due to  $\Delta N$  cycles with a cyclic shear stress  $\tau_c = \tau_{c,N+1}$  is the same as that which would be obtained from a constant stress test with  $\tau_c = \tau_{c,N+1}$  from  $\gamma_{c,N+1}$   $\left[ = \gamma_{c,N} + \Delta\gamma_{c,i} \right]$  and for  $\Delta N$  cycles. (See Figure 4.5.8).

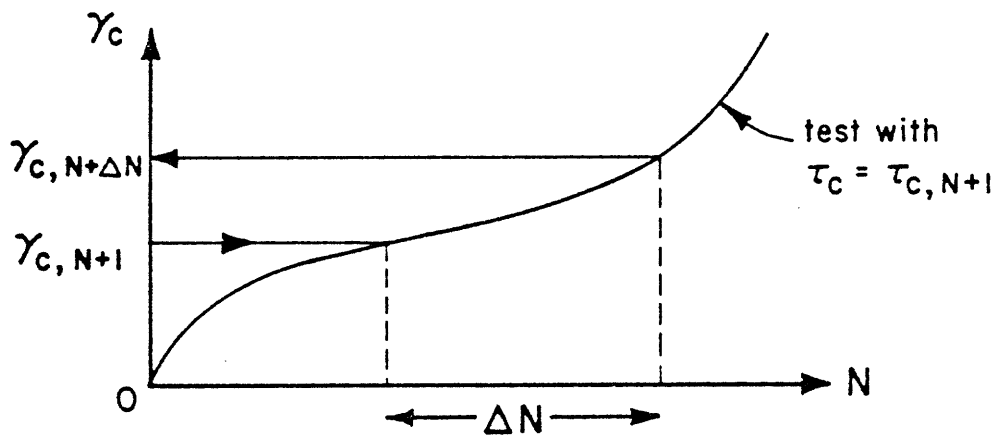


Figure 4.5.8 Use of data base in Andersen's procedure.

#### 4.5.2.B. Extension to $\gamma_{ave} \neq 0$

Every step of Andersen's procedure can be extended to the consideration of both  $\gamma_{ave}$  and  $\gamma_c$  except his second assumption. If we fix the test conditions to  $\tau_c = \tau_{co}$  and  $\tau_{ave} = \tau_{ave o}$  and look for the cycle at which  $\gamma_{ave} = \gamma_{ave o}$  and  $\gamma_c = \gamma_{co}$ , where  $\gamma_{ave o}$  and  $\gamma_{co}$  are also predetermined, we usually will find no solution. We can always fit one of the strains but not both. In the case of tests (9) and (10) we have adopted Andersen's procedure with a fit on  $\gamma_{ave}$ . The construction is thus made by fitting parts of test results (1), (2) and (8) so that the continuity of  $\gamma_{ave}$  is maintained (the immediate changes of  $\gamma_{ave}$  due to changes in  $\tau_c$  are negligible and there is no change of  $\tau_{ave}$ ). The resulting predictions are shown in Figures 4.5:8 and 4.5.9.

The "prediction" of test (9) on the basis of Andersen's procedure and the fitting of  $\gamma_{ave}$  is found to be very satisfactory. The maximum error over 90 % of the test is less than 20 % and the number of cycles at failure is established with an error of 10 cycles (but an extrapolation of the results of test (1) is necessary). Furthermore the prediction is seen to be consistently somewhat conservative.

The "prediction" of test (10) requires the extrapolation of the results from test (1) as well as the estimation of the  $\left\{ \tau_{ave} = 0.60 \tau_{strength} \right\}$  test results. A posteriori it can be said that the choice of this test was not justified, and that it is too complex. However it should be noted that the first 175 cycles of loading reproduce very well the result of test (9), and that the  $\gamma_{ave}$  fitting appears to work well. The prediction of the number of cycle to failure is in error by roughly 10 % on the conservative side.

These two tests suggest that Andersen's procedure can be used with the fit on  $\gamma_{ave}$  to provide a very reasonable first approximation of the clay deformation behavior for this range of loading. This condition might have to be revised however in the case of loadings producing rupture in combined cyclic and average deformations.

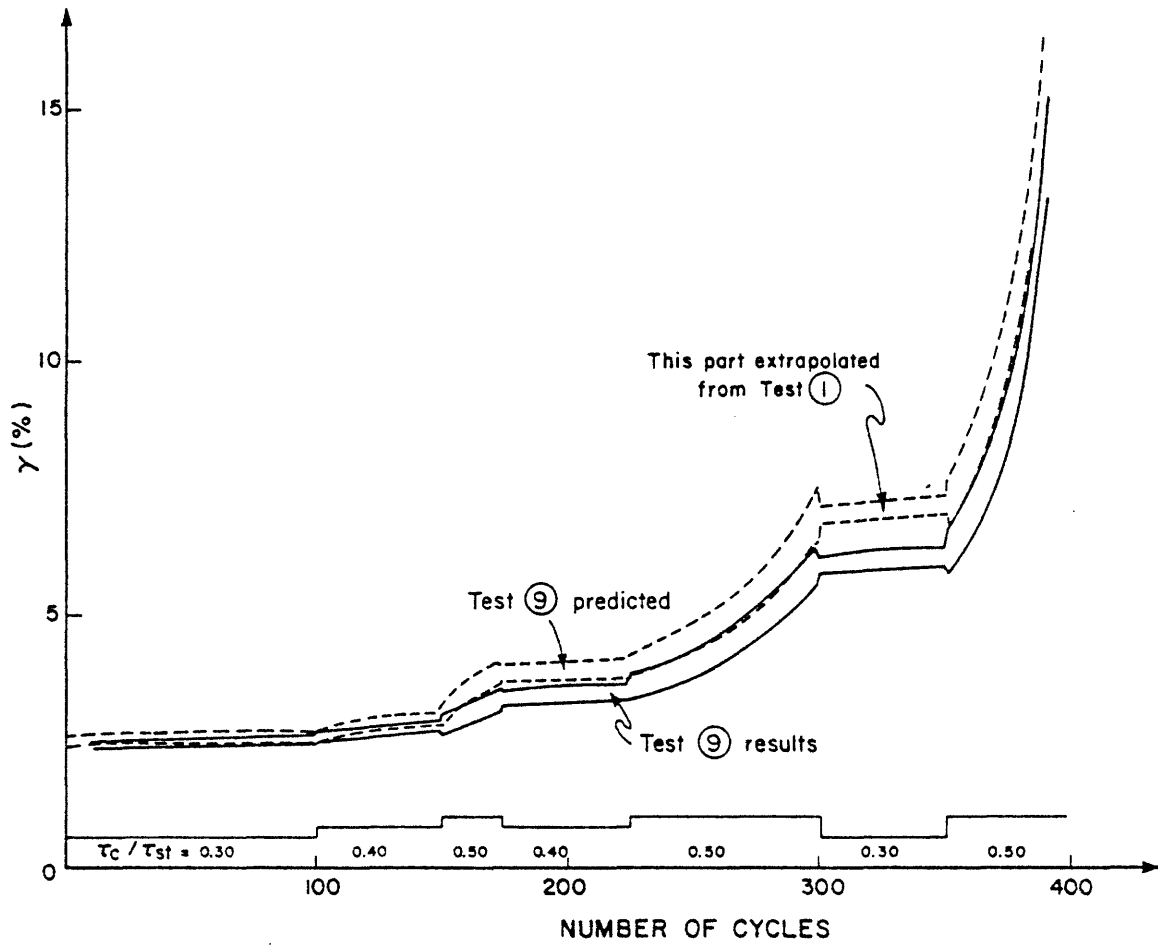


Figure 4.5.9 Prediction of test (9) Andersen's procedure with fit on  $\gamma_{ave}$ .

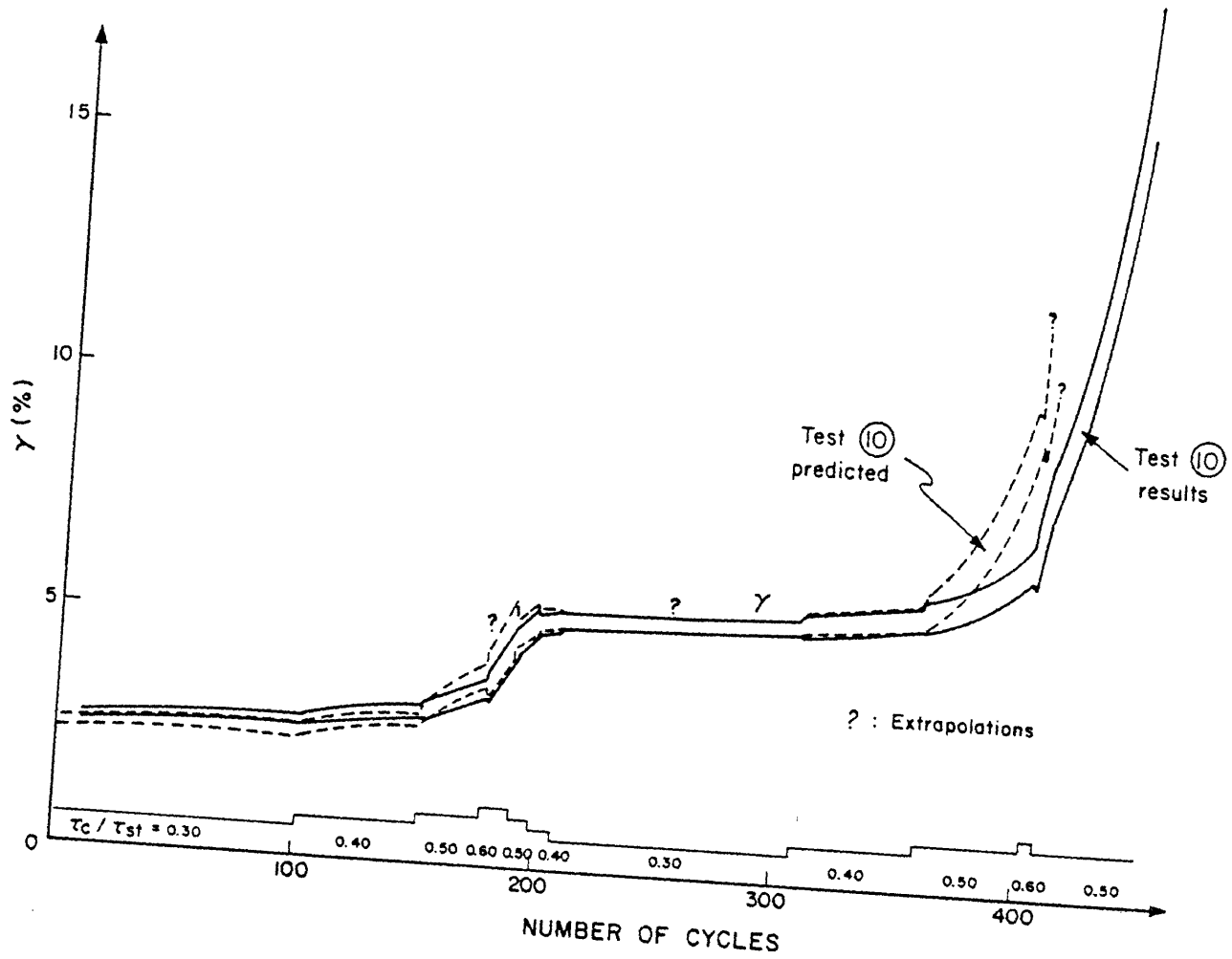


Figure 4.5.10. Prediction of test 10 Andersen's procedure with fit on  $\gamma_{ave}$

## 4.6 SUMMARY

This chapter presents original results on the cyclic behavior of plastic Drammen Clay tested with  $\tau_{ave} = \tau_{cons}$ . The concept of 3-D strain contour diagrams greatly expands our ability to use these data by allowing for easy interpolations and extrapolations as well as a visualisation of the degradation occurring over a wide range of loading. All the results reported here-in are compatible with those obtained during Andersen's 1975 program. It is interesting to note that all the failures occurred in an average deformation mode. (large  $\gamma_{ave}$ ). Furthermore the extension of Andersen's procedure with a fit on  $\gamma_{ave}$  permits a satisfactory estimation of the clay behavior under variable cyclic loading (with  $\tau_{ave} = \tau_{cons}$ ).

---

## 5. TLPILE : THE ANALYTICAL TOOL

TLPILE is the name of the computer code which has been developed to integrate the Pile Model of Chapter 3 and the Soil Degradation data of Chapter 4 into an engineering tool specifically adapted to the analysis of a tension pile under cyclic loading. The organization of the chapter is as follows : first we shall present the modification of the soil-pile parameters resulting from the soil degradation, secondly we shall reconsider the results obtained in the preceding chapters from a numerical point of view - i.e. how the Pile Model is implemented and how the soil degradation data are stored and used - then we shall consider TLPILE and the Iteration Procedure in itself. Finally a detailed example of application to a typical offshore pile will be treated.

### 5.1 MODIFICATION OF THE SOIL-PILE PARAMETERS

As already mentioned the soil-pile parameters are the stiffnesses and the yield strengths of the generalized P-bodies representing the DSS zone (see Chapter 3). They determine the elasto-plastic characteristics of the soil-pile system. It was also shown in Chapter 3 that these parameters are obtained on the basis of a DSS stress-strain relationship, and it is the study of the evolution of such stress-strain relationships under cyclic loading that will now be used to estimate the modification of the soil-pile parameters.



Experimental evidence of the effect of cycling on the stress-strain relationship is provided by immediate changes of stress level during storm loadings and by static loadings run after a period of cycling. The results that we shall consider are for a symmetric stress loading ( $\tau_{ave} = 0$ ). Figures 5.1.1.a and b show storm loading results obtained by Hicher on an Illite and a Bentonite. During the storm build-up period the  $N = 1$  curve can be used to estimate the change of cyclic strain associated with an immediate change of cyclic stress as proposed in the Andersen procedure (Figure 5.1.2). However when the stresses are decreased as the storm fades away, a clear softening occurs. The same effect is seen when a static loading is performed after a cyclic period. Figure 5.1.3.a shows the stress-strain curves obtained by Andersen | 2 | at the end of five cyclic tests. Straight lines join the origin to the last summits reached during the cycling, and thus represent the cyclic stiffnesses at these instants. There is obviously some scatter but one can detect a clear tendency for softening and lower strength with decreasing cyclic stiffness (Andersen | 2 | and Hicher | 41|, among others, have pointed out that the soil behaves as if it were in an overconsolidated state after cyclic loading, the maximum past pressure being given by the original effective stresses existing before cycling).

Our intention is to model the results of Figure 5.1.3.a using only the first loading curve (for the normally consolidated case). A scaling factor, SF, is applied to the strain coordinates of this first loading curve as shown in Figure 5.1.3.b for SF = 2, 4, 8 and 16. The range of strain of interest spans the whole figure ( $\gamma$  varying between 0 and 15 %), and it can be seen that over this range the scaling technique represents both the softening and the reduction in strength observed above. Once the position

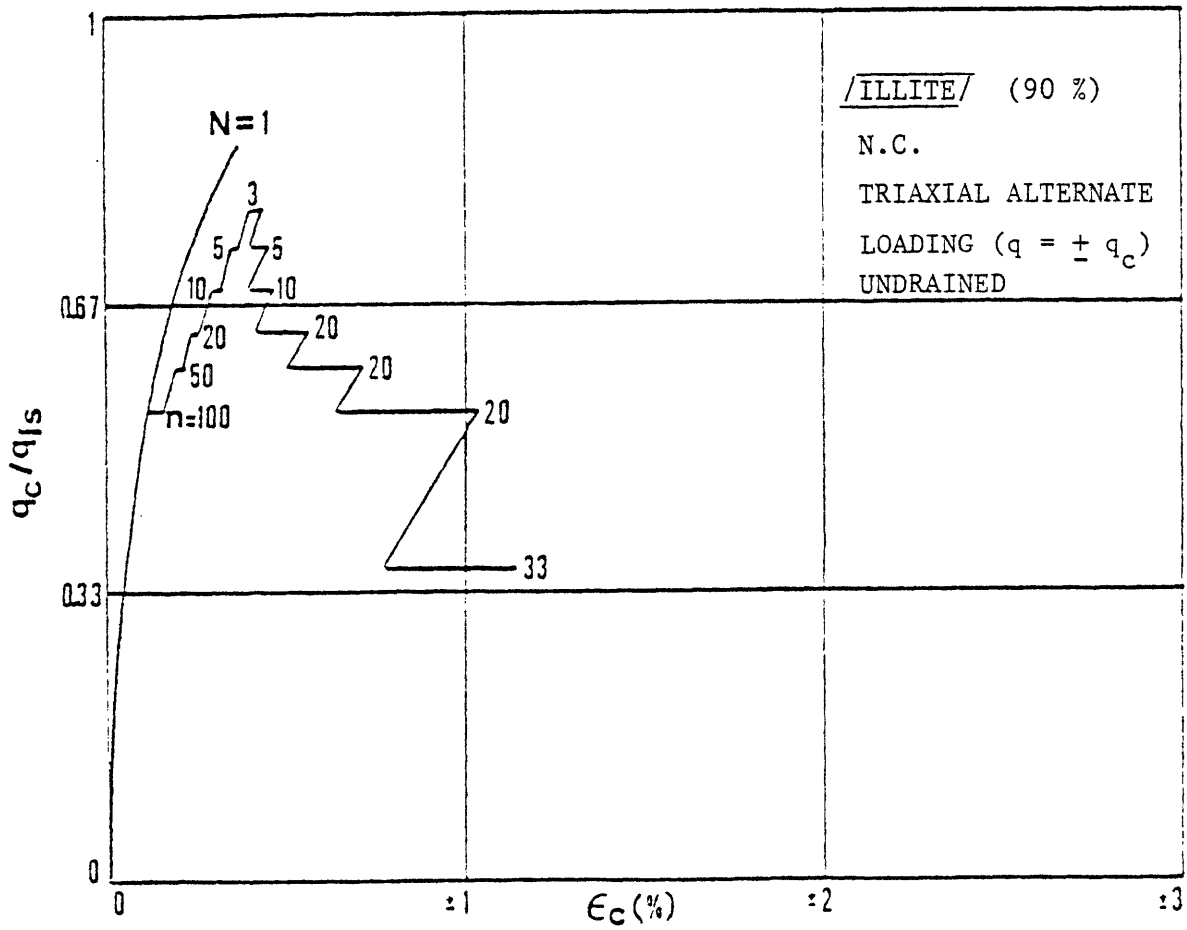


Figure 5.1.1.a Storm loading on Illite ( $\tau_{ave} = 0$ ).  
(|41|).

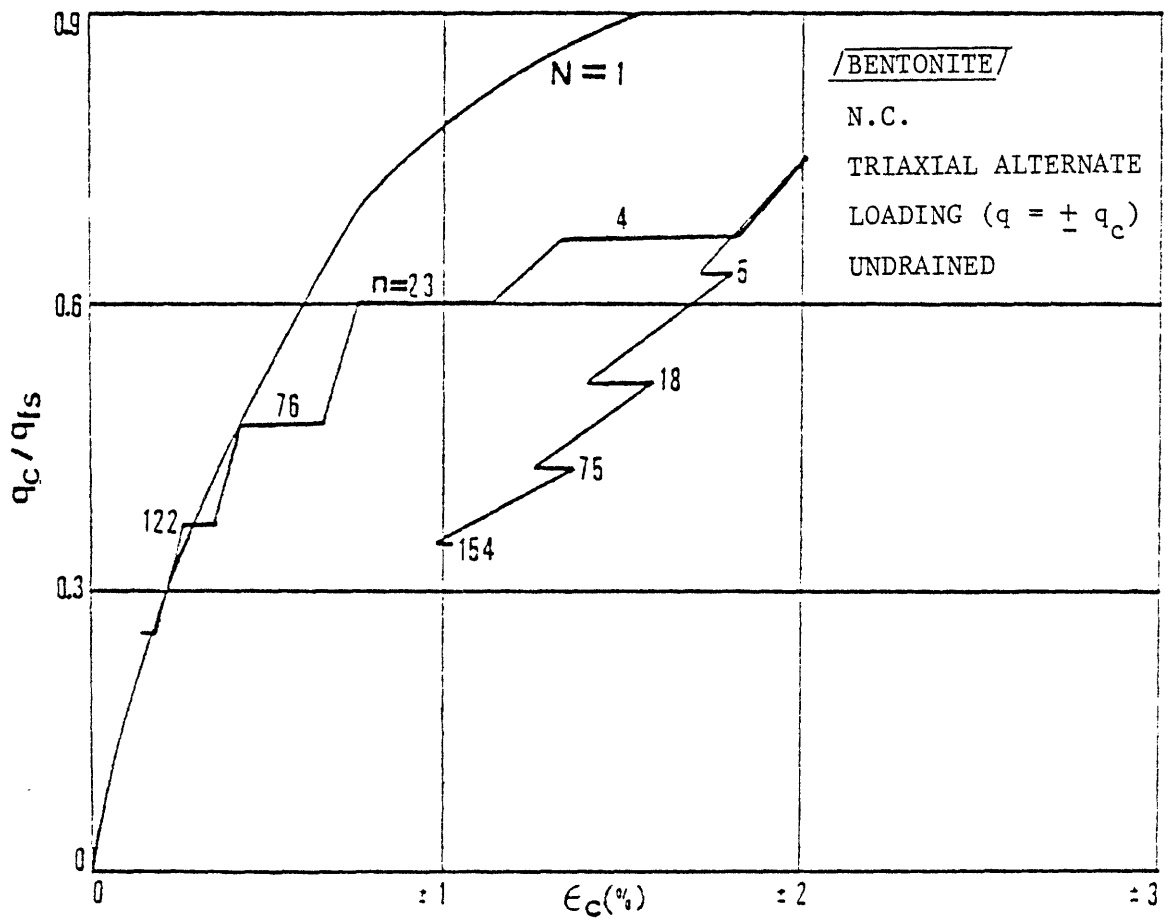


Figure 5.1.1.b Storm loading on Bentonite ( $\tau = 0$ ).

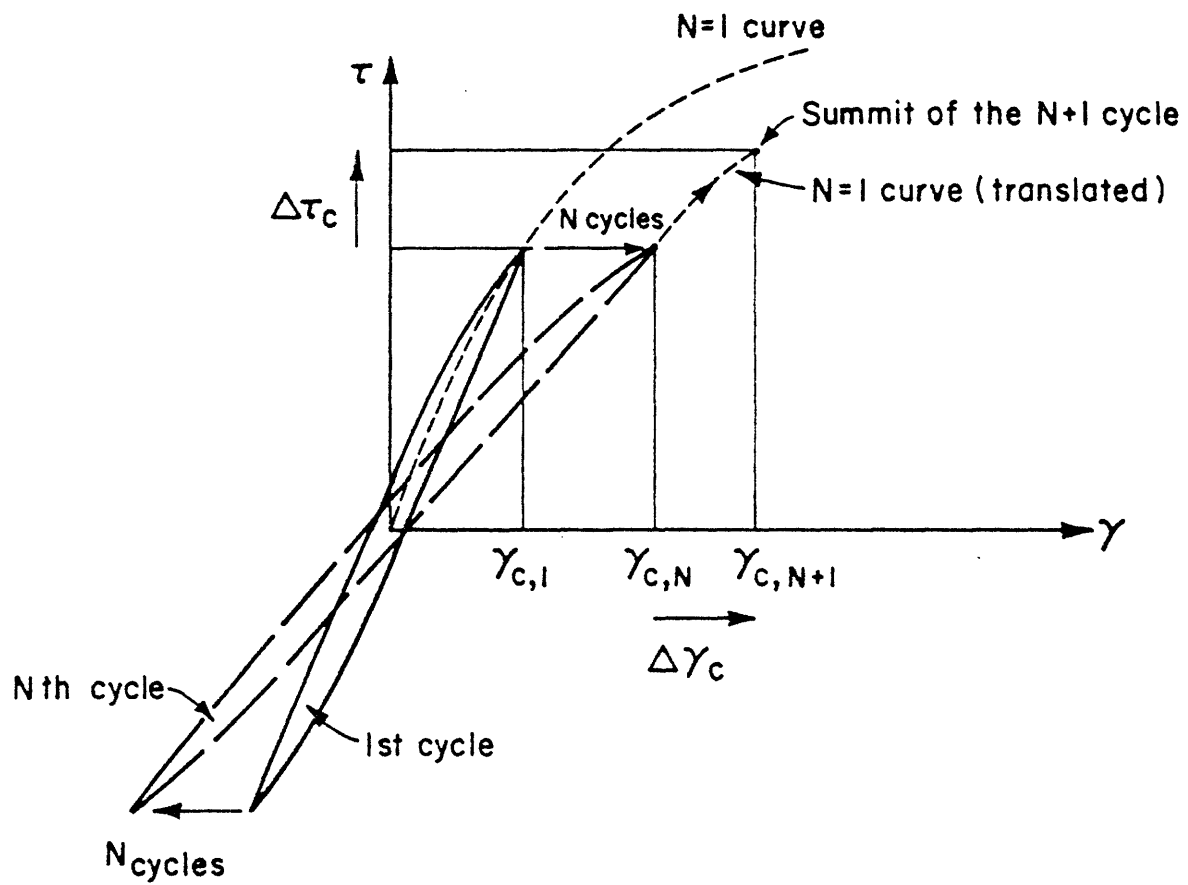
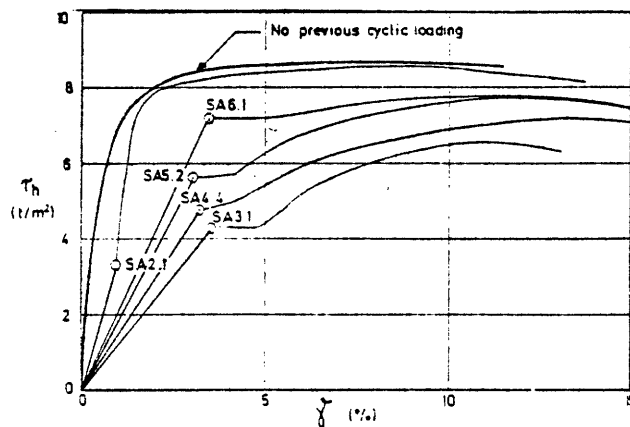
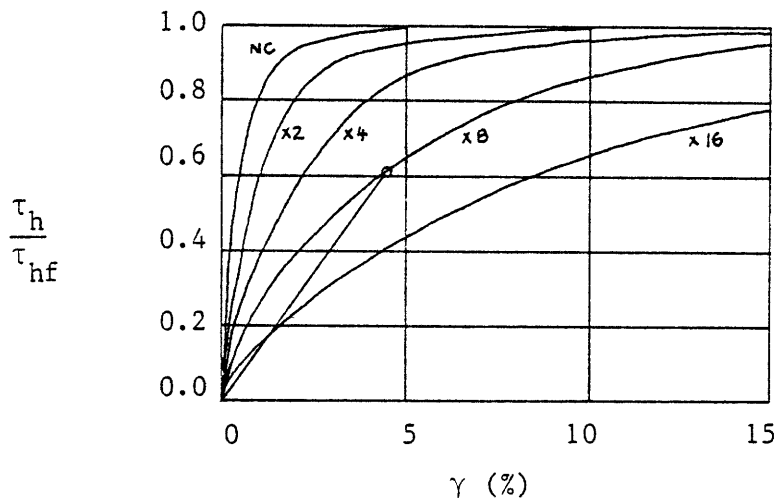


Figure 5.1.2 Andersen's procedure.  
Use of the  $N = 1$  curve.



Plastic Drammen Clay  
DSS tests

Figure 5.1.3.a Static loading after cycling. (After Andersen [2]).



NC curve from  
test SA 1.5  
 $\sigma'_{vc} = 40 \text{ t/m}^2$   
 $\tau_{hf} = 8.7 \text{ t/m}^2$

Figure 5.1.3.b Construction of stress-strain relationships after cycling.

of the last summit is given the proposed construction allows for a very reasonable estimate of the stress-strain relationship during subsequent static loading.

Now consider the case of an asymmetric stressing with  $\tau_{ave} \neq 0$ . Figure 5.1.4 shows the original stress strain curve (OABC) at some point along the pile. The explicit procedure is applied between points BC and B'C' to represent the effect of N cycles of loading (chapters 2 and 3). The cyclic stiffness given by B'C' is now different from the one obtained from BC. We assume that the elasto-plastic properties of the soil are preserved after cycling. By scaling curve OABC along the strain axis so that the image of BC has the same slope as B'C' we can obtain the stress-strain curve O'A'B'C' which inherently contains the stress-strain properties necessary to follow its evolution under a subsequent (static) loading. The fit of the image of BC with B'C' requires the translation OO' of the origin. The scaling factor determined from the evolution of the cyclic stiffness controls the modification of the soil-pile parameters while the translation OO' is equivalent to a global slippage of all the St Venant bodies of a generalized P-body. The modification of the soil-pile parameters requires the change of the stiffnesses of the P bodies and of the plastic strains but the yield strengths are not affected. We have represented the translation OO' by imposing a permanent displacement to the "fixed" references to which the soil nodal points are attached (Chapter 3). Figure 5.1.5 shows the schematics of the artifice employed : a very stiff spring is added in series together with a very large internal force (see Cook [20]). It is clear that the addition of these springs and forces does not change the fact that the Pile Model is an Iwan model.

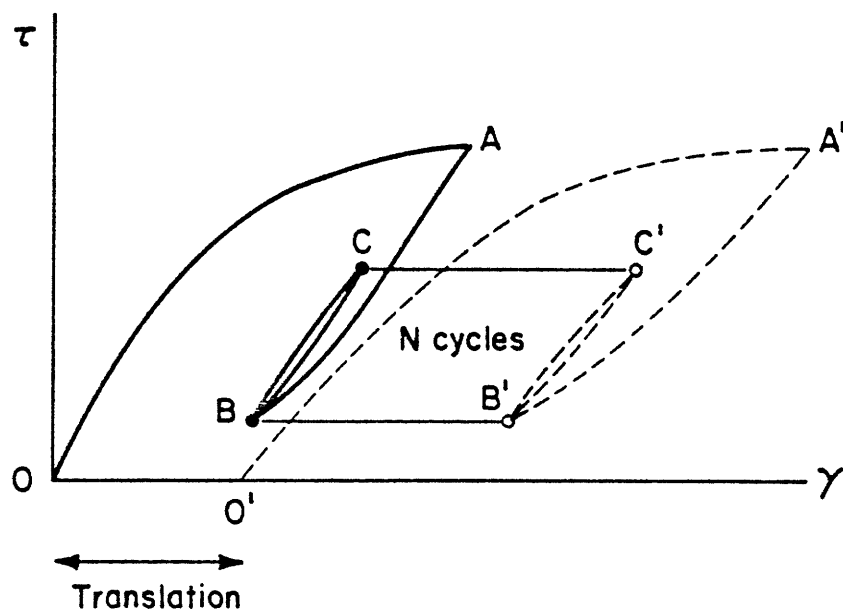


Figure 5.1.4 Modification of the stress-strain relationship with cycling.

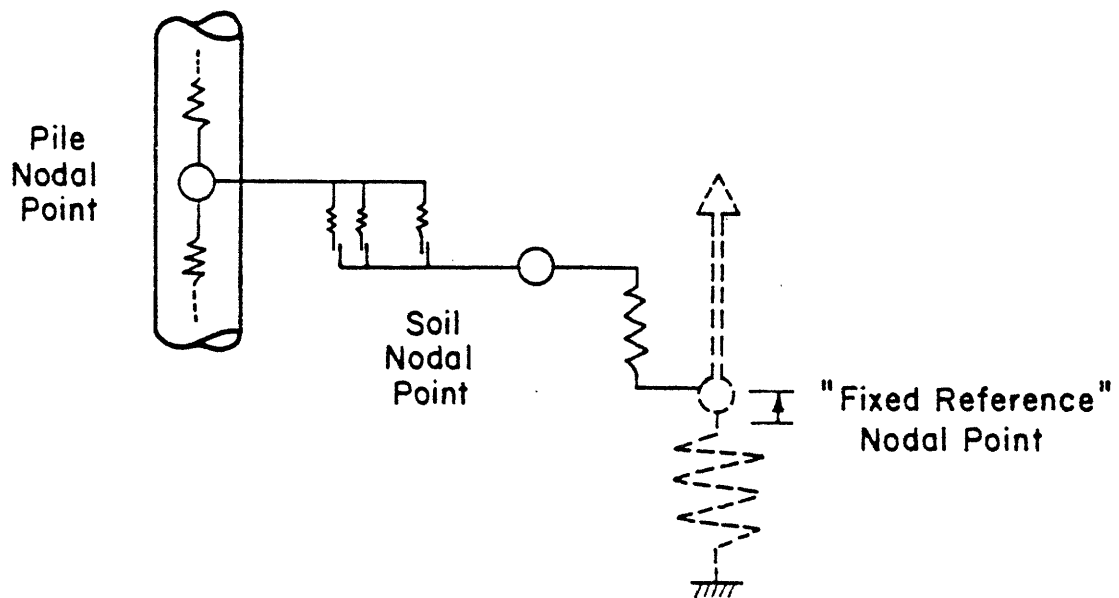


Figure 5.1.5 Artifice used to impose the permanent displacement to the "fixed" reference.

## 5.2 NUMERICAL ASPECTS OF THE PILE MODEL

How are we going to treat numerically the non-linearity of the Pile Model ? We shall proceed by successive solutions of linear problems. The idea is to replace a Prandtl body by a linear spring and set of internal forces proportional to the plastic strains. Figure 5.2.1.a shows the P-body on the left and both the equivalent linear spring and the internal forces on the right.

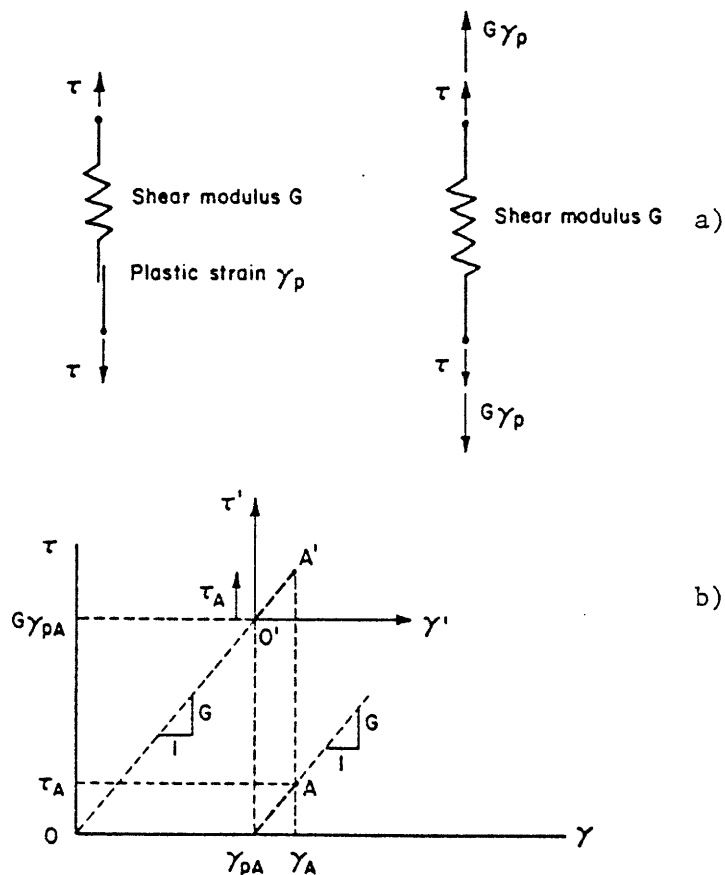


Figure 5.2.1 a) P-body and the equivalent linear force and internal forces,  
 b) stress-strain diagram explaining the equivalence.

Figure 5.2.1.b explains the equivalence on the stress-strain curve. The behavior at point A is studied in fact at point A' as a linear problem in the new system of coordinates ( $\tau'$ ,  $\gamma'$ ).

Consider the Pile Model of Figure 3.2.1 with a force P applied at its top, and study its evolution as force P is changed to P'. Before this force is changed we replace all the P bodies in the Model by their equivalent linear springs and sets of internal forces. A linear elastic analysis is then performed under load P'. The objective is to locate the first P-body that will yield as the external force is changed from P to P'. Since the system is linear any change in displacement, or force, is proportional to the change of external force. Let us consider the stress strain diagram of Figure 5.2.2, corresponding to Prandtl body number j.

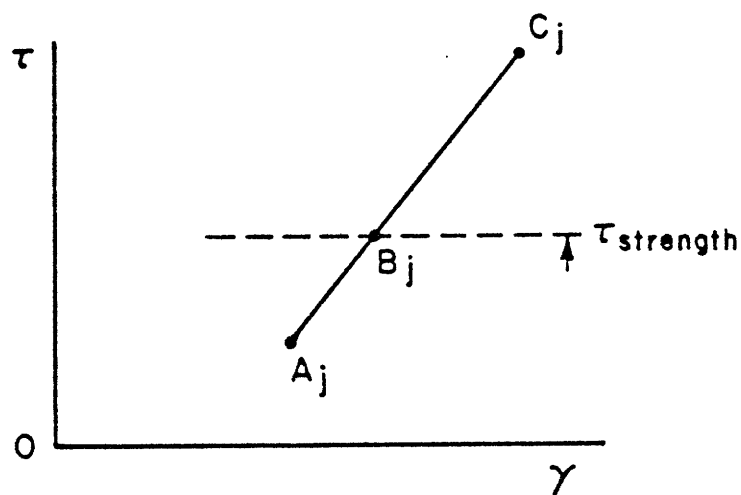


Figure 5.2.2 Relative position of the result of the elastic solution with respect to the starting and yield points.



Point  $A_j$  is the original condition under force  $P$ , point  $B_j$  corresponds to the yield strength and point  $C_j$  to the result of the elastic analysis under  $P'$ . The first P-body to yield will be the one for which the ratio  $AB/AC$  will be the smallest (in the case of Figure 5.2.3 it is P-body number 2).

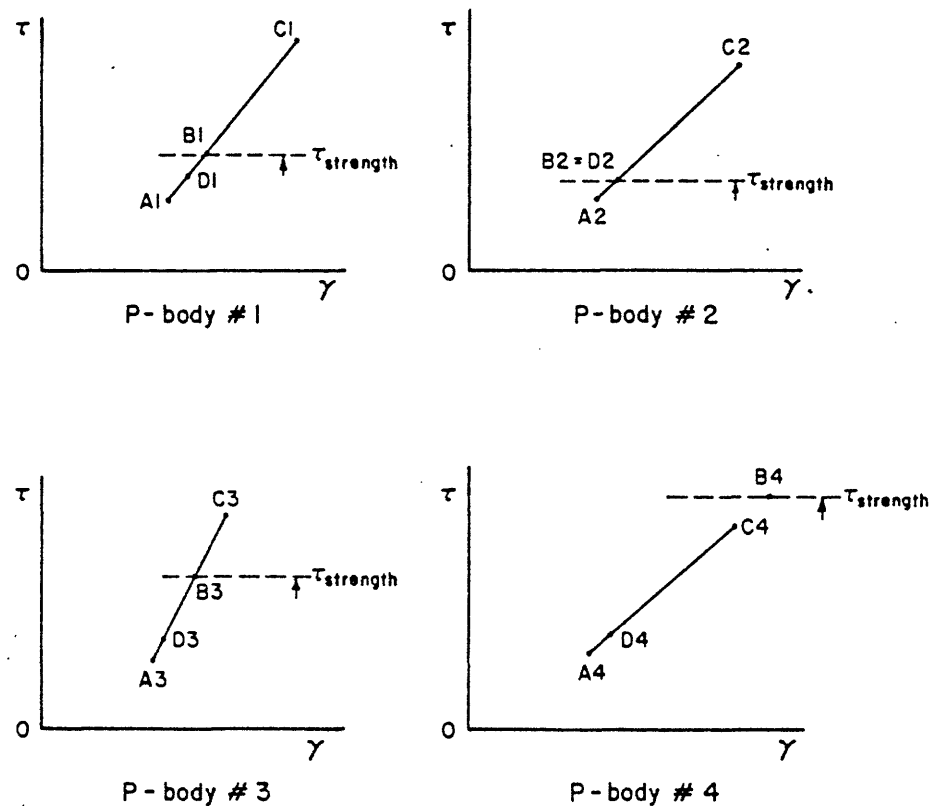


Figure 5.2.3 Example of determination of the next P-body to yield.

Once this P-body is located it is replaced by a constant reacting stress equal to its yield strength, and the stresses existing in the other P-bodies when the yielding first occurs are then calculated. These stresses correspond to a point  $D_i$  between  $A_i$  and  $C_i$  such that  $A_i D_i / A_i C_i$  is the smallest

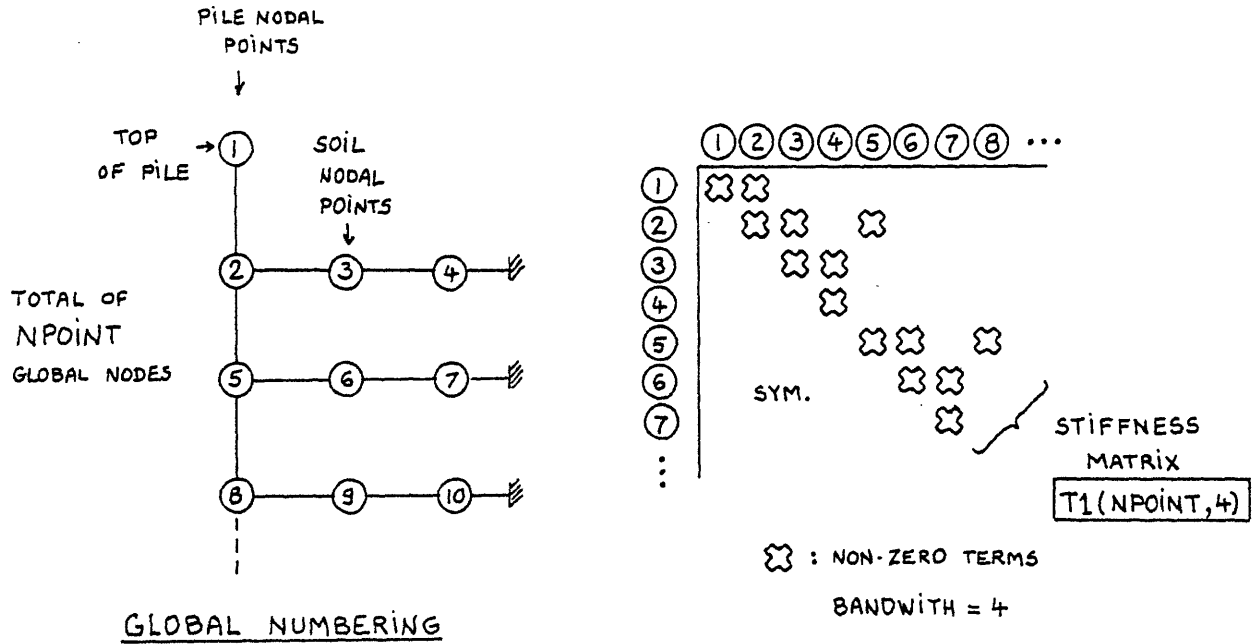


Figure 5.2.4 Global numbering and global stiffness matrix.

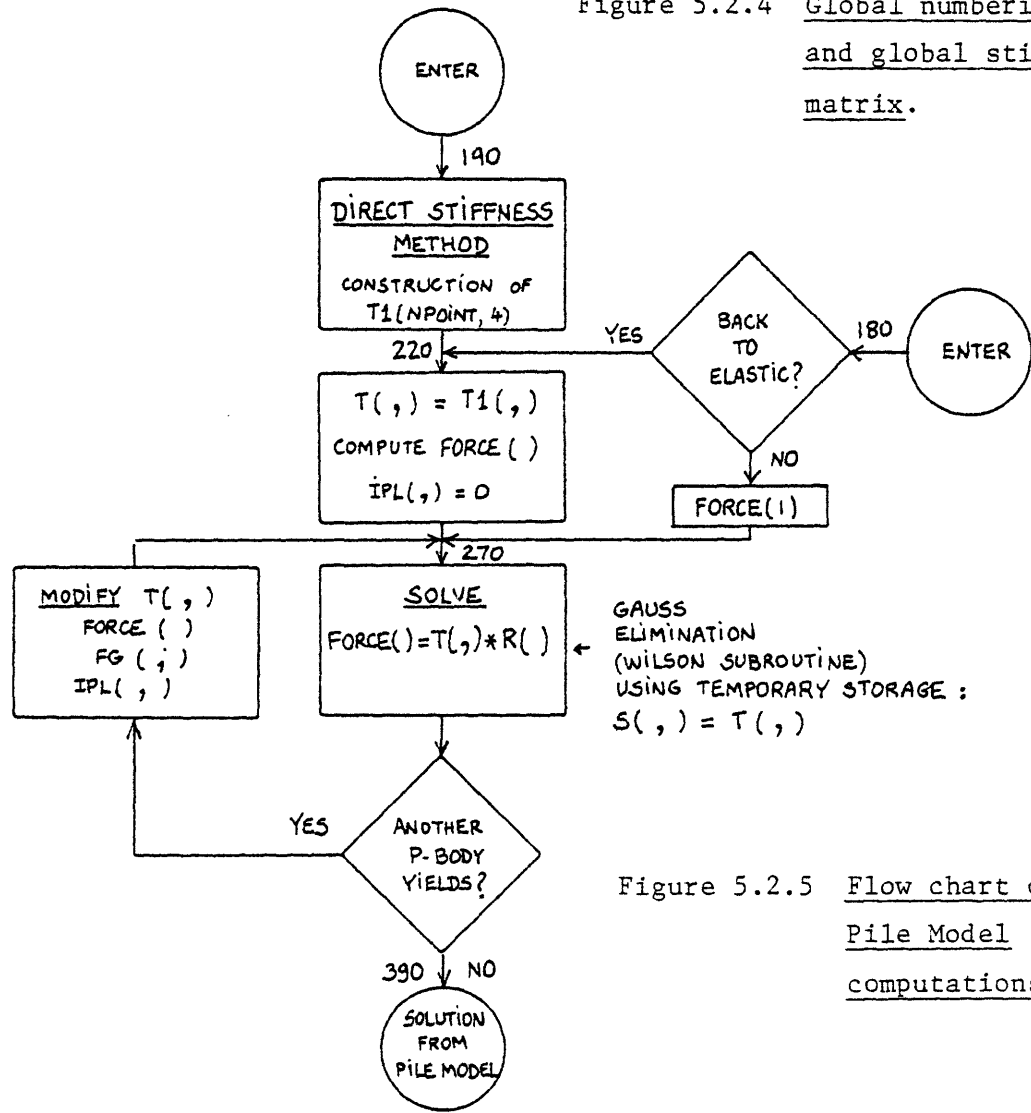


Figure 5.2.5 Flow chart of Pile Model computations.

ratio previously obtained ( $A_2 B_2 / A_2 C_2$  in the example of Figure 5.2.3). These points  $D_i$  are the new starting points. The new equivalent linear system (new since P-body number 2 has been replaced by a constant force and thus its stiffness is ignored) is then analyzed under  $P'$  and the previous procedure is repeated to obtain the next P-body to yield. If no P-body yields the solution has been found. The analysis requires therefore one iteration per element yielding.

If the force at the top is now changed from  $P'$  to  $P''$  we can differentiate between two cases : either the change from  $P'$  to  $P''$  is of the same sign as the change from  $P$  to  $P'$  in which case all the Prandtl elements that yielded during  $PP'$  are still yielding during  $P'P''$ , or the sign is different. In the first case we can simply pursue the preceding iteration procedure (keeping the last equivalent linear system obtained and its internal forces) while in the second case we start from the original equivalent linear system and a new set of internal forces ("Back to Elastic" option).

In the Pile Model the global nodes are numbered as shown on the left of Figure 5.2.4. The top of the pile is node number 1, and further down the pile-node number  $i$  is numbered as  $3 * (i - 2) + 2$  in the global system. A schematic representation of the global stiffness matrix is given on the right of the same figure. A banded matrix  $T1(NPOINT,4)$  can be used to store it (NPOINT is the total number of nodal points  $3 * NLAYER + 1$ ). This matrix is assembled by the Direct Stiffness Method (Cook |20|). The linear equation which is then to be solved is :

$$FORCE (i) = T1(i,j) R (j)$$

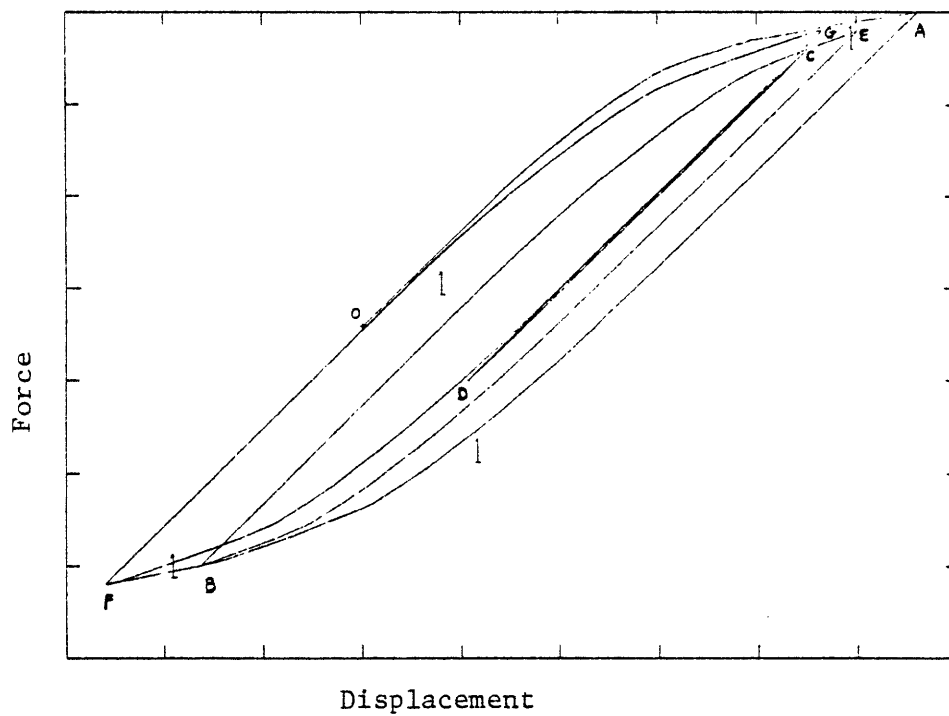


Figure 5.2.6 Numerical check of the behavior of the Pile Model subjected to a loading similar to the one of Figure 3.3.15.

where :

FORCE (i) is the global force on global node i and

R (j) is the global displacement on global node j.

The basic flow chart of the Pile Model is presented in Figure 5.2.5.

Tl(i,j) is the initial stiffness matrix while T (i,j) and S (i,j) are temporary storages. T (i,j) is the modified stiffness matrix at each iteration while S (i,j) is the stiffness matrix which is reduced during the Gauss elimination procedure. The calculated displacements R (j) are used to estimate the elastic forces FELAS in each P-body. If the force in P-body # K, in layer I was FG (I,K) and the strength FL (I,K) the P-body which yields in this iteration is the one for which

$$\left[ FL (I, K) - FG (I,K) \right] / \left[ FELAS - FG (I,K) \right] \text{ is minimum.}$$

Once it is determined the stiffness of the P-body is subtracted from the T (i,j) matrix and the strength is subtracted from the appropriate global forces ; then new values of FG (i,k) are obtained and the Gauss elimination is reactivated. The index IPL (I,K) is set to one to indicate that P-body # K in layer I has yielded. The numbers indicated on the flow chart correspond to the addresses in the TLPILE code (Figure 5.2.5).

A graphical check of the Pile Model is given in Figure 5.2.6 which shows the calculated force-displacement relationship for the whole Pile Model under a loading pattern similar to the one of Figure 3.3.15.

### 5.3 SOIL DEGRADATION DATA BASE

The data obtained in Chapter 4 have been stored as multilinear 3-D strain contour diagrams defined by their cross-sections at  $N = 1, 50, 100, 200, 500, 1000$  and  $5000$  cycles. This last value of  $N$  (5000) was added by extrapolation and corresponds to the iso- $\gamma$  networks of Figure 5.3.1.a and b.\* We have introduced the iso- $\gamma_{ave}$  networks for  $\gamma_{ave} = 2.5, 3, 4, 6$  and  $15\%$  as well as the iso- $\gamma_c$  networks for  $\gamma_c = 0.15, 0.25, 0.5$  and  $3\%$ . The digitization of networks at a particular number of cycles ( $N = 100$ ) is shown in Figure 5.3.2.a and b together with the description of the storage arrays. Figure 5.3.3 give a partial axisymmetric view of the  $\gamma_{ave} = 4\%$  network as it evolves with number of cycles.

A subroutine called CYCDEG (for cyclic degradation) has been developed to estimate the new values of  $\gamma_{ave}$  and  $\gamma_c$  (GAV and GCY) resulting from the application during DN cycles of a loading characterized by normalized values of  $\tau_{ave}$  and  $\tau_c$  (TAV and TCY) and initiating with an average strain  $\gamma_{ave,0}$  (= GAVO). CYCDEG is based on Andersen's procedure with a fit on  $\gamma_{ave}$  (Chapter 4). A simplified flow chart of CYCDEG is presented in Figure 5.3.4. The call of CYCDEG is represented by :

i n p u t	o u t p u t
CYCDEG	(TAV, TCY, GAVO, DN, GAV, GCY).

The complete listing of CYCDEG is provided in Appendix 5.A.

---

\*Extrapolations using Figures 4.4.7 through 4.4.8.

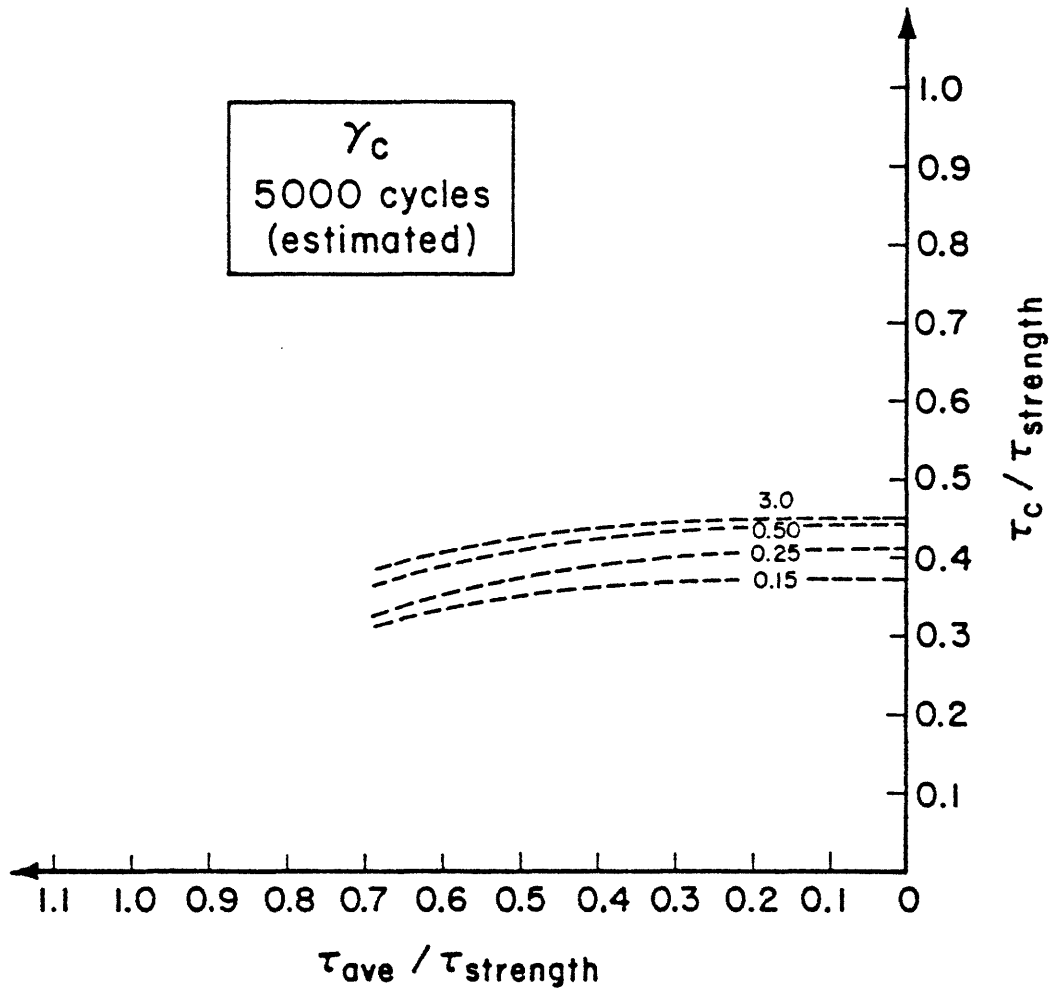


Figure 5.3.1.a Section of iso  $\gamma_c$  network at  $N = 5000$  cycles.  
(Estimated).

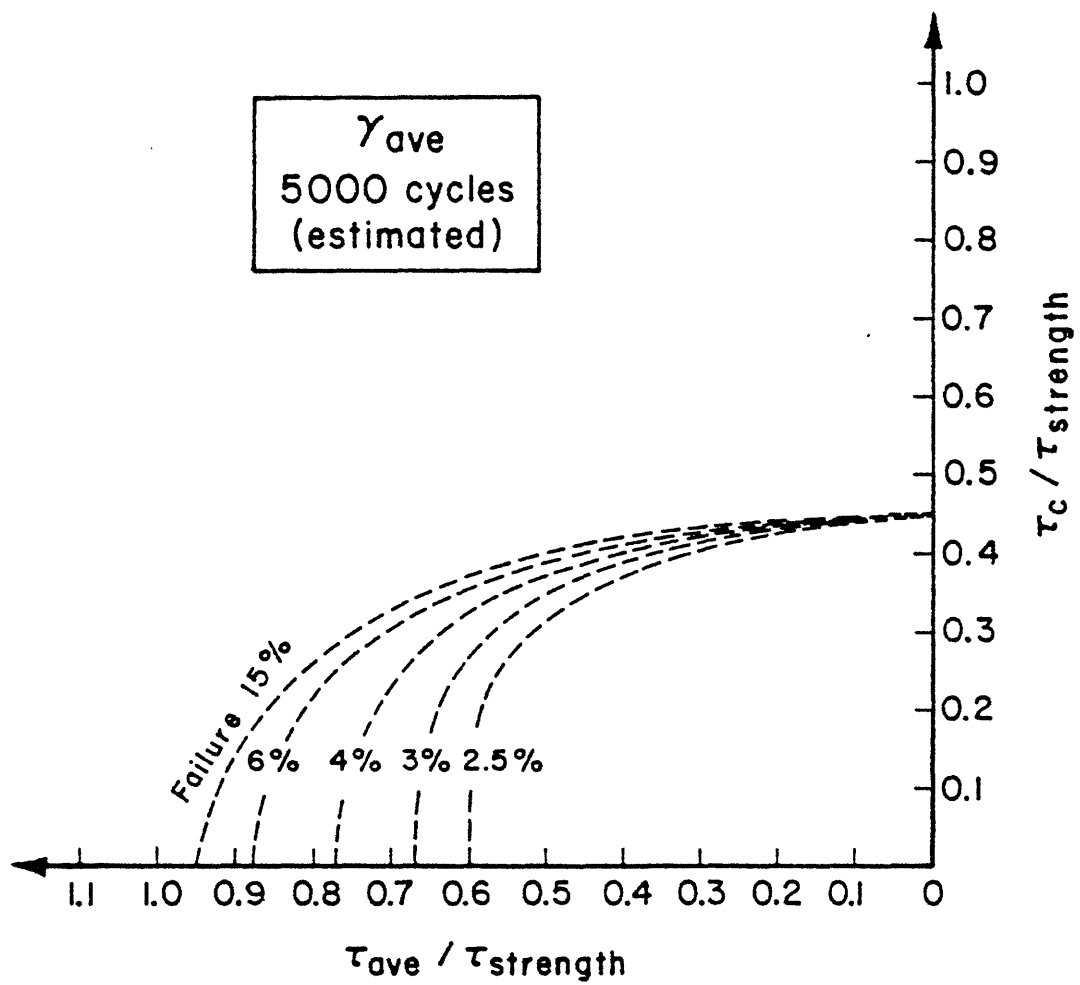


Figure 5.3.1.b Section of iso  $\gamma_c$  network at  $N = 5000$  cycles.  
 (Estimated).



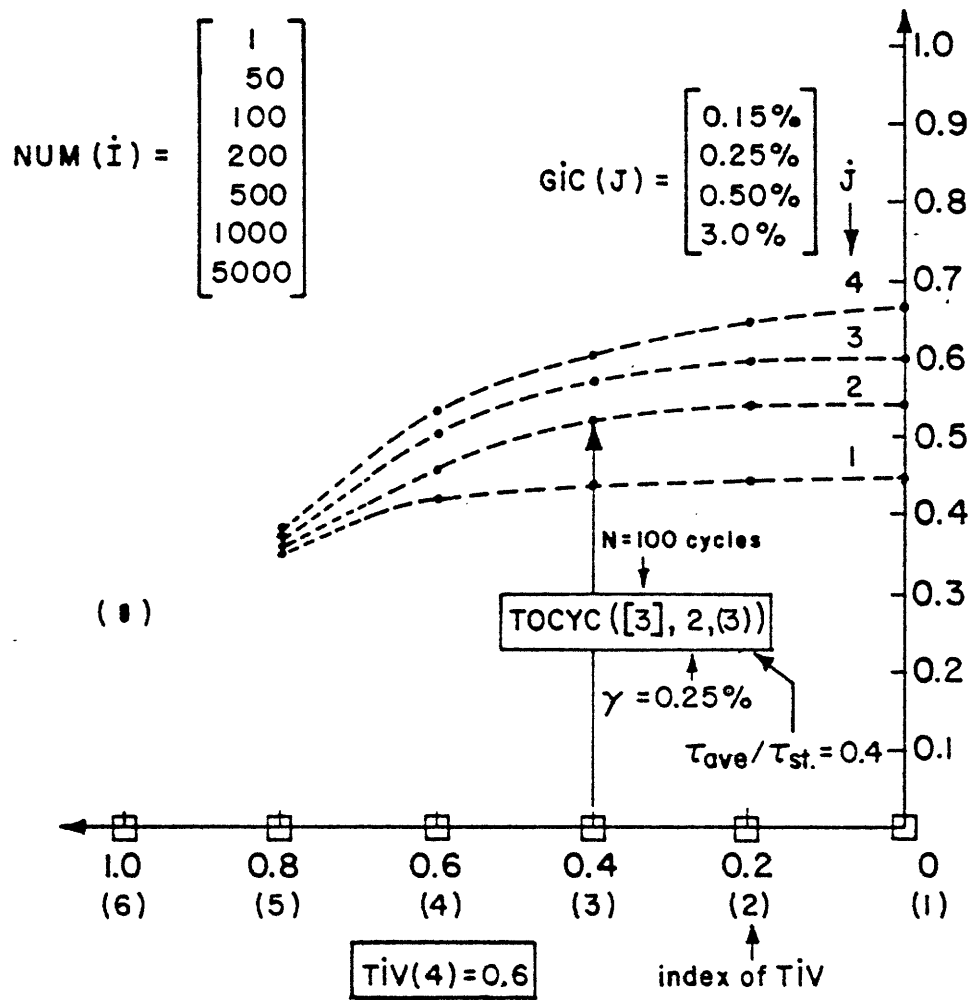


Figure 5.3.2.a Digitization of iso- $\gamma_c$  network at N = 100.

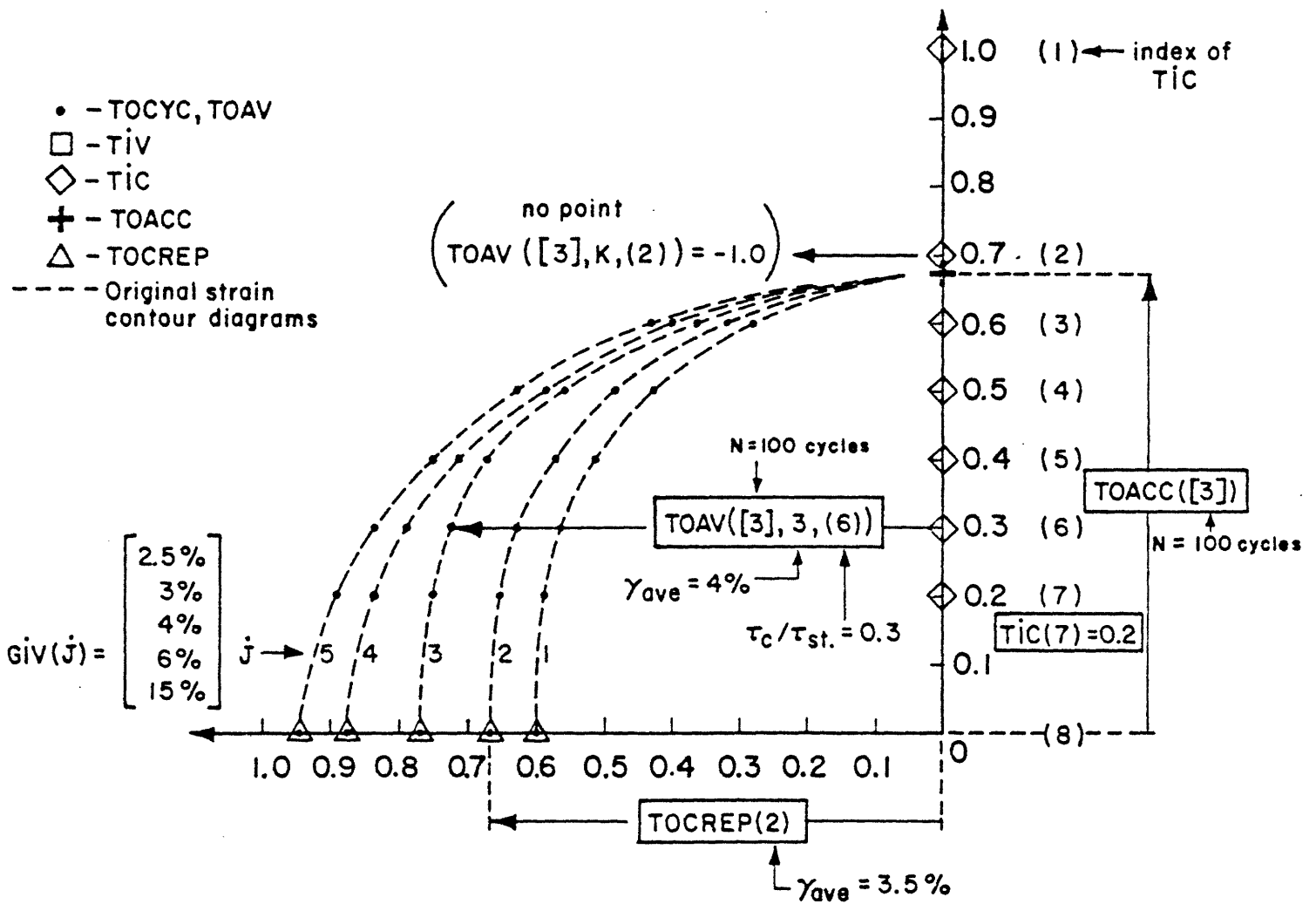


Figure 5.3.2.b Digitization of iso- $\gamma_{ave}$  network at N = 100.

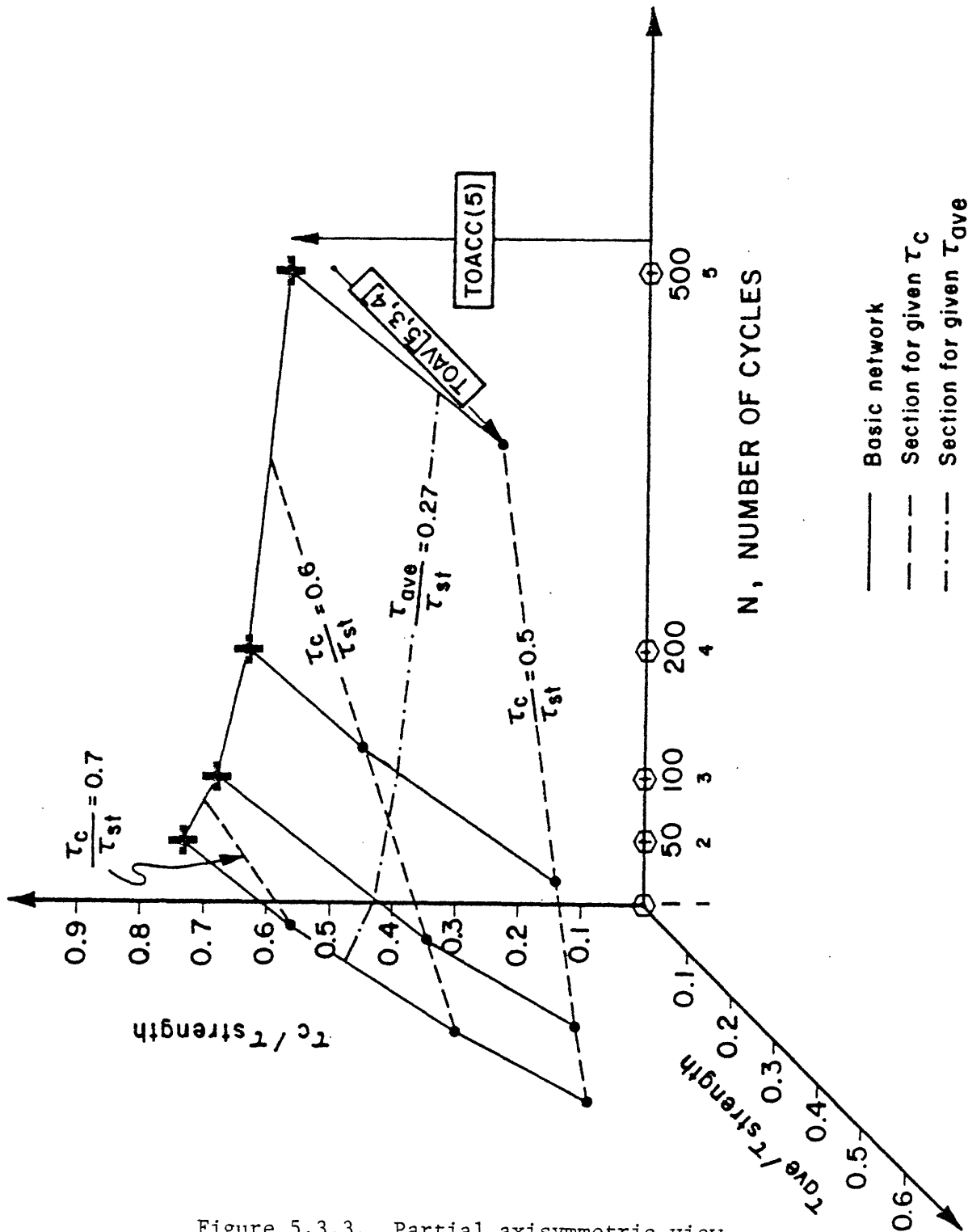


Figure 5.3.3. Partial axisymmetric view  
of the iso- $\gamma_{ave} = 4\%$  network.

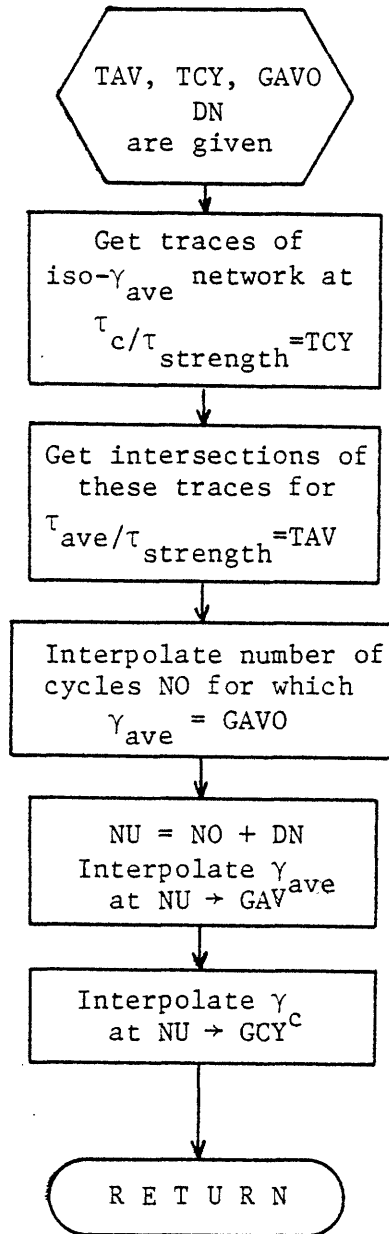


Figure 5.3.4 Simplified flow-chart of subroutine CYCDEG

#### 5.4 ORGANIZATION OF TLPILE AND ITERATION SCHEME

The present version of TLPILE differentiates between three stages :

- 1) a static pre-loading which generates the  $\tau_{\text{cons}}$  distribution, 2) a modification of the model parameters to account for the effects of consolidation on the future cyclic loading, and 3) the cyclic loading in itself.

The static preloading stage corresponds to the calm sea state condition during which the soil around the pile is subjected to "drained creep" : the stresses applied to the soil are almost constant, excess pore pressure dissipates, and some creep deformation accumulates. The soil is healing after the passage of the last storm (or after the pile installation). The purpose of this preliminary stage is to establish the  $\tau_{\text{cons}}$  distribution as well as some estimates of the strains and displacements that can exist before the passage of the storm. This period is represented in TLPILE by an equivalent static loading during which the soil parameters are adapted to account for the time of application of the load. The approximation consists in using stress-strain relationships of the type of the "19 hour curve" of Figure 4.5.2 in place of the regular loading curves obtained during static loading (and typically a strain rate of 5 % per hour, see the curve labelled "reference undrained loading" in this same figure). In the second stage the soil-pile parameters are modified to account for the stiffer and stronger response obtained during an undrained loading applied after consolidation under average shear stresses. These changes correspond to the two diagrams placed on the right hand side of Figure 4.5.2. As a consequence of these modifications the Iwan models become asymmetric.

From now on the analysis is performed incrementally.

Finally the cyclic loading stage involves the iteration procedure as such and will be given the major emphasis. The loading is specified by imposing the forces applied to the top of the pile while the degradation of the soil is estimated from a data base obtained from the tests reported in Chapter 4.

The procedure relies on the decomposition of the evolution of the shear stress distributions in successions of periods of constant average and cyclic shear stresses separated by instant modifications of the soil-pile parameters.

Figure 5.4.1 shows a schematic flow chart of the basic iteration scheme. Given some initial conditions and the loading  $P$ , representing both  $P_{ave}$  and  $P_{cyc}$ , the Pile Model is used to determine the stress and strain distributions  $\tau$  and  $\gamma$  (also representing both their average and cyclic components). These distributions are respectively in equilibrium (with  $P$ ) and compatible (in terms of displacements).

The soil degradation is estimated for the values of  $\tau$  just obtained and will result in a new distribution of shear strains,  $\gamma'$ , corresponding to  $N$  cycles of cyclic loading under  $P$ . This shear strain distribution  $\gamma'$  will usually not be compatible with the overall pile displacements.

The modifications of the soil-pile parameters are then made on the basis of this new  $\gamma'$  distribution (translations and scalings of section 5.1) before the Pile Model is used again to derive a set of new shear stress and shear strain distributions,  $\tau'$  and  $\gamma''$  (respecting equilibrium and compatibility).

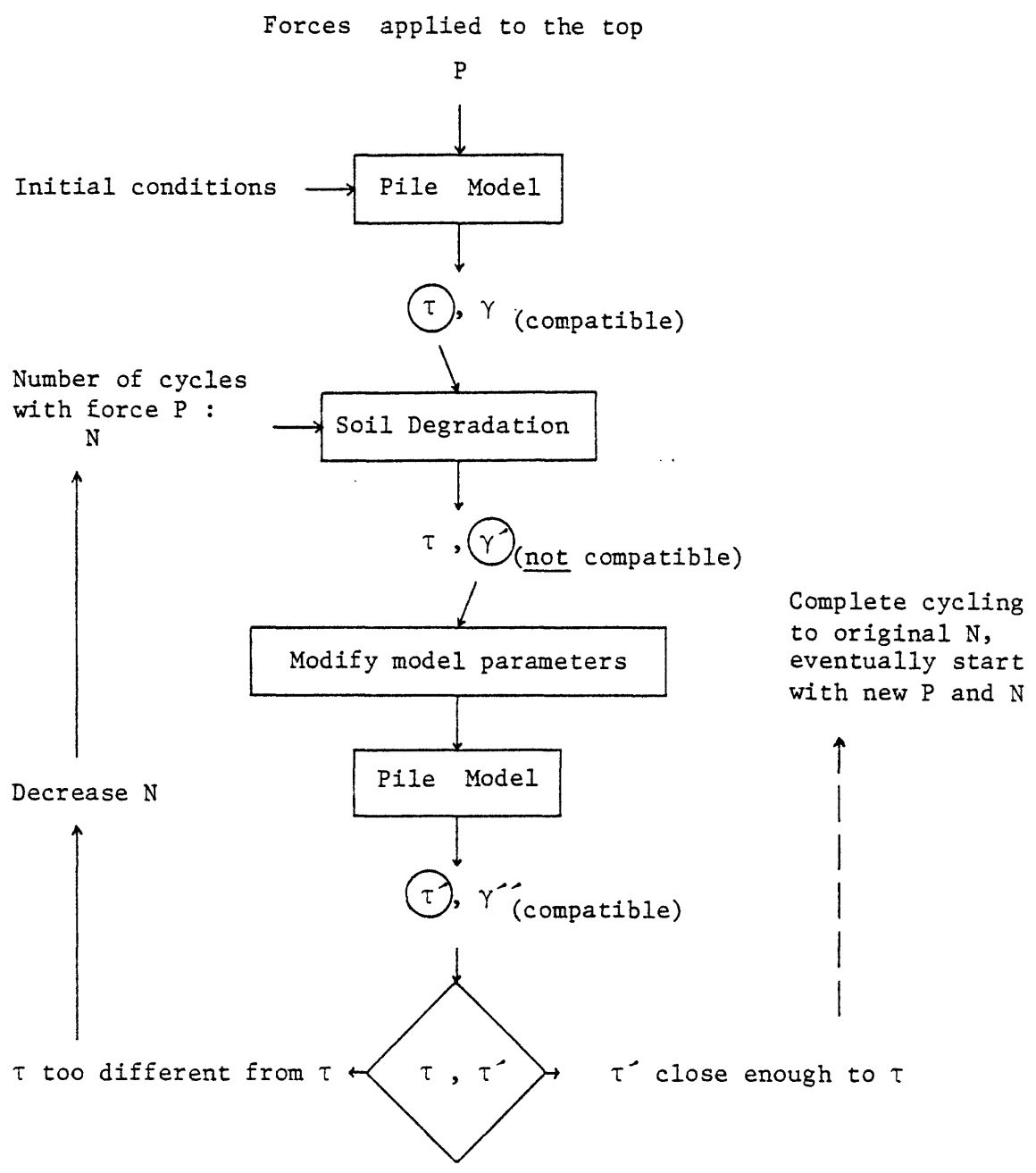


Figure 5.4.1 Iteration scheme

The criterion that will be used to decide whether  $\tau'$  and  $\gamma'$  are acceptable is based on the difference of  $\tau_{ave}$  and  $\tau'_{ave}$ . Since the degradation assumes a constant value of  $\tau_{ave}$  we feel it is logical to accept the iteration outcome when  $\tau'_{ave}$  is not too different from  $\tau_{ave}$ .\*

If  $\tau'_{ave}$  is too different from  $\tau_{ave}$  the number of cycles is decreased and the procedure is re-initiated on the basis of  $\tau$  and  $\gamma$ . When  $\tau'$  is satisfactory the cycling is completed to the original N value, and if necessary a new set (P, N) is considered.

The basic variables used in TLPILE are schematically defined in Figures 5.4.2 and 5.4.3. Figure 5.4.2 gives an overview of the discretization of the pile-soil system both vertically and horizontally. The boundaries of the layers used in the model correspond either to an actual soil layer change or to a pile wall thickness change. The pile nodal points are placed at the center of the model layers. The top of the pile is a pile nodal point while the tip is not.

The bottom part of Figure 5.4.2 shows the geometrical description and the horizontal decomposition in layer number i while Figure 5.4.3 introduces the variables used in the computation. There are three global nodal points in each layer : one for the pile on the left, one for the soil (at the demarcation of the DSS and elastic zones) in the center of the figure and one for the "fixed" reference on the right. The bottom of Figure 5.4.3 gives the basic first-deformation curve of the DSS zone in layer i and the force-displacement diagram of one of the P bodies.

Figure 5.4.4 presents the TLPILE general flow chart as a support for the listing provided in Appendix 5.B (variables appearing in the flow chart and not previously described are introduced in COMMENTS as they appear in the listing).

---

\*  $|\tau_{ave} - \tau'_{ave}| < \epsilon * \tau_{strength}$  ;  $\epsilon = 10\%$  was subjectively selected in our analyses.



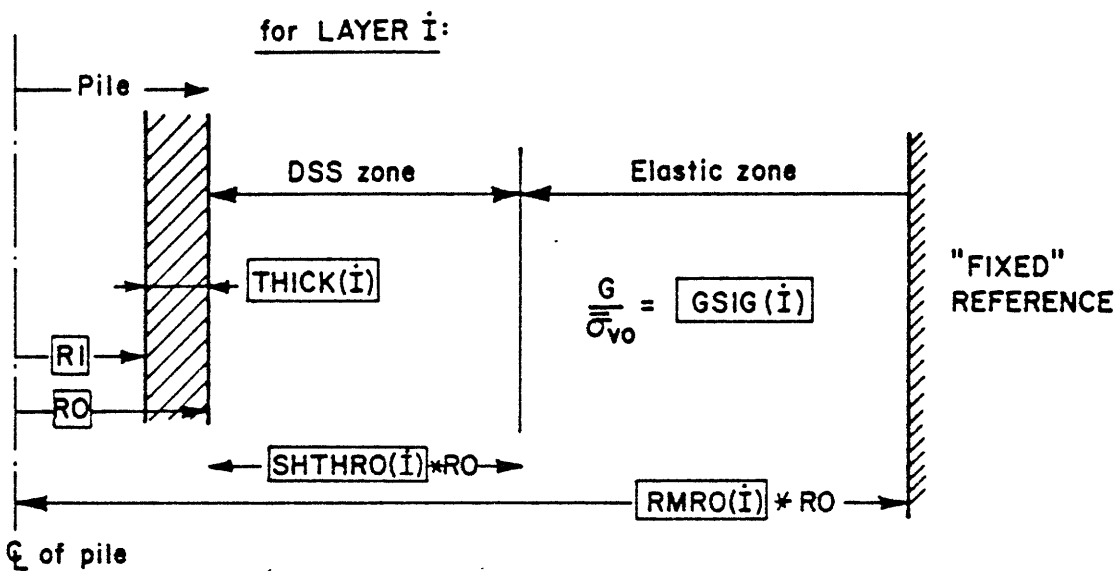
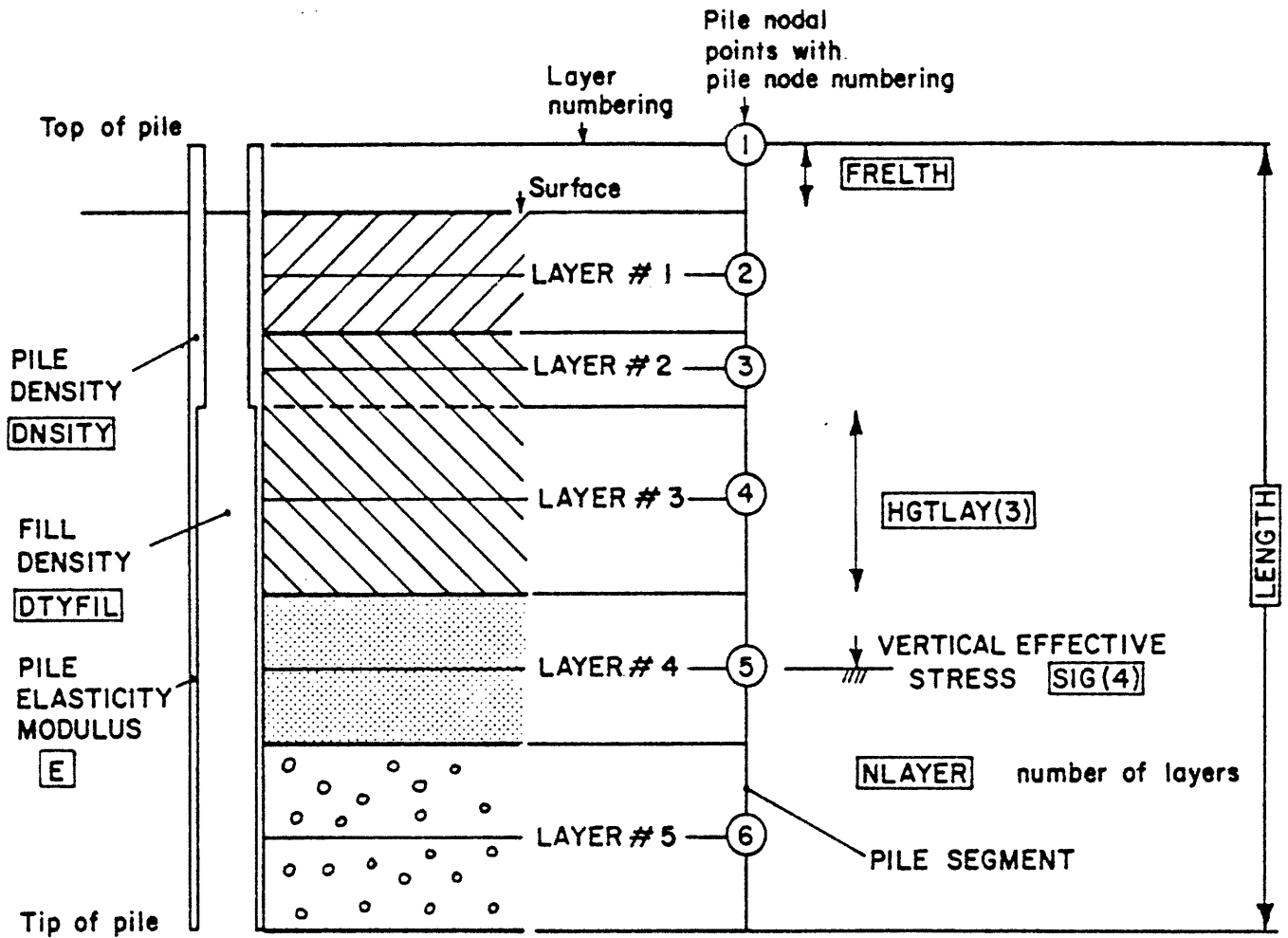


Figure 5.4.2 Basic variables used in TLPPILE (1).

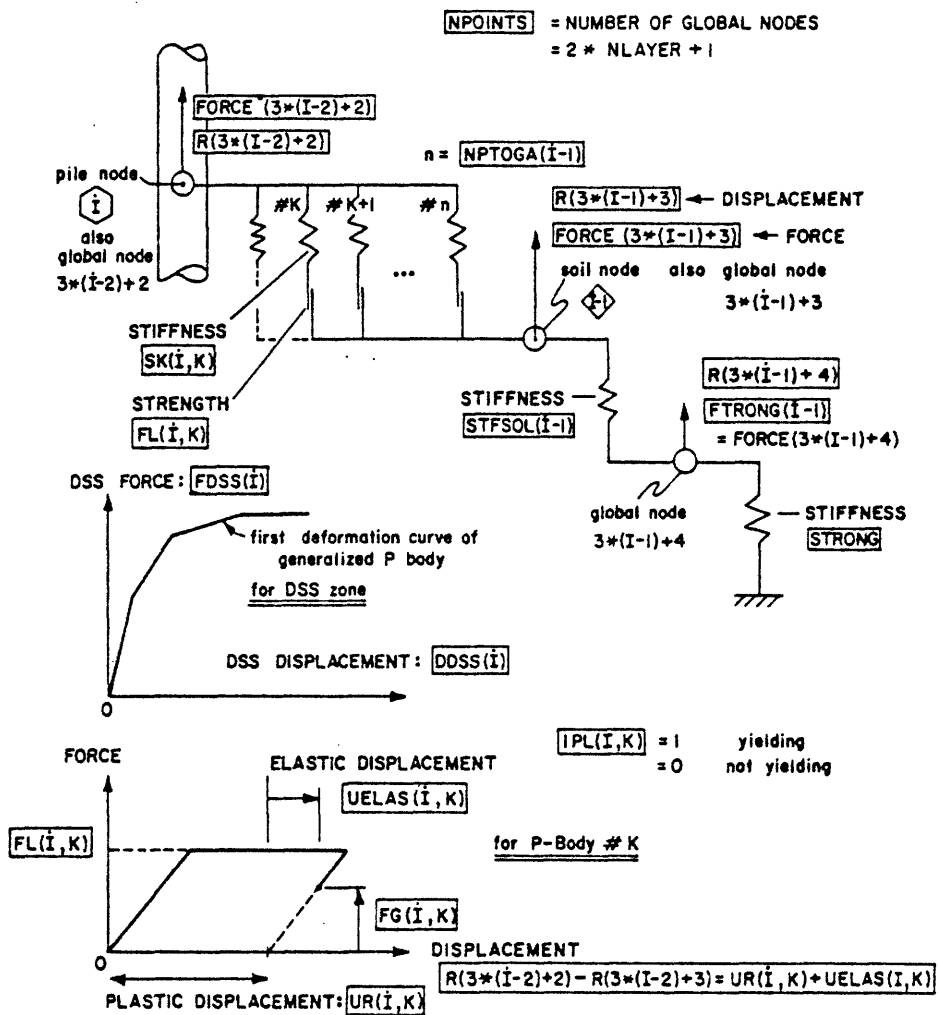


Figure 5.4.3 Basic variables used in TLPILE (2).

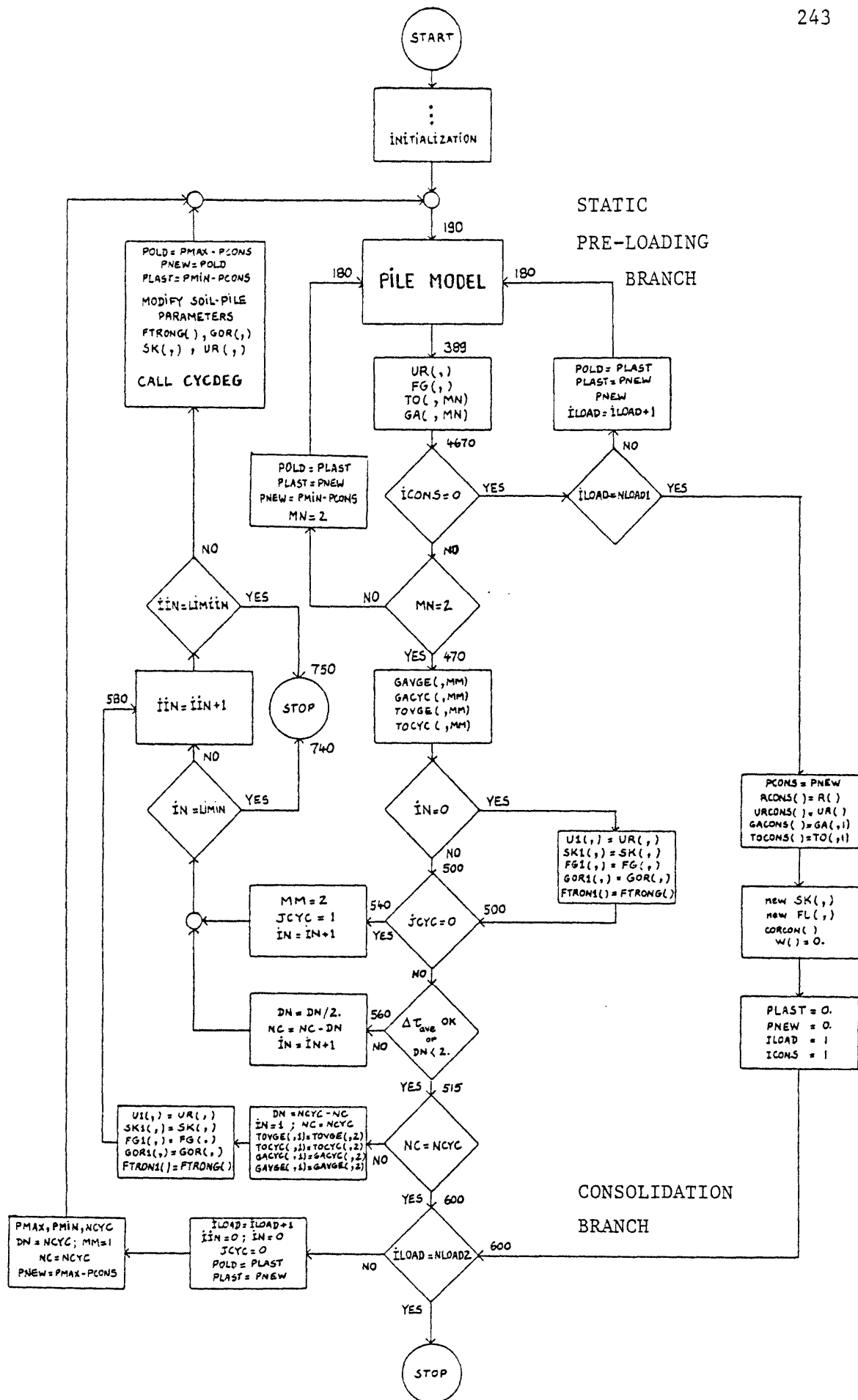


Figure 5.4.4 Flow chart of TLPILE.

## 5.5 EXAMPLES OF APPLICATION OF TLPILE

The objective of this section is to study the storm behavior of a pile foundation designed according to the state-of-the-art.

### 5.5.1 Presentation of the examples

The profile under study is composed of Normally Consolidated Clay (exhibiting normalized behavior) as can be encountered in several deep water environments such as the Norwegian Trench and offshore Western Australia. These clays will usually fall in the category of "low to moderate plasticity" of the API RP2A\*, recommendations, as does Plastic Drammen Clay (the properties of the clay used in the examples will be those of Plastic Drammen Clay). The  $\alpha$ -method will therefore be the same for all these clays. This method considers average values of the soil shear strength and of the ultimate skin friction over the whole pile length. In the present case of a linear distribution of shear strength with depth this will be equivalent to using the values at mid-depth (typically around - 50 m) where the shear strength is slightly larger than the  $72 \text{ KN/m}^2$  corresponding to the transition to  $\alpha = 0.5$ . We shall use this value of  $\alpha$  in all our examples and over the whole pile length.

The loading applied at the template level\*\*, and per foundation template, is characterized by :

- an average tension of 5600 tonnes (54.93 MN)
- and a maximum tension of 10000 tonnes (98.10 MN).

---

\* By contrast with the highly plastic clays of the Gulf of Mexico.

\*\* The weight of the template has already been considered.

Two design options will be considered : an 8-pile template and a 12-pile template. Neglecting group effects, the resulting loadings per pile are :

. for the 8-pile template :

maximum	1250 tonnes (12.26 MN)
average	700 tonnes ( 6.87 MN)
minimum	150 tonnes ( 1.47 MN),

. and for the 12-pile template :

maximum	835 tonnes ( 8.19 MN)
average	470 tonnes ( 4.61 MN)
minimum	105 tonnes ( 1.03 MN).

The load package which we shall apply to the pile top is composed of two successive levels : the first one corresponds to 73 % (of the cyclic component,  $P_{cyc}$ ) of the maximum loads and is effective over  $1 + 2 + 50 + 500 = 553$  cycles, then the maximum load is applied over  $1 + 2 + 5 + 50 = 58$  cycles. This loading pattern is obviously very simple - much too simple in fact to satisfactorily represent a storm - but it has been selected for two reasons :

1 We want to study the effect of a sustained loading comparable to those applied in the in-situ tests (section 2.2) which were extremely simple.

2 We do not know the site and the sea conditions.

The loading at the lower level (553 cycles) is characterized by :

. for the 8-pile template :

maximum	1100 tonnes (10.79 MN)
average	700 tonnes ( 6.87 MN)
minimum	300 tonnes ( 2.94 MN),

and for the 12-pile template :

maximum	735 tonnes ( 7.21 MN)
average	470 tonnes ( 4.61 MN)
minimum	205 tonnes ( 2.01 MN).

The choice of the factor of safety\* (F.S.) is delicate (as usual).

We shall adopt  $FS = 1.5$  as recommended in the RP2A rules for extreme environmental conditions. An additional factor of safety will be introduced in the form of the material coefficient  $k_{cy} = 0.85$  (see Chapter 2). The ultimate pile capacities are therefore given by :

for the 8-pile template :  $1250 * 1.5 = 1875$  tonnes (18.39 MN),

and for the 12-pile template :  $835 * 1.5 = 1250$  tonnes (12.26 MN).

The RP2A rules explicitly include the effective weight of the pile in the ultimate capacity.

The length of the pile is then governed by the choice of the pile diameter (and to a lesser extent by the wall thickness since it affects the pile weight). We shall consider two pile diameters typically used offshore : 72" (183 cm) and 48" (122 cm). The reference thickness will be taken as 2" (5.08 cm), and later increased up to 3" (7.62 cm).

The basic example (number 1) has the following characteristics :

$FS = 1.5,$

$k_{cy} = 0.85,$

diameter = 72 ",

wall thickness = 2 ", and it

belongs to an 8-pile template.

---

\* This factor of safety corresponds to the ratio of the ultimate pile capacity to the allowable pile capacity as defined by the RP2A rules (section 2.26).

Let us evaluate its length to meet the ultimate capacity of 18.39 MN. The ultimate skin friction of depth  $z$  (in meters) is :

$$\begin{aligned} C_a &= \alpha * k_{cy} * 0.22 * \bar{\sigma}_{vo} \text{ (KN/m}^2\text{)} \\ &= \alpha * k_{cy} * 0.22 * .7 * 9.81 * z \text{ (KN/m}^2\text{)} \end{aligned}$$

or :

$$C_a = .755 * .85 z \text{ (KN/m}^2\text{)},$$

so that the ultimate capacity is given by :

$$18393 \text{ (KN)} = .755 * 0.85 * \frac{1^2}{2} * p + 1 (A_{\text{steel}} * 6 + A_{\text{soil}} * .7) * 9.81$$

where  $p$  is the pile perimeter,

$l$  is the pile length,

$A_{\text{steel}}$  is the cross-sectional area of steel,

$A_{\text{soil}}$  is the cross-sectional area of soil inside the pile,

→  $l = 90.69$  meters.

The other examples will constitute variations around this basic example. We shall study the effect of varying five of the key parameters :

1.  $k_{cy}$ , by using both  $k_{cy} = 0.85$  and  $k_{cy} = 1.00$
2. FS, by considering FS = 1.5, 1.3, 1.1, 1.0 and 0.9
3. the pile diameter by using 72" and 48"
4. the type of template (8 piles or 12 piles)
5. the wall thickness by considering two uniform thickness of 2" and 3" and a variable thickness of 2" at the tip and 3" at the top.

We therefore have a total of 10 examples has presented in Table 5.5.1.

We therefore have a total of 10 examples has presented in Table 5.5.1 :

<u>Pile diameter</u>	<u>8-pile template</u>		<u>12-pile template</u>
72 " (183 cm)	FS = 1.5 <u>/1/</u> k <sub>cy</sub> = 0.85 2" uniform l = 90.69 m	FS = 1.5 <u>/2/</u> k <sub>cy</sub> = 1.0 2" uniform l = 84.80 m	FS = 1.5 <u>/3/</u> k <sub>cy</sub> = 0.85 2" uniform l = 73.19 m
	FS = 1.5 <u>/4/</u> k <sub>cy</sub> = 0.85 variable thickness l = 90.56 m	FS = 1.5 <u>/5/</u> k <sub>cy</sub> = .85 3" uniform l = 89.61 m	
48 " (122 cm)	FS = 1.5 <u>/6/</u> k <sub>cy</sub> = 0.85 2" uniform l = 115.29 m		

k <sub>cy</sub> = 0.85 2" uniform 72" Ø 8-pile template	FS = 1.3	l = 84.48 m	<u>/7/</u>
"	FS = 1.1	l = 77.07 m	<u>/8/</u>
"	FS = 1.0	l = 73.11 m	<u>/9/</u>
"	FS = 0.9	l = 68.95 m	<u>/10/</u>

Table 5.5.1 Definition of examples.



## 5.5.2 The basic example

### 5.5.2.A. Description of the input

The pile is composed of 10 segments. It has a free standing length of 5 meters, so that the total length is 95.69 meters. The fixed boundary is taken 10 radii away from the pile, while the DSS zone is half a radius in width. The ratio  $G/\bar{\sigma}_{vo}$  is taken as 100, which is representative of Plastic Drammen Clay at a strain of  $10^{-3}$ .

The DSS stress-strain relationship used in each layer is multilinear with 6 intermediate points, excluding the origin. It is obtained from Figure 4.5.2 so that, with the strain rate correction factor of 1.1, it fits the fast undrained test curve. The ultimate friction (on the t-z curve) is reached for a displacement of 0.91 % of the pile diameter.

Since the clay exhibits normalized properties these parameters are applied all along the pile. Appendix 5.C presents the data file corresponding to example/1/ and can be used together with the Fortran listing to complete the description of TLPILE (including the soil degradation data base).

### 5.5.2.B. Static loadings

It is useful to start our analysis by considering the behavior of the pile under static loading. Let us first recognize that the pile's true ultimate friction capacity is equal to 18.0 MN which corresponds to (18.39 MN - the effective weight of the pile : 3.1 MN) / 0.85. If the pile is loaded rapidly before consolidation the ultimate capacity can be estimated as :  $18.0 * 1.1 + 3.1 \approx 22.9$  MN. After consolidation under 6.87 MN applied at its top, the pile will have accumulated some additional resistance as shown in Figure 5.5.1 which gives the force-displacement curve to failure. The ultimate capacity in this case is 24 MN.

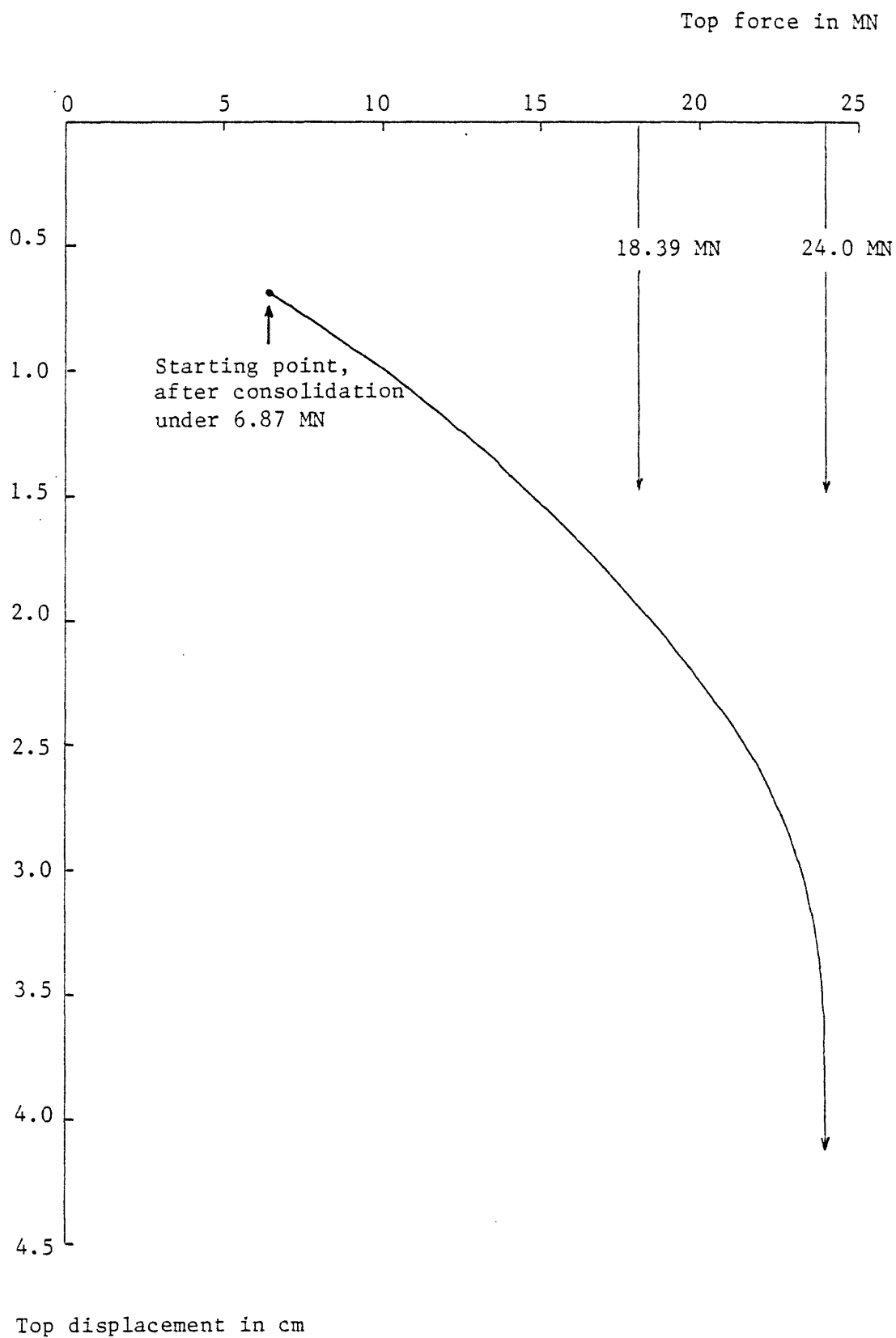


Figure 5.5.1 Force displacement curve to failure,  
basic example.

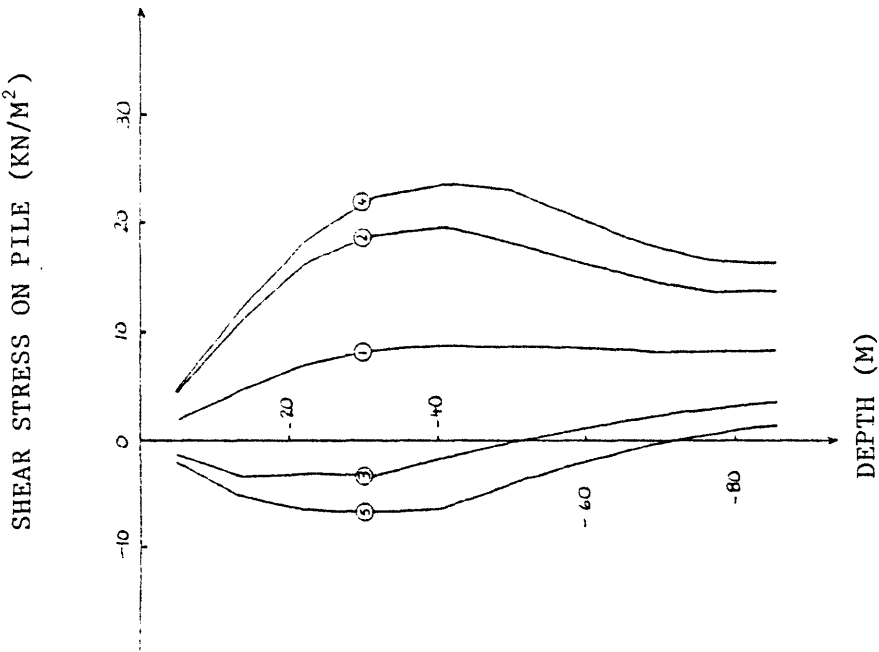
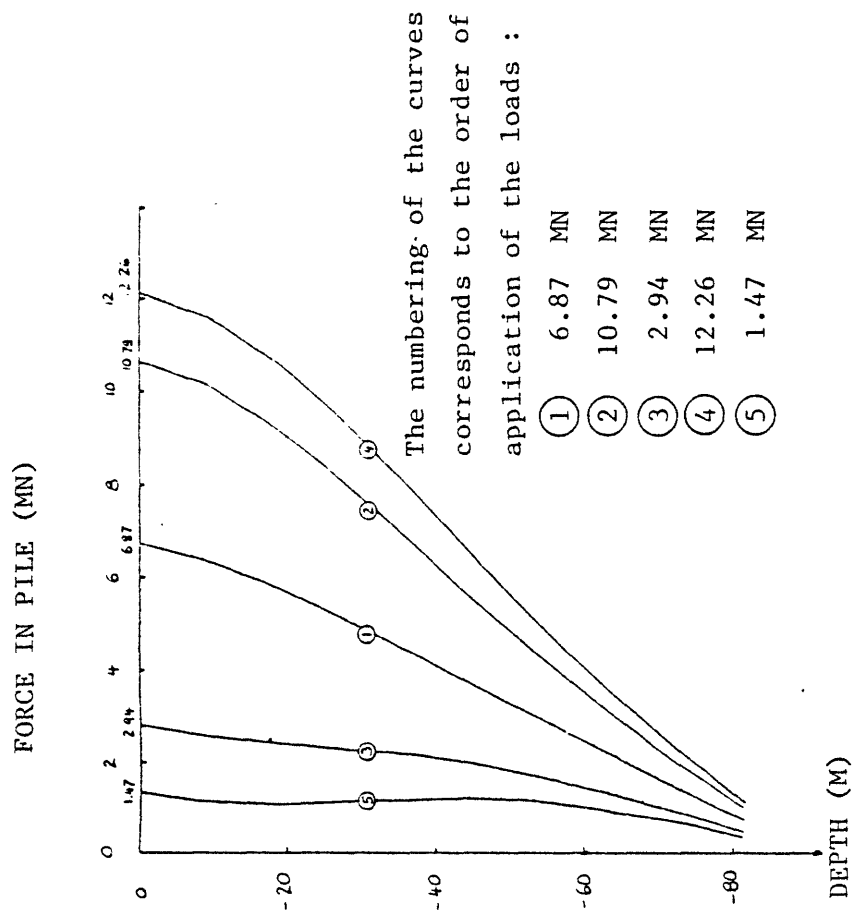


Figure 5.5.2.b Shear stress distribution on pile, static loading.



The numbering of the curves corresponds to the order of application of the loads :

- ① 6.87 MN
- ② 10.79 MN
- ③ 2.94 MN
- ④ 12.26 MN
- ⑤ 1.47 MN

Figure 5.5.2.a Force distribution in pile, static loading.

Of great interest to our research are the shear stress and force distributions along the pile. Let us consider the following (fast) loading : first we consolidate under 6.87 MN, then we go to 10.79 MN, down to 2.94 MN, up to 12.26 MN and finally down to 1.47 MN. This loading will define all the distributions which would be encountered during the first cycle of application of the lower load level (10.79 MN, 2.94 MN) and of the upper load level (12.26 MN, 1.47 MN) when applied just after consolidation. The corresponding distributions with depth of the force and of the shear stresses are shown in Figure 5.5.2.a and b. At a given depth the shear stress is proportional to the slope of the force distribution. These curves will be used later on to estimate the changes associated with the cycling.

#### 5.5.2.C. Cyclic loading

The results of the analysis will be presented graphically through four types of diagrams :

- 1 the force-displacement relationship at the top of the pile,
- 2 the history of the displacement at the top of the pile,
- 3 the distribution of the force in the pile, and finally
- 4 the distribution of the shear stresses along the pile.

The first two diagrams are given in Figure 5.5.3.a and b. The force-displacement diagram of Figure 5.5.3.a shows\* :

- . a very small permanent displacement (0.45 mm) accumulated during the cycling (this displacement is a lower bound since it is obtained by reloading from the minimum load to the consolidation load),
- . a very small change of the cyclic stiffness of the pile.

---

\* The preliminary loading curve shown on the figure leads to the consolidation load of 6.87 KN and its associated displacement. Also represented are the permanent displacement and the cyclic stiffness at the end of each load level.

The history of the top displacement (Figure 5.5.3.b) shows in addition that :

- the main changes in the rate of displacement seems to occur in the first 50 to 100 cycles of the initiation of the cycling (even though these changes are small).

Let us consider the distributions of the force and shear stresses along the pile, first by considering the lower level of loading in Figure 5.5.4.a and b. The curves corresponding to  $N = 1$  are evidently the same as those obtained during the static loadings of the last section (Figure 5.5.2.a and b). The load distribution diagram (Figure 5.5.4.a shows that :

- the maximum load is progressively transferred towards the tip of the pile,
- the minimum load distribution is rather stable.

The shear stress distribution curves of Figure 5.5.4.b allows us to add that :

- there is a systematic loss of cyclic shear stress in the top 30 meters of the pile,
- under the maximum load, the effect of the first 50 cycles is very similar to that of the last 500 cycles,
- the tip of the pile is subjected to an increase of both cyclic and average shear stresses.

Similar distributions for the upper load level are given in Figure 5.5.5.a and b. Figure 5.5.5.a clearly indicates :

- a loss of residual stresses under the minimum load (comparison with curve ⑤ of Figure 5.5.2.a),

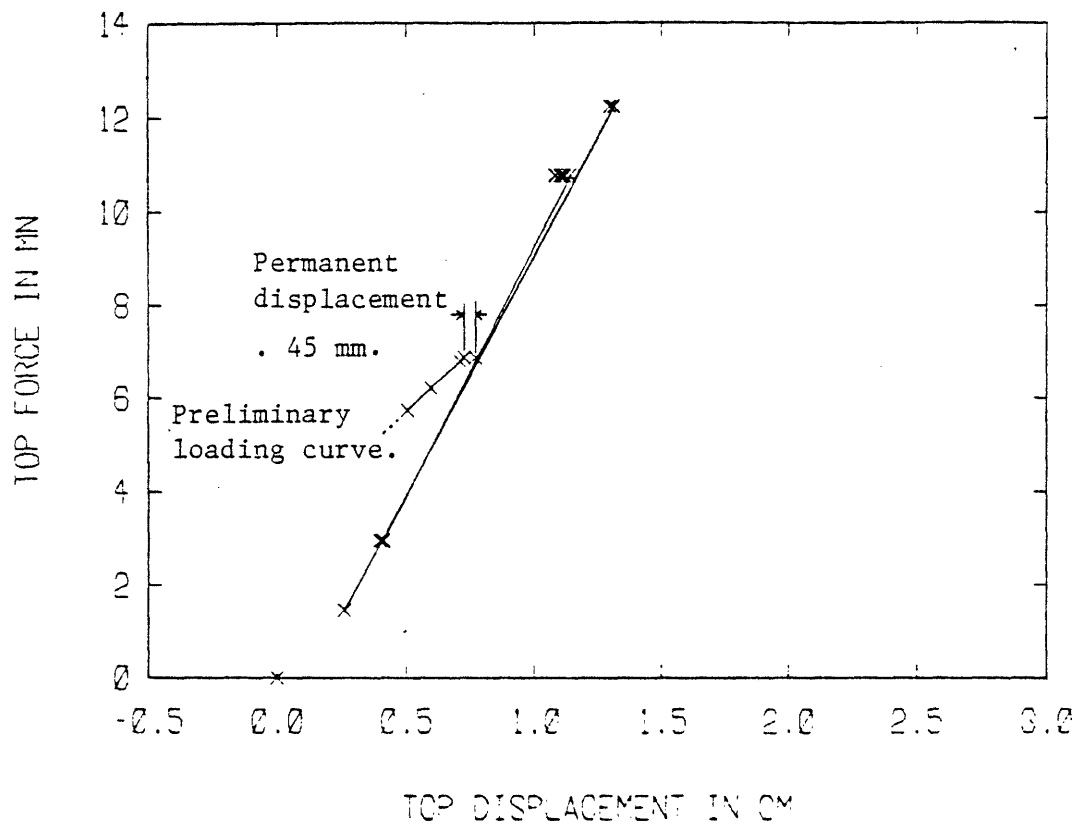


Figure 5.5.3.a Force-displacement at pile top, example /17/.

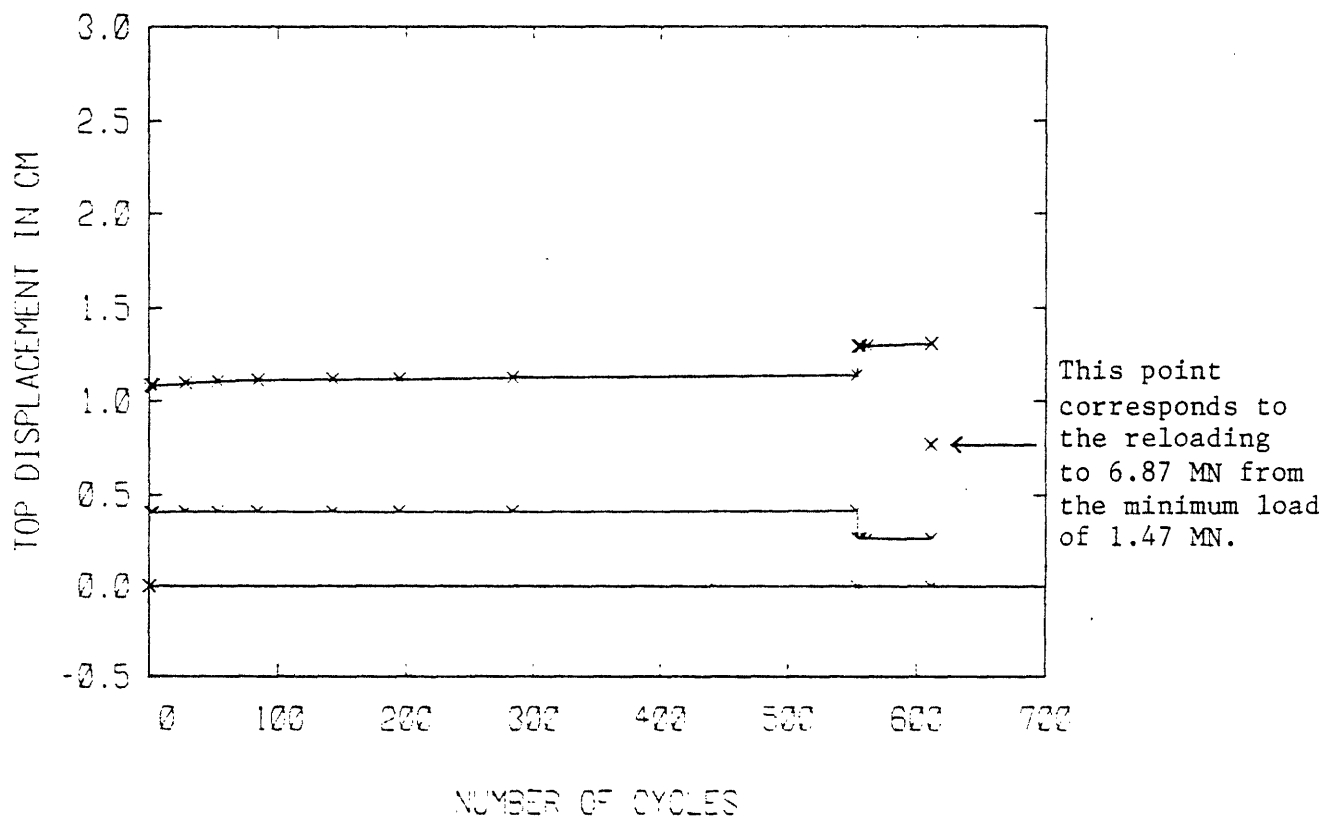
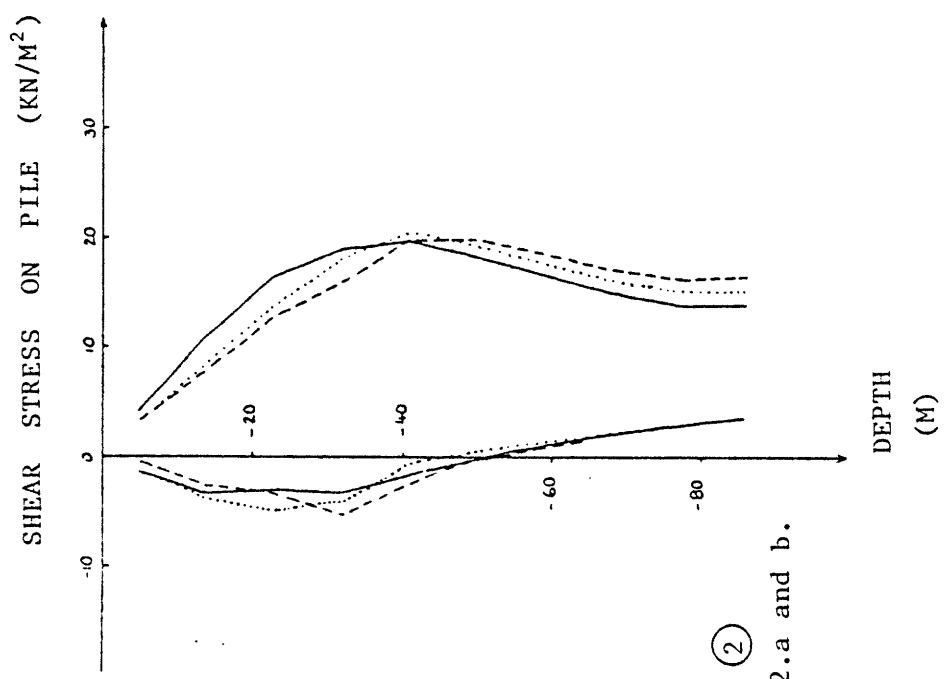


Figure 5.5.3.b History of displacement at pile top, example /17/.



\_\_\_\_\_ N = 1, corresponds also to (2)  
 and (3) of Figure 5.5.2.a and b.  
 ..... N = 53,  
 ----- N = 553.

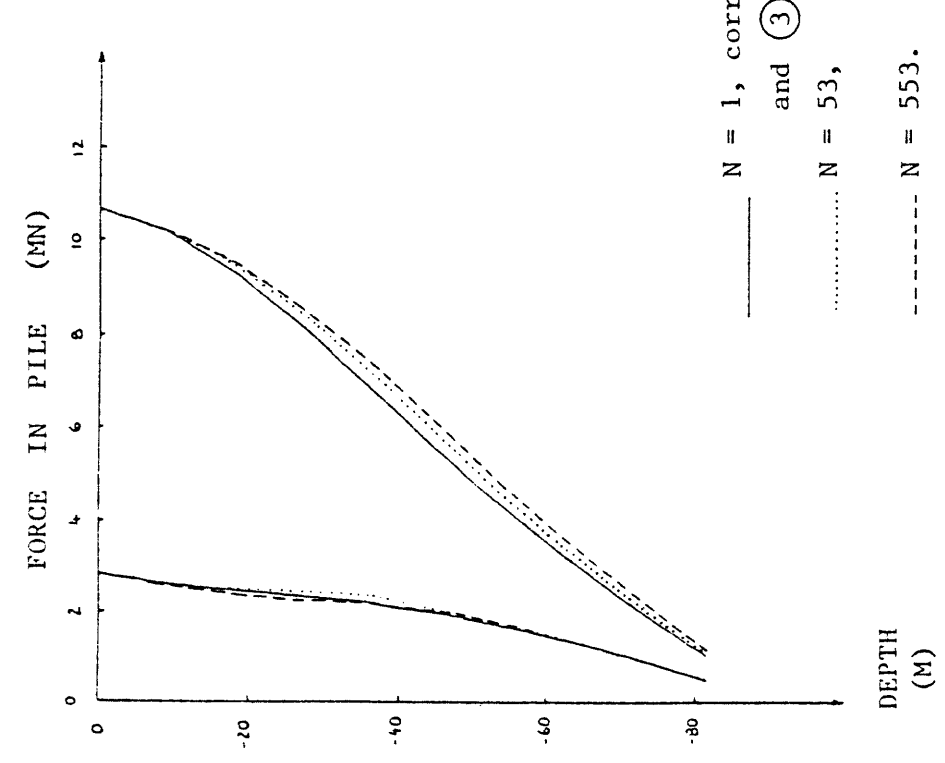


Figure 5.5.4.a Force distribution in pile, example /1/, lower load level.

Figure 5.5.4.b Shear stress distribution on pile, example /1/, lower load level.

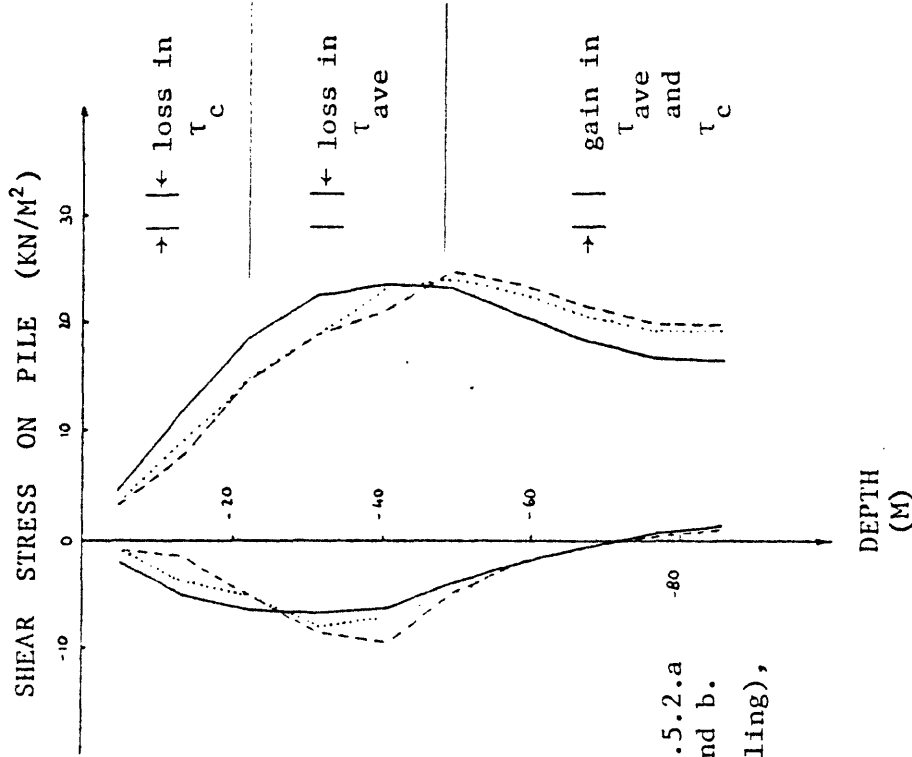
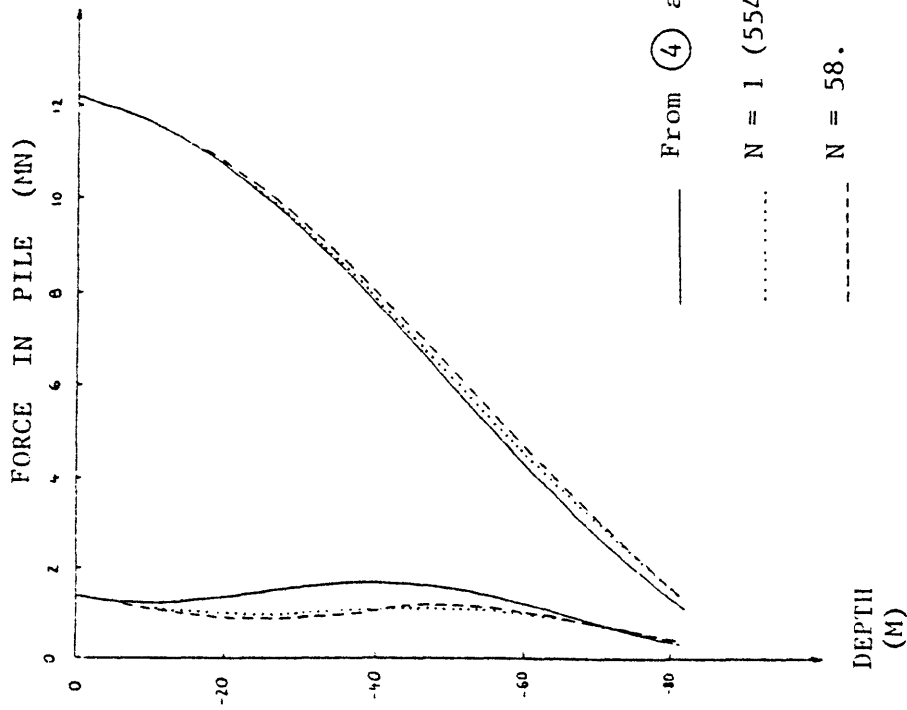


Figure 5.5.5.a Force distribution in pile, example /1/, upper load level.

Figure 5.5.5.b Shear stress distribution on pile, example /1/, upper load level.



and finally Figure 5.5.5.b allows us to distinguish between :

- three zones along the pile corresponding to a loss of  $\tau_c$  at the top, a loss of  $\tau_{ave}$  in the middle and a gain in both  $\tau_{ave}$  and  $\tau_c$  at the tip of the pile.

This schematic description of the results of example /1/ will now serve as references in our study of some design variations.

### 5.5.3 Variations around the basic example

We shall differentiate between geometric parameters such as thickness, diameter of the pile and the choice of the template type and safety parameters such as the factor of safety F.S. and the material coefficient  $k_{cy}$ .

#### 5.5.3.A. A geometric parameters

##### a) Thickness :

Example /5/ corresponds to a uniform thickness of 3", all the other parameters being essentially the same as those of example /1/ (with the exception of the total length of  $89.61 + 5 = 94.61$  meters). The pile is therefore stiffer than in the basic example.

The force displacement relationship of Figure 5.5.6.a greater cyclic stiffness and leads to a permanent displacement of 0.31 mm. At the same time the history of the displacement (Figure 5.5.6.b) is very similar in evolution to that of example /1/ with the exception of the displacement range ; very little degradation actually occurs.

Figure 5.5.7 compares the shear stress distributions in example /1/ (5.5.7.a) and those of example /5/ (5.5.7.b). (The format of

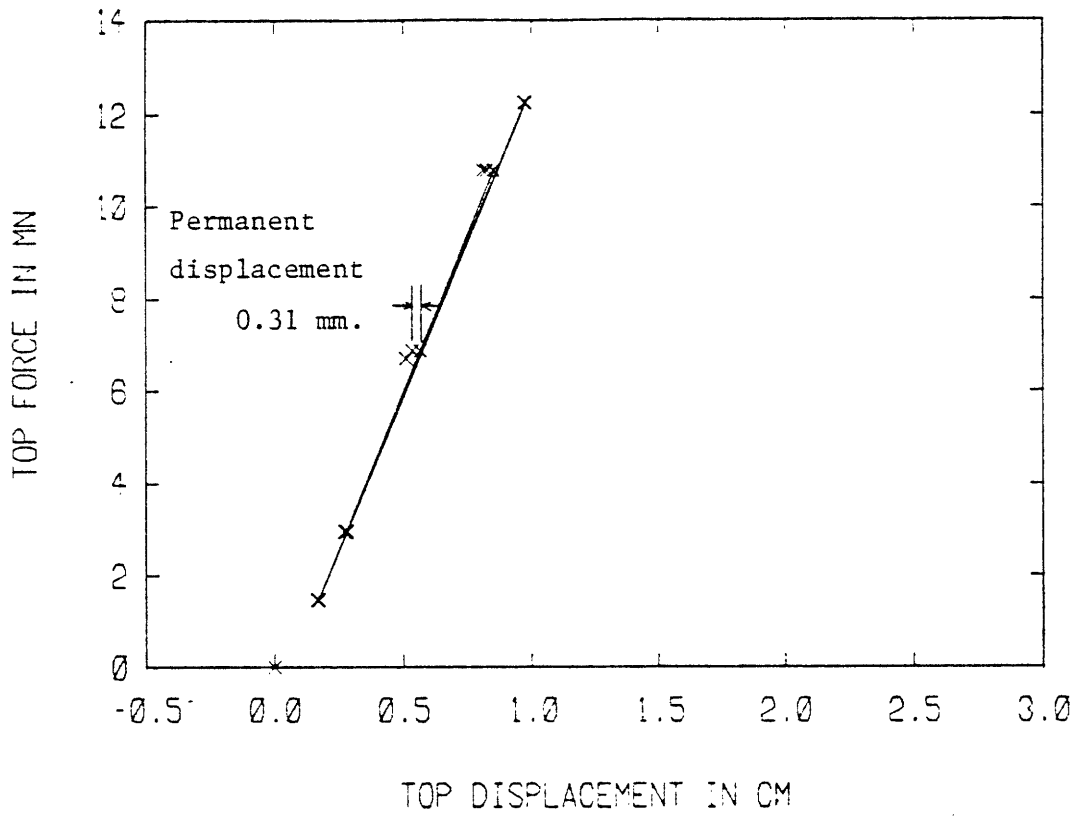


Figure 5.5.6.a Force-displacement at pile top, example /5/ uniform wall thickness of 3".

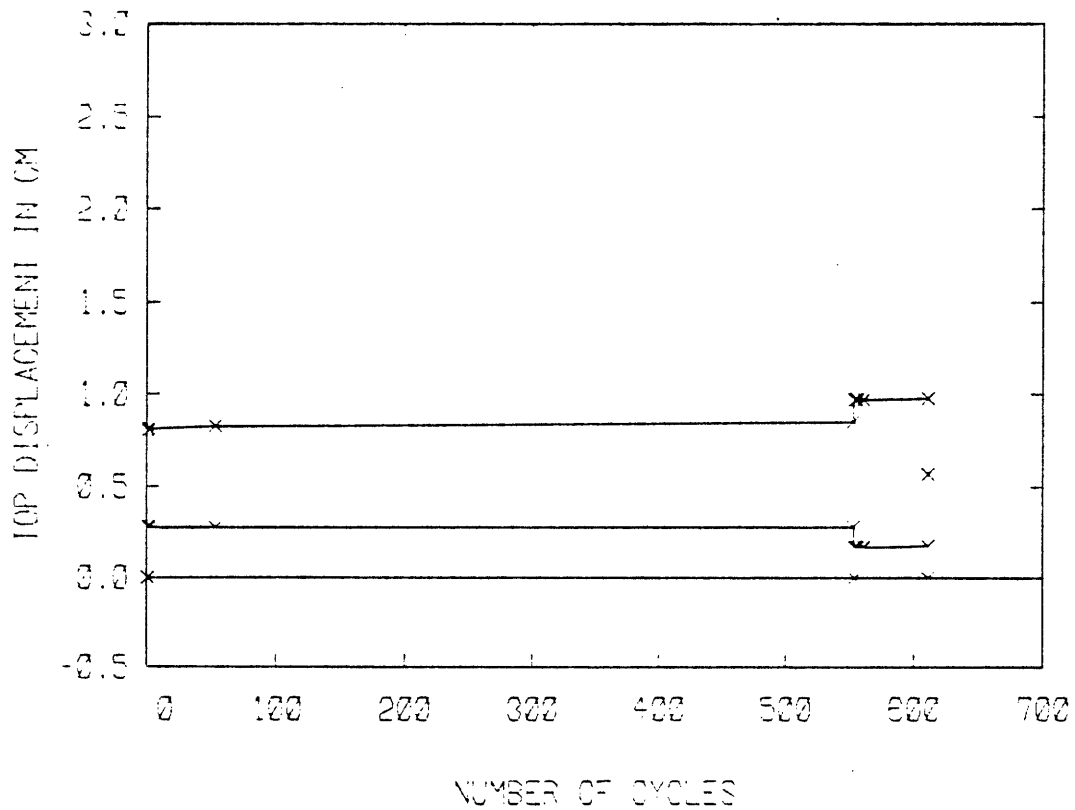


Figure 5.5.6.b History of displacement at pile top, example /5/ uniform wall thickness of 3".

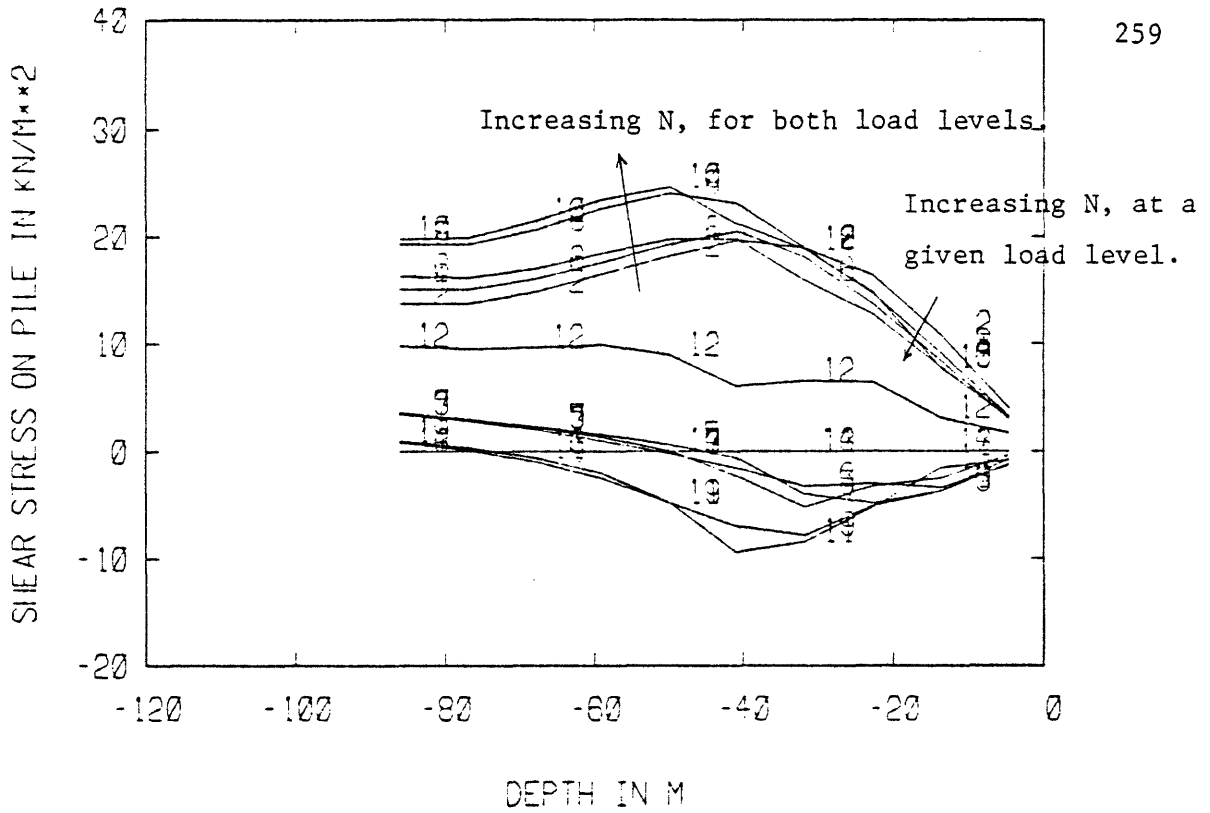


Figure 5.5.7.a Shear stress distribution in pile, example /1/  
uniform wall thickness of 2".

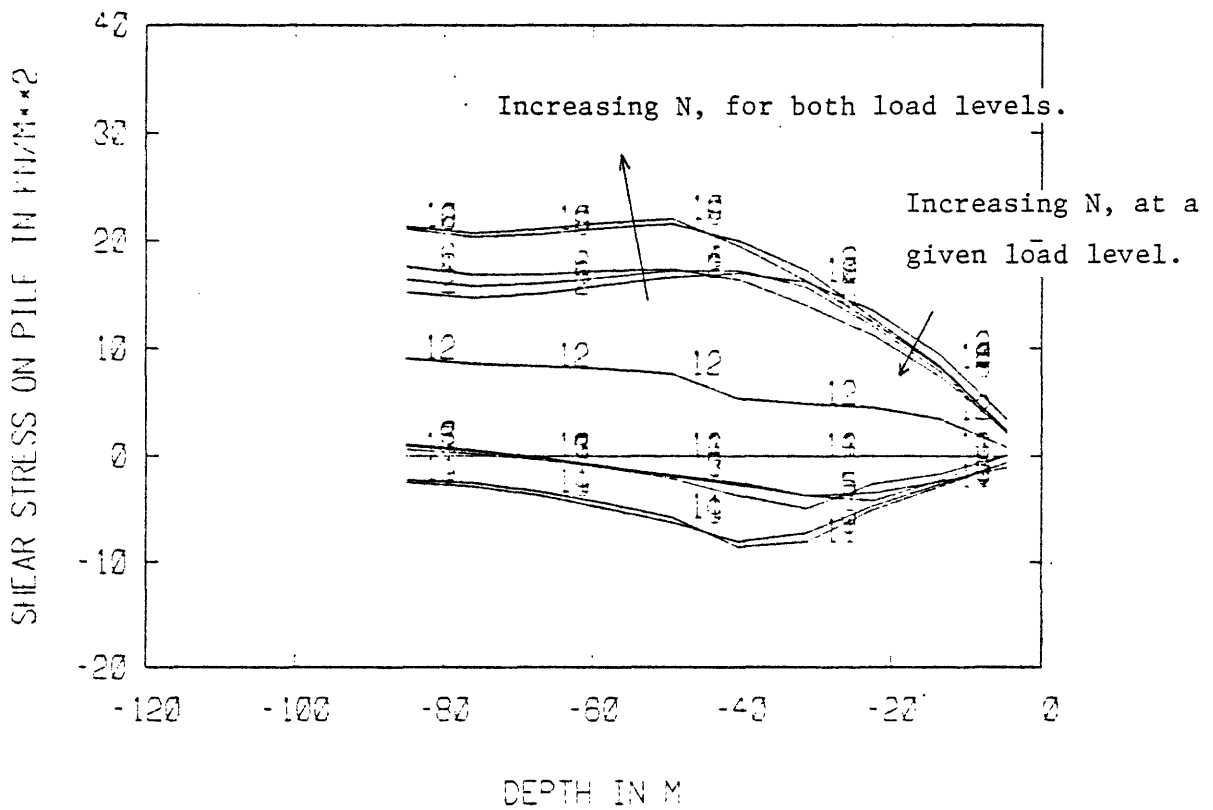


Figure 5.5.7.b Shear stress distribution in pile, example /5/  
uniform wall thickness of 3".

presentation is different\* but the scaling is the same as before). The two patterns are also very similar ; the stiffer pile of example /5/ leads to more linear distributions (recall Figure 4.1.1 for an infinitely rigid pile). In the lower part of the pile the shear stresses under maximum load increase regularly with time, while at the top of the pile, there is a decrease of shear stress at each load level (but a higher stress at the beginning of the upper load level than at the end of the lower one). Example /4/ dealt with a variable thickness (3" of top 30 % of pile, 2.5" over next 30 % and 2" over the remaining 40 %). It led to a permanent displacement of 0.35 mm, and in general as was expected, to a behavior intermediate to those of example /1/ and /5/. Overall the change of thickness was not found to affect significantly the pile response.

b) Diameter :

A change of pile diameter, keeping the other parameters constant, affects both the length and the section of steel, and results in a much softer response as we shall now see.

Example /6/ considered a 48" (122 cm)-diameter pile of 115.29 meters. The force-displacement at the top (Figure 5.5.8.a) indicates a

---

\* The numbering on the plots corresponds to the following sequence :

	<u>-lower level-</u>			<u>-upper level-</u>	
number of cycles	1	53	553	1	58
max. load ...	2	4	6	8	10
min. load ...	3	5	7	9	11

number 12 is assigned to the reloading to the mean load (6.87 MN),  
number 13 and 14 are ignored.

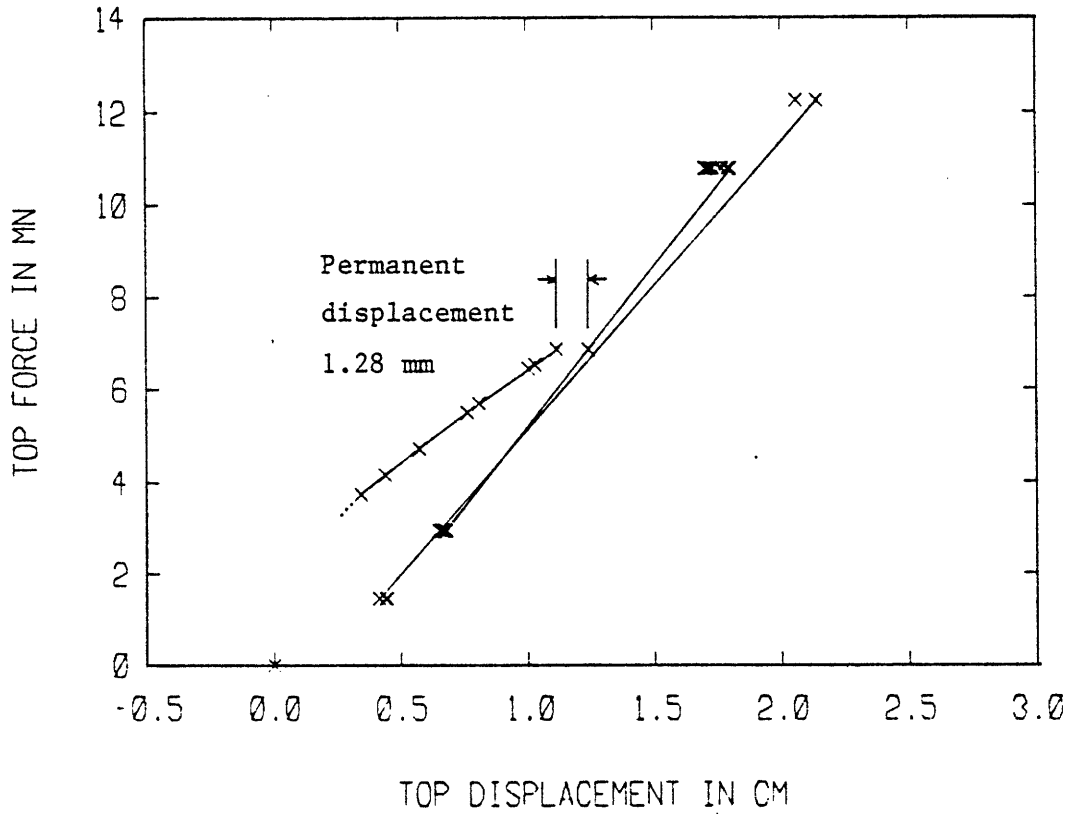


Figure 5.5.8.a Force-displacement at top, example /6/  
pile diameter 48".

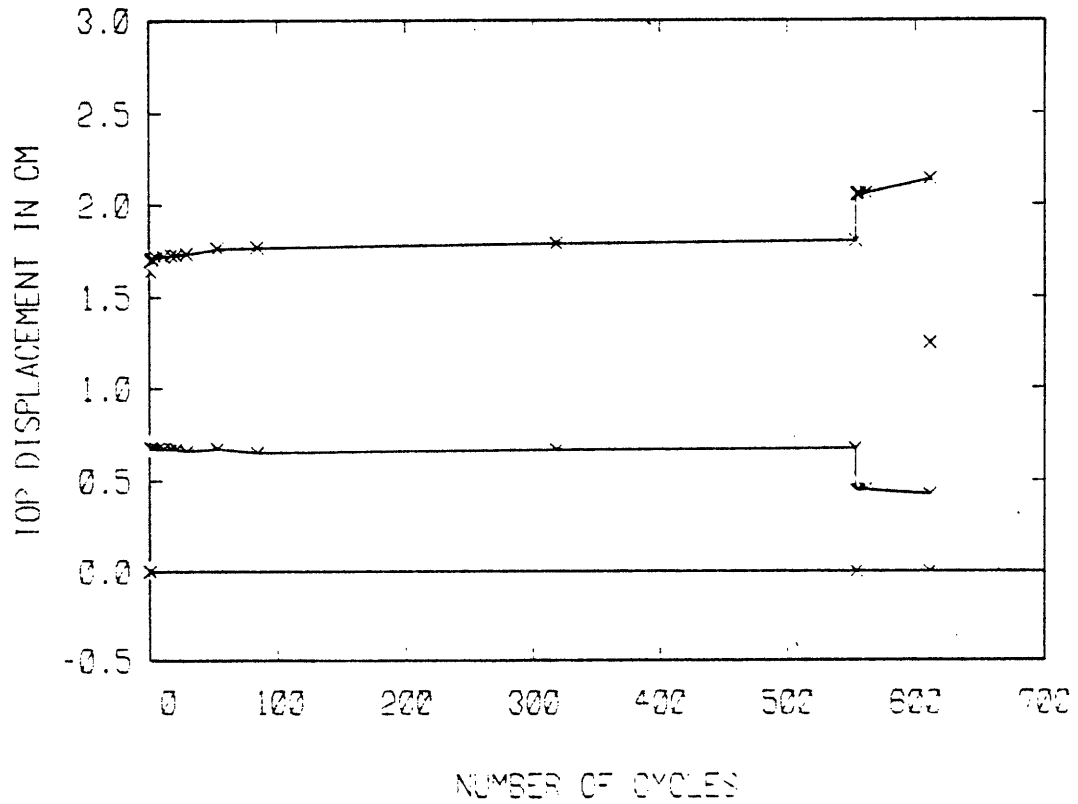


Figure 5.5.8.b History of displacement at pile top, example /6/  
pile diameter 48".

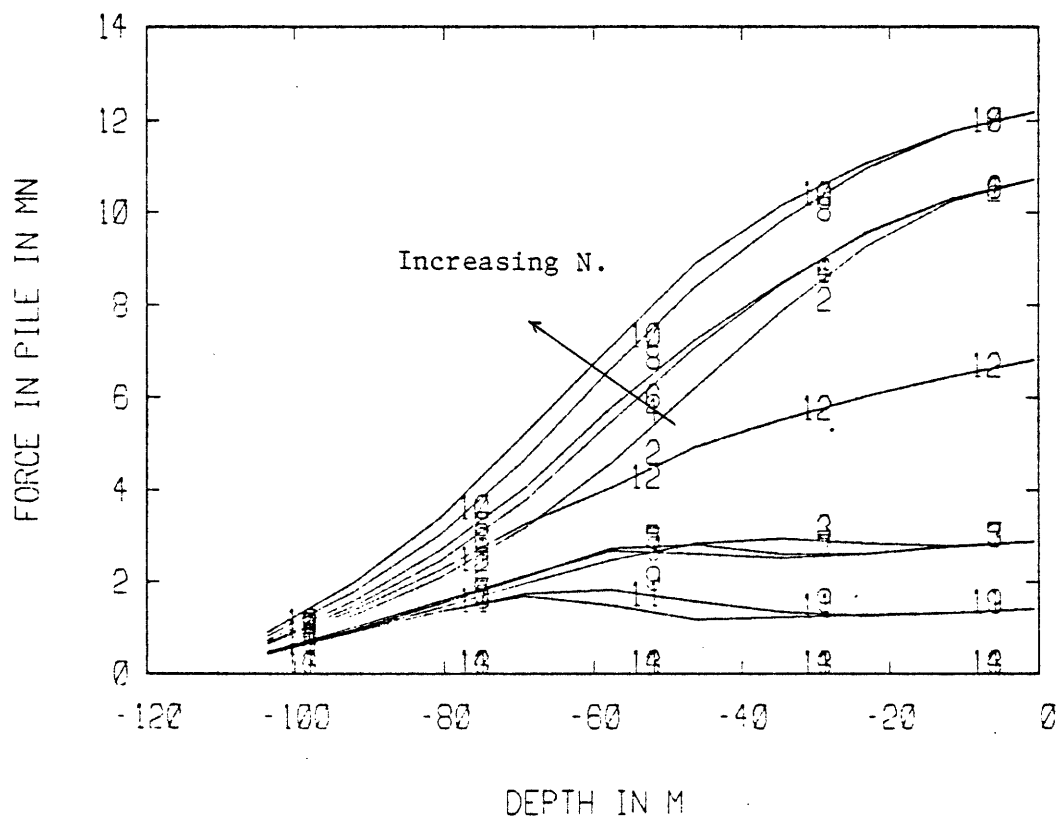


Figure 5.5.9.a Force distribution in pile, example  $\sqrt{6}$  pile diameter 48".

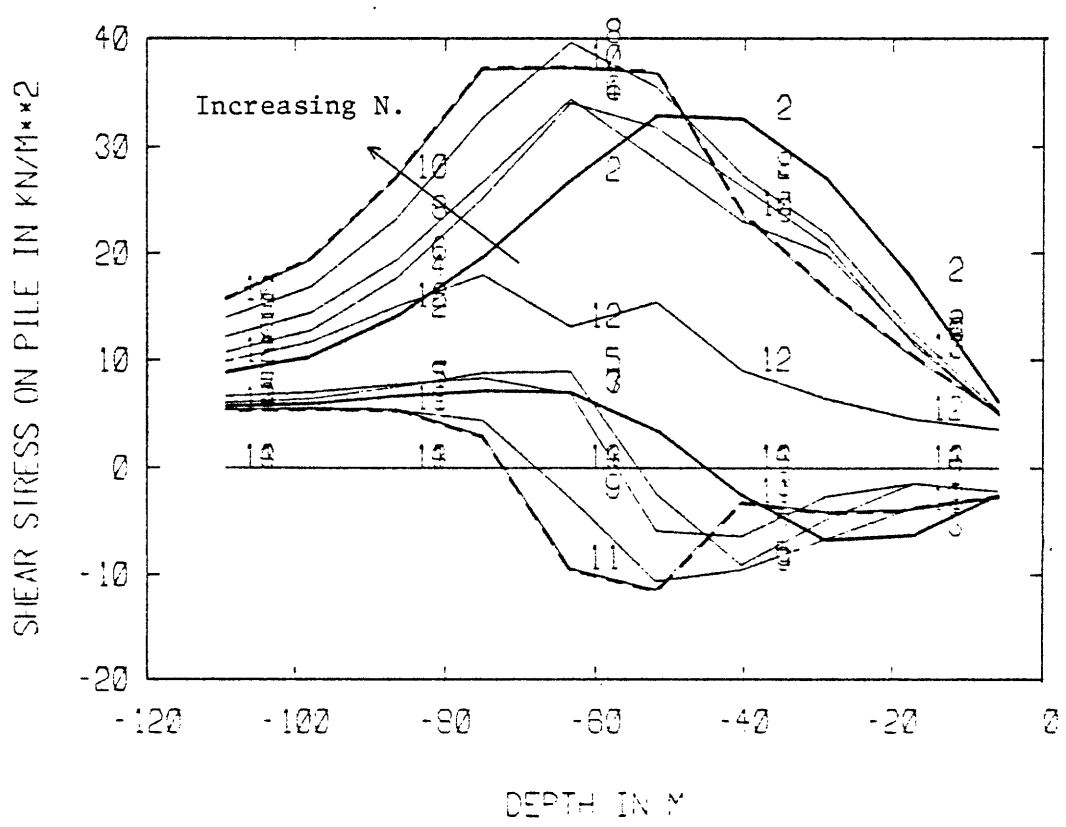


Figure 5.5.9.b Shear stress distribution on pile, example  $\sqrt{6}$  pile diameter 48".

marked increase in the permanent displacement to 1.28 mm and noticeable changes of cyclic stiffness at both load levels. It is interesting to note that once again the response during the 50 to 100 first cycles cannot be extrapolated to cover the remaining cycles at the lower load level. Also the minimum displacement seems to actually decrease during the first cycles of application of each load level, this period corresponding to a sharp decrease of the cyclic stiffness which then seem to stabilize after 100 cycles in the case of the lower load level.

The force distribution (Figure 5.5.9.a) and the shear stress distribution\* (Figure 5.5.9.b) confirm the significant changes occurring along the pile. The shear stress distributions corresponding to the first cycle at the lower load level have been highlighted by thicker lines whereas dotted lines have been used for the last cycle curves (of the upper load level). The shift of the distributions towards the tip of the pile is obvious and the loss of resistance at the pile top is severe.

The pile diameter is thus viewed as an important parameter affecting the pile response. A smaller diameter, and thus a slender pile, results in more cyclic degradation.

c) Choice of template :

Example /3/ analyzed the case of a pile belonging to a 12-pile template. Its length was 73.19 meters and its section characteristics

---

\* Note that the change of diameter results in higher stresses on the pile. The scaling of the plot is still the same as for example /1/.

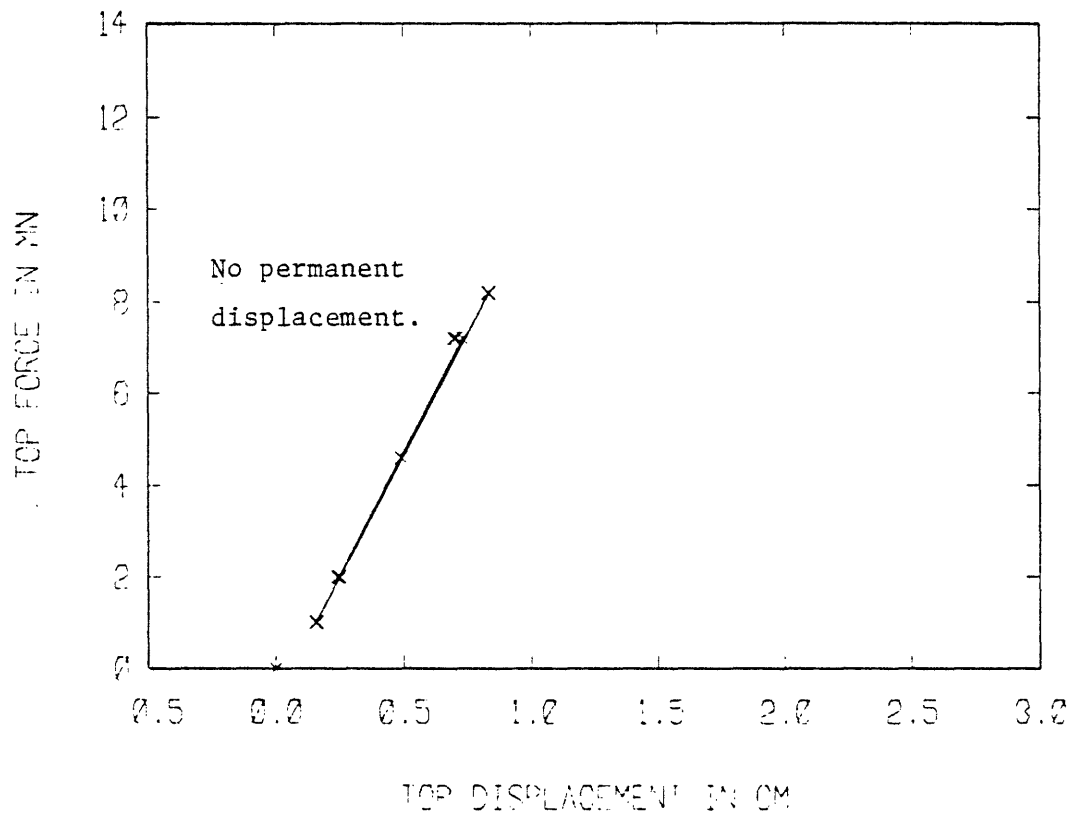


Figure 5.5.10.a Force-displacement at top, example /3/  
12-pile template.

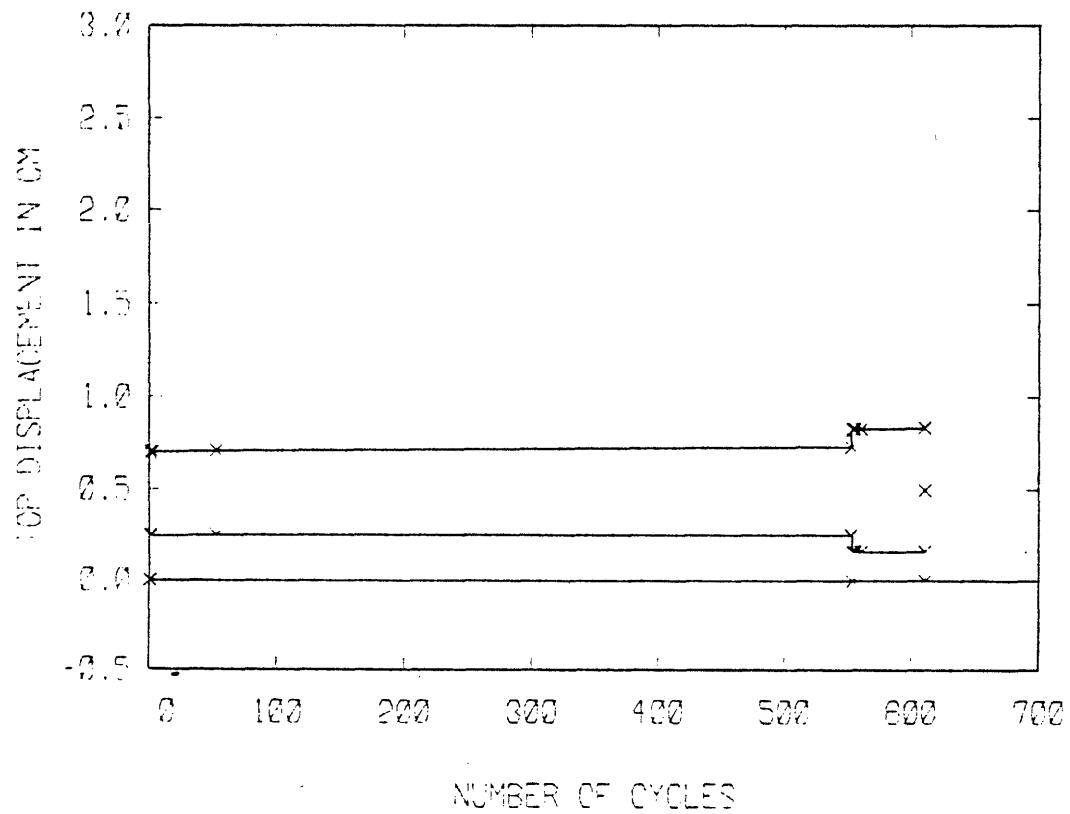


Figure 5.5.10.b History of displacement at pile top, example /3/  
12-pile template.



were those of example /1/. The shortening of the pile affects the behavior as would the increase of the thickness (example /5/). The force-displacement at the top (Figure 5.5.10.a) shows an essentially elastic response with no permanent displacement (our lower bound is 0.0 mm) and no degradation of the cyclic stiffness. The same results are found from the history of the displacement (Figure 5.5.10.b). The shear stress distribution was almost identical to that of example /5/ (Figure 5.5.7.b).

### 5.5.3.B. Safety parameters

The change of  $k_{cy}$  from 0.85 to 1.00 with FS = 1.5 is equivalent to keeping  $k_{cy} = 0.85$  and changing FS to  $\approx 1.3$ , and therefore example /2/ and example /7/ lead to essentially the same results. In other words, we can restrict ourselves to the variation of F.S. while maintaining  $k_{cy} = 0.85$ .

Table 5.5.1 sketches the different types of ultimate capacities which can be considered :

- there is the design ultimate capacity obtained with  $k_{cy} = 0.85$ ,  
the "actual" ultimate capacity obtained with  $k_{cy} = 1.00$ ,
- and its correction for strain rate effects.

We do not consider in this table the gains accumulated during consolidation. It can be seen that the design factor of safety F.S. (column # 2) is well lower than the effective factor of safety against a fast pull-out as given by column # 7. Now what will be the effect of F.S. on the cyclic behavior of the pile ? Figure 5.5.11 presents a comparison of the force displacement relationships and of the histories of displacement at the pile top for tests /7/ through /10/. It can be seen

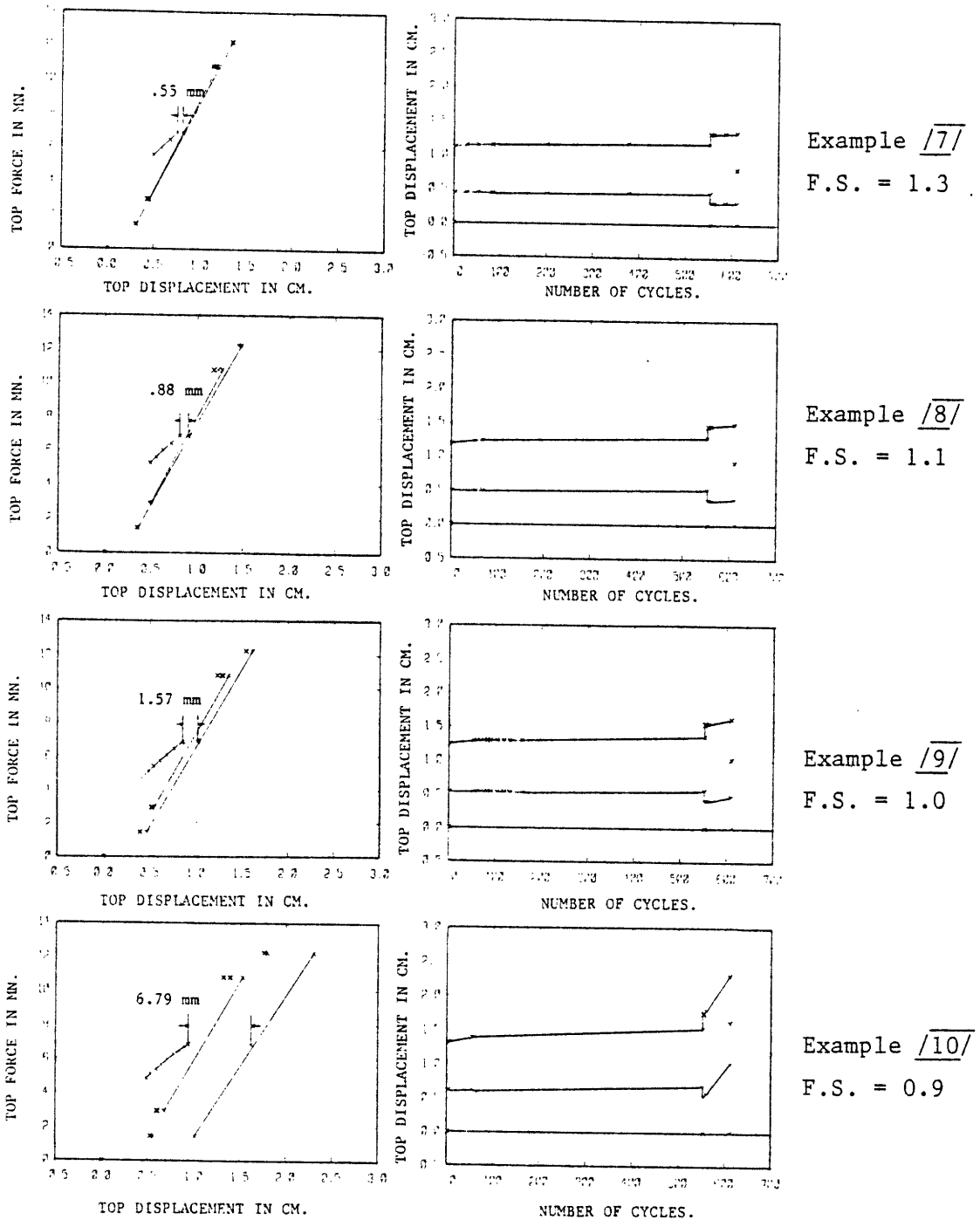


Figure 5.5.11 Force displacement relationships and histories of the displacement at the pile top for various values of the factor of safety F.S.

<u># 1</u>	<u># 2</u>	<u># 3</u>	<u># 4</u>	<u># 5</u>	<u># 6</u>	<u># 7</u>	
<u>Example</u>	<u>F.S.</u>	Ultimate capacity with $k_{cy}=0.85$	<u>Actual ultimate capacity</u>	<u>Estimate actual ultimate capacity + strain rate effect</u>	<u>Weight</u>	<u>Total</u>	<u>Results column # 7 divided 12.26 MN</u>
2,7	1.3	13.170	15.495	17.05	2.77	19.82	1.60
8	1.1	10.960	12.895	14.18	2.53	16.71	1.36
9	1.0	9.860	11.60	12.76	2.34	15.10	1.23
10	0.9	8.770	10.32	11.34	2.26	13.60	1.11

Does not consider gains from consolidation.

Table 5.5.2 Various definitions of the ultimate capacities and factors of safety.

that at the lower load level the evolution with decreasing F.S. is steady but such is not the case for the upper load level where cyclic rupture is clearly initiated in example /10/. The cyclic stiffness does not change very much, even upon reaching this zone of quick degradation. The permanent displacements have been also plotted versus F.S. in Figure 5.5.12. The results of the analyses are very consistent and demonstrate a tendency for a abrupt change of behavior around F.S. = 1. The state-of-the-art design corresponds to a very safe situation in terms of accumulation of displacements.

#### 5.5.4 Conclusions

The results of these analyses should not be accepted as such before confirmation of their validity is granted by experimental means. Many

PERMANENT  
DISPLACEMENT (MM)

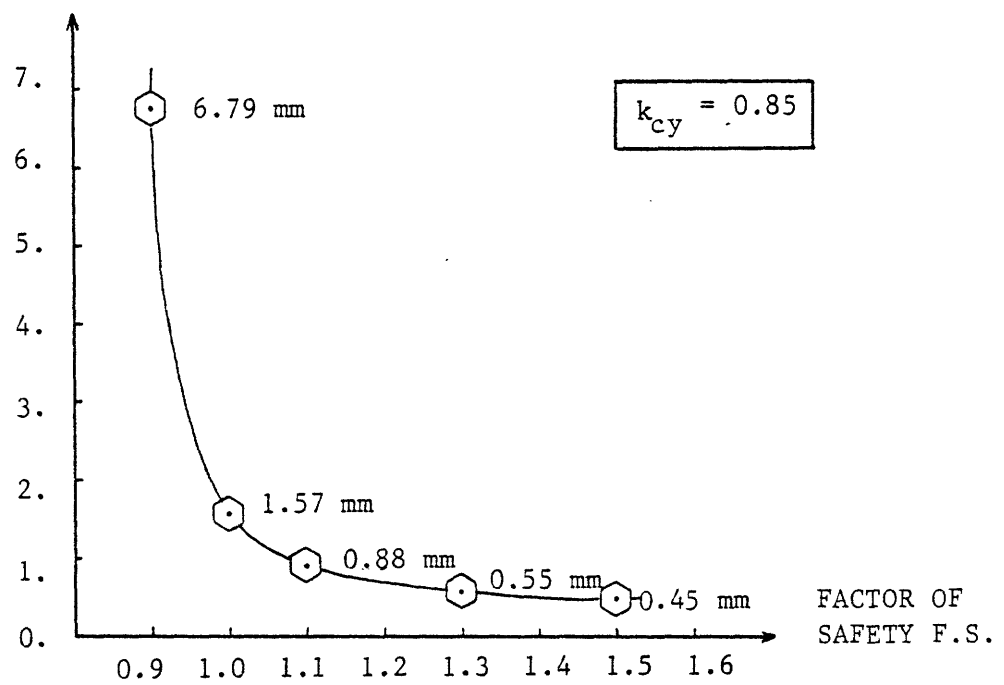


Figure 5.5.12 Permanent displacement versus factor of safety F.S.

delicate assumptions had to be made throughout the construction of the methodology on which TLPiLE is based, and we cannot overlook the fact that some fundamental aspects of soil behavior have been crudely represented (drained and undrained cyclic creep for example). However it is legitimate to express some satisfaction in view of the apparent fit existing between our results and the experimental evidence.

The limited degradation of the cyclic stiffness, the importance of the first 50 to 100 cycles (forbidding extrapolation), the transfer of force and shear stresses down the pile under maximum load and the complex distributions under minimum load are all key elements of actual pile behavior under cyclic loading.

Finally, a word should be said of the cost of running an analysis. The preparation of the input, without previous knowledge of the program, is a matter of 3 hours and the actual running takes 46 seconds of CPU time on the VAX 11/782. Most of the plots shown in this section are provided on request by the program as well as print outs of the results of various levels of sophistication.

---

## 6 SUMMARY, CONCLUSIONS AND RECOMMENDATIONS

### 6.1 SUMMARY

#### 6.1.1 Recapitulation of objectives

The thesis focuses on the behavior of a tension pile embedded in clay and subjected to undrained cyclic loading. The motivation behind this study is the development of foundations for Tension Leg Platforms (TLPs). The objective of the research was stated as follows in the introductory chapter :

"to contribute to the development of a methodology that will ultimately allow us to follow the evolution of the pile-soil contact degradation and to estimate the redistributions of stresses and strains occurring during a storm as well as the resulting displacements of the foundation".

#### 6.1.2 Contributions

The key contributions of this work can be reviewed within the framework of the trilogy used throughout the thesis : the Pile Model, which deals with the theoretical behavior of the mechanical component of the methodology, the Soil Degradation Data, which relate to the experimental study of the fatigue of soil, and the analytical tool TLPILE.

#### 6.1.2.A. The Pile Model

The Pile Model, title of chapter 3, is composed of a one-dimensional segmented elastic pile embedded in a soil represented by elasto-perfectly-plastic elements (the P-bodies) grouped in assemblages (the Iwan models) which are decomposable in branches placed in series and in parallel. These assemblages are representing the behavior of Direct Simple Shear (DSS) zones located directly in contact with the pile and where plastic strains are concentrated so that away from this zone the soil remains elastic. The Pile Model is an extension of traditional models used to study piles under static loading and based on the concept of "t-z" curves. A construction of these "t-z" curves, which relate the local displacement of the pile to the local force applied by the soil to the pile, was proposed on the basis of local DSS stress-strain relationships. The concept of "t-z" curves was then adapted to cyclic loading by considering them as first-deformation curves of Iwan models. These models respect, in their symmetrical form, the extended Masing rules, but are restricted to time-independent elasto-plastic parameters. In other words the soil degradation per se (the soil fatigue) is not considered at this stage.

It was shown that the Pile Model as a whole could be viewed as an Iwan model. Properties of symmetrical Iwan models under cyclic loading can be summarized by the following points.

1. Stabilization to a closed loop occurs in one-and-one-half cycle of loading.
2. This loop is convex and symmetrical with respect to its center.
3. The equations of the unloading and reloading branches of the closed

loop correspond to translations of the first deformation curve with a scaling factor of two.

In the case of an asymmetrical Iwan model this last result does not hold but the first two are still applicable. Random assemblies of P-bodies (which are not Iwan models) subjected to cyclic loading will stabilize either after one-and-one-half cycle of loading or never. A physical analog of an Iwan model was also presented ; it allows for a visualization of the intricate memorization of the model strain history.

Parallel to these results the conditions of application of shakedown analysis were examined but led to comparatively minor benefits for the specific type of model considered (a more detailed discussion of shakedown analysis and examples of its use in geotechnical engineering can be found in Appendix 3).

The results showed that a tension pile represented by this Pile Model could not be pulled out by application at its top of a cyclic loading which never reaches the pile's ultimate capacity.

#### 6.6.2.B. The soil degradation data

Chapter 4 introduced the experimental component of the methodology in the form of a study of the contribution of average shear stresses to the cyclic degradation of Plastic Drammen Clay.

A series of 12 Direct Simple Shear tests was run, using the Geonor device and NGI procedures, to investigate the combined effect of  $\tau_{ave} = \tau_{cons}$  and  $\tau_c$  on the cyclic behavior of the clay. These tests involved a  $K_o$ -consolidation to a Normally Consolidated State, followed by a "drained" shear and consolidation under  $\tau_{cons}$ . The cyclic loading



was applied under constant volume condition. A detailed description of the testing is provided in chapter 4 and Appendix 4. Ten out of 12 tests were run to failure which occurred in an average displacement mode (defined as  $\gamma_{ave}$  reaching 10 %). The results proved to be quite consistent, and were perfectly compatible with those of the 1975 NGI program. They also validated the use of the concept of 3-D strain contour diagrams as a convenient way to interpolate and extrapolate the clay behavior to a wide range of loadings. Numerous charts presenting cross-sections of these 3-D strain contour diagrams at chosen number of cycles are found in the body of chapter 4. Also included is the estimation of the behavior during the first cycle over the whole range of stresses. Note that undrained creep was neglected throughout the cycling.

Two tests were run with variable cyclic loading and were used satisfactorily to check the validity of the use of Andersen's procedure with a fit on the average shear strain to predict the strain evolution with number of cycles. Many more tests would however be necessary to insure a proper verification over a large range of loadings.

#### 6.2.3.C. TLPILE

TLPILE is the name of the computer code integrating the mechanics of the Pile Model and the degradation of the soil. It can be viewed as the numerical - or the analytical - component of the methodology, and was treated in chapter 5.

The modification of the soil-pile parameters due to the cyclic degradation of the soil was based on the evolution of the cyclic stiffness. Then the numerical treatment of the Pile Model was documented, and the

key parameters introduced. The data storage capacity and the implementation of Andersen's procedure with a fit on  $\gamma_{ave}$  was presented in an introduction to subroutine CYCDEG which estimates the parameters of the soil degradation along the pile. Then the iteration procedure which is the backbone of TLPILE was detailed before specific examples of application to an offshore pile were given.

These examples have shown that a stiffer pile minimizes the cyclic degradation. An increase in the pile wall thickness or in the number of piles per foundation template results in beneficial effects on the overall cyclic behavior, but the increase of the pile diameter has the most significant impact since it affects both the length (for a given ultimate capacity) and the cross sectional area.

The use of a factor of safety of 1.5 as defined by the RP2A regulations for extreme environmental conditions together with a material coefficient  $k_{cy} = 0.85$  applied on the shear strength give a satisfactory combination resulting in very small permanent displacement (of the order of 0.5 mm) under a simplified storm loading.

The code TLPILE allows for a thorough description of the redistribution of stresses and strains, and of the displacements and forces in the model at any desired number of cycles. The program is flexible in use and inexpensive to run. However at the present stage of development it should not be forgotten that it leads to results of only qualitative interest. Table 6.1.1 recaps the key points of this summary.

PILE MODEL

## Theoretical

- . Generalization of Iwan Models
  - decomposable assemblies
  - cyclic behavior (stabilization in  $1 \frac{1}{2}$  cycle to closed, symmetrical, loop, etc...)
  - asymmetry
- . Shakedown Analysis
- . Construction of t-z curve

SOIL DEGRADATION :

## Experimental

- . DSS Tests on Plastic Drammen Clay ( $\tau_{ave} = \tau_{cons}$ )
  - compatible with 1975 program
  - consistent set of data
- . 3-D strain contour diagrams
  - interpolation ; extrapolation ; visualization
  - wide range of stresses
- . Extension of Andersen's procedure for variable loading
  - direct use of data base

TLPILE :

## Analytical

- . Adaptation of t-z curves to cyclic loading
- . Code, explicit procedure, iteration scheme examples, compatible with experimental evidence.

Table 6.1.1 Summary.

## 6.2 CONCLUSIONS AND RECOMMENDATIONS

The behavior of tension piles under cyclic loading is still poorly understood both experimentally and analytically. This should come as no surprise since the static behavior of piles is itself far from being mastered despite the considerably larger experience that has been accumulated. While all the limitations encountered in modeling the static behavior of piles are clearly transferred to the cyclic case, one must also consider the precarious state of development of the study of creep and fatigue of soil. The problem is further complicated by our quest for a displacement approach.

One cannot however postpone the inquiry into the cyclic behavior of tension piles until their static behavior is fully understood. This unscientific conclusion is forced upon the engineer by the need to provide satisfactory answers to a continuous flow of new problems. In such circumstances experimental evidence and engineering judgment must guide the design of the new facilities. Exploratory modeling of a physical phenomenon such as presented in the thesis should be only considered as a support to engineering judgment.

How much confidence can be placed in the proposed methodology ? The main structure of the procedure is the development of a string of well-established geotechnical methods of analysis, and as such one can expect to at least preserve the quality of estimation acquired by its components. However acceptance of the model must be conditioned upon experimental verification of its validity. Unfortunately this check cannot be performed satisfactorily at this stage due to the lack of both pile test and laboratory data. Thus the results presented earlier are only judged qualitatively for their respect of observed trends. The author acknowledges this serious

limitation of his work and can only point out to the careful construction of the model on the basis of his best understanding of the physics of the phenomena involved.

The prime achievement of this work has perhaps been to correct some of the obvious limitations of existing analyses. Poulos (see section 2.3) had the great merit of initiating a quest for simple and flexible engineering models of pile cyclic behavior that would allow sensitivity analyses of the key design parameters to be performed quite easily. The governing idea of the approach is to maintain a uniform degree of sophistication over all the composite steps of the methodology. By no means it is suggested that more elaborate techniques of analysis (such as finite element approaches involving far more complex rheological laws, joint elements and numerical algorithms) should not be developed, but in view of the present weakness of some of the elements in the chain of calculations (initial conditions, cyclic data...), it may be useful to develop simpler tools which lead, at the present time, to only slightly less accurate answers. Having selected this orientation, this work has attempted to :

- 1 improve and develop the limited soil mechanics background of methods of analysis traditionally biased towards structural considerations by revising the method of construction of the "t-z" curves and by establishing a consistent soil data base,
- 2 propose an engineering tool based on a rational iteration scheme and a detailed theoretical knowledge of the model cyclic behavior. The resulting program, which allows for

a great flexibility of use and requires only a marginal cost of implementation, permits the user to follow the pile behavior during the whole evolution of the cyclic loading,

3 include, and respect, experimental evidence. All the elements mentioned by Kraft et al. [56] have been considered in some way or another : the loading rate, the number of load cycles, the magnitude of the cyclic load, the loading history, and the magnitude of the sustained load. The failure mechanism by accumulation of average strains, the relative stability of the cyclic stiffness, the importance of the first few cycles of loading and the transfer of force towards the tip of the pile which have been observed by Puech [86] and McAnoy et al. [70], among others, are all accounted for,

4 define the assumptions the methodology is based upon in order to clearly state its limitations.

At each stage of the thesis results have been gathered in a form which permits direct applications to other fields of geotechnical engineering ; such is essentially the case of the study of Iwan Models, both from a theoretical and from a numerical standpoint, the introduction of shakedown analysis and, more importantly perhaps, the soil degradation data bank. Direct use of the concept of 3-D strain contour diagrams and of the specific charts provided in the body of this work can permit a rapid preliminary estimation of soil behavior under cyclic loading whenever

average shear stresses present a particular interest. Examples of possible fields of application of these data are given in Figure 6.2.1.

The overall conclusions of the research are believed to be summarized in the next three points.

- 1 The concept of "t-z" curve can be conveniently expanded to the consideration of cyclic loading by the use of Iwan models. The resulting pile model is particularly adapted to analyses uncoupling mechanical and cyclic degradation responses, and offers the advantage of insuring automatic recording of the strain history.
- 2 Average shear stresses have a significant effect on the cyclic behavior of clay. The crude differentiation between one-way and two-way cycling should be replaced by the systematic consideration of two components of stresses such as  $\tau_{ave}$  and  $\tau_c$ . Efforts to characterize the cyclic behavior of a clay by using only one parameter of the stress loading may be quite misleading.
- 3 There is no counter-indication to the use of the present state-of-the-art for the design of piles for TLP foundations in Normally Consolidated Clay.

Let us now consider some recommendations for future research.

Of paramount importance is the calibration of the methodology against actual pile test results, and in this domain the future release of the presently proprietary data accumulated throughout the world will represent an important breakthrough. However the methodology can be significantly improved before

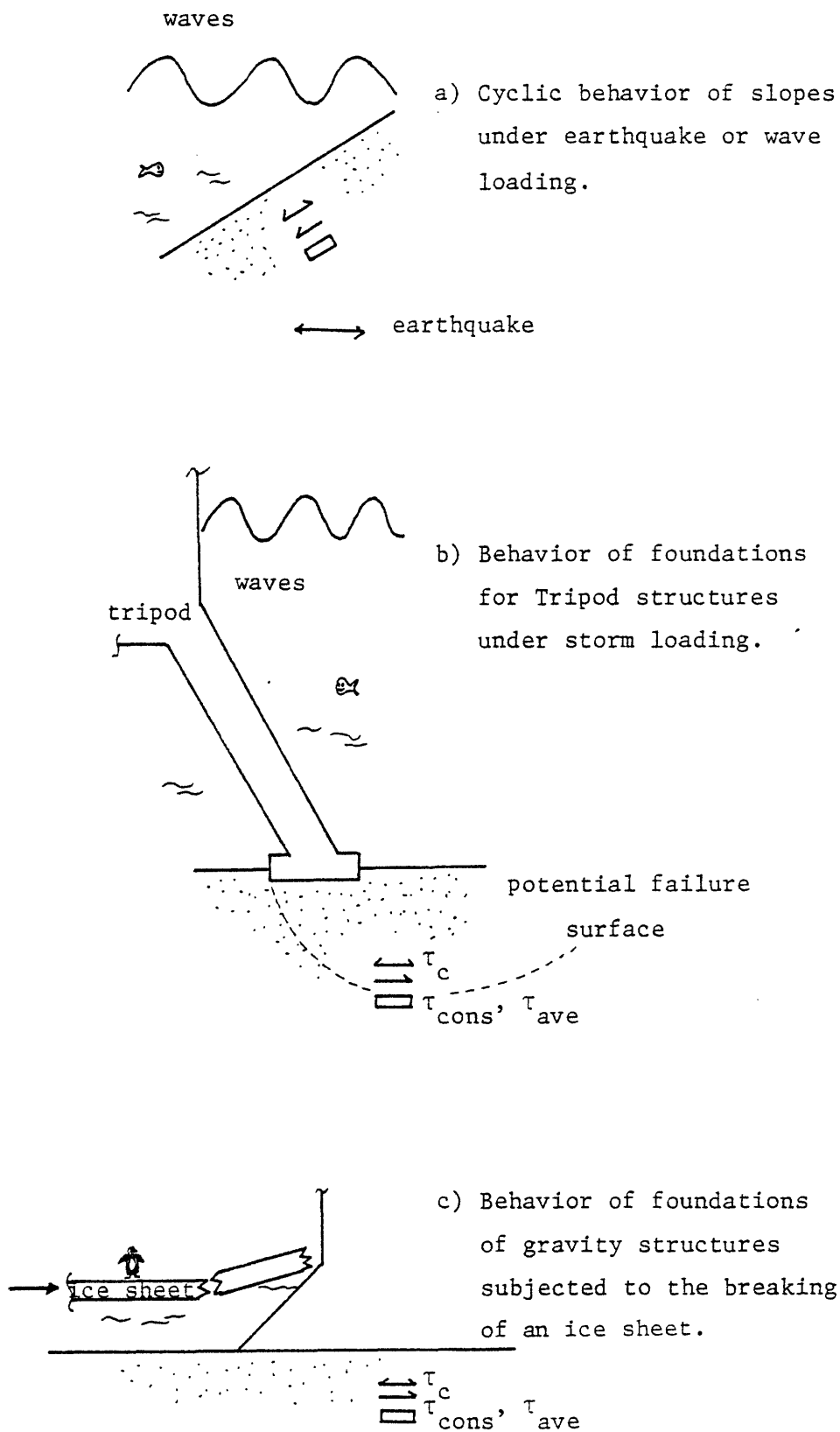


Figure 6.2.1 Potential domains of application of soil degradation data.



these data become available. The author firmly believes that the gathering of soil degradation data constitutes potentially the most valuable source of development. Laboratory tests of the type run in this thesis with the cyclic DSS of Geonor can lead to a tremendous improvement of our knowledge of many aspects of the cyclic behavior of soils which are relevant to our problem. One of the key objectives should be to relax the condition of maintaining  $\tau_{ave}$  equal to  $\tau_{cons}$ , especially in the case of variable cyclic loading. Thus the use of Andersen's procedure with a fit on  $\gamma_{ave}$  is still far from being justified, and many more variable cyclic tests must be performed before a definitive assessment of its validity is made.

In fact the pursuit of this major avenue of research should lead to the development of stress-controlled tests where the amplitude of the stresses applied are varied continuously during the loading. The idea is to bridge the gap existing between "constant stress" and "constant strain" testing.

Other very important questions meriting investigation relate to the validation of basic elasto-plastic laws under irregular loading. The effects of preloading, and especially those of consolidating a specimen under a given shear stress, are far from being properly quantified.

Finally the author wishes to point out the very important question of drainage, not only during the storm loading itself, but also in the repeated calm periods between storms. The use of the DSS equipment in its present stage of development may however prove to be unsatisfactory in this perspective and new techniques providing a more reliable measurement of excess pore pressures in the specimen must be envisioned.

As is so often the case in soil mechanics the number of parameters to be considered is overwhelming. While it would be useful to gather cyclic data for various soil types, different OCR's, different stress systems, etc... such an enterprise is totally unrealistic at the present time. It would be much more reasonable to start a systematic study of a reference clay such as for example reconsolidated Boston Blue Clay that would exhibit a more consistent structure than undisturbed Drammen Clay.

\_\_\_\_\_.

REFERENCES

Note : The following abbreviations have been used :

API	American Petroleum Institute
ASCE	American Society of Civil Engineers
BOSS	Behavior of Off-Shore Structures Conference
ICE	Institution of Civil Engineers
ICSMFE	International Conference on Soil Mechanics and Foundation Engineering
JGED	Journal of the Geotechnical Engineering division
JSMFD	Journal of the Soil Mechanics and Foundations Division
NGI	Norwegian Geotechnical Institute
OTC	Offshore Technology Conference

- 1 American Petroleum Institute. (1979) "Recommended Practice for Planning, Designing and Constructing Fixed Offshore Platforms". API RP2A.
- 2 Andersen K. (1975) "Research Project, Repeated Loading on Clay: Summary and Interpretation of Test Results". NGI. Report 74037-9.
- 3 Andersen K. (1976) "Behavior of Clay Subjected to Undrained Cyclic Loading" Boss'76, Vol. 1. Trondheim, Norway.
- 4 Andersen K., Pool J.H., Brown S.F. and Rosenbrand W.F. (1980) "Cyclic and Static Laboratory Tests on Drammen Clay". JGED. ASCE Vol. 106. GT5.
- 5 Aurora R.P., Peterson E.H., O'Neill M.W. (1981) "Model Studies of Long Piles in Clay". OTC Paper # 4149.
- 6 Baligh M.M. (1975) "Theory of Deep Site Static Cone Penetration Resistance" Research Report R75-56, No. 517, Department of Civil Engineering, MIT.
- 7 Baligh M.M. and Kavvas M. (1980) "Axial Static Capacity of Offshore Friction Piles in Clay : I. Evaluation of Existing Methods". Research Report R80-32, No. 681, Department of Civil Engineering, MIT.
- 8 Bea R.G. (1975) "Parameters Affecting Axial Capacity of Piles in Clays". OTC Paper # 2307.
- 9 Bea R.G. and Audibert J.N.E. (1979) "Performance of Dynamically Loaded Pile Foundations". Boss'79, London.
- 10 Bea R.G., Dover A.R. and Audibert J.M.E. (1982) "Pile Foundation Design Considerations for Deep water Fixed Structures". Boss'82. MIT.
- 11 Bjerrum L. and Kenney T.C. (1968) "Effect of Structure on the Shear Behavior of Normally Consolidated Quick Clays". Geotech. Conf. Oslo 1967 on Shear Strength Prop. of Natural Soils and Rocks. Proceedings Vol. 2.

- 12 Bleich F. (1936) Prel. Rep. 2nd Int. Congr. Bridge and Struct. Eng. Berlin.
- 13 Bogard D. and Matlock H. (1979) "A Model Study of Axially Loaded Pile Segments Including Pore Pressure Measurements". Report to API, Austin, Texas.
- 14 Boulon M. Darve F., Desrues J., Foray P. (1978) "Soil-Structure Coupling. Non Linear Rheological Relationships and Boundary Conditions in Soil Mechanics". Computers and Structures. Vol. 9. pp. 293-303.
- 15 Boulon M., Desrues J., Foray P. (1979) "Méthode de Calcul du Comportement des Pieux à l'Arrachement". Revue Française de Géotechnique No. 7.
- 16 Boulon M, Desrues J., Foray P., Forgue M. (1980) "Numerical Model for Foundations under Cyclic Loading - Application to Piles". Int. Symp. on Soils under Cyclic and Transient Loading. Vol. 2. Swansea.
- 17 Cambefort H., Chadeisson R. (1961) "Critère pour l'Evaluation de la Force Portante d'un Pieu". 5e ICSMFE. Paris.
- 18 Canadian Geotechnical Society (1978) "Canadian Foundation Engineering Manual".
- 19 Chan S.F. (1977) "Load Transfer Characteristics of an Instrumented Steel Pile in a Fill Ground". 5th Southeast Asian Conf. on Soil Eng. Bangkok, Thailand, pp 153-163, 1977.
- 20 Cook R.D. (1974) "Concepts and Applications of Finite Element Analysis". John Wiley.
- 21 Cox W.R., L.M. and Verner E.A. (1979) "Axial Load Tests on 14-in Pipe Piles in Clay". OTC Paper # 3491. Houston.
- 22 Coyle and Reese. "Load Transfer for Axially Loaded Piles in Clay". J.S.M.F.D., ASCE Vol. 92. SM2.
- 23 Darve F. (1978) "Une Formulation Incrémentale des Lois Rhéologiques, Application aux Sols". Thèse de Doctorat d'Etat. Institut de Mécanique de Grenoble.
- 24 Darve F. and Labanieh S. "Incremental Constitutive Law for Sands and Clays, Simulation of Monotonic and Cyclic Tests". To be published in Int. Jnal. Num. and Anal. Meth. in Geomechanics.
- 25 Desbordes O. and Nayroles B. (1976) "Sur la Théorie et le Calcul de l'Adaptation des Structures Elastoplastiques". J. de Mécanique 15.
- 26 Det Norske Veritas (1980) "Rules for the Design, Construction and Inspection of Offshore Structures".
- 27 Ecole Nationale des Ponts et Chaussées. Cours de Mécanique des Sols. Tome 1, Les Fondations. III Les Fondations Profondes. Bourges F. and Frank R.
- 28 Ellis W. and Hartman V.B. (1967) "Dynamic Soil Strength and Slope Stability" J.S.M.F.D. ASCE. SM4.

- 29 Flugge S. (1958) Encyclopedia of Physics. Vol. IV : Elasticity and Plasticity  
Ed. by Flugge S., Berlin, Springer.
- 30 Fritsche J. (1931) Baingenieur 12, 827.
- 31 Gallagher K.A. and St John (1980) "Field Scale Model Studies of Piles as  
Anchorages for Buoyant Platforms". Eur. Off. Pet. Conf. and Exhibit.  
London, England.
- 32 Gokhfeld D.A. and Cherniavsky O.F. (1980) Limit Analysis of Structures at  
Thermal Cycling. Sijthoff and Noordhoff Ed.
- 33 Grosh J.J. and Reese L.C. (1980) "Field Tests of Small-Scale Pile Segments in  
a Soft Clay Deposit under Repeated Axial Loading". OTC Paper # 3869.
- 34 Gruening M. (1926) Tragfähigkeit Statisch Unbest. Tragwerke etc. Berlin : Springer.
- 35 Hadge W.E. (1979) "A Relationship between the Drained and Undrained Cyclic  
Behavior of Sand". MS Thesis. MIT.
- 36 Haldar A.K., Reddy D.V. and Arockiasamy (1982) "Offshore Platform Foundation  
Shakedown Analysis". Boss'82. MIT.
- 37 Halphen B. (1978) Thèse d'Etat. Paris.
- 38 Hedberg J. (1977) "Cyclic Stress-Strain Behavior of Sand in Offshore Environment".  
Ph.D. Thesis. MIT.
- 39 Herrmann H.G. and Houston W.N. (1976) "Response of Seafloor Soils to Combined  
Static and Cyclic Loading". OTC. Houston.
- 40 Herrmann H.G. and Houston W.N. (1978) "Behavior of Seafloor Soils Subjected to  
Cyclic Loading". OTC. 3260.
- 41 Hicher P.-Y. (1979) "Contribution à l'Etude de la Fatigue des Argiles" Thèse de  
Docteur-Ingénieur. Ecole Centrale de Paris.
- 42 Hodge P.G. (1959) Plastic Analysis of Structures. Mc Graw-Hill, N.Y.
- 43 Hoeg K. (1982) "Geotechnical Issues in Off-Shore Engineering". Boss'82. MIT.
- 44 Holmquist D.V. and Matlock H. (1976) "Resistance-Displacement Relationships  
for Axially-Loaded Piles in Soft Clay". OTC. Paper # 2474.
- 45 Houston W.N. and Herrmann H.G. (1980) "Undrained Cyclic Strength of Marine  
Soils". J.G.E.D. ASCE. GT6.
- 46 Hujeux J-C., Aubry D. (1981) "A Critical State Type Stress-Strain Law for  
Monotonous and Cyclic Loading. Geotechnical and Numerical Considerations".  
Implem. of Comp. Proc. and Stress-Strain Laws in Geotech. Eng. Chicago.

- 47 Huslid J.M., Gudmestad O.T. and Alm-Paulsen A. (1982) "Alternate Deep Water Concepts for Northern North Sea Extreme Conditions". Boss'82. MIT.
- 48 Idriss I.M., Dobry R. and Singh R.D. (1978) "Nonlinear Behavior of Soft Clays During Cyclic Loading". JGED, ASCE, Vol. 104, GT 12.
- 49 Iwan W.D. (1966) "A Distributed-Element Model for Hysteresis and its Steady-State Dynamic Response". Journal of Applied Mechanics.
- 50 Iwan W.D. (1967) "On a Class of Models for the Yielding Behavior of Continuous and Composite Systems". Journal of Applied Mechanics.
- 51 Janbu N. (1976) "Static Bearing Capacity of Friction Piles". 6th Eur. Conf. on Soil Mech. and Found. Eng. Vol 1.2. Wien, Austria.
- 52 Karlsrud K. (1982). Discussion. 2nd Int. Conf. Num. Meth. Off Piling, Austin, Texas.
- 53 Kavvadas M. (1982) "Non-linear Consolidation around Driven Piles in Clays". D. Sc. Thesis, MIT.
- 54 Koiter W.T. (1960) "General Theorems for Elastic-Plastic Solids". Progress in Solid Mechanics. Vol. 2. North Holland, Amsterdam.
- 55 Koiter W.T. (1956) "A New General Theorem on Shakedown of Elastic-Plastic Structures". Proc. Konk, Ned. Akad. Wett, 1359.
- 56 Kraft L.M., Cox W.R. and Verner E.A. (1981) "Pile Load Tests : Cyclic Loads and Varying Load Rates". JGED, ASCE, Vol. 107, GT1.
- 57 Kraft L.M., Ray R.P. and Kagawa T. (1981) "Theoretical t-z Curves". JGED, ASCE, Vol. 107. GT 11.
- 58 Ladd C.C. and Edgers L. (1972) "Consolidated-Undrained Direct Simple Shear Tests on Saturated Clays". Contract Report 3-101, Phase Report 12, Department of Civil Engineering, MIT.
- 59 Ladd C.C. and Foott R. (1974) "New Design Procedure for Stability of Soft Clays". JGED, ASCE, Vol. 100, GT7.
- 60 Lassoudière F., Meimon Y., Hujeux J-C., Aubry D. (1982) "Cyclic Behavior of Soils and Application to Offshore Foundation Calculation". Boss'82. Vol. 1, MIT.
- 61 Lee K.L. and Focht J.A. (1976) "Strength of Clay Subjected to Cyclic Loading" Marine Geology, Vol. 1, No. 3.
- 62 Maier G. (1977) "Shakedown Analysis" in Engineering Plasticity by Mathematical Programming. Pergamon Press.
- 63 Mandel J. (1965) Cahiers du Groupe Francais de Rhéologie, I, No.1.

- 64 Marr A., Urzua A. and Bouckovalas G. (1982) "A Numerical Model to Predict Permanent Displacement from Cyclic Loading of Foundations". Boss'82, Vol. 1, MIT.
- 65 Martin J.B. (1975) "Plasticity : Fundamentals and General Results". MIT Press.
- 66 Masing G. (1926) Proc. 2n Int. Cong. of Applied Mechanics, pp. 332-335.
- 67 Matlock H., Bogard D. and Cheang L. (1982) "A Laboratory Study of Axially Loaded Piles and Pile Groups Including Pore Pressure Measurements". Boss'82, Vol. 1, MIT.
- 68 Matlock H. and Foo S.H.C. (1980) "Axial Analysis of Piles Using a Hysteric and Degrading Soil Model". 1st. Int. Conf. Num. Meth. Off. Piling, ICE, London.
- 69 Mattes N.S., Poulos H.G. (1969) "Settlement of Single Compressible Pile". Jnl. Soil Mech. and Found. Div. ASCE, Vol. 95, SMI.
- 70 McAnoy R.P.L., Cashman A.C. and Purvis D. (1982) "Cyclic Tensile Testing of a Pile in Glacial Till". 2nd Int. Conf. Num. Meth. in Off. Piling. Austin.
- 71 Meimon Y., Hicher P.Y. (1980) "Mechanical Behavior of Clays under Cyclic Loading". Int. Symp. on Soils Under Cyclic and Transient Loading. Swanses. 7.11.
- 72 Melan E. (1936) Prel. Rep. 2nd Int. Congr. Bridge and Struct. Eng. Berlin.
- 73 De Mello V.F.B. (1977) "Reflections on Design Decisions of Practical Significance to Embankment Dams". Seventeenth Rankine Lecture. Geotechnique 27, No.3.
- 74 Mercier J.A. (1982) "Evolution Tension Leg Platform Technology", Boss'82. MIT.
- 75 Mindlin R.D. (1936) "Force at a Point in the Interior of a Semi-Infinite Solid". Physics. Volume 7, pp. 195-202.
- 76 Nguyen Quoc Son (1973) Thèse d'Etat, Paris.
- 77 Olsen. Report to API.
- 78 Persoz B. (1958) "Modèles Plasto-Elastiques". Rheologica Acta, Band 1, Nr. 2-3.
- 79 Persoz B. (1969) La Rhéologie. Masson, Paris.
- 80 Poulos H.G. (1979) "Development of an Analysis for Cyclic Axial Loading of Piles". 3rd Int. Conf. on Num. Meth. in Geom. Aachen.
- 81 Poulos H.G. (1980) "Analysis of Cyclic Axial Response of a Single Pile" Univ. of Sydney, School of Civil Eng. Research Report # 362.

- 82 Poulos H.G. (1981) "Some Aspects of Skin Friction of Piles in Clay under Cyclic Loading". Geot. Eng., Vol. 12, No. 1, p. 1-17.
- 83 Poulos H.G. (1981) "Cyclic Axial Response of Single Pile". JGED, ASCE, Vol. 107, GT1.
- 84 Poulos H.G. (1982) "Influence of Cyclic Loading on Axial Pile Response" 2nd. Int. Num. Meth. Off. Piling. Austin.
- 85 Prevost J.H. (1977) "Mathematical Modelling of Monotonic and Cyclic Undrained Clay Behavior". Int. Jnal. Num. and Anal. Meth. in Geomechanics. Vol. 1.
- 86 Puech A. (1982) "Basic Data for the Design of Tension Piles in Silty Soils". Boss'82, Vol. 1, MIT.
- 87 Puech A., Boulon M. and Meimon Y. (1982) "Behavior of Tension Piles : Field Data and Numerical Modelling", 2nd Int. Conf. Num. Meth. Off Piling Austin, Texas.
- 88 Puech A., Foray P., Boulon M., Desrues J. (1979) "Calcul des Pieux a l'Arrachement à partir d'un modèle numérique en contraintes effectives, premiers résultats". Brighton Eng. 7th Eur. Conf. SMFE.
- 89 Puech A. and Jezequel J.F. (1980) "The Effects of Long Time Cyclic Loadings on the Behavior of a Tension Pile". OTC Paper # 3870. Houston.
- 90 Pyke R. (1979) "Nonlinear Soil Models for Irregular Cyclic Loadings". JGED, ASCE, GT6.
- 91 Randolph M.F. and Wroth C.P. (1978) "Analysis of Deformation of Vertically Loaded Piles". JGED, ASCE, Vol. 104, GT12.
- 92 Reiner M. (1971) "Advanced Rheology". Lewis, London.
- 93 Sawczuk A. (1974) "Shakedown Analysis of Elastic-Plastic Structures". Nuclear Eng. and Design 28.
- 94 Seed H.B., Chan C.K. (1966) "Clay Strength under Earthquake Loading Conditions". J.S.M.F.D., ASCE, SM2.
- 95 Sowa V.A. (1970) "Pulling Capacity of Concrete Cast in situ Bored Piles". Canadian Geotechnical Journal, Vol. 7, pp. 482-493.
- 96 Steenfelt J.S., Randolph M.F. and Wroth C.P. (1981) "Instrumented Model Piles Jacked into Clay". Paper 8/56. 10. ICSMFE. Stockholm, Sweden.
- 97 Swane I.C. and Poulos H.G. (1982) "A Theoretical Study of the Cyclic Shakedown of Laterally Loaded Piles". Num. Meth. in Geomechanics, Edmonton.



- 98 St John (1980) "A Review of Current Practice in the Design and Installation of Piles for Offshore Structures". Department of Energy. Report OT-R-8002, Offshore Technology, Paper 5.
- 99 Taylor P.W., Bartlett P.E. and Wiessing P.R. (1981) "Foundation Rocking Under Earthquake Loading". 10th ICSMFE, Vol. 3, Stockholm.
- 100 Timoshenko S.P. (1930) Strength of Materials. First Edition. Van Nostrand.
- 101 Urzua A. (1981) "Analysis of Permanent Displacements from Cyclic Loading Foundation". Ph. D. Thesis. MIT.
- 102 Van Eekelen H.A.M. and Potts D.M. (1978) "The Behavior of Drammen Clay under Cyclic Loading". Geotechnique, Vol. 238, No. 2.
- 103 Zarka J. (1979) "Sur l'Etude du Comportement Global des Matériaux Soumis a un Chargement Cyclique". Journal de Mécanique Appliquée. Vol. 3. No. 3.

APPENDICESNote :

Each appendix is numbered according to the chapter it refers to. Appendix 3.A is the first appendix corresponding to Chapter 3.

## APPENDIX 3

SHAKEDOWN ANALYSIS

## 3.A INTRODUCTION

The purpose of the present appendix is to introduce shakedown analysis and to demonstrate its potential in the field of geotechnical engineering.

It is our intention to evaluate the logical consequences of the choice of an elastic-plastic model for a given soil and to estimate its behavior when subjected to a specific loading range.

A straightforward way of studying this model is to follow its evolution over its complete loading history. The disadvantages of such a procedure are evident : it requires a lot of computation, therefore time and money, if it is even physically possible. The result obtained is a perfect description of the model behavior under the prescribed load history (with the exception of possible computational errors). This approach has been consistently used due to the availability of powerful computers.

Other approaches are possible. Among them are analyses "at-the-limit" and bounding techniques. These approaches are schematically compared in Figure 3.A.1.

Both the analyses at-the-limit and the bounding techniques require only a partial knowledge of the loading (such as the loading range).

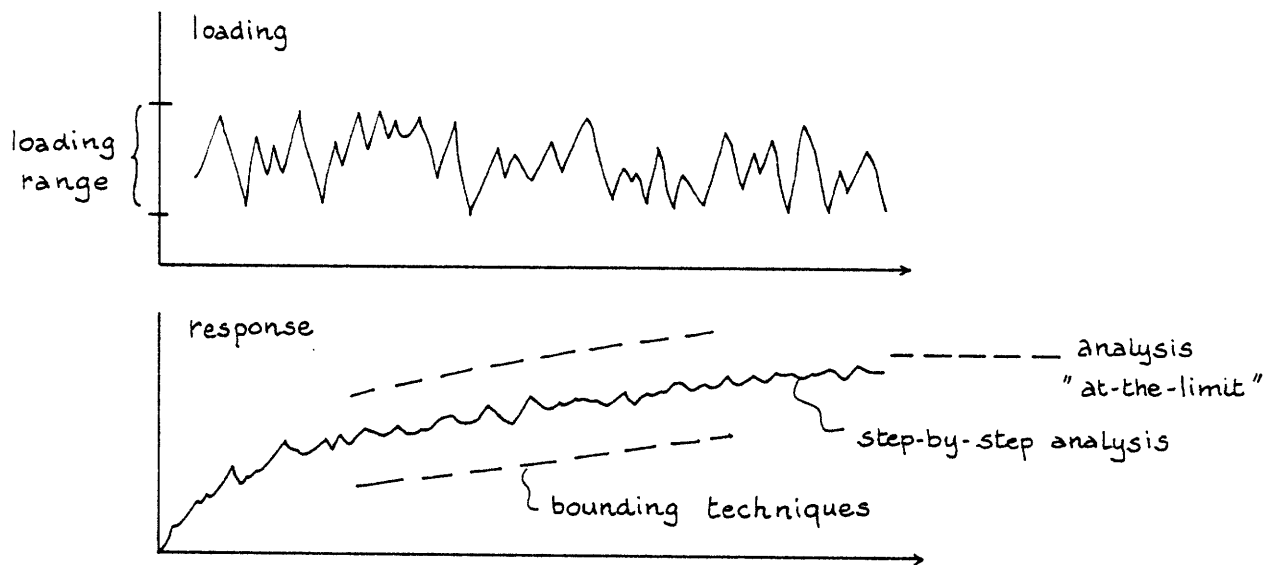


Figure 3.A.1

Classical shakedown analysis can be classified among the analyses at-the-limit. We shall be concerned by the existence of the limit and not by the time necessary to reach it. Clearly shakedown analysis will provide a limited description of the system behavior. However the analysis is quite simple. Only the loading range is required.

The historical development of shakedown analysis has been extensively described in the book of Gokhfeld and Cherniavsky [32], and by Maier [62], Martin [65] and Sawczuk [93]. The precursors in this domain of applied mechanics were Gruening (1926) [34], Fritsche (1931) [30], and Bleich (1932) [12] but the fundamental theorems were derived by Melan (1936) [72] and Koiter (1956) [55]. The key paper which contributed to the development of shakedown analysis as we know it today is due to Koiter (1960) [54]. Since its publication many different extensions of the basic results have been obtained (thermal effects,

dynamics, hardening, geometric effects, etc...) and shakedown analysis has now been applied in geotechnical engineering (Haldar et al. [36], Swane and Poulos [97]). The literature on shakedown analysis is voluminous and we shall not even attempt to present it here. Complete bibliographic lists were given by Maier [62], Gokhfeld and Cherniavsky [32] and Sawczuk [93] among others (this latter paper is certainly one of the most accessible and is recommended as an introduction on the subject).

We shall now formally introduce shakedown analysis. Some background theoretical information and assumptions will first be reviewed. Then the terminology will be explained before the general theorems are presented.

### 3.B SHAKEDOWN ANALYSIS

#### 3.B.1 Background

##### 3.B.1.A Basic assumptions and definitions

We shall assume that the deformations remain small. As a consequence the strain tensor will be define

$$\epsilon_{ij} = \left( u_{i,j} + u_{j,i} \right) / 2 \quad \text{Eq. 3.B.1}$$

with  $u_i$  = displacement in direction  $i$ .

Changes of geometry due to the deformation are also neglected in setting up the equation of equilibrium. As a direct consequence the conditions of equilibrium can be expressed by the virtual work equation\* :

$$\int_v \sigma_{ij} \epsilon_{ij} dv = \int_v X_i u_i dv + \int_{S_p} P_i u_i ds \quad \text{Eq. 3.B.2}$$

holding for any stress distribution  $\sigma_{ij}$  in equilibrium with the external loads  $X_i$  and  $P_i$ , and for any displacement field  $u_i$  with its corresponding strain distribution  $\epsilon_{ij}$ .

---

\* We restrict ourselves to zero imposed displacements on  $S_u$ , the complementary of  $S_p$ .

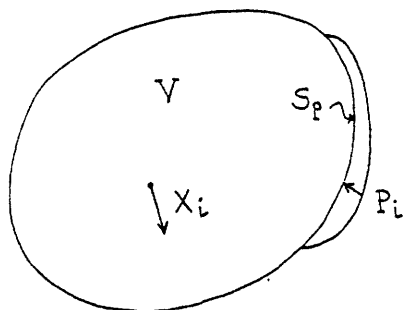


Figure 3.B.1

It is also assumed that the loads are applied slowly (pseudo-static loading) and that the actual strain  $\epsilon_{ij}$  may be written as :

$$\epsilon_{ij} = \epsilon_{ij}' + \epsilon_{ij}'' \quad \text{Eq. 3.B.3}$$

(elastic strain)      (plastic strain)

with  $\epsilon_{ij}' = A_{ijkl} * \sigma_{kl}$  (Hooke's law)

classical tensor of elastic coefficients assumed constant      actual stress tensor

The elastic domain  $D_E$  is limited by the yield surface  $S_Y$ . The equation of  $S_Y$  is  $\emptyset(\sigma) = 0$ , where  $\emptyset$  is called the yield function. The domain  $D_E$  is defined by  $\emptyset(\sigma) < 0$ .

By definition, when  $\left\{ \begin{array}{l} \sigma_{ij} \in D_E \\ \sigma_{ij} \notin S_Y \end{array} \right.$   $\sigma_{ij}$  is called "safe" and noted  $\sigma_{ij}^{(s)}$

when  $\left\{ \begin{array}{l} \sigma_{ij} \in S_Y \\ \sigma_{ij} \in D_E \end{array} \right.$   $\sigma_{ij}$  is called "allowable" and noted  $\sigma_{ij}^{(a)}$ .

And therefore, when  $\sigma_{ij} = \sigma_{ij}^{(s)}$ ,  $\dot{\epsilon}_{ij} = 0$

and  $\sigma_{ij} \in S_Y$  implies:  $\dot{\epsilon}_{ij} \neq 0$  ( $\dot{\epsilon}_{ij}$  is then governed by the flow rule).

Furthermore, a stress distribution  $\sigma_{ij}^*$  will be called statically admissible (S.A.) if it satisfies the equations of equilibrium in the interior of the body and the stress boundary conditions on  $S_p$ .

A strain distribution  $\epsilon_{ij}^*$  will be called kinematically admissible (K.A.) if it may be derived by (3.B.1) from a displacement field  $u_i^0$  satisfying the boundary condition  $u_i^0 = u_{i0}$  on  $S_u$ .

Finally, Drucker's postulate is also assumed valid. Therefore :

$$\therefore \text{with } \sigma_{ij} \in S_Y : \left\{ \begin{array}{l} (\sigma_{ij} - \sigma_{ij}^{(s)}) \dot{\epsilon}_{ij} > 0, \forall \sigma_{ij}^{(s)} \text{ Eq. 3.B.4.a} \\ (\sigma_{ij} - \sigma_{ij}^{(a)}) \dot{\epsilon}_{ij} \geq 0, \forall \sigma_{ij}^{(a)} \text{ Eq. 3.B.4.b} \end{array} \right.$$

$$\therefore \text{with } \sigma_{ij} \in S_Y : \dot{\sigma}_{ij} \dot{\epsilon}_{ij} \geq 0.$$

$$\therefore S_Y \text{ is convex.}$$

### 3.B.1.B Uniqueness of stresses

The state of stress in the body is unique if the complete loading history of the body is specified from its original state. Several different



stress distributions can usually satisfy a given set of final loads and prescribed surface displacements ; however uniqueness is insured if in addition the plastic strain distribution  $\epsilon_{ij}$ " in the body is specified.

Let  $\sigma_{ij}^{(e)}$  denote the (artificial) stress distribution (corresponding to the given body forces  $X_i$  in the interior, surface tractions  $P_i$  on  $S_p$  and surface displacements  $u_{i0}$  on  $S_u$ ) which would be obtained if the body were perfectly elastic. This elastic stress distribution is of course unique.

The actual stresses may now always be written in the form :

$$\sigma_{ij} = \sigma_{ij}^{(e)} + \rho_{ij} \quad \text{Eq. 3.B.5}$$

which defines the residual stresses  $\rho_{ij}$ .

These residual stresses are the permanent stress remaining in the body after complete unloading ( $X_u = 0, P_i = 0$ ) if this unloading would occur without further plastic deformation.

There can exist no more than one residual stress distribution  $\rho_{ij}$  corresponding to a given plastic strain distribution  $\epsilon_{ij}$ " and zero displacements on  $S_u$ . The converse is not true.

### 3.B.1.C. Note on stress and strain decompositions

Let us recap the definitions of the stress and strain with the following diagram (due to Mroz).

Remark : We have implicitly assumed no temperature effects, and in fact no time effect in the sense that the time scale could be change without changing the stresses and strains (however maintaining the pseudo-static condition -e.g. no dynamic effects or no strain rate effects on moduli and strength-). Prager speaks of inviscid plastic behavior "which

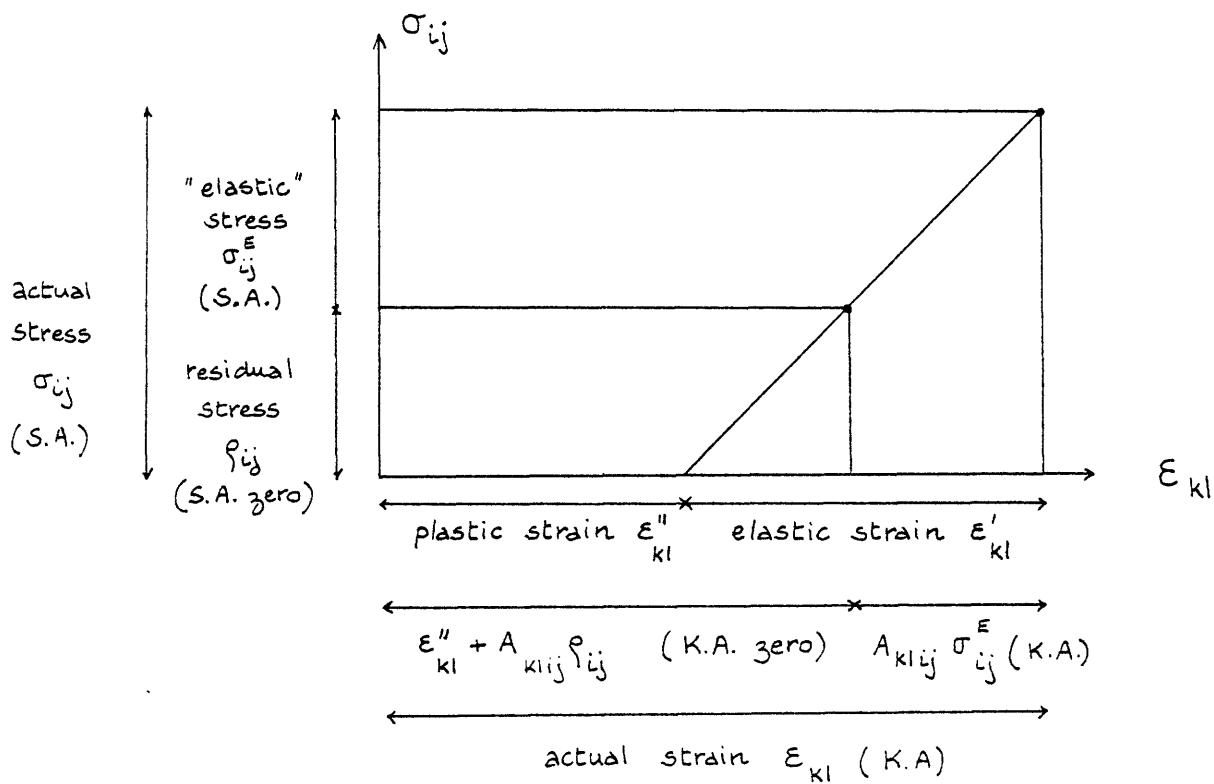


Figure 3.B.2 Decomposition of stress and strain

implies that the speed with which a program of straining is carried out does not affect the intensities of the accompanying stresses".

### 3.B.2 Terminology

Figure 3.B.3 offers a overview of elastic-plastic structure analysis. The branch of interest is the variable loading which includes cyclic loading as a special case. (As already mentioned we shall only need to consider the loading range and therefore the distinction is unimportant).

Classical shakedown analysis is restricted to elastic-plastic systems with constant material properties, e.g. these properties are independent of time (number of cycles). Shakedown analysis leaves aside the transient stage to focus on the steady-state condition (final stage). The term steady-state is in fact only adapted to cyclic loading, and in the case of a non-cyclic loading the transition between transient and final stages may indeed be delicate to establish. As a matter of fact depending on the loading history several repetitions of transient-then-shakedown-stages may occur, and would only be observable in a step-by-step analysis. Shakedown analysis considers only the ultimate final stage. The transient stage happens to be extremely important in practice since the plastic deformations accumulated during this period may be large enough to endanger the serviceability of the structure. Several methods have been proposed to establish bounds on these deformations. Global measures of plastic strain energy exist but criteria governing the magnitude of local deformations are far more complex to establish.

In parallel to this area of interest we find the estimation of transient stage duration. Very little work has been done in this domain on a theoretical

E L A S T I C P L A S T I C S T R U C T U R E

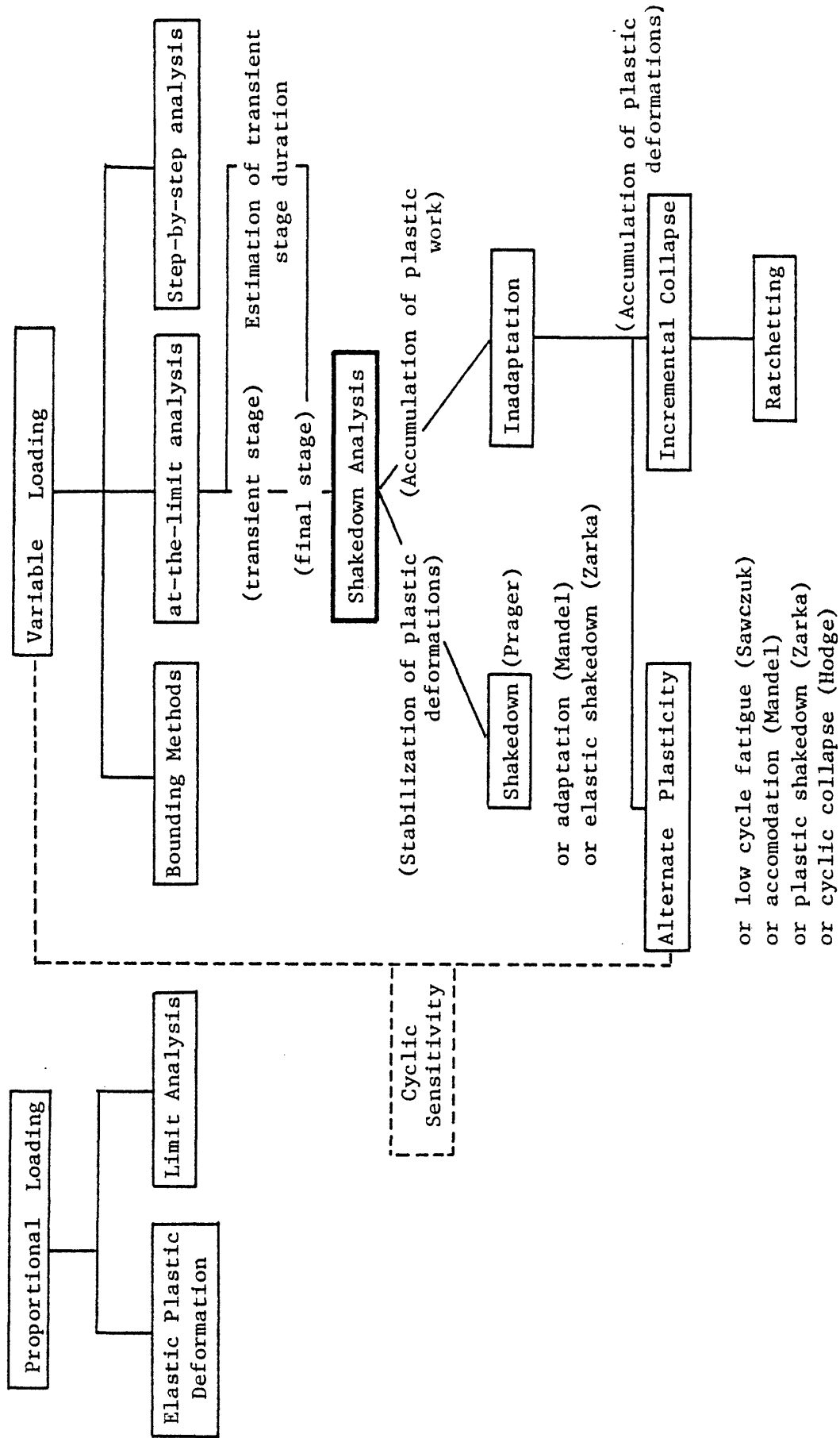


Figure 3.B.3 Overview of Elastic-Plastic Analysis (adapted from A. Sawczuk 93 |).

basis. Shakedown analysis differentiates between the stabilization of plastic deformations and their accumulation.

The amounts of plastic deformation that occur in consecutive "cycles" of loading may decrease as the terms of a convergent infinite series, or plastic deformation may stop altogether after the first "cycle" or the first few "cycles" of loading. In either case, the structure is said to shakedown : it will respond to further "cycling" in a purely elastic manner provided that the loads remain within the prescribed range. If shakedown\* does not occur the plastic deformations are said to be unstable ; we have inadaptation. There are then two possibilities : either no increment of plastic strain occurs in a "cycle" of loading, and we have alternate plasticity, or we have further accumulation of plastic strain increments and incremental collapse.

In the case of alternate plasticity plastic strains in the zone at yield develop repeatedly in opposite directions and eventually result in a low cycle fatigue. Plastic deformations remain bounded, but the plastic strain work does not. Note that in the zone that is not at yield the structure may have locally shaken down or may have remained elastic.

In the case of incremental collapse although no overall collapse can be produced at any load combination it may happen that the plastic zones formed in sequence would constitute a mechanism had they all occurred simultaneously. Such a mode of inadaptation includes ratchetting where a same element is repeatedly yielding in the same direction.

---

\* Written shakedown or shake down. Introduced by Prager in 1948.

Note that a structure subjected to incremental collapse may be locally in alternate plasticity, or shakedown or elasticity. This hierarchy in the global terminology is summarized in the following Table 2.1.

	<u>/LOCAL/</u>			
	<u>Elast.</u>	<u>Shake.</u>	<u>Alt. Plast.</u>	<u>Incr. Coll.</u>
<u>Elasticity</u>	X			
<u>Shakedown</u>	(X)	X		
<u>/GLOBAL/</u> <u>Alt. plasticity</u>	(X)	(X)	X	
<u>Incr. collapse</u>	(X)	(X)	(X)	X
	X = necessary			
	(X) = possible			

Table 2.1 Local vs global properties

A major concern to us is the ignorance in classical shakedown analysis of the cyclic sensitivity of material properties. This problem is especially important in the case of alternate plasticity. The consideration of this effect within the framework of the analysis of elastic-plastic structures under variable loading constitutes the essence of the present thesis. Shakedown analysis is obviously one of the important components of this puzzle.

### 3.B.3 Theorems

These theorems are based (quoting from S. Flugge [29]) "on the consideration that if a system of self-equilibrating elastic residual stresses in the redundant structure can be found such that the sum of these stresses and the maximum positive or negative stresses produced by the loads in the assumedly perfectly elastic structure at every point for all possible load combinations does nowhere exceed the yield stress, the structure will "shakedown" to such a distribution of residual stresses that all subsequent load applications of the same (or lower) intensity will produce a purely elastic response".

To further clarify the context let us already mention the fact that the theorems to be presented can be considered as extensions of the classical limit theorems of plasticity. As such we shall have a static theorem : Melan's theorem, and a kinematic theorem : Koiter's.

#### 3.B.3.1 Melan's theorem

##### 3.B.3.1.A. Classical form :

Several versions of Melan's theorem are available. We shall use Martin's formulation [65].

If, and only if, any time - independent distribution of residual stress  $\bar{\rho}_{ij}$  can be found such that

$$\emptyset \left[ \sigma_{ij}^E(t) + \bar{\rho}_{ij} \right] < 0 \quad \text{Eq. 3.B.6}$$

the structure will shakedown.

There is the proof by Koiter [54] of this theorem. (For a perfectly rigorous proof the reader is referred to Desbordes and Nayroles [25]).

Proof :

- A. It is of course evident that if shakedown occurs a residual stress  $\rho_{ij}$  does exist that satisfies Eq. 3.B.6. In other words shakedown is clearly impossible if no distribution of residual stresses exists on which the stresses due to an elastic response to the external loads may always be superimposed without violation of the yield condition. This gives the necessary condition of the theorem.
- B. The sufficient condition will be proved by introducing the essentially positive elastic strain energy  $A$  corresponding to the residual stresses  $\rho_{ij} - \bar{\rho}_{ij}$ , where  $\rho_{ij}$  denotes the actual momentaneous residual stress, and  $\bar{\rho}_{ij}$  is the time-independent residual stress satisfying Melan's criterion :

$$A = \int_v \frac{1}{2} \left( \rho_{ij} - \bar{\rho}_{ij} \right) A_{ijkl} \left( \rho_{kl} - \bar{\rho}_{kl} \right) dv.$$

We have :

$$\sigma_{ij}(t) = \sigma_{ij}^E(t) + \rho_{ij}(t) \quad \text{by definition of } \rho_{ij}(t)$$

and :

$$\varepsilon_{ij}(t) = \varepsilon_{ij}'(t) + \varepsilon_{ij}''(t) = A_{ijkl} \rho_{kl}(t) + A_{ijkl} \sigma_{kl}^E(t) + \varepsilon_{ij}''(t) ;$$

hence :

$$A_{ijkl} \rho_{kl}(t) = \varepsilon_{ij}(t) - A_{ijkl} \sigma_{kl}^E(t) - \varepsilon_{ij}''(t).$$



Consider the time derivative of  $A'$  written  $\dot{A}$ ,

$$\dot{A} = \int \left( \rho_{ij} - \bar{\rho}_{ij} \right) A_{ijkl} \dot{\rho}_{kl} dv.$$

Therefore :

$$\dot{A} = \int \left( \underbrace{\rho_{ij} - \bar{\rho}_{ij}}_{\substack{\uparrow \\ \text{This is a statically} \\ \text{admissible stress field,} \\ \text{in equilibrium with zero body and surface forces (on } S_p \text{)}}} \right) \left( \underbrace{\dot{\epsilon}_{ij} - A_{ijkl} \dot{\sigma}_{kl}^E - \dot{\epsilon}_{ij}''}_{\substack{\text{This is a kinematically} \\ \text{admissible velocity field.}}} \right) dv.$$

This is a statically  
admissible stress field,  
in equilibrium with zero body and surface forces (on  $S_p$ ).

The virtual work equation gives :

$$\int \left( \rho_{ij} - \bar{\rho}_{ij} \right) \left( \dot{\epsilon}_{ij} - A_{ijkl} \dot{\sigma}_{kl}^E \right) dv = 0,$$

and as a result  $\dot{A}$  can be written as :

$$\dot{A} = - \int \left( \rho_{ij} - \bar{\rho}_{ij} \right) \dot{\epsilon}_{ij}'' dv.$$

This is nothing but Drucker's expression after the following substitutions :

$$\rho_{ij} = \sigma_{ij} - \sigma_{ij}^E$$

$$\text{and } \bar{\rho}_{ij} = \sigma_{ij}^{(S)} - \sigma_{ij}^E \quad (\text{from Eq. 3.B.6}).$$

Then by subtraction :

$$\rho_{ij} - \bar{\rho}_{ij} = \sigma_{ij} - \sigma_{ij}^{(S)}.$$

From Drucker's first inequality (Eq. 3.B.4.a) we have

$$\dot{A} = - \int \left( \sigma_{ij} - \sigma_{ij}^{(S)} \right) \dot{\epsilon}_{ij}'' dv < 0.$$

(Note importance of minus sign in front of integral).

We therefore have  $A \geq 0$  and  $\dot{A} < 0$

that proves that  $\lim_{t \rightarrow \infty} A$  exists and that  $\lim_{t \rightarrow \infty} \dot{A} = 0$ .

Let us interpret this last result :

assuming that these limits are attained for  $t > t_1$ , with  $t_1$  finite, ( $t_1$  infinite presents no physical interest). We then have :

$$\forall t > t_1 \int \left( \rho_{ij}(t) - \bar{\rho}_{ij} \right) \dot{\epsilon}_{ij}''(t) dt = 0. \quad \text{Eq. 3.B.7}$$

If  $\rho_{ij}(t) = \bar{\rho}_{ij}$ ,  $\forall t$ , we know from Eq. 3.B.6 that  $\dot{\epsilon}_{ij}'' = 0$  everywhere.

If  $\rho_{ij}(t) \neq \bar{\rho}_{ij}$ , we must have  $\boxed{\dot{\epsilon}_{ij}''(t) = 0 \text{ everywhere for } t > t_1}$

to insure the validity of Eq. 3.B.7. Which proves the theorem.

### 3.B.3.1.B. The integral form :

Melan's theorem can also be worded in a different way ; using Sawczuk's [93] formulation :

A structure will shakedown to the prescribed loading range, if, and only if, there exists a time-independent residual stress distribution  $\bar{\rho}_{ij}$  and a safety factor  $m > 1$  such that :

$$\emptyset \left[ m \left( \sigma^E(t) + \bar{\rho}_{ij} \right) \right] \leq 0. \quad \text{Eq. 3.B.8}$$

The proof of this form of the theorem will not be given here, but it is worth noting that a (somewhat crude) bound on the total plastic work can be obtained. For a system having an initial stress distribution  $\rho_{ij0}$ , the total plastic work, TPW, produced between  $t = 0$  and  $t = T$  is given by :

$$\text{TPW} = \int_0^T \int_V \sigma_{ij}(t) \dot{\epsilon}_{ij}(t') dv dt' \leq \frac{m}{2(m-1)} \int_V \left[ \bar{\rho}_{ij} - \rho_{ij0} \right] A_{ijkl} \left[ \bar{\rho}_{kl} - \rho_{klo} \right] dv.$$

Eq. 3.B.9

### 3.B.3.2 Koiter's theorem

Koiter first recognized that Melan's theorem could be interpreted as an extension of the static theorem of plastic limit analysis. It was then logical to look for a similar extension of the kinematic theorem.

#### 3.B.3.2.A. Admissible plastic strain rate cycle :

Koiter's analysis is structured around the concept of an admissible plastic strain rate cycle,  $\dot{\epsilon}_{ij0}''(t)$ . By definition  $\dot{\epsilon}_{ij0}''(t)$  is such that :

$$\Delta \epsilon_{ij0}'' = \int_0^T \dot{\epsilon}_{ij0}''(t) dt \quad \text{Eq. 3.B.10}$$

where  $\Delta \epsilon_{ij0}''$  is a kinematically admissible strain distribution. T is indicative of the "cycle" of loading.

#### 3.B.3.2.B. Formulation of theorem (Koiter |54|) :

"The body will not shakedown ; i.e. it will fail ultimately by cyclic plastic deformations, if any admissible plastic strain rate cycle  $\dot{\epsilon}_{ij0}''(t)$  and any external loads  $X_i(t)$ ,  $P_i(t)$  within the prescribed limits can be found for which :

$$\int_0^t \left( \int_V X_i \dot{u}_{i0} dv + \int_{Sp} P_i \dot{u}_{i0} ds \right) dt > \int_0^t \int_V F \left( \dot{\epsilon}_{ij0}'' \right) dv \quad \text{Eq. 3.B.11}$$

where  $F \left( \dot{\epsilon}_{ij0}'' \right)$  is the plastic energy dissipation function in the strain rate cycle  $\dot{\epsilon}_{ij0}''(t)$ .

$$F \left( \dot{\epsilon}_{ij}'' \right) = \sigma_{ij} \dot{\epsilon}_{ij}'' \quad \text{Eq. 3.B.12}$$

"On the other hand, the structure will shakedown if a number  $k > 1$  can be found with the property that for all admissible plastic strain rate cycle  $\dot{\epsilon}_{ij0}''(t)$  and all external loads  $X_i(t)$ ,  $P_i(t)$  within the prescribed limits

$$k \int_0^T \left( \int_V X_i \dot{u}_{i0} dv + \int_{Sp} P_i \dot{u}_{i0} ds \right) dt \leq \int_0^T \int_V F \left( \dot{\epsilon}_{ij0}'' \right) dv dt.$$

$$\text{Eq. 3.B.13}$$

The upper bound of such numbers  $k$  is then obviously the factor of safety with respect to shakedown".

### 3.C EXAMPLES OF APPLICATION OF SHAKEDOWN ANALYSIS

#### 3.C.1 Presentation of the examples

The objective of this section is to present simple applications of shakedown analysis to problems of interest to the geotechnical engineer.

We shall consider the rocking behavior of a rigid rectangular foundation placed on a bed of Winkler springs representing underlying clay. The weight of the structure is constant and equal to  $N$ . The external moment  $M$ , varying between  $-M^*$  and  $M^*$ , is also applied to the foundation. Our goal is to characterize the behavior of this foundation for any couple  $(N, M^*)$  (Figure 3.C.1.a).

Two cases will be treated. The first one corresponds to Winkler springs having the same strength in tension and in compression. It could be associated to a piled foundation placed under the mat (Figure 3.C.1b). The second case allows for separation of the foundation and the underlying soil (Figure 3.C.1.c). In both cases the Winkler springs have uniform properties over the entire foundation. They are P-bodies with a modulus  $K$  and a strength  $\sigma_0$ . The movements are assumed small and the forces are applied in a quasi-static way.

These examples are directly inspired by the work reported by Taylor et al. [99] and will show how an elementary manipulation of stress distribution diagrams and the use of Melan's theorem can allow us to completely describe the foundation behavior.

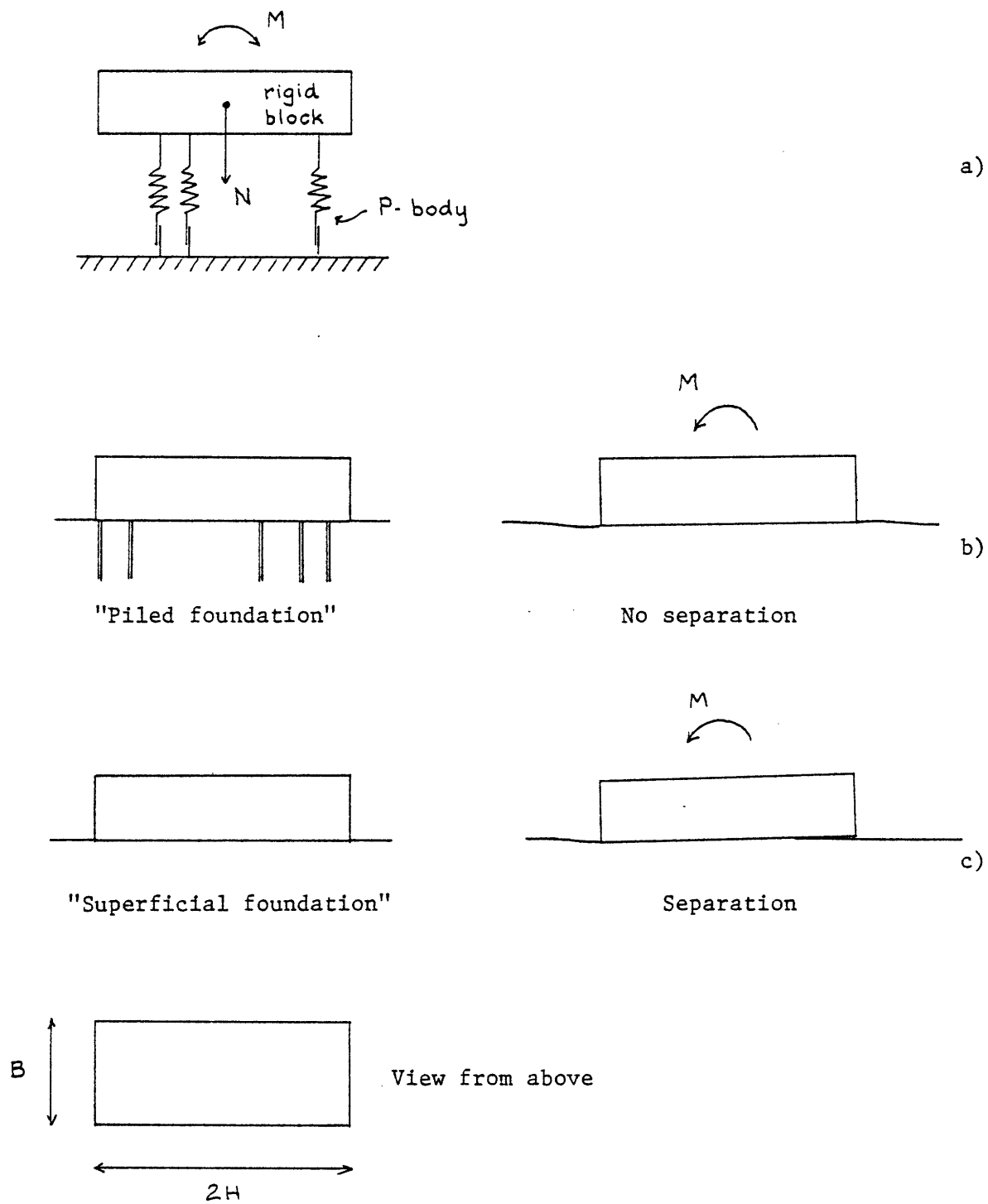


Figure 3.C.1 Presentation of examples.

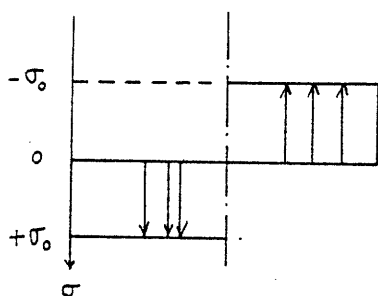
### 3.C.2 No separation : the "pile foundation" case :

#### 3.C.2.1 Normalizing factors

We shall normalize both  $N$  and  $M^*$  by their maximum values  $N_{\max}$  and  $M_{\max}$  which are obtained as follows.

$N_{\max}$  corresponds to no moment applied to the foundation and to a uniform distribution of  $\sigma = \sigma_0$ , and therefore  $N_{\max} = 2HB \sigma_0$ .

$M_{\max}$  corresponds to no vertical load applied to the foundation and a stress diagram as shown in Figure 3.C.2.



$$|M_{\max}| = 2 \frac{H}{2} BH |\sigma_0| = H^2 B |\sigma_0|$$

Figure 3.C.2

The normalized vertical load  $n$  and normalized moment  $m$  are then defined as :

$$n = \frac{N}{N_{\max}} \quad \text{and} \quad m = \frac{M^*}{M_{\max}}$$

#### 3.C.2.2 Elastic range

The elastic range is obtained using the principle of superposition.

We have on the extreme fiber a maximum stress of :

$$\sigma = \frac{N}{2HB} + \frac{3}{2} \frac{M^*}{H^2 B} = \sigma_N^E + \sigma_{M^*}^E$$

and therefore the equation limiting the elastic range is :

$$\underline{1 = n + \frac{3}{2} m} \quad (\text{see Figure 3.C.12})$$

### 3.C.2.3 Shakedown

From Melan's theorem the foundation will shakedown under the prescribed loading if we can find a time-independent residual stress distribution  $\bar{\rho}$  such that :

$$-\sigma_0 < \sigma^E(t) + \bar{\rho} < \sigma_0, \quad \text{at all time.} \quad \text{Eq. 3.C.1}$$

To define the shakedown range let us first assume that  $N = 0$  and then for each value of  $M^*$  find the maximum value of  $N$  which we can add and still have shakedown.

Let us first observe that we cannot have  $\sigma^E(t) > \sigma_0$ , or otherwise Eq. 3.C.1 would lead to :

$$\sigma^E(t) + \bar{\rho} < \sigma_0 \implies \bar{\rho} < 0$$

and

$$-\sigma_0 < -\sigma^E(t) + \bar{\rho} \implies \bar{\rho} > 0$$

which is impossible

This is evidently valid for  $\sigma^E(t) = \sigma_{M^*}^E(t)$

so that  $\sigma_{M^*}^E(t) \leq \sigma_0$  if shakedown is to occur.

Consider therefore two cases :

a.  $\underline{\sigma_{M^*}^E = \sigma_0}$



The elastic stress distribution is shown in Figure 3.C.3 for  $M = M^*$  and  $M = -M^*$ .

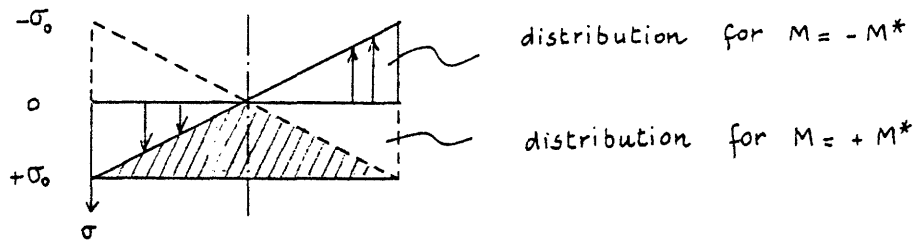


Figure 3.C.3

We can show that the maximum value of  $N$  compatible with shakedown correspond to the shaded area of Figure 3.C.3 by simply recognizing that it can be seen as the sum of an elastic stress distribution due to  $N$  and of an acceptable residual stress distribution (Figure 3.C.4).

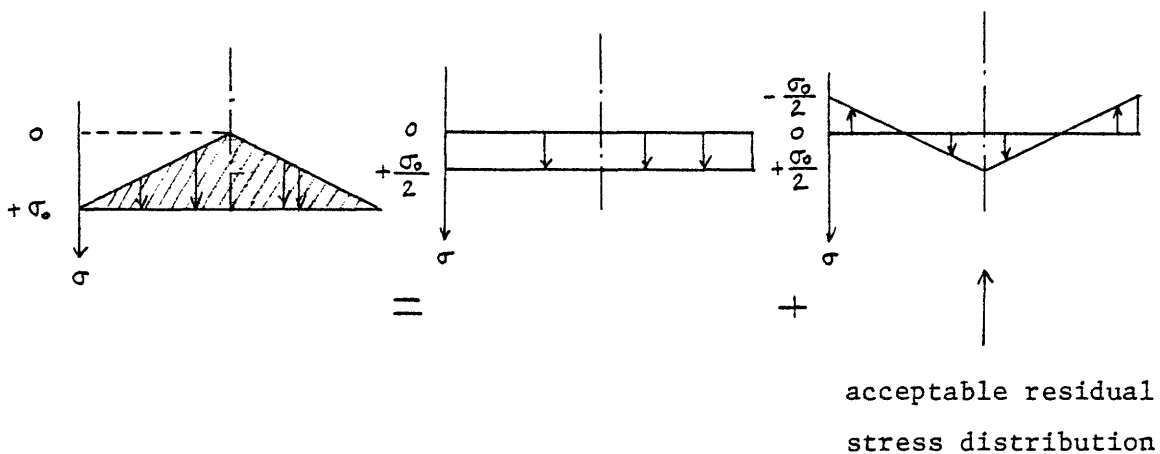


Figure 3.C.4

We are therefore in the condition of application of Melan's theorem.

Adding N does not modify the moment which is such that

$$\sigma_{M^*}^E = \frac{3}{2} \frac{M^*}{H^2 B} = \sigma_0 \quad \text{and thus :} \quad \underline{m = \frac{2}{3}}$$

and N is limited by  $0 < N < \sigma_0 HB$  ,

or,  $\underline{0 < n < \frac{1}{2}}$  .

The procedure which has just been employed will be called the "technique of the shaded area".

b.  $\sigma_{M^*}^E < \sigma_0$

Let us apply this technique once again. The elastic stress distributions for  $M = + M^*$  and  $- M^*$  are shown in Figure 3.C.5.

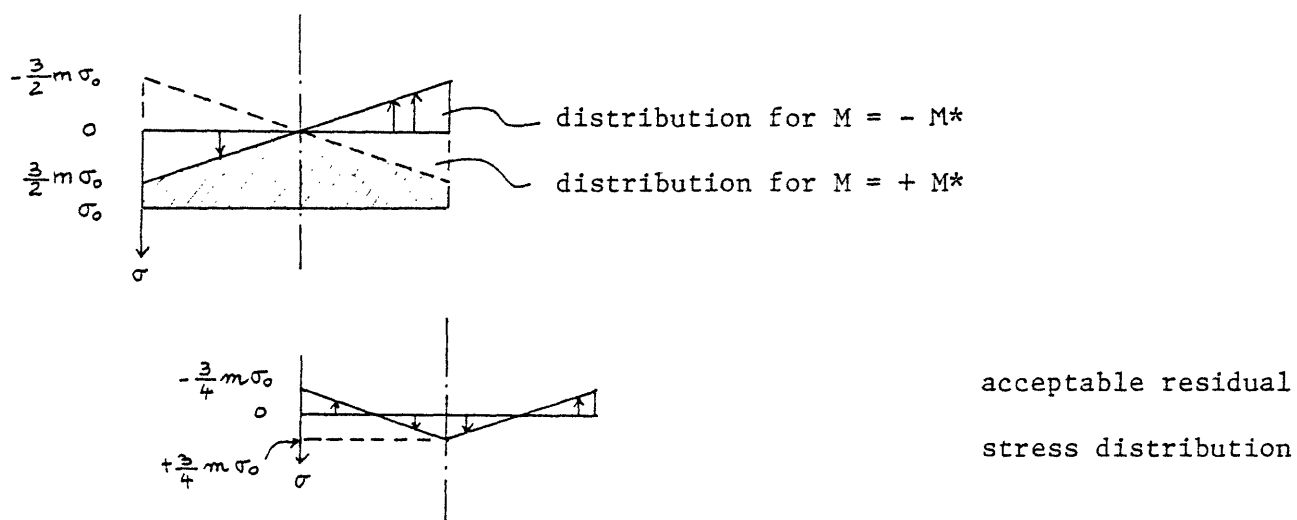


Figure 3.C.5

$$\begin{aligned} \text{Maximum } N &= \left( \sigma_0 - \frac{3}{2} m \sigma_0 \right) 2HB + \frac{3}{2} m \sigma_0 HB \\ &= 2HB \sigma_0 \left( 1 - \frac{3}{4} m \right) \end{aligned}$$

$$\text{or } \underline{n = 1 - \frac{3}{4} m}$$

$$\text{valid for } \underline{\frac{1}{2} < n < 1}$$

The complete shakedown domain is now defined (see recap in Figure 3.C.12).

### 3.C.2.4 Ultimate capacity

The failure condition under M and N is characterized by a stress diagram of the type shown in Figure 3.C.6.

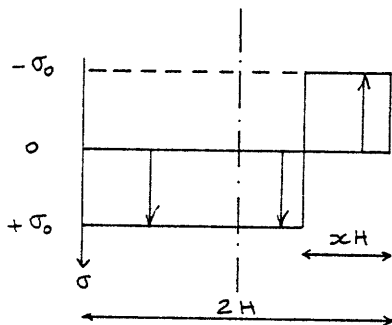


Figure 3.C.6

$$N = 2B (H - xH) \sigma_0 = 2HB \sigma_0 (1 - x)$$

$$\text{or } n = 1 - x$$

$$\text{and } M = 2H \left( 1 - \frac{x}{2} \right) x HB \sigma_0$$

$$\text{or } m = 2x \left( 1 - \frac{x}{2} \right)$$

By eliminating  $x$  we obtain the failure curve :  $\underline{m = 1 - n^2}$

(see Figure 3.C.12).

The problem now becomes to study the behavior of the foundation for a load combination  $(m, n)$  located in between the shakedown domain and the failure curve.

### 3.C.2.5 Alternate plasticity

Let us first establish the transition curve between shakedown and alternate plasticity. This limit is characterized by

$$\begin{aligned}\sigma_{\max}^E - \bar{p} &= \sigma_0 \\ \sigma_{\min}^E - \bar{p} &= -\sigma_0\end{aligned}$$

which, by subtraction yields :

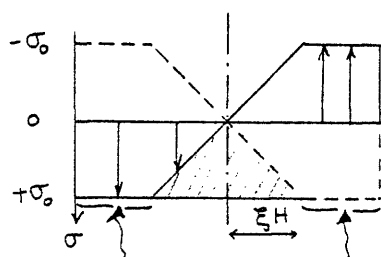
$$\sigma_{\max}^E - \sigma_{\min}^E = 2\sigma_0 \quad , \text{ and, in our case,}$$

$\frac{3}{2} m\sigma_0 + \frac{3}{2} m\sigma_0 = 2\sigma_0$  or  $\underline{m = \frac{2}{3}}$ , equation of the boundary between shakedown and alternate plasticity (Figure 3.C.12).

Alternate plasticity can only occur for  $m > \frac{2}{3}$ , and it will occur at the edges of the foundation. Where there is no alternate plasticity there is shakedown or elasticity.

Again starting with  $N = 0$ , we have a stress distribution of the type shown in Figure 3.C.7 for  $M = \pm M^*$ .

elastic zone



zones of alternate plasticity

Figure 3.C.7

The center part of the foundation remains elastic. We can now consider the shaded area as the maximum value of  $N$  which can be added while insuring the shakedown of the center of foundation. This value of  $N$  is

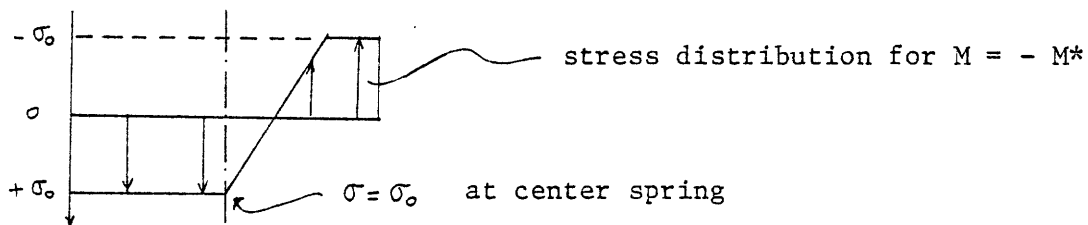
$$N = \xi H B \sigma_0 \quad \text{or } n = \frac{\xi}{2} \quad \text{valid for } 0 < n < \frac{1}{2}$$

$$M \text{ is given by : } M = \sigma_0 B H^2 \left( 1 - \frac{\xi^2}{3} \right) ; \quad m = 1 - \frac{\xi^2}{3}$$

Eliminating  $\xi$  we find the boundary of the alternate plasticity domain :

$$\text{corresponding to the equation : } \underline{m = 1 - \frac{4}{3} n^2} \quad (\text{see Figure 3.C.12}).$$

It is easy to show that this same equation corresponds to the stress diagram of Figure 3.C.8, corresponding to the yielding of the center spring



for each passage at  $M^*$  or  $-M^*$ .

Figure 3.C.8

### 3.C.2.6 Incremental collapse

By incremental collapse we mean any condition that is neither elasticity, shakedown, nor alternate plasticity. In this particular example we have ratchetting since the center spring yields each time the moment  $M$  covers the range  $\left[ -M^*, +M^* \right]$ .

Ratchetting leads to a memory loss. A partial stress distribution under  $-M^*$  is given in Figure 3.C.9.

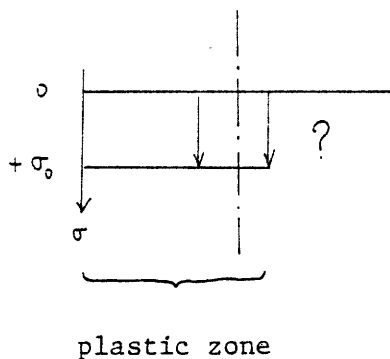


Figure 3.C.9

In the plastic zone the displacements are given by :

$$u = u'' + u' \quad \text{where} \quad u' = \sigma_0/k = \text{cte.}$$

Since the rigid block imposes a linear distribution of the displacement  $u$ , it is clear that the distribution of the plastic displacement  $u''$  is linear in this zone and that the distribution of residual stresses will itself be linear. Therefore the stress distribution placed at the right of the plastic zone in Figure 3.C.9 can only be linear or constant (plastic), and will correspond to one of the cases of Figures 3.C.10 a and b.

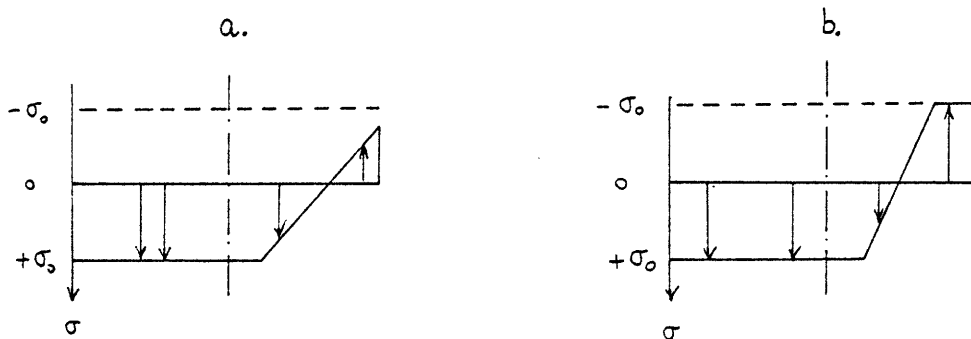


Figure 3.C.10

The limiting diagram is given by Figure 3.C.11

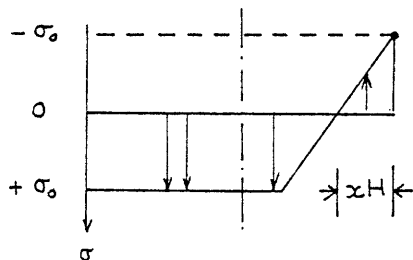


Figure 3.C.11

The corresponding limiting curve is obtained by elimination of  $z$  from the following relations :

$$n = (1 - x)$$

$$m = 2x - \frac{4}{3}x^2$$

or 
$$\underline{m = \frac{4}{3} (1 - n) \left(n + \frac{1}{2}\right)}$$
 see Figure 3.C.12.

We have now completely defined the nature of the behavior of this foundation according to the couple  $(m, n)$ .

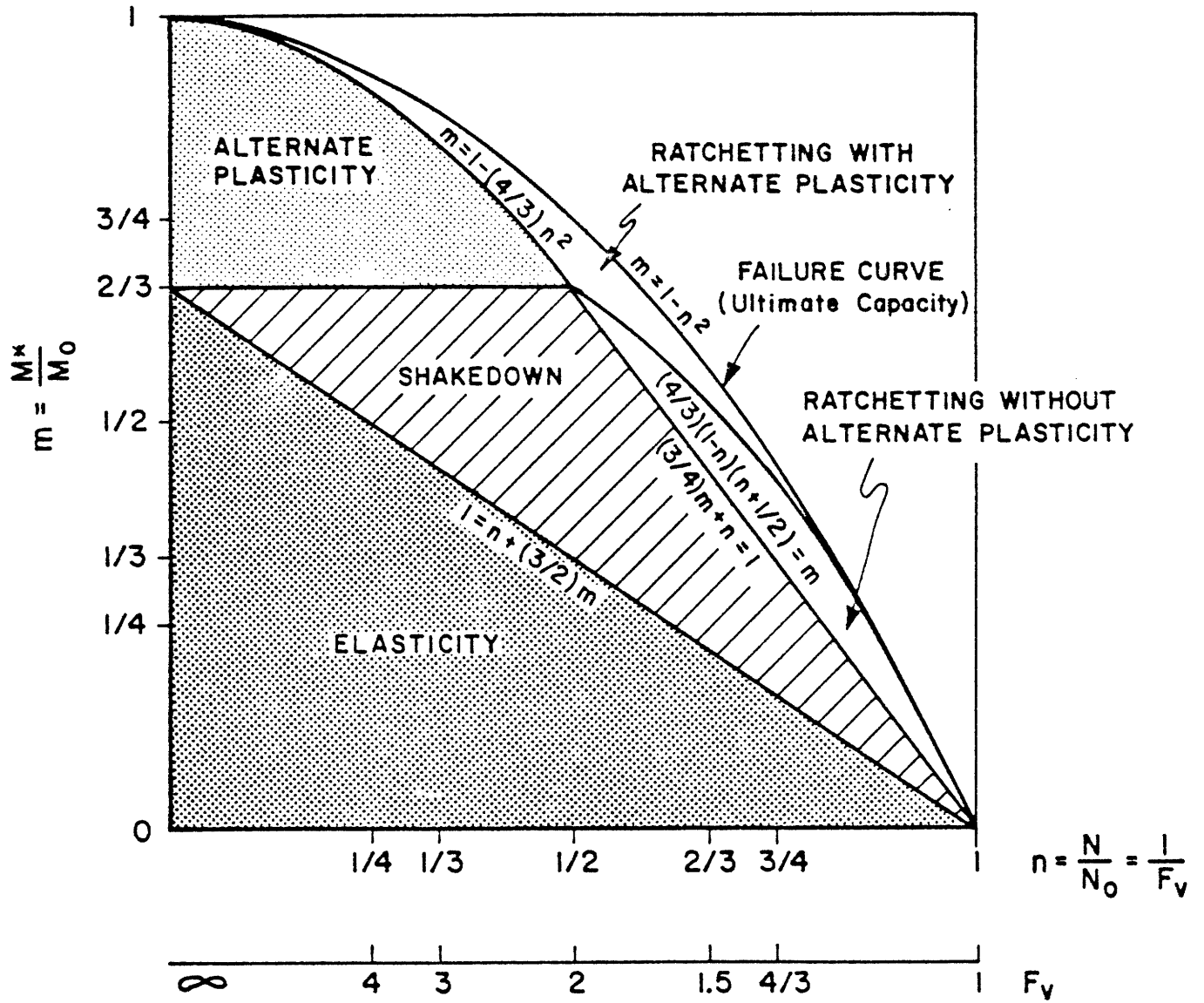


Figure 3.C.12 Rocking behavior of rigid foundation without separation.



### 3.C.3 Separation : the superficial foundation case

#### 3.C.3.1 General remarks on separation

It is assumed that the soil underneath the rigid foundation does not transmit tension loads. As a result as soon as the stress under the foundation drops to zero separation occurs.

In such a case we may have the temptation to assimilate the separation operation to a zero strength in tension for the Winkler elasto-plastic springs. This should not however be done. It is essential to see that when  $\sigma = 0$  no plastic strains occur in tension.

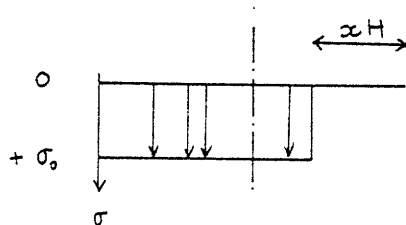
As the soil is reloaded, i.e. the contact is re-established, the plastic strains are those existing at separation. In this respect the separation is equivalent to an "infinite" yield strength in tension. The past observation results in the impossibility to obtain a state of alternate plasticity.

#### 3.C.3.2 Normalizing factors

The same normalizing factors used in the case of no separation will be used for comparison purposes.

#### 3.C.3.3 Ultimate capacity

At ultimate capacity the stress distribution is of the form of Figure 3.C.13.



$$N = H(2-x) B \sigma_0$$

$$x = 2(1-n)$$

$$M = N \frac{xH}{2} \sigma_0 B$$

Figure 3.C.13

Hence,  $\underline{m = 2 n (1 - n)}$  (see Figure 3.C)

### 3.C.3.4 Elastic range

We shall differentiate between the true elastic range and the pseudo-elastic range which will be associated with separation.

I - True elastic range (no separation)

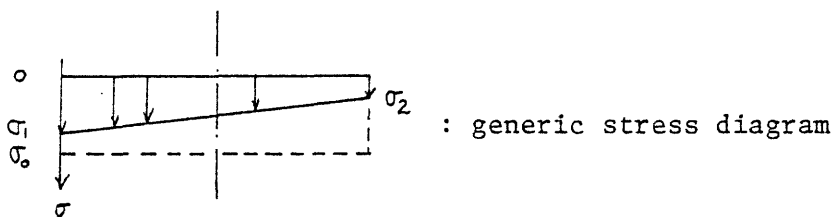


Figure 3.C.14

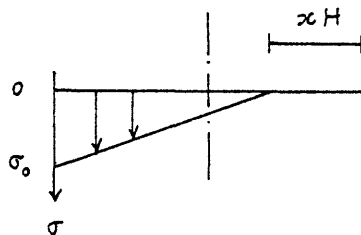
$$\begin{aligned}
 \text{a) } \underline{\sigma_2 = 0} \quad & N = \sigma \, 2HB \, \frac{1}{2} \quad n = \frac{\sigma}{\sigma_0} \, \frac{1}{2} \\
 & M = \sigma \, HB \, \frac{H}{3} \quad m = \frac{\sigma}{\sigma_0} \, \frac{1}{3} \\
 & \sigma \leq \sigma_0 \quad \frac{\sigma}{\sigma_0} \leq 1 \quad n \leq \frac{1}{2} \\
 & \underline{m = \frac{2}{3} n \quad ; \quad n \leq \frac{1}{2}}
 \end{aligned}$$

This limit corresponds to the onset of separation (Figure 3.C.19).

$$\begin{aligned}
 \text{b) } \underline{\sigma_1 = \sigma_0} \quad & \left\{ \begin{aligned} N &= 2H \, \frac{\sigma + \sigma_0}{2} \, B \\ M &= (\sigma_0 - \sigma) \, \frac{2HB}{2} \, \frac{1}{3} \end{aligned} \right. \\
 & \underline{n + \frac{3}{2} m = 1 \quad ; \quad n \geq \frac{1}{2}}
 \end{aligned}$$

This limit corresponds to the onset of yield (Figure 3.C.19)

II - Pseudo elastic range (separation)



$$N = H (2-x) B \sigma_0 \frac{1}{2}$$

$$x = 2(1-2n)$$

$$M = NH \frac{1}{3} (1+x)$$

$$m = \frac{2}{3} \left(1 - \frac{x}{2}\right) (1+x)$$

$$\underline{m = \frac{2}{3} n (3 - 4n) \quad ; \quad n \leq \frac{1}{2}}$$

Figure 3.C.15

For a given  $n$  (which has to be less than  $\frac{1}{2}$  by construction) this equation gives the maximum value of  $m$  which will still maintain elasticity (in the sense of pseudo-elasticity, i.e. with separation).

3.C.3.5 - Shakedown

In a similar manner we shall treat true shakedown and pseudo-shakedown (associated with separation) separately.

I - True shakedown

Since we do not want separation we must have  $n > \frac{1}{2}$ .

In the zone of true shakedown we can find a residual stress distributions  $\rho$  such that :

$$\sigma_{max}^E + \rho \leq \sigma_0$$

$$\sigma_{min}^E + \rho \geq 0$$

where  $\sigma^E$  is the elastic stress.

Therefore

$$\sigma_{max}^E - \sigma_{min}^E \leq \sigma_0$$

at the extreme fiber:

$$\sigma_{max}^E - \sigma_{min}^E = 2 \frac{3}{2} m \sigma_0 \leq \sigma_0$$

$$\rightarrow \underline{m < 1/3}$$

Let us now consider the stress distribution due to the moment, and especially its envelop as M varies :

For a given m :

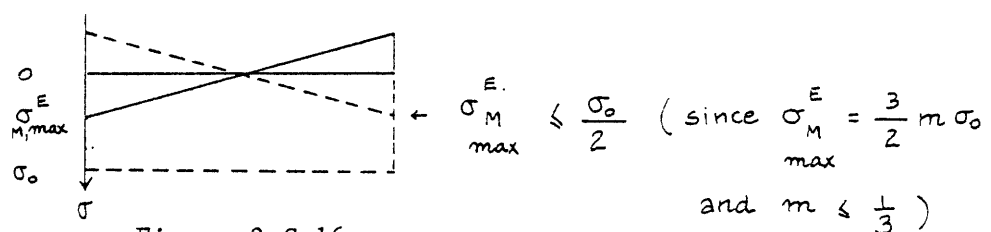


Figure 3.C.16

The maximum value of  $n$  corresponding to this  $m$  and leading to true shakedown is given by the shaded area, (technique of the shaded area).

$$\text{For a given } m \text{ the shaded area} = 2HB \sigma_0 - HB \frac{3}{2} m \sigma_0$$

$$n \sigma_0 2HB = \sigma_0 2HB \left(1 - \frac{3}{4} m\right)$$

$$\text{therefore the limit is given by } n = 1 - \frac{3}{4} m$$

$$\text{or } m = \frac{4}{3} [1 - n]$$

The true shakedown zone is defined by :

$$\left| \begin{array}{l} n \geq \frac{1}{2} \\ m \leq 1/3 \\ m \leq 4/3 [1 - n] \end{array} \right. \quad (\text{See Figure 3.C.19}).$$

## II - Pseudo-shakedown

Pseudo-shakedown is the zone where we would have had alternative plasticity.

It is sufficient to show that no incremental collapse occurs in this zone.

### 3.C.3.6 - Incremental collapse

As in the case of no separation we shall have incremental collapse when the center spring yields. The same argumentation holds concerning the loss of memory from one cycle to another and the linearity of the stress distribution in the elastic range.

The limiting lines for ratchetting are given by :

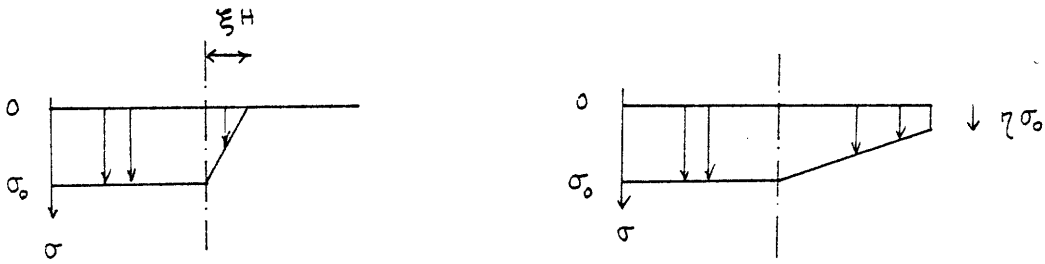


Figure 3.C.17

a) Separation

$$N = NB\sigma_0 + \frac{\xi HB\sigma_0}{2}$$

$$N = 2HB\sigma_0 \left( \frac{1}{2} + \frac{\xi}{4} \right)$$

$$n = \frac{1}{2} \left( 1 + \frac{\xi}{2} \right) \quad \xi = 2(2n-1)$$

$$M = \frac{1}{2} H^2 B \sigma_0 + \frac{\xi HB\sigma_0}{2} \xi H \frac{1}{3}$$

$$m = \frac{1}{2} \left( 1 + \frac{1}{3} \xi^2 \right)$$

eliminating  $\xi$   $m = \frac{1}{2} \left( 1 + \frac{1}{3} 4(2n-1)^2 \right)$

transition between  
ratchetting with  
separation and  
pseudo-shakedown

$$m = \frac{1}{2} + \frac{2}{3} (2n-1)^2$$

$$n \geq \frac{1}{2} \quad n \leq \frac{3}{4}$$

b) No separation

$$N = 2H\sigma_0 B - (1-\eta)\sigma_0 \frac{HB}{2}$$

$$N = 2H\sigma_0 B \left( 1 - \frac{1-\eta}{4} \right)$$

$$n = \frac{3}{4} + \frac{\eta}{4} \quad \eta = 4n-3$$

$$M = (1-\eta)\sigma_0 \frac{HB}{2} \frac{2H}{3} \quad m = \frac{1-\eta}{3}$$

$$m = \frac{4}{3} (1 - n)$$

Transition between ratchetting  
without separation and  
shakedown

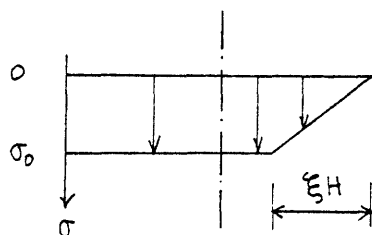
$$m = \frac{4}{3} (1 - n)$$

$$\frac{3}{4} \leq n \leq 1$$

it is the  
limit of the  
shakedown  
analysis.

(Figure 3.C.19)

c) Let us now consider the boundary between the two types of ratchetting



$$N = 2H\sigma_0 B - \xi \frac{H\sigma_0 B}{2}$$

$$N = 2H\sigma_0 B \left(1 - \frac{\xi}{4}\right)$$

$$n = 1 - \frac{\xi}{4}$$

$$M = \xi \frac{HB\sigma_0}{2} H \left(1 - \frac{\xi}{3}\right)$$

$$m = \frac{\xi}{2} \left(1 - \frac{\xi}{3}\right)$$

Figure 3.C.18

$$\underline{m = \frac{2}{3} (1 - n) (4n - 1)} \quad \text{See Figure 3.C.19.}$$

The complete loading range is now defined.

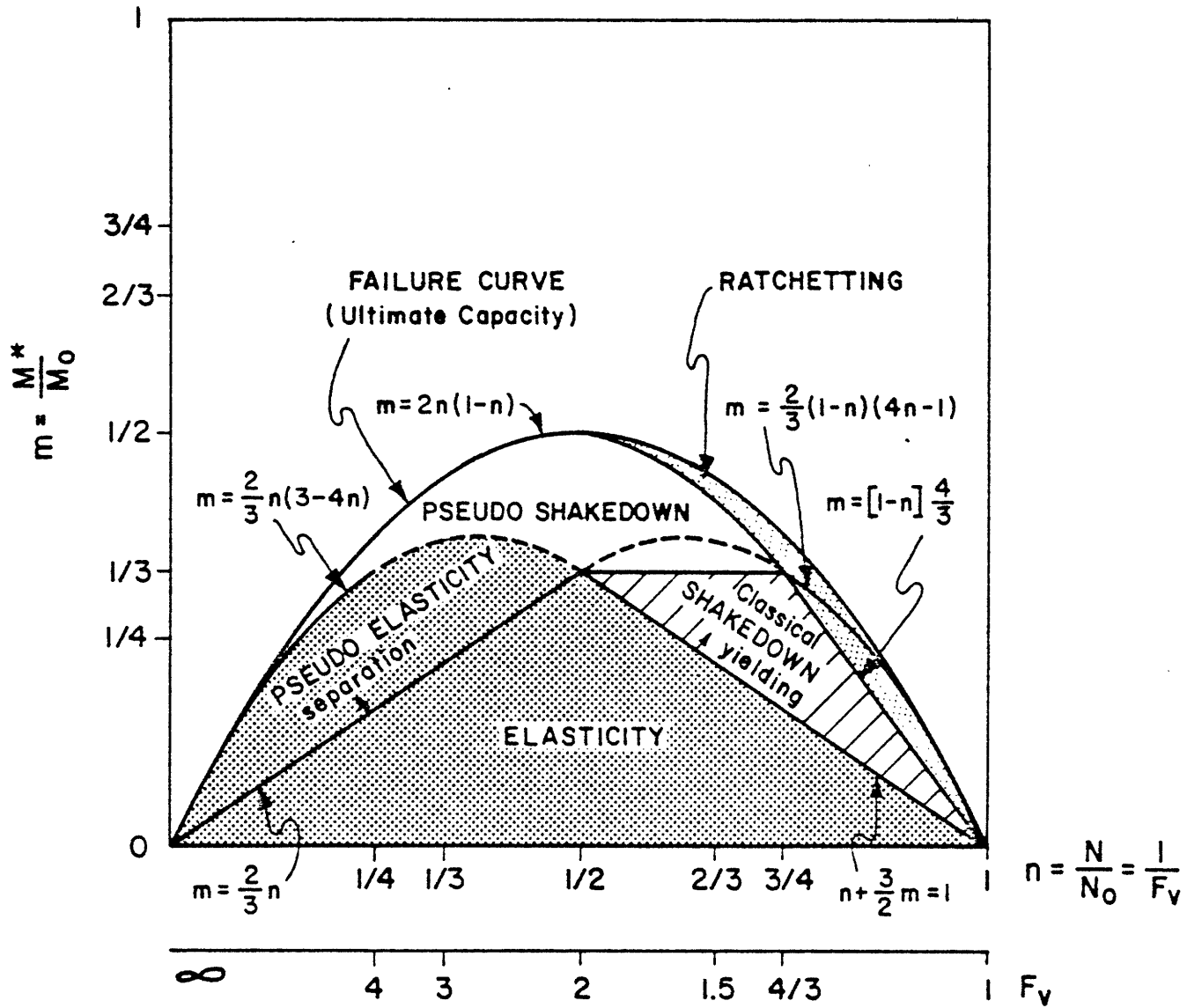


Figure 3.C.19 Rocking behavior of rigid foundation with separation.



## APPENDIX 4

COMPLEMENTARY EXPERIMENTAL RESULTS

## 4.A GENERAL DATA

Table 4.A.1 : Typical Plastic Drammen Clay Properties\*Average propertiesnatural water content  $\omega = 52 \%$ liquid limit  $\omega_L = 55 \%$ plastic limit  $\omega_P = 28 \%$ plasticity index  $I_P = 27 \%$ clay content ( $< 2 \mu$ ) 45 - 55 %specific gravity  $G_S = 2.76$ 

$$\left( s_{u,DSS} / \sigma'_{vc} \right)_{NC} = .215$$

Mineralogy

K-feldspar 25 - 30 %

Na-feldspar 5 %

quartz 20 %

hydromica 40 %

hornblende 5 %

chloride 5 %

\* After Andersen, 1975 | 2 | .

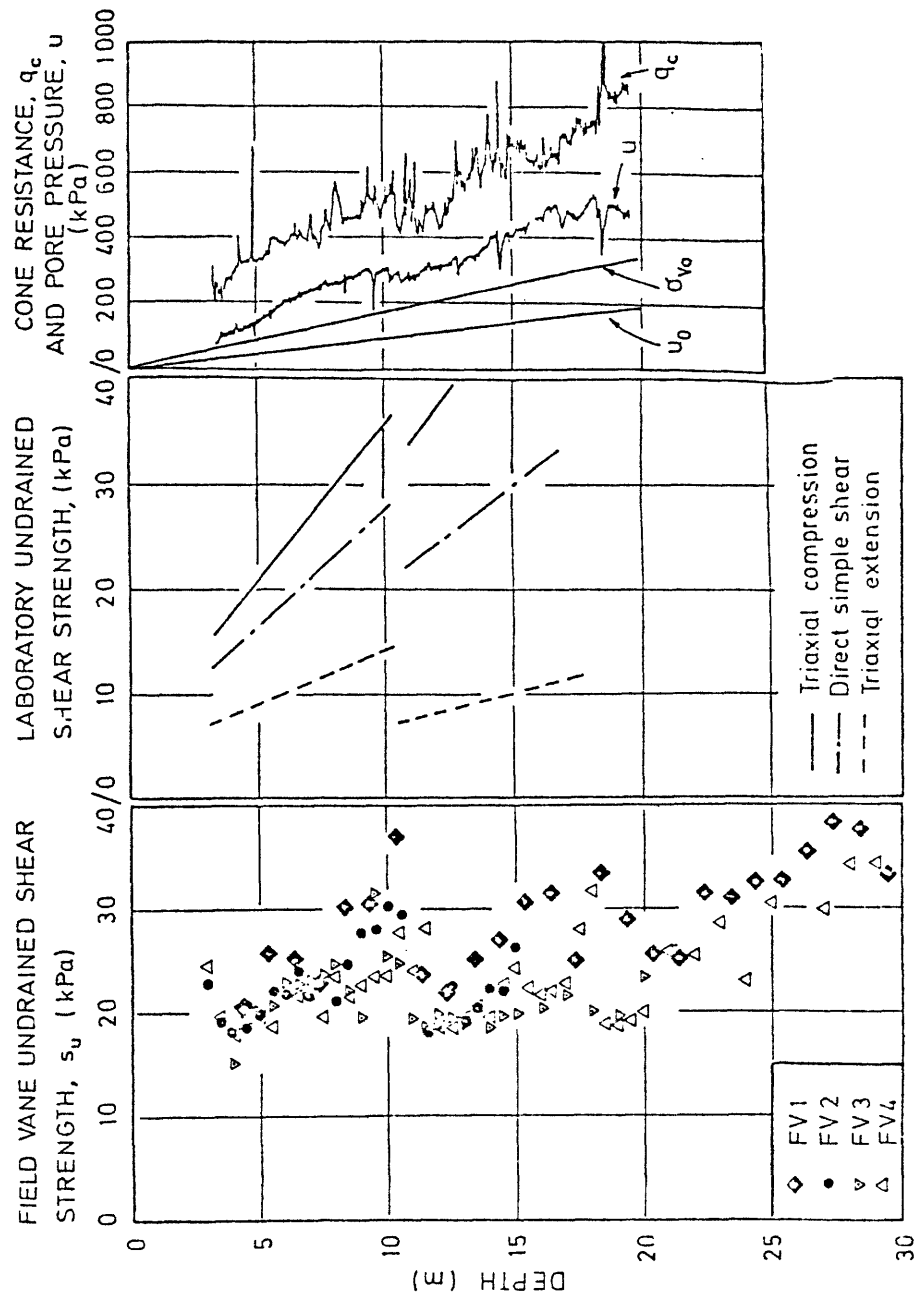


Figure 4.A.1 Additional strength parameters from the Danviksgt. site. (After NGI).

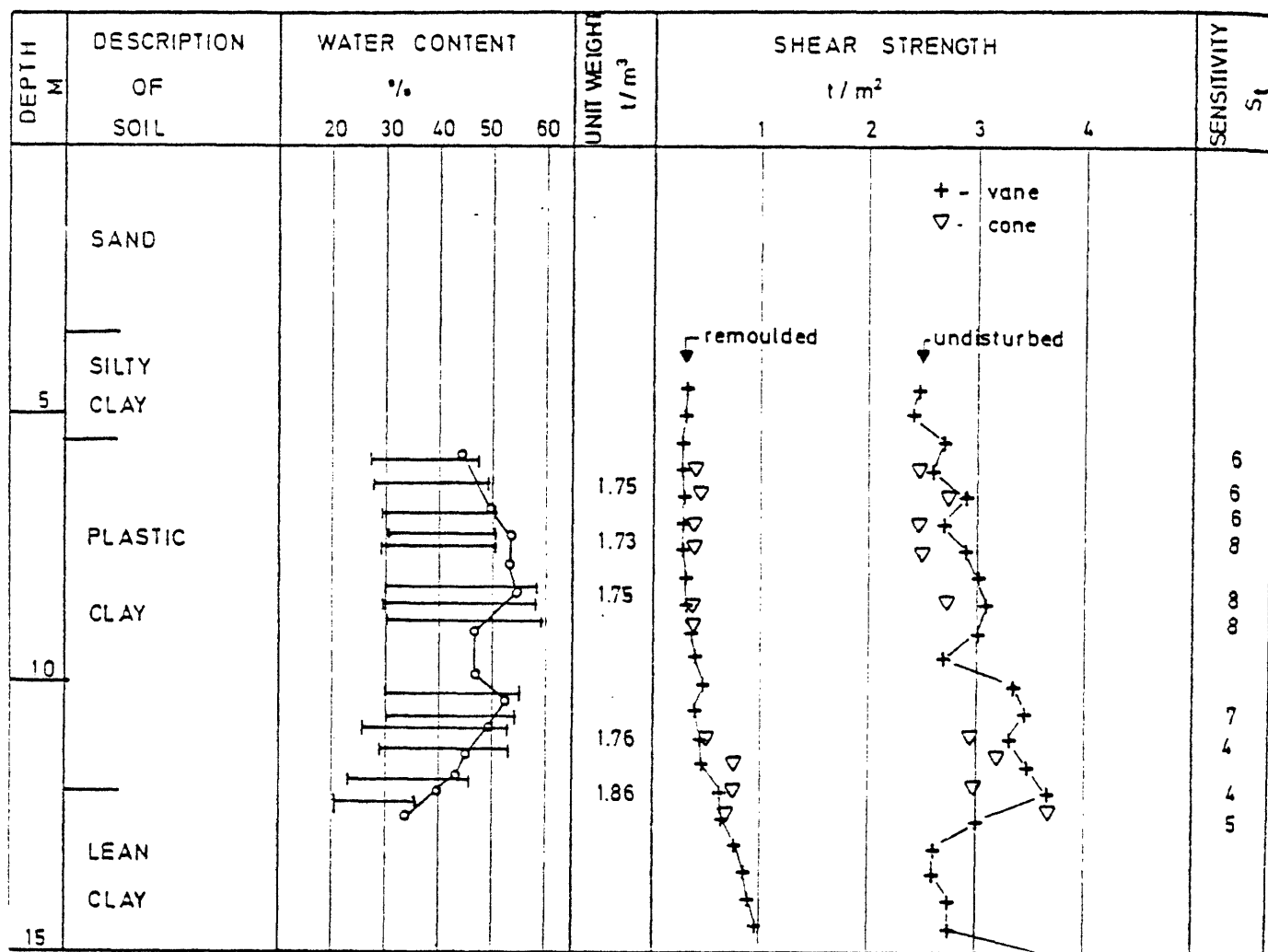


Figure 4.A.2 Soil profile from Museumsparken in Drammen, Norway

#### 4.B PREPARATION AND INDEX PROPERTIES

The clay was extruded from two tubes, 200 mm in diameter and 1 m long, from boring 39 made on May 6, 1981 at 50301 Danviksgt. in Drammen, Norway. These two tubes correspond to the depth ranges 6.2 - 7.2 m and 7.3 - 8.3 m. They were stored in NGI humid room at a temperature of 8°C. The first tube had been opened previously to our testing, while the second one was intact.

One 10 cm high cake was extruded from each tube on Friday, April 2, 1982. Each cake was immediately sliced on four parts and placed in liquid paraffin at 8°C. The procedure is presented in Figures 4.B.1 and 4.B.2 where the relative positioning of the specimens and the locations of shell fragments and organic matters are also indicated. The slicing of the cake quarters was made whenever needed.

The aspect of the two cakes was quite different, the first one (39-1) presenting a rim of yellowish color (oxidation) and deep vertical marks on its side. Chips of clay were obviously unstable and some silty parts were also visible. The second cake (39-2) was apparently perfect.

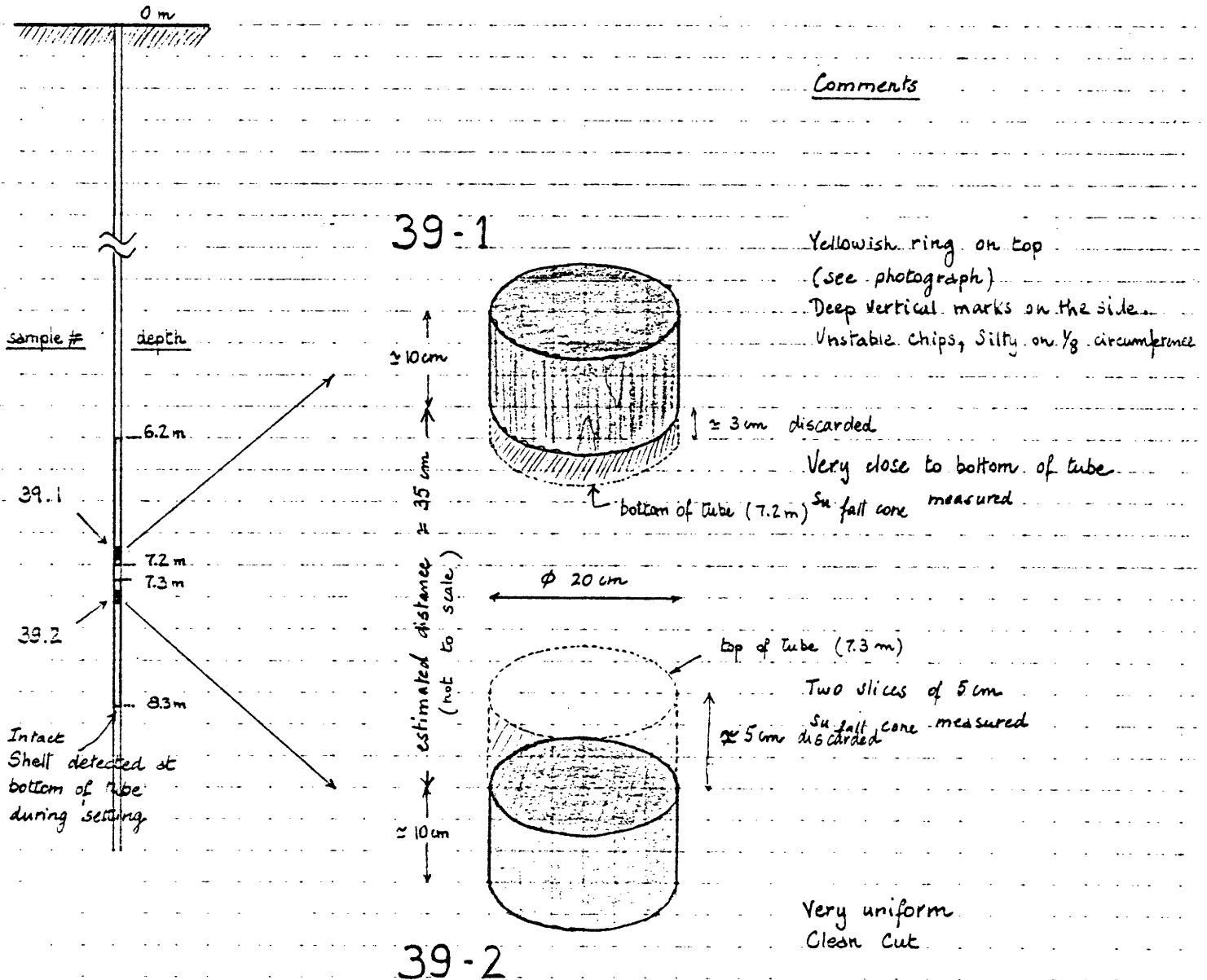
The actual preparation of a typical specimen took around 10 minutes. The membranes used were too thick and as a result some clay was systematically removed on the outer periphery of the specimen during the placement of the membrane. The routine measurement of the initial height was also found to be somewhat unreliable and a direct check was made which yielded a very systematic height of 16.0 mm.

date: 6/5 1981  
 location: DRAMMEN  
 50301 DANVIKSGT.  
 BORING 39

Figure 4.B.1

Preparation

Comments



Both samples prepared on the 3<sup>rd</sup>, April 1982.

Storage in liquid paraffin around 8°C after cutting each "cake" in 4 slices (see detail on fig. )

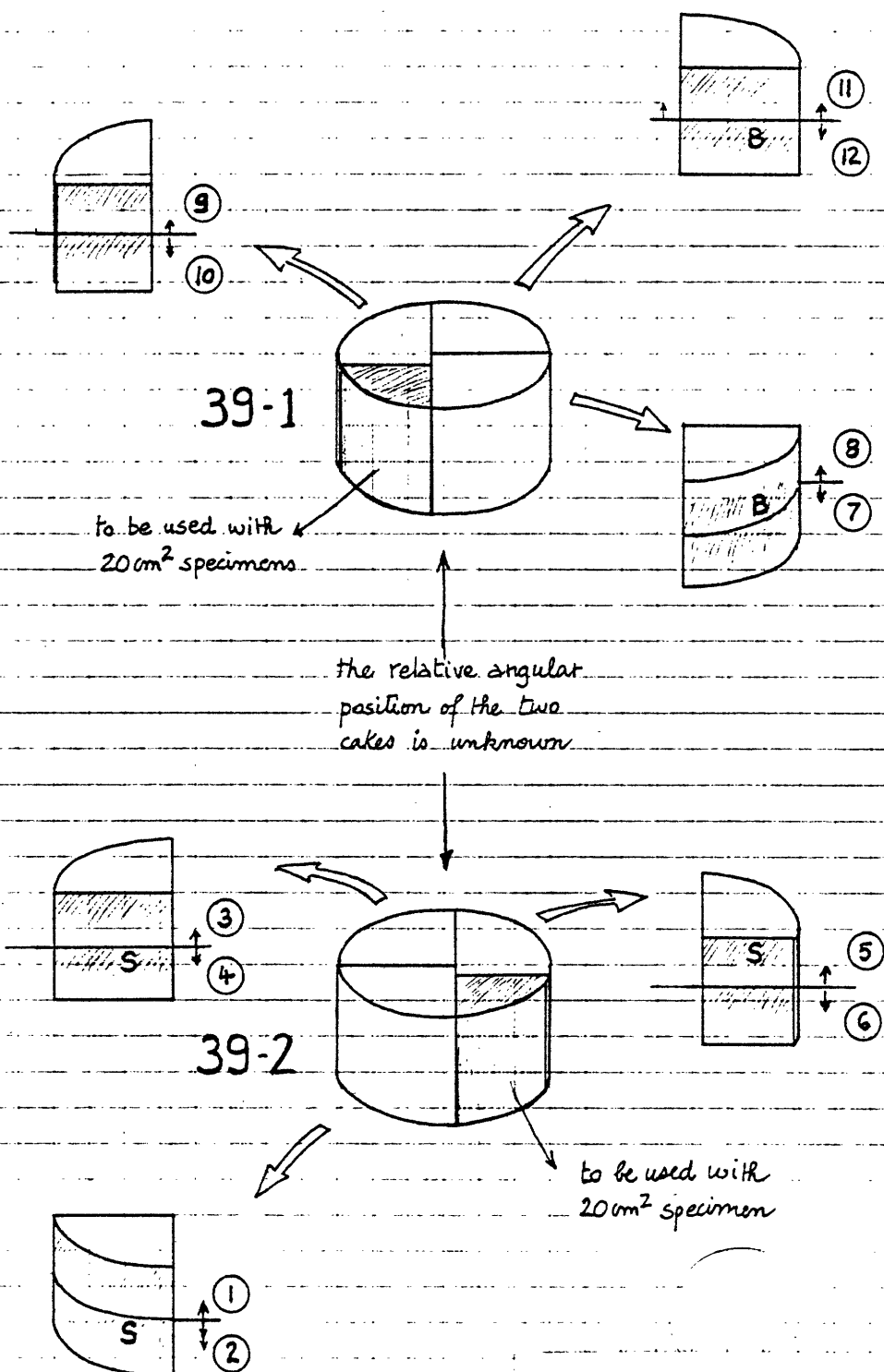


Figure 4.B.2

Specimen Distribution

- ③ Test number
- B Brown, probably organic spots
- S Shell
- Actual location of specimens

Clay index properties were obtained for each specimen. During trimming the larger chunks were kept for Atterberg limit estimations while the closest clay was quickly stored for natural water content measurement. Most of the relevant results were reported in Table 4.3.1. A comparison of the two different cakes can be made on the basis of Figure 4.B.3 and the Casagrande's chart of Figure 4.B.4. The two cakes correspond to somewhat different clays. This finding is confirmed by the fall cone measurements of Table 4.B.1 and the correlation diagram of Figure 4.B.5. Sample 39.2 yields a far better correlation with respect to natural water content ; however the "strengths" do not appear too different.

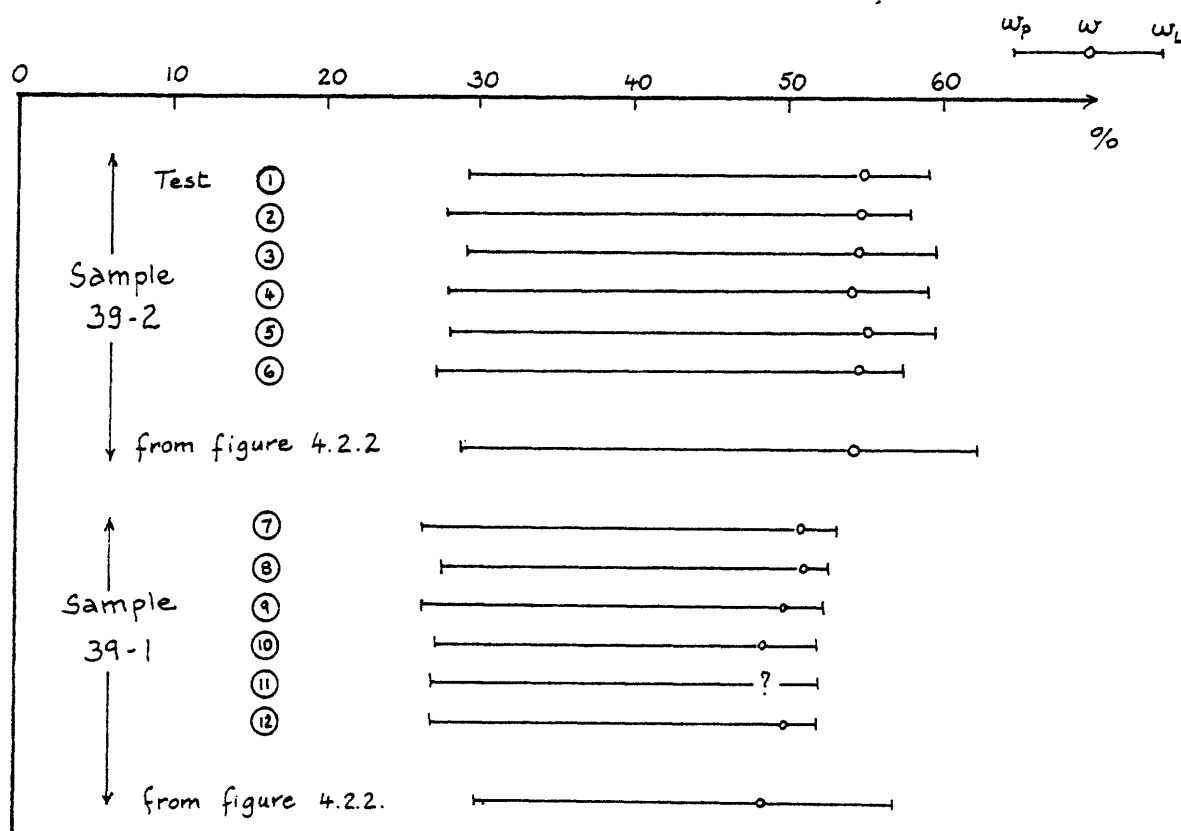


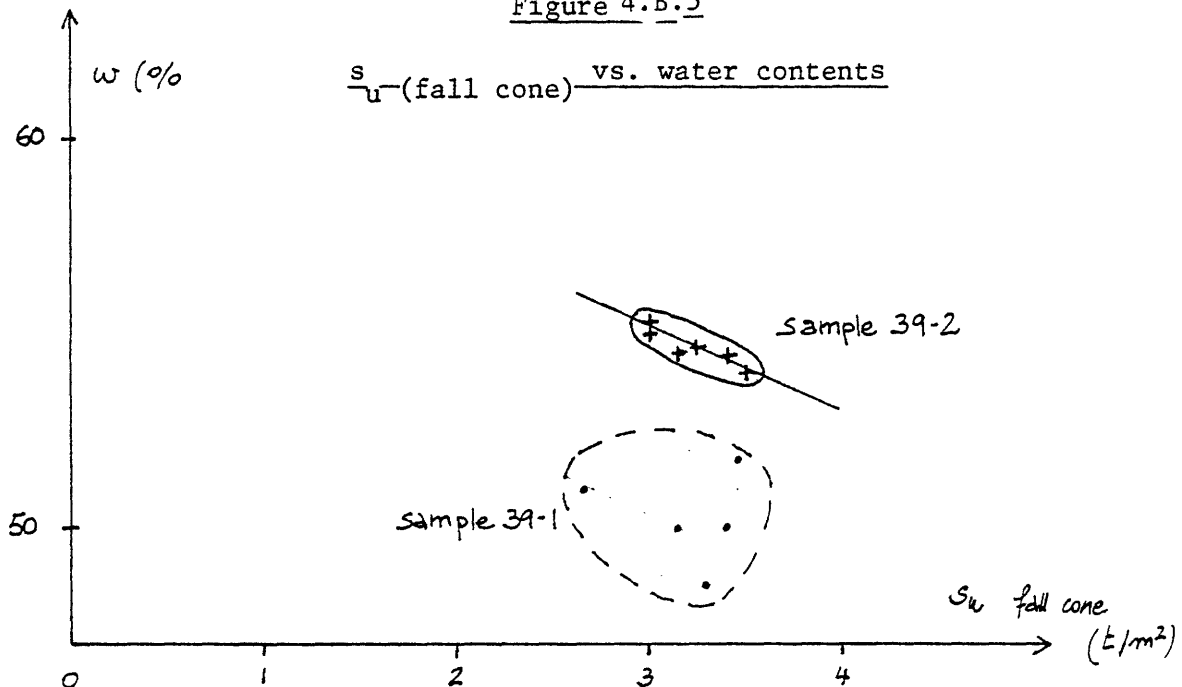
Figure 4.B.3 Water contents and Atterberg limits.

Table 4.B.1

$S_u$  fall cone (100 g cone) in  $t/m^2$

IN DENT P T A H J I N G	mean for the test ( $\sigma$ = stand. deviation)		
	8	9	11
39-1	$\begin{matrix} 3.35 \\ 3.35 \\ 3.65 \end{matrix} \downarrow$ <u>3.46</u>	$\begin{matrix} 3.10 \\ 3.35 \\ 3.75 \end{matrix} \downarrow$ <u>3.40</u>	$\begin{matrix} 2.95 \\ 2.90 \\ 2.95 \end{matrix} \downarrow$ <u>2.93</u>
			$\rightarrow$ <u>3.26</u> $\sigma = .24$
	$\begin{matrix} 2.75 \\ 2.50 \\ 2.75 \end{matrix} \downarrow$ <u>2.66</u>	$\begin{matrix} 3.50 \\ 3.25 \\ 3.10 \end{matrix} \downarrow$ <u>3.28</u>	$\begin{matrix} 3.10 \\ 3.10 \\ 3.25 \end{matrix} \downarrow$ <u>3.15</u>
			$\rightarrow$ <u>3.03</u> $\sigma = .27$
	$\begin{matrix} 2.45 \\ 2.45 \\ 3.10 \end{matrix} \downarrow$ <u>3.00</u>	$\begin{matrix} 3.50 \\ 3.10 \\ 3.10 \end{matrix} \downarrow$ <u>3.23</u>	$\begin{matrix} 3.10 \\ 2.95 \\ 2.95 \end{matrix} \downarrow$ <u>3.00</u>
			$\rightarrow$ <u>3.07</u> $\sigma = .11$
39-2	$\begin{matrix} 3.25 \\ 3.10 \\ 3.10 \end{matrix} \downarrow$ <u>3.15</u>	$\begin{matrix} 3.50 \\ 3.50 \\ 3.50 \end{matrix} \downarrow$ <u>3.50</u>	$\begin{matrix} 3.50 \\ 3.50 \\ 3.25 \end{matrix} \downarrow$ <u>3.41</u>
			$\rightarrow$ <u>3.35</u> $\sigma = .15$

Figure 4.B.5





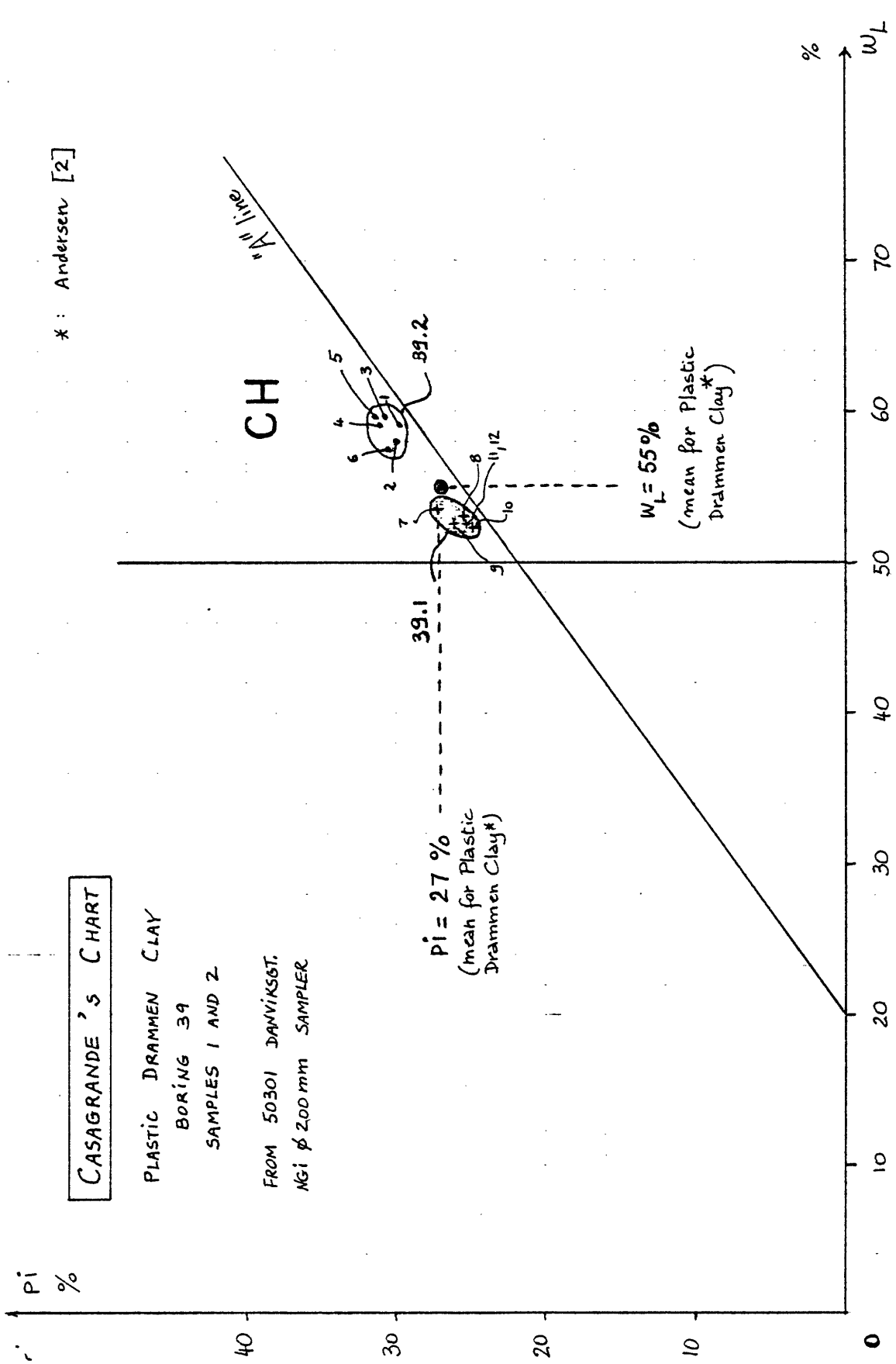


Figure 4.B.4.

## 4.C CONSOLIDATION, SHEAR AND CREEP

4.C.1 Consolidation

The consolidation stage followed closely the NGI procedure. The key results are presented in the form of increments of displacements, heights and strains in Table 4.C.1 and in the  $\left[ \varepsilon - \log \sigma'_{vc} \right]$  diagram of Figure 4.C.1 where the mean (and standard deviation) points are reported for each cake. Again it can be seen that while each cake yields very consistent results some discrepancy exists between the two cakes.

The measurements at each step loading are taken at 6,15 and 30 seconds, 1 and 30 minutes. Figure 4.C.1 corresponds to the 30 minutes reading. This procedure is oriented towards the estimation of the "false" deformation by a Taylor  $\log(t)$  fit\*. The total corrected deformation is then used to estimate the correction for vertical deformation of the membrane.

$$\Delta \text{ weight to be applied} \\ \text{on level arm hanger} = \frac{\sigma_m \times A \times C}{10}$$

$\sigma_m$  is obtained from Figure 4.C.2 by entering the corrected deformation

A is the surface of the specimen (50 cm<sup>2</sup>)

C is a parameter of the membrane, here 1.3

---

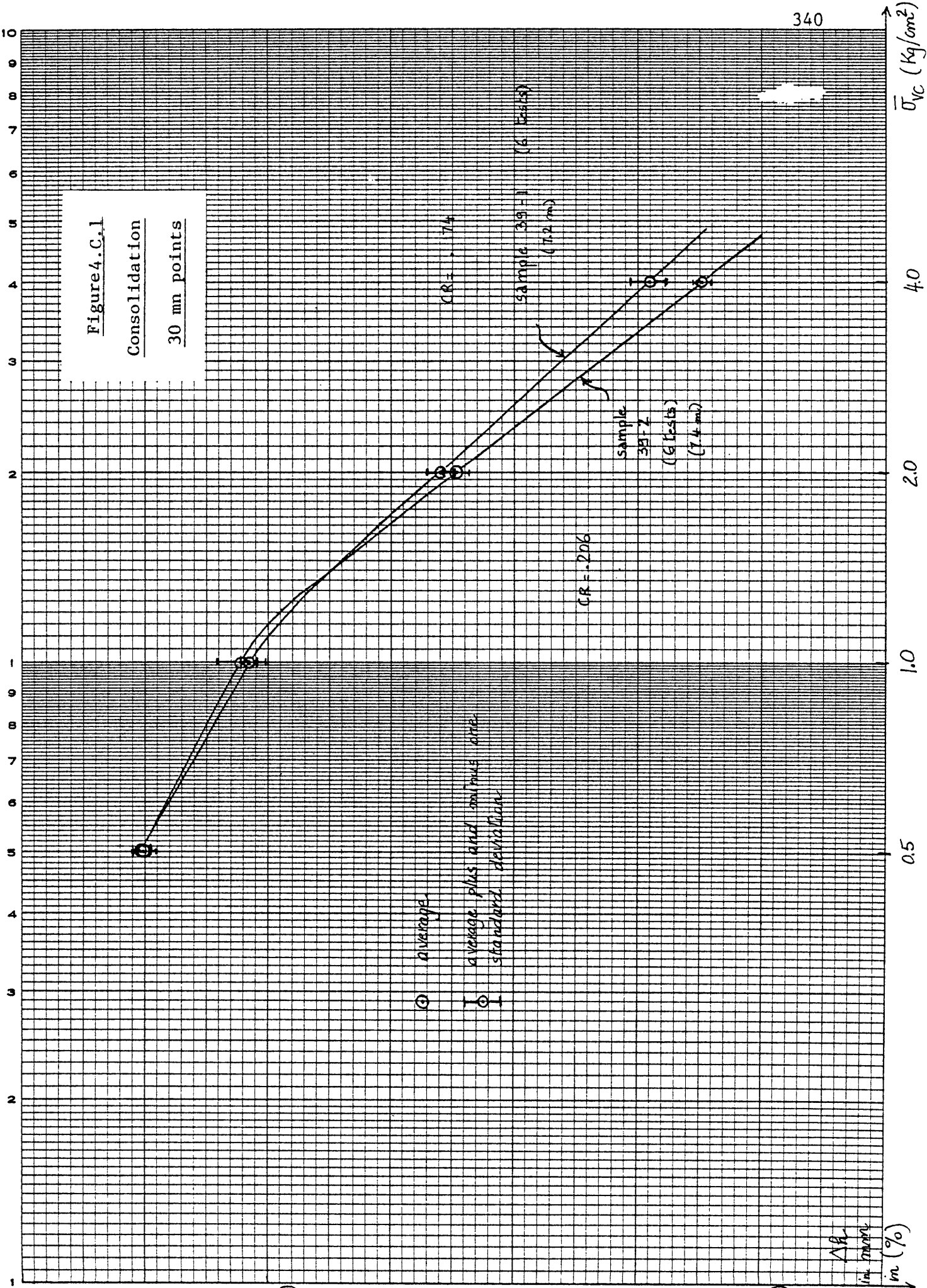
\* False deformation : initial deformation as obtained from Taylor's fit - deformation before application of load.

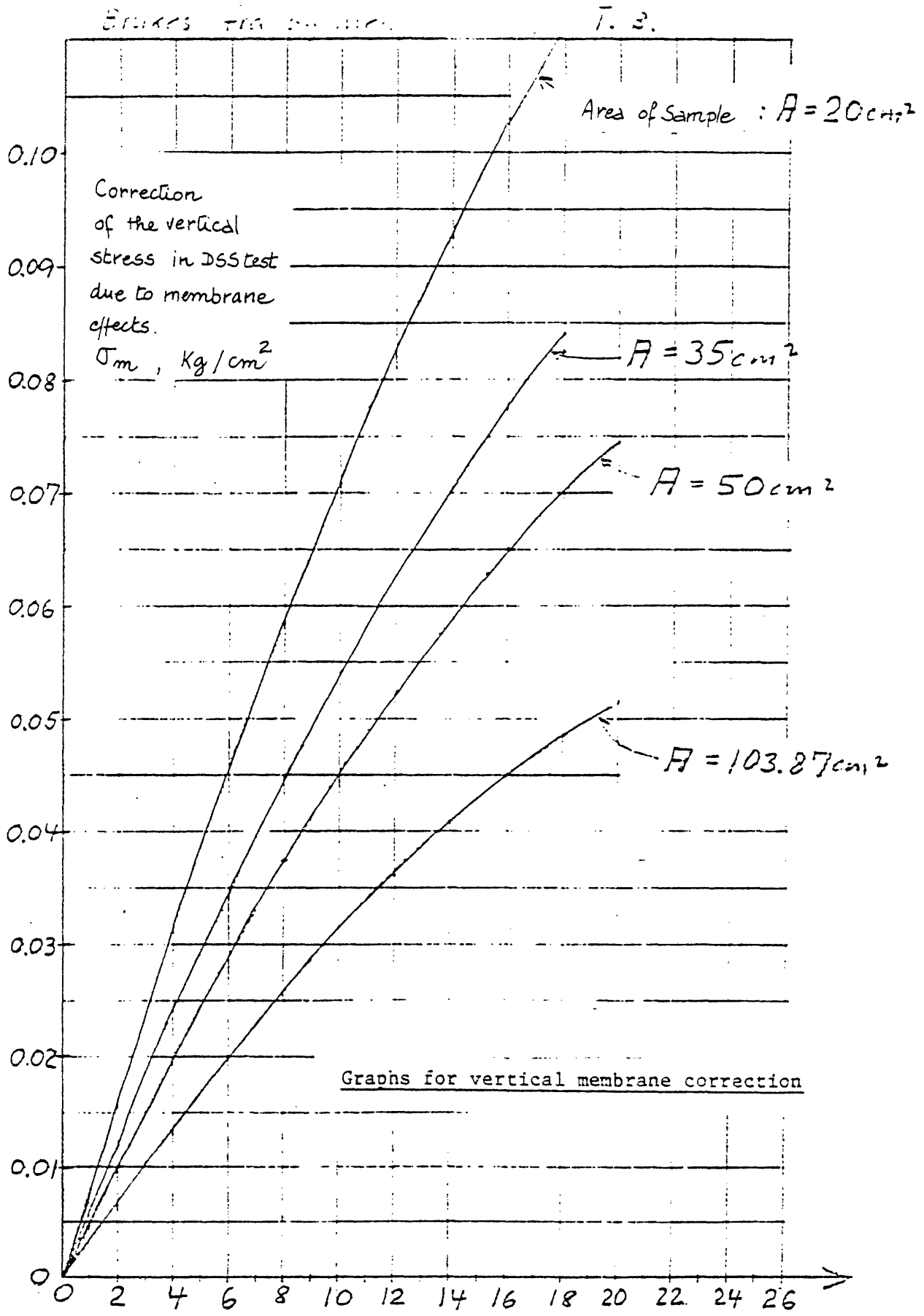
$\bar{\sigma}_{vc}$ (kg/cm <sup>2</sup> )	Time increment min $\Delta$	①	②	③	④	⑤	⑥	⑦	⑧	⑨	⑩	⑪	⑫
		(**)	(**)	(**)	(**)	(**)	(**)	(**)	(**)	(**)	(**)	(**)	(**)
.5	06	.200	.199	.182	.200	.190	.208	.206	.183	.200	.200	.190	.195
	15	.050	.050	.050	.045	.050	.045	.045	.045	.040	.045	.045	.050
	30	.060	.045	.055	.040	.045	.045	.055	.055	.035	.045	.045	.045
	1	.065	.055	.065	.055	.065	.050	.065	.065	.050	.060	.045	.070
1.0	30	.169	.104	.200	.109	.180	.100	.168	.137	.116	.146	.122	.146
	06	.096	.076	.080	.071	.075	.080	.072	.078	.084	.084	.088	.079
	15	.040	.030	.035	.035	.040	.035	.035	.040	.035	.040	.035	.035
	30	.050	.035	.040	.035	.035	.035	.045	.040	.060	.040	.045	.040
2.0	1	.055	.039	.055	.045	.050	.045	.055	.050	.055	.050	.055	.045
	30	.228	.156	.234	.162	.220	.152	.228	.200	.219	.207	.248 (*)	.195
	06	.152	.147	.111	.128	.120	.133	.122	.135	.131	.133	.127	.125
	15	.060	.055	.070	.060	.060	.065	.060	.065	.065	.065	.060	.065
4.0	30	.085	.090	.070	.085	.070	.075	.075	.080	.080	.075	.080	.070
	1	.090	.110	.095	.100	.095	.105	.100	.110	.100	.100	.115	.095
	30	.470	.548	.442	.533	.470	.548	.420	.425	.400	.371	.458	.375
	06	.190	.207	.183	.192	.170	.192	.165	.180	.175	.184	.177	.177
$\Delta R$ consolidation (mm)		.085	.095	.085	.085	.095	.095	.085	.095	.095	.090	.095	.090
		.105	.115	.100	.105	.105	.110	.100	.105	.095	.095	.110	.100
$R_0 - \Delta R$ cons. (mm)		.140	.145	.130	.155	.135	.145	.125	.135	.115	.115	.130	.115
		.432	.487	.435	.500	.457	.520	.350	.350	.340	.350	.364	.345
$\Delta h$ start dr. shear (mm)		2.822	2.788	2.717	2.740	2.727	2.783	2.591	2.573	2.490	2.490	2.644	2.457
		13.178	13.212	13.283	13.260	13.273	13.217	13.409	13.427	13.510	13.510	13.556	13.543
$\Delta h$ start cyc. shear (mm)		-	-	.145	.146	.138	.123	.128	.114	.112	.112	.121	.100
		-	-	.185	.196	.145	.156	.223	.206	.192	.198	.168	.198
$E_v$ end of consol. (%)		17.6	17.4	17.0	17.1	17.0	17.4	16.2	16.0	15.6	15.6	16.5	15.4
$E_v$ end of dr. shear (%)		-	-	19.0	19.3	18.8	19.1	18.4	18.1	17.5	17.5	18.3	17.2

VERTICAL DISPLACEMENT INCREMENTS in mm. VERTICAL DISPLACEMENTS AND STRAINS.

(\*) 5 minutes late  
(\*\*) no membrane correction

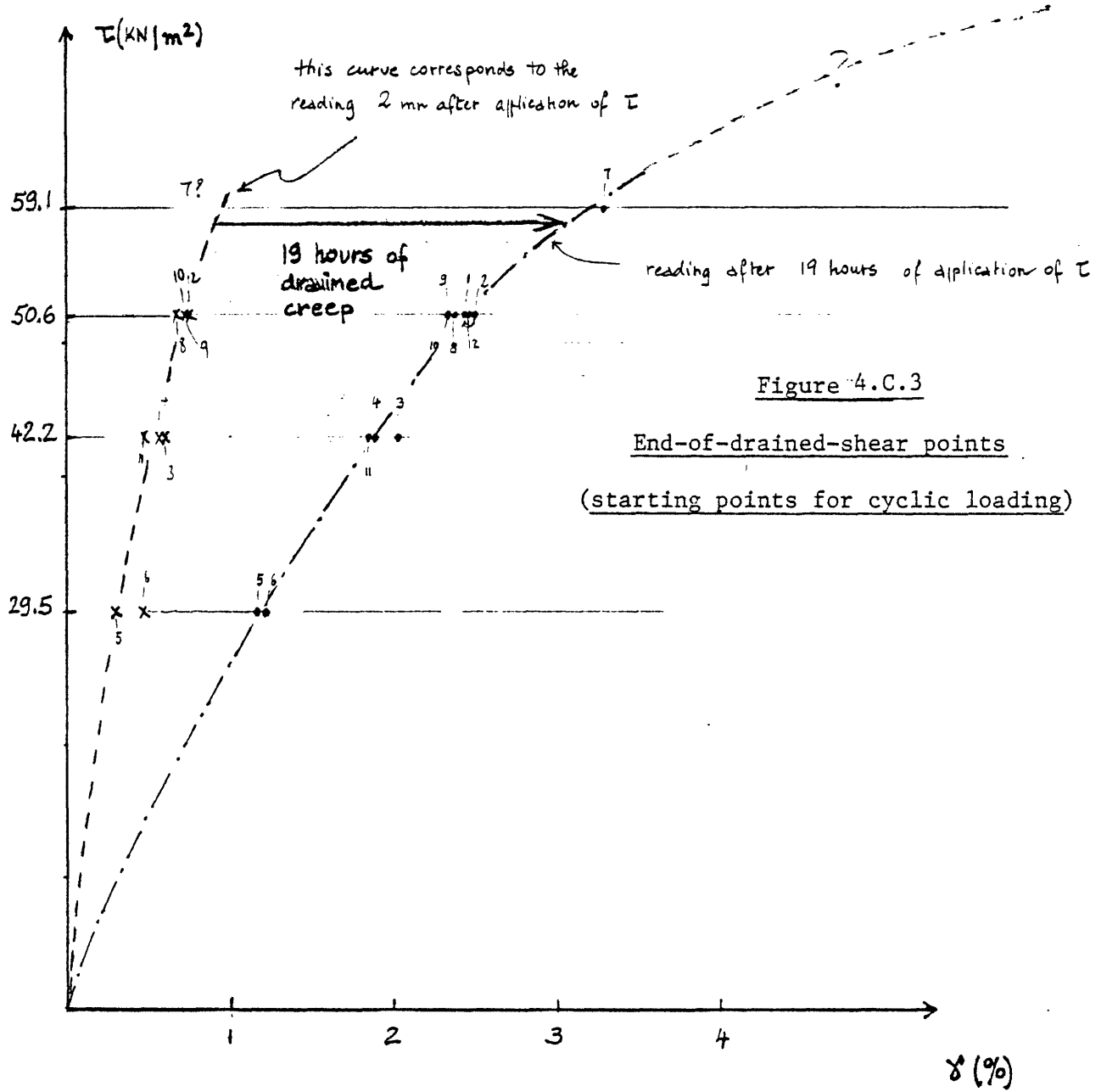
Table 4.C.1 Consolidation data.





Vertical Deformation of Membrane in % of Sample Height

Figure 4.C.2.



The resulting load increase was only 2 %. This correction was not applied to tests ①, ② and ⑫.

Contact with the specimen was insured by placing a load of 150 g on the arm hangar during 10 mn. The apparatus had been previously checked for levelness and sensitivity of the vertical displacement reading.

#### 4.C.2 Drained shear and creep

Figure 4.C.3 presents in a  $\tau$ - $\gamma$  diagram the points corresponding to the end of drained shear and the end of creep (19 hours difference). Vertical deformation measurements were reported in Table 4.C.1.

The horizontal (shear) displacements do not show evidence of a significant difference between cakes 39.1 and 39.2

A horizontal correction of the same type as in section 4.C.1 is also applied to all the shear deformations. Figure 4.C.4 gives the correction factor on the shear load as a function of the shear strain.

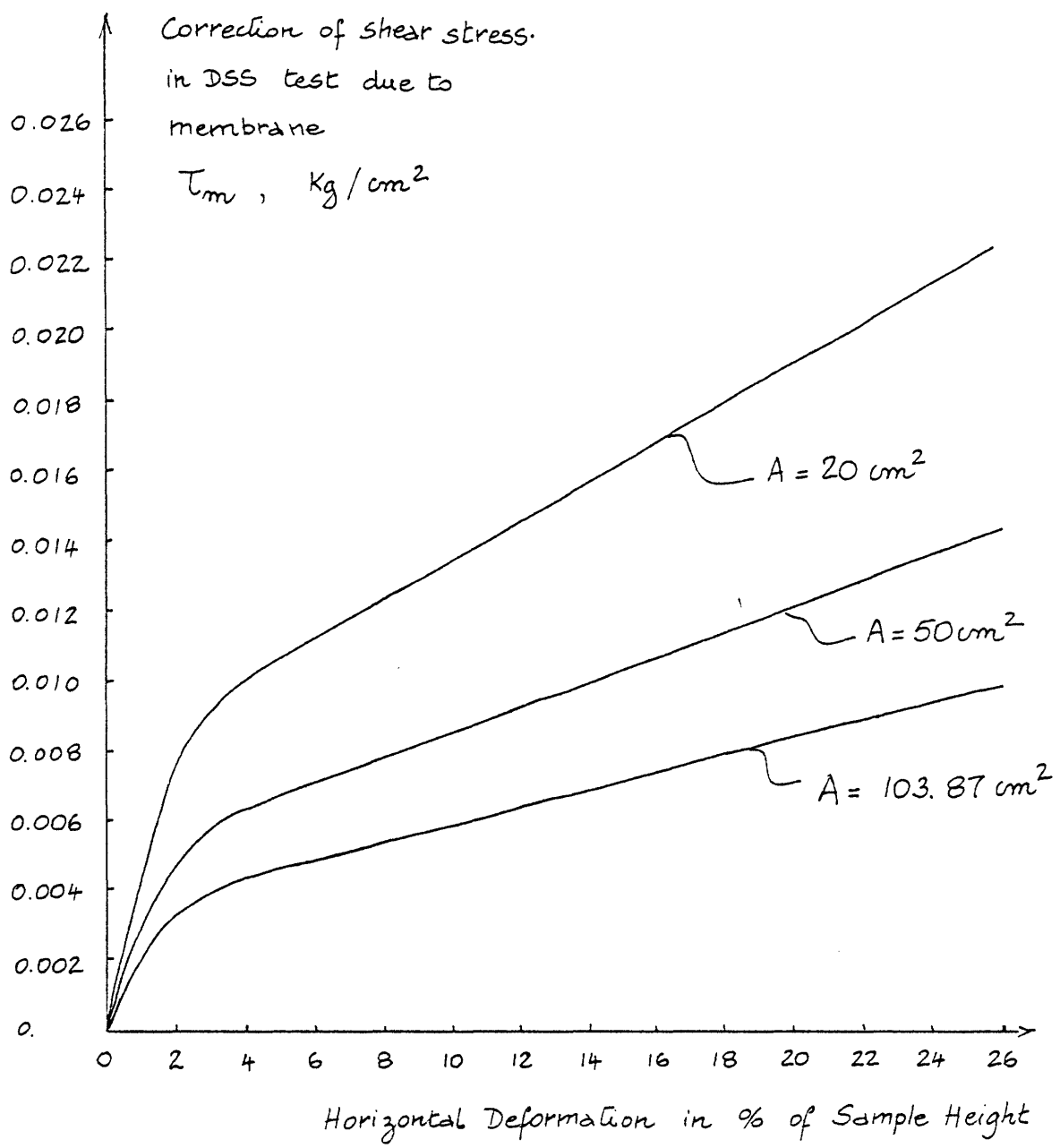


Figure 4.C.4.

(after NGI)



#### 4.D CYCLIC LOADING

Tables 4.D.1 through 4.D.12 give the shear stresses, deformations and pore pressures at selected cycles. Both stresses and deformations have been corrected for horizontal membrane deformation.

SHEAR STRESSES, DEFORMATIONS (*) AND PORE PRESSURES AT SELECTED CYCLES.						NGI 82 59000-6		TEST NUMBER 1			
						PLASTIC DRAMMEN CLAY NORMALLY CONSOLIDATED $\bar{\sigma}_{ve} = 4 \text{ kg/cm}^2 = 392.4 \text{ KN/m}^2$					
N	$\tau_{max}$ (KN/m <sup>2</sup> )	$\delta_{max}$ (%)	$\delta_c$ (%)	$\delta_{ave}$ (%)	$u_{ave}$ (KN/m <sup>2</sup> )	N	$\tau_{max}$ (KN/m <sup>2</sup> )	$\delta_{max}$ (%)	$\delta_c$ (%)	$\delta_{ave}$ (%)	$u_{ave}$ (KN/m <sup>2</sup> )
	$\tau_{min}$ (KN/m <sup>2</sup> )	$\delta_{min}$ (%)					$\tau_{min}$ (KN/m <sup>2</sup> )	$\delta_{min}$ (%)			
0	$\tau_{ave} = 50.6$			2.43	0						
50	75.84 25.29	2.66 2.46	.1	2.56	24.5						
100	75.82 25.28	2.71 2.49	.11	2.60	31.8						
150	75.82 25.28	2.72 2.50	.11	2.61	36.7						
200	75.82 25.28	2.73 2.51	.11	2.62	41.6						
300	75.80 25.27	2.78 2.54	.12	2.66	46.5						
400	75.74 25.25	2.83 2.60	.12	2.72	51.4						
500	75.77 25.23	2.90 2.66	.12	2.78	57.5						
750	75.74 25.22	2.98 2.72	.13	2.85	67.3						
1000	75.73 25.20	3.01 2.78	.13	2.90	73.4						
1250	75.72 25.19	3.07 2.81	.13	2.94	79.5						
1500	75.70 25.18	3.13 2.84	.14	2.99	79.5						

(\*) all deformations relative to height after  $K_0$ -consolidation  
after membrane correction

Table 4.D.1

$$\tau_{ave} = 50.62 \text{ KN/m}^2$$

$$\tau_c = 25.31 \text{ KN/m}^2$$

SHEAR STRESSES, DEFORMATIONS (*) AND PORE PRESSURES AT SELECTED CYCLES.						NGI 82 59000-6		TEST NUMBER (2)			
						PLASTIC DRAMMEN CLAY NORMALLY CONSOLIDATED $\bar{\sigma}_{vc} = 4 \text{ kg/cm}^2 = 392.4 \text{ KN/m}^2$					
N	$\tau_{max}$ (KN/m <sup>2</sup> )	$\delta_{max}$ (%)	$\delta_c$ (%)	$\delta_{ave}$ (%)	$u_{ave}$ (KN/m <sup>2</sup> )	N	$\tau_{max}$ (KN/m <sup>2</sup> )	$\delta_{max}$ (%)	$\delta_c$ (%)	$\delta_{ave}$ (%)	$u_{ave}$ (KN/m <sup>2</sup> )
	$\tau_{min}$ (KN/m <sup>2</sup> )	$\delta_{min}$ (%)					$\tau_{min}$ (KN/m <sup>2</sup> )	$\delta_{min}$ (%)			
0	$\tau_{ave} = 50.6$			2.42	0						
50	84.14 16.73	3.11 2.88	.12	3.00	68.4						
100	84.07 16.68	3.33 3.07	.13	3.22	88.0						
200	84.01 16.60	3.64 3.33	.15	3.48	112.5						
300	83.95 16.54	3.95 3.60	.17	3.77	129.6						
400	83.90 16.44	4.25 3.87	.19	4.06	146.7						
500	83.86 16.44	4.56 4.18	.19	4.37	158.9						
750	83.77 16.34	5.47 5.01	.23	5.24	188.4						
1000	83.68 16.22	6.85 6.24	.30	6.54	220.2						
1100	83.61 16.19	7.84 7.15	.34	7.49	239.5						
1200	83.53 16.09	9.67 8.91	.38	9.29	249.7						
1300	83.41 15.97	13.49 12.54	.48	13.02	271.7						
1350	83.22 15.79	19.06 18.00	.53	18.53	271.7						
1360	83.14 15.71	21.51 20.20	.65	20.95	271.7						

note: T = 12 seconds

(\*) all deformations relative to height after Ko-consolidation  
after membrane correction

Table 4.D.2

$$\tau_{ave} = 50.62 \text{ KN/m}^2$$

$$\tau_c = 33.75 \text{ KN/m}^2$$

SHEAR STRESSES, DEFORMATIONS (*) AND PORE PRESSURES AT SELECTED CYCLES.						NGI 82 59000-6	TEST NUMBER <b>3</b>				
						PLASTIC DRAMMEN CLAY NORMALLY CONSOLIDATED $\bar{\sigma}_{vc} = 4 \text{ kg/cm}^2 = 392.4 \text{ kN/m}^2$					
N	$\tau_{max}$ (kN/m <sup>2</sup> )	$\delta_{max}$ (%)	$\delta_c$ (%)	$\delta_{ave}$ (%)	$u_{ave}$ (kN/m <sup>2</sup> )	N	$\tau_{max}$ (kN/m <sup>2</sup> )	$\delta_{max}$ (%)	$\delta_c$ (%)	$\delta_{ave}$ (%)	$u_{ave}$ (kN/m <sup>2</sup> )
	$\tau_{min}$ (kN/m <sup>2</sup> )	$\delta_{min}$ (%)					$\tau_{min}$ (kN/m <sup>2</sup> )	$\delta_{min}$ (%)			
0	$\tau_{ave} = 42.17$			2.02	0						
50	84.04 -0.16	3.05 2.58	.24	2.82	101.8						
100	83.99 -0.24	3.35 2.82	.27	3.09	126.2						
200	83.88 -0.34	3.93 3.28	.33	3.61	156.6						
300	83.82 -0.43	4.51 3.81	.35	4.16	183.5						
400	83.75 -0.51	5.31 4.46	.43	4.89	208.0						
500	83.69 -0.59	6.33 5.28	.53	5.81	227.5						
600	83.57 -0.69	8.27 6.92	.68	7.60	259.5						
650	83.49 -0.79	10.56 8.80	.88	9.68	280.0						
700	83.28 -0.97	17.02 14.26	1.38	15.64	293.6						
710	83.19 -1.06	19.78 16.84	1.47	18.31	310.8						

(\*) all deformations relative to height after  $K_0$ -consolidation  
after membrane correction

Table 4.D.3

$$\tau_{ave} = 42.19 \text{ kN/m}^2$$

$$\tau_c = 42.19 \text{ kN/m}^2$$

SHEAR STRESSES, DEFORMATIONS (*) AND PORE PRESSURES AT SELECTED CYCLES.						NGI 82 59000-6		TEST NUMBER (4)			
						PLASTIC DRAMMEN CLAY NORMALLY CONSOLIDATED $\bar{\sigma}_{vc} = 4 \text{ Kg/cm}^2 = 392.4 \text{ KN/m}^2$					
N	$\tau_{max}$ (KN/m <sup>2</sup> )	$\delta_{max}$ (%)	$\delta_c$ (%)	$\delta_{ave}$ (%)	$u_{ave}$ (KN/m <sup>2</sup> )	N	$\tau_{max}$ (KN/m <sup>2</sup> )	$\delta_{max}$ (%)	$\delta_c$ (%)	$\delta_{ave}$ (%)	$u_{ave}$ (KN/m <sup>2</sup> )
	$\tau_{min}$ (KN/m <sup>2</sup> )	$\delta_{min}$ (%)					$\tau_{min}$ (KN/m <sup>2</sup> )	$\delta_{min}$ (%)			
0	$\tau_{ave} = 42.17$			1.88	0						
10	92.44 -8.65	3.11 2.61	.25	2.86	68.9						
20	92.27 -8.77	4.12 3.11	.50	3.62	152.1						
30	92.22 -8.88	4.73 3.73	.51	4.23	179.0						
40	92.15 -8.95	5.73 4.50	.62	5.12	203.5						
50	92.05 -9.05	7.26 5.57	.85	6.42	228.1						
60	91.93 -9.17	10.20 7.50	1.35	8.85	252.6						
70	91.70 -9.36	17.28 12.66	2.31	14.97	268.9						
75	91.46 -9.54	24.60 18.21	3.20	21.41	296.7						

(\*) all deformations relative to height after Ko-consolidation after membrane correction

(\*) motor not working (bad connection for a few cycles)

$\tau_{ave} = 42.19 \text{ KN/m}^2$   
 $\tau_c = 50.62 \text{ KN/m}^2$

Table 4.D.4

SHEAR STRESSES, DEFORMATIONS (*) AND PORE PRESSURES AT SELECTED CYCLES.						NGI 82 59000-6		TEST NUMBER <b>5</b>			
						PLASTIC DRAMMEN CLAY NORMALLY CONSOLIDATED $\bar{\sigma}_{vc} = 4 \text{ Kg/cm}^2 = 392.4 \text{ KN/m}^2$					
N	$\tau_{max}$ (KN/m <sup>2</sup> )	$\delta_{max}$ (%)	$\delta_c$ (%)	$\delta_{ave}$ (%)	u (KN/m <sup>2</sup> )	N	$\tau_{max}$ (KN/m <sup>2</sup> )	$\delta_{max}$ (%)	$\delta_c$ (%)	$\delta_{ave}$ (%)	u (KN/m <sup>2</sup> )
	$\tau_{min}$ (KN/m <sup>2</sup> )	$\delta_{min}$ (%)					$\tau_{min}$ (KN/m <sup>2</sup> )	$\delta_{min}$ (%)			
0	$\tau_{ave} = 29.52$			1.17	0						
10	75.72 -16.93	1.82 1.37	.23	1.60	68.5						
50	75.58 -17.04	2.35 1.76	.30	2.06	132.1						
100	75.51 -17.13	2.77 2.05	.36	2.41	166.4						
150	75.43 -17.21	3.24 2.41	.42	2.83	186.0						
200	75.36 -17.28	3.89 2.83	.53	3.36	215.3						
250	75.31 -17.36	4.60 3.35	.63	3.98	230.0						
300	75.23 -17.44	5.84 4.21	.82	5.03	259.4						
310	75.20 -17.46	6.25 4.48	.84	5.37	269.1						
320	75.17 -17.48	6.79 4.84	.98	5.82	274.0						
330	75.13 -17.51	7.50 5.25	1.13	6.38	278.9						
340	75.10 -17.55	8.38 5.84	1.27	7.11	283.8						
350	75.05 -17.61	9.87 6.79	1.54	8.33	298.5						
360	74.97 -17.67	12.23 8.33	1.95	10.28	308.3						
370	74.82 -17.76	16.79 10.99	2.90	13.89	327.9						
375	74.68 -17.84	21.05 13.35	3.85	17.20	332.9						

(\*) all deformations relative to height after Ko-consolidation  
— — — — — after membrane correction

Table 4.D.5

$$\tau_{ave} = 29.53 \text{ KN/m}^2$$

$$\tau_c = 46.40 \text{ KN/m}^2$$

SHEAR STRESSES, DEFORMATIONS (*) AND PORE PRESSURES AT SELECTED CYCLES.						NGI 82 59000-6	TEST NUMBER <b>6</b>				
						PLASTIC DRAMMEN CLAY NORMALLY CONSOLIDATED $\bar{\sigma}_{vc} = 4 \text{ kg/cm}^2 = 392.4 \text{ KN/m}^2$					
N	$\tau_{max}$ (KN/m <sup>2</sup> )	$\delta_{max}$ (%)	$\delta_c$ (%)	$\delta_{ave}$ (%)	u (KN/m <sup>2</sup> )	N	$\tau_{max}$ (KN/m <sup>2</sup> )	$\delta_{max}$ (%)	$\delta_c$ (%)	$\delta_{ave}$ (%)	u (KN/m <sup>2</sup> )
	$\tau_{min}$ (KN/m <sup>2</sup> )	$\delta_{min}$ (%)					$\tau_{min}$ (KN/m <sup>2</sup> )	$\delta_{min}$ (%)			
0	$\tau_{ave} =$ 29.52			1.21	0						
10	75.72 -16.94	1.83 1.44	.20	1.64	72.1						
50	75.58 -17.05	2.37 1.83	.27	2.10	124.7						
100	75.50 -17.15	2.84 2.17	.34	2.51	163.8						
150	75.43 -17.22	3.30 2.52	.39	2.91	190.3						
200	75.37 -17.29	3.91 2.91	.50	3.41	217.8						
250	75.30 -17.37	4.84 3.52	.66	4.18	244.2						
300	75.17 -17.47	6.77 4.76	1.01	5.77	275.6						
310	75.13 -17.50	7.46 5.15	1.16	6.31	280.5						
320	75.10 -17.54	8.55 5.77	1.39	7.16	286.4						
330	75.04 -17.60	10.40 6.77	1.82	8.59	300.1						
340	74.92 -17.68	13.96 8.55	2.71	11.26	319.6						
345	74.80 -17.73	17.44 10.18	3.63	13.81	324.2						
350	74.57 -17.84	24.62 13.57	5.53	19.10	348.9						

(\*) all deformations relative to height after Ko-consolidation  
after membrane correction

Table 4.D.6

$$\tau_{ave} = 29.53 \text{ KN/m}^2$$

$$\tau_c = 46.40 \text{ KN/m}^2$$

SHEAR STRESSES, DEFORMATIONS (*) AND PORE PRESSURES AT SELECTED CYCLES.						NGI 82 59000-6		TEST NUMBER (7)			
						PLASTIC DRAMMEN CLAY NORMALLY CONSOLIDATED $\bar{\sigma}_{vc} = 4 \text{ kg/cm}^2 = 392.4 \text{ KN/m}^2$					
N	$\tau_{max}$ (KN/m <sup>2</sup> )	$\delta_{max}$ (%)	$\delta_c$ (%)	$\delta_{ave}$ (%)	u (KN/m <sup>2</sup> )	N	$\tau_{max}$ (KN/m <sup>2</sup> )	$\delta_{max}$ (%)	$\delta_c$ (%)	$\delta_{ave}$ (%)	u (KN/m <sup>2</sup> )
	$\tau_{min}$ (KN/m <sup>2</sup> )	$\delta_{min}$ (%)					$\tau_{min}$ (KN/m <sup>2</sup> )	$\delta_{min}$ (%)			
0	$\tau_{ave} = 59.04$			3.29	0						
50	92.53 25.14	4.11 3.84	.13	3.98	61.2						
100	92.47 25.06	4.37 4.11	.14	4.24	78.3						
200	92.38 24.97	4.84 4.52	.16	4.68	107.7						
300	92.30 24.88	5.34 5.02	.16	5.18	132.1						
400	92.24 24.81	5.93 5.52	.20	5.73	147.8						
500	92.18 24.74	6.64 6.23	.21	6.44	167.4						
600	92.11 24.67	7.75 7.28	.24	7.52	191.8						
650	92.05 24.61	8.69 8.16	.27	8.43	200.6						
700	91.98 24.53	10.04 9.46	.29	9.75	215.3						
750	91.91 24.46	12.34 11.66	.34	12.00	225.1						
800	91.78 24.33	16.27 15.51	.38	15.39	249.6						
810	91.74 24.30	17.50 16.62	.44	17.06	255.4						
820	91.68 24.24	19.44 18.39	.53	18.92	260.3						
825	91.61 24.18	21.32 20.03	.65	20.68	265.2						

(\*) all deformations relative to height after  $K_0$ -consolidation  
after membrane correction

Table 4.D.7

$$\tau_{ave} = 59.06 \text{ KN/m}^2$$

$$\tau_c = 33.75 \text{ KN/m}^2$$





NGI 82  
59000-6

TEST NUMBER

9

SHEAR STRESSES, DEFORMATIONS (\*) AND  
PORE PRESSURES AT SELECTED CYCLES.

PLASTIC DRAMMEN CLAY  
NORMALLY CONSOLIDATED

$\bar{\sigma}_{vc} = 4 \text{ kg/cm}^2 = 392.4 \text{ KN/m}^2$

N	$T_{max}$ (KN/m <sup>2</sup> )	$\delta_{max}$ (%)	$\delta_c$ (%)	$\delta_{ave}$ (%)	u (KN/m <sup>2</sup> )	N	$T_{max}$ (KN/m <sup>2</sup> )	$\delta_{max}$ (%)	$\delta_c$ (%)	$\delta_{ave}$ (%)	u (KN/m <sup>2</sup> )
	$T_{min}$ (KN/m <sup>2</sup> )	$\delta_{min}$ (%)					$T_{min}$ (KN/m <sup>2</sup> )	$\delta_{min}$ (%)			
0	$T_{ave} = 50.60$			2.33	0	325	75.28 24.69	6.28 5.96	.16	6.12	210.4
10	75.86 25.29	2.47 2.36	.06	2.42	24.5	349	75.27 24.69	6.33 5.99	.17	6.16	210.4
50	75.85 25.28	2.53 2.39	.07	2.46	29.4	350	92.12 7.83	6.65 5.81	.42	6.23	210.4
98	75.83 25.26	2.59 2.47	.06	2.53	39.2	360	92.06 7.79	7.53 6.53	.50	7.03	220.2
100	84.25 16.84	2.65 2.44	.11	2.55	44.0	370	91.99 7.71	8.86 7.68	.59	8.27	230.0
125	84.20 16.79	2.80 2.59	.11	2.70	61.2	380	91.92 7.63	11.18 9.64	.77	10.41	244.7
149	84.17 16.17	2.91 2.68	.12	2.80	73.4	390	91.78 7.51	15.37 13.25	1.06	14.31	269.1
150	92.57 8.34	3.03 2.65	.19	2.84	73.4	395	91.66 7.41	18.89 16.26	1.32	17.58	278.9
173	92.45 8.21	3.52 3.08	.22	3.30	107.7						
174	84.02 16.62	3.49 3.17	.16	3.33	112.6						
200	84.00 16.59	3.57 3.28	.15	3.43	122.3						
223	83.99 16.58	3.67 3.31	.18	3.49	122.3						
225	92.40 8.14	3.83 3.31	.26	3.57	127.2						
260	92.27 8.01	4.65 4.06	.30	4.36	161.5						
298	92.14 7.85	6.33 5.52	.41	5.93	200.6						
300	75.28 24.70	6.18 5.84	.17	6.01	205.5						

(\*) all deformations relative to height after  $K_0$ -consolidation  
after membrane correction

Table 4.D.9

SHEAR STRESSES, DEFORMATIONS (*) AND PORE PRESSURES AT SELECTED CYCLES.						NGI 82 59000-6		TEST NUMBER (10)			
						PLASTIC DRAMMEN CLAY NORMALLY CONSOLIDATED $\bar{\sigma}_{vc} = 4 \text{ kg/cm}^2 = 392.4 \text{ KN/m}^2$					
N	$\tau_{max}$ (KN/m <sup>2</sup> )	$\delta_{max}$ (%)	$\delta_c$ (%)	$\delta_{ave}$ (%)	u (KN/m <sup>2</sup> )	N	$\tau_{max}$ (KN/m <sup>2</sup> )	$\delta_{max}$ (%)	$\delta_c$ (%)	$\delta_{ave}$ (%)	u (KN/m <sup>2</sup> )
	$\tau_{min}$ (KN/m <sup>2</sup> )	$\delta_{min}$ (%)					$\tau_{min}$ (KN/m <sup>2</sup> )	$\delta_{min}$ (%)			
0	$\tau_{ave} =$ 50.60			2.34	0	260	75.34 24.76	5.35 5.09	.13	5.22	190.8
10	75.80 25.24	2.72 2.56	.08	2.64	18.4	307	75.33 24.75	5.47 5.17	.15	5.32	190.8
50	75.76 25.20	2.83 2.68	.08	2.76	34.2	308	83.76 16.32	5.55 5.13	.21	5.34	190.8
101	75.75 25.19	2.87 2.71	.08	2.79	41.5	330	83.75 16.31	5.69 5.21	.24	5.45	190.8
102	84.17 16.76	2.90 2.72	.09	2.81	41.5	357	83.74 16.30	5.85 5.38	.24	5.62	194.8
125	84.11 16.71	3.13 2.86	.14	3.00	63.0	358	92.16 7.86	6.03 5.35	.34	5.69	194.8
152	84.07 16.69	3.24 2.94	.15	3.09	73.3	402	92.08 7.79	7.32 6.49	.42	6.91	200.6
153	92.49 8.26	3.32 2.94	.19	3.13	74.5	403	100.48 -0.64	7.77 6.38	.70	7.08	200.6
177	92.39 8.12	3.85 3.42	.22	3.64	117.3	407	100.42 -0.71	8.98 7.54	.72	8.26	230.0
178	100.79 -0.31	4.04 3.42	.31	3.73	129.1	408	91.99 7.70	9.05 7.84	.61	8.45	234.9
187	100.67 -0.45	5.05 4.22	.42	4.64	156.5	420	91.91 7.62	11.24 9.81	.72	10.53	254.5
188	92.23 7.96	5.05 4.42	.32	4.74	161.4	430	91.82 7.54	14.04 12.30	.87	13.67	269.3
197	92.21 7.93	5.33 4.71	.31	5.02	171.2	440	91.67 7.42	18.6 15.9	1.36	17.21	284.2
198	83.78 16.35	5.29 4.83	.23	5.06	176.1	450	91.35 7.14	28.23 24.45	1.89	26.34	298.6
207	83.77 16.34	5.33 4.90	.22	5.12	176.1	452	74.47 23.90	28.61 27.70	.46	28.16	298.6
208	75.34 24.77	5.32 4.98	.17	5.15	181.0	460	74.40 23.83	30.95 29.81	.57	30.38	308.4

(\*) all deformations relative to height after Ko-consolidation  
after membrane correction

Table 4.D.10

SHEAR STRESSES, DEFORMATIONS (*) AND PORE PRESSURES AT SELECTED CYCLES.						NGI 82 59000-6		TEST NUMBER 11			
						PLASTIC DRAMMEN CLAY NORMALLY CONSOLIDATED $\bar{\sigma}_{ve} = 4 \text{ kg/cm}^2 = 392.4 \text{ KN/m}^2$					
N	$\tau_{max}$ (KN/m <sup>2</sup> )	$\delta_{max}$ (%)	$\delta_c$ (%)	$\delta_{ave}$ (%)	u (KN/m <sup>2</sup> )	N	$\tau_{max}$ (KN/m <sup>2</sup> )	$\delta_{max}$ (%)	$\delta_c$ (%)	$\delta_{ave}$ (%)	u (KN/m <sup>2</sup> )
	$\tau_{min}$ (KN/m <sup>2</sup> )	$\delta_{min}$ (%)					$\tau_{min}$ (KN/m <sup>2</sup> )	$\delta_{min}$ (%)			
0	$\tau_{ave} = 42.17$			1.84	0						
10	75.81 8.40	2.16 1.95	.11	2.06	28.9						
50	75.76 8.36	2.34 2.10	.12	2.22	60.7						
100	75.71 8.31	2.51 2.25	.13	2.38	75.4						
250	75.63 8.24	2.78 2.48	.15	2.63	95.4						
500	75.57 8.16	3.10 2.78	.16	2.94	126.7						
750	75.51 8.11	3.40 3.01	.20	3.21	146.3						
1000	75.46 8.06	3.71 3.31	.20	3.51	163.9						
1500	75.39 7.96	4.34 3.87	.24	4.11	183.5						
2000	75.31 7.89	5.22 4.63	.30	4.93	213.8						

(\*) all deformations relative to height after  $K_0$ -consolidation  
after membrane correction

Table 4.D.11

$$\tau_{ave} = 42.19 \text{ KN/m}^2$$

$$\tau_c = 33.75 \text{ KN/m}^2$$

SHEAR STRESSES, DEFORMATIONS (*) AND PORE PRESSURES AT SELECTED CYCLES.						NGI 82 59000-6		TEST NUMBER (12)			
						PLASTIC DRAMMEN CLAY NORMALLY CONSOLIDATED $\bar{\sigma}_{vc} = 4 \text{ kg/cm}^2 = 392.4 \text{ KN/m}^2$					
N	$\tau_{max}$ (KN/m <sup>2</sup> )	$\delta_{max}$ (%)	$\delta_c$ (%)	$\delta_{ave}$ (%)	u (KN/m <sup>2</sup> )	N	$\tau_{max}$ (KN/m <sup>2</sup> )	$\delta_{max}$ (%)	$\delta_c$ (%)	$\delta_{ave}$ (%)	u (KN/m <sup>2</sup> )
	$\tau_{min}$ (KN/m <sup>2</sup> )	$\delta_{min}$ (%)					$\tau_{min}$ (KN/m <sup>2</sup> )	$\delta_{min}$ (%)			
0	$\tau_{ave} =$ 50.60			2.47	0						
10	84.19 16.78	2.97 2.78	.10	2.88	39.1						
50	84.05 16.67	3.46 3.16	.15	3.31	78.2						
100	83.97 16.56	3.88 3.58	.15	3.73	103.9						
200	83.87 16.46	4.46 4.11	.18	4.29	139.4						
300	83.80 16.37	5.18 4.76	.21	4.97	163.9						
400	83.73 16.30	6.06 5.53	.27	5.80	183.5						
500	83.64 16.21	7.43 6.78	.33	7.11	208.0						
600	83.51 16.07	10.41 9.57	.42	9.99	239.8						
650	83.37 15.93	14.73 13.62	.56	14.18	259.4						
670	83.27 15.84	17.75 16.52	.62	17.14	274.2						
690	83.12 15.69	22.37 20.88	.75	21.63	279.1						
700	82.99 15.57	26.22 24.62	.80	25.42	293.7						

(\*) all deformations relative to height after  $K_0$ -consolidation  
after membrane correction

Table 4.D.12

$$\tau_{ave} = 50.62 \text{ KN/m}^2$$

$$\tau_c = 33.75 \text{ KN/m}^2$$

## 4.E COMPARISON OF TESTS (2) AND (12)

It has been decided to discard test (12) for two reasons :

Specimens (2) and (12) were obtained from two different cakes.

Specimen (2) appeared very homogeneous whereas specimen (12) showed a significant heterogeneity in the form of a large circular trace (5 mm in diameter) of black organic (?) matter. Traces of shells were also clearly apparent in this specimen and in the adjacent clay during preparation.

Specimen (12) was located only 5 cm above the bottom of tube 39.1 (see Figure 4.B.1).

The behavior of test (12) does not appear to be consistent with the neighboring tests while test (2) is. This can be shown by considering Figures 4.E.1 and 4.E.2 where the tests (2), (12), (7) and (11), i.e. all the test corresponding to

$\frac{\tau_c}{\tau_{\text{strength}}} = 40 \%$ , are presented in the form of the curves of  $\gamma_c$  and  $\gamma_{\text{ave}}$  versus time. Tests (1), (2), (12), and (8) corresponding to  $\frac{\tau_{\text{ave}}}{\tau_{\text{strength}}} = 60 \%$  can also be considered. Figure 4.E.3 shows some discrepancy in the evolution of  $\gamma_c$  in test (12). Figure 4.E.4 shows the corresponding graph of  $\gamma_{\text{ave}}$  for information, but does not permit drawing of any conclusions.

Figure 4.E.1

$\gamma_c$  vs. time for tests (2), (7), (11) and (12)

$N$   
number of cycles

$$\frac{\tau_c}{\tau_{st}} = 40\%$$

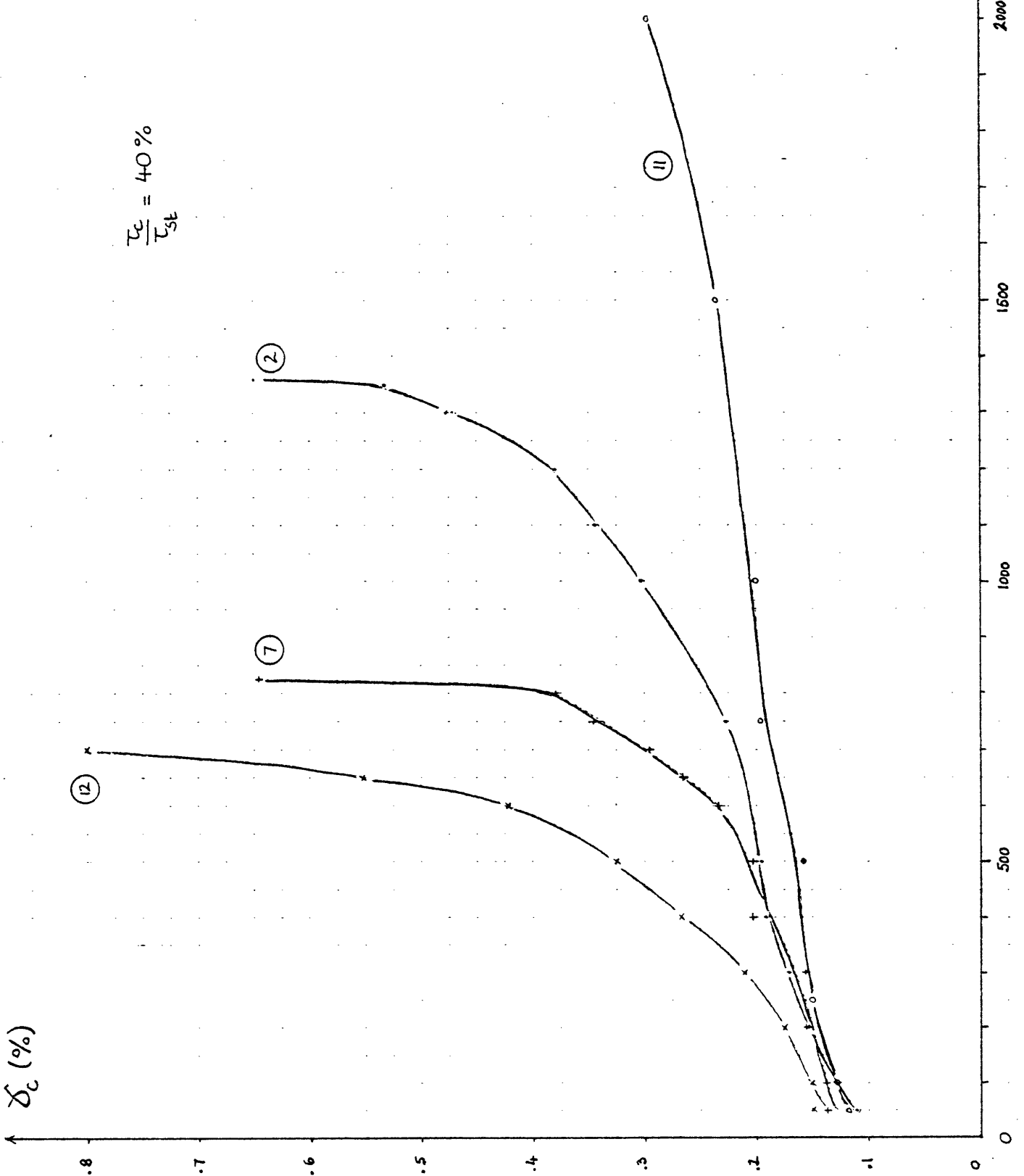


Figure 4.E.2

$\gamma_{ave}$  vs. time for tests (2), (7), (11) and (12).

$$\frac{L_c}{L_{3E}} = 40\%$$

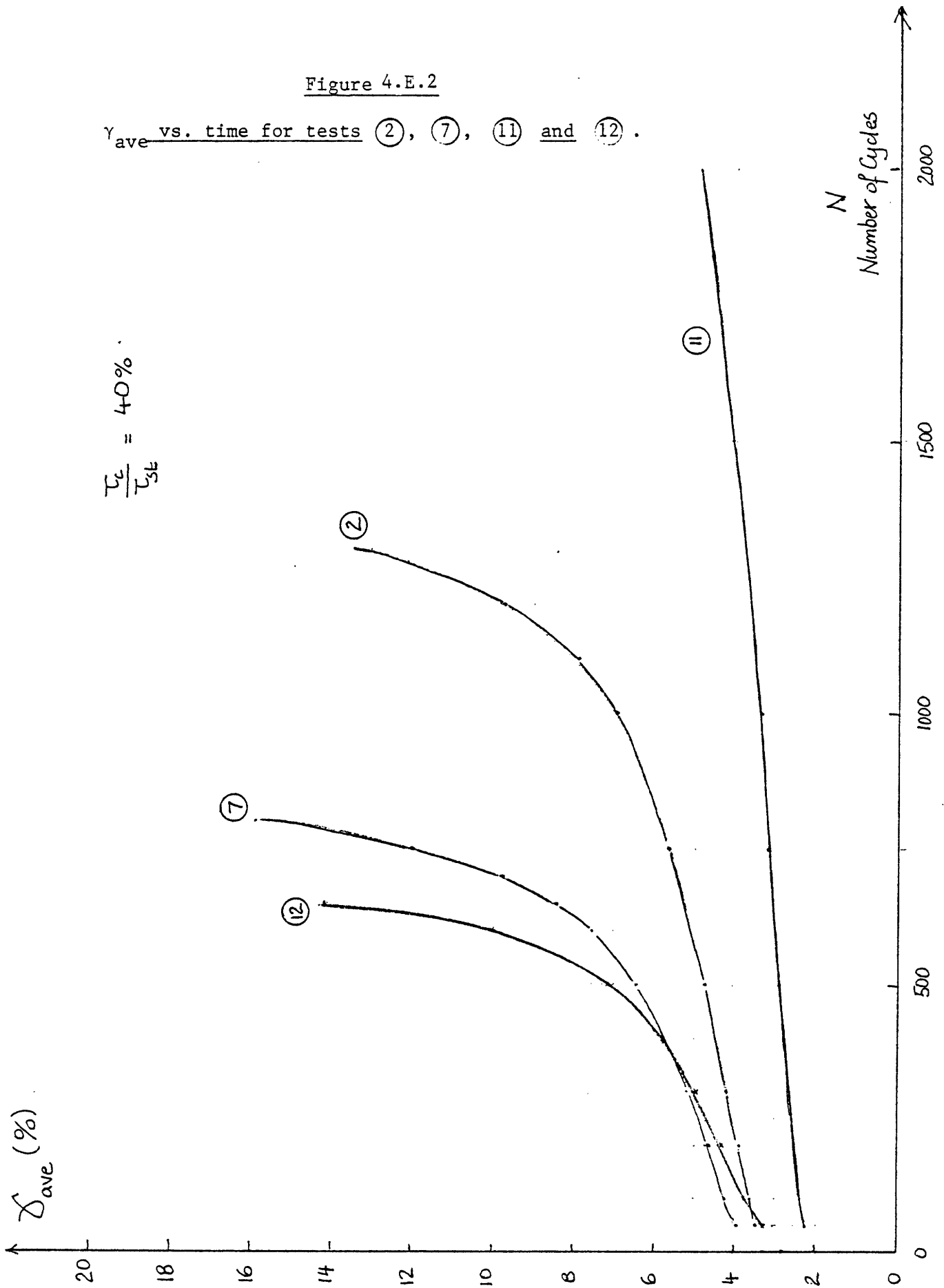




Figure 4.E.3

$\gamma_c$  vs. time for tests (1), (2), (8) and (12)

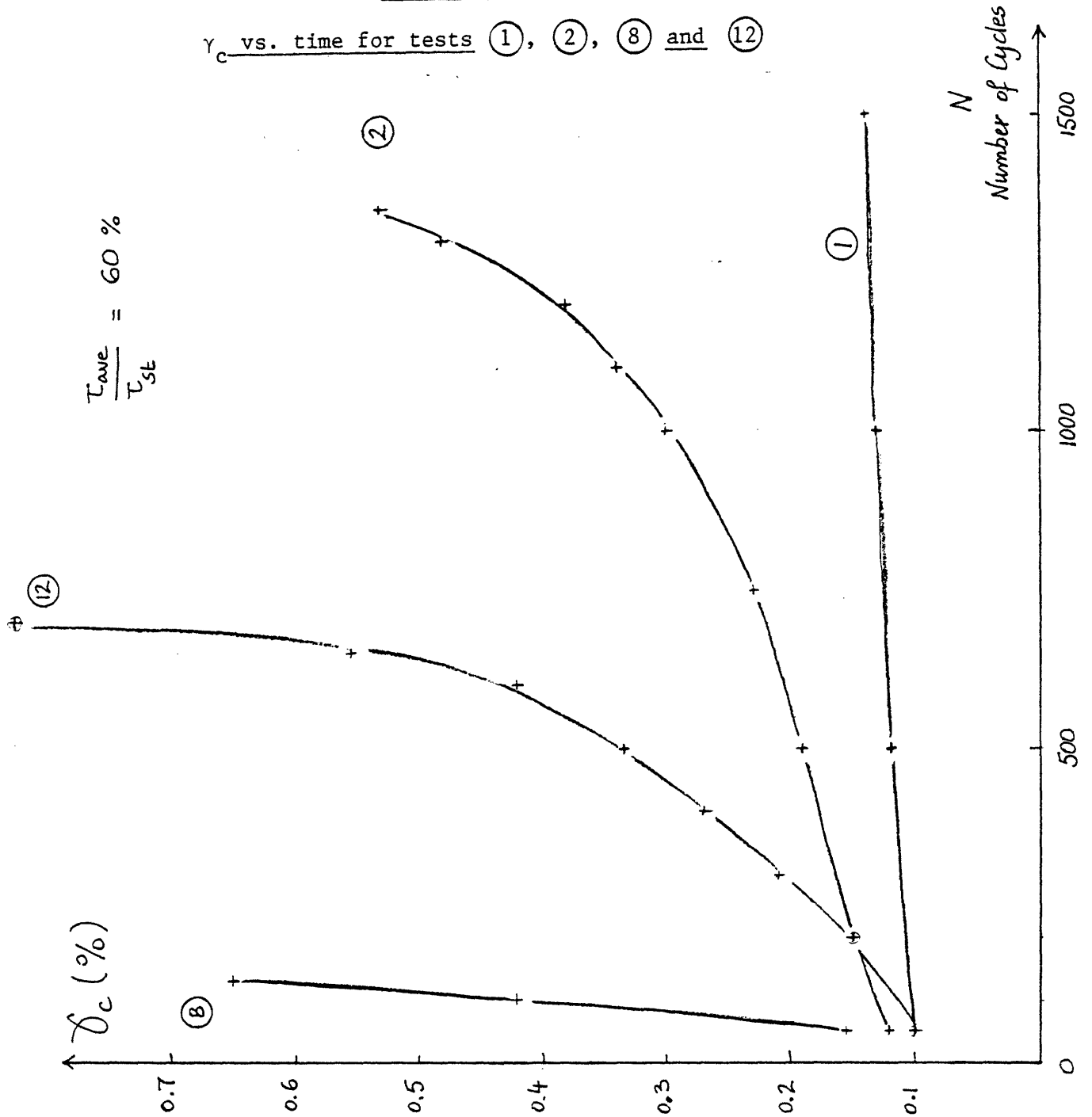
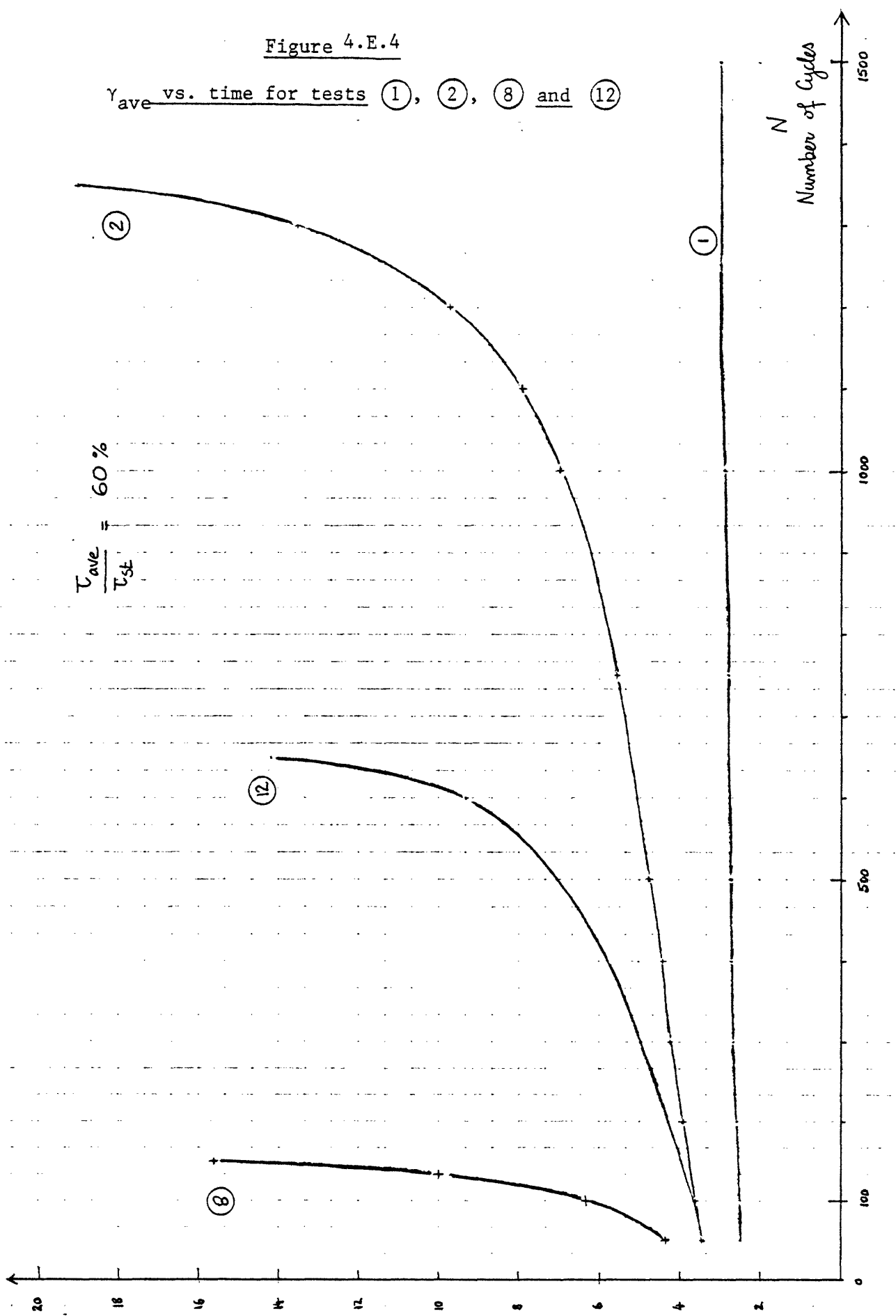


Figure 4.E.4

$\gamma_{ave}$  vs. time for tests (1), (2), (8) and (12)



## APPENDIX 5

LISTINGS OF COMPUTER PROGRAMS AND DATA FILE

## 5.A SUBROUTINE CYCDEG

```

C *****
C SUBROUTINE CYCDEG(TAV,TCY,GAVO,DN,GAV,GCY,IWRITE)
C *****
C VERSION NOV 9, 1982
C *****
C GIVEN A PAIR TAU-AVE (TAV), TAU-CYC (TCY), THIS SUBROUTINE WILL:
C 1. FIND THE NUMBER OF CYCLES (NO) AT WHICH THE AVERAGE
C DEFORMATION (GAVO) WILL BE OBTAINED,
C 2. ADD THE INCREMENT OF CYCLES (DN) TO GET THE NEW NUMBER OF CYCLES
C NU (NO+DN) AND FIND THE CORRESPONDING DEFORMATIONS, AVERAGE
C (GAV) AND CYCLIC (GCY).
C *****

REAL NUM(7),NINT(5),NO,NU,NUMB
COMMON TOACC(7),TOCREP(5),TIC(8),TIV(6),TOAV(7,5,6)
COMMON GIV(5),GIC(4),NUM,TOCY(7,4,6)
DIMENSION T(4),TAVINT(5,7),TCYNT(4,7),GCYN(7)

IF(IWRITE.EQ.1) WRITE(6,800) TAV,TCY,GAVO,GCY,DN
800 FORMAT(/5X,'TAV=',F6.2,2X,'TCY=',F6.2,2X,'GAVO=',F6.3,'(%)',2X,
1 'GCYO=',F6.3,'(%)',2X,'DN=',F5.0,'(CYCLES)')

DO 50 I=1,5
NINT(I)=-1.
DO 50 J=1,7
50 TAVINT(I,J)=-1.

ITACHI=7

IF(TCY.LT.TOACC(7)) GO TO 102

C*****
C LOCATE TCY VIS A VIS TOACC(I)
C TOACC(ITACHI)>TCY>TOACC(ITACLO)
C*****

DO 100 I1=2,7
I=I1
IF(TCY.GE.TOACC(I)) GO TO 101
100 CONTINUE
101 ITACLO=I
ITACHI=I-1

C*****
C LOCATE TCY VIS A VIS TIC(I)
C TIC(ITACHI)>TCY>TIC(ITICLO)
C*****

102 DO 103 I1=2,8
I=I1
IF(TCY.GE.TIC(I)) GO TO 104
103 CONTINUE
104 ITICLO=I
ITACHI=I-1

```

Page 2

```

C
      ALO=(TCY-TIC(ITICHI))/(TIC(ITICLO)-TIC(ITICHI))
      AHI=(TIC(ITICLO)-TCY)/(TIC(ITICLO)-TIC(ITICHI))

C*****
C      LOCATE GAVO VIS A VIS GIV(I)
C      GIV(IGHI)>GAVO>GIV(IGLO)
C*****

      DO 700 II=1,4
      I=5-II
      IF(GAVO.GE.GIV(I)) GO TO 701
700  CONTINUE
C      *****
C      GAVO < 2.5 %
C      *****

      IGHI=1
      IGLO=1
      GO TO 702
C      *****
C      GAVO > 2.5 %
C      *****

701  IGHI=I+1
      IGLO=I
702  CONTINUE

C*****
C      OBTAIN X-SECTIONS OF 3D GAV SURFACES FOR TCY
C      TAVINT(K,N) & NINT(K)
C*****

      DO 200 K=1,5
      IF(ITICHI.EQ.1) GO TO 106
      IF(ITICHI.EQ.7) GO TO 110
C      *****
C      .2 < TCY < .7
C      *****

      IHI=ITICHI-1
      ILO=ITICLO-1
      DO 105 N1=1,7
      N=N1
      IF( TOAV(N,K,ILO).EQ.-1.OR.TCY.GT.TOACC(N) ) GO TO 114
      IF( TOAV(N,K,IHI).NE.-1. ) GO TO 80
      TAVINT(K,N)=TOAV(N,K,ILO)*(TOACC(N)-TCY)/(TOACC(N)-TIC(ITICLO))
      GO TO 105
80  TAVINT(K,N)=ALO*TOAV(N,K,ILO)+AHI*TOAV(N,K,IHI)
105  CONTINUE
      M=7
      GO TO 115
C      *****
C      .7 < TCY
C      *****

106  N=ITACLO
      DO 107 I=1,ITACHI
107  TAVINT(K,I)=(TCY-TOACC(I))/(TIC(2)-TOACC(I))*TOAV(I,K,1)

```

Page 3

```

      GO TO 114
C          *****
C          .2 >TCY
C          *****
110 DO 113 N1=1,7
      N=N1
      IF(TOAV(N,K,6).EQ.-1.) GO TO 114
113 TAVINT(K,N)=ALO*TOCREP(K)+AHI*TOAV(N,K,6)
      M=7
      GO TO 115

C*****
C      M IS THE LAST INDEX OF N FOR WHICH WE HAVE A VALUE OF TAVINT
C*****

114 M=N-1
115 IF(TAV.GT.TAVINT(K,1)) GO TO 195
      IF(TAV.LT.TAVINT(K,7)) GO TO 190
      IF(TAV.LT.TAVINT(K,M)) GO TO 120

C*****
C      INTERSECTION TAVINT & TAV EXISTS
C*****

      DO 117 I1=2,M
      I=I1
      IF(TAV.GE.TAVINT(K,I)) GO TO 118
117 CONTINUE
118 BLO=(TAV-TAVINT(K,I))/(TAVINT(K,I-1)-TAVINT(K,I))
      BHI=(TAVINT(K,I-1)-TAV)/(TAVINT(K,I-1)-TAVINT(K,I))
      NINT(K)=BLO*NUM(I-1)+BHI*NUM(I)
      GO TO 200

C*****
C      INTERPOLATE WITH TOACC NETWORK
C*****

120 CLO=(TCY-TOACC(ITACHI))/(TOACC(ITACLO)-TOACC(ITACHI))
      CHI=(TOACC(ITACLO)-TCY)/(TOACC(ITACLO)-TOACC(ITACHI))
      NUMB=CLO*NUM(ITACLO)+NUM(ITACHI)*CHI
      DLO=(TAVINT(K,M)-TAV)/TAVINT(K,M)
      DHI=TAV/TAVINT(K,M)
      NINT(K)=NUMB*DLO+NUM(M)*DHI
      GO TO 200

C          *****
C          NINT(K) > 5000
C          *****
190 NINT(K)=10000.
      IF(NINT(IGLO).EQ.10000.AND.IGLO.NE.IGHI) GO TO 9025
      GO TO 200

C          *****
C          TAV > TAVINT(K,1)
C          *****
195 NINT(K)=1.
C

```

Page 4

200 CONTINUE

```

C*****
C   THE NINT(K) ARE AVAILABLE, NOW WE WANT NO CORRESPONDING TO GAVO
C*****
C   GET GAV1: AVERAGE DEFORMATION AT 1ST CYCLE
C*****

```

```

      IF(TAV.GE.TAVINT(5,1)) GO TO 900
      DO 205 K=1,4
      K1=5-K
      IF(TAV.GE.TAVINT(K1,1)) GO TO 206

```

205 CONTINUE

```

C   *****
C   TAV<TAVINT(1,1)
C   *****
      GAV1=GIV(1)*TAV/TAVINT(1,1)
      IF(GAV1.GT.GAVO) GAV1=GAVO
      GO TO 207

```

```

C   *****
C   TAVINT(K1+1,1)>TAV>TAVINT(K1,1)
C   *****

```

```

206 T1=TAVINT(K1+1,1)-TAVINT(K1,1)
      GAV1=(TAV-TAVINT(K1,1))/T1*GIV(K1+1)
      GAV1=GAV1+(TAVINT(K1+1,1)-TAV)/T1*GIV(K1)
207 CONTINUE

```

```

C*****
C   GET GAV7: AVERAGE DEFORMATION AT 5000 CYCLES
C*****

```

```

      GAV7=15.
      IF(NINT(5).NE.10000.) GO TO 350
      DO 220 KK=1,4
      K=5-KK
      IF(TAV.GT.TAVINT(K,7)) GO TO 221

```

220 CONTINUE

```

C   *****
C   TAVINT(1,7)>TAV
C   *****
      GAV7=TAV/TAVINT(1,7)*GIV(1)
      GO TO 350

```

```

C   *****
C   TAVINT(K+1,7)>TAV>TAVINT(K,7)
C   *****

```

```

221 GAV7=(TAV-TAVINT(K,7))/(TAVINT(K+1,7)-TAVINT(K,7))*GIV(K+1)
      GAV7=GAV7+(TAVINT(K+1,7)-TAV)/(TAVINT(K+1,7)-TAVINT(K,7))*GIV(K)

```

```

C
      IF(GAVO.GT.GAV7) GO TO 219
350 IF(GAVO.GT.GAV7) GO TO 218

```

```

C
      IF(GAVO.LE.GAV1) GO TO 217

```

```

C   *****
C   GAVO>GAV1
C   *****

```

Page 5

```

IF(IGHI.EQ.1) GO TO 210
IF(NINT(IGHI).EQ.10000.) GO TO 211
IF(GAV1.GE.GIV(IGLO)) GO TO 216
C          *****
C          GIV(IGHI)>GAVO>GIV(IGLO)
C          *****
NO=(GAVO-GIV(IGLO))/(GIV(IGHI)-GIV(IGLO))*NINT(IGHI)
NO=NO+(GIV(IGHI)-GAVO)/(GIV(IGHI)-GIV(IGLO))*NINT(IGLO)
GO TO 230
C          *****
C          GIV(1)>GAVO>GAV1
C          *****
210 IF(NINT(1).EQ.10000.) GO TO 215
NO=(GAVO-GAV1)/(GIV(1)-GAV1)*NINT(1)+(GIV(1)-GAVO)/(GIV(1)-GAV1)
GO TO 230
C          *****
C          GAV7>GAVO>GAV1
C          *****
215 NO=(GAVO-GAV1)/(GAV7-GAV1)*5000.+(GAV7-GAVO)/(GAV7-GAV1)
GO TO 230
C          *****
C          GAV1>GIV(IGLO)
C          *****
216 NO=(GAVO-GAV1)/(GIV(IGHI)-GAV1)*NINT(IGHI)
NO=NO+(GIV(IGHI)-GAVO)/(GIV(IGHI)-GAV1)
GO TO 230
C          *****
C          GAV1>GAVO
C          *****
217 NO=1.
GO TO 230
211 NO=(GAVO-GIV(IGLO))/(GAV7-GIV(IGLO))*5000.
NO=NO+(GAV7-GAVO)/(GAV7-GIV(IGLO))*NINT(IGLO)
GO TO 230
218 NO=NINT(5)
GO TO 230
219 NO=10000.

230 NU=NO+DN

```

```

IF(NU.GE.5000.AND.NINT(5).EQ.10000.) GO TO 398
IF(NU.GT.NINT(5)) GO TO 404
C*****
C FIND NEW GAV CORRESPONDING TO NU CYCLES
C*****
DO 235 I=1,5
I1=I
IF(NINT(I1).GT.1.) GO TO 236
235 CONTINUE
236 IF(NU.LT.NINT(I1)) GO TO 397
DO 240 KK=1,5
K=6-KK
IF(NINT(K).EQ.10000.) GO TO 240

```



Page 6

```

      IF(NU.GE.NINT(K)) GO TO 241
240  CONTINUE
241  IF(NINT(K+1).EQ.10000.) GO TO 250
      IF(NINT(K).EQ.NINT(K+1)) GO TO 777
      GAV=(NU-NINT(K))/(NINT(K+1)-NINT(K))*GIV(K+1)
      GAV=GAV+(NINT(K+1)-NU)/(NINT(K+1)-NINT(K))*GIV(K)
      GO TO 399
250  GAV=(NU-NINT(K))/(5000.-NINT(K))*GAV7
      GAV=GAV+(5000.-NU)/(5000.-NINT(K))*GIV(K)
      GO TO 399
C
397  IF(NINT(I1).EQ.10000.) GO TO 252
      GAV=(NU-1.)/(NINT(I1)-1.)*GIV(I1)
      GO TO 399
252  GAV=(NU-1.)/4999.*GAV7+(5000.-NU)/4999.*GAV1
      GO TO 399
C
398  GAV=GAV0
      IF(GAV7.GT.GAV0) GAV=GAV7
      NU=10000.
      GO TO 399
777  GAV=GIV(K)
      GO TO 399
404  GAV=15.
      NU=NINT(5)

C*****
C   GET GCY
C*****

399  DO 400 II=1,5
      I=6-II
      IF(TAV.GE.TIV(I)) GO TO 401
400  CONTINUE

C           *****
C           TIV(IHI)>TAV>TIV(ILO)
C           *****
401  IHI=I+1
      ILO=I

C
      ALO=(TAV-TIV(IHI))/(TIV(ILO)-TIV(IHI))
      AHI=(TIV(ILO)-TAV)/(TIV(ILO)-TIV(IHI))

      IF(NU.GT.5000.) GO TO 411
C
      DO 402 II=1,6
      I=7-II
      IF(NU.GT.NUM(I)) GO TO 403
402  CONTINUE
C           *****
C           NUM(NHI)>NU>NUM(NLO)
C           *****
403  NHI=I+1
      NLO=I

```

Page 7

```

405 DO 410 N=NLO,NHI
      DO 410 L=1,4
        TCYNT(L,N)=ALO*TOCY(N,L,ILO)+AHI*TOCY(N,L,IHI)
410 CONTINUE
      GO TO 412
411 DO 413 L=1,4
413 TCYNT(L,7)=TOCY(7,L,ILO)*ALO+AHI*TOCY(7,L,IHI)

```

```

C*****
C   GET GCYN(N) IF IWRITE = 1
C*****

```

```

412 IF(IWRITE.EQ.0) GO TO 419
      DO 415 N=1,7
        IF(TCY.GE.TCYNT(4,N)) GO TO 416
        DO 417 L=1,3
          LL=4-L
          IF(TCY.GE.TCYNT(LL,N)) GO TO 418
417 CONTINUE
        GCYN(N)=GIC(1)*TCY/TCYNT(1,N)
        GO TO 415
418 T1=TCYNT(LL+1,N)-TCYNT(LL,N)
        GCYN(N)=GIC(LL)*(TCYNT(LL+1,N)-TCY)/T1
        GCYN(N)=GCYN(N)+GIC(LL+1)*(TCY-TCYNT(LL,N))/T1
        GO TO 415
416 GCYN(N)=3.
415 CONTINUE

419 IF(NU.GT.5000.) GO TO 422
      DO 420 L=1,4
        T(L)=(NU-NUM(NLO))
        T(L)=T(L)+(NUM(NHI)-NU)/(NUM(NHI)-NUM(NLO))*TCYNT(L,NLO)
420 CONTINUE
      GO TO 425
422 DO 423 I=1,4
423 T(I)=TCYNT(I,7)
C
425 IF(TCY.GT.T(4)) GO TO 9100
      DO 430 II=1,3
        I=4-II
        IF(TCY.GE.T(I)) GO TO 431
430 CONTINUE
        GCY=TCY/T(1)*GIC(1)
        GO TO 999
431 GCY=(TCY-T(I))/(T(I+1)-T(I))*GIC(I+1)
        GCY=GCY+(T(I+1)-TCY)/(T(I+1)-T(I))*GIC(I)
        GO TO 999
9025 NO=10000.
      NU=10000.
9020 GAV=GAVO
      GO TO 999
9100 GCY=3.

999 IF(IWRITE.EQ.0) RETURN

```

Page 8

```
      WRITE(6,801) (NINT(I),I=1,5)
801  FORMAT(/5X,'#CYCLES:  1',6X,5(F5.0,3X),'5000')
      WRITE(6,806) GAV1,(GIV(I),I=1,5),GAV7
806  FORMAT(7X,'GAV  : ',F6.3,6(2X,F6.3)/)
      WRITE(6,804)
804  FORMAT(5X,'#CYCLES:  1',7X,'50',6X,'100',5X,'200',5X,'500',
1     5X,'1000',4X,'5000')
      WRITE(6,805) (GCYN(I),I=1,7)
805  FORMAT(7X,'GCY  : ',F5.3,6(3X,F5.3)/)
      WRITE(6,802) NO,NU,GAV,GCY
802  FORMAT(5X,'NO=',F6.0,'(CYCLES)  NU=',F6.0,'(CYCLES)  GAV=',
1     F6.3,'(%)  GCY=',F6.3,'(%)')
      RETURN

900  GAV=15.
      GCY=3.
      IF(IWRITE.EQ.1) WRITE(6,807)
807  FORMAT(/5X,'TAV>TAVINT(5,1),  GAV=15 %  GCY=3%')
      RETURN
      END
```

5.B PROGRAM TLPILE

```

C *****
C * *
C *** PROGRAM TLPIL3 *****
C * *
C *****
C
C (UPDATED VERSION OF TLPIL)
C
C VERSION NOVEMBER 30, 1982 © ALAIN M. GOULOIS COPYRIGHT
C *****
C
C UNITS USED IN THE CODE ARE METERS & KILONEWTONS, BUT INPUTS
C AND OUTPUTS UNITS CAN BE DIFFERENT.
C
C *****
C
C DOUBLE PRECISION STFPIL(11),U1(11,6),UR(11,6)
C DOUBLE PRECISION R(31),RCONS(31),T(31,4),T1(31,4),FORCE(31)
C DOUBLE PRECISION S(31,4),FTRONG(10),FTRON1(10),STRONG,ROO
C DOUBLE PRECISION SK(11,6),C,SKM,CORCON(10),FLM,FELAS
C DOUBLE PRECISION DELAS,DF(11,6),FL(11,6),FG(11,6),FRATIO
C DOUBLE PRECISION CIGN,X,BMIN,AA,BB,FG1(11,6),SK1(11,6)
C DOUBLE PRECISION FTRON2(10)
C
C DIMENSION THICK(10),XAREA(5),WF(10),WP(10),TITLE(40)
C DIMENSION HGTLAY(10),SHTHRO(10),DENSOL(10),GSIG(10),RMRO(10)
C DIMENSION NPTOGA(10),SIG(10),TOSIG(6),GA1(6),STFSOL(10)
C DIMENSION FDSS(11,6),DDSS(11,6),W(11)
C DIMENSION SOFT(10),TMAX(10),ALPHA(10),BETA(10)
C DIMENSION GA(10,2),TO(10,2),GACONS(10)
C DIMENSION GAVGE(11,2),GACYC(11,2),TOVGE(11,2)
C DIMENSION SOFCON(10),DMAX(10),Q(6),GAVEC(10)
C DIMENSION TOCYC(11,2),IPL(11,6),FOPILE(10)
C DIMENSION FOSOL(10),FODSS(10),UELAS(11,6),TIMEFC(10),TOCONS(10)
C DIMENSION GOR(11)
C DIMENSION GOR1(11),DOR(11),GG(10),PDEF(5,10)
C DIMENSION ARRAY1(2,150),ARRAY2(15,10),ARRAY3(15,10)
C DIMENSION ARRAY4(3,50)
C DIMENSION XSCL1(4),XSCL2(4),XSCL3(4),XSCL4(4)
C
C REAL NUM(7),NCYC,LENGTH,NC,LCYC
C
C COMMON TOACC(7),TOCREP(5),TIC(8),TIV(6)
C COMMON GIV(5),GIC(4),NUM,TOCY(7,4,6)
C
C CHARACTER*40 XLAB1,XLAB2,XLAB3,YLAB1,YLAB2,YLAB3,XLAB4
C *****
C
C PI=3.14159
C WPILE=0.
C WFILL=0.
C PLIMIT=0.

```

```

C
C*****
C TITLE
C*****
C
      READ(5,8610)(TITLE(I),I=1,40)
8610 FORMAT(20A4)
      WRITE(6,8615)(TITLE(I),I=1,40)
8615 FORMAT(1X,20A4/1X,20A4/1X,80(1H*)///)
C
C*****
C LABELS OF PLOTS
C*****
C
      READ(5,8802)XLAB1
      READ(5,8802)YLAB1
      READ(5,8802)XLAB2
      READ(5,8802)YLAB2
      READ(5,8802)XLAB3
      READ(5,8802)YLAB3
      READ(5,8802)XLAB4
8802 FORMAT(A40)
      READ(5,8898) (XSCL1(I),I=1,4)
      READ(5,8898) (XSCL2(I),I=1,4)
      READ(5,8898) (XSCL3(I),I=1,4)
      READ(5,8898) (XSCL4(I),I=1,4)
8898 FORMAT(4F10.2)
C
C*****
C SOIL PILE DESCRIPTION STARTS *****
C*****
C
      READ(5,4010) DIAM,DNSITY,DTYFIL,FRELTH,E,ITEST,IWRITE
      READ(5,5000) LIMIN,LIMIIN
5000 FORMAT(I5,I5)
      LENGTH=FRELTH
      RO=DIAM/200.
C
      IF(ITEST.EQ.1) IWRITE=1
C
      READ(5,4050) NLAYER,NLOAD1,NLOAD2,ACC,LCYC,ALPFAC
      IF(NLOAD1.GT.10.OR.NLOAD2.GT.10) GO TO 775
      NSEG=NLAYER
      NNODES=NSEG+1
      NPOINT=NNODES+NLAYER*2
C
C*****
C LOADING
C*****
C
      READ(5,8620)(PDEF(1,I),I=1,NLOAD1)
8620 FORMAT(F10.4)
      WRITE(6,8630)
      WRITE(6,8635)(PDEF(1,I),I=1,NLOAD1)
8635 FORMAT(5X,F10.4)

```

```

8630 FORMAT(2X,'STATIC LOADING IN MN'/)
      IF(NLOAD2.EQ.0) GO TO 7
      DO 5 I=1,NLOAD2
      READ(5,8625)(PDEF(J,I),J=2,5)
      5 CONTINUE
8625 FORMAT(2F10.4,F10.0,F5.0)
C
      WRITE(6,8640)
8640 FORMAT(//2X,'CYCLIC LOADING IN MN,MN & CYCLES'/)
      DO 6 I=1,NLOAD2
      WRITE(6,8645) PDEF(2,I),PDEF(3,I),PDEF(4,I)
      6 CONTINUE
8645 FORMAT(5X,2(F10.4,5X),F10.0)
C
C*****
C BASIC DSS ELEMENTS
C*****
C
      7 SI=0.
C
      DO 20 I=1,NLAYER
      READ(5,4080)HGTLAY(I),SHTHRO(I),DENSOL(I),GSIG(I),RMRO(I),NPTOGA(I)
      1)
      READ(5,4081)TIMEFC(I),SOFT(I),ALPHA(I),BETA(I),SOFCON(I)
      READ(5,4082)THICK(I)
      LENGTH=LENGTH+HGTLAY(I)
      SI=SI+HGTLAY(I)*(DENSOL(I)-1.)*9.81/2.
      SIG(I)=SI
      SI=SI+HGTLAY(I)*(DENSOL(I)-1.)*9.81/2.
      BUF=SIG(I)*HGTLAY(I)*DIAM*PI/100.
      N=NPTOGA(I)
C
      DO 10 J=1,N
      READ(5,4030) TOSIG(J),GA1(J)
      FDSS(I+1,J)=TOSIG(J)*BUF*LCYC*ALPFAC
      DDSS(I+1,J)=GA1(J)*.01*RO*ALOG(SHTHRO(I)+1.)
      10 CONTINUE
C
      STFSOL(I)=2.*PI*HGTLAY(I)*GSIG(I)*SIG(I)/ALOG(RMRO(I)/(SHTHRO(I)+1.))
      TMAX(I)=TOSIG(N)*SIG(I)*LCYC*ALPFAC
      DMAX(I)=DDSS(I+1,N)+FDSS(I+1,N)/STFSOL(I)
C
      R1=RO-THICK(I)/100.
      XAREA(I)=PI*(RO*RO-R1*R1)
      WF(I)=(DTYFIL-1.)*PI*R1*R1*HGTLAY(I)*9.81
      WP(I)=DNSITY*XAREA(I)*HGTLAY(I)*9.81
      WFILL=WFILL+WF(I)
      WPILE=WPILE+WP(I)
C
      20 CONTINUE
C
C*****
C DECOMPOSITION IN Prandtl BODIES
C*****

```

```

C
  DO 60 I=1,NLAYER
  N=NPTOGA(I)
  IF(N.EQ.1) GO TO 50
  Q(1)=FDSS(I+1,1)/DDSS(I+1,1)
C
  DO 30 J=2,N
  Q(J)=(FDSS(I+1,J)-FDSS(I+1,J-1))/(DDSS(I+1,J)-DDSS(I+1,J-1))
30 SK(I+1,J-1)=Q(J-1)-Q(J)
C
  SK(I+1,N)=Q(N)
C
  DO 40 J=1,N
40 FL(I+1,J)=DDSS(I+1,J)*SK(I+1,J)
C
  GO TO 60
C
50 SK(I+1,1)=FDSS(I+1,1)
  FL(I+1,1)=FDSS(I+1,1)
C
60 CONTINUE
C
  NSPR=0
  DO 70 I=1,NLAYER
  N=NPTOGA(I)
  NSPR=NSPR+N
70 PLIMIT=PLIMIT+FDSS(I+1,N)
C
C*****
C STIFFNESSES OF PILE SEGMENTS
C*****
C
  DO 80 I=2,NSEG
  A1=E*XAREA(I-1)/(HGTLAY(I-1)/2.)
  A2=E*XAREA(I)/(HGTLAY(I)/2.)
  STFPIL(I)=A1*A2/(A1+A2)
80 CONTINUE
C
  A1=1.
  XA=0.
  IF(FRELTH.EQ.0.) GO TO 90
  READ(5,4083) XA
  EA=RO-XA/100.
  XA=PI*(RO*RO-EA*EA)
  A1=E*XA/FRELTH
90 A2=E*XAREA(1)/(HGTLAY(1)/2.)
  STFPIL(1)=A1*A2/(A1+A2)
  IF(FRELTH.EQ.0.) STFPIL(1)=A2
C
C*****
C WEIGHT DISTRIBUTION
C*****
C
  WPILE=WPILE+XA*DNSITY*FRELTH*9.81
  WPH20=WPILE*(DNSITY-1.)/DNSITY

```



```

      WTH20=WFILL+WPH20
C
      W(1)=-FRELTH*WPH20/LENGTH
C
      DO 100 I=2,NNODES
100  W(I)=-HGTLAY(I-1)*(WTH20+W(1))/(LENGTH-FRELTH)
C
      PTENS=PLIMIT+WTH20
      PCOMP=-PLIMIT+WTH20
C
C*****
C WRITE PILE SOIL CHARACTERISTICS
C*****
C
      EA=E/1000.
      WRITE(6,8000)LENGTH,FRELTH,DIAM,DNSITY,DTYFIL,EA
      WRITE(6,8300)XA,LCYC,ALPFAC
      WRITE(6,8001)NLAYER,NNODES,NPOINT,NLOAD1,NLOAD2,ITEST,IWRITE
      DO 115 I=1,NLAYER
      WRITE(6,8500)I
      RATIO=DMAX(I)/(2.*RO)*100.
      EA=DMAX(I)*100.
      WRITE(6,8004)I,HGTLAY(I),I,SHTHRO(I),I,TMAX(I),I,EA,RATIO
      WRITE(6,8005)I,DENSOL(I),I,GSIG(I),I,RMRO(I),I,NPTOGA(I)
      WRITE(6,8006)I,TIMEFC(I),I,SOFT(I),I,ALPHA(I),I,BETA(I)
      WRITE(6,8007)I,SIG(I),I,SOFCON(I),I,STFSOL(I),I,W(I)
      WRITE(6,8010)I,THICK(I),I,XAREA(I)
      N=NPTOGA(I)
      J=I+1
      DO 110 K=1,N
      EA=DDSS(J,K)*100.
      WRITE(6,8008)J,K,FDSS(J,K),J,K,EA,J,K,FL(J,K),J,K,SK(J,K)
110  CONTINUE
      EA=STFPIL(I)/1000.
      WRITE(6,8009)I,EA
115  CONTINUE
      WRITE(6,8040)NNODES,W(NNODES)
      A1=PLIMIT/1000.
      A2=WTH20/1000.
      A3=WPH20/1000.
      A4=WPILE/1000.
      A5=WFILL/1000.
      WRITE(6,8011)A1,A2,A3,A4,A5
      A1=PTENS/1000.
      A2=PCOMP/1000.
      WRITE(6,8012)A1,A2
      IF(ITEST.EQ.1)STOP
C
      DO 120 I=2,NNODES
      N=NPTOGA(I-1)
      DO 120 K=1,N
      SK(I,K)=SK(I,K)/SOFCON(I-1)
120  CONTINUE
      WRITE(6,8505)
C

```

```

C*****
C SOIL DEGRADATION DATA
C*****
C
  READ(5,810)(TIC(I),I=1,8)
  READ(5,820)(TIV(I),I=1,6)
  READ(5,830)(GIV(I),I=1,5)
  READ(5,840)(GIC(I),I=1,4)
  READ(5,850)(NUM(I),I=1,7)
  READ(5,825)(TOACC(I),I=1,7)
  READ(5,830)(TOCREP(I),I=1,5)
C
  DO 130 I=1,7
  DO 130 J=1,5
  READ(5,870)(TOAV(I,J,K),K=1,6)
130 CONTINUE
C
  DO 140 I=1,7
  DO 140 J=1,4
  READ(5,871)(TOCY(I,J,K),K=1,6)
140 CONTINUE
C
C*****
C INITIALIZATIONS
C*****
C
  ARRAY1(1,1)=0.
  ARRAY1(2,1)=0.
  ARRAY3(15,1)=-HGTLAY(1)/2.
  ARRAY2(15,1)=(FRELTH-HGTLAY(1)/2.)/2.
  DO 145 I=2,NLAYER
  ARRAY3(15,I)=ARRAY3(15,I-1)-(HGTLAY(I-1)+HGTLAY(I))/2.
  ARRAY2(15,I)=(ARRAY3(15,I-1)+ARRAY3(15,I))/2.
145 CONTINUE
  LLL=0
  ROO=0.
  STRONG=1000.*STFPIL(2)
  DO 150 I=1,NPOINT
150 RCONS(I)=0.
  DO 170 I=1,NLAYER
  N=NPTOGA(I)
  DO 160 K=1,N
160 FG(I+1,K)=0.
  GOR(I+1)=0.
  GOR1(I+1)=0.
  FTRON2(I)=0.
  FTRONG(I)=0.
  GACONS(I)=0.
  TOCONS(I)=0.

170 CONTINUE
  ILOAD=1
  JP=1
  IN=0
  IIN=0

```

```

    PLAST=0.
    POLD=0.
    ICONS=0
    TNCYC=1.
    TN=0.
    KLM=1
    MN=1
C
    PNEW=PDEF(1,1)
    WRITE(6,8032) PNEW
    PNEW=PNEW*1000.
    GO TO 190
C
C*****
C PILE *****
C*****
C
C*****
C TEST FOR RETURN TO ELASTIC RANGE
C*****
C
    180 IF(PNEW.GT.PLAST.AND.POLD.GT.PLAST) GO TO 220
        IF(PNEW.LT.PLAST.AND.POLD.LT.PLAST) GO TO 220

        GO TO 260
C
C*****
C DIRECT STIFFNESS METHOD
C*****
C
    190 STFPIL(NNODES)=0.
        T1(1,1)=STFPIL(1)
        T1(1,2)=-STFPIL(1)
C
        DO 210 I=2,NNODES
            I1=3*(I-2)+2
            I2=I1+1
            I3=I1+2
            T1(I1,1)=STFPIL(I-1)
            T1(I1,4)=-STFPIL(I)
            T1(I2,1)=STFSOL(I-1)
            T1(I3,1)=STRONG+STFSOL(I-1)
            T1(I2,2)=-STFSOL(I-1)
            T1(I1,2)=0.
            N=NPTOGA(I-1)
C
        DO 200 K=1,N
            T1(I1,1)=T1(I1,1)+SK(I,K)
            T1(I2,1)=T1(I2,1)+SK(I,K)
    200 T1(I1,2)=T1(I1,2)-SK(I,K)
C
    210 CONTINUE
C
C*****
C BACK TO ELASTIC ZONE

```

```

C*****
C
  220 JJ=0
      DO 230 I=2,NNODES
      DO 230 K=1,6
  230 IPL(I,K)=0
      DO 240 I=1,NPOINT
      DO 240 J=1,4
  240 T(I,J)=T1(I,J)
C
      DO 250 I=2,NNODES
      I1=3*(I-2)+2
      I2=I1+1
      I3=I1+2
      FORCE(I1)=W(I)
      FORCE(I2)=0.
      FORCE(I3)=FTRONG(I-1)

C
C*****
C RESIDUAL FORCES
C*****
C
      DO 250 K=1,N
      FORCE(I1)=FORCE(I1)+UR(I,K)*SK(I,K)
      FORCE(I2)=FORCE(I2)-UR(I,K)*SK(I,K)

C
  250 CONTINUE
C
C*****
C SOLVE FOR DISPLACEMENTS BY Gauss ELIMINATION (WILSON SUBROUTINE)
C*****
C
  260 FORCE(1)=PNEW+W(1)
C
  270 IF(IWRITE.EQ.0.OR.IWRITE.EQ.1) GO TO 281
      WRITE(6,8800) FORCE(1)
  8800 FORMAT(10X,'FORCE( 1)=' ,F12.2,'(KN)')
      DO 280 I=2,NNODES
      I1=3*(I-2)+2
      I2=I1+1
      I3=I1+2
      WRITE(6,8801) I1,FORCE(I1),I2,FORCE(I2),I3,FORCE(I3)
  280 CONTINUE
  8801 FORMAT(2(10X,'FORCE(' ,I2,')=' ,F12.2,'(KN)'),
  1 10X,'FORCE(' ,I2,')=' ,E10.3,'(KN)')
C
  281 DO 282 I=1,NPOINT
  282 R(I)=FORCE(I)
C
      DO 285 I=1,NPOINT
      DO 285 J=1,4
  285 S(I,J)=T(I,J)
C
C

```

C\*\*\*\*\*

C FORWARD REDUCTION

C\*\*\*\*\*

C

```

      DO 310 N=1,NPOINT
      DO 300 L=2,4
      IF(S(N,L).EQ.0.) GO TO 300
      I=N+L-1
      C=S(N,L)/S(N,1)
      J=0
      DO 290 K=L,4
      J=J+1
290  S(I,J)=S(I,J)
      S(N,L)=C
300  CONTINUE
310  CONTINUE
      DO 340 N=1,NPOINT
      DO 330 L=2,4
      IF(S(N,L).EQ.0.) GO TO 330
      I=N+L-1
      R(I)=R(I)-S(N,L)*R(N)
330  CONTINUE
340  R(N)=R(N)/S(N,1)

```

C

C\*\*\*\*\*

C BACK-SUBSTITUTION

C\*\*\*\*\*

C

```

      DO 360 M=2,NPOINT
      N=NPOINT+1-M
      DO 350 L=2,4
      IF(S(N,L).EQ.0.) GO TO 350
      K=N+L-1
      R(N)=R(N)-S(N,L)*R(K)
350  CONTINUE
360  CONTINUE

```

C

C\*\*\*\*\*

C DETECT NEXT Prandtl SPRING TO YIELD

C\*\*\*\*\*

C

```

      X=0.
      KMIN=0
      IMIN=0
      BMIN=1.

```

C

```

      DO 380 I=2,NNODES
      I1=3*(I-2)+2
      I2=I1+1
      I3=I1+2
      N=NPTOGA(I-1)
      DO 370 K=1,N
      CIGN=1.
      IF(IPL(I,K).EQ.1.OR.IPL(I,K).EQ.-1) GO TO 370
      DELAS=R(I1)-R(I2)-UR(I,K)

```

```

FELAS=DELAS*SK(I,K)
DF(I,K)=FELAS-FG(I,K)
IF(DF(I,K).LT.0.)CIGN=-CORCON(I-1)
IF(DF(I,K).EQ.0.) GO TO 370
FRATIO=(FL(I,K)*CIGN-FG(I,K))/DF(I,K)
IF(FRATIO.GE.BMIN) GO TO 370
BMIN=FRATIO
IMIN=I
KMIN=K

C
C*****
C POSSIBILITY OF STRAIN-SOFTENING
C*****
C
      X=-FL(I,K)*CIGN*SOFT(I-1)
370 CONTINUE
380 CONTINUE

C
C*****
C CORRECT FOR STIFFNESS AND FORCE OF YIELDING SPRING
C*****
C
      I=IMIN-1
      IF(IWRITE.EQ.1) WRITE(6,8033) KMIN,I
      IF(IMIN.EQ.0) GO TO 383
      JJ=JJ+1
      IF(JJ.EQ.NSPR) GO TO 760
      I1=3*(IMIN-2)+2
      I2=I1+1
      FORCE(I1)=FORCE(I1)+X-UR(IMIN,KMIN)*SK(IMIN,KMIN)
      FORCE(I2)=FORCE(I2)-X+UR(IMIN,KMIN)*SK(IMIN,KMIN)
      T(I1,1)=T(I1,1)-SK(IMIN,KMIN)
      T(I2,1)=T(I2,1)-SK(IMIN,KMIN)
      T(I1,2)=T(I1,2)+SK(IMIN,KMIN)
      IPL(IMIN,KMIN)=1
      IF(CIGN.NE.1.) IPL(IMIN,KMIN)=-1
      FG(IMIN,KMIN)=-X
383 A1=0.
      DO 385 I=2,NNODES
      N=NPTOGA(I-1)
      DO 385 K=1,N
      IF(IPL(I,K).EQ.1.OR.IPL(I,K).EQ.-1) GO TO 384
      FG(I,K)=FG(I,K)+DF(I,K)*BMIN
384 A1=A1+FG(I,K)
385 CONTINUE
      IF(IMIN.EQ.0) GO TO 389
      ROO=ROO+(R(1)-ROO)*BMIN
      IF(ICONS.EQ.1.AND.ITEST.NE.3) GO TO 270
      IF(ICONS.EQ.1.AND.ITEST.EQ.3) GO TO 386
      JJJ=JJ+JP
      IF(JJJ.GT.150) JJJ=150
      A1=A1+WTH20
      ARRAY1(1,JPJ)=A1/1000.
      ARRAY1(2,JPJ)=ROO*100.
      IF(IWRITE.EQ.0) GO TO 270

```

```

      WRITE(6,8989)A1,ARRAY1(2,JJJ)
8989 FORMAT(10X,'F AT TOP=',F10.5,'(MN)',5X,'& D AT TOP=',F6.3,
1      '(CM) WHEN YIELDING OCCURS')
      GO TO 270

```

```

386 JJJ=JLM+JJ
      JPP=JJJ
      IF(JJJ.GT.150) JJJ=150
      A1=A1+PCONS
      ARRAY1(1,JJJ)=A1/1000.
      ARRAY1(2,JJJ)=(ROO+RCONS(1))*100.
      GO TO 270

```

```

C
C*****
C RESULTS FROM PILE
C*****
C

```

```

389 CONTINUE
      ROO=R(1)
      IF(ICONS.EQ.1) GO TO 392
      WRITE(6,8888) JJ
8888 FORMAT(5X,I2,' P-BODIES HAVE JUST YIELDED'/)
      JP=JP+JJ+1
      IF(JP.GT.150)JP=150
      ARRAY1(1,JP)=PNEW/1000.
      ARRAY1(2,JP)=R(1)*100.
      GO TO 390
392 IF(ITEST.EQ.3) JLM=JJJ
      JPP=JLM+MN
      IF(ITEST.EQ.3) JPP=JJJ+1
      IF(ITEST.EQ.3) JLM=JPP
      IF(JPP.GT.150) JPP=150
      ARRAY1(1,JPP)=(PNEW+PCONS)/1000.
      ARRAY1(2,JPP)=(R(1)+RCONS(1))*100.
390 FOPILE(1)=FORCE(1)

```

```

C
      DO 391 I=2,NSEG
      I1=3*(I-2)+2
      FOPILE(I)=STFPIL(I)*(R(I1)-R(I1+3))
391 CONTINUE

```

```

C
      DO 420 I=2,NNODES
      I1=3*(I-2)+2
      I2=I1+1
      I3=I1+2
      FOSOL(I-1)=STFSOL(I-1)*(R(I2)-R(I3))
      N=NPTOGA(I-1)
      DO 410 K=1,N
      AA=R(I1)-R(I2)
      IF(IPL(I,K).EQ.0) GO TO 407
      BB=FL(I,K)/SK(I,K)
      IF(IPL(I,K).EQ.-1) BB=-BB

```

```

C
C*****
C DISPLACEMENTS , FORCES , STRESSES & STRAINS

```

```

C*****
C
      UR(I,K)=AA-BB
C
407 FG(I,K)=SK(I,K)*(R(I1)-R(I2)-UR(I,K))
      UELAS(I,K)=AA-UR(I,K)
C
410 CONTINUE
      TO(I-1,MN)=FOSOL(I-1)/(HGTLAY(I-1)*2.*RO*PI)
      GA(I-1,MN)=(R(I1)-R(I2)+R(I3))*100./(RO*ALOG(SHTHRO(I-1)+1.))
420 CONTINUE
      IF(IWRITE.EQ.0) GO TO 4670
C
      DO 4660 I=2,NNODES
        J=I-1
        N=NPTOGA(I-1)
        FODSS(I-1)=0.
C
        I1=3*(I-2)
        I2=I1+1
        I3=I1+2
        DO 4650 K=1,N
C
          FODSS(I-1)=FODSS(I-1)+SK(I,K)*UELAS(I,K)
          A1=UR(I,K)*100.
          A2=UELAS(I,K)*100.
          IF(K.NE.1.AND.UR(I,K).EQ.0.) GO TO 4650
          WRITE(6,8514)I,K,A1,I,K,A2
4650 CONTINUE
C
          WRITE(6,8515)J,J,FODSS(J),J,FOPILE(J)
          A1=TO(J,MN)/TMAX(J)*100.
          WRITE(6,8516)J,GA(J,MN),J,TO(J,MN),A1
4660 CONTINUE
C
C*****
C END OF PILE *****
C*****
C
4670 IF(ICONS.EQ.0.AND.ILOAD.NE.NLOAD1) GO TO 610
      IF(ICONS.EQ.0.AND.ITEST.NE.3) GO TO 610
      IF(KLM.GT.50) KLM=50
      ARRAY4(3,KLM)=TNCYC
      ARRAY4(MN,KLM)=(R(1)+RCONS(1))*100.
      IF(MM.EQ.1) KLM=KLM+1
C
C*****
C GET ABSOLUTE RESULTS
C*****
C
      IF(MN.EQ.2) GO TO 422
      WRITE(6,8041)
      GO TO 424
422 WRITE(6,8042)
424 CONTINUE

```



```

C
  DO 430 I=1,NPOINT
  A1=R(I)*100.
  A2=(R(I)+RCONS(I))*100.
  WRITE(6,8531)I,A1,I,A2
430 CONTINUE
C
  FOPILE(1)=STFPIL(1)*(R(1)+RCONS(1)-R(2)-RCONS(2))
  FOSOL(1)=STFSOL(1)*(R(3)+RCONS(3)-R(4)-RCONS(4))
  FODSS(1)=FOSOL(1)
  DO 440 I=2,NLAYER
  I1=3*(I-1)+2
  I2=I1+1
  I3=I1+2
  FOPILE(I)=STFPIL(I)*(R(I1-3)-R(I1)+RCONS(I1-3)-RCONS(I1))
  FOSOL(I)=STFSOL(I)*(R(I2)+RCONS(I2)-R(I3)-RCONS(I3))
440 FODSS(I)=FOSOL(I)
C
  WRITE(6,8049)
C
  DO 460 I=2,NNODES
  J=I-1
  N=NPTOGA(I-1)
C
  WRITE(6,8515)J,J,FODSS(J),J,FOPILE(J)
  A1=(TO(J,MN)+TOCONS(J))/TMAX(J)*100.
  A2=GA(J,MN)+GACONS(J)
  A3=TO(J,MN)+TOCONS(J)
  WRITE(6,8561)J,A2,J,A3,A1
460 CONTINUE
C
  LMN=LLL+MN
  IF(LMN.GE.14) LMN=14
  DO 462 I=1,NLAYER
  ARRAY3(LMN,I)=TO(I,MN)+TOCONS(I)
  ARRAY2(LMN,I)=FOPILE(I)/1000.
462 CONTINUE
C
  IF(ICONS.EQ.0.AND.ILOAD.EQ.NLOAD1) GO TO 610
  IF(ITEST.EQ.3) GO TO 601
  IF(NCYC.EQ.0.) GO TO 770
C
  IF(MN.EQ.2) GO TO 470
C
C*****
C RETURN TO PILE WITH PNEW=PMIN-PCONS
C*****
C
  MN=2
  POLD=PLAST
  PLAST=PNEW
  PNEW=PMIN-PCONS
  A1=PNEW/1000.
  A2=PLAST/1000.
  A3=POLD/1000.

```

```

        WRITE(6,8812)A1,A2,A3,MN
        GO TO 180
C
C*****
C CONSIDER CYCLIC DEGRADATION OF THE SOIL
C*****
C
  470 MN=1
        IF(IN.EQ.0.AND.PDEF(5,ILOAD).NE.0.) LLL=LLL+2
  471 A1=PMAX/1000.
        A2=PMIN/1000.
        IF(MM.EQ.2) GO TO 472
        WRITE(6,8545)
        WRITE(6,8540)A1,A2,NC
        GO TO 474
  472 WRITE(6,8546)
        WRITE(6,8542)A1,A2,NC,IN
  474 CONTINUE
        DO 480 I=1,NLAYER
          GAVGE(I,MM)=(GA(I,1)+GA(I,2))/2.+GACONS(I)
          GACYC(I,MM)=ABS((GA(I,1)-GA(I,2))/2.)
          TOVGE(I,MM)=(TO(I,1)+TO(I,2))/2.+TOCONS(I)
          TOCYC(I,MM)=ABS((TO(I,1)-TO(I,2))/2.)
          TCY=TOCYC(I,MM)/TMAX(I)*100.
          TAV=TOVGE(I,MM)/TMAX(I)*100.
          TT=(TOVGE(I,2)-TOVGE(I,1))/TMAX(I)*100.
C
          WRITE(6,8500)I
          WRITE(6,8501)I,MM,GAVGE(I,MM)
          WRITE(6,8502)I,MM,GACYC(I,MM)
          IF(MM.EQ.1) WRITE(6,8503)I,MM,TOVGE(I,MM),TAV
          IF(MM.EQ.2) WRITE(6,8803)I,MM,TOVGE(I,MM),TAV,TT
          WRITE(6,8504)I,MM,TOCYC(I,MM),TCY
C
  480 CONTINUE
C
        IF(MM.EQ.2) WRITE(6,8546)
        IF(MM.EQ.1) WRITE(6,8545)
C
C*****
C STORE PLASTIC DISPL. AND PRANDTL STIFFNESSES FOR 1ST CYCLE
C*****
C
        IF(IN.NE.0) GO TO 500
        IF(IWRITE.EQ.1) WRITE(6,8543)
        DO 490 I=2,NNODES
          N=NPTOGA(I-1)
          DO 490 K=1,N
            U1(I,K)=UR(I,K)
            SK1(I,K)=SK(I,K)
            FG1(I,K)=FG(I,K)
            GOR1(I)=GOR(I)
            FTRON1(I-1)=FTRONG(I-1)
  490 CONTINUE
C

```

```

      IF(IWRITE.EQ.1)WRITE(6,8505)
    500 IF(JCYC.EQ.0) GO TO 540
  C
  C*****
  C IS THE CHANGE OF AVERAGE SHEAR STRESS ACCEPTABLE?
  C*****
  C
      IF(DN.LT.2.) GO TO 515
      DO 510 I=1,NLAYER
      IF(TOVGE(I,2).LT.0.) GO TO 550
      TT=(TOVGE(I,2)-TOVGE(I,1))/TMAX(I)*100.
      TT=ABS(TT)
      IF(TT.GT.ACC) GO TO 560
    510 CONTINUE
  C
    515 IF(IWRITE.EQ.1)WRITE(6,8037)
      DO 1700 I=1,NLAYER
    1700 FTRON2(I)=FTRONG(I)
      TN=TN+DN
      KLM=KLM+1
      JLM=JLM+2
  C
  C*****
  C ARE ALL THE CYCLES OF THIS PACKAGE COMPLETED?
  C*****
  C
      IF(NC.EQ.NCYC) GO TO 600
      DN=NCYC-NC
      TNCYC=TN+DN
      NC=NCYC
      DO 520 I=1,NLAYER
      TOVGE(I,1)=TOVGE(I,2)
      TOCYC(I,1)=TOCYC(I,2)
      GACYC(I,1)=GACYC(I,2)
    520 GAVGE(I,1)=GAVGE(I,2)
  C
  C*****
  C STORE PLASTIC DISPL. AND Prandt1 STIFFNESSES FOR INTERMEDIATE CYCLE
  C*****
  C
      DO 530 I=2,NNODES
      N=NPTOGA(I-1)
      DO 530 K=1,N
      U1(I,K)=UR(I,K)
      SK1(I,K)=SK(I,K)
      FG1(I,K)=FG(I,K)
      GOR1(I)=GOR(I)
      FTRON1(I-1)=FTRONG(I-1)
    530 CONTINUE
  C
      WRITE(6,8999)NCYC, DN
    8999 FORMAT(5X, 'NEW ITERATION TO COMPLEMENT NCYC=',F6.0,
    1', NOW DN=',F6.0, 'CYCLES. ENTER CYCDEG' /)
      IN=1
      GO TO 580

```

```

C
  540 MM=2
      TNCYC=TN+DN
      JCYC=1
      GO TO 570
C
  550 IF(IWRITE.EQ.1) WRITE(6,8508)I,TOVGE(I,2)
C
C*****
C REDUCE NUMBER OF CYCLES TO HALF AND START AGAIN
C*****
C
  560 DN=DN/2.
      TNCYC=TN+DN
      NC=NC-DN
      IF(IWRITE.EQ.1)WRITE(6,8509)I,TT,DN,NCYC
C
C*****
C IN AND IIN ARE INDEXES LIMITING THE NUMBER OF ITERATIONS
C*****
C
  570 IN=IN+1
      IF(IN.EQ.LIMIN) GO TO 740
  580 IIN=IIN+1
      IF(IIN.EQ.LIMIIN) GO TO 750
      IF(IWRITE.EQ.1) WRITE(6,8510)IN,IIN
      IF(IWRITE.EQ.1) WRITE(6,8547)
C
C*****
C ENTER DO LOOP IN WHICH THE CYCLIC DEGRADATION IS CONSIDERED FOR
C EACH SOIL LAYER.
C*****
C
      IA=0
C
      DO 590 I=1,NLAYER
      IF(IWRITE.EQ.1) WRITE(6,8500) I
      GAVO=GAVGE(I,1)
      TCY=TOCYC(I,1)/TMAX(I)
      TAV=TOVGE(I,1)/TMAX(I)
      GCY=GACYC(I,1)
      GG(I)=(GAVO-GACONS(I))*RO*(ALOG(SHTHRO(I)+1.))/100.
      IF(GG(I).LT.0.) GG(I)=0.
      IF(TAV.LE.0.) GO TO 595
C
      *****
      CALL CYCDEG(TAV,TCY,GAVO,DN,GAV,GCY,IWRITE)
C
      *****
      GO TO 598
  595 GAV=GAVO
  598 CONTINUE
      GAVEC(I)=GAV
      AB=GCY/GACYC(I,1)
      IF(AB.LT.1.)AB=1.
      GOR(I+1)=GAV-(GAVO-GACONS(I)-GOR1(I+1))*AB-GACONS(I)
      IF(GOR(I+1).LT.0.) GOR(I+1)=0.

```

```

DOR(I+1)=GOR(I+1)*RO*(ALOG(SHthro(I)+1.))/100.
C
IF(GAV.GE.15.)IA=IA+1
C
N=NPTOGA(I)
C
A1=DOR(I+1)*100.
A3=GG(I)*100.
IF(IWRITE.EQ.1) WRITE(6,9000)A3,AB,GOR(I+1),GOR1(I+1),A1
9000 FORMAT(5X,'GG=',F10.6,2X,'AB=',F10.6,2X,'GOR=',
1F10.6,2X,'GOR1=',F10.6,2X,'DOR=',F10.6/)
C
DO 590 K=1,N
SK(I+1,K)=SK1(I+1,K)/AB
UR(I+1,K)=U1(I+1,K)*AB
590 CONTINUE
IF(IWRITE.EQ.1) WRITE(6,8505)
C
A1=DOR(NNODES)
IF(A1.LT.0.)A1=0.
A2=A1*STRONG
DO 596 I=2,NNODES
DOR(I)=DOR(I)-A1
IF(DOR(I).LT.0.) DOR(I)=0.
596 FTRONG(I-1)=A2
DO 597 I=2,NNODES
I1=3*(I-2)+2
BUF=GG(I-1)+GACONS(I-1)/SOFCO(I-1)*RO*ALOG(SHthro(I-1)+1.)/100.
IF(DOR(I).GT.BUF) DOR(I)=BUF
FTRONG(I-1)=FTRONG(I-1)+DOR(I)*STRONG
C
I2=I-1
A3=(DOR(I)+A1)*100.
IF(IWRITE.EQ.1) WRITE(6,9001)I2,A3,FTRONG(I2)
9001 FORMAT(5X,'LAYER #',I2,5X,'DISPL. FIXED REF.=',
1F10.6,'(CM)',5X,'FTRONG=',E10.3,'(KN)')
597 CONTINUE
C
J3=1
DO 5090 I=2,NLAYER
I2=NLAYER+1-I
FADD=PCONS/STFPIL(I2+1)*STRONG
IF(GAVEC(I2).GE.15.) GO TO 5190
IF(FTRONG(I2).GE.FTRONG(I2+1).AND.J3.EQ.1) GO TO 5090
IF(FTRONG(I2).LT.FTRONG(I2+1).AND.J3.EQ.1) GO TO 5096
IF(FTRONG(I2).LE.FTRONG(J3+1)) GO TO 5094
J1=I2+1
DO 5095 K=J1,J3
FTRONG(K)=-FLOAT(K-I2)*(FTRONG(I2)-FTRONG(J3+1))
5095 FTRONG(K)=FTRONG(K)+FTRONG(I2)
J3=1
GO TO 5090
5096 J3=I2
5094 IF(I.NE.NLAYER) GO TO 5090
DO 5098 K=1,J

```

```

5098 FTRONG(K)=FTRONG(J3+1)
5090 CONTINUE
      GO TO 5192

5190 DO 5191 L=1,I2
      L1=I2+1-L
5191 FTRONG(L1)=FTRONG(L1+1)

5192 DO 5193 I=1,NLAYER
      IF(FTRONG(I).LT.FTRONG(I)) FTRONG(I)=FTRONG(I)
5193 GOR(I)=(FTRONG(I)/STRONG)/(RO*(ALOG(SHthro(I-1)+1.))/100.)

      IF(IWRITE.EQ.0) GO TO 5100
      WRITE(6,8505)
      DO 5101 I=1,NLAYER
5101 WRITE(6,5099) I,FTRONG(I)
      WRITE(6,8505)
5100 CONTINUE
5099 FORMAT(5X,'FTRONG(',I2,')=',E10.3,'(KN)')

      IF(IA.EQ.NLAYER) GO TO 765
C
      IF(IWRITE.EQ.1) WRITE(6,8505)
C
      POLD=PMAX-PCONS
      PNEW=POLD
      PLAST=PMIN-PCONS
      A1=PNEW/1000.
      A2=PLAST/1000.
      A3=POLD/1000.
      WRITE(6,8812)A1,A2,A3,MN
8812 FORMAT(5('*'),'ENTER PILE MODEL WITH PNEW=',F9.4,'(MN)'
1,5X,'PLAST=',F9.4,'(MN)',5X,
2'POLD=',F9.4,'(MN)',5X,'MN=',I2/)
C
      GO TO 190
C
C*****
C END OF LOADING - STOP
C*****
C
601 LLL=LLL+1
      JLM=JLM+1
600 IF(ILOAD.EQ.NLOAD2) GO TO 770
      ILOAD=ILOAD+1
      IF(ILOAD.NE.1.AND.PDEF(5,ILOAD).NE.0.) LLL=LLL+2
      IIN=0
      IN=0
      JCYC=0
      POLD=PLAST
      PLAST=PNEW
      MM=1
      WRITE(6,8038)
C
      PMAX=PDEF(2,ILOAD)

```

```

      PMIN=PDEF(3,ILOAD)
      NCYC=PDEF(4,ILOAD)
      IF(NCYC.EQ.0.) LLL=LLL+2
      WRITE(6,8035)PMAX,PMIN,NCYC
      PMAX=PMAX*1000.
      PMIN=PMIN*1000.
      DN=NCYC
      NC=NCYC
      TNCYC=TN+DN
C
      PMA=PMAX-PCONS
      PMI=PMIN-PCONS
      IF(PMA.EQ.POLD.AND.PMI.EQ.PLAST) GO TO 606
C
C*****
C GO TO PILE WITH PNEW=PMAX-PCONS
C*****
C
      PNEW=PMAX-PCONS
      A1=PNEW/1000.
      A2=PLAST/1000.
      A3=POLD/1000.
      WRITE(6,8812)A1,A2,A3,MN
      IF(ILOAD.EQ.1) GO TO 190
      GO TO 180
C
606 PNEW=PMI
      PLAST=PMA
      POLD=PMI
      MN=1
      GO TO 471
C
C*****
C STATIC LOADING BEFORE CONSOLIDATION
C*****
C
610 CONTINUE
      A1=PNEW/1000.
      A2=PLAST/1000.
      A3=POLD/1000.
      WRITE(6,8512)A1,A2,A3,MN
      DO 615 I=1,NPOINT
      A1=R(I)*100.
615 WRITE(6,8513)I,A1
C
      IF(ILOAD.EQ.NLOAD1) GO TO 680
      POLD=PLAST
      PLAST=PNEW
      ILOAD=ILOAD+1
      PNEW=PDEF(1,ILOAD)
      PNEW=PNEW*1000.
C
      GO TO 180
C
C*****

```

## C CONSOLIDATION

C\*\*\*\*\*

C

```

680 PCONS=PNEW
    LLL=LLL+1
    JLM=JJJ+1
    DO 690 I=1,NPOINT
690 RCONS(I)=R(I)
    DO 710 I=1,NLAYER
    N=NPTOGA(I)
    GACONS(I)=GA(I,1)
    TOCONS(I)=TO(I,1)
710 CONTINUE

```

C

```

    IF(IWRITE.EQ.1) WRITE(6,8517)
    A1=0.

```

C

```

    DO 730 I=1,NLAYER
    N=NPTOGA(I)
    B=TO(I,1)/TMAX(I)
    FLM=(1.+(ALPHA(I)-1.)*B)*TIMEFC(I)
    CORCON(I)=2.*TIMEFC(I)/FLM-1.
    SKM=FLM/(1.-BETA(I)*B)

```

C

```

    DO 720 K=1,N
    FL(I+1,K)=FL(I+1,K)*FLM
    A1=A1+FL(I+1,K)
    SK(I+1,K)=SK(I+1,K)*SKM*SOFCON(I)

```

C

```

    J=I+1
    IF(IWRITE.EQ.0) GO TO 721
    WRITE(6,8518)J,K,FL(J,K),J,K,SK(J,K)

```

C

```

721 FG(I+1,K)=0.
720 UR(I+1,K)=0.
    W(I+1)=0.
730 CONTINUE
    W(1)=0.
    ROO=0.

```

C

```

    A1=(A1+PCONS)/1000.
    WRITE(6,8060)A1

```

C

```

    IF(IWRITE.EQ.0) GO TO 736
    WRITE(6,8505)
    DO 735 I=1,NLAYER
735 WRITE(6,8550)I,CORCON(I)
736 WRITE(6,8548)
    IF(ITEST.EQ.2) STOP

```

C

```

    PLAST=0.
    PNEW=0.
    ILOAD=0
    ICONS=1
    GO TO 600

```



```

C
C*****
C END OF CONSOLIDATION GO TO CYCLIC LOADING
C*****
C
  740 WRITE(6,8600)
      STOP
  750 WRITE(6,8601)
      STOP
  760 IF(ITEST.EQ.3) GO TO 770
      WRITE(6,8521)
      STOP
  765 WRITE(6,8560)
  770 IF(ITEST.EQ.3.OR.NLOAD2.EQ.0) GO TO 772
      CALL QPICTR(ARRAY1,2,JPP,QY(1),QX(2),QXLAB(XLAB1),
  1 QYLAB(YLAB1),QLABEL(1014),QISCL(-2),QXSCL(XSCL1))
      GO TO 774
  772 CALL QPICTR(ARRAY1,2,JPP,QY(1),QX(2),QXLAB(XLAB1),
  1 QYLAB(YLAB1),QLABEL(1014))
      IF(NLOAD2.EQ.0) STOP
  774 CALL QPICTR(ARRAY2,15,NSEG,QX(15),
  1 QY(1,2,3,4,5,6,7,8,9,10,11,12,13,14),QXLAB(XLAB2),
  2 QYLAB(YLAB2),QLABEL(4),QISCL(-2),QXSCL(XSCL2))
      CALL QPICTR(ARRAY3,15,NSEG,QX(15),
  1 QY(1,2,3,4,5,6,7,8,9,10,11,12,13,14),QXLAB(XLAB3),
  2 QYLAB(YLAB3),QLABEL(4),QISCL(-2),QXSCL(XSCL3))
      IF(ITEST.EQ.3) STOP
      CALL QPICTR(ARRAY4,3,KLM,QX(3),QY(1,2),QXLAB(XLAB4),
  1 QYLAB(XLAB1),QLABEL(1014),QISCL(-2),QXSCL(XSCL4))
      STOP
  775 WRITE(6,8700)
  8700 FORMAT(//2X,'NLOAD1 OR NLOAD2 > 10  STOP')
C
C
C
C
C
  4010 FORMAT(4F10.2,1PE10.2,2I10)
  4050 FORMAT(3I10,3F5.2)
  4030 FORMAT(2F10.4)
  4080 FORMAT(5F10.2,I10)
  4081 FORMAT(5F10.2)
  4082 FORMAT(F10.2)
  4083 FORMAT(F10.2)
  8000 FORMAT(///2X,'LENGTH=' ,F7.2,' (m)' ,2X,'FRELTH=' ,F5.2,' (m)' ,
  12X,'DIAM=' ,F7.2,' (cm)' ,
  22X,'DNSITY=' ,F5.2,2X,'DTYFIL=' ,F5.2,2X,'E=' ,1PE10.2,' (MPa)')
  8300 FORMAT(2X,'XA=' ,F7.4,' (m2)' ,2X,'LCYC=' ,F5.2,2X,'ALPFAC=' ,
  1F5.2)
  8001 FORMAT(/2X,'NLAYER=' ,I2,2X,'NNODES=' ,I2,2X,'NPOINT=' ,I2,2X,
  1 'NLOAD1=' ,I2,2X,'NLOAD2=' ,I2,2X,'ITEST=' ,I1,2X,'IWRITE=' ,I1//)
  8004 FORMAT(/2X,'HGTLAY(' ,I2,' )=' ,F5.2,' (m)' ,2X,'SHTHRO(' ,I2,' )=' ,F5.2,
  12X,'TMAX(' ,I2,' )=' ,F9.2,' (kPa)' ,2X,'DMAX(' ,I2,' )=' ,F7.4,' (cm)' ,
  22X,'DMAX IN % OF DIAM=' ,F7.4)

```

```

8005 FORMAT(2X,'DENSOL(' ,I2,' )=' ,F5.2,2X,'GSIG(' ,I2,' )=' ,F10.2,2X,
1'RMRO(' ,I2,' )=' ,F5.2,2X,'NPTOGA(' ,I2,' )=' ,I2)
8006 FORMAT(2X,'TIMEFC(' ,I2,' )=' ,F5.2,2X,'SOFT(' ,I2,' )=' ,F5.2,2X,
1'ALPHA(' ,I2,' )=' ,F5.2,2X,'BETA(' ,I2,' )=' ,F5.2)
8007 FORMAT(2X,'SIG(' ,I2,' )=' ,F10.2,'(kPa)',2X,'SOFCON(' ,I2,' )=' ,F5.2,
12X,'STFSOL(' ,I2,' )=' ,F12.2,'(kN/m)',2X,'W(' ,I2,' )=' ,F9.2,
2'(kN)')
8010 FORMAT(2X,'THICK(' ,I2,' )=' ,F5.2,'(cm)',2X,'XAREA(' ,I2,' )=' ,
1F7.4,'(m2)')
8008 FORMAT(2X,'FDSS(' ,I2,' ,',I2,' )=' ,F10.4,'(kN)',2X,'DDSS(' ,I2,' ,',
1I2,' )=' ,F5.2,'(cm)',2X,'FL(' ,I2,' ,',I2,' )=' ,F10.2,'(kN)',2X,
2'SK(' ,I2,' ,',I2,' )=' ,F10.2,'(kN/m)')
8009 FORMAT(2X,'STFPIL(' ,I2,' )=' ,F15.2,'(MN/m)')
8040 FORMAT(2X,'W(' ,I2,' )=' ,F9.2,'(kN)')
8041 FORMAT(/10X,'DISPLACEMENTS OF NODAL POINTS UNDER PMAX-PCONS')
8042 FORMAT(/10X,'DISPLACEMENTS OF NODAL POINTS UNDER PMIN-PCONS')
8049 FORMAT(/5X,'ABSOLUTE RESULTS')
8011 FORMAT(///2X,'PLIMIT=' ,F10.5,'(MN)',2X,'WTH20=' ,F10.5,'(MN)',
12X,'WPH20=' ,F10.5,'(MN)',2X,'WPILE=' ,F10.5,'(MN)',2X,
2'WFILL=' ,F10.5,'(MN)')
8012 FORMAT(2X,'PTENS=' ,F10.5,'(MN)',5X,'PCOMP=' ,F10.5,'(MN)')
8030 FORMAT(2X,'SK(' ,I2,' ,',I2,' )=' ,F10.2,'(kN/m)')
8031 FORMAT(2X,'CORRECT SK WITH SOFCON')
810 FORMAT(8F5.1)
820 FORMAT(6F5.2)
830 FORMAT(5F5.2)
840 FORMAT(4F5.2)
850 FORMAT(7F5.0)
825 FORMAT(7F5.2)
870 FORMAT(6F6.3)
871 FORMAT(6F5.3)
6011 FORMAT(F10.2)
8032 FORMAT(80('*')/ ,2X,'PNEW=' ,F9.4,'(MPa)',5X,
1'ENTER PILE FOR 1ST TIME')
8033 FORMAT(10X,'P-BODY #',I2,5X,'HAS JUST YIELDED IN LAYER #',I2)
8034 FORMAT(/5X,'MN=' ,I2/)
8037 FORMAT(/20('*') ,1H ,2X,'THE CHANGE OF SHEAR STRESS IS OK',
11H ,2X,'GET NEW VALUES OF NC AND DN ,IF NECESSARY')
8038 FORMAT(2X,80('*'))
8035 FORMAT(/5('*') ,1H ,2X,'NEW PACKAGE : PMAX=' ,F10.4,5X,'PMIN=' ,
1F10.4,5X,'NCYC=' ,F10.0/)
8060 FORMAT(/2X,'NEW PLIMIT=' ,F10.6,'(MN)')
8600 FORMAT(2X,'IN=10')
8601 FORMAT(2X,'IIN=50')
8521 FORMAT(2X,'ALL SPRINGS YIELDED')
8500 FORMAT(5X,'LAYER #',I2)
8501 FORMAT(20X,'GAVGE(' ,I2,' ,',I2,' )=' ,F9.3,'(%)')
8502 FORMAT(20X,'GACYC(' ,I2,' ,',I2,' )=' ,F9.3,'(%)')
8503 FORMAT(20X,'TOVGE(' ,I2,' ,',I2,' )=' ,F9.3,'(kPa)',3X,
1 F6.2,'(%) OF TMAX')
8803 FORMAT(20X,'TOVGE(' ,I2,' ,',I2,' )=' ,F9.3,'(kPa)',3X,
1 F6.2,'(%) OF TMAX',3X,'CHANGE =' ,F6.2,'(%)')
8504 FORMAT(20X,'TOCYC(' ,I2,' ,',I2,' )=' ,F9.3,'(kPa)',3X,
1 F6.2,'(%) OF TMAX')
8505 FORMAT(//)

```

```

8506 FORMAT(2X,'U1(' ,I2,' ,',I2,')=' ,F7.4,' (cm)' ,5X,'SK1(' ,I2,' ,',I2,
1')=' ,F12.2,' (kN/m)' )
8507 FORMAT(5X,'LAYER=' ,I2,5X,'REL. CHANGE OF SHEAR STRESS =' ,F6.2,
1' (%)' )
8508 FORMAT(///5X,'NEGATIVE AV. SHEAR STRESS IN LAYER #' ,I2,
15X,'TOVGE=' ,F10.2,///)
8509 FORMAT(///2X,'LAYER #' ,I2,5X,'TT=' ,F7.4,5X,'NEW DN=' ,F7.0,5X,
1'NCYC=' ,F7.0//)
8510 FORMAT(///2X,'IN=' ,I2,5X,'IIN=' ,I2)
8511 FORMAT(2X,'UR(' ,I2,' ,',I2,')=' ,F7.4,' (cm)' ,5X,'SK(' ,I2,' ,',
I2,')=' ,F12.2,' (kN/m)' )
8512 FORMAT(/5('*') ,RESULTS FROM PILE MODEL,STATIC PRELOADING STAGE' /,
12X,'PNEW=' ,F9.4,' (MN)' ,5X,'PLAST=' ,F9.4,' (MN)' ,5X,
2'POLD=' ,F9.4,' (MN)' ,5X,'MN=' ,I2/)
8513 FORMAT(20X,'R(' ,I2,')=' ,F10.6,' (cm)' )
8514 FORMAT(15X,'UR(' ,I2,' ,',I2,')=' ,F7.4,' (cm)' ,5X,'UELAS(' ,I2,' ,',I2,
1')=' ,F7.4,' (cm)' )
8515 FORMAT(10X,'LAYER #' ,I2,5X,'FODSS(' ,I2,')=' ,F8.2,' (kN)' ,
1 5X,'FOPILE(' ,I2,')=' ,F10.2,' (kN)' )
8516 FORMAT(10X,'GA(' ,I2,' ,',1)=' ,F6.2,' (%)' ,5X,'TO(' ,I2,' ,',1)=' ,F8.2,
1' (kPa)' ,5X,'SHEAR STRESS RATIO=' ,F9.4,' (%)' )
8517 FORMAT(/10X,'CONSOLIDATION (SEE R() ABOVE FOR ORIGIN) ' /)
8518 FORMAT(10X,'FL(' ,I2,' ,',I2,')=' ,F10.2,' (kN)' ,5X,'SK(' ,I2,' ,',I2,
1')=' ,F12.2,' (kN/m)' )
8520 FORMAT(2F10.4,F10.0)
8525 FORMAT(10X,'FORCE(' ,I2,')=' ,F12.2,' (KN)' )
8531 FORMAT(10X,'R(' ,I2,')=' ,F10.6,' (cm)' ,10X,'ABSOLUTE R(' ,I2,')=' ,
1F10.6,' (cm)' )
8540 FORMAT(10X,'DEFORMATIONS & SHEARS AT DEFINITE POINT' ,5X,
1'PMAX=' ,F9.4,5X,'PMIN=' ,F9.4,5X,'NC=' ,F6.0/)
8541 FORMAT(10X,'UR(' ,I2,' ,',I2,')=' ,F7.4,' (cm)' ,5X,'ABS.UR(' ,I2,' ,',
I2,')=' ,F7.4,' (cm)' )
8542 FORMAT(10X,'DEFORMATIONS & SHEARS AT POTENTIAL POINT' ,5X,
1'PMAX=' ,F9.4,' (MN)' ,2X,'PMIN=' ,F9.4,' (MN)' ,2X,'NC=' ,F6.0,2X,
2'IN=' ,I2/)
8543 FORMAT(///5X,'STORE VALUES OF UR & SK FOR 1ST CYCLE OF NEW PACK.' /
1)
8544 FORMAT(///5X,'STORE VALUES OF UR & SK FOR INTERM. CYCLE OF NEW PA'
1'CK.' /)
8545 FORMAT(/5X,75('1')/)
8546 FORMAT(/5X,75('2')/)
8547 FORMAT(2X,18('-')/)
8548 FORMAT(//2X,20('*') ,CONSOLIDATION COMPLETED' ,20('*'))
8549 FORMAT(1H1)
8550 FORMAT(2X,'CORCON(' ,I2,')=' ,F7.4)
8560 FORMAT(/2X,'THE PILE IS FAILING, ALL SOIL ELEMENTS' ,
1'HAVE REACHED A DEFORMATION OF 15% STOP!' )
8561 FORMAT(10X,'ABS.GA(' ,I2,' ,',1)=' ,F5.2,' (%)' ,5X,'ABS.TO(' ,I2,' ,',1)=' ,
1F10.2,' (kPa)' ,5X,'ABS.SHEAR STRESS RATIO=' ,F8.4,' (%)' )

```

C  
C  
C

END

5.C DATA FILE FOR EXAMPLE /1/

\*\*\*\*\*  
Input file for the basic example of chapter 5.  
\*\*\*\*\*

BASIC EXAMPLE

\*\*\*\*\* F.S.= 1.5, kcy= 0.85, wall thick.= 2", diam.= 72", L= 90.69 meters

TOP DISPLACEMENT IN CM

TOP FORCE IN MN

DEPTH IN M

FORCE IN PILE IN MN

DEPTH IN M

SHEAR STRESS ON PILE IN KN/M\*\*2

Plot descriptors

NUMBER OF CYCLES

-0.50	3.00	0.00	14.00
-110 00	0.00	0 00	12.50
-110.00	0.00	-15.00	35.00
0.00	700.00	-0 50	3 00

183.	7.	1.7	5.	2.1E08	0	0
10 75						
10	1	9	10.	1.	.5	Global parameters

6.87 Static loading

10.79	2.94	1.	1.
10.79	2 94	2.	
10.79	2.94	50.	
10.79	2 94	500.	1.
12.26	1.47	1.	1.
12 26	1.47	2.	
12.26	1.47	5.	
12 26	1 47	50.	

Cyclic loading

6.87

9.07	.5	1.7	100.	10.	6
1.1	1 0	.52	48	10.	

5.08

0.089

0.138

0.172

0.196

0.211

0.215

Layer parameters

Repeate desription of Layer 9 other times ( since there is a total of 10 layers )

9.0

1. .7 .6 .5 .4 .3 .2 0.

0.	.2	4	6	.8	1.
2.5	3.	4.	6.	15.	
.15	25	5	3.		
1.	50.	100.	200.	500.	1000.
1.1	.73	.68	.63	.57	.52
.60	.67	.77	.88	.95	

Data global parameters

.55	.57	58	.585	.59	.595
.63	.65	.655	.66	.665	.668
.70	.72	74	.75	.76	.765
.76	.79	.82	.84	.85	.86
.765	.805	.86	.89	.91	.93
.15	.35	.47	.54	.58	.59
.175	.38	.52	.59	.635	.655
.20	.43	.59	.70	.74	.755
.225	.48	.65	.75	.815	.85
.25	.53	.70	.79	.86	.91
-1.	.29	.43	.52	.57	.585
-1.	.33	.49	.58	.63	.652
-1.	.37	.56	.67	.73	.75
-1.	.40	.60	.72	.80	.84
-1.	.45	.64	.76	.84	.90
-1.	.15	.36	.49	.56	.582
-1	.18	.41	.55	.625	.65
-1.	.22	.52	.64	.70	.745
-1.	.26	.57	.71	.79	.835
-1.	.30	.59	.74	.82	.89
-1.	-1.	.27	.45	.54	.58
-1.	-1.	.325	.50	.61	.645
-1.	-1.	.39	.57	.68	.74
-1.	-1.	.50	.695	.77	.83
-1.	-1.	.53	.73	.81	.88
-1.	-1.	.15	.40	.53	.575
-1.	-1.	.175	.46	.60	.64
-1.	-1.	.20	.54	.67	.735
-1.	-1.	.225	.595	.74	.82
-1.	-1.	.25	.67	.79	.87
-1.	-1.	-1.	.30	.51	.57
-1.	-1.	-1.	.35	.57	.635
-1.	-1.	-1	.40	.64	.73
-1.	-1.	-1.	.45	.70	.815
-1.	-1.	-1.	.50	.75	.865

TOAVE network

50	.50	.50	.50	.50	.50
.62	.62	.62	.62	.62	.62
.87	.87	.87	.87	.87	.87
1 08	1.08	1.08	1.08	1.08	1 08
.46	.455	.45	.43	.38	.27
.575	.57	.54	.52	.39	.275
.645	.635	.61	.57	.40	.28
.73	.70	.64	.60	.41	.285
.45	.45	.44	.425	.35	.27
.545	.54	.525	.46	.36	.275
.60	.595	.575	.505	.37	.28
.67	.65	.61	.54	.38	.285

TOCYC network

425	.425	.42	.40	.34	.27
525	.52	50	.45	.35	.275
.57	.565	.54	.48	.36	.28
.625	60	.57	51	.37	.285
.41	.41	.40	.39	.33	.27
.48	475	465	.44	.34	.275
.55	.54	.52	.47	.35	.28
.565	.56	.54	.48	.36	.285
.39	.385	.375	.35	.32	.27
.46	.45	.43	.39	.33	.275
.49	.48	.46	.42	.34	.28
.52	50	485	.45	.35	.285
.37	.37	.36	.33	.31	.27
.41	.41	39	.36	.32	.275
.445	.445	.43	.39	.33	.28
.45	45	44	.41	.34	.285